Aushiq Ali Memon

Communication-Based Adaptive Protection of AC Microgrids with Converter-Based Distributed Energy Resources

ACTA WASAENSIA 529

Vaasan yliopisto
UNIVERSITY OF VAASA

ISBN 978-952-395-130-3 (print)
978-952-395-131-0 (online)

ISSN 0355-2667 (Acta Wasaensia 529, print)
2323-9123 (Acta Wasaensia 529, online)

URN https://urn.fi/URN:ISBN:978-952-395-131-0

Hansaprint Oy, Turenki, 2024.

ACADEMIC DISSERTATION

To be presented, with the permission of the Board of the School of Technology and Innovations of the University of Vaasa, for public examination on the 23rd of February, 2024, at noon.

Article based dissertation, School of Technology and Innovations, Electrical Engineering

Author	Aushiq Ali Memon https://orcid.org/0000-0003-1290-6312
Supervisor(s)	Professor Kimmo Kauhaniemi University of Vaasa. School of Technology and Innovations, Electrical Engineering. Professor Timo Vekara University of Vaasa. School of Technology and Innovations, Electrical Engineering.
Custos	Professor Kimmo Kauhaniemi University of Vaasa. School of Technology and Innovations, Electrical Engineering.
Reviewers	Professor Tarlochan Sidhu University of Ontario Institute of Technology. Faculty of Engineering and Applied Science, Department of Electrical, Computer and Software Engineering. Professor Nathaniel Taylor KTH Royal Institute of Technology. Faculty of Electrical Engineering and Computer Science EECS, Department of Electromagnetic Engineering EME.
Opponent	Professor Francisco Gonzalez-Longatt University of South-Eastern Norway. Department of Electrical Engineering, Information Technology and Cybernetics. Loughborough University. School of Mechanical, Electrical and Manufacturing Engineering.

Tiivistelmä

Vaihtovirtaan (AC) perustuvien mikroverkkojen käyttöönottoon liittyy monia taloudellisia ja teknisiä haasteita. Merkittävimmät tekniset haasteet koskevat järjestelmän ohjausta ja suojausta. AC-mikroverkkojen toiminta sekä muuhun verkkoon kytkeytyneenä että itsenäisenä saarekkeena, hajautettujen energiaresurssien (DER) kytkeminen ja irrottaminen sekä niiden rajallinen kyky syöttää vikavirtaa edellyttävät mukautuvia ohjaus- ja suojausjärjestelmiä. Eri ohjaus- ja suojalaitteiden välillä on oltava tietoliikenneyhteydet adaptiivisten suojausjärjestelmien toteuttamiseksi. Suojalaitteiden tulee pystyä käsittelemään ennakoimattomia viiveitä ja virheitä tietoliikenteessä. DER-yksiköiden säädön tulee toimia normaalin verkkoa seuraavan tilan lisäksi myös verkon muodostavassa tilassa toimittaessa saarekekäytössä. Lisäksi tarvitaan strategia energian varastointiin kuormituksen ja tuotantovaihteluiden tasoittamiseksi saareketilanteessa. Verkkoonliitynnän määräykset ovat yleensä saatavilla verkkoon kytketylle toimintatavalle, joten saarekekäytölle on kehitettävä uusia ohjeita. Tarvetta olisi myös kehittää suunnattu suojausjärjestelmä, joka toimisi erilaisilla mikroverkoilla ja eri toimintatiloissa.

Edellä mainitut tekijät huomioon ottaen tässä väitöskirjassa ehdotetaan, analysoidaan ja validoidaan verkkovaihtosuuntaajiin perustuvia energiaresursseja sisältävien AC-mikroverkkojen tietoliikennepohjaisia adaptiivisia suojausratkaisuja sekä ei-reaaliaikaisilla simuloinneilla että reaaliaikaisilla hardware-in-the-loop (HIL) -simuloinneilla. Työssä on tarkasteltu Ethernet-pohjaisia viestintäprotokollia, ja IEC 61850 -standardin mukainen GOOSE-protokolla on valittu käytettäväksi adaptiivisissa suojausjärjestelmissä. Simulointitulosten perusteella työssä ehdotetaan käytettäväksi ylivirtasuojareleiden vakioaikaan perustuvaa koordinointia saareketilassa. Saareketilan osalta on tutkittu DER-yksiköiden ja akkuenergiavarastojen (BESS) tuottaman vikavirran lisäämistä niin, että adaptiivinen ylivirtasuojaus voitaisiin välttää ja varmistettaisiin nopea sulakesuojauksen toiminta. Lisäksi työssä on ehdotettu ja arvioitu virran suuruusvertailuun ja symmetristen komponenttien käyttöön perustuvia suunnattuja suojausjärjestelmiä. Väitöskirjassa ehdotetaan myös menetelmiä vaihekatkosten havaitsemiseksi sekä uusia rajakäyriä vaihtosuuntaajapohjaisten DER-yksiköiden jännitekuopan (LVRT) ja jännitteen nousun (HVRT) sietoisuudelle.

Avainsanat: AC-mikroverkot, adaptiivinen suojaus, saareketila, vaihtosuuntaajaliitäntäiset hajautetut energiaresurssit, IEC 61850 tietoliikenne, GOOSE-protokolla, HIL-simulaatiot

Abstract

The implementation of AC microgrids has many economic and technical challenges. The most prominent technical challenges of AC microgrids include those of control and protection. The operation of AC microgrids in both grid-connected and islanded modes, the connection and disconnection of distributed energy resources (DERs) due to operational and economic reasons, and the limited fault current contribution of converter-based DERs require adaptive control and protection schemes. Communication links between control and protection devices need to be provided to implement adaptive control and protection schemes. The protection devices should be capable of handling unwarranted and nondeterministic communication delays and failures. In addition to the grid-following control of DERs, the grid-forming control of DERs is also required for the islanded mode of operation. Additionally, some kind of energy storage is also required for smoothing load and generation variations in the islanded mode. The grid codes are usually available for the grid-connected mode of operation, therefore new grid codes for the islanded mode of operation need to be developed, as well as directional protection schemes for various configurations and modes of AC microgrids.

Considering the above factors, a communication-based adaptive protection of radial AC microgrids with converter-based DERs is proposed, analyzed and validated using offline and real-time hardware-in-the-loop (HIL) simulations in this thesis. Various Ethernet-based communication protocols have been reviewed, and the IEC 61850 communication based generic object-oriented substation event (GOOSE) protocol has been selected for application in adaptive protection schemes. The method of handling communication failures by intelligent electronic devices (IEDs) or protection relays is also proposed. Based on simulation results, the definite-time coordination of overcurrent protection relays is suggested for the islanded mode of radial AC microgrids. The extent of fault current contributions from DERs and battery energy storage systems (BESS) to avoid definite-time adaptive overcurrent protection scheme and ensuring fast fuse operations is investigated for different islanded modes. Directional protection schemes based on current magnitude comparison and symmetrical component methods have been proposed and evaluated. Also, methods for the detection of open phase faults and new low voltage ride-through (LVRT) and high voltage ride-through (HVRT) curves for converter-based DERs are suggested in this thesis.

Keywords: AC microgrids, Adaptive protection, Islanded mode, Converter-based DERs, IEC 61850 communication, GOOSE protocol, HIL simulations

ACKNOWLEDGEMENT

This doctoral thesis has been developed from full-time and part-time research work done in various research projects conducted at the University of Vaasa, Finland during the years 2014-2020 and 2022-23. The financial support provided by the research projects including SGEM (Apr 2014-Aug 2014), ECV-eCharge (Sep 2014-May 2016), ProtectDG (Jun 2016-Jun 2017), FESSMI (Jun 2016-Oct 2017), SESP (Jun 2017-Sep 2018), VINPOWER (Oct 2018-Aug 2020), SolarX (Sep 2019-Dec 2020) and CIRP-5G (Sep 2022-Feb 2023) is acknowledged.

This thesis work has also been funded by the Quaid-e-Awam University of Engineering, Science and Technology, Nawabshah, Pakistan through Faculty Development and other Immediate Needs Project (FDINP) scholarship of Higher Education Commission (HEC), Islamabad, Pakistan. The financial support provided is acknowledged.

First of all, I would like to thank Almighty Allah for His utmost kindness and blessings in providing me plenty of strength, ability and hope to face all challenges in life. Then, I would like to thank my supervisor *Prof. Kimmo Kauhaniemi* for providing an opportunity to work in his team and later providing a continuous and unwavering support, a proper guidance, a timely and critical feedback, encouraging remarks during low times and good compliments after a success. I would also like to thank my second supervisor and chairman of the Department of Electrical Engineering at the University of Vaasa, *Prof. Timo Vekara* for maintaining a conductive work and research environment, taking keen interest in my research and providing valuable feedback. I am also thankful to all Deans of Faculty of Technology, now School of Technology and Innovations, for providing necessary resources, and facilities to carry out the research and course work smoothly.

I am thankful to my co-authors including Prof. Hannu Laaksonen and Mazaher Karimi from the University of Vaasa and Sadegh Mahmoudi tabar, and Mohammad Mohammadi from the Shiraz University, Iran for good research cooperation. I am also thankful to other co-authors and colleagues of the Smart Electric Systems (SES) research group including Lauri Kumpulainen, Katja Sirviö, Mike Mekkanen, Amir Farughian, Jagdesh Kumar, Omid Palizban, and Sampo Voima for an additional support and cooperation. Also, thanks to colleagues from industries and other partner universities for listening to my ideas in project meetings and workshops and providing important feedback. I am also thankful to all reviewers of my published articles and thesis for providing quality feedback.

Thanks to Mike Mekkanen for sharing his ideas and experience about IEC 61850 communication standard and helping in FREESI Lab setup to conduct Hardware-In-the-Loop testing. Also, thanks to Technobothnia lab technicians and IT people at the University of Vaasa for providing necessary help when required.

Thanks to Amir Farughian for giving a good company during lunch times and Haresh Kumar for a phone talk during thesis writing to give me necessary breaks in keeping my work stress levels under control. I am also thankful to all classmates, friends and colleagues from Pakistan and other countries connected via social media for their continuous support and feedback to keep my morale high. Thanks to all my teachers too who always believed in me, inspired and guided me to achieve goals in life.

Last but not least thanks to my proud family members back in Pakistan, they remained steadfast and supportive even during hard times in life and prayed unconditionally for my success. My father, grandmother and uncle died during these times, may Allah rest their souls in peace and paradise, Aameen. This thesis is dedicated to all my family members.

Contents

Figures

Tables

Abbreviations

AC	Alternating Current
ACB	Air Circuit Breaker
AI	Artificial Intelligence
ANN	Artificial Neural Network
ANSI	American National Standards Institute
BES	Bulk Electric System
BESS	Battery Energy Storage System
CB	Circuit Breaker
CHIL	Control Hardware-In-the-Loop
CHP	Combined Heat and Power
CID	Configured IED Description
CIGRE	Conseil International des Grandes Reseaux Electriques (International Council on Large Electric Systems)
CT	Current Transformer
CTI	Coordination Time Interval
DC	Direct Current
DER	Distributed Energy Resource

DG	Distributed Generation
DMS	Distribution Management System
DNP	Distributed Network Protocol
EN	Europäische Normen (European Standards)
ENTSO-E	European Network of Transmission System Operators for Electricity
ESS	Energy Storage System
EU	European Union
EV	Electric Vehicle
FCL	Fault Current Limiter
GHG	Green House Gas
GOOSE	Generic Object-Oriented Substation Event
GPS	Global Positioning System
HF	High Frequency
HIF	High Impedance Fault
HIL	Hardware-In-the-Loop
HSR	High-availability Seamless Redundancy
HV	High Voltage
HVRT	High Voltage Ride-Through
ICD	IED Capability Description
IDMT	Inverse Definite Minimum Time
IEC	International Electrotechnical Commission
IED	Intelligent Electronic Device
IEEE	Institution of Electrical and Electronics Engineers
IGBT	Insulated Gate Bipolar Transistor
IP	Internet Protocol
IRENA	International Renewable Energy Agency
ISO	International Organization for Standardization
LAN	Local Area Network
LD	Logical Device
LF	Low Frequency
LG	Line-to-Ground
LL	Line-to-Line
LLG	Line-to-Line-to-Ground

LLL	Line-to-Line-to-Line
LLLG	Line-to-Line-to-Line-to-Ground
LN	Logical Node
LV	Low Voltage
LVRT	Low Voltage Ride-Through
MC	Microgenerator Controller
MCB	Miniature Circuit Breaker
MCCB	Molded Case Circuit Breaker
MGCC	Microgrid Central Controller
MGMS	Microgrid Management System
ML	Multi-Level
MMS	Manufacturing Message Specification
MTTR	Mean Time To Repair
MU	Merging Unit
MV	Medium Voltage
MVA	Megavolt-Ampere
MW	Megawatt
NERC	North American Electricity Reliability Corporation
NPC	Neutral Point Clamped
OC	Overcurrent
OF	Overfrequency
OSI	Open Systems Interconnections
OV	Overvoltage
PCC	Point of Common Coupling
PHIL	Power Hardware-In-the-Loop
PLC	Power-Line Carrier
PLL	Phase-Locked Loop
PMSG	Permanent Magnet Synchronous Generator
PMU	Phasor Measurement Unit
PRP	Parallel Redundancy Protocol
PSCAD	Power Systems Computer Aided Design
PSIL	Power System-In-the-Loop
p.u.	per unit

PV	Photovoltaic
PWM	Pulse Width Modulation
RCA	Relay Characteristic Angle
RES	Renewable Energy Sources
RT	Real-Time
SC	Subcommittee
SCADA	Supervisory Control And Data Acquisition
SCD	Substation Configuration Description
SCIG	Squirrel Cage Induction Generator
SCL	Substation description Configuration Language
SCR	Silicon-Controlled Rectifier
SIL	Software-In-the-Loop
SSCB	Solid-State Circuit Breaker
SSD	System Specification Description
SV	Sampled Value
TC	Technical Committee
TCP	Transmission Control Protocol
TDS	Time Dial Setting
THD	Total Harmonic Distortion
TR	Technical Report
TS	Technical Specification
UF	Underfrequency
UN	United Nations
U.S.	United States
UV	Undervoltage
Var	Volt-Ampere Reactive
VPP	Virtual Power Plant
VSC	Voltage Source Converter
VT	Voltage Transformer
WAMS	Wide-Area Measurement Systems
WAN	Wide Area Network
WG	Working Group
WRIG	Wound Rotor Induction Generator

WTG	Wind Turbine Generator
XML	eXtensible Markup Language

List of symbols

f	Frequency (Hz)
G	Measured value of the characteristic quantity
G_S	Setting value of the characteristic quantity
I	Current (A)
I_P	Pickup current
$I>$	Overload stage or function
$I>>$	Time overcurrent stage or function
$I>>>$	Instantaneous overcurrent stage or function
I_0	Zero-sequence current
I_1	Positive-sequence current
I_2	Negative-sequence current
k	Time dial setting (TDS)
k_1	Gradient for additional positive-sequence reactive current
k_2	Gradient for additional negative-sequence reactive current
P	Active power (W)
Q	Reactive power (VAr)
t	Time or operating time (s)
U or V	Voltage (V)
U_C	Voltage at connection point
U_0 or V_0	Zero-sequence voltage
U_1 or V_1	Positive-sequence voltage
U_2 or V_2	Negative-sequence voltage
U_{1_1min}	One minute average of the pre-fault positive-sequence voltage

U_{2_1min}	One minute average of the pre-fault negative-sequence voltage
ω	Angular or rotating frequency
ΔI_{Q1}	Additional positive-sequence reactive current
ΔI_{Q2}	Additional negative-sequence reactive current
ΔU_1	Sudden jump or change of positive-sequence voltage
ΔU_2	Sudden jump or change of negative-sequence voltage
67P	Positive-sequence directional element
67Q	Negative-sequence directional element

Publications

This doctoral thesis is based on the following appended papers.

I. Memon, A. A., & Kauhaniemi, K. (2015). A critical review of AC Microgrid protection issues and available solutions. E*lectric Power Systems Research*, 129, 23–31. https://doi.org/10.1016/j.epsr.2015.07.006. © 2015 Elsevier B.V.

II. Memon, A. A., & Kauhaniemi, K. (2020). An Adaptive Protection for Radial AC Microgrid Using IEC 61850 Communication Standard: Algorithm Proposal Using Offline Simulations. *Energies*, 13(20). https://doi.org/10.3390/en13205316. © 2020 by the authors, CC BY.

III. Memon, A. A., Laaksonen, H., & Kauhaniemi, K. (2021). Microgrid Protection with Conventional and Adaptive Protection Schemes. In A. Anvari-Moghaddam, H. Abdi, B. Mohammadi-Ivatloo, & N. Hatziargyriou (Eds.), Microgrids: Advances in Operation, Control, and Protection (pp. 523–579). Springer International Publishing. https://doi.org/10.1007/978-3-030-59750-4_19. © 2021 Springer Nature Switzerland AG.[1]

IV. Memon, A. A., & Kauhaniemi, K. (2021). Real-Time Hardware-in-the-Loop Testing of IEC 61850 GOOSE-Based Logically Selective Adaptive Protection of AC Microgrid. *IEEE Access*, 9, 154612–154639. https://doi.org/10.1109/ACCESS.2021.3128370. CC BY.

V. Memon, A. A., Karimi, M., & Kauhaniemi, K. (2022). Evaluation of New Grid Codes for Converter-Based DERs From the Perspective of AC Microgrid Protection. *IEEE Access*, 10, 127005–127030. https://doi.org/10.1109/ACCESS.2022.3226653. CC BY.

VI. Memon, A. A., & Kauhaniemi, K. (2023). Protection of the Future Harbor Area AC Microgrids Containing Renewable Energy Sources and Batteries. *IEEE Access*, 11, 57448-57469. https://doi.org/10.1109/ACCESS.2023.3283575. CC BY.

VII. tabar, S. M., Memon, A. A., Karimi, M., Mohammadi, M., & Kauhaniemi, K. (2023). Hardware in the loop testing for power systems. In J. García (Ed.), *Encyclopedia of Electrical and Electronic Power Engineering* (pp. 294–309). Elsevier. https://doi.org/10.1016/B978-0-12-821204-2.00146-X. © 2023 Elsevier Inc.

[1] Reproduced with permission from Springer Nature.

Author's contribution

Aushiq Ali Memon is the main author as well as the corresponding author of the first six publications (Publication I-VI) and the second author of Publication VII. The specific contributions of authors for Publication I-VII are described below:

Publication I: *Memon* defined the research design and layout, collected and managed research material, analyzed data, defined methodology and research methods, verified and analyzed research findings, visualized results, wrote the body text of the original article and edited the article. *Kauhaniemi* acquired research resources and funding, managed and guided in the research process, reviewed, commented and edited the article.

Publication II: *Memon* defined the research design and layout, collected and managed research material, analyzed data, defined methodology and research methods, verified and analyzed research findings, visualized results, wrote the body text of the original article and edited the article. *Kauhaniemi* acquired research resources and funding, managed and guided in the research process, reviewed, commented and edited the article.

Publication III: *Memon* defined the research design and layout, collected and managed research material, analyzed data, defined methodology and research methods, verified and analyzed research findings, visualized results, wrote the body text of the original article and edited the article. *Laaksonen* wrote some sections and subsections of the original article, analyzed data, verified and analyzed research findings and edited the article. *Kauhaniemi* acquired research resources and funding, managed and guided in the research process, reviewed, commented and edited the article.

Publication IV: *Memon* defined the research design and layout, collected and managed research material, analyzed data, defined methodology and research methods, verified and analyzed research findings, visualized results, wrote the body text of the original article and edited the article. *Kauhaniemi* acquired research resources and funding, managed and guided in the research process, reviewed, commented and edited the article.

Publication V: *Memon* defined the research design and layout, collected and managed research material, analyzed data, defined methodology and research methods, verified and analyzed research findings, visualized results, wrote the body text of the original article and edited the article. *Karimi* collected research material, analyzed data, reviewed and edited the article. *Kauhaniemi* acquired

research resources and funding, managed and guided in the research process, reviewed, commented and edited the article.

Publication VI: *Memon* defined the research design and layout, collected and managed research material, analyzed data, defined methodology and research methods, verified and analyzed research findings, visualized results, wrote the body text of the original article and edited the article. *Kauhaniemi* acquired research resources and funding, managed and guided in the research process, reviewed, commented and edited the article.

Publication VII: *Mehmoudi tabar* defined the research design and layout, collected and managed research material, analyzed data, defined methodology and research methods, verified and analyzed research findings, visualized results, wrote the body text of the original article and edited the article. *Memon* collected and managed research material, analyzed data, defined methodology and research methods, verified and analyzed research findings, visualized results, wrote the body text of the original article and edited the article. *Karimi* verified and analyzed research findings, visualized results, wrote the body text of the original article and edited the article. *Mohammadi* guided in the research process, reviewed, commented and edited the article, *Kauhaniemi* guided in the research process, reviewed, commented and edited the article.

1 INTRODUCTION

1.1 Background

During the last decade, various research and development activities around the world have been focused on renewable energy technologies commonly known as renewable energy sources (RES), and their integration into transmission and distribution systems. The key driving forces behind the development of RES technology are the reduction of greenhouse gas (GHG) emissions and meeting the constantly growing energy and electricity demand. The GHG emissions are largely produced by the burning of fossil fuels for heat, electricity and transportation (United States Environmental Protection Agency (EPA), n.d.-b). According to the earlier projections of the International Energy Agency (IEA) and World Energy Council, the primary energy demand will increase between 40% and 150% and electricity consumption will increase between 110% and 260% by 2050 (Metz et al., 2007). The most prominent economic benefits of RES technology are less dependency on fossil fuel imports and getting cheap and clean energy from renewable sources to meet the growing energy demand. The recent goals related to RES technology development are the United Nations (UN) sustainable development goals (SDGs) set in 2015 as part of UN 2030 Agenda for Sustainable Development including affordable and clean energy (SDG7), industry, innovation and infrastructure (SDG9), and climate action (SDG13) (United Nations (UN), n.d.); (European Commission, n.d.-c).

According to the recently published global renewable energy outlook by the International Renewable Energy Agency (IRENA), the share of renewable electricity generation with current pace will grow from 26% in 2018 to 38% in 2030 and 55% in 2050. However, this share of renewable electricity will probably grow even faster from current rates of 26% to 57% in 2030 and 86% in 2050 due to declining costs, and thus cheaper electricity generation from RES compared to the generation from fossil fuels. The variable RES (VRES) like wind energy and solar photovoltaic (PV) would supply 33% and 25% of the total global electricity demand respectively by 2050. The increasing share of wind energy and solar PV will also require some kind of energy storage to smooth out the power variability and provide the needed flexibility of operations to behave like dispatchable energy sources (IRENA, 2020).

Every region and every country of the world has its own targets and timelines for reducing GHG emissions and increasing the RES share for energy and electricity

production. For example, the existing ambitious targets of the European Union (EU) for the year 2030 are at least 40% cuts in emissions from the 1990 levels, and at least a 32% share for renewable energy and at least 32.5% improvements in energy efficiency (European Commission, n.d.-a). By the year 2050, the EU aims to be climate-neutral, and an economy with net-zero GHG emissions (European Commission, n.d.-b). Finland sets an ambitious target to be carbon neutral by the year 2035 (Finnish Government Valtioneuvosto, 2020).

According to renewable energy statistics, the share of RES in gross final energy consumption already reached 19.7% in 2019 in the EU-27 Member States which was only 0.3% short of the year 2020 target of 20%. Fourteen EU-27 member states have already surpassed their national targets of RES share in gross final energy consumption for 2020. Sweden leads with a 56.1% share of RES in gross final consumption of energy, followed by Finland with 43.1%, Latvia with 41%, Denmark with 37.2%, and Austria with 33.6%. In 2019, the share of RES became 34% in terms of gross electricity consumption in the EU-27. Wind energy and hydropower accounted for two-thirds of the total electricity generated from RES with a 35% share of each. The remaining one-third of electricity generated from RES came from solar PV with a 13% share, solid fuels with an 8% share, and other RES with a 9% share. Solar PV is the fastest growing RES for electricity generation. The consumption of electricity generated from RES is also growing among the EU-27 Member States. In 2019, 75% of electricity consumed in Austria was generated from RES, followed by 71% in Sweden, 65% in Denmark, 54% in Portugal, and 53% in Latvia (Eurostat, 2020).

With the ever-growing amount of RES integration in electrical networks, the power generation is gradually shifting from large and distant centralized generation towards small distributed generation (DG) present at or near the load centers (Palizban, 2016). However, large wind and solar PV farms with hundreds of megawatt (MW) capacity will still be operated as centralized generation as part of a megagrid (Marnay et al., 2015). Small kilowatt scale or few MW scale RES including wind turbine generators (WTGs), solar PV systems, combined heat and power (CHP) capable reciprocating engine generators, fuel cells and microturbines can be used as DG. These DG may provide electrical power to a single structure like a home or business facility, or it may be a part of an industrial, military, or campus microgrid (United States Environmental Protection Agency (EPA), n.d.-a).

The North American Electric Reliability Corporation (NERC) defines DG as “Any non-Bulk Electric System (non-BES) generating unit or multiple generating units at a single location owned and/or operated by 1) the distribution utility, or 2) a

merchant entity". A distributed energy resource (DER) is defined as: "... any resource on the distribution system that produces electricity and is not otherwise included in the formal NERC definition of the Bulk Electric System (BES)" (NERC, 2017). The BES as defined by NERC includes "all transmission elements operated at 100 kV or higher and real power and reactive power resources connected at 100 kV or higher. The BES does not include facilities used in the local distribution of electric energy" (NERC, 2018). So, according to these definitions, DER is usually connected at a distribution voltage of less than 100 kV, and includes any DG, generating unit, multiple generating units at a single location, energy storage systems (ESSs), microgrid, etc. connected within the sole boundary of a distribution system. In the context of this thesis, the acronym DERs for distributed energy resources includes both the RES type of DG units and ESSs, and DERs are considered as components of a medium voltage (MV) or low voltage (LV) microgrid. The BES or megagrid is referred to as the "main grid" in this thesis.

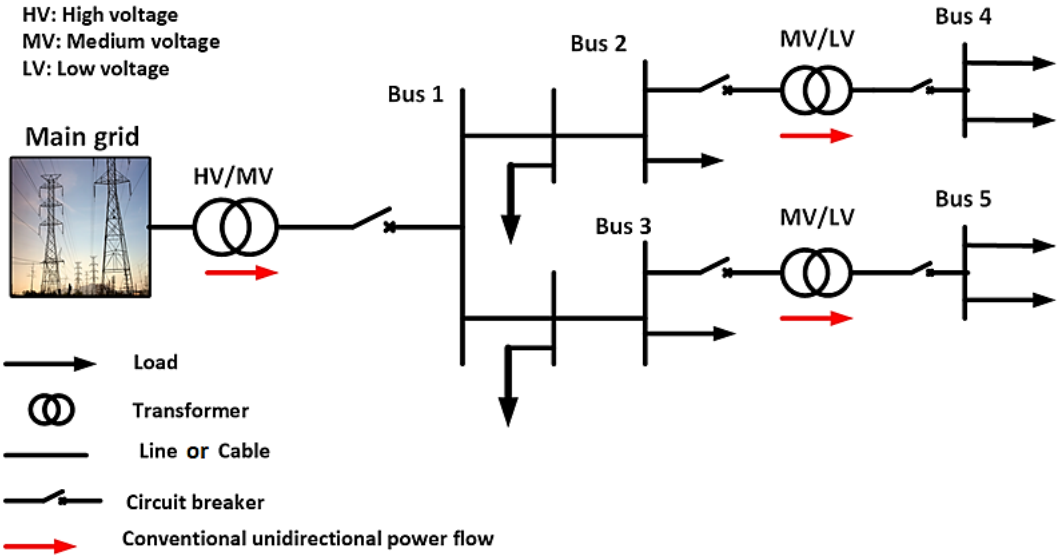

Figure 1. A conventional distribution network without DERs.

The conventional three-phase distribution systems of electricity with unidirectional power flow and without any DERs (Figure 1) are going through various stages of development with an increasing integration of DERs. The integration stages of DERs in distribution systems can be broadly classified into two categories in terms of the number and capacities of DERs: 1) Distribution networks embedded with a limited share of DERs (Figure 2) and 2) Distribution networks embedded with an extensive share of DERs (Figure 3). The share of DERs can be measured in terms of percentage of load (Enayati et al., 2018) or peak load (K. A. W. Horowitz et al., 2018) of a circuit or a feeder supplied by the DERs, referred to as the "penetration level" of DERs. A limited share of DERs can be connected to the existing distribution networks without any violations of operating

conditions using the “fit and forget” principle. The power flow direction in a distribution network with a limited share of DERs (Figure 2) will be unidirectional such that the large amount of additional active power will still be imported from the main grid. At times of low consumption and high generation from DERs locally, the DERs are either totally disconnected or their active power output is limited or curtailed to avoid overloading and overvoltage. During faults, DERs are disconnected immediately by anti-islanding protections, for example, as per Institute of Electrical and Electronics Engineers (IEEE) 1547-2003 requirements, or due to safety reasons and the non-availability of advanced control and protection equipment to manage the situation.

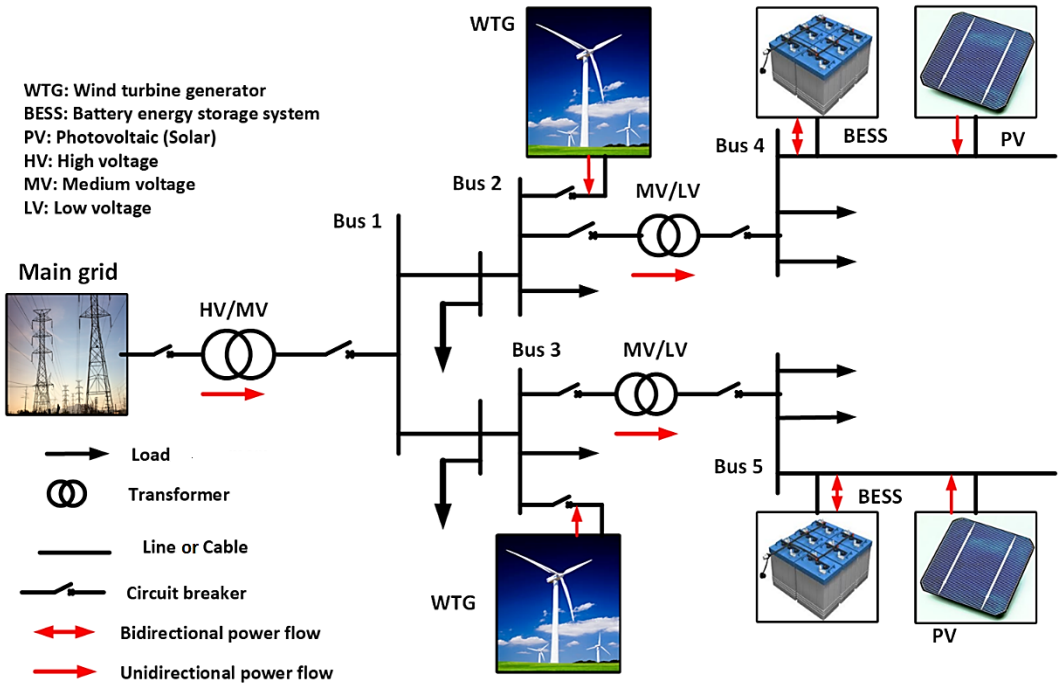

Figure 2. The distribution network embedded with a limited share of DERs.

For distribution networks with an extensive share of DERs (with a peak load capacity of 100% and beyond) and an increased chance of the bidirectional power flow (Figure 3), the short-term measures of DERs disconnection or curtailment will not be sufficient, and other advanced solutions will be required including the upgrading of existing passive DERs to more active or dynamic DERs with advanced or smart converter technologies (NERC, 2017). For example, in the United States (U.S.), the states of California and Hawaii have already observed the highest penetration levels of DERs and have adopted smart solar PV inverters with features like voltage and frequency ride-through, dynamic voltage support, power quality , etc. (Enayati et al., 2018).

The impact of DERs' penetration on the local distribution network is usually measured in terms of "hosting capacity." The penetration level of DERs at which the upgrades of a given feeder or circuit will be required is termed as the "hosting capacity" (K. A. W. Horowitz et al., 2018). In other words, the hosting capacity can be defined as the amount of new DERs and loads connected to the feeder without affecting the reliability, safety and power quality for other customers (M. H. J. Bollen & Häger, 2004); (M. Bollen & Hassan, 2011). This means that a limited amount of DERs can be connected to the existing distribution network without reaching a hosting capacity limit causing any considerable deviation to the operating conditions like local overvoltage, the overloading of lines and transformers, or power quality and protection issues which may require mitigation measures or equipment upgrades. The traditional measures employed to avoid adverse effects like the voltage variations and overloading include limiting or curtailing the active power of DERs, adding voltage regulators or changing their set points, shifting the connections of new DERs to strong networks near substations, and reconductoring lines or upgrading the power transformers (Masters, 2000); (Bignucolo et al., 2008); (K. A. W. Horowitz et al., 2018).

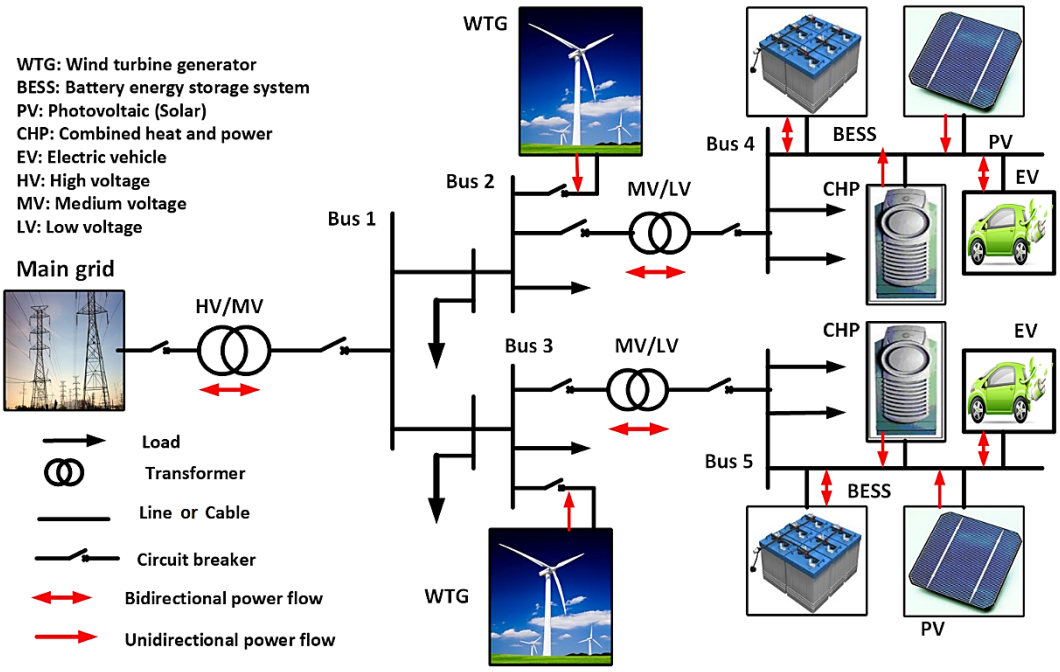

Figure 3. The distribution network embedded with an extensive share of DERs.

The emerging mitigation strategies to avoid the adverse effects of the extensive share of DERs include the application of advanced communication and control methods to collect information from every component of the distribution network and then provide the necessary control actions. Other emerging mitigation

strategies include the application of distribution static synchronous compensators (D-STATCOMs), advanced inverters for DERs with fixed power factor or local voltage–reactive power (Volt–Var) control capability, and battery energy storage systems (BESS). The costs of distribution upgrades not only depend on the choice of the mitigation measure, but also on the characteristics of the feeder, the location of the DERs, the size of DERs, and the unit cost of each mitigation scheme (K. A. W. Horowitz et al., 2018). The use of these mitigation measures will increase the hosting capacity of the distribution feeders for connection of an increasing amount of DERs without operational disturbances. The use of storage and communication for increasing the hosting capacity of DERs for existing electrical grids have been suggested by (Etherden, 2014). Details of the use of the hosting capacity approach as a planning tool for increasing the amount of PV panels and electric vehicle (EV) chargers in two rural and suburban LV networks in Sweden using both undervoltage and overvoltage as limiting factors have been discussed in (M. H. J. Bollen & Rönnberg, 2017). The detailed cost of distribution system upgrades for the accommodation of high penetration of PV systems at different locations in three different types of real feeders in the U.S. applying minimum mitigation measures has been discussed in (K. A. W. Horowitz et al., 2018).

In parallel to the above-mentioned mitigation measures for the integration of DERs, the concept of microgrid has emerged to provide a flexible architecture for the deployment of DERs in order to meet the wide-ranging needs of different communities whether living in metropolitan cities or remote rural areas. The integration of various individual DERs into conventional distribution systems creates different technical challenges. These technical challenges could be better addressed by co-locating variable DERs with controllable loads and storage technologies in microgrids, so that the generation and consumption can be better managed locally. In this way, a microgrid will appear as a single producer or consumer of electricity to the main grid which is capable of modifying its net load profile such that it provides benefit to the main grid (R. Lasseter et al., 2002); (Hirsch et al., 2018).

The natural disasters that increasingly occur due to climate change and the resulting power outages, cause an estimated loss of $150 billion per annum to the U.S. economy. Moreover, currently occurring threats of cyber-attacks and ageing infrastructure force the development of more advanced solutions of power continuity, as traditional standby generators are not enough to meet these challenges. Microgrids provide the necessary infrastructure to keep the power on for extended durations of time after the isolation from a failed or damaged main grid (Baier et al., 2017). According to the CIGRE (Conseil International des Grandes Reseaux Electriques) Working Group C6.22, microgrids offer many

benefits to customers and the utilities, including the enhancement of energy efficiency, a reduction in overall energy consumption and purchase, a deferral of grid expansion and investments, reductions in emissions, improvements in supply reliability, operational benefits of loss reduction, congestion management, voltage control, and a more cost-efficient replacement of electricity infrastructure for Smart Grids. These benefits can also be obtained through other methods, but microgrids offer them in a single coordinated ecosystem for different stakeholders (Marnay et al., 2015). The prominent benefits offered by microgrids are shown in Figure 4.

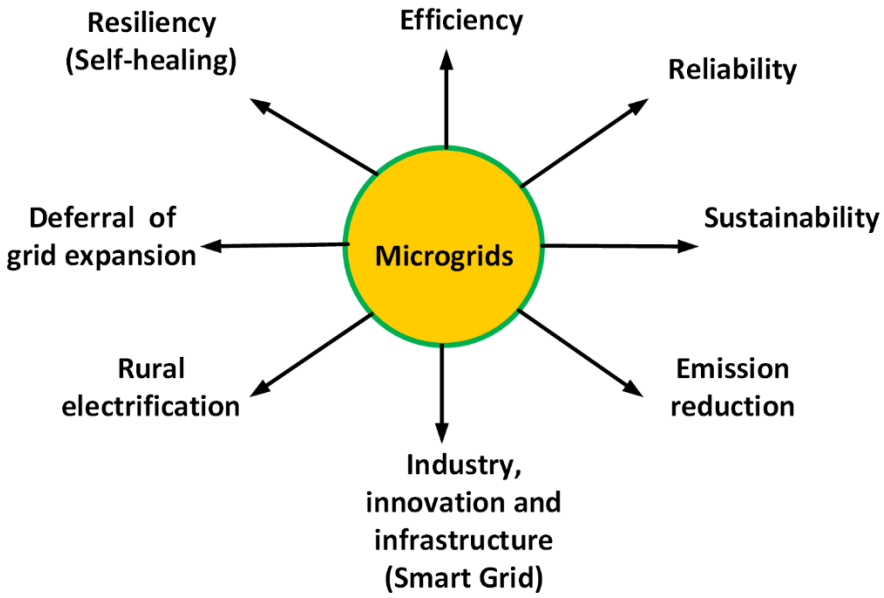

Figure 4. The prominent benefits of microgrids.

In Europe, the key driving forces behind microgrid research and development activities have been the reduction of emissions and the integration of enormous amounts of sustainable RES into the electric grid. Whereas, in the U.S. and Japan, the main drivers of microgrid developments have been the improvement of the resiliency and reliability of critical facilities (transport, communication, drinking water and waste treatment, and hospitals) during natural disasters. Resiliency can be defined as the ability to bounce back quickly after a problem. In other words, resiliency is a measure of robustness during extreme events and the speed of subsequent restoration. In smart grids, the term “self-healing” has been used to describe the recovery from power disturbance events. However, resiliency is a more general term which includes the ability to withstand and recover from deliberate attacks, weather or climate disturbances, power disaster events, and thus the need for forecasting these events. Power resiliency is the capability of sustaining power and recovering from adverse events which is very necessary for

critical business, industrial or healthcare facilities. From the global perspective, about 760 million people in the world lacked access to electricity in 2019 (Ritchie et al., 2020), and it is estimated that about 670 million people will still be without electricity in 2030 (International Energy Agency, IEA, n.d.). Therefore, for developing countries, the microgrid provides a viable platform for rural electrification. Irrespective of the reasons behind the microgrid development initiatives, all markets (including the U.S., Europe and the developing world) can achieve various common benefits from microgrids. Additionally, the fuel savings and ancillary services provided by microgrids could be important components of future business cases (Marnay et al., 2015); (Ton & Wang, 2015); (Zielinski, 2016); (Baier et al., 2017); (Hirsch et al., 2018).

1.2 Microgrid definitions

The CIGRE working group WG6.22 finds that most microgrids contain two fundamental requirements: The first is that a microgrid contains sources and sinks under local control; and the second is that a microgrid can operate either grid-connected or islanded. Therefore, CIGRE WG6.22 defines microgrids by way of a single sentence as follows:

"Microgrids are electricity distribution systems containing loads and distributed energy resources, (such as distributed generators, storage devices, or controllable loads) that can be operated in a controlled, coordinated way either while connected to the main power network or while islanded" (Marnay et al., 2015).

The U.S. department of energy (DOE) considers microgrid as a key building block for a Smart Grid, and defines the microgrid as:

"A group of interconnected loads and distributed energy resources within clearly defined electrical boundaries that acts as a single controllable entity with respect to the grid. A microgrid can connect and disconnect from the grid to enable it to operate it in both grid-connected and island-mode" (Ton & Smith, 2012).

The above two definitions of microgrids do not indicate the size of DERs, voltage levels, the form of electric current (alternating current [AC] or direct current [DC]), and hence the technologies that can be used for microgrids. However, the CIGRE WG6.22 explains that the generators within the context of microgrids include all sources such as fossil or biomass-fired CHP units, solar PV modules, small WTGs, and mini-hydro generators. The storage devices in the CIGRE definition of microgrids include all electrical (superconducting magnetic energy storage),

electrochemical (batteries), mechanical (flywheels) and heat storage technologies. The controllable loads include the automatic dimmable lights, building heating, ventilating, and air conditioning loads, water boilers, delayed irrigation pumping, pumped hydropower storage, plug-in EVs, and BESS (Marnay et al., 2015).

In earlier research (R. H. Lasseter & Piagi, 2004), the microgrid was considered as a better and systematic approach to exploit the potential of DG, and viewed as a subsystem comprised of generation and associated loads. During any disturbance in the distribution system, a microgrid can intentionally isolate itself from the disturbance providing higher local reliability without any harm to the transmission grid. This approach was based on the controls provided by the generators enabling a plug-and-play model without communication or custom engineering for each side.

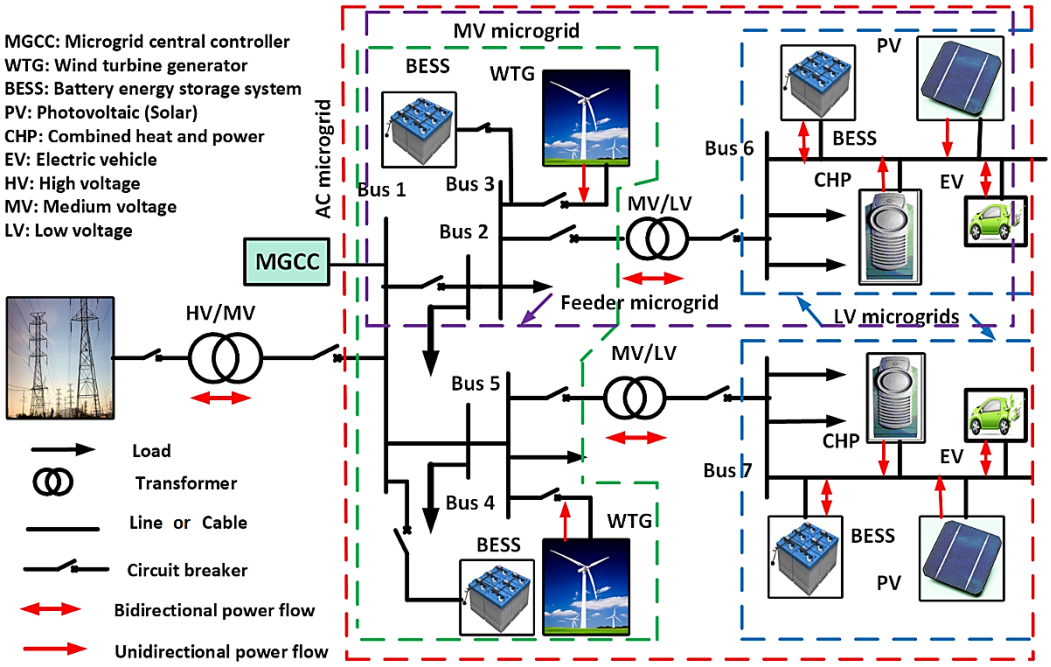

Figure 5. The distribution network embedded with MV and LV AC microgrids.

According to another earlier definition:

"*Microgrids comprise Low Voltage distribution systems with distributed energy sources, such as micro-turbines, fuel cells, PVs, etc., together with storage devices, i.e., flywheels, energy capacitors and batteries, and controllable loads, offering considerable control capabilities over the network operation. These systems are interconnected to the Medium Voltage Distribution network, but they can also be operated isolated from the main grid, in case of faults in the upstream network. From the customer point of view, Microgrids provide both thermal and electricity needs, and in addition enhance local reliability, reduce emissions,*

improve power quality by supporting voltage and reducing voltage dips, and potentially lower costs of energy supply" (Hatziargyriou et al., 2006).

In more general way, the modern microgrid is an integral part of the smart distribution grid with an islanded operation capability. From that perspective, a microgrid can be a separate geographically islanded grid, a small household or LV customer, LV microgrid with all LV feeders connected to an MV–LV transformer, MV feeder microgrid, or a high voltage (HV)–MV substation microgrid comprised of all MV feeders; but each with their own local smart microgrid management system (MGMS) or microgrid central controller (MGCC) (Laaksonen, 2011). Therefore, future distribution networks embedded with an extensive share of DERs (Figure 3) will transform to distribution networks embedded with MV and LV microgrids (Figure 5).

1.3 Microgrid types and operational modes

Microgrids are categorized into three types according to the nature of the electric current: AC microgrids, DC microgrids, and hybrid AC–DC microgrids. In AC microgrids the electric power is distributed and consumed in AC form, whereas in DC microgrids the electric power is distributed and consumed in DC form irrespective of the form of the generated electric power.

In AC microgrids, the generated DC power is first converted to AC power through DC–AC converters before being distributed through AC lines or cables and being consumed. In DC microgrids, the generated AC power is first converted to DC power before being distributed through DC lines or cables and being consumed. In hybrid AC–DC microgrids (Figure 6), a small part of the system (for example an LV distribution system) consists of DC sources, lines or cables and loads, whereas the rest of the MV and HV distribution system consists of AC sources, lines or cables and loads. The other possibility of a hybrid AC–DC microgrid is that MV and HV distribution systems consist of DC sources, lines or cables and loads, and the rest of the LV distribution system consists of AC sources, lines or cables and loads. In this thesis, only the MV and LV substation or feeder type of radial AC microgrids are considered.

AC microgrids can be further classified as radial and looped or ring AC microgrids, depending on the nature of the network configuration. A looped or ring AC microgrid provides higher levels of reliability compared to a radial AC microgrid, mainly due to the fact that the looped or ring network topology provides alternative paths for electric power flow to the loads. In the case of faults in one section of the looped or ring topology and a subsequent tripping of the lines or cables, the electric

power flows to the loads through an alternative path. Just like conventional radial distribution, radial AC microgrid systems could be operated, managed and protected in a simpler way compared to the looped or ring AC microgrids. However, it all depends on the location of the DERs connected to the lines or cables in the radial AC microgrids. If the DERs are connected to both ends of the lines or cables, then the operation, management and protection of the radial AC microgrids will have the same degree of complexity as that of the looped or ring AC microgrids.

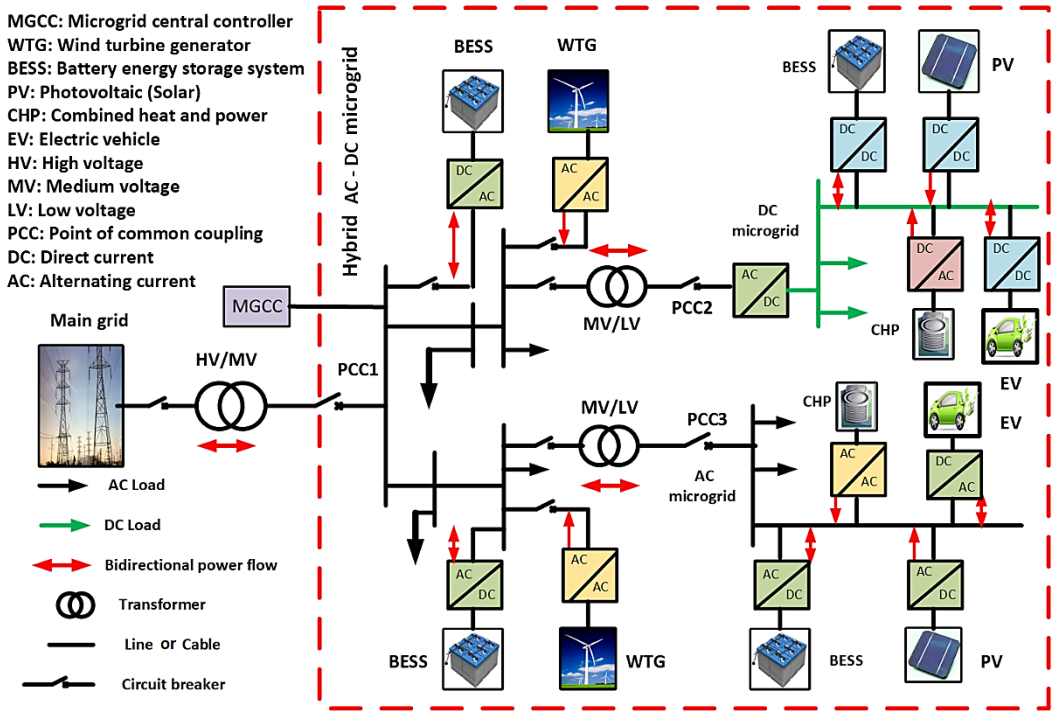

Figure 6. Hybrid AC–DC microgrid.

The AC microgrid has three operational modes: 1) steady state grid-connected mode, 2) steady state islanded mode, and 3) transition mode where the transition is either from the grid-connected to the islanded mode or from the islanded mode to the grid-connected mode. The later type of transition mode is also called the re-synchronization mode. Another, emergency operational mode can be the black start mode. AC microgrids may lose stability due to unforeseen reasons, and a blackout may happen during the islanded mode. However, the black start mode can be initiated by the microgrid controller in order to restart or re-synchronize the disconnected DERs of the AC microgrid.

1.4 Motivation for the work

There are various technical issues that need to be solved before the practical implementation of AC microgrid with an extensive share of converter-based DERs.

One of the crucial issues is the design of a proper protection scheme for AC microgrids, which should not only be capable of meeting the basic protection requirements of selectivity, sensitivity and reliability, but also the new requirements of adaptivity and high-speed. These protection requirements should be met not only during the grid-connected mode, but also during the islanded mode of operation. Since the introduction of the microgrid concept, researchers have introduced a variety of new concepts for protection schemes to be incorporated into MV and LV AC microgrids. A vast majority of the researchers agree on a point that conventional protective devices usually based on a single setting overcurrent principle are inadequate to provide complete protection for AC microgrids during both grid-connected and islanded modes of operation. Therefore, new protection techniques based on other principles and approaches must be developed.

The new protection schemes should not only be adaptive according to the operational modes of the AC microgrid, but also be sensitive enough to detect and clear the lowest possible fault currents within microgrid quickly, ensuring minimum supply disruption to customers. A literature survey shows that it is difficult to provide complete protection to the AC microgrid in both grid-connected and islanding modes against every disturbance or fault by using only one type of protection scheme. Therefore, a combination of various protection schemes based on different principles of operation will be required for future AC microgrids. Moreover, the use of communication means is inevitable for the fast, safe and reliable operation of an AC microgrid. Therefore, new protection schemes must be based on some kind of communication link. The International Electrotechnical Commission (IEC) 61850 communication standard is considered as the most suitable protocol to implement both centralized and decentralized control and protection schemes. However, the problems of unwarranted and non-deterministic communication delays, communication failures and cyber-attacks also require alternate techniques, in order to avoid a complete failure of protection schemes.

The inherent limited fault current contribution from the converter-based DERs, and a lack of inertia and variable fault current contribution due to the connection and disconnection of the converter-based DERs for different operational purposes increase the challenges for the protection schemes of AC microgrids. These phenomena result in limited fault current magnitudes for a limited duration of time, even during a three-phase ungrounded balanced shunt fault that usually results in the maximum fault current magnitude in the conventional distribution systems. The conventional protection devices of distribution systems like fuses and overcurrent (OC) relays with a single setting become slow or fail to operate. The

higher fault current contribution from the main grid during the grid-connected mode and the limited fault current contribution from the DERs for a short time during the islanded mode require fast and adaptive protection schemes for AC microgrids, with various levels of sensitivity depending on the connection and disconnection status of DERs.

The majority of the previously proposed protection strategies are applicable for either the grid-connected or the islanded mode of operation, and only a few schemes are suitable for both modes of operation. Moreover, those schemes either become ineffective for certain fault types like unbalanced line-to-line (LL) shunt faults and open phase or series faults or have not been investigated enough for these conditions. Furthermore, the vast majority of previously proposed schemes are based on technical assumptions, and still require extensive simulation and validation testing. Previously proposed protection schemes for AC microgrids also lack suitable grid codes or standardization for implementation, specifically for the islanded mode operation with the grid-forming and grid-following converter-based DERs. The integration of BESS into AC microgrids is also expected for the operational flexibility and islanded mode of operation. This means that fault current contribution from DERs will increase due to additional BESS as fault current sources. Moreover, in the future, new grid codes are expected to demand higher than the rated fault current contribution from DERs and BESS. These factors need to be considered for the development of new protection schemes for AC microgrids.

1.5 Objectives of the thesis

There are three key objectives of this thesis:

1. The development of suitable protection schemes for MV–LV AC microgrids with an extensive share of the converter-based DERs compatible for both grid-connected and islanded modes of operation. The developed protection schemes will ensure selectivity, sensitivity, reliability, adaptivity and high-speed requirements. The protection schemes are based on the combination of existing but rarely used and novel adaptive protection principles. The directional protection schemes for radial AC microgrids are developed which in future can also be applied in looped AC microgrids with little or no modifications.

2. Benchmarking the protection schemes against grid codes during different operational modes, validated through offline and real-time simulations. Proposals for the new grid codes of converter-based DERs, and particularly for the islanded mode of operation, are suggested.

3. An analysis of the role of IEC 61850 communication standard and BESS for protection coordination among various protective devices. Alternative protection strategies to cope with communication link failures are proposed.

In relation to the above objectives, following six research questions are addressed:

1) To what extent are conventional overcurrent protections suitable for the protection of AC microgrid with converter-based DERs?

2) What type of communication-based adaptive protection schemes will be required in radial AC microgrids with converter-based DERs?

3) To what extent will the adaptivity of protection schemes in AC microgrids with converter-based DERs be affected or avoided when BESS are used as fault current sources?

4) What types of directional protection schemes are required for the grid-connected and islanded modes of operation of AC microgrids with converter-based DERs?

5) How can the IEC 61850 communication-based adaptive protection schemes of AC microgrids be tested and validated?

6) What kind of grid codes and communication standards will be required for future AC microgrids, particularly for the islanded mode of operation to ensure the proper protection of AC microgrids?

1.6 Methodology and scope

The following research methodology is used in this thesis:

1) The analysis, evaluation and benchmarking of the protection schemes against the grid code requirements are carried out using the current-limiting generic and average type of converter-based DER models using offline simulations in PSCAD (Power Systems Computer Aided Design), MATLAB/Simulink and the real-time (RT) hardware-in-the-loop (HIL) simulations using the OPAL-RT simulator and the actual relays. Protection relay models are also developed for different case studies.

2) The combination of grid-forming and grid-following converter models are utilized as the limited fault current sources for the AC microgrids with an extensive share of the converter-based DERs. This enables the simulation-

based analysis of protection schemes in both grid-connected and islanded modes.

The scope of the thesis is limited to:

1) The most challenging symmetrical and unsymmetrical phase faults, including three-phase or line-to-line-to-line (LLL) shunt faults, two-phase or LL shunt faults, and ungrounded open phase or series faults.

2) MV and LV radial AC microgrids with only converter-based DERs.

3) IEC 61850 communication standard, mainly GOOSE protocol, which is considered for the centralized and decentralized communication-based protection schemes of AC microgrid.

1.7 Scientific contribution

The scientific contributions of this doctoral thesis reported in seven original published scientific articles can be subdivided into three parts as summarized next.

1. The first part of contributions consists of reviews about the state of the art and challenges including:

   a) A comprehensive literature review of the latest protection challenges, new requirements and available protection schemes of AC microgrids with converter-based DERs is provided. A critical analysis of the available protection schemes of AC microgrids with converter-based DERs is presented.

   b) The operational performance of the conventional single-setting overcurrent protection schemes of AC microgrids with converter-based DERs in both grid-connected and islanded modes of operation with and without the application of an additional centralized grid-forming BESS as a fault current source is analyzed.

   c) A comprehensive review of real-time simulation methods used for power system development, testing and validation is presented.

2. The second part of contributions consists of new solutions and validations including:

a) The potential application of BESS as fault current sources for the protection of radial AC microgrids in both grid-connected and islanded modes is analyzed. Particularly, the use of available BESS resources to quickly blow fuses during three-phase balanced shunt faults in the islanded mode of operation is analyzed to defer investment in advanced adaptive protection schemes, while still maintaining the proper protection coordination between all protection devices.

b) A novel and generic communication-dependent adaptive protection algorithm for radial AC microgrids with an extensive share of converter-based DERs using the IEC 61850 communication standard is proposed. The suggested solution can be implemented with both centralized and decentralized communication-based architectures.

c) A communication-based logically selective adaptive protection algorithm for radial AC microgrids is validated through a real-time HIL testing of an actual relay with IEC 61850 GOOSE communication protocol and Ethernet link. The communication delays between two intelligent electronic devices (IEDs) or relays are also estimated for the practical implementation of the proposed adaptive protection scheme.

d) The common European standards or EN grid codes and IEEE grid codes applicable for converter-based DERs from the perspective of AC microgrid protection are evaluated. In this regard, the role of reactive power contribution from DERs during ungrounded unbalanced shunt and series faults is analyzed for the detection of these faults. The symmetrical-component based protection functions are evaluated using standardized settings.

e) New symmetrical-component based directional protection schemes for radial AC microgrids with converter-based DERs are proposed and evaluated. These can also be applied to looped or ring AC microgrids with little or no modification.

3. The third part of contributions consists of future perspectives including:

a) New grid codes for the islanded mode of operation of future AC microgrids are proposed.

b) The latest and future trends of the protection schemes of microgrids in general and AC microgrids in particular are presented.

1.8 Outline of the thesis

This doctoral thesis is composed of seven independent published and appended original publications. The rest of the research material is comprised of additional four chapters (Chapters 2–5).

Chapter 2 explains four main functional components of AC microgrids, and provides a comprehensive literature review about DERs and related converters in addition to the controls and communications used in AC microgrids. AC microgrid protection challenges, requirements and solutions are discussed separately using illustrations. The focus of this chapter is to give background information about the protection schemes' challenges when new renewable energy generators called distributed energy resources (DERs) are connected to the local distribution networks and microgrids. These challenges produce new operational requirements for the protection schemes. Therefore, the development of new advanced protection methods and the modification of existing protection schemes are inevitable for the complete protection of microgrids. This chapter also offers a critical review of existing methods for the protection of AC microgrids in grid-connected and islanded modes. Based on the literature review, research gaps have been identified and new trends for AC microgrid protection are also summarized.

Chapter 3 gives an overview of new IEC/EN and IEEE standards and grid codes for AC microgrids in general, and protection systems in particular. In this regard, EN 50549-1-2019, EN 50549-2-2019 and IEEE 1547-2018 grid codes are briefly summarized. This chapter briefly explains the IEC 61850 communication standard, related protocols, and their applications for the protection of AC microgrids. This chapter also gives a brief description of different real-time testing methods for the control and protection of AC microgrids.

Chapter 4 presents comprehensive simulation-based case studies for different selected configurations of radial AC microgrids. The short-circuit fault studies are divided into two categories in this chapter: symmetrical short-circuit faults and unsymmetrical or unbalanced short-circuit faults. The solutions presented are not only based on offline simulations, but also on real-time hardware-in-the-loop (HIL) simulations consisting of real-time digital simulator and actual protection relay exchanging information using IEC 61850 GOOSE communication protocol. Moreover, standardized communication protocols and new grid codes of DERs are also evaluated and adopted to enhance the applicability of the presented solutions in real-world implementations. This chapter presents contributions of this thesis divided into eight main parts in relation to the respective published articles.

Chapter 5 presents the conclusions of the thesis, and suggestions of future work.

1.9 Summary of publications

In the following the Publications I–VII are briefly summarized according to scientific contributions of this thesis.

Publication I entitled as "A critical review of AC microgrid protection issues and available solutions" belongs to the literature review part of contributions.

This paper reviews protection issues in AC Microgrids, and presents state of the art and new protection schemes for AC Microgrids. It also gives a critical analysis of each proposed method, and categorizes the protection issues and schemes on the basis of the grid-connected and islanded operational modes of AC Microgrid. The majority of the newly proposed protection schemes were found to be communication-based adaptive protection schemes. The paper concludes that more effort is required to overcome the limitations of proposed protection schemes and to improve the reliability of communication system for adaptive protection schemes or provide alternate means to cope with communication failures. Moreover, protection against cyber-attacks is crucial for the safe and secure operation of future microgrids due to the extensive use of communication-dependent schemes.

Publication II entitled as "An adaptive protection for radial AC microgrid using IEC 61850 communication standard: Algorithm proposal using offline simulations" is related to new solutions and validations as well as future perspectives parts of contributions.

This paper proposes a new logically selective adaptive protection scheme for radial AC microgrid with an application of the IEC 61850 generic object-oriented substation event (GOOSE) protocol. The focus of the paper is to utilize the existing low voltage ride-through (LVRT) characteristic of distributed generators (DGs) with reactive power supply during the three-phase ungrounded shunt faults and communication between IEDs at different locations for adaptive overcurrent (OC) protection. The adaptive overcurrent IEDs detect the faults with two different preplanned settings groups: a lower setting group with a tripping threshold of 1.15 times rated load current for the islanded mode, and a higher setting group with a tripping threshold of 2.5 times rated load current for the grid-connected mode considering limited fault contributions of 1.2 times the rated current from the converter-based DGs. The setting groups are changed to lower values quickly using the circuit breaker status signal (XCBR) after a loss-of-mains, loss-of-DG, or islanding is detected. The methods of fault detection and isolation for two different kinds of communication-based IEDs (adaptive–nonadaptive) are explained for three-phase faults at two different locations. The communication-based IEDs take

decisions in a decentralized manner, using information about the circuit breaker status, fault detection (OC pickup signal), and a current magnitude comparison of signals obtained from other IEDs. However, the developed logically selective algorithm can also be implemented with the centralized system. The proposed algorithm assumes a one-way GOOSE transfer time delay of 10–20 milliseconds (ms) from one IED to the other. The paper also suggests a new LVRT characteristic curve of converter-based DGs for the islanded mode of operation, which helps in maintaining a proper protection coordination among IEDs. The results presented in this paper are based on PSCAD simulations.

Publication III entitled as "Microgrid protection with conventional and adaptive protection schemes" also belongs to the literature review part of contributions.

This publication is a book chapter, which presents a comprehensive review and challenges of the conventional and adaptive protection schemes for microgrids. The focus of this work is on protection schemes used for the AC microgrids, but protection schemes used for DC microgrids are also considered. The book chapter presents the protection issues and schemes for the grid-connected and islanded modes of operation. The basic requirements of protection schemes like sensitivity, selectivity and reliability along with the new requirements of adaptivity, re-synchronization and the selection of circuit breaker technology for microgrids are defined. The protection coordination performance of inverse-time and definite-time overcurrent relays is compared for the radial AC microgrid before the connection of the converter-based distributed energy resources (DERs) and after the connection of the converter-based DERs in the grid-connected mode, and with an additional connection of the centralized battery energy storage system (BESS) in the islanded mode of operation. The book chapter categorizes the adaptive protection schemes into two types: communication-based and communication-less adaptive protection schemes. The communication-based adaptive protection schemes are further classified as centralized and decentralized adaptive protection schemes from the implementation point of view. The chapter presents potential protection schemes for low voltage (LV) and medium voltage (MV) microgrids, based on the latest research articles. The paper emphasizes the need for specific grid codes for the islanded mode of operation to have the standardized requirements of DERs. The book chapter ends with a brief but comprehensive review of DC microgrid protection schemes and the challenges for the implementation of these schemes.

Publication IV entitled as "Real-Time hardware-in-the-loop testing of IEC 61850 GOOSE-based logically selective adaptive protection of AC microgrid" is mainly related to new solutions and validations part of contributions.

This paper reviews the HIL testing methods and applications covered in recent literature, and presents a step-by-step documentation of a new HIL testing setup for a specific case study. The case study evaluates the real-time implementation of the previously proposed communication-dependent logically selective adaptive protection algorithm of AC microgrids featured in Publication II using HIL testing of the IEC 61850 generic object-oriented substation event (GOOSE) protocol. The previous algorithm is updated for the application according to the new European standards entitled as "Requirements for generating plants to be connected in parallel with distribution networks. Part 1: Connection to a LV distribution network. Generating plants up to and including Type B" (EN 50549-1-2019) and "Requirements for generating plants to be connected in parallel with distribution networks. Part 2: Connection to a MV distribution network. Generating plants up to and including Type B" (EN 50549-2-2019). An RT model of AC microgrid that includes the converter-based DERs and battery storage along with IEC 61850 GOOSE protocol implementation is created in MATLAB/Simulink and RT-LAB software using the OPAL-RT simulator platform. Local area network (LAN) at the laboratory acts as the IEC 61850 station bus for exchanging GOOSE Boolean signals between the RT target and the actual digital relay. An evaluation of the round-trip delay using the RT simulation is performed. The main finding of the paper is that using Ethernet communication-based IEC 61850 GOOSE protocol, the whole process of fault detection, isolation and adaptive setting is possible within the standard LVRT curve maintaining a seamless transition to the islanded mode. The signal monitoring inside the relay is suggested to avoid a false tripping of the relay due to the signal modification or missing data transfer.

Publication V entitled as "Evaluation of new grid codes for converter-based DERs from the perspective of AC microgrid protection" is related to new solutions and validations as well as future perspectives parts of contributions.

The ever-increasing penetration levels of converter-based distributed energy resources (DERs) in medium and low voltage distribution networks necessitates new and revised standards or connection requirements of generating units. The standardized connection requirements to be met by DERs are called grid codes. This paper reviews new European and IEEE grid codes of MV–LV converter-based DERs, and presents an evaluation of selected grid codes applicable for AC microgrid protection. The selected grid codes are evaluated for both grid-connected and islanded modes of AC microgrid operation. The standardized settings of different protection schemes including symmetrical components-based protection schemes are evaluated for quick fault detection and isolation during the most challenging unbalanced faults in grid-connected and islanded modes. The extent of dynamic reactive power (Q) injection by DERs according to European

grid codes is evaluated, and the effect of Q-injection on fault detection and protection coordination is observed. The generic grid-forming DER model with coupled dq-control has been enabled to provide enough reactive current during the unbalanced faults with the help of an additional Q-source. It is concluded that the grid code requirement of dynamic Q-injection can be met by converter-based DERs with an additional Q-source of minimum capacity equal to twice the apparent power of individual DER in the grid-connected mode. The same extent of Q-injection is also useful for fault detection and reliable directional element design in the islanded mode. A new five-cycle high voltage ride-through (HVRT) curve is also suggested for a smooth transition to the islanded mode.

Publication VI entitled as "Protection strategies for the future harbor area AC microgrids containing renewable energy sources and batteries" is mainly related to new solutions and validations part of contributions.

A significant share of global carbon emissions is related to marine vessels running solely on fossil fuels. The hybrid or fully electrified marine vessels using battery energy storage systems (BESS) both for onboard propulsion systems and for cold-ironing during docking at harbor areas will significantly reduce marine-related carbon emissions. However, the transformation of marine vessels' operations from diesel engines to BESS will necessarily require charging stations and other electric power infrastructure at harbor areas. The sustainable and cheap energy of renewable energy sources like wind turbine generators (WTGs), photovoltaic (PV) systems and related BESS could be used at harbor areas for charging depleted vessel-BESS and supplying power to cold-ironing loads. For this purpose, two new harbor area smart grid or AC microgrid models have been developed by our research group. This paper presents a comprehensive analysis of three-phase short-circuit faults for one of the proposed AC microgrid models using PSCAD/EMTDC (Electromagnetic Transients including DC) simulations. A fault study of harbor area AC microgrid-1 is done for both grid-connected and islanded modes. The main purpose of the fault study is to check if grid-connected mode overcurrent settings of intelligent electronic devices (IEDs) will also be valid for different islanded mode fault cases with different fault current contributions from converter-based distributed energy resources (DERs) including WTG, PV and BESS. The extent of fault current contributions from DERs and BESS to avoid adaptive protection settings and to ensure definite-time protection coordination and fast fuse operations during different islanded modes is investigated.

Publication VII entitled as "Hardware in the loop testing of power systems" also belongs to the literature review part of contributions.

This review article addresses the modern Hardware-In-the-Loop (HIL) simulation methods used for testing the control and protection of power systems. In this regard, the basic specifications required for the HIL simulation of power systems are explained in this article. The article presents the general concept of HIL simulation and defines the common framework for the controller HIL and power HIL types of simulations. The article also gives an overview of the Ethernet-based and SCADA (Supervisory Control And Data Acquisition) communication protocols, in addition to the latest real-time simulators used for HIL testing. Additionally, the article also highlights the most common application areas of HIL simulation in power systems and presents different methods of improving the stability of HIL simulation experiments.

1.10 Other publications by the author

The author also contributed as the co-author of the following conference papers, research reports and journal articles on closely related topics during different stages of the research work. However, these publications are not directly related to the main objectives of the thesis, and are therefore not included in this thesis.

Mekkanen, M., Kauhaniemi, K., Kumpulainen, L., Memon, A. (2018). Light-Weight IEC 61850 GOOSE Based LOM Protection for Smart Grid. CIRED Workshop-Ljubljana, 7-8 June 2018. http://dx.doi.org/10.34890/314

Raipala, O., Hovila, P., Leminen, J., Farughian, A., Memon, A., Kauhaniemi, K. (2019). Utilization of a mixture of CTs and current sensors in line differential protection applications. Proceedings of 25th International Conference on Electricity Distribution: CIRED 2019, Madrid, 3-6 June 2019, Paper No. 292. http://dx.doi.org/10.34890/1026

Memon, A. A., Kauhaniemi, K. (2019). Modelling of grid-friendly charger topologies for electric vehicles. Article in Electric Commercial Vehicles ECV 2012-2016, final report, pp.189-198. https://www.vtt.fi/inf/pdf/technology/2019/T348.pdf

Kumpulainen, L., Kauhaniemi, K., Farughian, A., Sirviö, K., Memon, A., Voima, S. Mekkanen, M., Kumar, H., (2019). VINPOWER Vaasa innovation platform for future power systems: Final report (summary) http://urn.fi/URN:NBN:fi-fe2020081250941

Kumar, J., Memon, A. A., Kumpulainen, L., Kauhaniemi, K., Palizban, O. (2019). Design and Analysis of New Harbour Grid Models to Facilitate Multiple Scenarios

of Battery Charging and Onshore Supply for Modern Vessels. Energies, 12, 2354. https://doi.org/10.3390/en12122354

Sirviö, K., Kauhaniemi, K., Memon, A. A., Laaksonen, H., & Kumpulainen, L. (2020). Functional Analysis of the Microgrid Concept Applied to Case Studies of the Sundom Smart Grid. Energies, 13(16), 4223. http://dx.doi.org/10.3390/en13164223

2 THEORETICAL BACKGROUND

This chapter introduces the state-of-the-art functional components of an AC microgrid including DERs and related power electronics converters, distribution components and protective devices, controllable and uncontrollable loads, and control and communication means. The protection challenges and new requirements of an AC microgrid protection are explained with examples and illustrations. The protection solutions for grid-connected and islanded modes of operation along with their advantages and limitations are reviewed. Also, the advanced protection solutions of future using the optimization algorithms, AI methods and wide-area measurements are reviewed in this chapter. Based on literature review, research gaps in AC microgrid protection solutions will be identified.

2.1 Functional components of an AC microgrid

Although a microgrid is viewed as a local small distribution system, the architecture of a microgrid is a system of various complex systems. The functional components of an AC microgrid can be subdivided into four main categories as shown in Figure 7: (1) DERs and related power electronic converters, (2) Distribution components and protective devices, (3) Controllable and uncontrollable loads, and (4) Control and communication. These functional components are further explained separately in Sections 2.1.1–2.1.4.

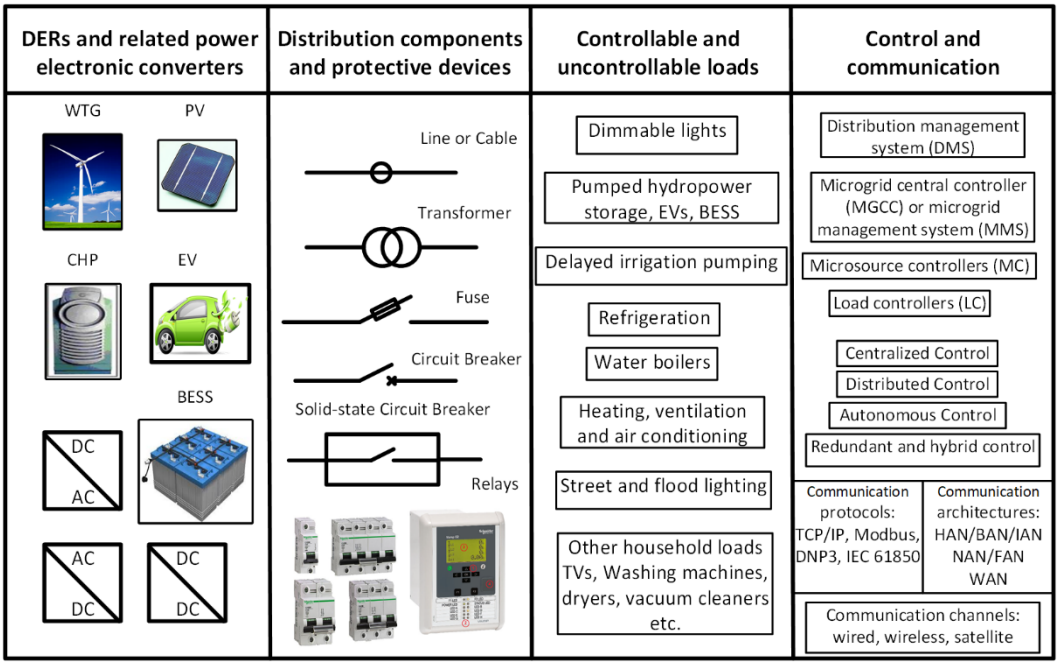

Figure 7. Functional components of an AC microgrid.

Four functional components of an AC microgrid (Figure 7) are derived from three of five layers of smart grid architecture (Kuzlu et al., 2014): power system, control and communication layers. So, functional components (1)–(3) belong to the power system layer and functional component (4) to control and communication layers.

2.1.1 DERs and related power electronic converters

DERs (and particularly variable RES like WTGs and solar PV systems and related power electronics) have gone through various technological development stages, the details of which can be found in (Ackermann, 2005); (H. Li & Chen, 2008); (Kim & Lu, 2010); and (Teodorescu et al., 2011). However, a brief review is provided here in Section 2.1.1 based on the literature review for the utility scale DERs connected to the main grid.

Power electronic converters required in microgrids are DC–DC, AC–AC, AC–DC and DC–AC converters, or any suitable combinations of these converters. However, it all depends on the type of DER and its output power characteristics, the magnitude and the form of electric current and voltage (AC or DC) at the network connection point, and the type of load which determine the particular selection of the converter type. In traditional distribution networks, the form of electric current and voltage is AC, therefore for the connection of the DERs with an inherent DC power output with DC voltage and DC current (solar PV, fuel cells, batteries), DC–AC converters (also called inverters) are usually required. However, since solar PV, fuel cells and batteries generate electric power at low voltage DC, a step-up DC–DC converter (also called a boost converter) is therefore usually required before the DC–AC conversion stage. The other types of DERs like WTGs and the CHP microturbines generate power at variable and high frequency AC, therefore two stage AC–DC and DC–AC or AC–AC converters are required for these types of DERs (Keyhani et al., 2010).

Power electronic converters have been developed over the years, ranging from simple diode rectifiers to the thyristor-based H-bridge topology which can be used for DC–DC and DC–AC or AC–DC converters either in half-bridge or full-bridge form. Today's advanced converter topologies consist of insulated gate bipolar transistors (IGBTs) and metal-oxide-semiconductor field-effect transistors (MOSFETs) for MV and LV applications (Teodorescu et al., 2011). For EVs and BESS, either separate AC–DC charging and DC–AC discharging converters or a single bidirectional converter with both charging and discharging capabilities are required, depending on the application. Different converter topologies for EVs can be found in (Musavi et al., 2012); (Khaligh & Dusmez, 2012); (Yilmaz & Krein, 2013); and (Koushki et al., 2014).

WTGs have been available in at least four standard types: type 1 through type 4 (or type A through type D) WTGs (Ackermann, 2005); (Australian Energy Market Operator, AEMO, 2013). The earlier type 1 WTGs are fixed speed type (with no speed control) using an asynchronous squirrel cage induction generator (SCIG) designed to be connected directly to the grid via a three-phase transformer. The problem with type 1 WTG is that the SCIG always absorbs a variable reactive power from the grid during wind fluctuations causing voltage fluctuations to the grid. Therefore, reactive power compensation needs to be provided by capacitor banks at the connection point of type 1 WTGs. Moreover, for a smoother grid connection, a soft-starter device is also required to reduce the inrush current. The type 2 WTGs provide a limited variable speed control, and hence output power control using a variable generator rotor resistance called an OptiSlip® (a registered trademark of Vestas Wind Systems A/S). The type 2 WTG uses a wound rotor induction generator (WRIG), and it is also connected directly to the grid via a three-phase transformer like type 1 WTGs. Moreover, the type 2 WTG also requires capacitor banks for reactive power compensation and needs a soft-starter device for a smoother grid connection.

The type 3 WTG (Figure 8) is commonly known as the doubly fed induction generator (DFIG), and provides a limited variable speed control and consists of a WRIG and a partial scale frequency converter with a rated power of about 25–35% of nominal generator power. The stator of the type 3 WTG is directly connected to the grid, and the rotor is connected to the grid via a back-to-back voltage source converter (VSC), also called the frequency converter. The type 3 WTG can be connected to the grid using a three-phase three-winding transformer, or a three-phase inductor (for frequency converter connection) and a two-winding transformer. The partial scale frequency converter provides the reactive power compensation, a smoother grid connection, and a wider range of speed control compared with the type 2 WTGs. The two-stage partial frequency converter of type 3 WTGs has two independently controlled VSCs: AC–DC converter from the rotor-side and DC–AC converter from the grid-side, both separated by a common DC link capacitor. The rotor-side AC–DC converter is usually used to control the active and reactive power, whereas the grid-side DC–AC converter is used to maintain a constant DC link voltage and operates at unity power factor. In most cases, no external reactive power compensation is required for type 3 WTGs when connected to strong networks near substations. However, when connected to distant weak networks, type 3 WTGs require dynamic reactive support for compliance with the technical requirements like voltage and power factor control. The grid code requirements compliance of type 3 WTGs have been studied in (Memon, 2013) for voltage and power factor control at the connection point of a weak distribution

network. The type 3 WTG has been the leading WTG concept with a market share of 85% in 2008 (Rechsteiner, 2008).

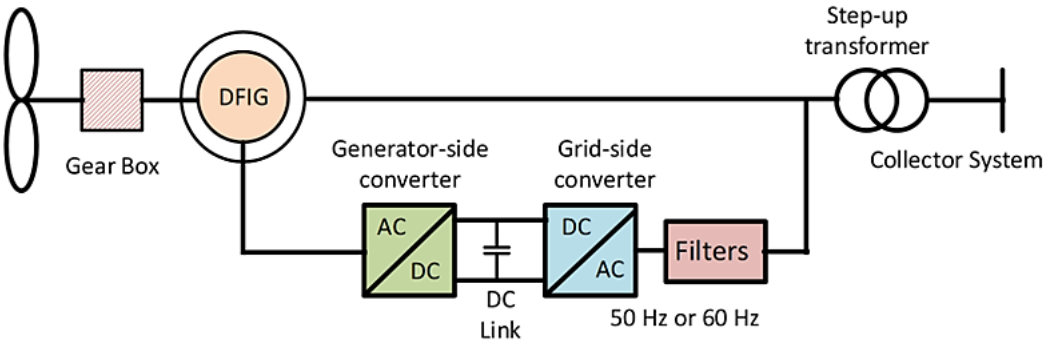

Figure 8. Type 3 wind turbine generator.

The type 4 WTG (Figure 9) is a full variable speed WTG that uses a full-scale frequency converter (usually a back-to-back VSC) for the reactive power compensation and a smooth connection to the grid. The type 4 WTG can use a WRIG, a wound rotor synchronous generator (WRSG), or a permanent magnet synchronous generator (PMSG). With the advantage of having a frequency converter of the same rating as the generator, the type 4 WTG provides generator operation from zero to the full rated speed with an improved reactive power capability compared with the type 3 WTG. Moreover, a generator of the type 4 WTG is completely decoupled from the grid, hence the control of the active and reactive power is completely dependent on the frequency converter which is usually faster than the type 3 WTG. Due to the complete decoupling provided by the frequency converter, the impact of the grid voltage and frequency disturbances on the generator and mechanical drive is negligible in the type 4 WTG. Because of these obvious advantages, the type 4 WTG was expected to replace the future market share of the type 3 WTG (Teodorescu et al., 2011); (Australian Energy Market Operator, AEMO, 2013). Presently, direct drive PMSG based type 4 WTGs are dominant in the offshore wind turbine market (Ibrahim & Zakzouk, 2022).

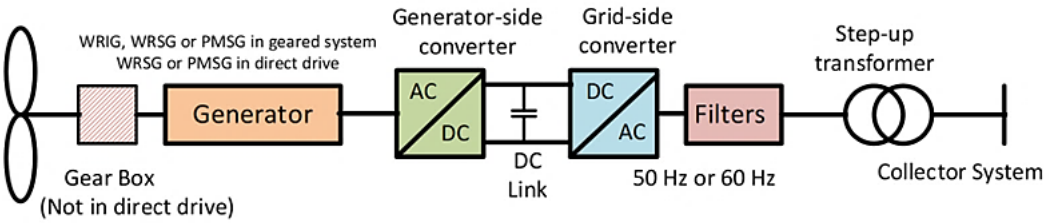

Figure 9. Type 4 wind turbine generator.

Power electronic converters for multi-megawatt (5 MW or greater) WTGs have been divided into three categories: Back-to-back pulse width modulation (PWM)

or two-level converters, multi-level (ML) converters, and matrix converters. The back-to-back PWM converter is the most cost effective and mature technology with two VSCs separated by a DC link capacitor, hence providing separate control for generator-side and grid-side converters. However, the DC link capacitor reduces the overall life of the converter and due to high frequency harmonics, additional filters are required. Moreover, a back-to-back converter has more switching losses compared with the other two topologies. The ML (the neutral point clamped, NPC) converters have three or more voltage levels, and hence produce less total harmonic distortion (THD) compared with two-level converters. Moreover, ML converters have about 25% less switching losses than the two-level converters. The major disadvantages of the ML converters are the voltage imbalance created by the capacitors, and uneven stress on switches due to its design. The matrix converter has the advantage that it is a direct AC–AC converter without any DC link capacitor and inductor in its design. Therefore, the matrix converter has an increased efficiency and overall life in addition to the reduced size. The matrix converter also has reduced switching losses and harmonic emissions compared with the two-level converter. However, the increased number of switches and cost, reduced output voltage (86% of the input voltage), higher sensitivity to the grid disturbances, rapid input voltage variations, and high conduction losses are obvious disadvantages of the matrix converter (Kim & Lu, 2010).

From the grid connection point of view, PV converters (inverters) can be broadly classified into two categories: transformer-based (Low frequency [LF] or high frequency [HF]) topologies and transformer-less topologies. The transformer-less topologies are more attractive from the viewpoint of a 1–2% higher efficiency and reduced weight due to the absence of an LF or HF transformer than transformer-based topologies, particularly in single-phase and partial load applications. However, transformer-less topologies are more complex in structure and control due to the requirements of keeping the leakage current and DC current injection under control due to safety reasons. Various transformer-less PV inverter topologies are derived from two well-proven converter families: H-bridge and NPC topologies. For three-phase applications, it is usual practice to use three independent single-phase PV inverters in three-phase four-wire connection instead of three-phase three-wire connection, since it allows the use of the existing single-phase inverters and mild anti-islanding requirement. However, using single-phase building blocks, three-phase three-wire PV inverter units can also be made, but the DC link voltage required is in the range of 600–1000 V compared with only 400 V in single-phase topologies. From the solar PV power plant configuration point of view, the PV inverters can be categorized into two types: string or multistring PV inverters (0.4–6 kW) and mini central or central PV inverters (6–1000 kW) (Teodorescu et al., 2011). The single-phase PV inverter

topologies has been described in more detail in (Teodorescu et al., 2011), and the details about the three-phase grid-connected PV inverters are given in (Mechouma et al., 2012).

2.1.2 Distribution components and protective devices

The power distribution components in microgrids include the lines, cables and power transformers for the distribution of electric power from the grid or the DERs to the loads. The power distribution components also include auxiliary equipment like capacitor banks, inductors and other voltage control and reactive power compensation equipment. These power distribution components need to be protected from abnormal conditions like short-circuit currents during the faults. Therefore, suitable switching and protective devices are installed at the selected locations in order to protect the expensive electric equipment like lines, cables and transformers, as well as loads installed at the consumer premises. The protective devices include the simple fuses, simple sensing and switching circuit breakers (CBs) like miniature circuit breakers (MCBs), molded case circuit breakers (MCCBs) and air circuit breakers (ACBs) for LV levels and mechanical circuit breakers operated by separately installed sensing relays such as overcurrent relays for the MV levels. Modern numerical protection relays (also called intelligent electronic devices [IEDs]) provide different protection functions such as overcurrent, overvoltage, undervoltage etc. in a single device. These IEDs, mechanical CBs and instrument transformers (current transformer [CT] and voltage transformer [VT]) are essential components of modern MV and HV protection schemes. Recently, solid-state circuit breakers (SSCBs) have also been developed for MV and LV levels and for both AC and DC applications. The choice of protective devices for microgrids is an important and challenging task because the safety of the equipment and personnel and the continuity of supply depend on the proper working of the protection schemes. Various factors need to be considered for the proper selection of protective devices including the cost, location, type, sensitivity and worth of the equipment under protection, network topology, type of supply (AC or DC), voltage level, minimum and maximum magnitude of short-circuit current, as well as the types of DERs and their connections. These mentioned factors and other challenges are further discussed in Sections 2.2–2.4.

2.1.3 Controllable and uncontrollable loads

Controllable loads are those loads which can be continuously monitored, and hence their operation or usage can be changed, reduced, optimized, interrupted or

delayed for other times. The controllable loads can actively participate in the demand side management of the microgrid, thus helping to stabilize and optimize the operation of the microgrid overall. The controllable loads include dimmable lights, building heating, ventilation and air conditioning loads, water boilers, delayed irrigation pumping, pumped hydropower storage, plug-in EVs, and BESS. Other time- and weather-dependent, high priority, continuous and uninterrupted operating loads fall under the category of uncontrollable loads.

2.1.4 Control and communication

As mentioned in Section 1.2, a microgrid is considered as the building block of a smart grid, therefore its interactive platform consists of all five essential layers of smart grid architecture (Kuzlu et al., 2014): i.e. the power system layer (for generation, distribution and utilization of power), control layer (for monitoring, control and management functions), communication layer (for two-way communication), security layer (for data confidentiality, integrity, authentication and availability) and application layer (for delivering applications to customers and the utility). The power system layer elements have already been described in Sections 2.1.1–2.1.3. Section 2.1.4 briefly describes the control and communication layers of a microgrid's architecture.

The main task of microgrid control is to balance the power supply and demand in the microgrid during different operational modes, while maintaining good power quality and stability through different control actions or functions. The control actions or functions include the voltage control, frequency control, power sharing among DERs, demand-side management, protection of personnel and equipment, power quality improvement, smooth transition of different operational modes (grid-connected, islanded, transitory, black-start), energy management, economic power dispatch, optimization of operation, market participation, and multi-microgrid interaction and coordination (Sen & Kumar, 2018); (Sirviö et al., 2020).

Three alternative control strategies for microgrids have been mentioned in (IEEE Std 1547.4, 2011): centralized control, distributed control and autonomous control. In the centralized control, the central controller gives commands to the distributed devices in the entire system in a master-slave configuration. In the distributed control, various independent controllers communicate with each other in order to control the entire system. The distributed control uses intelligent devices strategically located at various places to detect abnormal conditions and initiate corrective actions. In the autonomous control, the control actions are performed with independent controls without communication with each other. The Consortium for Electric Reliability Technology Solutions (CERTS) microgrid

autonomous control concept uses traditional voltage vs reactive power droop and active power vs frequency droop in combination with DC storage at the DC bus of each DER to avoid a master-controller or a central storage unit (Piagi & Lasseter, 2006).

Three hierarchical control levels are found in the centralized control of grid-connected microgrids (Hatziargyriou et al., 2006): (1) Local controller for individual DER or controllable load called a microgenerator controller (MC) or load controller (LC), (2) MGCC or MGMS, and (3) Distribution management system (DMS). All these control levels should coordinate and communicate with each other to optimize the microgrid operation.

In a recent review (Sen & Kumar, 2018), microgrid control has been divided into four broad types: centralized control, decentralized control, distributed control and hierarchical control. Each of these four control types consists of different functional layers. The centralized control architecture is divided into three layers: DMS, MGCC, and LC. The decentralized control architecture is divided into only two layers of upper- or higher-level controllers and lower-level controllers. The distributed control architecture is divided into three layers: droop or lower layer, secondary or intermediate layer, and auxiliary or upper layer. The hierarchical control is also divided into three layers: primary, secondary, and tertiary control. The hierarchical control is derived from the ANSI/ISA-95 (American National Standards Institute–International Society of Automation) and its structure is based upon the different time scales required for different control requirements. The primary control used for voltage-frequency (V-f) control operates within a milliseconds and seconds time scale. The secondary control eliminates steady state fluctuations as a result of primary control actions with a response time of minutes. The tertiary control used for the management of power exchange with the main grid operates within a time scale of several minutes to an hour.

Novel hybrid controls for microgrids are also being suggested, as seen in (Bintoudi et al., 2017) which features a hybrid control system for AC microgrid consisting of both centralized and decentralized control methods. The proposed method uses a three-level (primary, secondary and tertiary) hierarchical control with the application of intelligent agent-based components. The proposed method uses the decentralized agent-based control as a backup in case the centralized control such as the MGCC fails. In future, hybrid or redundant controls for microgrids (Figure 10) will be necessary that use both communication-based and local non-communication-based methods like droop controls to avoid power supply interruptions due to cyberattacks and communication failures.

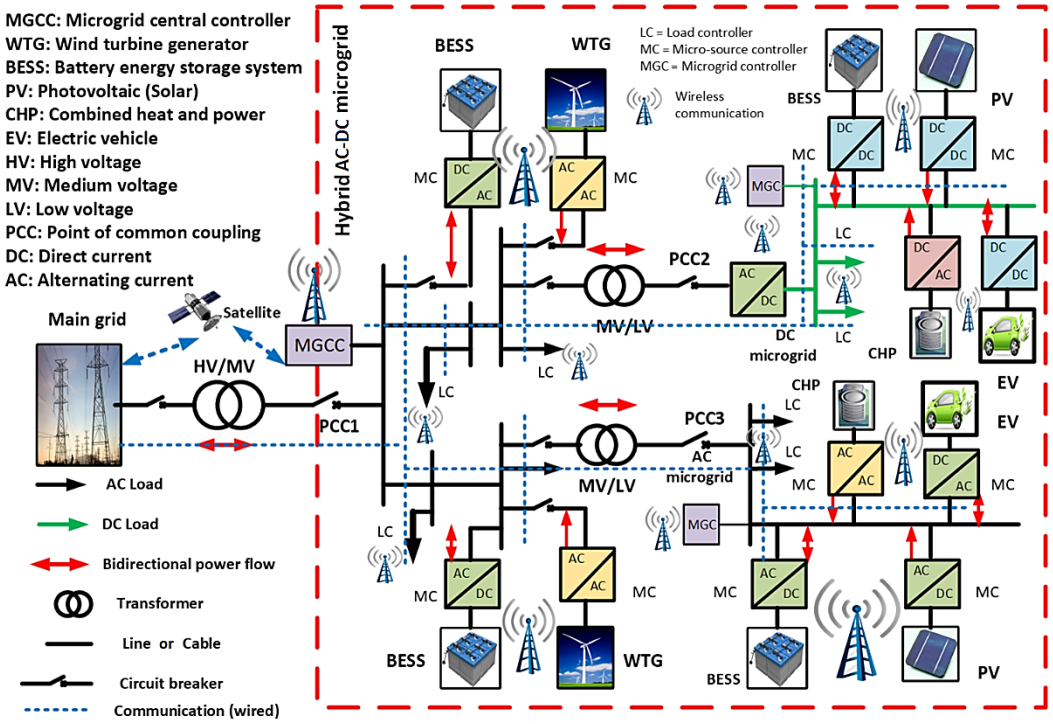

Figure 10. Hybrid microgrid with redundant control and communication.

The communication architecture in microgrids can be divided into three multi-layered hierarchical network levels: 1) HAN (Home Area Network), BAN (Building Area Network) or IAN (Industrial Area Network), 2) NAN (Neighborhood Area Network) or FAN (Field Area Network), and 3) WAN (Wide Area Network). These network levels can be implemented using any or a combination of three types of communication technologies or channels depending on the application and the coverage range: wired communication technologies, wireless communication technologies, and satellite communication technologies (Kuzlu et al., 2014). For a successful communication between devices in different network and control levels, standardized rules and regulations are required for the exchange of information, and these systematically defined rules are called communication protocols. The most common communication protocols used for microgrids include TCP/IP (Transmission Control Protocol–Internet Protocol), Modbus, DNP3 (Distributed Network Protocol version 3.3), IEC 61850, and IEC 60870. The Ethernet-based communication protocols are briefly reviewed in Publication VII. The IEC 61850 standard of communication is described in Section 3.3.

2.1.5 Grid-following and grid-forming controllers

For the essential capability of an AC microgrid to operate smoothly during both grid-connected and islanded modes of operation, two different micro-source or

microgenerator controllers (MCs) for DER converters are generally required. The MC required during the grid-connected mode is called the grid-following controller because its voltage (V) and frequency (f) is only controlled by the main grid. With the grid-following controller, the converter-based DERs are capable of feeding or generating fixed magnitudes of active power (P) and reactive power (Q) according to their set points to meet the local load requirements. The rotating frequency signal (ωt, where $\omega = 2\pi f$) is extracted from the measured three-phase grid-side voltage at the DER terminals using a phase-locked loop (PLL) based on a synchronous reference frame to generate the power of the same frequency of the main grid. The majority of the converter-based DERs connected in MV–LV distribution grids use grid-following controllers because DERs are usually not allowed to operate in the islanding mode. Figure 11 shows a grid-following controller of a generic three-phase converter-based DER. The different other types of the grid-following controllers for converters of PV and WTGs can be found in (Teodorescu et al., 2011).

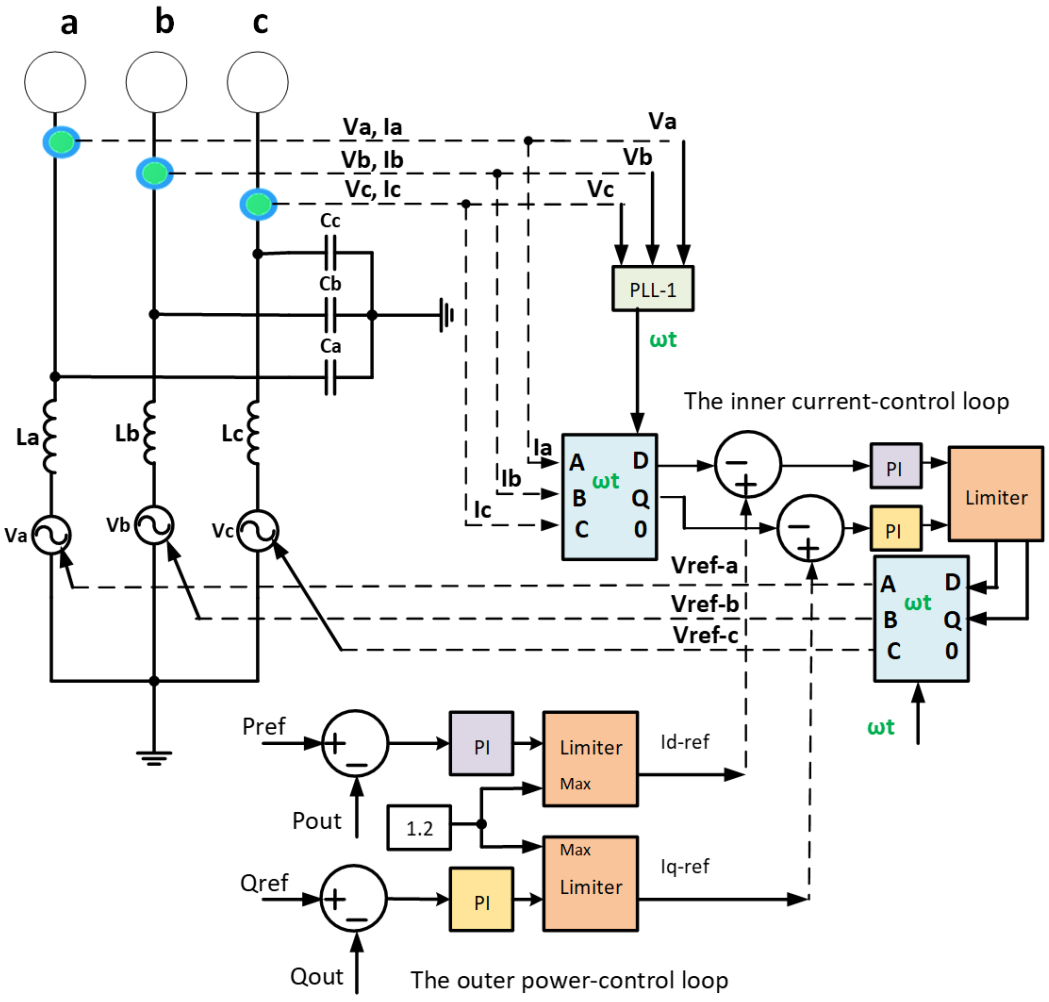

Figure 11. Grid-following controller of a generic converter-based DER.

The MC required during the islanded mode is called the grid-forming controller because it enables the converter-based DER to be used as a reference generator controlling the local voltage (V) and frequency (f) of the islanded AC microgrid. Anyone or all of the converter-based DERs or ESS in an islanded AC microgrid can be used as the reference generators by changing their control from the grid-following mode to the grid-forming mode. Since the three-phase grid-side voltage at the DER terminals is not available during the islanded mode, therefore, the rotating frequency signal (ωt) has to be locally generated. A voltage-controlled oscillator (VCO) with a fixed or constant input signal of the required frequency can be used to generate the reference frequency sinusoidal signal or the rotating frequency signal (ωt) for the grid-forming controller. This will enable the converter or the inverter of the grid-forming DER to work as a controlled-frequency VSC, generating the AC power with the required 50 Hz or 60 Hz frequency. Figure 12 shows a grid-forming controller of a generic three-phase converter-based DER.

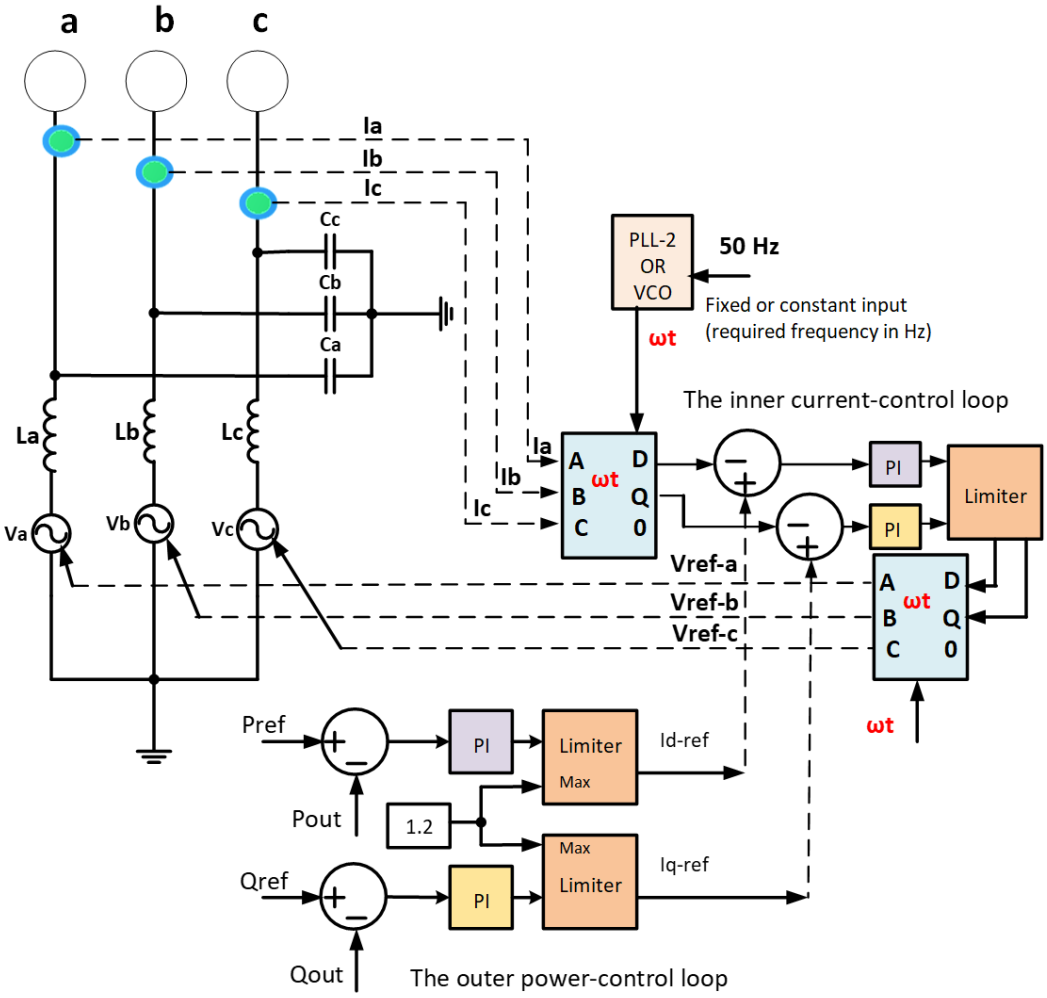

Figure 12. Grid-forming controller of a generic converter-based DER.

The grid-forming controllers of DERs in earlier research have been considered for only the islanded mode, and reported with different names such as isolated mode controllers (Chandorkar et al., 1993), decentralized controllers (Guerrero et al., 2013), islanded mode controllers (Rasheduzzaman et al., 2014), autonomous mode controllers (Sadeghkhani et al., 2017), and standalone mode controllers (Fusero et al., 2019), etc. But in the most recent research, these are more commonly referred to as "grid-forming" controllers applicable for both grid-connected and islanded modes.

According to (Guerrero et al., 2013), the controllers of grid-forming converters are generally required to ensure that:
1) The total linear and non-linear load is shared in the desired way.
2) The stability is guaranteed on a global scale within the islanded section.
3) Any DC voltage offsets on the microgrid is prevented.
4) The oscillations between the output filters are actively damped.

The grid-forming controllers can be divided into three main categories: Droop-based controllers, synchronous machine-based controllers, and virtual oscillator-based controllers. The droop-based controllers are further categorized into frequency-based droop, angle-based droop, and power synchronization controllers (Rathnayake et al., 2021). The conventional droop-based controllers lack the inertia support and are not suitable for sharing non-linear loads. To solve the harmonic current sharing problem, output virtual reactors and resistors are suggested for proper sharing of harmonic currents due to non-linear loads. The load-dependent frequency and voltage amplitude deviation are other disadvantages of droop-based controllers (Guerrero et al., 2013).

The synchronous machine-based controllers are further categorized into virtual synchronous machine controllers, swing equation emulation controllers, augmented virtual synchronous generator controllers, synchronverter controllers, and matching controllers. These grid-forming converters address the lack of inertia support that is often seen as a problem of conventional droop controllers. The virtual oscillator-based controllers can be categorized into dead-zone virtual oscillator-based, dispatchable virtual oscillator-based, and unified virtual oscillator-based controllers. Several other grid-forming controllers are also reviewed and summarized in the latest review articles including (Rathnayake et al., 2021) and (H. Zhang et al., 2021).

The general challenges addressed in the latest grid-forming converters are related to stability issues (both small signal and transient stability), capability to work during both grid-connected and islanded modes, current limitation to avoid over-sized converters, fault recovery, and large-signal transient stability. The stability

of grid-forming converters is addressed in (Rasheduzzaman et al., 2014), (Alipoor et al., 2015), (Du et al., 2019), (Gouveia et al., 2019), (Yang et al., 2021), (H. Zhang et al., 2021), (Z. Jin & Wang, 2022), and (C. Li et al., 2022). The operation of grid-forming converters during both grid-connected and islanded modes are addressed in (Chandorkar et al., 1993), (Zhong & Weiss, 2011), (Zhong et al., 2014), (Zhong et al., 2015), and (Fusero et al., 2019). The current limitation of grid-forming converters is addressed in (Sadeghkhani et al., 2017), (Meng et al., 2021), and (Du et al., 2022). The dynamic performance and frequency support functions of grid-forming converters are addressed in (J. Liu et al., 2016), (Zhou et al., 2021), (Sajadi et al., 2021), (Du et al., 2021), (Amin et al., 2021), and (M. Li et al., 2022). The comparison of grid-forming and grid-following controllers is presented in (Pattabiraman et al., 2018), and (Gao et al., 2021).

As briefly reviewed above, there are various grid-forming controllers proposed in the latest research articles. The choice mainly depends on how the controller meets the maximum technical requirements including the latest grid code requirements of DERs, as discussed in Section 3.4. From a protection point of view, most of the well-designed grid-forming and grid-following converters behave similarly during faults. The fault current contribution from the converter-based DERs is limited to 1–2 per unit (p.u.) of the rated current. This causes various protection challenges during grid-connected and islanded modes as discussed in Sections 2.2.1 and 2.2.2, respectively. Related to this thesis, the generic current limiting grid-following and grid-forming controllers of Figure 11 and Figure 12 are used for the simulation-based analysis featured in Publications II–VI.

2.2 Protection challenges

The protection challenges of AC microgrids are divided into two main categories on the basis of steady state operational modes: protection challenges during the grid-connected mode, and protection challenges during the islanded mode. These are explained separately in Sections 2.2.1 and 2.2.2.

2.2.1 Protection challenges during grid-connected mode

In the grid-connected mode of AC microgrids, the highest fault current contribution comes from the main grid through point of common coupling (PCC) during short-circuit faults. However, depending on the size and type of the DERs connected inside the AC microgrid, the fault current contribution from the main grid is decreased due to the fault current contribution of DERs. The fault current contribution from the main grid is decreased up to the maximum extent when

majority of the synchronous generators (gas, diesel or hydropower) are connected inside the AC microgrid. Due to the reduced fault current from the main grid, the sensitivity and operational speed of conventional single setting overcurrent (OC) protection devices like fuses and inverse-time OC relays installed upstream of the fault location are affected. This means the fuses and inverse-time OC relays may take a longer than expected time to operate during short-circuit faults, particularly for providing coordinated backup protection. This will expose the electrical equipment and loads to the short-circuit fault currents for a longer than expected duration of time. Therefore, the equipment may either be damaged, or its effective lifespan will be reduced. The converter-based DERs inside the AC microgrid with a limited fault current contribution of 1.2 p.u. may produce a lesser effect to the operation of fuses and inverse-time OC relays than synchronous generators in the grid-connected mode. However, the extensive share of the converter-based DERs inside the AC microgrid with a fault current contribution of greater than 1.2 p.u. of the nominal current may still produce a combined adverse effect on the operation of fuses and inverse-time OC relays.

The connection and disconnection of the converter-based DERs inside the AC microgrid due to various operational, technical and economic requirements will also change the fault contribution from the main grid. This means that OC protection devices will see different fault current levels depending on the connection and disconnection status of converter-based DERs. Figure 13 shows the phenomenon when all BESS and DERs are connected inside the grid-connected radial AC microgrid. When all of the BESS and DERs are connected inside the radial AC microgrid, then during the short-circuit fault between breakers 6 and 7, the fault current contribution from the main grid is reduced due to the fault current contribution of BESS1 and WTG. Consequently, the breakers 2 and 6 will experience an unequal level of fault currents, whereas the breaker 1 will experience a lower fault current magnitude than in a case without BESS and DERs. This may cause inverse-time OC protection devices at breakers 1 and 2 to respond with slower speeds and at breaker 6 with higher speed during the fault, depending on current magnitude reduction and extra fault current contribution of BESS1 and WTG. This means the selectivity or coordination of protection devices will be affected due to the connection of the converter-based DERs. Due to current magnitude dependency, converter-based DERs cause the inverse-time OC relays upstream to the fault point to be less or more sensitive depending on the location and fault current contribution of BESS and DERs.

The reverse fault current flow during short-circuit faults at some protection devices can also be observed in the grid-connected mode when the converter-based DERs are connected at both ends of the fault point. The reverse fault current flow

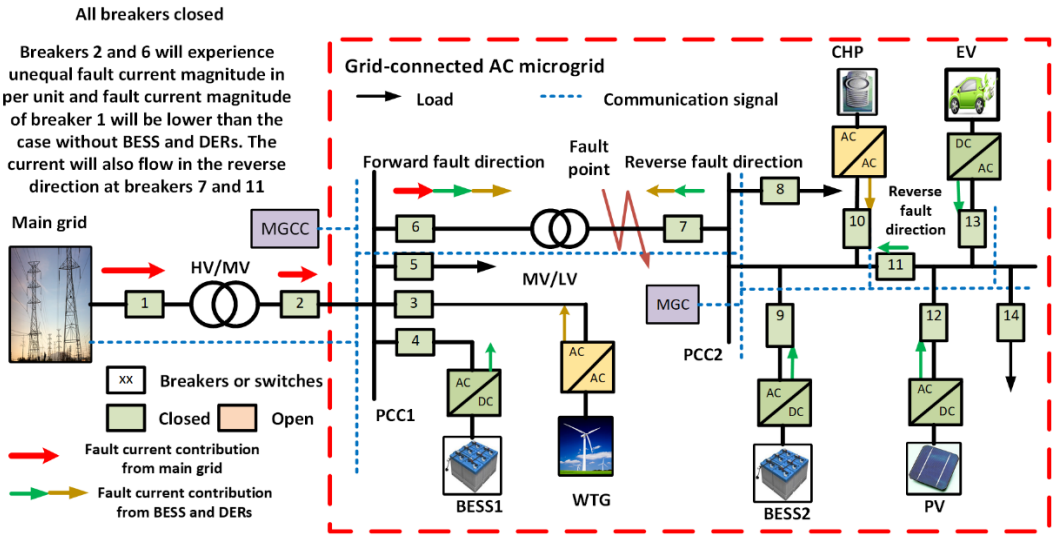

Figure 13. Fault current variation in the grid-connected radial AC microgrid with all DERs connected during the fault.

can be observed at the protection devices of breakers 7 and 11 in Figure 13 during the short-circuit fault at a location between breakers 6 and 7. Primarily, the protection device at breaker 6 has to detect and isolate the mentioned short-circuit fault. However, protection devices at breakers 7 and–or 11 may respond earlier than the protection device at breaker 6 due to the reverse fault current flow, depending on the settings, control and fault current contribution of BESS2, and the DERs including CHP, PV and EV. This will result in an unintentional islanded condition at the LV sections due to a false tripping of breaker 7 and–or 11. This will be an unwanted islanding condition if grid-forming converters and MGC at PCC2 are not available. To avoid this false operation, some directional detection scheme will also be required for protection devices at breakers 6, 7 and 11. With the directional detection function available, only protection devices detecting a forward fault direction will operate. Hence, a false operation of protection devices will be avoided.

The traditional method is to disconnect or cease to energize all of the converter-based DERs during short-circuit faults in the grid-connected mode. This way the single settings of inverse-time OC relays will be useful during short-circuit faults. This phenomenon is described in Figure 14 where all of the converter-based DERs are disconnected by opening the related breakers or switches (red color boxes) during the short-circuit fault. For the same purpose, fault current limiters (FCLs) are also suggested to be used at output terminals of DER units, in order to limit or reduce the fault current contribution of DERs. With the extensive share of converter-based DERs in the grid-connected mode, the option of disconnecting all DERs during the faults will result in a network instability problem, unwarranted

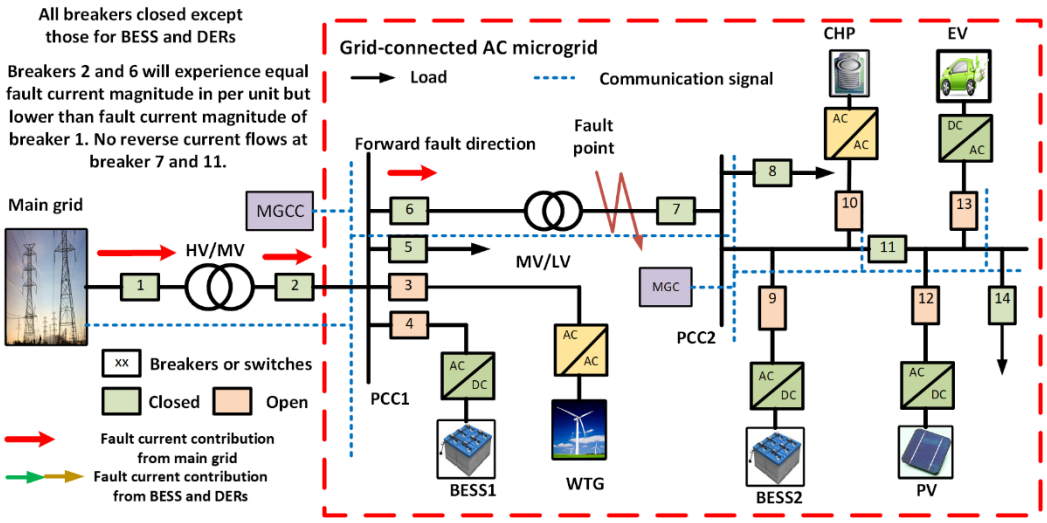

Figure 14. Fault current variation in the grid-connected radial AC microgrid with all DERs disconnected during the fault.

power outages for the customers, and a reduced level of renewable power generation in the energy mix. Therefore, adaptive OC relays are usually required to change the active setting groups in real time, based on the connection and disconnection status of the converter-based DERs in the grid-connected mode. Usually, the predefined reliable setting groups are changed in real time depending on the connection or disconnection status of DERs. Both definite-time and inverse-time OC relays can be used for the implementation of adaptive protection schemes.

The substation type of radial AC microgrids (Figure 13 and Figure 14) with BESS and DERs connected to the MV and LV side of the distribution transformer may be designed or go through transformation into five possible configurations as shown in Figure 15. This thesis considers the first four types of realistic radial AC microgrid configurations.

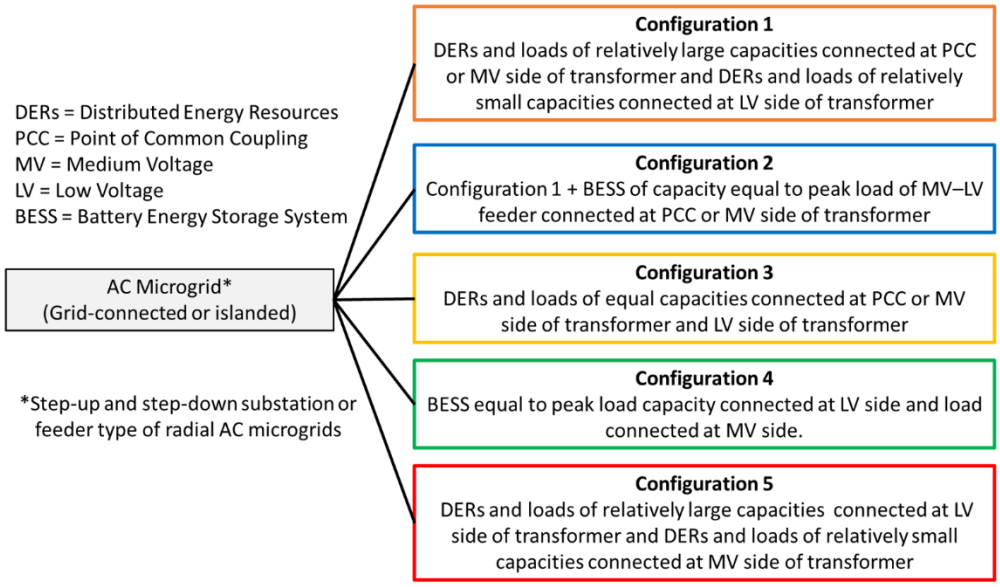

Figure 15. Five configurations of substation type of radial AC microgrids.

The radial AC microgrid configurations mentioned in Figure 15 may have different settings or capabilities for the fault current contribution of DERs. The fault current contribution of converter-based DERs is mainly dependent on the size, capacity or the capability of the converters to handle the short-circuit fault current. A capacity larger than the peak, rated or average load capacity of the converters of DERs means a higher short-circuit fault current contribution capability. The short-circuit fault current contribution is mainly dictated by the grid codes of DERs. The grid codes also demand other capabilities of DERs such as low voltage ride-through (LVRT), high voltage ride-through (HVRT), frequency ride-through, etc. and these requirements are explained separately in the next Chapter 3. Figure 16 outlines the main protection challenges in grid-connected radial AC microgrids.

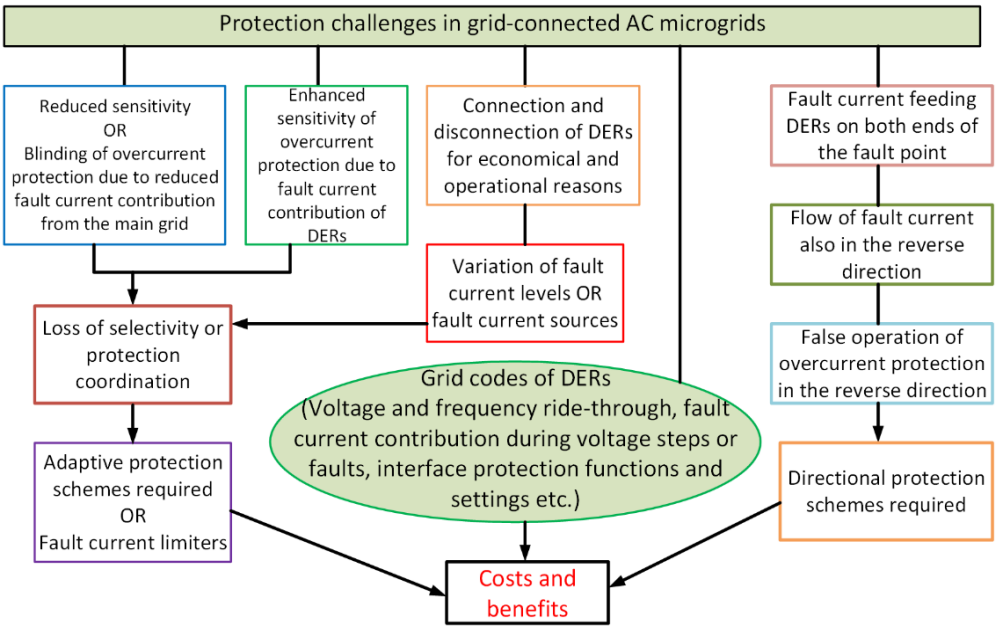

Figure 16. Main protection challenges in grid-connected radial AC microgrids.

2.2.2 Protection challenges during islanded mode

In the islanded mode of AC microgrid operation, the protection challenges mainly depend on the fault current contribution of the local grid-forming and the grid-following DERs. The nature of the protection challenges will also depend on the design or the network configuration of the islanded AC microgrid, and the type of protection device such as definite-time or inverse-time OC relays. The main challenge in the islanded mode will be the reduced fault current sensed by protection devices compared with the grid-connected mode. This means that current magnitude dependent inverse-time OC relays with same grid-connected mode settings will generally operate slower in the islanded mode compared with the grid-connected mode, irrespective of network configuration. Consequently, the protection coordination among protection devices will be either altered or lost during short-circuit faults in the islanded mode. For the network configurations 1 and 2 (shown in Figure 15) the protection challenges will be less compared with configurations 3 and 4 when keeping the same fault current contribution levels or settings of DERs. This is because of the fact that relatively large and therefore strong DERs and BESSs connected at the MV side of the distribution transformer in configurations 1 and 2 will help detect the short-circuit faults at the LV side of the distribution transformer by providing enough of a short-circuit fault current contribution. However, local short-circuit faults at the isolated MV and LV sections of AC microgrid configurations 1 and 2, for example seen in Figure 13 with breakers 2, 6 and 7 open, will still be difficult to detect and isolate.

Due to operational, technical and economic reasons, the connection and disconnection of DERs in the islanded mode will further change the fault current contribution levels. This will require more sensitive adaptive settings of the OC protection devices in the islanded mode due to the lower fault current contribution from the DERs. The only protection devices suitable for providing adaptive protection settings will be OC relays with multiple setting groups. Thus, OC relays will change the active setting group in real time to lower or raise sensitivity values depending on the connection and disconnection status of the DERs. The essential requirement to implement an adaptive protection scheme is to have a reliable communication link to collect the connection or disconnection status of DERs, and then change the appropriate OC relay settings. The adaptive protection can be implemented with centralized communication through MGCC, with decentralized communication through distributed IEDs with enough processing power to save and process the data, or in a hybrid manner using both centralized and decentralized communications. This is further discussed in Section 2.3.

The grid codes of DERs for the islanded mode of operation are still not fully available. AC microgrids with only converter-based grid-forming and grid-following DERs may require some advanced control schemes or additional devices to provide or limit the fault current contribution, depending on the type and setting of OC protection schemes or the type and location of faults. The provision of maximum fault current contribution provided by the grid-forming and grid-following DERs to provide complete protection during balanced and unbalanced faults also depends on the type of protection scheme used. The size of the converters for DERs is usually limited to the rated capacity of DERs with a fault current contribution of only 1–1.2 p.u of the rated full load current. In future, more oversized converters of DERs may be required for the islanded mode due to the majority of converter-based DERs being able to provide a high enough level of fault current for quick fault detection and isolation. These issues are further addressed in Chapter 4. Figure 17 outlines the main protection challenges in islanded radial AC microgrids.

It should be noted that only technical challenges of grid-connected and islanded radial AC microgrids have been addressed in this thesis. The cost–benefit analysis is not considered due to various uncertain factors, for example, variable cost of equipment and different power reliability requirements of loads etc.

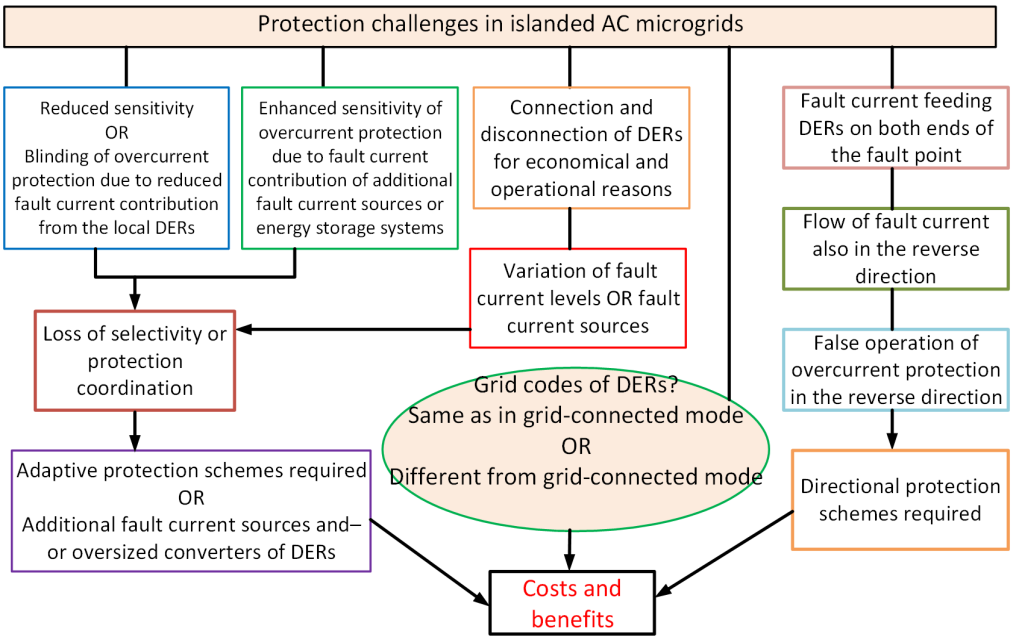

Figure 17. Main protection challenges in islanded radial AC microgrids.

2.3 Protection requirements

Three main requirements of traditional protection schemes include the sensitivity, selectivity or protection coordination, and reliability. A fourth and comparatively new requirement is the adaptivity of protection schemes. The adaptivity requirement will ensure that the first three requirements are met, even after the connection or disconnection of DERs or during different operation modes like grid-connected and islanded modes. It is a well-known fact that the higher the speed of operation of a protection device or scheme, the less damage happens to property and personnel. The speed of fault detection and isolation will be much improved if high-speed circuit breakers and switches are used. Therefore, the selection of the most suitable switching technology is also an important protection requirement. These requirements previously defined in Publication III are discussed in Sections 2.3.1–2.3.5 with some additional information.

2.3.1 Sensitivity

The sensitivity of the protection device or scheme is the capability to sense or respond to the lowest possible operating quantity variation that is somewhat above or below from the point of a set threshold during the fault or operational disturbance. The lower the set threshold, the more sensitive the protection device. Ideally, the more sensitive the protection device, the higher probability of correct

operation. This applies in general to all protection devices including OC, overvoltage (OV), undervoltage (UV), overfrequency (OF), underfrequency (UF), etc. The protection devices are usually set at such thresholds of operating quantities which are to a fair degree beyond the normal operating points on the measurement scale. This will ensure that the protection devices do not operate falsely during normal operations causing unnecessary supply interruptions. For example, the OC protection devices are usually selected for or set at current magnitudes above the maximum possible overload current or inrush current, whichever is larger of the two. A fuse is widely used as the protection device in traditional power systems, particularly at secondary distribution systems due to its simplicity and low cost. However, the use of fuses in modern active distribution systems and microgrids may be limited because their operation is not adaptive according to the dynamically changing configurations of the network. This is also true for other single-setting devices like MCCBs, MCBs, and ACBs.

As mentioned in Sections 2.2.1 and 2.2.2, the connection and disconnection of the DERs as well as the grid-connected and islanded modes of the AC microgrid change the fault current levels and affect the sensitivity of single-setting OC protection devices. This means that OC devices with only one level of sensitivity or set threshold (also called the pickup current) may not operate as required. Therefore, the sensitivity or set threshold has to be changed according to changing operational modes for the correct operation of the OC protection devices. This means that OC relays should be made to be adaptive with multiple setting groups, in order to be useful for AC microgrid protection. For AC microgrids in general, less sensitive OC protection settings are required during the grid-connected mode and more sensitive OC protection settings are required during the islanded mode. This will prevent the false operation of OC relays during the grid-connected mode, and avoid the blinding of OC relays during the islanded mode.

2.3.2 Selectivity or protection coordination

The selectivity or protection coordination among different protection devices distributed across traditional distribution systems ensures that only the faulty section of the system is isolated, and that the power supply of a minimum number of customers is interrupted during the faults. For this purpose, the primary or the local protection device close to the fault location has to operate first after a fault detection within its zone. The backup protection device usually located remotely upstream of the primary protection device operates after a predefined time delay called the coordination time interval (CTI) only if the primary protection device fails to operate.

Although selectivity or protection coordination is possible between fuses with different operating curves, this is usually only required locally at the load ends of distribution feeders. This is also true for MCBs, MCCBs and ACBs. For the long transmission and distribution lines, protection coordination among the various protection relays is usually required. The most commonly used protection relays in distribution systems are the definite-time OC relays and inverse-time OC relays also called inverse definite minimum time (IDMT) OC relays. The definite time-based coordination is used for protection coordination between the definite-time OC relays.

Definite time-based coordination has one drawback that for faults at the source or the substation end of the feeder, the OC relays have longer tripping times. However, definite time-based coordination is simple and independent of the fault current magnitude, and it provides complete protection coordination as long as the OC relay is able to sense or detect the fault. Definite time-based coordination is usually used for three-phase short-circuit faults in radial distribution feeders.

For properly coordinated IDMT OC relays, a CTI of 0.2–0.3 s is maintained throughout the whole operational or fault current range of the relays in order to avoid nuisance tripping. The total operating time of the primary definite-time OC relay (0.2–0.4 s) is dependent on pickup current (I_P), CB opening time (0.04–0.1 s), and security factors (0.12–0.22 s). However, the operating time of the primary or backup IDMT relay is dependent on different families of inverse characteristic curves such as standard inverse, very inverse, and extremely inverse characteristics. The operating time of IDMT relays is mainly defined by the two sets of standard inverse-time relay characteristics, IEC and ANSI (in the U.S.). The inverse-time relay characteristic is defined by equation (1) according to IEC 255–3 (Kannuppaiyan & Chenniappan, 2015):

$$\boldsymbol{t} = \frac{\boldsymbol{k\,a}}{\left(\frac{\boldsymbol{I}}{\boldsymbol{I_P}}\right)^{\boldsymbol{b}} - \boldsymbol{1}} \tag{1}$$

where t denotes the operating time of the relay, k denotes the time dial setting (TDS), I denotes the current sensed by the relay, I_P denotes the pickup current, and the constants a and b define the relay characteristics (types of curves). For a given current, the higher the TDS value, the longer the time to tripping contact closure. On the coordination plots, the up and down adjustment of inverse-time OC relay characteristics is done with TDS, and the left and right adjustment of characteristics is done with the pickup current. Therefore, a proper CTI can be ensured by the proper selection of TDS and I_P values. For the same pickup current value higher than the minimum pickup value and the same time dial setting, the operating time of an extremely inverse IDMT relay is faster than a very inverse

relay, and the operating time of a very inverse relay is faster than the standard inverse. The most common types of IDMT relays use an inverse or very inverse characteristic. Ideally, relays with identical inverse characteristics are used and coordinated throughout the power system (IEEE Std 242, 2001).

The old standard IEC 255–3 entitled *"Electrical relays-Part 3: Single input energizing quantity measuring relays with dependent or independent time"* has been replaced with new standard IEC 60255-151:2009 entitled "*Measuring relays and protection equipment-Part 151: Functional requirements for over/under current protection"*. Table 1 mentions the equation and constants for different IEC and IEEE inverse-time relay characteristic curves according to IEC 60255-151:2009. However, from the context of this thesis, the inverse-time characteristic according to equation (1) is used for evaluation in Publication III.

Table 1. Constants for dependent time operating characteristics according to IEC 60255-151:2009 (Bonetti et al., 2020).

Curve types	**Operating time** $t\,(G) = TMS\left[\frac{k}{\left(\frac{G}{G_S}\right)^{\alpha} - 1} + c\right]$		
	k (s)	**c (s)**	**α**
A (Inverse)	0.14	0	0.02
B (Very inverse)	13.5	0	1
C (Extremely inverse)	80	0	2
D (IEEE Moderately inverse)	0.0515	0.114	0.02
E (IEEE Very inverse)	19.61	0.491	2
F (IEEE Extremely inverse)	28.2	0.1217	2
t (G) = Operating time, TMS = Time Multiplier Setting, k, c, α = constants, G = Measured value of the characteristic quantity, G_S = Setting value of the characteristic quantity.			

Due to inverse time characteristics, IDMT relays have a faster operating time for faults near the source or substation, and a slower operating time for faults away from the substation. However, compared with definite-time OC relays, it is more complicated and time-intensive work to properly coordinate IDMT OC relays depending on the methodology used. Trial and error, curve fitting, and optimization techniques using different algorithms are the most common methodologies used for coordinating IDMT relays (Beheshtaein et al., 2019).

For achieving the required levels of sensitivity, speed and reliability, even multi-stage time-graded OC protection relays using both definite-time and inverse-time characteristics can be used. According to (ABB, 2011a), the grading time or a CTI of at least 150 ms should be used for numerical definite-time OC relays, and 360 ms for numerical IDMT OC relays. The mentioned minimum grading times include

the CB operating time of 50 ms and various other security and safety margin time delays.

In traditional passive distribution systems with power flow in one direction, the coordination of OC relays may work properly if the protection grading is done in the right way. However, after the connection of a considerable amount of DERs and depending on their capacity, type and location, the OC relay coordination may either be changed or completely lost (Doyle, 2002); (Brahma & Girgis, 2004). For AC microgrids with 100% power supply by DERs and majority of the DERs being converter-based, the loss of protection coordination means a reduced security of supply to consumers because it may cause the disconnection of large portions of consumers connected in the AC microgrid. Therefore, AC microgrid protection must be well coordinated in both the grid-connected and islanded modes of operation. The extent to which the protection coordination is disturbed by the connection of a large amount of converter-based DERs is discussed in Publication III with a simulation-based case study.

2.3.3 Reliability

The reliability of the protection scheme is its capability to operate correctly. The reliability is often defined in terms of the *dependability* and *security* of the protection relay operations. The dependability defines that the protection relay will operate and trip for all types of faults it is designed for, with no or minimum level of uncertainty. The security ensures that the protection relay will not operate and trip incorrectly. The protection schemes are usually designed to provide an increased level of dependability with some degree of compromise on security. That is why the probability of false or unwanted operations of protection schemes increases. Large interconnected power systems are usually redundant in providing several alternative paths of power flow, hence the loss of a generator or a line (n-1 criterion) due to an unwanted tripping is more acceptable than a sustained fault causing considerable damage to the faulty component (Gers & Holmes, 2004); (S. H. Horowitz & Phadke, 2008); (Altuve et al., 2016).

The reliability of the protection scheme, particularly in terms of the security, is a very important requirement for active distribution networks with several DERs or microgrids. The false tripping of the protection relay in active distribution networks and microgrids means an increased probability of operational instability. Because the false tripping of a breaker at the PCC of the main grid and microgrid during the grid-connected mode causes an unwanted islanding condition, a sudden disconnection of grid-following converter-based DERs with no grid-forming capability, increased re-synchronization operations for supply

restoration, unwarranted power supply disruptions to consumers, and power quality problems (R. Lasseter et al., 2002); (Chowdhury et al., 2009) are possible. During the islanded mode of operation, the false tripping of the grid-forming DER(s) may cause a complete blackout due to the consequent tripping of other grid-following DERs not equipped with grid-forming controllers.

The reliability of modern multifunctional numerical relays or IEDs using communication links not only depends on the dependability and security of the related hardware and software, but also on the reliability of the communication system. Furthermore, the reliability of hardware is not only dependent on physical failures of components due to manufacturing defects and subsequent exposure to various physical stresses during the operation, but also on the proper functioning of the software that is used. The reliability of the communication system means that the data or information is exchanged with the required speed or within the required time period (dependability issue), and without a compromise, modification or corruption of the data or information exchanged (security issue).

During the initial stages of development and manufacturing, *routine factory production tests* of protection relays are conducted in several stages to find and fix any manufacturing defects. Then, various rigorous *type tests* are performed to determine that the protection relay under test meets the specifications and follows all of the relevant standard requirements. These type tests include various electrical, environmental, as well as functional tests including various tests of software used for the protection relay operations. The *commissioning tests* are conducted during the installation process to check the overall protection configuration after each individual item of the protection scheme is checked. The *periodic maintenance tests* are conducted regularly throughout the operational life cycle of the protection relay to identify component failures and service degradation. All of these measures help in improving the overall reliability of the protection relays, particularly the dependability factor so that the relay is able to perform tripping when required to do so.

The modern microprocessor-based protection relays also include a built-in *self-test* or *self-supervision* feature to check if the critical components or subsystems of protection relays work properly. The self-test can be performed using automatic watchdog, checksum or other software functions for the selected checks and verifications, and diagnostic messages can be made available both locally and remotely. The self-test in general includes tests of the main active components like memory circuits, analog to digital converter, power supply, and microprocessor. Due to the built-in self-test feature in microprocessor-based protection relays, about 90% of all component failures are detected immediately and thus repaired

quickly within 48 hours. This means, with the self-test, the mean time to repair (MTTR) of protection relays is reduced to 2 days instead of 365 days without the self-test. With the reduction of MTTR, the availability of the protection relay is increased. After an abnormal condition is detected by a self-test, the protection relay closes an output contact, sends a message, or provides another indication of the failure (such as an alarm, etc.). After the detection of certain failures by the self-test, corrective measures are initiated like the trip and control functions being disabled by the protection relay. In this way the self-test increases the security of the protection relay by blocking the abnormal or unwanted function. The self-test feature cannot completely replace the periodic maintenance tests; however, it can significantly increase the maintenance test intervals from 1–4 years without self-test to 4–8 years with self-test. In order to maintain high level of reliability and low cost, the self-test should be as simple as possible (Kumm et al., 1994); (ABB, 2009).

According to NERC PRC-005-6 (NERC, n.d.), the periodic maintenance testing interval for unmonitored protection relays is once every six years, while that for fully monitored microprocessor-based protection relays is once every twelve years. The microprocessor-based protection relays are considered to be fully monitored if the monitoring includes:
1) Internal self-diagnosis and alarming.
2) Voltage and current waveform sampling three or more times per power cycle, and a conversion of samples to numeric values for measurement calculations by microprocessor electronics.
3) Alarming for power supply failure.

After meeting the three monitoring requirements listed above, the periodic maintenance testing of microprocessor-based protection relays after twelve years will include three key verifications: the settings as specified, the operation inputs and outputs of the relay that are essential for its proper functioning, and an acceptable measurement of power system input values. If the full monitoring of relays also includes the continuous verification of AC measurements by comparison to an independent AC measurement source with alarming for excessive error, the monitoring of some or all binary or status inputs and control outputs by a process that continuously demonstrates the ability to perform as designed with alarming for failure and alarming for change of settings, then only the unmonitored inputs and outputs of relays essential for its proper functioning are verified (Wester & Smith, 2011); (NERC, n.d.).

The trip coil, close coil, and lockout relay monitoring, the usage of alarm contacts of the IED self-test, the failure detection of instrument transformers based on

analog GOOSE messaging and other comparison methods, the monitoring of station battery, the oscillography cross-triggering, automated testing of input and output contacts, and the relay sequence of the event recorder etc. can increase the periodic testing interval, and increase the reliability of the protection and control system (Wester & Smith, 2011). Different tools can be used for the analysis of the dependability and security of protection schemes. The fault tree analysis (IEC 61025) is one of the useful tools by which to compare the relative reliability of protection schemes. The starting point for a fault tree construction is to identify which component failures may cause a dependability problem (e.g., a tripping failure) or a security problem (e.g., an unwanted tripping). The combinations of failure rates can be represented using AND, OR, or other logic gates. The usage of an OR gate means that any of several failures can cause the protection scheme failure. The usage of an AND gate means that all components fail simultaneously to cause a protection scheme failure. The dependability and security analyses of various combinations of protection schemes using fiber-optic channels have been conducted using the fault tree analysis in (Altuve et al., 2016). The fault tree analysis will also be a useful tool for the reliability assessment of protection schemes in microgrids.

The latest trends of using the digital twin (a virtual replica of the physical system) for predictive maintenance using the big data from field sensors, artificial intelligence (AI) and machine learning based feature extraction algorithms for condition monitoring and information update using real-time communication will considerably help to improve the reliability of the protection and control systems. However, this is still an emerging area of research with many challenges to overcome including standardization, improved and accurate digital modelling for multi-component and multi-level complex systems, etc. (Tao et al., 2019); (Luo et al., 2020); (You et al., 2022). The redundancy of protection relays and communication by using duplication, triplication, etc. will also help in elevating the reliability of protection schemes, but with extra cost (Ward et al., 2010). Figure 18 represents the present and future approaches of the reliability of protection relays and lists the testing methods which contribute to the improvement of protection reliability. In general, a more balanced approach between dependability and security will be required in future for maintaining an acceptable level of the reliability of protection relays. From the context of this thesis, the reliability of IEC 61850 GOOSE message is tested using Ethernet-based real-time simulations, and a method of Boolean signal continuity check is suggested to avoid false tripping of the protection relay as reported in Publication IV.

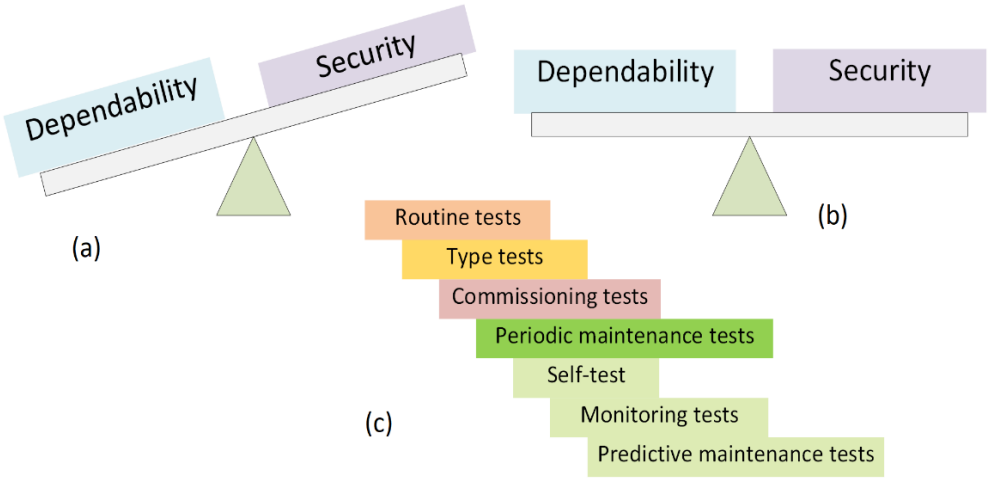

Figure 18. Reliability of protection relays (a) present approach (b) future approach (c) testing methods to improve reliability.

2.3.4 Adaptivity

Adaptivity (in the context of this thesis) is the ability of the protection scheme to change its settings according to changing operational modes such as grid-connected to an islanded mode and vice versa, or due to the connection and disconnection of DERs. An adaptive protection scheme usually makes online changes of protection settings to obtain a preferred response in accordance with the changing states or requirements of the system. The adaptive protection schemes are usually automated; however, the inclusion of some necessary human interventions is also possible. An adaptive protection scheme requires protection devices or relays with different groups of settings, characteristics or logics that can quickly be modified online using external control signals or commands. The modern numerical or microprocessor-based relays, also called IEDs, offer a variety of protection functions (overcurrent, overvoltage and undervoltage, etc.) with multiple setting groups for each protection function. The setting groups of IEDs can be changed adaptively using IED-to-IED, MGCC-to-IED and CB-to-IED communication links (Rockefeller et al., 1988).

As mentioned in Section 2.2, the connection and disconnection of DERs and operational mode changes from grid-connected to islanded mode and vice versa cause variations in the magnitudes of fault current sensed by OC relays. This may cause either a slow- or no-fault detection and isolation by OC relays due to the reduced magnitude of fault current, or result in unwanted tripping by OC relays due to an increased magnitude of fault current. The first situation of reduced fault current may affect the operation of both definite-time and inverse-time OC relays. The second situation of increased fault current will most likely affect the operation

of only the inverse-time OC relays due to their dependence on fault current magnitude. This is why adaptive relays are necessarily required for active distribution networks and AC microgrids to be equally protected in both the grid-connected and islanded modes of operation. Adaptive lower settings or reduced pickup current values will be required during the islanded mode due to the reduced fault current contribution from the converter-based DERs. Adaptive higher settings or increased pickup values will be required during the grid-connected mode due to the increased fault current contribution from the main grid. Moreover, after the connection or disconnection of one or more DERs in grid-connected or islanded mode, new revised settings may be required, particularly if inverse-time OC relays are used for AC microgrid protection.

The open or close status signals from CBs, particularly the CB at the PCC, determine the microgrid operational mode. If the CB at the PCC is closed, it indicates the grid-connected mode, and if the CB at the PCC is open then it indicates an islanded mode. The protection relays in an AC microgrid need to adapt their active setting groups based on the microgrid mode of operation. Adaptive protection can be either communication-based or communication-less adaptive protection. Although communication-based adaptive protection provides quick and dynamic service, it suffers from nondeterministic delays in the transmission, reception and processing of data, in addition to communication link failures. Therefore, communication-less adaptive protection will also be required to serve in those conditions.

The communication-based adaptive protection can be implemented using either centralized or autonomous–decentralized communication, although a combination of centralized and decentralized communications can also be used. Figure 19 shows the centralized communication-based adaptive protection that uses an MGCC to change the active setting group 1 or 2 of all IEDs based on the closed or open status of CB0 and–or CB1. During the grid-connected mode, after the occurrence of an LLL short-circuit fault between CB0 and CB1, the IED0 will detect the fault using the active setting group 1, open CB0, and transfer trip CB1. The MGCC will collect the open status of CB0 and CB1 and send a command to all IEDs in the islanded microgrid (IED2–IED6) to change settings to active setting group 2 (red). After the removal of the fault, the MGCC will close CB0 and CB1 after a synchronization check to operate in the grid-connected mode. The MGCC will collect the closed status of CB0 and CB1 and send commands to all IEDs (IED2–IED6) to change settings to active setting group 1 (green). The MGCC may also decide on other setting groups based on the status of DERs.

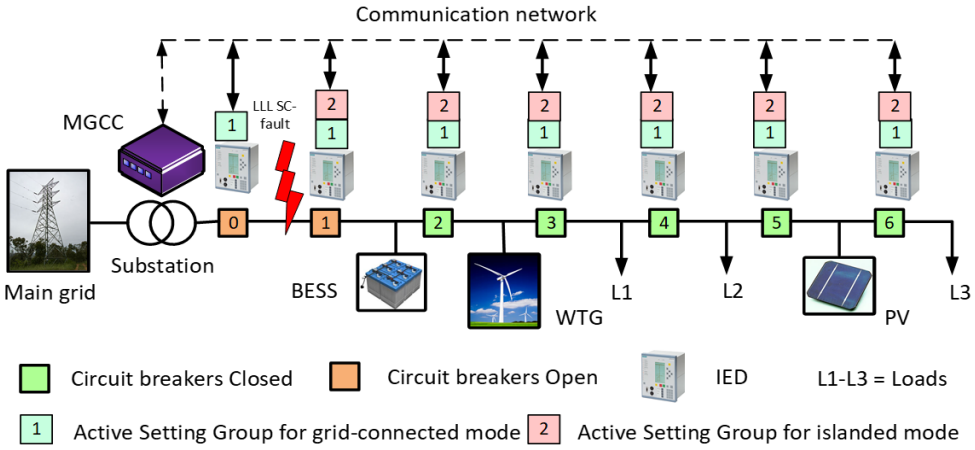

Figure 19. Centralized communication-based adaptive protection.

Figure 20 shows the decentralized communication-based adaptive protection, where each IED autonomously monitors the status of CBs after communication with the other IEDs and then decides to change its active setting group 1 or 2. Actually, each IED continuously monitors the status of its own CB and then sends this information to other IEDs via the communication network. During the grid-connected mode, after the occurrence of an LLL short-circuit fault between CB0 and CB1, the IED0 will detect the fault with active setting group 1, open CB0 and transfer trip CB1. The IED1 will send the open status of CB1 to all IEDs in the islanded microgrid (IED2–IED6). After receiving the open status of CB1, each IED will change its settings to active setting group 2 (red). After the removal of the fault, IED0 will close CB0 and CB1 after a synchronization check to operate in the grid-connected mode. The IED0 and IED1 will send the closed status of CB0 and CB1 to all IEDs (IED2–IED6). After receiving the closed status of CB0 and CB1, each IED will change its settings to active setting group 1 (green). Each IED may also decide other setting groups based on the status of DERs.

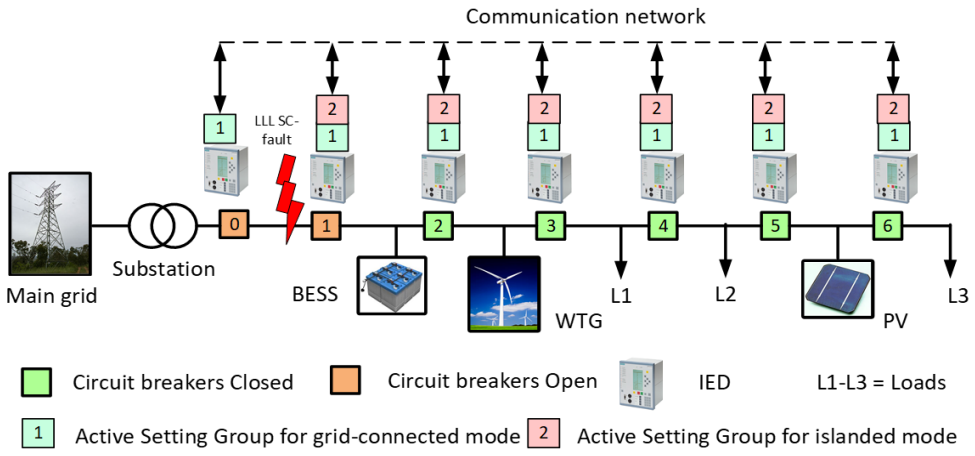

Figure 20. Decentralized communication-based adaptive protection.

Both the centralized and the decentralized communication-based adaptive protection schemes have their own advantages and disadvantages. The centralized controller (MGCC) has the advantage that it decreases the burden of computing on individual IEDs, and hence, simple control and protection IEDs can be used. However, a very powerful centralized controller or IED acting as a centralized controller is required for saving, processing and communicating data with other components or systems. Additionally, the redundancy of a centralized controller is also required because the failure of a centralized controller means the failure of the entire control and protection scheme. Centralized communication-based adaptive protection is the conventional and most widely used approach supported by different communication protocols including IEC 60870-5-101/104, Modbus, DNP3, and IEC 61850 and it can be implemented using serial bus communication, power-line carrier (PLC), or an Ethernet network (Dimeas et al., 2013).

The decentralized communication-based adaptive protection decreases the burden on a centralized controller, but requires very powerful individual IEDs with increased storage, computing and processing capabilities. Fast and reliable communication links between IEDs are also required for the decentralized communication-based adaptive protection scheme. The decentralized communication-based adaptive protection is a new method which relies on direct communication between the IEDs or multi-agents, and is currently supported by the IEC 61850 communication protocol. The decentralized communication-based adaptive protection requires an Ethernet network for implementation, however, PLC and 4G or 5G wireless communications can also be used (Dimeas et al., 2013).

Some of the proposed centralized communication-based adaptive protection schemes can be found in (Oudalov & Fidigatti, 2009), (Ustun et al., 2012), (Zamani et al., 2012), (Laaksonen et al., 2014), and (Coffele et al., 2015). The decentralized or localized communication-based adaptive protection scheme can be found in (Che et al., 2014). The simulation-based case studies of centralized and decentralized communication-based adaptive protection schemes for radial AC microgrids are discussed in more detail in Publication II and Publication IV.

2.3.5 Switching technology

The selection of the switching device for an AC microgrid depends on the required speed of operation, the voltage level, and the magnitude of fault current. The required speed of operation for a protection scheme depends on the sensitivity of the connected load. Loads sensitive to power quality problems during faults include variable frequency motor drives, computers, electronics, and communication devices in data centers etc. Additionally, the DERs in AC

microgrids specifically synchronous generators may be sensitive to voltage dips during faults, and may cause loss of stability problems. Therefore, an overall reduction in the operational time delay of the protection scheme is required. This means that the higher the speed of the switching device, the shorter the overall time delay of protection schemes and the more stable the operation of the AC microgrid (R. Lasseter et al., 2002); (Chowdhury et al., 2009); (Laaksonen et al., 2011).

Presently, the technology of AC circuit breakers and switches has reached quite an advanced stage of development and various types of CBs and switches are available. These switches include the single protection devices with combined functions of relays and CBs, like MCBs, MCCBs, and ACBs for LV applications up to 600 V. The mechanical CBs that use a vacuum or SF6 gas as an arc-extinguishing medium are available for MV applications. The mechanical CBs use spring, pneumatic, hydraulic, and electromagnetic mechanisms for electrode separation. The majority of MV mechanical CBs have an operational time delay of 3–5 cycles of AC supply voltage after the reception of a tripping command from the relays. A new prototype of MV mechanical CB, using a Thomson coil and permanent magnet actuators, has also been developed to decrease the operational time delay to one cycle of AC supply voltage, but it is rather an expensive solution. Another developed prototype, with a Thomson coil actuator and spring mechanism has the normal tripping time delay of 13.5–15 ms (Jeong et al., 2013).

The advancement of power electronic switches has paved the way for the development of AC solid-state circuit breakers (AC-SSCBs) with a faster tripping response (half-cycle or less) than high-speed mechanical CBs. The other advantages of AC-SSCBs include silent operation, longer life, and no mechanical wear and tear. There are two main types of AC-SSCBs: noncurrent-limiting and current-limiting (Krstic et al., 2007). Figure 21 shows the single-phase units of noncurrent-limiting and current limiting AC-SSCBs.

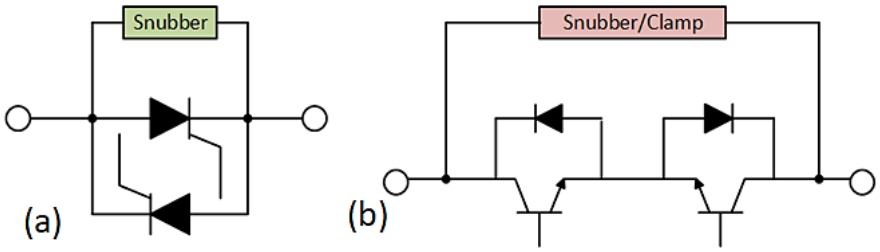

Figure 21. AC-SSCBs: (a) noncurrent-limiting (b) current-limiting (Krstic et al., 2007).

The noncurrent-limiting AC-SSCBs require inverse-parallel silicon-controlled rectifiers (SCRs) or thyristors, and can be used and coordinated with traditional

OC protection relays, CBs and fuses. However, the SCRs require fuse protection during worst-case asymmetrical fault currents of 200kA peak or higher (Krstic et al., 2007). A new improved design of noncurrent-limiting AC-SSCB (46 kW, 380 V) has been proposed by (Song et al., 2018) that offers the reclosing and rebreaking operational features using some additional switching devices.

The current-limiting AC-SSCBs require faster power electronic switches like IGBTs or integrated gate-commutated thyristors (IGCTs). The current-limiting AC-SSCBs generate higher power losses than noncurrent-limiting AC-SSCBs and face many design challenges. The selection of suitable snubbers, metal-oxide varistors (MOVs), and dynamic braking resistors for energy dissipation, voltage control during interruption, and the accurate differentiation between the fault current and load transients to avoid false tripping are the main challenges of current-limiting AC-SSCBs. Additionally, current-limiting AC-SSCBs are not suitable for the protection coordination with traditional OC relays, CBs and fuses. Hence, the complete design of the protection scheme of active distribution grids and microgrids has to be exclusively based on the current-limiting AC-SSCBs (Krstic et al., 2007).

The technical and economic aspects of different topologies of AC-SSCBs for MV applications have been compared in (Meyer et al., 2003), and it is concluded that the economic aspects like the reliability and operational costs are the decisive factors in the choice of topology of AC-SSCBs. The development of new silicon carbide (SiC) based power electronics switches has further improved the performance of SSCBs, and bidirectional SSCBs have also been developed (Urciuoli et al., 2011).

2.4 Protection solutions in literature

Section 2.4 is based on the literature review done in Publication I and Publication III of this thesis, with appropriate updates from the latest literature. In Publication I, the protection solutions or schemes for AC microgrids have been divided into three main categories: protection schemes for only the grid-connected mode, protection schemes for only the islanded mode, and protection schemes for both the grid-connected and islanded modes. Similarly, these schemes are briefly discussed in Sections 2.4.1–2.4.3. Section 2.4.4 presents other advanced solutions.

2.4.1 Protection schemes for only grid-connected mode

The solutions in Section 2.4.1 include the earlier proposed solutions to reduce the impact of DER connections on the performance of inverse-time OC relays in the grid-connected mode of microgrids and distribution networks. Table 2 lists the proposed schemes for the grid-connected mode with the prominent advantages and limitations or challenges for the implementation of each scheme. Further details can be found in Publication I and Publication III.

Table 2. Protection schemes for only grid-connected mode.

Proposed Scheme	Advantages	Limitations or Challenges
Time-dependent OC (Jager et al., 2004)	Reduced fault clearing time and increased DER connections.	Only for radial networks with synchronous DERs and looped networks with converter-based DERs. Increased number of relays required. Does not consider high impedance faults (HIF).
Adaptive OC pickup (Baran & El-Markabi, 2004)	Improves inverse-time OC relay sensitivity, reach or tripping time response with dynamic configurations of the radial network.	Better performance when some DERs are disconnected. Uses offline power flow method but requires communication to implement.
Definite-time grading of OC relays (Jenkins et al., 2005)	Does not use communication. Economical because existing relays can be used.	Only for LV microgrids with both synchronous and converter-based DERs.
Intelligent agents (Y. T. Jin et al., 2011)	Improves speed of backup relays. Autonomous monitoring and adjustment of parameters.	Only for radial networks without DERs or looped networks with DERs. Requires high-speed communication.
Fault current limiters in series with DERs (El-Khattam & Sidhu, 2008); (El-khattam & Sidhu, 2009); (Khederzadeh, 2009)	No disconnection of DERs. Use of same relay settings. No equipment upgrading.	Increased impedance of FCL with increased capacity of individual DER, hence costly. Transient response of FCL.

2.4.2 Protection schemes for only islanded mode

The protection solutions in Section 2.4.2 include the earlier proposed solutions to protect the AC microgrid during the islanded mode of operation. Table 3 lists the proposed schemes for the islanded mode with the prominent advantages and limitations or challenges for the implementation of each scheme. Further details can be found in Publication I and Publication III.

Table 3. Protection schemes for only islanded mode.

Proposed scheme	Advantages	Limitations or challenges
Adaptive directional OC (Voima et al., 2011)	Adaptive according to the operational mode of the microgrid and status of DERs. Can be used for radial as well as looped networks. Highly selective and speedy due to directional fault detection and communication.	Requires higher number IEDs, each one for a different zone. Requires high-speed communication (IEC 61850) for change of settings, locking/interlocking, transfer trip, and CB status signals including prior knowledge of all possible configurations. Measurement of both voltage and current, therefore CTs as well as VTs are required.
Voltage based (Al-Nasseri et al., 2006)	Useful for close-in short-circuit faults near DERs. Can be used for any type of network topology and DER type. Only voltage measurement, hence an economical choice.	Requires higher number voltage sensors and relays, each for a different zone or DER. Requires communication between relays for selectivity or discrimination of in-zone and out-zone faults. HIF and single-pole tripping not considered.
Harmonics content based (Al-Nasseri & Redfern, 2008)	Simple to implement because only the measurement of converter voltage is required to calculate the total harmonic distortion (THD) and frequency.	Hard to set threshold values of THD during different types of faults. Fault impedance variation causes sensitivity problems. Not suitable for synchronous DERs and dynamic loads. False tripping of DERs if a large non-linear load is switched on.
Symmetrical components and residual current (Nikkhajoei & Lasseter, 2007)	No use of communication. Good protection from line-to-ground (LG) faults by residual and zero-sequence currents. Good protection from LL faults by negative-sequence current.	Does not consider single-pole tripping, three-phase faults and HIF. Requires I^2t protection as the first backup and undervoltage as the second backup. False tripping of residual current protection during unbalanced load.

2.4.3 Protection schemes for both grid-connected and islanded modes

The protection solutions in Section 2.4.3 include the earlier proposed solutions to protect the AC microgrid during both the grid-connected and islanded modes of operation. Of course, these schemes can use a combination of the protection schemes mentioned in the previous two Sections (2.4.1 and 2.4.2) with some working only during the grid-connected mode and some working only during the islanded mode, but also other schemes using new principles of operation like differential, distance, inverse-time admittance, travelling waves and pattern recognition schemes, etc. Table 4 lists the proposed schemes for both the grid-connected and islanded modes with the prominent advantages and limitations or challenges for the implementation of each scheme. Further details can be found in Publication I and Publication III.

Table 4. Protection schemes for grid-connected and islanded modes.

Proposed scheme	Advantages	Limitations or Challenges
Adaptive directional OC (Oudalov & Fidigatti, 2009)	See Table 3	Centralized control requires redundancy, hence costly. Moreover, HIF not considered.
Multiagent protection (Perera & Rajapakse, 2006)	No centralized controller and VTs. No time synchronized measurements. Effective for all types of faults including HIF.	Requires differentiation between the switching transients and faults to avoid false tripping. Requires high-speed communication.
Differential protection (Conti et al., 2009)**;** (Sortomme et al., 2010)**;** (M. Dewadasa et al., 2011)	High-speed response to in-zone faults. Economical if OC relays and existing communication is used.	Ineffective when loads are unbalanced. No selective coordination of relays. LG fault at upstream zone remains energized by DERs at downstream zone in islanded mode due to no significant differential current when CB is not used between zones. Transfer trip is required.
Distance protection (J. M. Dewadasa et al., 2008)	Highly selective. Effective for three-phase and two-phase short-circuit faults.	False tripping during all types of ground faults if star-connected load at downstream of fault point. Requires some directional feature. Affected by an intermediate DER infeed. Needs communication link.
Inverse-time admittance (M. Dewadasa et al., 2009)	Highly selective. No use of communication link. Effective for all types of short-circuit faults.	Slow response for HIF and higher DER infeed. Measurement errors due to harmonics, transients and decaying DC component. Requires some directional feature.
Pattern recognition (Samantaray et al., 2012)**;** (Kar & Samantaray, 2014)	More robust than differential scheme. Effective for all types of faults, DERs and network configurations. Immune to noise and less sensitive to synchronization errors.	Requires more data for decision. Only for wide-area protection.
Current travelling waves (Shi et al., 2010)**;** (X. Li et al., 2012)**;** (Velaga et al., 2021)	Use or no use of communication link. Not affected by power swings, fault current, load unbalance, CT saturation, line compensation & mode of operation.	Affected by frequent taps, high attenuation, presence of transformers and capacitors. Requires wide-band CTs and VTs.

2.4.4 Other advanced protection solutions

In the new research literature, there is an increasing trend of using different optimization techniques mainly for the improvement of selectivity among inverse-time OC relays in active distribution networks and microgrids. Artificial

intelligence (AI) techniques are also frequently used for the solution of problems in different areas of modern power systems with DERs such as adaptive control and protection applications. The latest advancements in wireless telecommunication technology such as the fifth-generation or 5G broadband cellular networks (Gore & Valsan, 2018); (Erunkulu et al., 2021) and cheap, high-speed and low-latency internet connectivity via the low earth orbit (LEO) satellite constellations (Qu et al., 2017); (Leyva-Mayorga et al., 2020); (Daehnick et al., 2020); (S. Liu et al., 2021) are paving the way for a practical implementation of wide-area measurement-based control and protection solutions. However, these technologies are still in their earlier stages of development and applications. Global navigation satellite systems (GNSS) including the U.S.-based Global Positioning System (GPS), the EU's Galileo, China's BEIDOU, Japan's QZSS (Quasi-Zenith Satellite System), and Russia's GLONASS geostationary earth orbit (GEO) systems can be used alternatively for time synchronization in wide-area measurement systems (WAMS). The GPS has been the most popular and accurate system among them for WAMS applications. The EU's Galileo system is compatible with GPS, GLONASS and other mobile telecommunication systems like 3G, 4G and 5G, etc. These advanced solutions are briefly reviewed next in Section 2.4.4 from the viewpoint of AC microgrid protection.

Optimization techniques for selectivity

A comparative study of the directional OC relay coordination algorithms including differential evolution algorithm, genetic algorithm, particle swarm optimization, harmonic search, and seeker optimization algorithm is reported in (Alam et al., 2015). The performance of differential evolution algorithm has been found to be superior compared with other optimization algorithms. The differential evolution algorithm has also been proposed in (Shih et al., 2017) for the improved coordination and sensitivity of directional OC relays. The particle swarm optimization and nonlinear interior point trust region algorithms are used in (Papaspiliotopoulos et al., 2015) to optimize the coordination OC relays for distribution networks with DERs. The ant colony optimization algorithm for the OC relay coordination is suggested in (Shih et al., 2015) as a better choice than the genetic algorithm. The differential search algorithm is used in (Singh et al., 2016) for the offline optimization of OC and distance relays settings. The linear programming and optimization based coordination of inverse-time directional OC relays is suggested in (Lin et al., 2016) for the grid-connected and islanded modes of radial and looped microgrids.

A modified particle swarm optimization is suggested in (Atteya et al., 2017) to solve the OC relay coordination problem in distribution networks with DERs. The mixed

integer nonlinear programming based optimal coordination of inverse-time OC relays is suggested in (Javadi et al., 2018). A particle swarm optimization and integer linear programming based hybrid algorithm has been recently proposed in (Samadi & Chabanloo, 2020) for the proper coordination of OC relays in active distribution networks. A new method for the gradual improvement of protection coordination of inverse-time OC relays has been proposed in (Ghadiri & Mazlumi, 2020) that uses the Kohonen map or self-organizing map clustering algorithm. The proposed method is applicable for distribution networks with changing loads and varying unit commitments of converter-based DERs.

Artificial Intelligence based solutions

An artificial neural network (ANN) implementation at the data concentrator for fault detection and location is proposed in (Lin et al., 2016). An adaptive fuzzy algorithm has been proposed for online adaptive protection in (El Naily et al., 2017) that updates and optimizes the protection coordination according to changing network topology. The proposed algorithm is dependent on CB status and pre-fault power flow. A hybrid method using an adaptive fuzzy inference module and genetic algorithm is proposed in (Kumar & Srinivasan, 2018) for optimal protection settings and minimizing the operating time of directional OC relays during different operational modes of DERs. The fuzzy logic has been used for adaptive protection in (Momesso et al., 2019) for the adjustment of the pickup current of OC relays in distribution systems with DERs. A real-time fuzzy system has been proposed in (Momesso et al., 2020) for the decentralized directional adaptive protection scheme of a transmission system. The dynamically adaptive fuzzy system decreases the operating time of the relays using the adaptive pickup current, while maintaining the stability and coordination during the dynamic conditions of the system.

An interval type-2 fuzzy logic with two different fuzzy systems is proposed in (Bukhari et al., 2018) for the detection, classification and location of faults in microgrids. The fuzzy system uses the phase angle between superimposed modal voltage and modal current as an input for the identification of fault direction. The Hilbert-Huang transform for feature extraction and machine learning models for classification of the fault events are suggested for microgrid protection in (Mishra & Rout, 2018). The used machine learning models include Naive Bayes classifier, the support vector machine, and the extreme learning machine. The windowed fast Fourier and wavelet transforms for feature extraction, correlation analysis for feature selection, and bagged decision trees for fault detection are suggested for microgrid protection in (Netsanet et al., 2018). The data mining-based machine learning method is proposed for the adaptive protection of MV microgrids in (Lin

et al., 2019). The proposed method uses the ANN for the detection and support vector machine (SVM) for the location of the fault. The mathematical morphology based feature extraction and extreme machine learning based classifiers are suggested for differential protection in (Mishra et al., 2019). The intelligent microgrid protection scheme proposed in (Yu et al., 2019) uses the discrete wavelet transform for feature extraction, and deep neural networks for fault classification, detection and location.

Wide-area measurement-based solutions

Phase comparison differential protection based on time synchronized WAMS is proposed in (F. Zhang & Mu, 2015) for active distribution networks with a high amount of DERs. The wide area monitoring system has been suggested in (Phadke et al., 2016) to improve the performance of backup relays. The monitoring system of distribution systems using the micro phasor measurement unit (micro-PMU) for fast and accurate synchronized phasor measurements, and parallel computation for screening, gathering and processing of big data for state estimation is suggested in (Sun et al., 2017). The application of micro-PMUs for online adaptive coordination of OC relays in microgrids is suggested in (Ghalei Monfared Zanjani et al., 2018). The scheme proposes the installations of micro-PMUs at the PCC and various locations inside the microgrid for the detection of uncertainties due to line and DER outages. An online smart adaptive protection scheme using the micro-PMUs, MGCC and a highly reliable communication system between them is suggested in (Elbana et al., 2019) for fault detection and isolation in microgrids. A special protection scheme based on a voltage stability index calculated through the synchronized measurements of micro-PMUs is suggested for distribution networks in (Kumar et al., 2020).

A centralized wide-area monitoring system based on PMUs and distance relays for fault detection and protection of single and parallel double-circuit transmission lines is proposed in (Eissa, 2018a). The performance of the protection scheme is enhanced by three-dimensional (3D)-Phase Surface. The wide-area protection-based distance relay for transmission systems is also suggested in (Maneekorn et al., 2020). An integrated impedance angle based protection scheme for microgrid using wide-area positive sequence components of voltages and currents collected from PMUs is suggested in (Sharma & Samantaray, 2020). An extensive review of the challenges of wide-area protection due to RES integration into the smart grid presented in (Eissa, 2018b) is suggested for further insightful information.

Figure 22 presents a summary of the advanced protection solutions and related applications based on the current updated literature review. These solutions will be more relevant and applicable for future distribution systems with multi-

microgrids and a large number of IEDs that will not be easily set, planned and managed using conventional methods. It should be noted that Section 2.4.4 was included at the final stage of thesis to present the latest research trends of AC microgrid protection. Therefore, it is less relevant to the solutions proposed in this thesis.

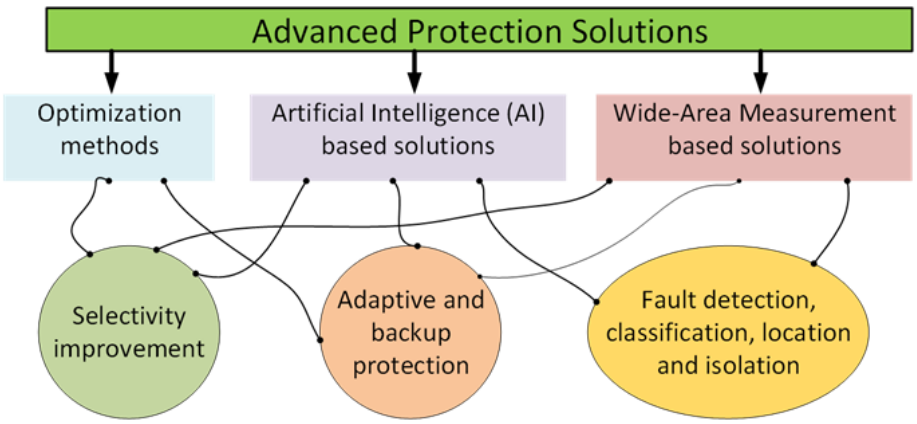

Figure 22. A summary of advanced protection solutions with applications.

2.5 Research gaps

Based on the literature review presented in Section 2.4, various research gaps have been found as summarized in the six broad categories shown in Figure 23.

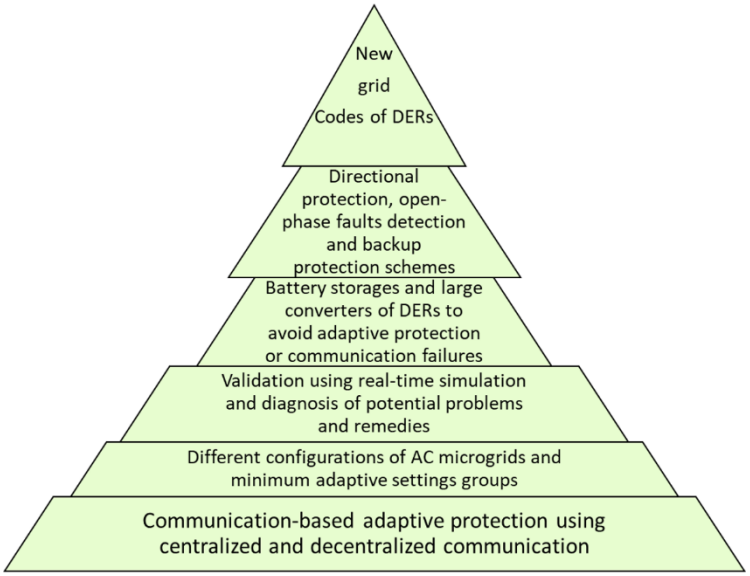

Figure 23. Research gaps in AC microgrid protection solutions.

The decentralized adaptive protection scheme along with the traditional centralized adaptive protection scheme using only two setting groups is considered

and validated using the real-time HIL simulation in this thesis. The increasing use of BESS along with DERs and the potential large sizes of converters for DERs to avoid adaptive protection scheme and communication failures are also investigated. In addition, new directional protection, open phase faults detection and coordinated backup protection schemes for AC microgrids with converter-based DERs are suggested. More importantly, the present grid codes of converter-based DERs are evaluated and new grid codes are suggested for the protection of AC microgrids.

3 GRID CODES, COMMUNICATION AND TESTING METHODS

Literature review presented in the previous Chapter 2 indicates that a majority of proposed protection solutions for AC microgrids lack proper standards and grid codes for practical implementation. Additionally, a proper validation testing of proposed protection solutions is also missing. In this regard, IEC/EN and IEEE standards and grid codes for AC microgrids and power system protection are briefly introduced in this chapter. Among these, the most related standards and grid codes including IEC 61850, EN 50549-1. EN 50549-2 and IEEE 1547-2018 are summarized. The real-time testing methods used for validation of proposed protection solutions of AC microgrids are described in Section 3.5.

3.1 IEC standards for AC microgrids

The IEC technical committee TC 8, administered by the IEC National Committee of Italy, is mainly responsible for the development of IEC standards for the *System aspects of electrical energy supply*. The basic standards developed by IEC TC 8 are generally related to the grid-connected mode of AC microgrids. IEC TC 8 is subdivided into three subcommittees SC 8A, SC 8B, and SC 8C, all three SCs being administered by the IEC National Committee of China. Additionally, the IEC TC 8 is comprised of one Working Group (WG 11), two Maintenance Teams (MT 1 and MT 8), five Joint Working Groups (JWG 1, JWG 9, JWG 10, JWG 12 and JWG 44), and two Advisory Groups (AG 1 and AG 13). Table 5 lists the currently active IEC standards, technical reports (TR) and technical specifications (TS) for system aspects of grid-connected AC microgrids developed by IEC TC 8.

Table 5. IEC standards for AC microgrids developed by TC 8.

IEC standards for the system aspects of electrical energy supply	
Standard	**Description**
IEC 60038:2009+AMD1:2021 CSV	IEC standard voltages
IEC 60059:1999+AMD1:2009 CSV	IEC standard current ratings
IEC 60196:2009	IEC standard frequencies
IEC TR 62511:2014	Guidelines for the design of interconnected power systems
IEC TS 62786:2017	Distributed energy resources connection with the grid
IEC 62559-2:2015	Use case methodology–Part 2: Definition of the templates for use cases, actor list and requirements list
IEC TS 63060:2019	Electric energy supply networks – General aspects and methods for the maintenance of installations and equipment
IEC TS 62749:2020 RLV	Assessment of power quality – Characteristics of electricity supplied by public networks
IEC TS 63222-1:2021	Power quality management–Part 1: General guidelines
AMD1 = Amendment 1, CSV = Consolidated version, TR = Technical Report, TS = Technical Specification, RLV = Redline version.	

The IEC SC 8A develops IEC standards related to the *Grid Integration of Renewable Energy Generation*. The main areas of focus of IEC SC 8A are the main grid level requirements of interconnection for renewable energy sources, the impact of a high amount of variable DERs on the main grid, grid code compliance tests, and best practices for the main grid level planning, modeling, forecasting, control, protection, scheduling and dispatching of renewable generators. The IEC SC 8A also coordinates with IEC TC 8 and IEC SC 8B on issues related to DER interconnection with the main grid, as well as the design and operation of microgrids.

The IEC SC 8B develops IEC standards related to *Decentralized electrical energy systems* including but not limited to AC, DC, AC-DC hybrid microgrids, DGs, distributed ESS, virtual power plants (VPPs), and other DERs. The IEC SC 8B also coordinates with IEC TC 8, IEC SC 8A and IEC SC 8C on the issues related to the interaction of renewable generators, VPPs and microgrids with the interconnected main grid. Table 6 lists the currently active IEC standards, TR and TS for AC microgrids developed by IEC SC 8A and IEC SC 8B.

The IEC SC 8C develops IEC standards related to *Network Management in Interconnected Electric Power Systems* including their design, planning, operation, control, and market integration. The IEC SC 8C focuses on issues related to the resilience, reliability, security, and stability of the interconnected electric power systems. The IEC SC 8C also coordinates with IEC TC 8, IEC SC 8A and IEC SC 8B on issues related to the connection and impact of renewable generators and microgrids to the interconnected main grid. Currently, IEC SC 8C does not have any published documents (standards, TR and TS).

Table 6. IEC standards for AC microgrids developed by SC 8A and SC 8B.

IEC standards for the grid integration of renewable energy generation (SC 8A)	
Standard	**Description**
IEC TR 63043:2020	Renewable energy power forecasting technology
IEC 62934:2021	Grid integration of renewable energy generation – Terms and definitions
IEC TS 63102:2021	Grid code compliance assessment methods for grid connection of wind and PV power plants
IEC TR 63401-2:2022	Dynamic characteristics of inverter-based resources in bulk power systems – Part 2: Sub- and Super-synchronous control Interactions
IEC TR 63401-4:2022	Dynamic characteristics of inverter-based resources in bulk power systems – Part 4: Behavior of inverter-based resources in response to bulk grid faults
IEC standards for the decentralized electrical energy systems (SC 8B)	
Standard	**Description**
IEC TS 62898-1:2017	Microgrids – Part 1: Guidelines for microgrid projects planning and specification
IEC TS 62898-2:2018	Microgrids – Part 2: Guidelines for operation
IEC TS 62898-3-1:2020	Microgrids – Part 3-1: Technical requirements–Protection and dynamic control

3.2 IEEE standards for AC microgrids

The selected active IEEE standards related to AC microgrids are listed in Table 7. The IEEE standards listed in Table 7 include the most relevant general IEEE standards for AC microgrids of series 1547 and 2030. Table 8 contains IEEE standards of series 2030, 1588 and C37 related to AC microgrid protection. The *Power System Relaying and Control Committee* develops the IEEE standards of series C37, and the complete list of power system protection standards can be found at (IEEE Standards Association, n.d.).

Table 7. The active IEEE Standards for AC microgrids.

Standard	Description
1547-2018	IEEE Standard for Interconnection and Interoperability of Distributed Energy Resources with Associated Electric Power Systems Interfaces.
1547.1-2020	IEEE Standard Conformance Test Procedures for Equipment Interconnecting Distributed Energy Resources with Electric Power Systems and Associated Interfaces.
1547.7-2013	IEEE Guide for Conducting Distribution Impact Studies for Distributed Resource Interconnection.
2030.2-2015	IEEE Guide for the Interoperability of Energy Storage Systems Integrated with the Electric Power Infrastructure.
2030.2.1-2019	IEEE Guide for Design, Operation, and Maintenance of Battery Energy Storage Systems, both Stationary and Mobile, and Applications Integrated with Electric Power Systems.
2030.3-2016	IEEE Standard Test Procedures for Electric Energy Storage Equipment and Systems for Electric Power Systems Applications.
2030.5-2018	IEEE Standard for Smart Energy Profile Application Protocol.
2030.6-2016	IEEE Guide for the Benefit Evaluation of Electric Power Grid Customer Demand Response.
2030.7-2017	IEEE Standard for the Specification of Microgrid Controllers.
2030.8-2018	IEEE Standard for the Testing of Microgrid Controllers.
2030.9-2019	IEEE Recommended Practice for the Planning and Design of the Microgrid.
2030.11-2021	IEEE Guide for Distributed Energy Resources Management Systems (DERMS) Functional Specification.

Table 8. The active IEEE Standards for an AC microgrid protection.

Standard	Description
P2030.12/D1.4-2022	IEEE Draft Guide for the Design of Microgrid Protection Systems.
2030.100-2017	IEEE Recommended Practice for Implementing an IEC 61850-Based Substation Communications, Protection, Monitoring, and Control System.
2030.101-2018	IEEE Guide for Designing a Time Synchronization System for Power Substations.
1588-2019	IEEE Standard for a Precision Clock Synchronization Protocol for Networked Measurement and Control Systems.
PC37.2/D1.1-2022	IEEE Approved Draft Standard Electrical Power System Device Function Numbers, Acronyms, and Contact Designations.
C37.95-2014	IEEE Guide for Protective Relaying of Utility-Consumer Interconnections.
C37.103-2015	IEEE Guide for Differential and Polarizing Relay Circuit Testing.
C37.112-2018	IEEE Standard for Inverse-Time Characteristics Equations for Overcurrent Relays.
C37.17-2012	IEEE Standard for Trip Systems for Low Voltage (1000 V and below) AC and General Purpose (1500 V and below) DC Power Circuit Breakers.
C37.13.1-2016	IEEE Standard for Definite-Purpose Switching Devices for Use in Metal-Enclosed Low Voltage (600 V AC and Below) Power Circuit Breaker Switchgear.
C37.230-2020	IEEE Guide for Protective Relay Applications to Distribution Lines.

3.3 IEC 61850 standard of communication

As discussed in Chapter 2, adaptive protection schemes are necessarily required for AC microgrids for maintaining a proper protection coordination between primary and backup relays in both grid-connected and islanded modes. The adaptive protection schemes can be centralized, decentralized, or hybrid centralized and decentralized protection schemes. The centralized adaptive protection schemes for AC microgrids can be implemented using different Ethernet-based and SCADA communication standards and protocols including IEC 60870, DNP3 (IEEE 1815), Modbus, SPA-bus, and IEC 61850. These communication standards and protocols are reviewed in Publication VII of this thesis. The details of SCADA protocols can be found in (Clarke et al., 2004). Presently, applications of IEC 61850 communication standard are rapidly growing due to its suitability for both centralized and decentralized adaptive protection schemes for AC microgrids. Therefore, the IEC 61850 communication standard is selected for research in this thesis and briefly explained in Sections 3.3.1–3.3.6.

3.3.1 Main and additional parts of IEC 61850 series

The IEC 61850 communication standard entitled *Communication networks and systems for power utility automation*, developed by the IEC TC 57, is an Ethernet-based communication standard for real-time data exchange between IEDs of different vendors supporting the IEC 61850 based data structures. The IEC 61850 standard consists of ten main parts: *IEC 61850-1 to IEC 61850-10* as listed in Table 9.

Table 9. Main parts of the IEC 61850 communication standard.

Part	Description
IEC TR 61850-1:2013	Part 1: Introduction and overview
IEC TS 61850-1-2:2020+AMD1:2022 CSV	Part 1-2: Guideline on extending IEC 61850
IEC TS 61850-2:2019	Part 2: Glossary
IEC 61850-3:2013	Part 3: General requirements
IEC 61850-4:2011+AMD1:2020 CSV	Part 4: System and project management
IEC 61850-5:2013+AMD1:2022 CSV	Part 5: Communication requirements for functions and device models
IEC 61850-6:2009+AMD1:2018 CSV	Part 6: Configuration description language for communication in power utility automation systems related to IEDs
IEC 61850-7-1:2011+AMD1:2020 CSV	Part 7-1: Basic communication structure - Principles and models
IEC 61850-7-2:2010+AMD1:2020 CSV	Part 7-2: Basic information and communication structure – Abstract communication service interface (ACSI)
IEC 61850-7-3:2010+AMD1:2020 CSV	Part 7-3: Basic communication structure – Common data classes
IEC 61850-7-4:2010+AMD1:2020 CSV	Part 7-4: Basic communication structure – Compatible logical node classes and data object classes
IEC TR 61850-7-5:2021	Part 7-5: IEC 61850 modelling concepts

IEC TR 61850-7-6:2019	Part 7-6: Guideline for definition of Basic Application Profiles (BAPs) using IEC 61850
IEC TS 61850-7-7:2018	Part 7-7: Machine-processable format of IEC 61850-related data models for tools
IEC 61850-7-410:2012+AMD1:2015 CSV	Part 7-410: Basic communication structure – Hydroelectric power plants – Communication for monitoring and control
IEC 61850-7-420:2021	Part 7-420: Basic communication structure – Distributed energy resources and distribution automation logical nodes
IEC TR 61850-7-500:2017	Part 7-500: Basic information and communication structure – Use of logical nodes for modeling application functions and related concepts and guidelines for substations
IEC TR 61850-7-510:2021	Part 7-510: Basic communication structure – Hydroelectric power plants, steam and gas turbines – Modelling concepts and guidelines
IEC 61850-8-1:2011+AMD1:2020 CSV	Part 8-1: Specific communication service mapping (SCSM) – Mappings to MMS (ISO 9506-1 and ISO 9506-2) and to ISO/IEC 8802-3
IEC 61850-8-2:2018	Part 8-2: Specific communication service mapping (SCSM) – Mapping to Extensible Messaging Presence Protocol (XMPP)
IEC 61850-9-2:2011+AMD1:2020 CSV	Part 9-2: Specific communication service mapping (SCSM) – Sampled values over ISO/IEC 8802-3
IEC/IEEE 61850-9-3:2016	Part 9-3: Precision time protocol profile for power utility automation
IEC 61850-10:2012	Part 10: Conformance testing
IEC TR 61850-10-3:2022	Part 10-3: Functional testing of IEC 61850 systems

The additional parts (TS and TR) of the IEC 61850 series including IEC TS 61850-80-1, IEC TR 61850-80-3, and IEC TS 61850-80-4 generally deal with the interoperability aspects of IEC 61850 with other communication protocols. *IEC TS 61850-80-1* provides guidelines for the information exchange between the IEC 61850 protocol used in substations and other protocols like IEC 60870-5-101 and IEC 60870-5-104 used at control centers. *IEC TR 61850-80-3* gives the requirements of new communication mapping (Specific Communication Service Mapping, SCSM) of web protocols. *IEC TS 61850-80-4* defines the translation of IEC 62056 object models used for smart metering to IEC 61850 logical nodes for other smart grid applications. The other additional parts of the IEC 61850 series including *IEC TR 61850-90-1 to IEC TR 61850-90-17* deal with the use of the IEC 61850 standard for communication between substations.

3.3.2 Data modeling and mapping in IEC 61850

Part 7 of IEC 61850 provides definitions of abstract data and service models to achieve the interoperability between IEDs without any dependency on communication systems or related protocols. The logical nodes (LNs) are defined as the smallest possible functional pieces of the logical device (LD), for example a relay inside the physical device or an IED. Each logical node consists of different data objects (DOs) and data attributes (DAs). The hierarchal structure of the IED 61850 data model is shown in Figure 24.

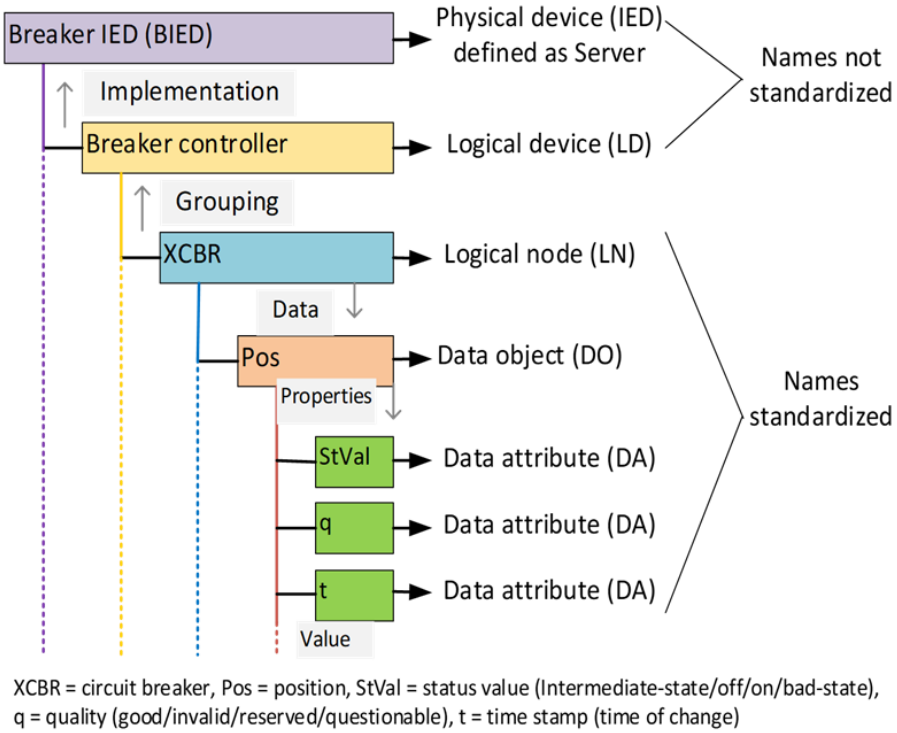

Figure 24. Hierarchical data model of IEC 61850, adapted from (Terwiesch et al., 2010).

The semantics of all exchanged values are provided by the standardized class names of LNs and the standardized full names of data objects and data attributes in IEC 61850. The grouping of different standardized LNs may be done inside the logical devices (LDs) with non-standardized names. The implementation of LDs is done in servers inside the physical devices or IEDs. The physical device (IED) with a non-standardized name is usually defined as a server with a network address. The data objects inside the LNs may be mandatory, optional or conditional depending on the application (Terwiesch et al., 2010); (R. Mackiewicz, n.d.).

The grouping of logical nodes in IEC 61850 is done such that the names of logical nodes related to automatic control begin with the letter “A” and the names of logical nodes related to metering and measurement begin with the letter “M”. In the same way, other logical nodes are grouped into Supervisory Control (C), Generic Functions (G), Interfacing/Archiving (I), Protection (P), Protection Related (R), Sensors (S), Instrument Transformers (T), Switchgear (X), Power Transformers (Y), Other Equipment (Z), etc. (R. Mackiewicz, n.d.); (R. E. Mackiewicz, 2006); (Adamiak et al., 2009). Table 10 lists some of the logical nodes related to Control (C), Protection (P), and Switchgear (X).

Table 10. IEC 61850 logical nodes (control, protection and switchgear).

Logical nodes for Control (C)		**Logical nodes for Switchgear (X)**	
CALH	Alarm handling	XCBR	Circuit breaker
CILO	Interlocking	XSWI	Circuit switch
CPOW	Point-on-wave switching	XFUS	Fuse
CSWI	Switch controller	**Protection Related functions (R)**	
CSYN	Synchronizer controller	RDIR	Directional element
Logical nodes for Protection (P)			
PDIF	Differential	PSDE	Sensitive directional earth-fault
PDIR	Direction comparison	PTOC	Time overcurrent
PDIS	Distance	PTOF	Overfrequency
PFRC	Rate of change of frequency	PTOV	Overvoltage
PIOC	Instantaneous overcurrent	PTUF	Underfrequency
PSCH	Protection scheme	PTUV	Undervoltage

The IEC 61850 standard uses the mainstream seven-layer ISO/OSI (International Organization for Standardization–Open Systems Interconnections) communication stack model for the data mapping. The ISO/OSI communication stack model consists of Ethernet Link layers 1 and 2, TCP/IP layers 3 and 4, and manufacturing message specification (MMS) layers 5, 6 and 7 (Brand, 2004); (Terwiesch et al., 2010); (Adamiak et al., 2009). According to (ISO/IEC 7498-1, 1994), the seven layers of the ISO/OSI communication model are defined individually as: Physical Layer (layer 1), Data Link Layer (layer 2), Network Layer (layer 3), Transport Layer (layer 4), Session Layer (layer 5), Presentation Layer (layer 6), and Application Layer (layer 7).

The IEC 61850 standard uses the MMS protocol at application layer 7 for mapping of the object model and its services for client-server communication. Part 8-1 of IEC 61850 defines the method of mapping objects to the MMS. For example, the data object name of the current measurement “MX” with data attribute “A” of the logical node “MMXU1” of the logical device “Relay1” of the physical device IED1 is mapped as IED1:Relay1/MMXU1.MX.A. The IEC 61850 standard uses the Ethernet link layer 2 for the direct mapping of only the time-critical services including GOOSE (generic object oriented substation event) and SV (sampled values) data messages (Brand, 2004); (R. Mackiewicz, n.d.); (Adamiak et al., 2009); (R. E. Mackiewicz, 2006). Figure 25 shows the mapping of IEC 61850 services to ISO/OSI communication stack.

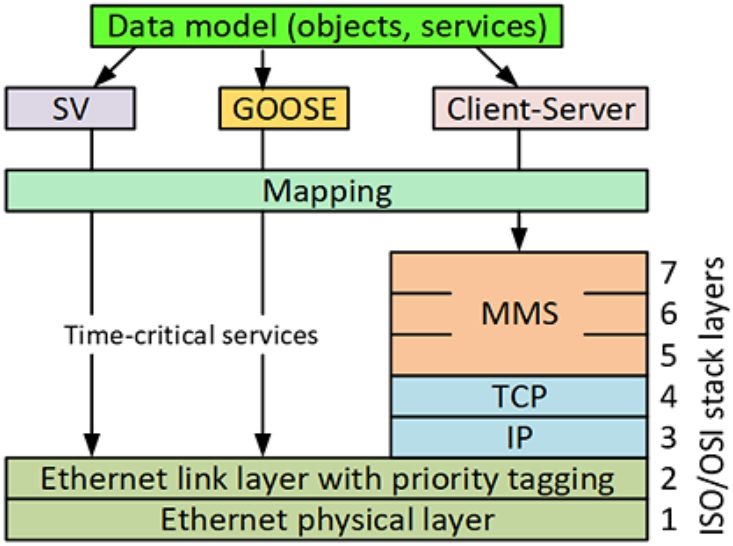

Figure 25. IEC 61850 mapping to ISO/OSI communication stack.

The IEC 61850 mapped data models are described in XML (eXtensible Markup Language) based Substation description Configuration Language (SCL) files. The SCL files include the IED capability description (ICD), configured IED description (CID), substation configuration description (SCD), and system specification description (SSD) files. These SCL files are created using the same methods and formats, but have different scopes depending on the requirements (R. E. Mackiewicz, 2006); (R. Mackiewicz, n.d.). The ICD file contains an XML description of items supported by an IED, the CID file contains the XML configuration of a specific IED, the SCD file contains an XML description of a single substation, and the SSD file contains an XML description of the entire system (Khavnekar et al., 2015). Any of these SCL files contains five sections as defined in IEC 61850-6 clause 9: Header, substation section, communication section, IED section and data type template section, the details of which can be found in (ABB, 2011b); (ABB, 2014).

Usually, the vendor-specific software tools are used for the configuration of IEC 61850 protocols and generate different SCL files. For example, the software tools used for IEC 61850 standard configuration of ABB protection IEDs and to generate different SCL files include PCM600 (IED tool) and CCT600/IET600 (system tool) software. The IED tool (PCM600) provides the ICD or CID file for each IED, then these ICD/CID files are imported into the system tool (CCT600/IET600) and merged into an SCD file that represents the complete substation or a part of the substation (ABB, 2011b); (ABB, 2014). The VAMPSET software tool is used for VAMP protection IEDs to configure the IEC 61850 standard and generate different SCL files. The common vendor-independent software tools have been missing for IEC 61850 protocol configuration for interoperability between IEDs of different

manufacturers. However, Helinks STS (an IEC 61850 Power System Engineering Tool) offers the IED manufacturer independent generation of SSD, SCD and other SCL files to support customized top-down and bottom-up engineering processes (Helinks LLC, n.d.). Other such tools include Siemens IEC 61850 System Configurator (Siemens, n.d.).

From the context of this thesis, only ICD files are created and used for the real-time testing of GOOSE messages between the IEDs. The complete procedure of GOOSE configuration is mentioned in Publication IV.

3.3.3 GOOSE and SV protocols of IEC 61850

The IEC 61850 standard offers two real-time peer-to-peer Ethernet-based communication protocols and services for the exchange of time-critical messages between IEDs: GOOSE and SV or SMV (sampled measured value) messages. The GOOSE messages may contain time-critical data like circuit breaker status, fast bus tripping, interlocking, blocking or releasing signals, whereas the SV messages contain the measured sample values of voltages and currents.

The modern GOOSE message can transfer both binary and analog types of data for different control and protection applications, but with different transmission time performance requirements. For example, the fast tripping and blocking GOOSE messages within a substation should be transmitted in 3 ms, and release and status change signals between the substations should be transmitted in 10 ms (Hou & Dolezilek, 2010); (IEC 61850-5, 2003). Other control and protection functions and their transmission time requirements can be found in the latest version of part-5 of IEC 61850 (IEC 61850-5, 2013) along with the definition of transmission time. The selected protection functions, related LNs and performance requirements are listed in Publication II.

The information or data exchange in GOOSE protocol happens in a publisher-subscriber manner. The IED at the sending-end publishes the status change GOOSE message over the Ethernet link, and any receiving-end IED connected to the same Ethernet link can subscribe to the GOOSE message to receive the data (Apostolov & Vandiver, 2015). For a successful GOOSE subscription, the subscriber IED needs the GOOSE ID, App ID and MAC (media access control) address of the published GOOSE message. These parameters are already known by the subscriber IEDs during the configuration process.

The GOOSE message is a multicast (one-to-many) type of message transmitted via Ethernet link layer-2 that can only be routed inside a LAN because it is sent to a

network address instead of a device address. Therefore, it cannot be known which IEDs will receive the GOOSE message, and because no acknowledgement is issued from the receiving-end IEDs, the delivery of the GOOSE message is not guaranteed. This means that it is the responsibility of an individual IED to survive the lost, duplicated and delayed GOOSE message in addition to out-of-order reception and a loss of connectivity (Hou & Dolezilek, 2010).

In order to address the above mentioned challenges and maintain a high level of dependability of GOOSE message delivery, a retransmission methodology is specified in IEC 61850-8-1 (Figure 26). According to the retransmission method, the normal GOOSE message is transmitted after the expiry of the configured maximum transmission time (*mt*), for example 100 ms, as the heartbeat data stream at regular intervals denoted by T_0 in Figure 26. When the status of data changes due to circuit breaker tripping or fault detection, the GOOSE message is transmitted with very short intervals, called the burst of GOOSE messages. This means that the time of transmission (*tot*) between GOOSE messages is reduced to T_1=0.5–5 ms after the data status is changed (Bekker et al., 2015). This is done to increase the chance of GOOSE data subscription by each IED through the nondeterministic Ethernet. After few quick initial data publications, the time of transmission between GOOSE messages is gradually increased to $T_2>T_1$, $T_3>T_2$ and so on until the time of transmission eventually becomes stable at T_0=*mt*=*tot*. The same procedure is repeated on occurrence of a new event or a status change (Hou & Dolezilek, 2010); (Bekker et al., 2015); (Aftab et al., 2018).

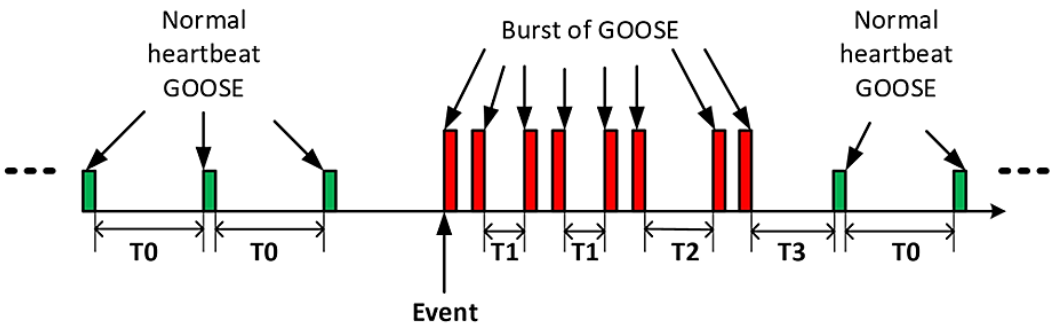

Figure 26. Retransmission principle of an IEC 61850 GOOSE message.

The publisher IED calculates a time to live (*ttl*) based on the next *tot* and publishes the *ttl* along with each GOOSE message so that subscriber IEDs can monitor a correct flow of data. The subscriber IED calculates the time to wait (*ttw*) based on the *ttl* included in each GOOSE message. On the expiry of the *ttw*, the subscriber IED assumes that a communication failure or delay has occurred and then adapts its logical functions according to this situation or issues an alarm. The *ttl* value is twice the *tot* value during the normal heartbeat mode when *tot*=T_0 and three times

during the burst mode when $tot=T_1, T_2, \ldots, T_n$. The increased value of *ttl* will prevent nuisance alarms due to frequent and small Ethernet delays. The health of the communication channel can be monitored by monitoring the cyclic or heartbeat delay T_0 of the GOOSE message by the subscriber IED (Hou & Dolezilek, 2010).

Lost or missing data packets can be detected by the subscriber IED just by tracking the sequence number (SqNum) attribute of the GOOSE data. Once the status change happens, the SqNum resets to zero and starts the sequence 1, 2, 3 … Any gap in SqNum indicates missing data, for example, if SqNum is 1, 2, 3, 5 …, it indicates that SqNum 4 is missing and then an alarm for missing data can be activated (Bekker et al., 2015). The same method can be used to detect cyber security intrusion (Apostolov & Vandiver, 2015).

The number of Ethernet switches and servers in LAN, network traffic and configuration (topology) etc. may add further delays in GOOSE transmission. Therefore, several performance tests and measurements are required to determine the practical value of the final GOOSE message transmission or transfer delay for a particular protection and control function (Steinhauser & Vandiver, 2015).

The SV protocol of IEC 61850 is used to transmit the measured synchronized sampled values of voltage and current from the conventional CTs and VTs or sensors to protection relays or IEDs for various protection functions like overcurrent protection and differential protection etc. The data is sampled at 4 kHz for a 50 Hz system (80 samples/cycle) using merging units (MUs), and each frame of data is sent after every 250 microseconds over the Ethernet LAN as a multicast message (Mocanu & Thiriet, 2021). It should be noted that an 80 samples/cycle is the most common sampling rate based on IEC 61850-9-2 LE (Light Edition). The IEC 61850 standard also defines several other sampling rates.

Like the GOOSE protocol, the information or data exchange in SV protocol also happens in a publisher-subscriber manner. The MUs at the sending-end publish the SV message over the Ethernet link, and any receiving-end IED connected to the same Ethernet link can subscribe to the SV message in order to receive the data. The IEDs cannot receive all SV messages available over Ethernet link, but only configured SV messages (El Hariri et al., 2019). Due to heavy traffic and hard real-time requirements, two high availability redundant network protocols are proposed in IEC 61850 for SV messages: High-availability Seamless Redundancy (HSR) and Parallel Redundancy Protocol (PRP) (Mocanu & Thiriet, 2021). Further details of the SV protocol and its applications can be found in (IEC 61850-9-2, 2011); (Leitloff et al., 2016); (Wannous et al., 2019); (Palizban et al., 2020).

Only the GOOSE message protocol is related to this thesis. Publication II uses GOOSE message for adaptive protection. In Publication IV of this thesis, the round-trip transfer time delay of GOOSE message has been estimated using the real-time simulator as an IED that publishes, subscribes and stores GOOSE messages in real time as explained also later in Section 4.3.

3.3.4 Substation architecture of IEC 61850

The substation architecture of IEC 61850 is divided into three-levels: process level, bay level, and substation level. At the process level, the measured data from field devices (CTs, VTs etc.) is digitized and published by MUs to the process bus. At bay level, IEDs are located which can subscribe to the data from the process bus. At substation level, each IED can publish and subscribe to the data from the station bus. A remote access point for WAN, human machine interface (HMI), SCADA etc. is also available at the station bus. Figure 27 shows the substation architecture of IEC 61850. Publication II of this thesis explains the IEC 61850 substation architecture of AC microgrids. Further details on IEC 61850 substation architecture can be found in (IEC 61850-5, 2003); (R. E. Mackiewicz, 2006); (Skendzic et al., 2007); (Adamiak et al., 2009).

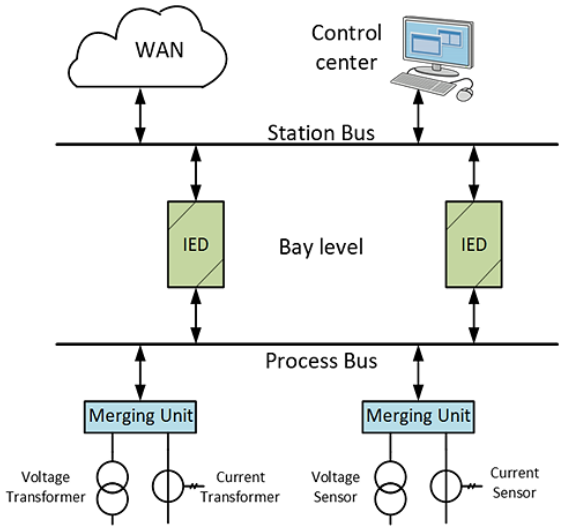

Figure 27. Substation architecture of IEC 61850.

3.3.5 Edition 1 and Edition 2 of IEC 61850

Edition 1 of IEC 61850 released in 2003 is the earlier version of the standard that contained various inconsistencies and technical issues for the implementation. Edition 2 of IEC 61850 released in 2010 addresses the shortcomings of Edition 1 and provides further improvements and inclusions. For example, Edition 1 was

limited to data models for only electrical devices in a substation, which has been extended to hydroelectric power plants, wind power plants, and other DERs in Edition 2. Network redundancy protocols like HSR and PRP are also added in Edition 2. Edition 1 was limited to communication between IEDs within a substation that has been extended to communication between substations in Edition 2. Edition 1 proposed and defined simple network time protocol (SNTP) for the time synchronization, whereas Edition 2 proposes and defines a more accurate precision time protocol (PTP) for time synchronization. Edition 2 also defines the data security mechanism that was not defied in Edition 1 (Khavnekar et al., 2015).

3.3.6 Benefits of IEC 61850

In addition to the application for both centralized and decentralized adaptive protection, automation, control, and monitoring functions, the IEC 61850 standard also offers other benefits. The main benefit offered by the IEC 61850 standard is the interoperability between IEDs from different manufactures and between different versions of IEDs from the same manufacturer. IEDs in conformance with the IEC 61850 standard would not need expensive protocol conversions as required in the earlier legacy protocols like DNP3 and IEC 60870-5-104 in order to exchange data. The use of peer-to-peer communication protocols like GOOSE messages over an Ethernet link, offers a two times faster execution of trip and blocking signals compared with traditional hardwired signals (Terwiesch et al., 2010). The replacement of copper control cables with fiber-optic cables will reduce the construction of trenches, ducts and cable raceways, and result in less commissioning labor (Moreno et al., 2010). The reduced costs of substation design, installation, commissioning, migration, extension, integration, operation and maintenance, an increased level of system reliability, and new functional capabilities like accurate time synchronization, self-supervision, wide-area protection etc. are other prominent benefits offered by the IEC 61850 standard (Hou & Dolezilek, 2010); (R. E. Mackiewicz, 2006); (R. Mackiewicz, n.d.); (Terwiesch et al., 2010).

3.4 Grid codes for DERs connected to distribution networks

The grid codes, in a general sense, define the rules for power systems and energy markets in order to enable network operators or transmission system operators (TSOs), generators, suppliers or distribution system operators (DSOs) and consumers an effective functioning across the market. In this way, the operational

stability, security of supply, and the smooth functionality of energy markets can be ensured. According to the ENTSO-E (European Network of Transmission System Operators for Electricity) classification (Figure 28), the grid codes are categorized into connection codes, operation codes, planning codes, and market codes. The connection codes are subdivided into generator connection code, demand connection code, and HVDC (high-voltage direct current) connection code (IRENA, 2016).

In modern power systems, the connections of generators (particularly the DERs) are distributed across the transmission and distribution systems. Therefore, the generator connection code can be further subdivided into the generator connection code for transmission systems and the generator connection code for distribution systems. The generator connection code for the distribution systems is more relevant to this thesis, and is therefore discussed in this section. In this regard, the active generator connection codes for the distribution systems related to EU and U.S. regions respectively named as “EN grid codes” and “IEEE grid codes” have been considered, as reviewed in Publication V.

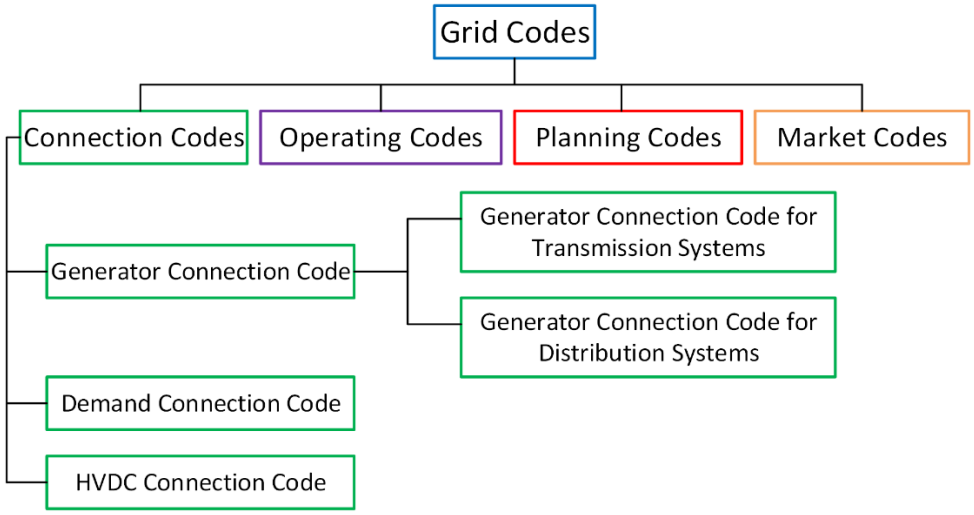

Figure 28. ENTSO-E classification of grid codes (IRENA, 2016).

3.4.1 EN grid codes

The harmonized EU standards EN 50549-1 and EN 50549-2, released in 2019, define the minimum connection requirements for type-A and type-B generators connected to LV and MV distribution systems, respectively. Type-A generators have a maximum active power capacity of 0.8 kW or more and these are connected at distribution networks of voltages below 110 kV. In the Nordic synchronous area, type-B generators have an active power capacity range of 1.5–10 MW. The active power capacity ranges of type-B generators connected to other synchronous areas

in Europe are given in Publication V. These grid codes define the technical requirements to be met by generators including synchronous as well as non-synchronous or converter-based generators. The technical requirements included in these grid codes are related to the operational behavior and the required capabilities of generators during normal as well as fault situations. The EN 50549-1 and EN 50549-2 grid codes define the separate technical requirements for synchronous and non-synchronous types of generators. In this regard, less stringent requirements from the synchronous generators and more stringent requirements from the non-synchronous generators are specified.

The grid code requirements for generators during normal continuous operation include the minimum and maximum voltage and frequency limits against the operating time limits. The grid code requirements for generators during disturbance or fault conditions include the voltage ride-through, frequency ride-through, rate-of-change-of-frequency ride-through, and the specific additional amount of reactive current provision during short-circuit events. The EN 50549-1 and EN 50549-2 grid codes also define the interface protection requirements with different voltage and frequency functions and their settings. The interface protection prevents overvoltage and islanding conditions, and helps the system to restore to normal state during voltage and frequency fluctuations beyond the normal limits. These grid codes emphasize that the interface protection requirements always overrule the technical limits and ride-through requirements. This means the connection and disconnection of a generator is mainly decided based on the settings of the interface protection. Further details can be found in Publication V of this thesis that also includes an evaluation of selected grid code requirements and interface protection settings.

3.4.2 IEEE grid codes

The IEEE standard 1547-2018 is widely accepted and adopted in the U.S. as a common grid code for the connection requirements of DERs. Standard 1547-2018 defines the technical requirements of DERs for interconnection with primary and secondary radial distribution systems. Unlike the EN grid codes, Standard 1547-2018 defines the technical requirements of DERs that are independent of the size of the generators. The categorization of the requirements is formed only on the basis of low (category-I), medium (category-II) and high (category-III) penetration levels of DERs.

The IEEE standard 1547-2018 defines the normal continuous ranges of operating frequency of DERs irrespective of the penetration level of the DERs. The normal continuous ranges of operating voltage of DERs are applicable for the point of

common coupling with the local distribution system. The requirements during abnormal operations or faults include the mandatory voltage ride-through, mandatory frequency ride-through, rate-of-change-of-frequency ride-through, multiple disturbance ride-through, and voltage phase angle change ride-through requirements. Additionally, two settings groups for each overvoltage, undervoltage, overfrequency, and underfrequency functions are also defined for "shall trip" category responses of DERs, but with thresholds higher than the mandatory ride-through settings. The IEEE standard 1547-2018 also defines enter service values of voltages and currents and resynchronization parameters for the already disconnected DERs that again want to be operating in parallel with the local distribution system. This standard also suggests the provision of dynamic reactive power during short-circuit faults for voltage support, provided that it shall not cause unwanted tripping of DERs. Last but not least, the IEEE standard 1547-2018 also defines different islanding conditions. Further details are included in Publication V of this thesis.

3.5 Testing methods for AC microgrids

The conventional state-of-the-art testing procedure for a new product, part of the product like the controller etc., or an entire system composed of various products and controllers in power systems involves a three step approach including offline simulations, lab testing with hardware prototypes of reduced size, and field testing. This conventional three step testing approach often lacks the coverage of smart grid functionalities and the realistic complexity level close to the actual power system. With the advent of real-time simulators, a new "testing chain" approach is being adopted that involves the whole range of testing possibilities with realistic levels of complexity, and a number of testing options for various functions and hardware interactions with the simulated reality of a power system. The real-time testing chain includes four stages (Heussen et al., 2020): Offline simulation, Software-in-the-loop (SIL), Control hardware-in-the-loop (CHIL), and combined CHIL and Power hardware-in-the-loop (PHIL) called Power System-in-the-loop (PSIL) as shown in Figure 29.

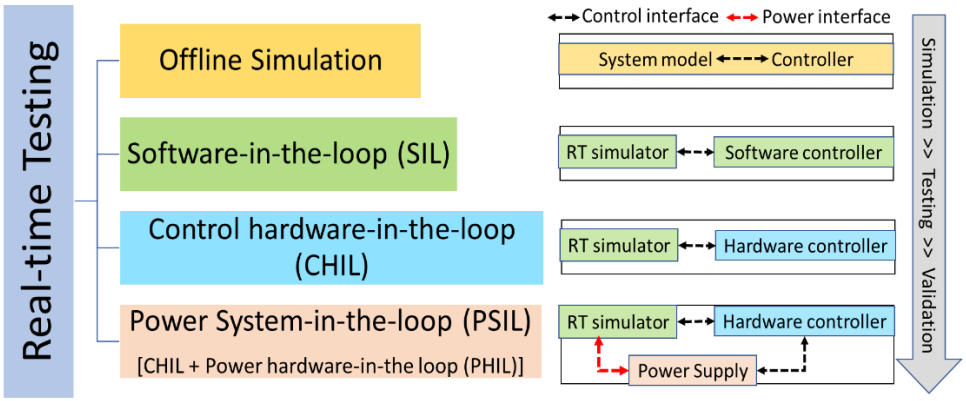

Figure 29. Real-time testing chain for power systems.

In the offline simulation, the power system model along with the controller is created in a pure software simulation environment (Simulink etc.). The functional testing of the control algorithm can be done in this stage without interaction with external software or hardware. In the SIL testing, two separate software tools can be used, one for the power system model (real-time simulator platform) and the other for the controller. The SIL setup enables the information exchange in a closed loop for verification of the behavior of the control algorithm. In the CHIL testing, the actual hardware controller can be tested with a physical control interface and real-time interaction with the simulated power system. The hardware controller can be an actual control or protection IED or the hardware controller of the power electronic converter. In the combined CHIL and PHIL testing (called PSIL testing), the actual power device like the PV converter or motor etc. controlled by the hardware controller can be tested, and meanwhile the impact of the controller on the simulated power system or its part can be observed in real-time. The PSIL testing setup is close to the field testing of a power system component, but can still be implemented in a laboratory (Heussen et al., 2020).

The real-time testing chain approach can also be used for AC microgrids for conformance testing of different communication protocols as well as functionality and system testing before the actual field testing during the commissioning of the project. The CHIL testing or even the PSIL testing using the real-time simulator can be useful for the whole range of IEC 61850 protocol testing, including compliance, functionality and interoperability tests in a multivendor testing environment. Such testing will help detect gray areas, and thus help revise and improve the protocols accordingly. For example, the Utility Communications Architecture (UCA) International Users Group, or UCAIug (a not-for-profit corporation consisting of utility users and supplier companies: UCAIug, n.d.), organize interoperability plugfest (IOP) sessions after every two years for IEC

61850 standard testing. In this event, feedback about the standard is collected and the companies get a chance to test the implementation of the latest features of the IEC 61850 standard. These IOP sessions have already brought various clarifications and improvements to the IEC 61850 standard (Brunner, 2015).

The simulation fidelity-based real-time simulations include electromagnetic transient (EMT) simulations, electromechanical transient or phasor simulations, and combined EMT and phasor simulations. The EMT simulations use discrete time average or detailed models of power systems and power electronic components. The average EMT models are useful for simulations of dynamic interactions between control systems and power systems. The detailed EMT models are useful for accurate simulations of harmonics in addition to dynamic interactions between control systems and power systems.

The scope of this thesis is only limited to the CHIL testing of the protection IED using average EMT simulation models. In this regard, the protection IED used as the “hardware controller under test” has been tested in real-time to verify the compliance of IEC 61850 GOOSE message protocol. The estimation of the round-trip transfer delay of a Boolean signal to and from the real-time simulator and protection IED has been performed in Publication IV. In this way, the implementation of an adaptive protection scheme of AC microgrid using IEC 61850 GOOSE protocol has been tested and validated. Further information about the real-time testing methods and case studies can be found in Publication IV and Publication VII.

4 DYNAMIC ASPECTS OF AC MICROGRID PROTECTION

The protection of AC microgrids has many twists and turns depending on the changing network configurations, the capacity (size), type, location and control of DERs, storage and related power electronic converters. The grid code requirements and economic limitations are other important factors. All of these factors make the choice of protection scheme for AC microgrids more challenging. The state-of-the-art review about the AC microgrid protection challenges and existing solutions has already been discussed in previous chapters. The main contributions of this thesis are summarized in Figure 30, and these are further elaborated in Sections 4.1–4.8.

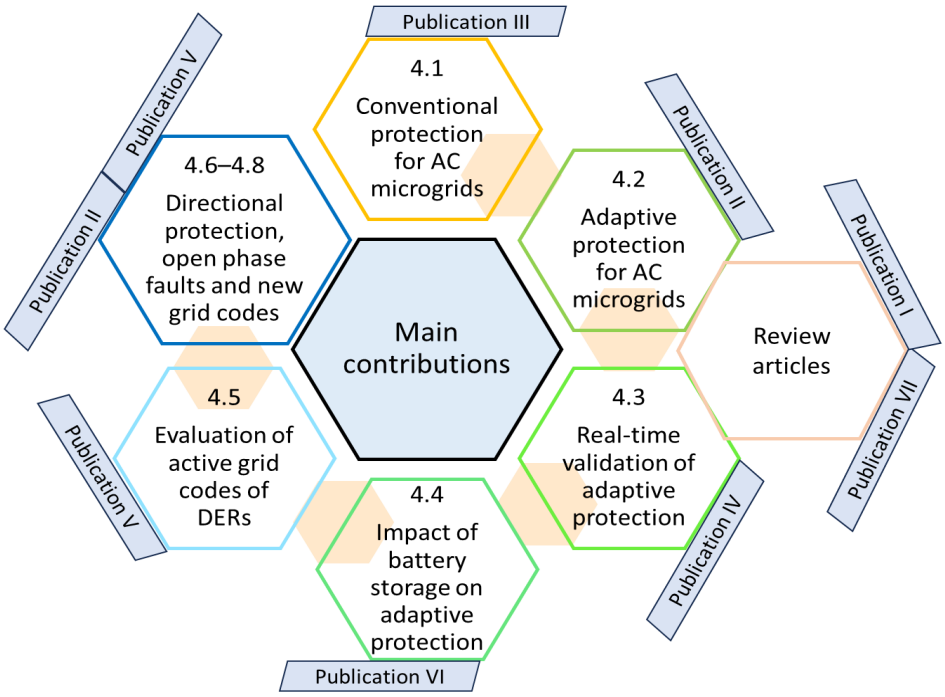

Figure 30. Main contributions of the thesis.

4.1 Conventional protection for AC microgrids

As mentioned in Section 2.2 of Chapter 2, the connection of an extensive share of DERs in distribution systems has an adverse effect on the performance of conventional overcurrent protection schemes. In support of this statement, Section 4.1 presents the case study results based on MATLAB/Simulink simulations to compare the performance of conventional definite-time and inverse-time overcurrent protection schemes before and after the connection of DERs in radial AC microgrids during faults in the grid-connected mode. The performance during the faults in the islanded mode is also compared. Figure 31

shows the single line diagram of a radial AC microgrid model used for this case study. The details of this case study can be found in Publication III of this thesis. In this section, only the results in terms of the tripping or operating time of definite-time and inverse-time overcurrent functions and coordination time interval (CTI) between IEDs are compared for three-phase short-circuit faults at three different locations (F1, F6, F8) of the considered AC microgrid (Figure 31).

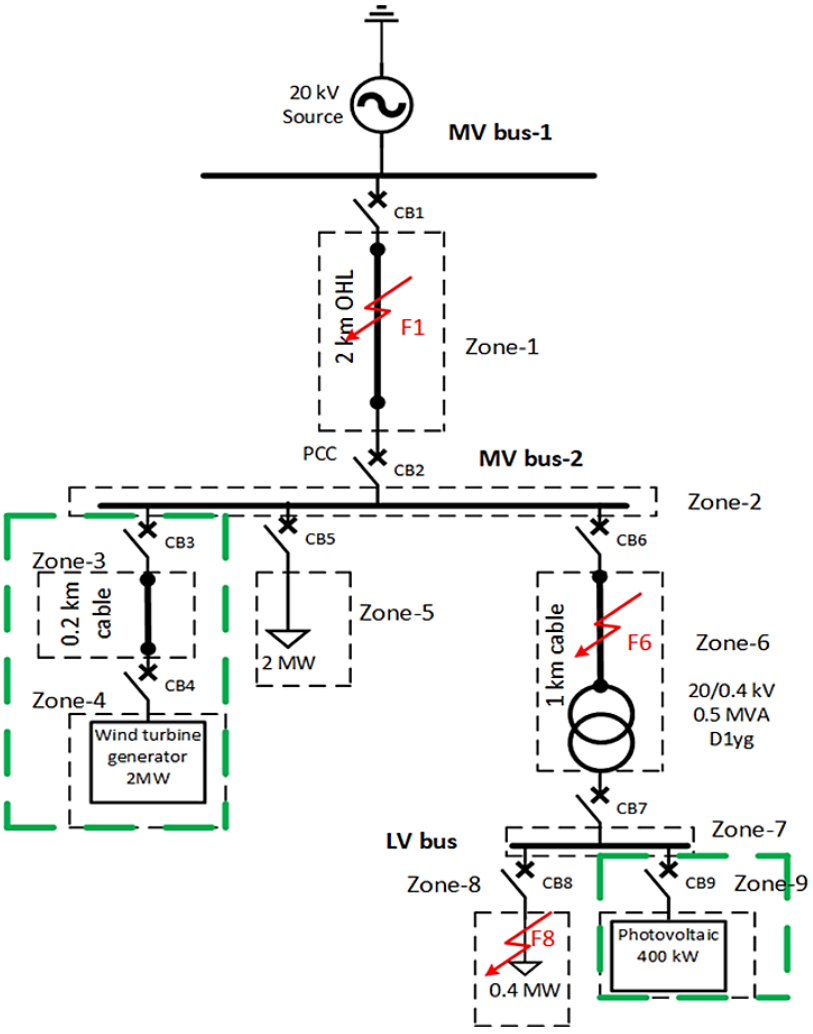

Figure 31. A radial AC microgrid in the grid-connected mode with DERs.

4.1.1 Faults in the grid-connected mode

Figure 32 shows the comparison of tripping or operating time of definite-time and inverse-time overcurrent IEDs 1, 2, 6, 7, and 8 (main and backup) during three-phase short-circuit faults F1, F6 and F8 in the grid-connected mode. IEDs 1–9 are located at CBs 1–9 locations in Figure 31. It is obvious from the results (Figure 32) that the inverse-time overcurrent IEDs have faster operating times (orange and

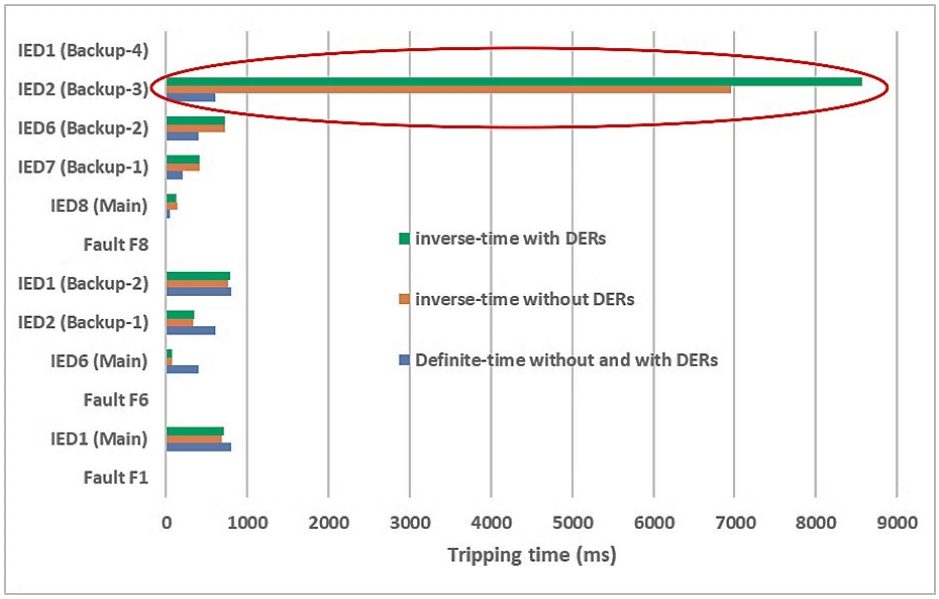

Figure 32. Comparison of tripping or operating time of definite- and inverse-time overcurrent IEDs in grid-connected mode.

green) than the definite-time IEDs (blue) during faults F1 and F6 closer to the main grid (20 kV source) compared with the operating times during the remote fault F8. The operating times of inverse-time overcurrent IEDs (main and backup) during faults F1 and F6 are negligibly delayed with the connection of DERs (wind turbine and PV system) than the cases without DERs (green vs orange). This negligible operating time delay is due to the limited fault current contribution of DERs (1–1.04 p.u.) during the faults F1 and F6 in the grid-connected mode with a 1.2 p.u. maximum fault current setting of DERs. Overall, this means that during the faults F1 and F6 in the grid-connected mode, the operating times of inverse-time overcurrent IEDs are nearly the same and faster than definite-time overcurrent IEDs in both cases of with and without the connection of DERs. However, during the remote fault F8 in the grid-connected mode, the operating times of inverse-time overcurrent IEDs are significantly delayed compared with the operating times of definite-time overcurrent IEDs. An unacceptable operating time delay of 7 s is observed at the inverse-time overcurrent IED2 (orange) acting as a remote backup-3 during the fault F8 in the grid-connected mode without DERs. The operating time delay at the inverse-time overcurrent IED2 is further aggravated and extends beyond 8 s with the connection of DERs (green). These significant operating time delays at the inverse-time overcurrent IED2 are encircled with the red line in Figure 32.

Figure 33 shows the comparison of CTI between successive definite-time and successive inverse-time overcurrent IEDs 6–2, 2–1, and 8–7, 7–6 and 6–2 during

three-phase short-circuit faults F6 and F8, respectively in the grid-connected mode.

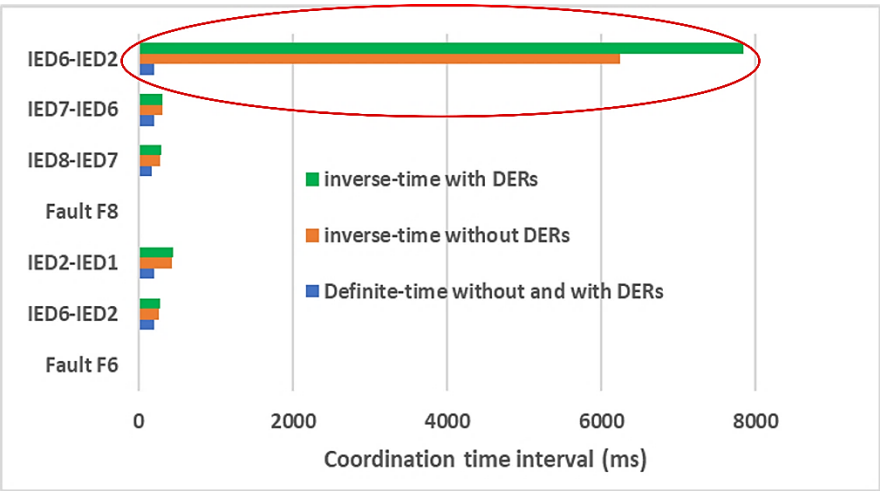

Figure 33. Comparison of coordination time interval between definite- and inverse-time overcurrent IEDs in grid-connected mode.

It is obvious that the CTI between successive definite-time IEDs remains fixed at 200 ms, whereas the CTI between the successive inverse-time overcurrent IEDs keeps changing. It can be observed from Figure 33 that in most cases the CTI between successive inverse-time overcurrent IEDs is 2–3 times greater than the CTI between successive definite-time IEDs. In the worst case, the CTI between successive inverse-time overcurrent IED6-IED2 (orange) acting as backup-2 and backup-3 during the fault F8 is observed to be 30 times greater (6000 ms) than that of definite-time IEDs at the same locations without DERs. The CTI between successive inverse-time overcurrent IED6–IED2 is further extended beyond 7000 ms during the fault F8 after the connection of DERs (green).

The results show that except for the fault F6, the performance of definite-time overcurrent IEDs is either comparable or better than the inverse-time overcurrent IEDs in the grid-connected mode with and without a connection of DERs.

4.1.2 Faults in the islanded mode

Figure 34 shows the single line diagram of a radial AC microgrid during the islanded mode with DERs and BESS (configuration 2 of Figure 15). In the islanded mode, the central BESS is operating as the grid-forming DER, and other DERs are operating as the grid-following DERs. The fault current contributions from the central BESS, WTG and PV system are 3.17 p.u., 1.2 p.u. and 1.17 p.u. respectively

during the fault F6, and 1.15 p.u., 1.2 p.u. and 1.17 p.u. respectively during the fault F8 in the islanded mode.

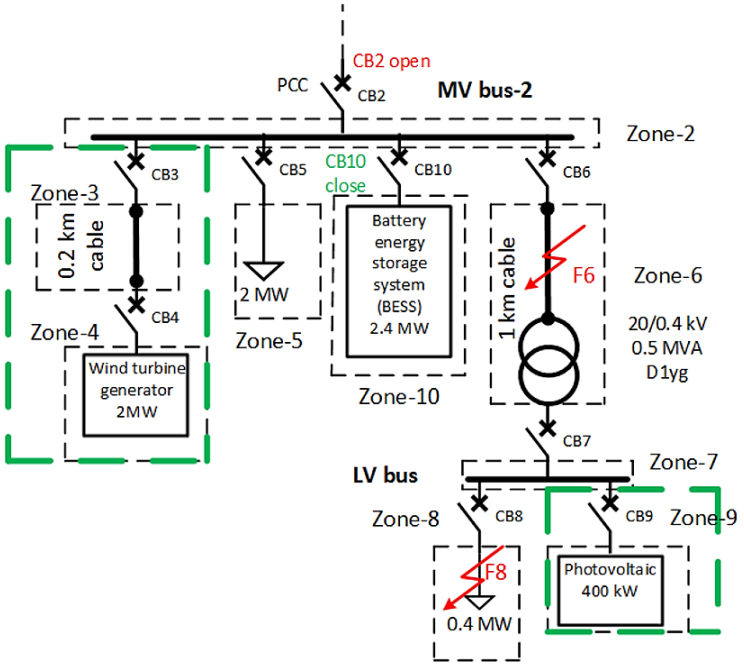

Figure 34. A radial AC microgrid in the islanded mode with DERs and BESS.

Figure 35 shows the comparison of tripping or operating time of definite-time and inverse-time overcurrent IEDs 6, 7, and 8 (main and backup) during three-phase short-circuit faults F6 and F8 in the islanded mode.

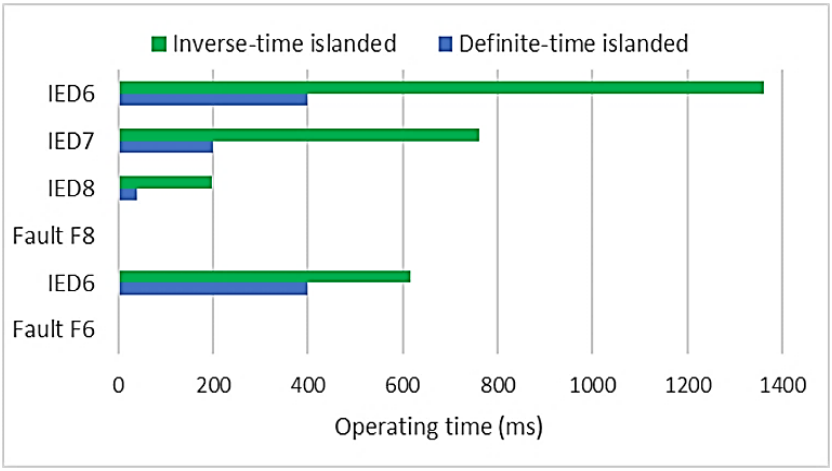

Figure 35. Comparison of tripping or operating time of definite- and inverse-time overcurrent IEDs in the islanded mode.

It is evident from the results (Figure 35) that during the faults F6 and F8 in the islanded mode, the operating times of both main and backup inverse-time overcurrent IEDs are significantly delayed compared with the operating times of

definite-time overcurrent IEDs. The slower operating times make inverse-time overcurrent IEDs unsuitable for a radial AC microgrid protection in the islanded mode of operation, even with a central BESS used as a fault current source.

Figure 36 shows the comparison of CTI between successive definite-time and successive inverse-time overcurrent IEDs 8–7, and 7–6 during three-phase short-circuit fault F8 in the islanded mode. It can be observed from Figure 36 that the CTI between successive inverse-time overcurrent IEDs is 3 times greater than the CTI between successive definite-time IEDs. This means that although the selective coordination of IEDs with inverse-time overcurrent function is possible, the unacceptable delayed operation of backup protection and resulting arc-fault has the potential to cause damage to the equipment (transformer windings etc.).

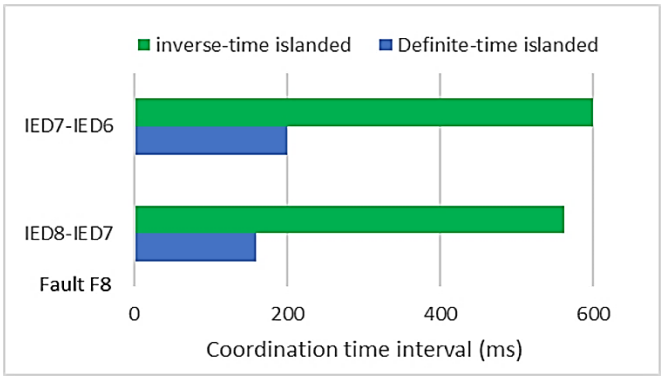

Figure 36. Comparison of coordination time interval between definite- and inverse-time overcurrent IEDs in the islanded mode.

It is concluded that the faster operating times and lower but acceptable CTI between IEDs makes the definite-time overcurrent function a better choice for the protection of radial AC microgrids in both the grid-connected and islanded modes for the considered conditions. However, the definite-time overcurrent function may also fail to operate if the LV bus section in Figure 34 is operated in the islanded mode (CB7 open) with a limited fault current contribution of 1.2 p.u. from the PV system and existing 2.25 p.u. tripping threshold setting of IED8 during the fault F8. In this situation, the only way forward will be to change the tripping setting of IED8 to a lower threshold value of 1.15–1.18 p.u. in order to detect and isolate the fault F8 in the islanded LV bus section (LV microgrid). This means that an adaptive protection setting will be required for an islanded mode operation of the LV bus section (Figure 34). The inverse-time overcurrent function will also need to be adaptive for getting faster operating times and lower CTI values in order to provide quicker main and backup protection, particularly in the islanded mode of operation. The adaptive protection using definite-time overcurrent is further discussed in the next Section 4.2.

4.2 Adaptive protection for AC microgrids

The adaptivity of the overcurrent protection scheme for an AC microgrid requires that the settings or tripping thresholds of IEDs need to be “adaptive” according to changing network configuration and the connection or disconnection status of DERs. The background information about the adaptivity and its implementation have already been discussed in Chapter 2 (Section 2.3.4) of this thesis. Section 4.2 will briefly present the proposed adaptive protection scheme for the radial AC microgrids using IEC 61850 communication standard based on Publication II of this thesis. Figure 37 shows the model of a radial MV–LV AC microgrid along with IEC 61850 substation architecture used for an adaptive protection case study.

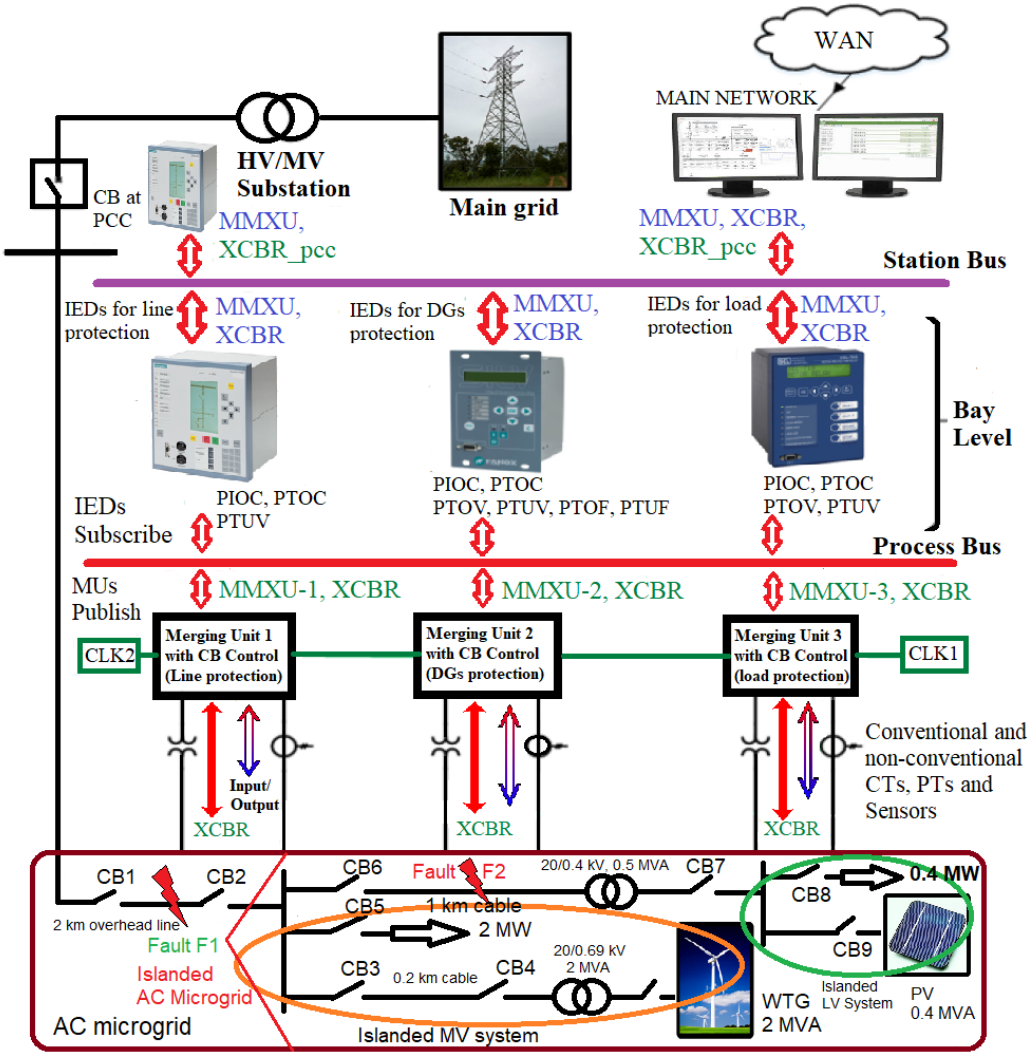

Figure 37. A radial MV-LV AC microgrid with IEC 61850 substation architecture used for an adaptive protection case study.

This case study is based on offline PSCAD simulations. The IEC 61850 substation architecture is briefly explained in Section 3.3.4 of the previous Chapter 3, and further details can be found in Publication II.

The considered radial AC microgrid model in Figure 37 is the same model as used in the previous case study of Section 4.1, but without using the central BESS. In this case study, the DER models including WTG and PV systems are provided with grid-forming and grid-following controls (explained in Section 2.1.5 of Chapter 2) in order to work also in the islanded mode without any central BESS (configuration 1 of Figure 15). The fault current contribution of DERs during short-circuit faults is limited to a maximum value of 1.2 p.u. of the rated current. Such an AC microgrid model will make the conventional overcurrent functions, particularly the inverse-time overcurrent, more challenging than when using an additional central BESS (configuration 2 of Figure 15). Thus, the considered radial AC microgrid model is assumed to be suitable for adaptive overcurrent protection case studies. For this case study, the AC microgrid model is only limited to definite-time overcurrent function based adaptive protection.

The protection IEDs used for the considered radial AC microgrid can be grouped into three broad types based on the system components protected by them: Line-IEDs, DER-IEDs, and Load-IEDs (Figure 38).

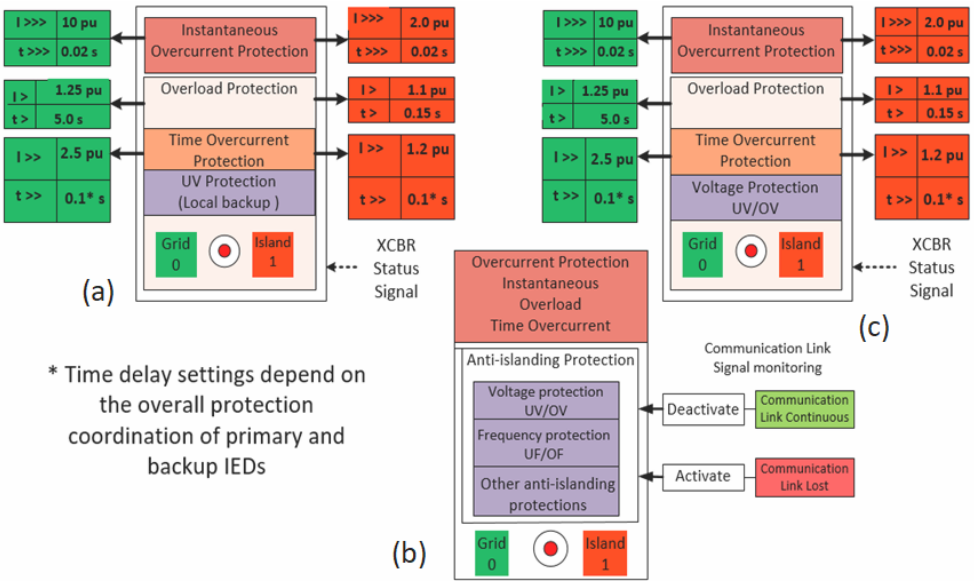

Figure 38. Adaptive protection IEDs with two setting groups: (a) Line-IED, (b) DER-IED and (c) Load-IED.

There are five Line-IEDs (IEDs 1, 2, 3, 6, and 7), two DER-IEDs (IEDs 4, and 9), and two Load-IEDs (IEDs 5, and 8) in the considered radial AC microgrid (Figure 37). Each of the Line-IEDs (except nonadaptive IED1), DER-IEDs and Load-IEDs

has at least two overcurrent setting groups or tripping thresholds as shown in Figure 38. The higher tripping threshold of 2.5 p.u. for the grid-connected mode (green) and the lower tripping threshold of 1.15–1.2 p.u. for the islanded mode (red) are considered for the definite-time overcurrent function. Additionally, the Line-IEDs are provided with UV protection, the Load-IEDs are provided with UV and OV protections, and DER-IEDs are provided with UV, OV, UF, OF and anti-islanding protections as local backup protections. The two setting groups (green and red) are changed adaptively using IEC 61850 GOOSE messages containing the circuit breaker status signals (XCBR/StVal).

In Figure 37, the three-phase short-circuit fault F1 is considered only in the grid-connected mode, and three-phase short-circuit fault F2 is considered only in the islanded mode of operation for the demonstration of IEC 61850 communication-based adaptive protection methodology. The proposed methodology uses the normal communication-less definite-time overcurrent coordination with 0.15 or 0.2 s time delay between each IED for fault detection and isolation during the communication link failures. In Figure 37, each CB is operated by the IED of the related number. For example, CB1 is operated by IED1, and so on. The proposed adaptive protection methods for the grid-connected and the islanded modes are explained in Sections 4.2.1 and 4.2.2, respectively.

4.2.1 Three-phase fault F1 in the grid-connected mode

Figure 39 shows the flow chart of a communication-based nonadaptive IED1 for the detection of three-phase fault F1 and other downstream faults for providing main and backup protection in the grid-connected mode. First, the fault is detected by IED1 using either an overcurrent function (during fault F1) or an undervoltage function (during other faults). Then, IED1 checks if the communication link-1 or link-2 is continuous. If there is no communication link-1 and link-2 failure signal, then IED1 checks if any downstream IED has detected the fault by checking GOOSE message data containing the fault detection signal received from other IEDs. If no status change is detected in any of the received GOOSE messages, IED1 assumes “No fault” at other IEDs and issues an immediate tripping command “Open CB1”.

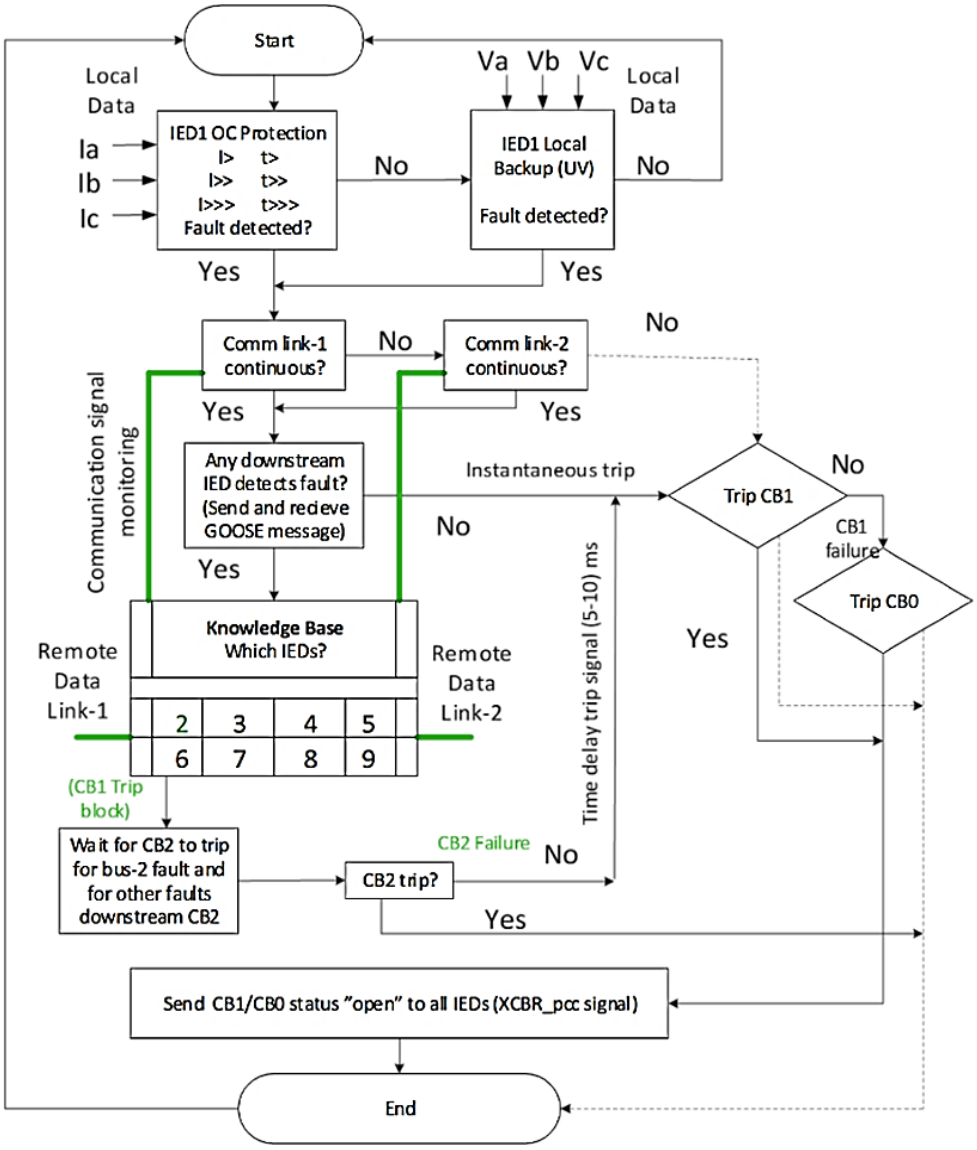

Figure 39. Flow chart of IED1 for providing main and backup protection.

If the status-change about the fault at any downstream IED, for example IED2, is detected, IED1 will wait until CB2 failure is declared by IED2 and then IED1 will issue a tripping command to CB1 to provide a backup protection. In case of communication link-1 and link-2 failure, IED1 will issue a tripping command to CB1 using the normal communication-less definite-time delay setting. The steps and timeline for the multicast (sent), subscribed (received) and tripping command GOOSE messages by IED1 are mentioned in events 1–6 of Figure 40.

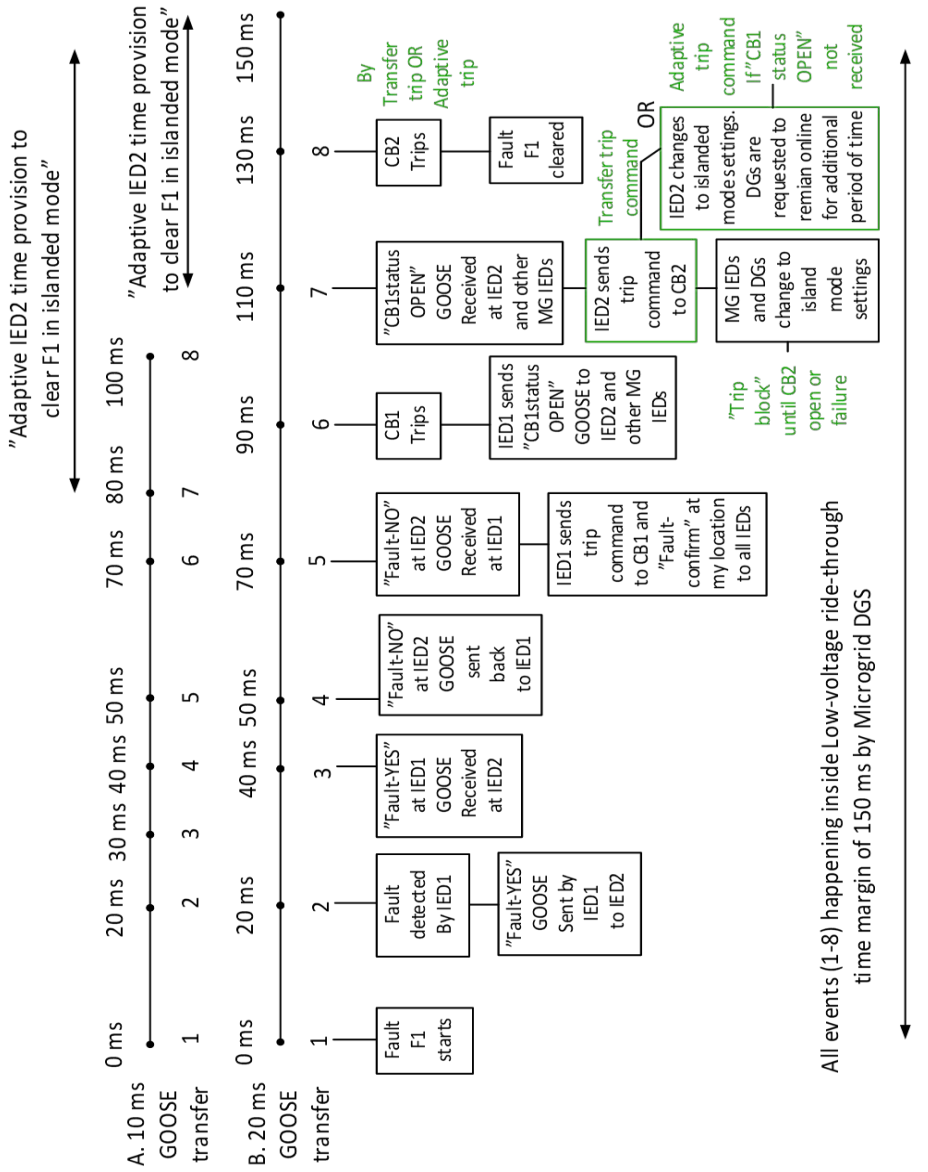

Figure 40. Three-phase fault F1 detection and isolation by IED1 and IED2 using GOOSE message with 10 ms and 20 ms transfer delay.

The communication-based algorithm of Figure 40 can be implemented assuming either a 10 ms or 20 ms transfer time delay for each GOOSE message, depending on practical latency (estimated in Publication IV). From event 7 to onwards is the tripping procedure by which adaptive IED2 isolates the fault F1 completely. The adaptive IED2 normally receives an "Open" status change of CB1 at event 7 and uses it as a transfer trip command by sending a tripping command "Open" to CB2. The fault F1 will clear completely at event 8 after the opening of CB2. At event 7 (transition mode), the control of DERs and the tripping thresholds of IEDs inside the AC microgrid (that is now partly islanded after the opening of CB1) will also change to islanded mode settings. If due to communication failure, IED2 does not

receive an “Open” status of CB1 (transfer trip) at event 7, then it will use adaptive lower settings to detect the fault F1 that is still being energized by the DERs of the AC microgrid, and will issue an adaptive tripping command “Open” to CB2. The adaptive IED2 will have 40–70 ms remaining from the initial 150 ms of the LVRT curve to clear the fault F1 in the transition or partly islanded mode with CB1 open and CB2 still in closed state. In this situation of a partial islanding condition, IED2 may stop the tripping of DERs happening at 150 ms by sending a trip block command in advance at event 7. Then IED2 will send a trip release command after the opening of CB2 for a smooth transition to the islanded mode without a blackout situation. Figure 41 shows the fault current magnitudes at main IED1 and main IED2 during the fault F1 in the grid-connected mode.

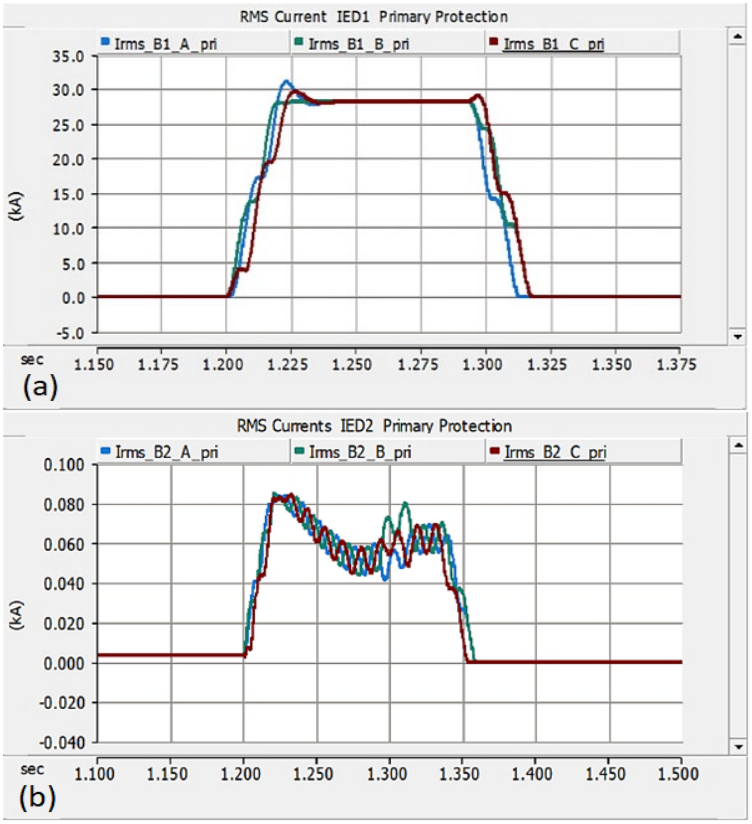

Figure 41. Fault current magnitudes at (a) main IED1 and (b) main IED2 during the fault F1 in the grid-connected mode.

Figure 42 shows the status of CB1 and CB2 with operating times of main IED1 (events 1–6) and main IED2 (events 1–8) during the fault F1 in the grid-connected mode. Figure 43 shows the fault current magnitude and operating time of IED2 providing backup for an unsuccessful transfer trip by IED1 or CB2 failure (event 8 onwards) during the fault F1 in the grid-connected mode. The presented simulation results during the fault F1 in the grid-connected mode prove the effectiveness of the proposed methodology.

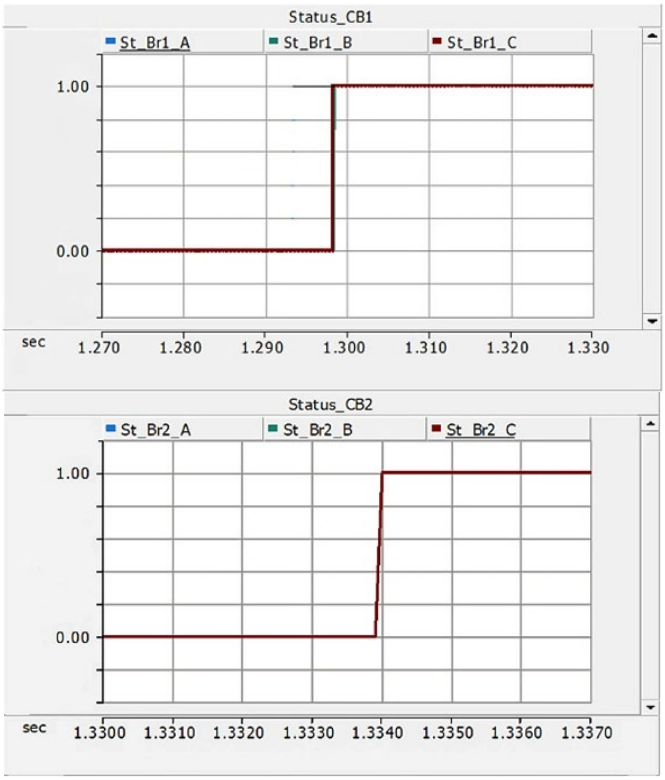

Figure 42. Status of CB1 and CB2 along with operating times of main IED1 and main IED2 during the fault F1 in the grid-connected mode.

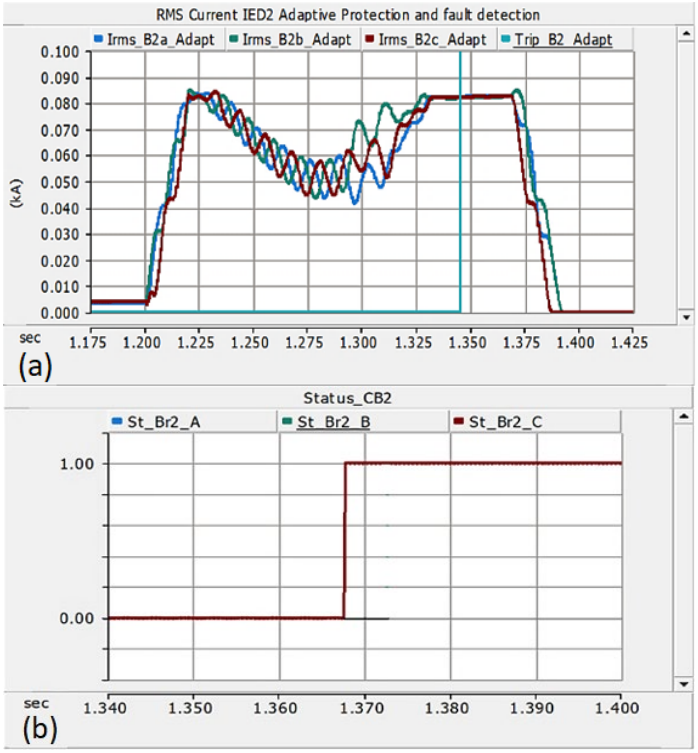

Figure 43. (a) fault current magnitude at IED2 (b) CB2 status and operating time of backup IED2 during the fault F1 in the grid-connected mode.

4.2.2 Three-phase fault F2 in the islanded mode

After the opening of CB1 and CB2, the AC microgrid (encircled with red lines in Figure 37) will transition to the islanded mode. In the islanded AC microgrid, the WTG (2 MVA capacity), a relatively strong source, operates with the grid-forming control, whereas the PV system (0.4 MVA capacity), a relatively weak source, operates with the grid-following control. Figure 44 shows the flow chart of communication-based adaptive IED6 for the detection of three-phase fault F2 and other downstream faults for providing main and backup protection in the islanded mode of an AC microgrid.

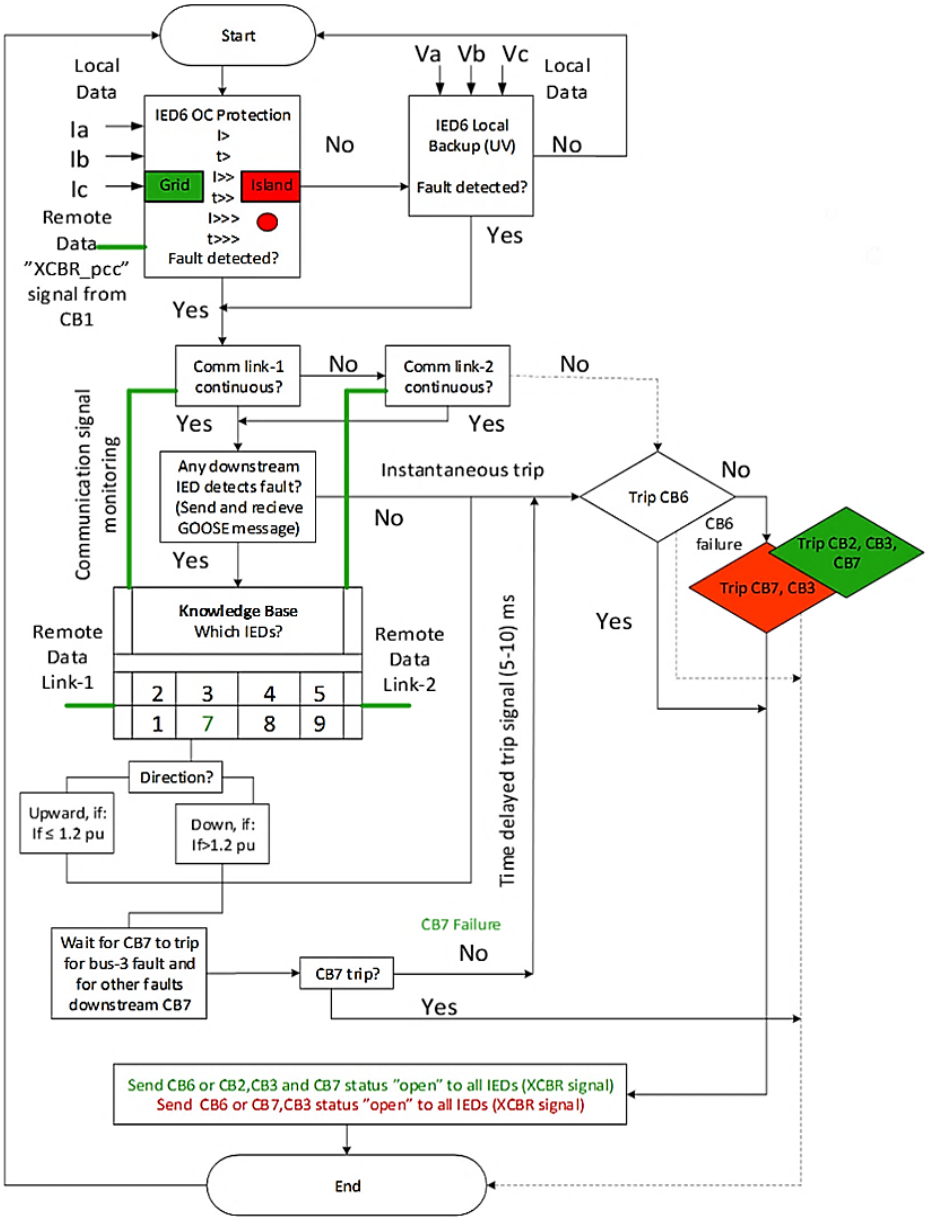

Figure 44. Flow chart of IED6 for providing main and backup protection.

It should be noted that during fault F2, a sufficient fault current magnitude is sensed by IED6 due to the limited but still sufficient fault contribution of the WTG. Therefore, only IEDs 3, 4 and 5 are provided with the lower overcurrent tripping thresholds (red settings), and the rest of the IEDs in the islanded AC microgrid (inside red lines in Figure 37) use the same higher tripping thresholds (green settings) as used in the grid-connected mode. If the WTG was of equal capacity as that of the PV system (configuration 3 of Figure 15), then all IEDs would have required lower overcurrent tripping thresholds in the islanded mode compared to that in the grid-connected mode for the detection of fault F2. Nevertheless, the rest of the communication-based methodology after the fault detection will be the same in both cases with configuration 1 (this case study) and configuration 3 of Figure 15 (Section 2.2.1) in the islanded mode.

According to the flow chart of Figure 44, IED6 will first detect the fault F2 in the islanded mode using the islanded mode overcurrent tripping thresholds or red settings, though in this case study the red settings are the same as the green settings for IED6. For the detection of other faults, an undervoltage function may be required. After the fault detection, IED6 will check if there is any communication link failure signal available. If the communication link is continuous then IED6 will check the received GOOSE messages from other IEDs, particularly downstream IEDs 7, 8, and 9 for a possible downstream fault. If no bursting of GOOSE messages and status changes for fault detection from other IEDs are available, then IED6 will assume “No fault” at the other IEDs and immediately issue a tripping command “Open” to CB6.

IED6 will additionally check the direction of the fault if a status-change about the fault at any downstream IED, for example IED7, is detected. It is assumed that IED6 also receives the magnitude of current at IED7 through an analog GOOSE message. IED6 will check the direction of fault in such a way that if the magnitude of current at IED7 is greater than 1.2 p.u. then the fault is assumed downstream of IED7, otherwise the fault is assumed to be upstream of IED7. This method of fault direction detection is called the “current magnitude comparison” scheme. If the fault is downstream of IED7, then IED6 will wait until a CB7 failure is declared by IED7. After the reception of the CB7 failure message, IED6 will issue a tripping command to CB6 to provide a backup protection. In case of communication link-1 and link-2 failure, IED6 will issue a tripping command to CB6 using the normal communication-less definite-time delay setting. In case CB6 failure happens, IED6 will issue a tripping command to CB3 and CB7 to isolate the fault F2 completely in the islanded mode. The steps and timeline for the multicast (sent), subscribed (received) and tripping command GOOSE messages by IED6 are mentioned in events 1–6 of Figure 45.

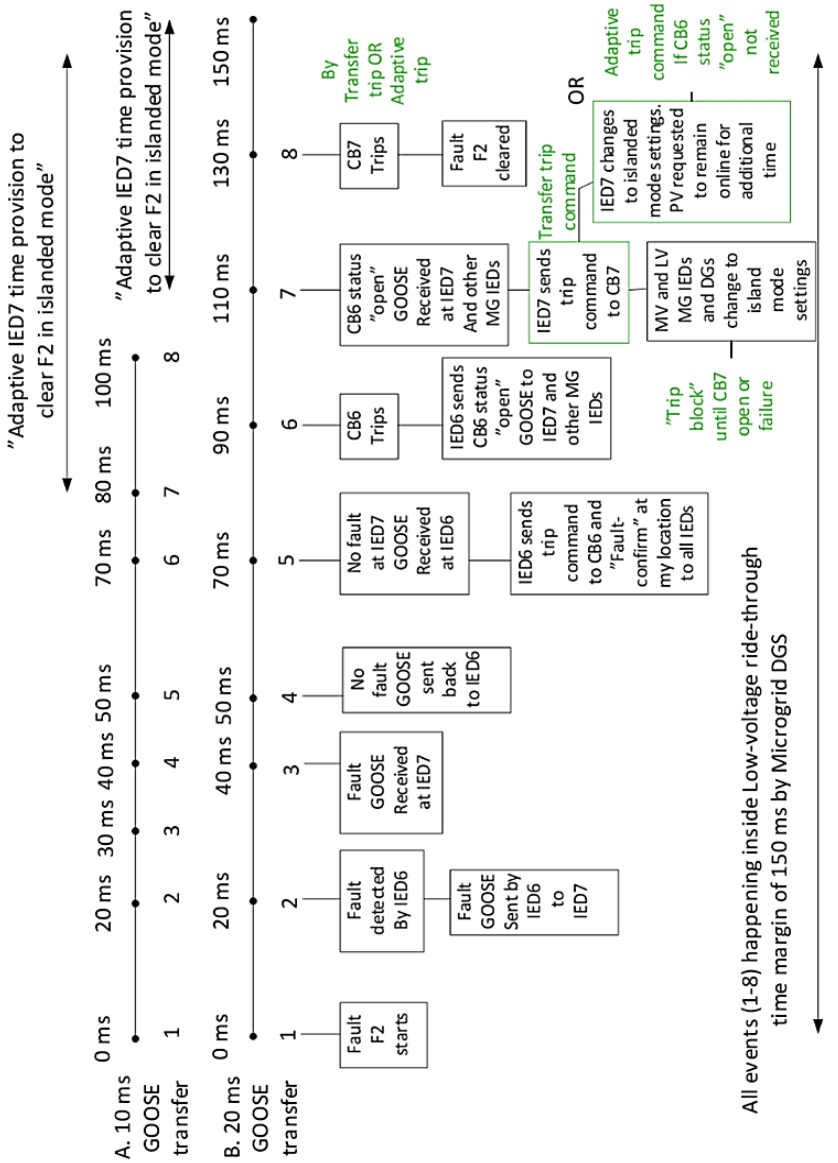

Figure 45. Three-phase fault F2 detection and isolation by IED6 and IED7 using GOOSE message with 10 ms and 20 ms transfer delay.

The communication-based algorithm of Figure 45 can be implemented assuming either a 10 ms or 20 ms transfer time delay for each GOOSE message, depending on practical latency. From event 7 to onwards is the tripping procedure by which adaptive IED7 isolates the fault F2 completely. All of the GOOSE communication procedures followed by IED6 and IED7 during the fault F2 in the islanded mode (Figure 45) will be the same as explained for IED1 and IED2 during the fault F1 in the grid-connected mode (Figure 40). This means that during fault F2 in the islanded mode, IED6 and IED7 will work respectively like IED1 and IED2 during fault F1 in the grid-connected mode.

The selective logic of IED7 for providing main, backup and transfer trip protection is presented in Figure 46. Such protection logics are also implemented for other IEDs in PSCAD simulation, and particularly IED1, IED2, and IED6 for the considered fault cases to produce the results.

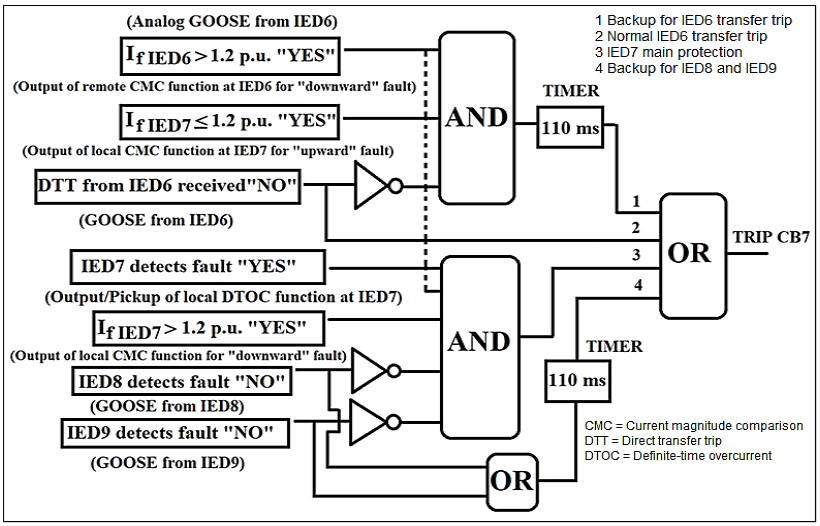

Figure 46. Selective logic of IED7 to provide main and backup protection functions and execution of transfer trip.

Figure 47 shows the fault current magnitudes at main IED6 and main IED7 during fault F2 in the islanded mode.

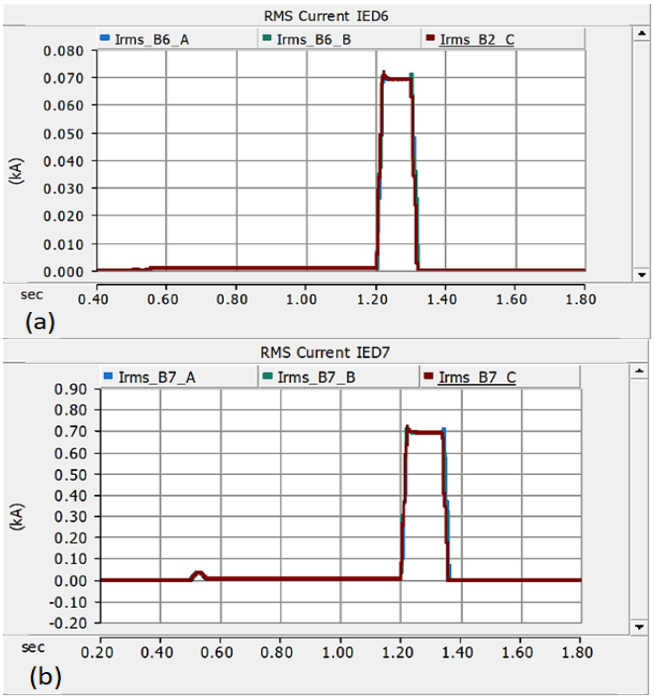

Figure 47. Fault current magnitudes at (a) main IED6 and (b) main IED7 during the fault F2 in the islanded mode.

Figure 48 shows the status of CB6 and CB7 with operating times of main IED6 (events 1–6) and main IED7 (events 1–8) during the fault F2 in the islanded mode. The main IED7 in this case (Figure 48) uses the normal IED6 transfer trip logic 2 of Figure 46. If the normal transfer trip fails, then IED7 will use transfer trip backup logic 1 of Figure 46 or use an adaptive local trip just like IED2. The presented simulation results during the fault F2 in the islanded mode prove the effectiveness of the proposed methodology.

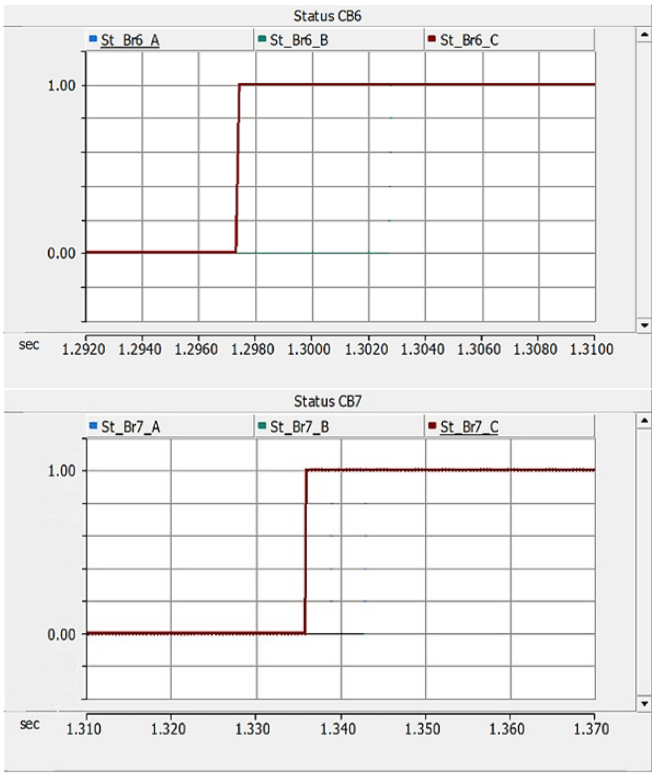

Figure 48. Status of CB6 and CB7 along with operating times of main IED6 and main IED7 during the fault F2 in the islanded mode.

After the successful detection and isolation of the fault F2 in the islanded mode, the already islanded AC microgrid (within red lines in Figure 37) will be further subdivided into two separate islanded sections: the islanded MV system supplied by the WTG and the islanded LV system supplied by the PV system. These newly created islanded systems within the islanded AC microgrid are encircled by orange and green color rings in Figure 37. In this situation, only the IEDs within the islanded LV section (IED8 and IED9) will need to change their settings to lower threshold settings, along with the control of PV system to be changed from the previous grid-following to the new grid-forming control. The WTG was already adapted to the grid-forming control and IEDs 3, 4 and 5 were already using lower setting groups in the combined islanded mode (within red lines in Figure 37).

4.3 Real-time validation of adaptive protection

In the previous case study of Section 4.2, an adaptive protection for radial AC microgrids using IEC 61850 communication standard was proposed using PSCAD-based offline simulations. In order to validate the proposed communication-based adaptive protection, a real-time (RT) CHIL simulation has been carried out using an actual IED (VAMP 52) and the RT simulator featured in Publication IV. Section 4.3 presents the results of the performed RT CHIL validation testing of logically selective adaptive protection in Publication IV. This case study also uses the same MATLAB/Simulink model with central BESS for the islanded mode of operation as was used in case study of Section 4.1. The Simulink model of a radial AC microgrid shown in Figure 49 has been converted into the required format of RT-LAB software, that is an OPAL-RT simulation platform software used for real-time simulation-based testing. Additionally, an IEC 61850 GOOSE protocol has been integrated into the model for an adaptive protection testing. The topmost view of the used RT simulation model and CHIL testing setup used in the laboratory are shown in Figure 50 (a) and (b), respectively. In Figure 49, each CB is operated by the IED of the related number. For example, CB1 is operated by IED1, and so on.Further details can be found in Publication IV.

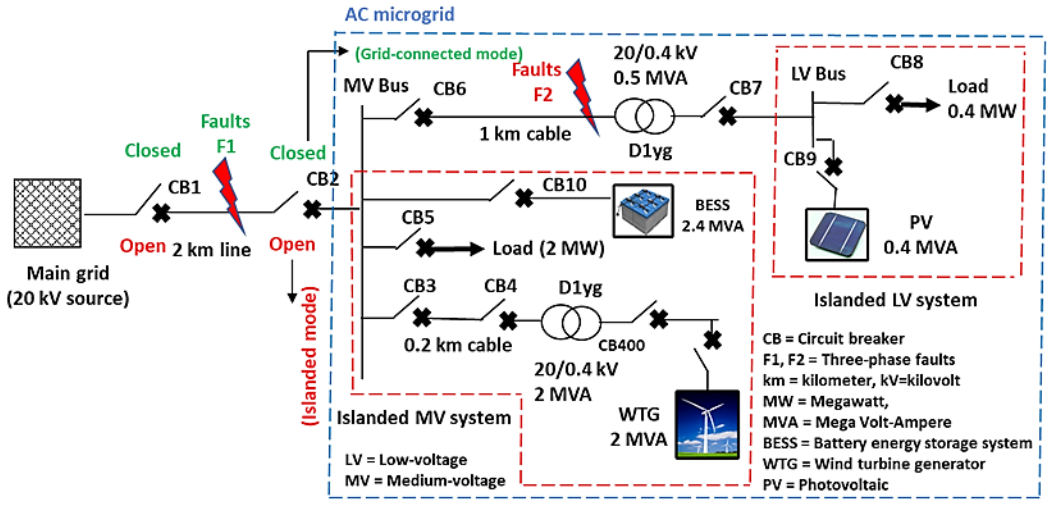

Figure 49. A radial AC microgrid model used for real-time simulation testing.

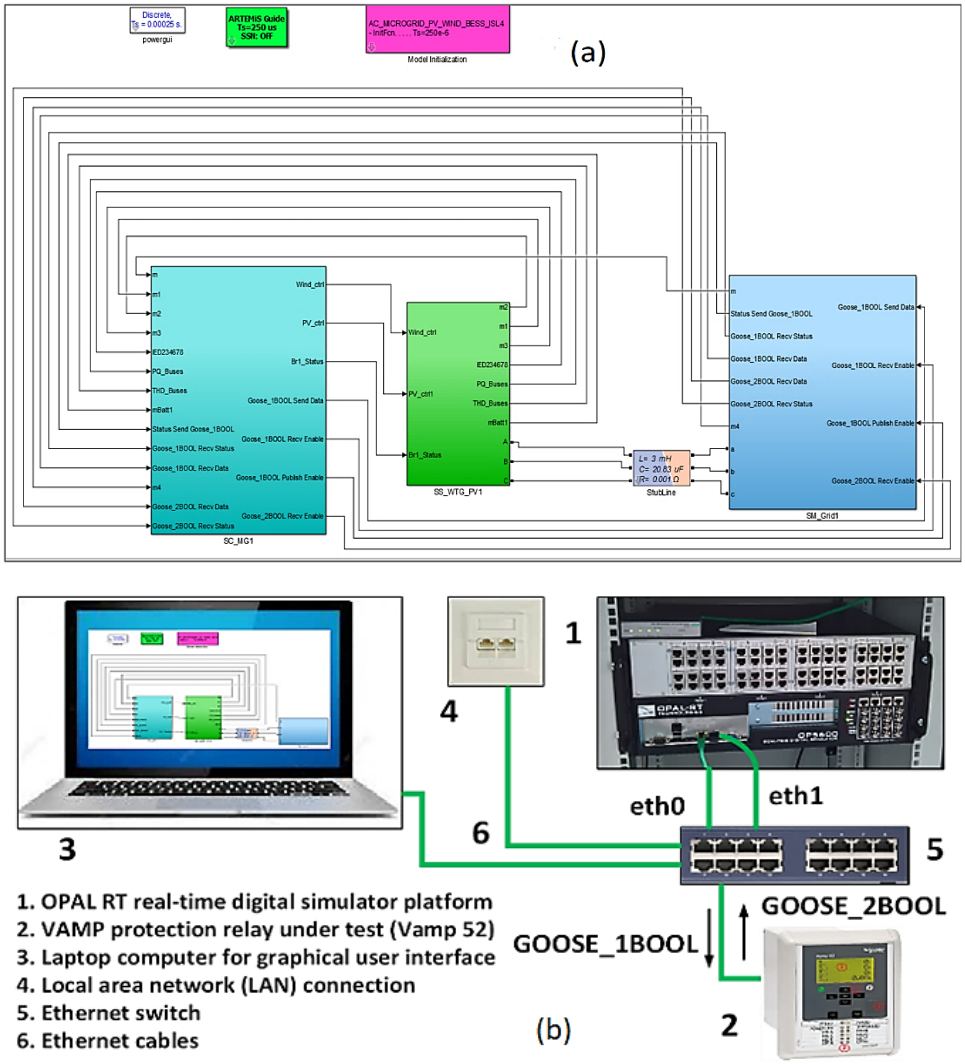

Figure 50. (a) RT simulation model and (b) CHIL testing platform.

One of the critical criteria for the acceptable performance of IEDs for IEC 61850 communication standard compliance is not only to test the successful publication and subscription of multicast messages, but also to test the minimum transfer and reception time delays of the time-critical signals including circuit breaker status signals, transfer trip commands, and pickup signals. Conventionally, the ping command using the IP address of the hosting computer or other device in the network is used for testing the IP-level network connectivity and an estimation of round-trip communication delay. The other method closely related to this case study is the analysis of the time delay of the stamped GOOSE messages saved in the buffer memory of IEDs. In this method, IEDScout or other software can be used for the round-trip delay estimation. The RT simulator offers a better method of round-trip delay estimation between two IEDs exchanging information using IEC 61850 communication protocols. Moreover, the use of an RT simulation model of the actual power system enables us to verify and validate the

communication protocols. Thus, the consequences of delayed trip messages can also be observed using the RT simulation method.

Figure 51 shows the procedure of estimation of round-trip communication delay of a Boolean GOOSE message between the RT simulator and VAMP protection relay. According to this method, the fault detection Boolean signal is first published by the RT simulator or target using a GOOSE-1BOOL message that is subscribed by VAMP relay, used for OR protection logic inside the relay, and the resulting "Logic output1" is then published as a GOOSE-2BOOL message by the VAMP relay and finally subscribed by the RT simulator or target and saved as a MAT file. The round-trip delay (t_{RTT}) is composed of seven individual delays: $t_{out\text{-}TARGET}$, $t_{net\text{-}GOOSE\text{-}1BOOL}$, $t_{in\text{-}HUT}$, $t_{app\text{-}LOGIC}$, $t_{out\text{-}HUT}$, $t_{net\text{-}GOOSE\text{-}2BOOL}$, and $t_{in\text{-}TARGET}$. It is a challenging task to estimate these seven individual delays because a time stamp is required at each input and output of the RT target, Ethernet switch, VAMP relay and OR logic inside the relay. The publication of a GOOSE message from one Ethernet port (eth0) of the RT target and the subscription of the same GOOSE message from the other Ethernet port (eth1) provides a method of estimating t_{Target} ($t_{out\text{-}TARGET} + t_{net\text{-}GOOSE\text{-}1BOOL} + t_{in\text{-}TARGET}$). The same method is used for the round-trip time delay (t_{RTT}) estimation (Figure 52).

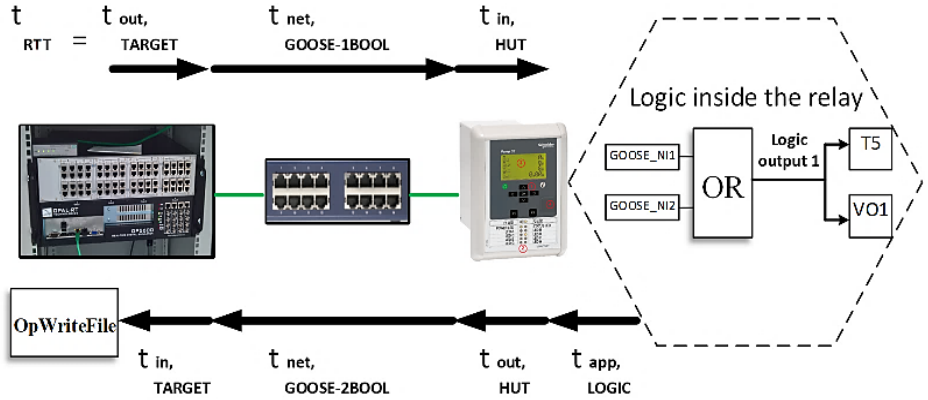

Figure 51. Round-trip time delay estimation using RT simulation.

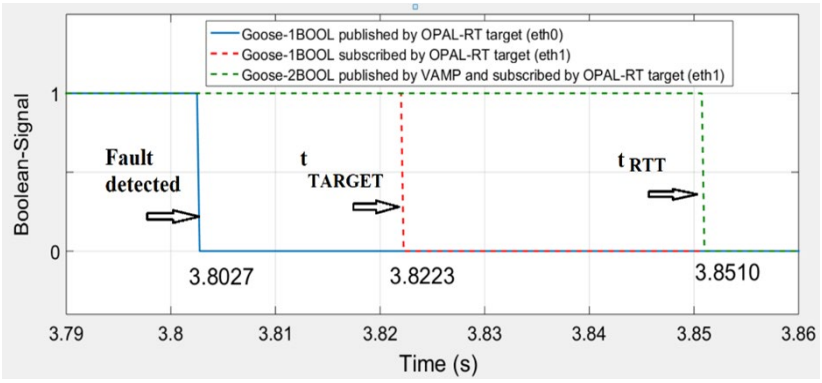

Figure 52. Estimated round-trip time delay (t_{RTT}) of Boolean signal.

The round-trip delay (t_{RTT}) is equivalent to the time delay between event 2 and event 5 (t_{25}) of the proposed adaptive protection algorithm presented in Figure 40 and Figure 45. The testing results are considered as validated if $t_{RTT} = t_{25}$ is estimated within the range of 30–50 ms considering 10 ms and 20 ms GOOSE transfer delays in the proposed algorithms (Figure 40 and Figure 45). Figure 53 shows the results of three best case test scenarios performed for the estimation of transfer delay $t_{RTT} = t_{25}$. The average transfer delay of three tests is 46.76 ms which is inside the range of 30–50 ms in the proposed algorithm, and therefore validates the application of the proposed algorithm.

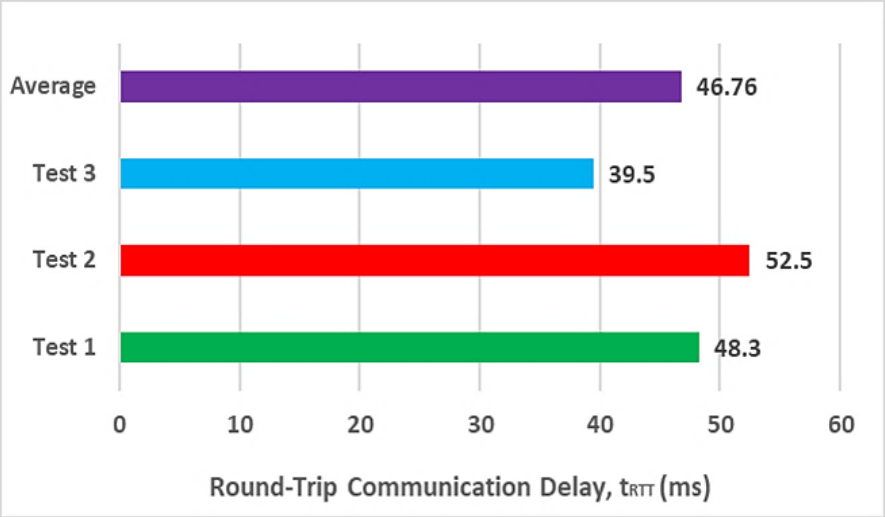

Figure 53. Three best case results of round-trip time delay testing.

The worst-case round-trip time delay of 90 ms was observed for the same testing case at another time of testing. This indicates the nondeterministic nature of the communication delays, and therefore several tests are required to find out the minimum and maximum transfer delay for the final control and protection applications. Another problem of missing data or communication failure for a brief time period of 10 ms was also observed during the tests. Therefore, a Boolean signal continuity check of status-0 for a duration of 20 ms was suggested as a remedy to avoid false tripping of the relay. This kind of missing data handling technique for Boolean as well as analog signals can be used inside relays as well as the simulation models to avoid false tripping. The signal continuity check will add security to relays, however, an extended LVRT curve up to 250 ms will be required.

The choice of changing the protection settings of IEDs and the activation of BESS in the islanded mode or transition to islanded mode are dependent on whether the “CB1 Open” or “CB2 Open” status signal is used as input to the algorithm during the fault F1 (Figure 49). In Publication II, “CB1 Open” signal is used as input for changing the protection settings of IEDs and an activation of grid-forming control

(event 7 of Figure 40) due to the absence of BESS in that case (Section 4.2). In Publication IV, “CB2 Open” signal is used for changing the protection settings of IEDs and the activation of BESS in the islanded mode. The choice also depends on whether the centralized or decentralized communication-based scheme is used for the AC microgrid. Using the centralized communication-based scheme the “CB1 Open” event occurs first, whereas using the decentralized communication-based scheme, the “CB2 Open” event happens first as shown in Figure 54 and Figure 55. So, using “CB1 Open” signal for the centralized communication-based scheme and “CB2 Open” for the decentralized communication-based scheme will be a natural choice. Nevertheless, using “CB2 Open” for the centralized communication-based scheme will only delay the process for just 10–20 ms, a shift from event 7 to event 8 as done in Figure 54. In any case, the IEDs will be in a “trip block” state until the voltage, frequency and current are restored to normal values after the transition to the islanded mode. The results look promising even though CB2 tripping was delayed up to 184 ms (Figure 56) after CB1 opening at 3.851 s due to RT simulation settings and limitations, but still the time taken for the complete transition to the islanded mode was 280 ms. The detailed simulation results are presented in Publication IV.

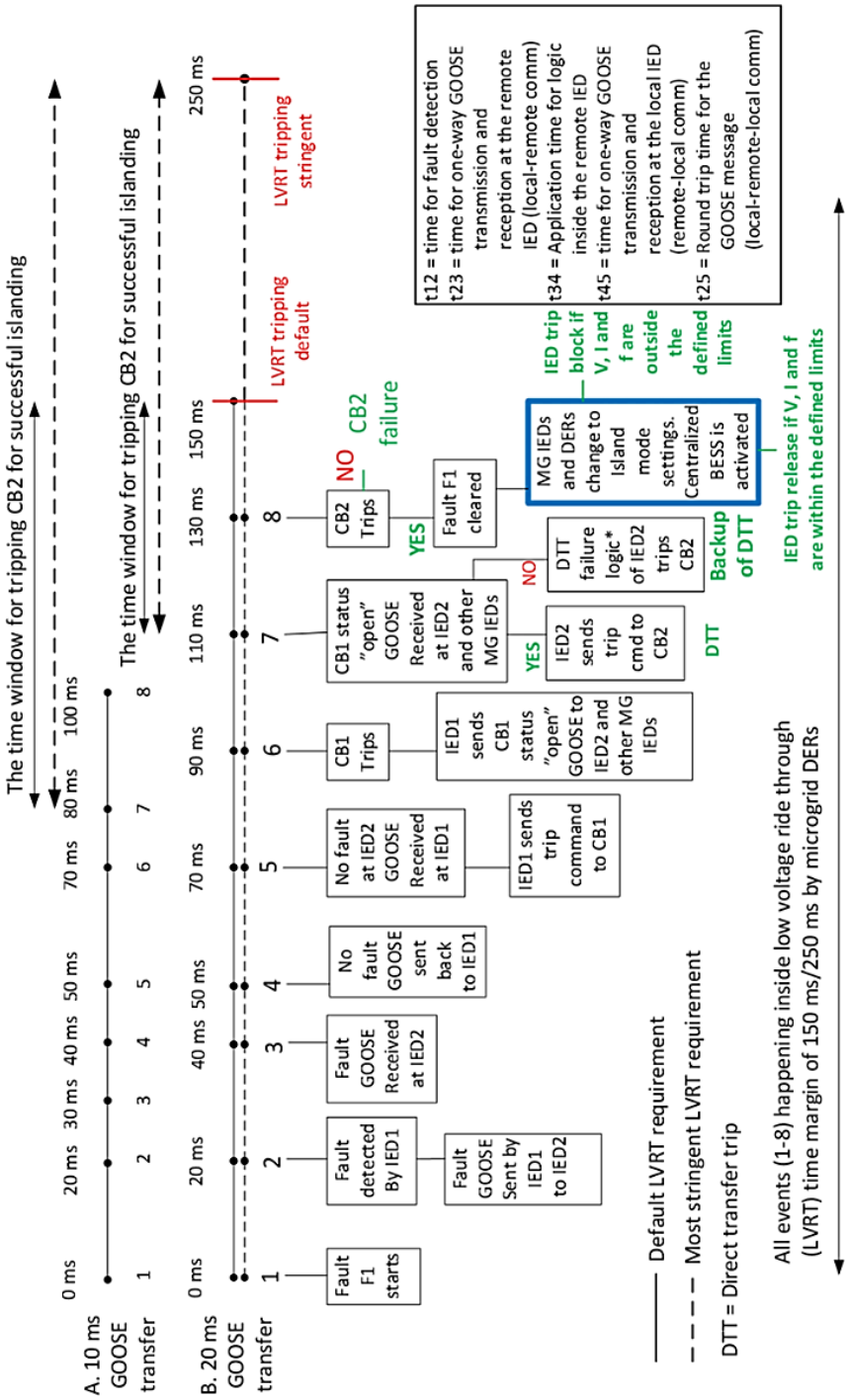

Figure 54. Communication-dependent logically selective adaptive protection algorithm using centralized communication.

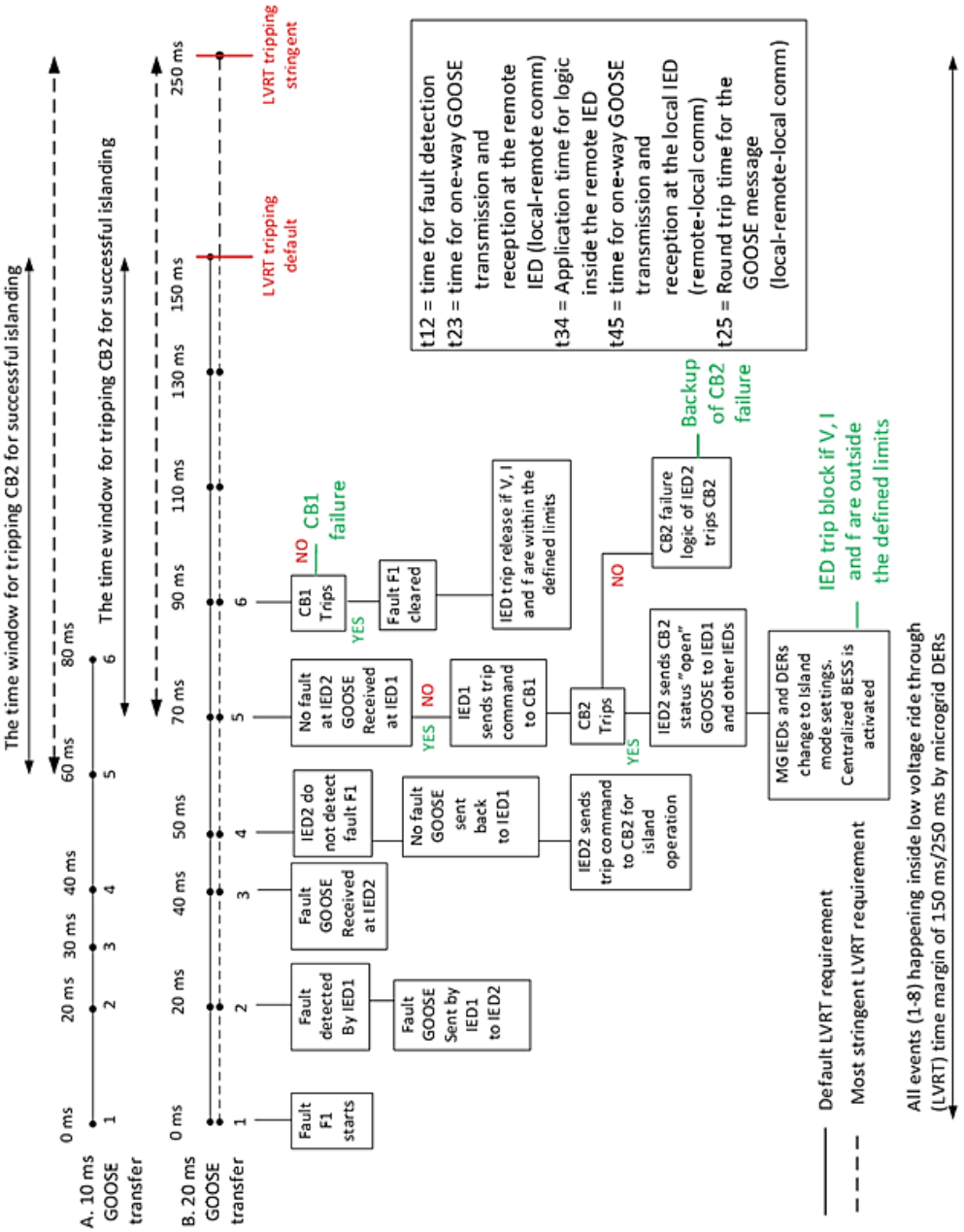

Figure 55. Communication-dependent logically selective adaptive protection algorithm using decentralized communication.

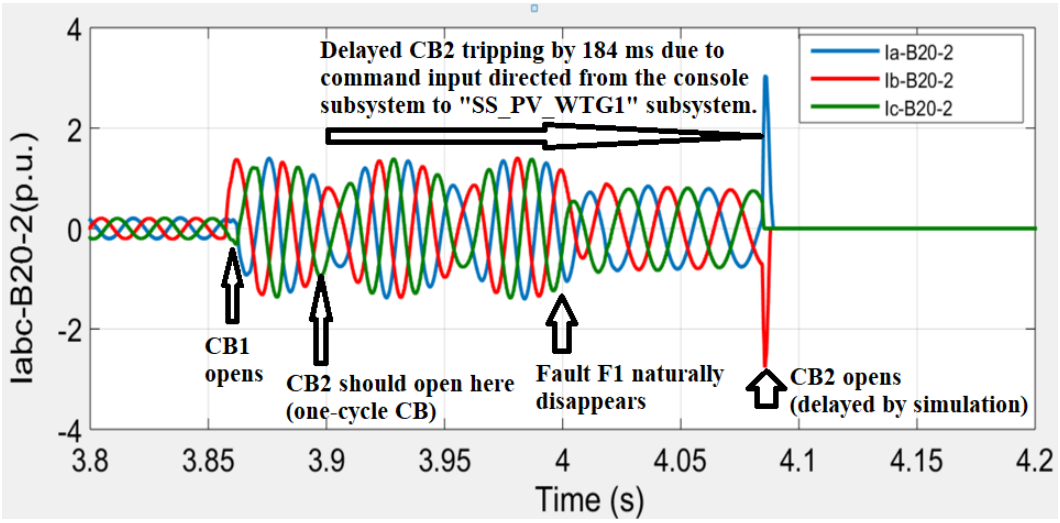

Figure 56. Three-phase current at CB2 during the grid-side fault F1.

4.4 Impact of battery storage on adaptive protection

In this section the results of a case study that evaluates the impact of distributed battery storages on adaptive protection of radial AC microgrids are presented as reported in Publication VI of this thesis. This case study is based on offline simulations with PSCAD software using the grid-forming and grid-following controls of DERs as discussed in Section 2.1.5, and as used in the previous case study of Section 4.2 in this thesis. The harbor area AC microgrid model used for this case study is presented in Figure 57. The focus of this case study is to evaluate whether the higher grid-connected mode settings of definite-time overcurrent IEDs could also be used in different islanded modes of a radial AC microgrid if distributed BESS and DERs provide a fault current contribution of 1.2–3 p.u. of the rated current. Thus, the case study serves to find out whether an adaptive protection scheme could be avoided with different fault current contribution levels of BESS and DERs. It is also checked whether fast acting fuses can operate in the islanded mode during remote three-phase short-circuit faults with the considered fault current contribution levels of DERs.

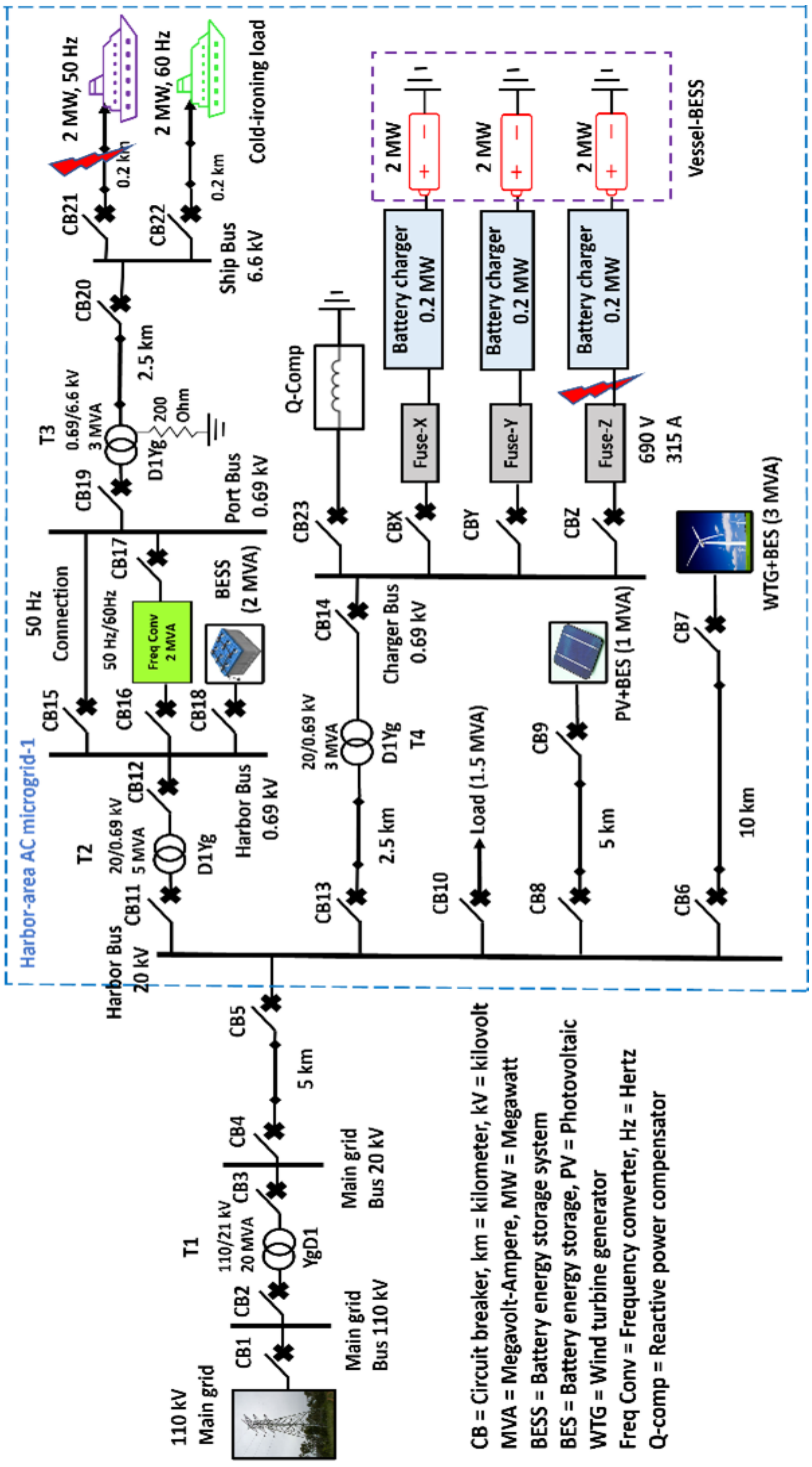

Figure 57. The harbor area radial AC microgrid with DERs and distributed BESS.

The operational modes of the harbor area AC microgrid-1 (Figure 57) can be broadly divided into two categories: grid-connected mode and islanded mode. Each of the two mentioned operational modes can be subdivided into two further modes: power supply to cold-ironing load with no slow-charging of vessel-BESS,

and slow-charging of vessel-BESS during the night with no cold-ironing load. Again, during the power supply to cold-ironing load, it should be considered if the vessel type or cold-ironing load type is 50 Hz or 60 Hz. If the vessel type or cold-ironing load type is 60 Hz, then it has to be supplied through a frequency converter that can only provide fault current up to twice the magnitude of the nominal current. However, only 50 Hz cold-ironing load is considered in this case study.

The number of overcurrent IEDs is equal to the number of CBs at various locations in Figure 57, and each CB is operated by the IED of the related number. For example, CB1 is operated by IED1, and so on. The frequency converter and battery chargers are primarily protected with fast acting fuses and local overcurrent IEDs act as backup for the fuses. In this paper, only the overcurrent function has been considered for the proposed radial AC microgrid-1 (Figure 57), therefore, all IEDs referred to in the following subsections are IEDs with definite-time coordination.

The magnitude of maximum load current ($I_{\text{max-load}}$) at each IED has been found with different combinations of DERs in the grid-connected mode as presented in Table 11. These magnitudes of maximum load currents ($I_{\text{max-load}}$) at each IED are selected for the grid-connected mode overcurrent settings. The pickup currents of all two-stage overcurrent IEDs have been set at 2.5 times $I_{\text{max-load}}$ for the overcurrent stage ($I>>$) and 1.25 times $I_{\text{max-load}}$ for the overload stage ($I>$). As mentioned earlier, the 60 Hz cold-ironing load is not considered in this case study, therefore, IED16, 17 and 22 are excluded from the fault analysis and evaluation. The harbor-BESS has been analyzed only in the islanded mode, hence, IED18 is not considered in the grid-connected mode. The details of how the magnitudes of $I_{\text{max-load}}$ at different IEDs have been determined and what threshold settings and protection coordination delays are used can be found in Publication VI.

Table 11. Magnitudes of maximum load currents at IEDs with different combinations of DERs in the grid-connected mode.

IED No.	$I_{\text{max-load}}$ (A)	IED No.	$I_{\text{max-load}}$ (A)	IED No.	$I_{\text{max-load}}$ (A)	IED No.	$I_{\text{max-load}}$ (A)
IED1	20.1	IED6	82.06	IED11	64.8	IED19	1790
IED2	20.1	IED7	79.68	IED12	1870	IED20	187
IED3	106.8	IED8	28.73	IED13	18.63	IED21	176.14
IED4	106.8	IED9	27.44	IED14	540		
IED5	107.5	IED10	45.42	IED15	1682.9		

In this case study, first the settings of overcurrent IEDs and the operating time of fuses during the remote three-phase short-circuit faults in the grid-connected mode are evaluated. Then, the evaluation of the same settings of overcurrent IEDs and the operating time of fuses are carried out during three-phase short-circuit

faults in six different islanded modes. These are discussed in the following Sections 4.4.1–4.4.2.

4.4.1 Three-phase faults in the grid-connected mode

There are two different operational configurations of the grid-connected mode considered for the harbor area AC microgrid-1 (Figure 57) as shown in Figure 58. The power supply to cold-ironing load with no slow-charging of vessel-BESS is shown in Figure 58 (a), and the slow-charging of vessel-BESS during the night with no cold-ironing load is shown in Figure 58 (b). The CBs shown in green color are active or closed CBs, and the CBs in red color are inactive or open CBs in Figure 58. A three-phase short-circuit fault at 50 Hz cold-ironing load is considered during the power supply to the cold-ironing load mode of operation. Similarly, a three-phase short-circuit fault at battery charger-Z terminal is considered during the slow-charging of the vessel-BESS mode of operation. The arrows in red color indicate the direction, flow or path of the fault current in Figure 58. The I_{fg} indicates the fault current contribution from the main grid, I_{fwtg} indicates the fault current contribution from the WTG and I_{fdg} indicates the combined fault current contribution from the WTG and PV system in Figure 58. The fuse used at the terminal of battery charger-Z in Figure 58 (b) is of gG-type with ratings of 690 V and 315 A.

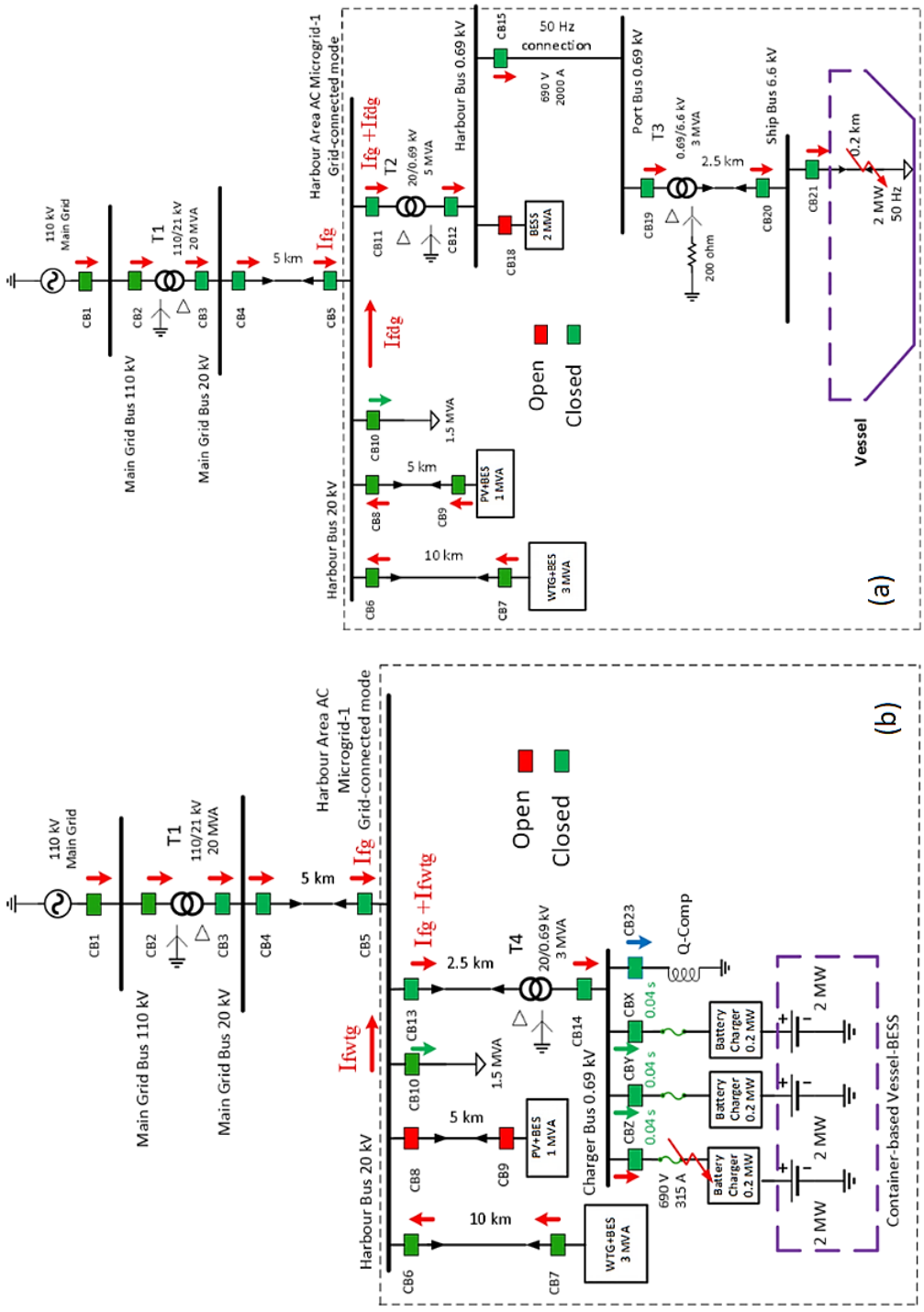

Figure 58. Two configurations of the harbor area radial AC microgrid-1 in the grid-connected mode: (a) power supply to 50 Hz cold-ironing load and (b) slow-charging of vessel-BESS.

Table 12 shows the magnitudes of fault currents at all active or closed IEDs during a three-phase short-circuit fault at 2 MW, 50 Hz cold-ironing load in the grid-connected mode of Figure 58 (a) when supplied by the main grid, WTG and PV

system. After comparing the magnitudes of fault currents in Table 12 with the magnitudes of maximum load currents in Table 11, it can be seen that except for IEDs 6, 7, 8, and 9, the magnitudes of fault currents at all other IEDs in the fault path are greater than 2.5 times $I_{\text{max-load}}$. Therefore, all IEDs in the fault path except IEDs 6, 7, 8, and 9 will pick up and trip the corresponding CBs according to the set definite-time coordination. Figure 59 shows the fault current magnitudes of each phase accompanied by the tripping signal of primary IED21 and the pickup signal of the first remote backup IED20. It is clear from Figure 59 (a) that during a three-phase short-circuit fault at 50 Hz cold-ironing load, the primary IED21 trips within 20 ms after the fault at a simulation time of 1.2 s (status changes from 0 to 1 at 1.22 s). Figure 59 (b) shows that the first remote backup IED20 also picks up during this fault and will provide backup for IED21 if it fails.

Table 12. Magnitudes of fault currents at active or closed IEDs during a three-phase short-circuit fault at 50 Hz cold-ironing load when supplied by main grid, WTG and PV system.

IED No.	I_{fault} (A)	IED No.	I_{fault} (A)	IED No.	I_{fault} (A)	IED No.	I_{fault} (A)
IED1	110.2	IED5	591.5	IED9	32.52	IED15	18554
IED2	110.2	IED6	94.81	IED10	38.1	IED19	18561.5
IED3	588	IED7	92.95	IED11	642	IED20	1937.47
IED4	588	IED8	33.55	IED12	18580	IED21	1937.47

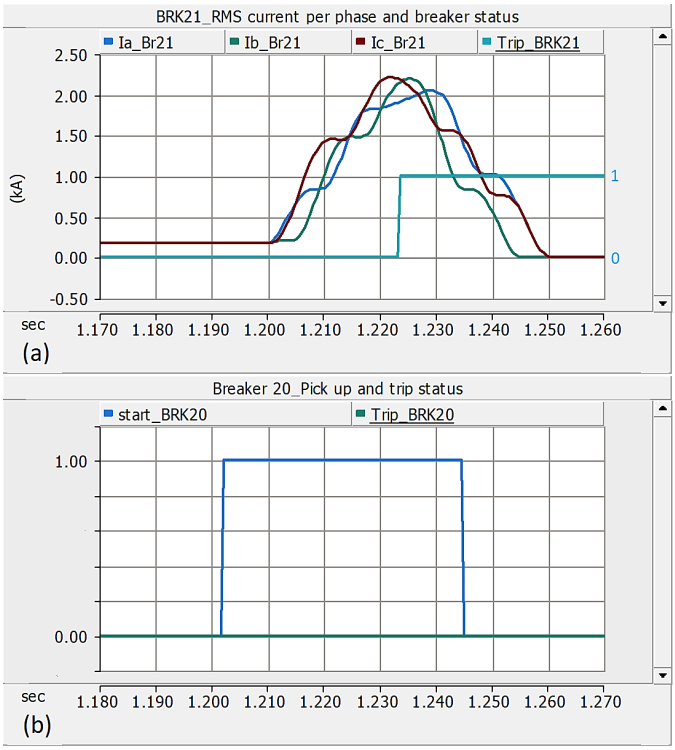

Figure 59. (a) magnitude of current and tripping signal of IED21 and (b) pickup signal of IED20 during a three-phase short-circuit fault at 50 Hz cold-ironing load in the grid-connected mode.

Table 13 shows the magnitudes of fault currents at all active or closed IEDs during a three-phase short-circuit fault at battery charger-Z terminal in the grid-connected mode of Figure 58 (b) when supplied by the main grid and WTG. After comparing the magnitudes of fault currents in Table 13 with the magnitudes of maximum load currents in Table 11, it can be seen that except for IEDs 6 and 7, the magnitudes of fault currents at all other IEDs in the fault path are greater than 2.5 times $I_{\text{max-load}}$. Therefore, all IEDs in the fault path except IEDs 6 and 7 will pick up and trip the corresponding CBs according to the set definite-time coordination. Figure 60 (a) shows the fault current flowing through fuseZ and Figure 60 (b) shows the tripping or blown status of fuseZ acting as the primary protection device. Figure 61 (a) shows the fault current magnitudes of each phase at IEDZ and Figure 61 (b) shows the tripping and pickup signals of the first remote backup IEDZ. It is clear from Figure 60 (b) that during a three-phase short-circuit fault at battery charger-Z terminal, fuseZ trips within 20 ms after the fault at simulation time of 1.2 s (status changes from 0 to 1 at 1.22 s). Figure 61 (b) shows that the first remote backup IEDZ also picks up during this fault and provides backup for fuseZ by tripping at a simulation time of 1.24 s that is within 20 ms after fuseZ fails to blow at 1.22 s.

Table 13. Magnitudes of fault currents at active or closed IEDs during a three-phase short-circuit fault at battery charger-Z terminal when supplied by main grid, and WTG.

IED No.	I_{fault} (A)	IED No.	I_{fault} (A)	IED No.	I_{fault} (A)	IED No.	I_{fault} (A)
IED1	213	IED5	1145	IED13	1210	IEDZ	35000
IED2	213	IED6	105	IED14	35100		
IED3	1144	IED7	103.5	IEDX	100		
IED4	1144	IED10	30.7	IEDY	100		

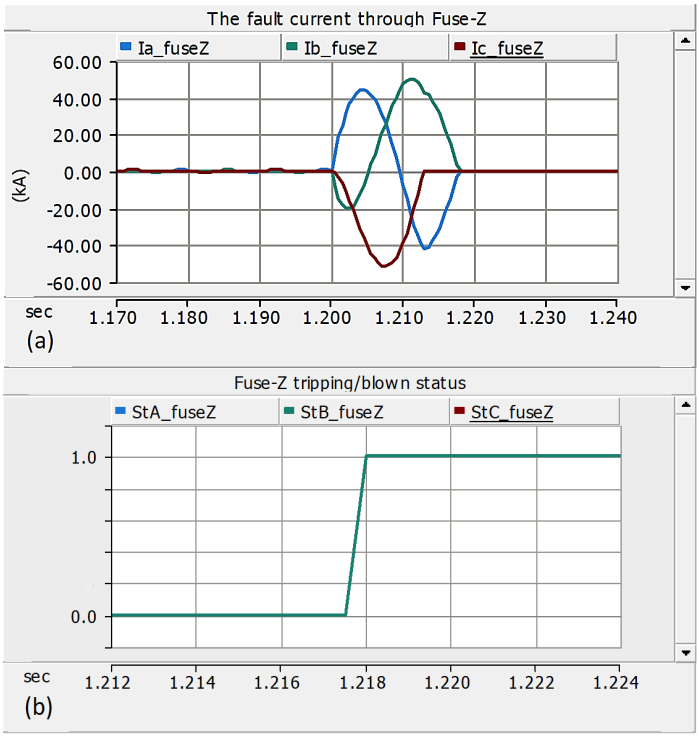

Figure 60. (a) magnitude of fault current through fuseZ and (b) tripping or blown status of fuseZ during a three-phase short-circuit fault at battery charger-Z terminal in the grid-connected mode.

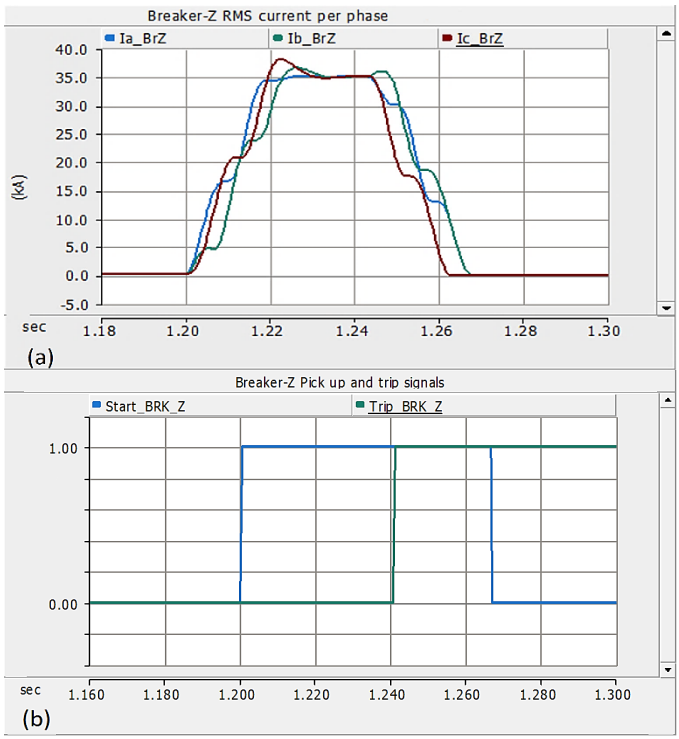

Figure 61. (a) magnitude of current at IEDZ and (b) pickup and tripping signals of backup IEDZ during a three-phase short-circuit fault at battery charger-Z terminal in the grid-connected mode.

4.4.2 Three-phase faults in the islanded mode

There are six different configurations considered for the islanded mode operation of the harbor area radial AC microgrid-1 (Figure 57) as shown in Figure 62.

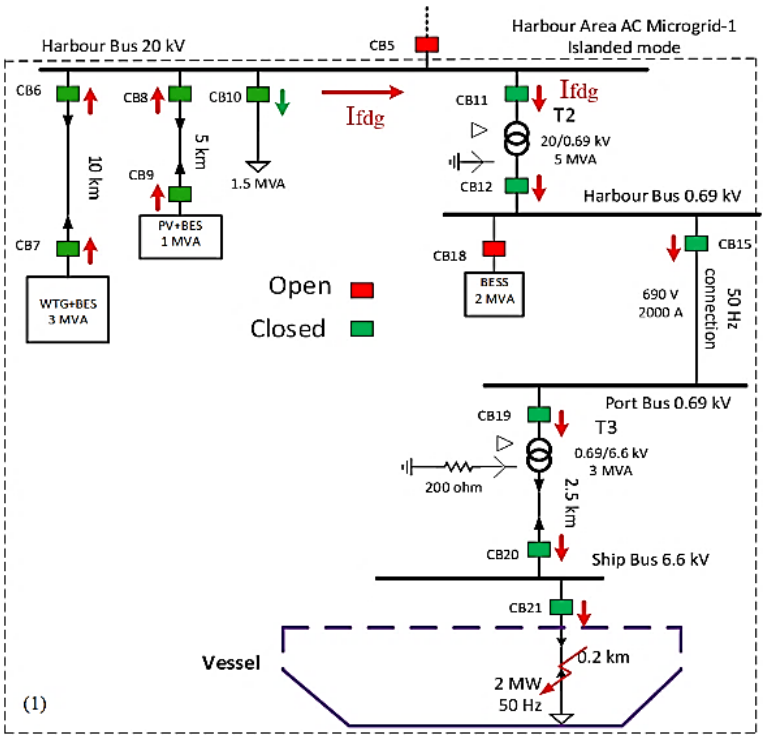

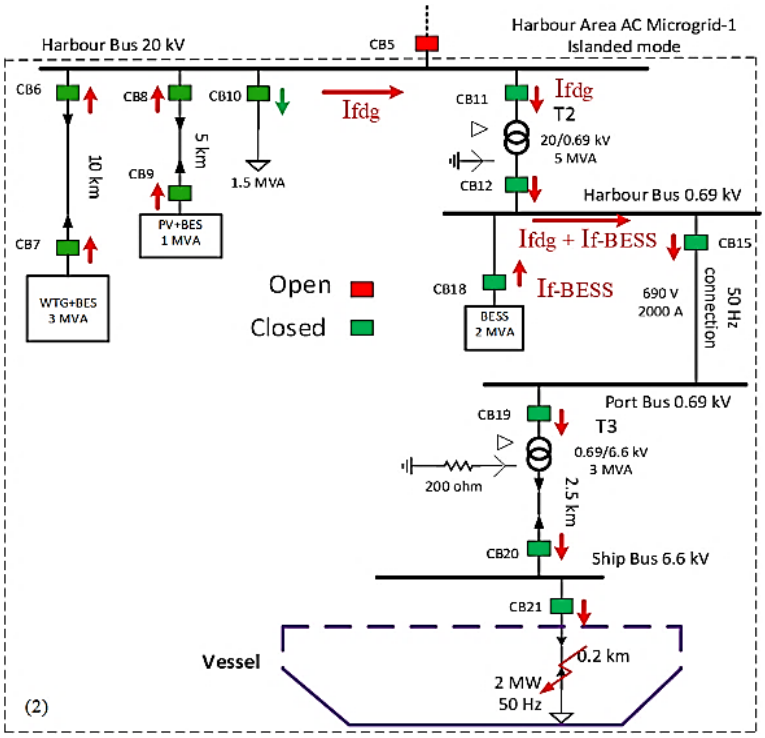

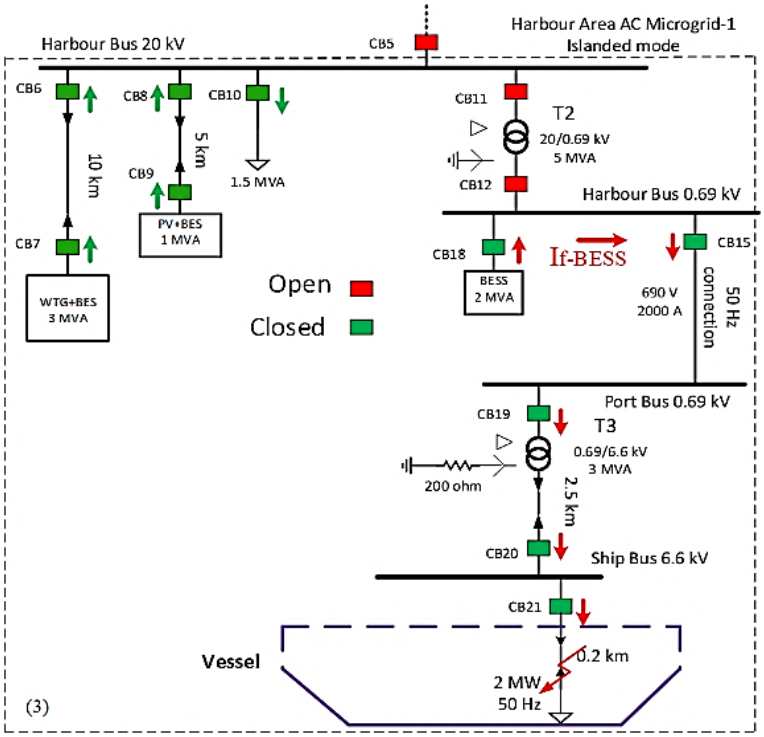
Harbour Bus 20 kV
CB5
Harbour Area AC Microgrid-1
Islanded mode
CB6
CB8
CB10
CB11
T2
20/0.69 kV
5 MVA
10 km
5 km
CB9
1.5 MVA
CB12
Harbour Bus 0.69 kV
PV+BES
1 MVA
CB7
CB18
If-BESS
CB15
WTG+BES
3 MVA
Open
Closed
BESS
2 MVA
690 V
2000 A
50 Hz
connection
Port Bus 0.69 kV
CB19
T3
0.69/6.6 kV
3 MVA
200 ohm
2.5 km
CB20
Ship Bus 6.6 kV
CB21
Vessel
0.2 km
2 MW
50 Hz
(3)

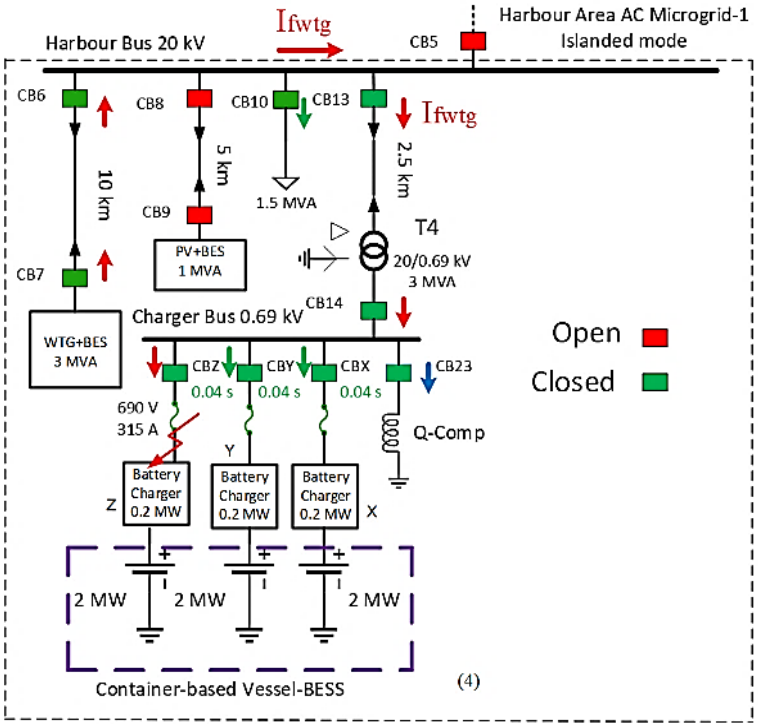
Ifwtg
Harbour Bus 20 kV
CB5
Harbour Area AC Microgrid-1
Islanded mode
CB6
CB8
CB10
CB13
Ifwtg
10 km
5 km
2.5 km
1.5 MVA
CB9
T4
PV+BES
1 MVA
20/0.69 kV
3 MVA
CB7
CB14
Charger Bus 0.69 kV
WTG+BES
3 MVA
Open
Closed
CBZ
CBY
CBX
CB23
0.04 s
0.04 s
0.04 s
690 V
315 A
Q-Comp
Y
Battery
Charger
0.2 MW
Z
X
2 MW
2 MW
2 MW
Container-based Vessel-BESS
(4)

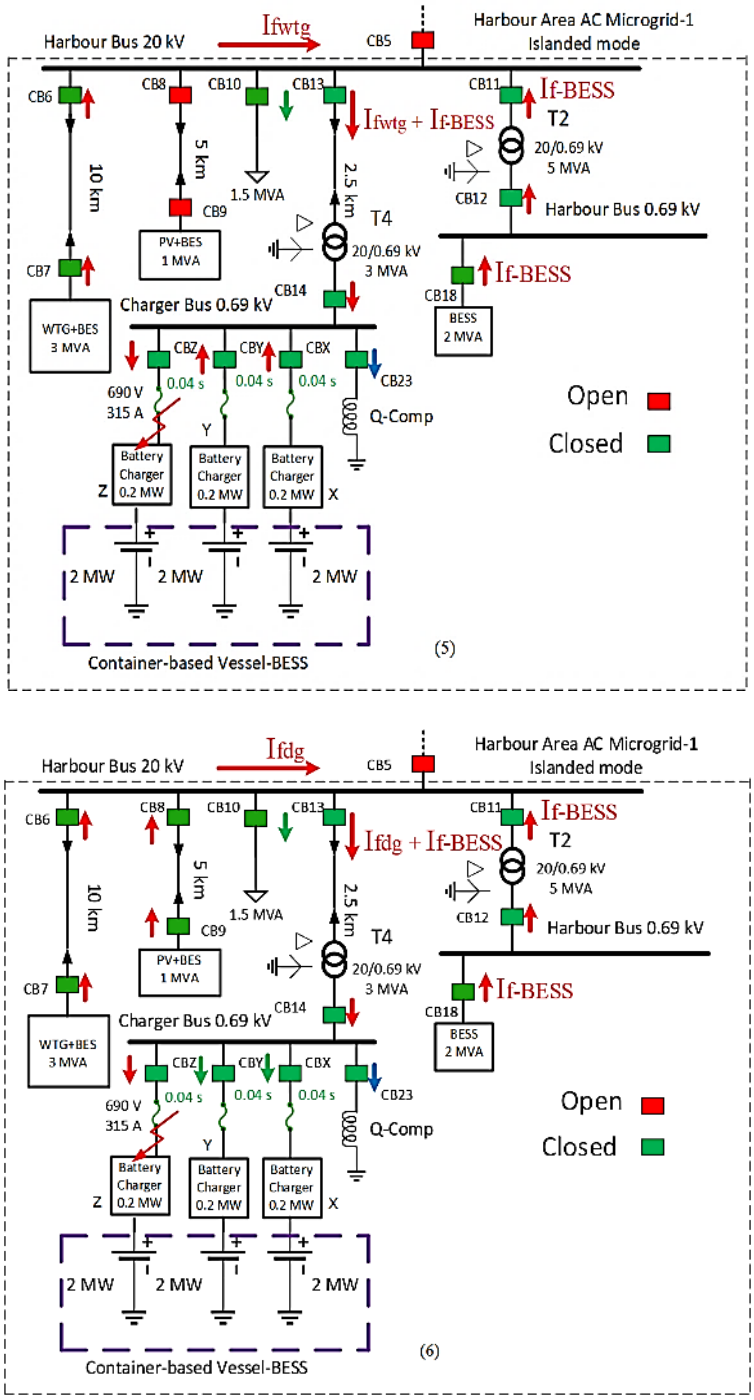

Figure 62. Six configurations (1)–(6) of the harbor area radial AC microgrid-1 in the islanded mode of operation.

The first three (1)–(3) of six considered configurations (Figure 62) for the islanded mode operation of the harbor area AC microgrid-1 are related to the power supply to cold-ironing load with no slow-charging of the vessel-BESS. The remaining three (4)–(6) of six considered configurations (Figure 62) for the islanded mode operation of the harbor area AC microgrid-1 are related to the slow-charging of the

vessel-BESS during the night with no cold-ironing load. In the islanded modes (1)–(3), a three-phase short-circuit fault is considered at the cold-ironing load of 2 MW 50 Hz. In the islanded modes (4)–(6), a three-phase short-circuit fault is considered at battery charger-Z terminal. The $I_{\text{f-BESS}}$ in Figure 62 denotes the fault current contribution from the harbor-BESS. Each of the considered six islanded modes is further subdivided into different cases based on fault current contribution scenarios of DERs and harbor-BESS. A summary of the islanded mode fault cases of the harbor area radial AC microgrid-1 is presented in Table 14. The results in terms of operating times of the IEDs and fuseZ in the considered islanded modes are presented in Table 15.

Table 14. Summary of the islanded mode fault cases.

Islanded mode fault cases	Fault current contributions from DERs	Are adaptive OC settings avoided?	Is protection coordination maintained?	Does the fuse operate within 20 ms?
1a	WTG & PV :1.2 p.u.	NO	NO	-
1b	WTG & PV: 2 p.u.	YES	YES (PARTIALLY)[1]	-
2a	WTG & PV: 2 p.u. H-BESS: 1.2 p.u.	YES	YES (PARTIALLY)	-
2b	WTG & PV: 2 p.u. H-BESS: 2 p.u.	YES	YES (PARTIALLY)	-
2c	WTG & PV: 2 p.u. H-BESS: 3 p.u.	YES	YES	-
3a	H-BESS: 2.5 p.u.	NO	NO	-
3b	H-BESS: 3 p.u.	NO	NO	-
		YES (25% additional MVA capacity)	YES (25% additional MVA capacity)	-
4a	WTG:	YES	YES (PARTIALLY)	NO (Delayed)
4b	WTG:	YES	YES (PARTIALLY)	NO (Delayed)
4c	WTG:	YES	YES (PARTIALLY)*	NO (Delayed)**
5a	WTG, PV-BES & H-BESS: 1.2 p.u.	YES	YES (PARTIALLY)	NO (Delayed)
5b	WTG, PV-BES & H-BESS: 2 p.u.	YES	YES (PARTIALLY)	NO (Delayed)
5c	WTG: 3 p.u. PV-BES & H-BESS: 2 p.u.	YES	YES	YES
5d	WTG, PV-BES & H-BESS: 2.5 p.u.	YES	YES	YES
6a	WTG, H-BESS & V-BESS: 1.2 p.u.	YES	YES (PARTIALLY)	NO (Delayed)
6b	WTG, H-BESS & V-BESS: 2 p.u.	YES	YES (PARTIALLY)*	NO (Delayed)**
6c	WTG, H-BESS & V-BESS: 2.5 p.u.	YES	YES (PARTIALLY)*	NO (Delayed)**
6d	WTG, H-BESS & V-BESS: 3 p.u.	YES	YES (PARTIALLY)*	NO (Delayed)**

WTG=Wind turbine generator, PV = Photovoltaic, BESS = Battery energy storage system, H-BESS = Harbor-BESS, PV-BES = PV-Battery energy storage, V-BESS = Vessel-BESS (both X and Y), MVA = Megavolt-Ampere.
*Can be improved by extending coordination delay between fuseZ and IEDZ to 40 ms
**FuseZ operating time is delayed up to 20 ms or less.
[1] Grid-forming control of both WTG and PV will improve the coordination delay of primary and backup IEDs closer to the setting limits in the islanded mode 1b.

Table 15. Operating times of IEDs and fuseZ in islanded mode cases.

Fault cases	Operating times (ms) during 3-phase short-circuit faults					
	IED21	IED20	IED19	IED15	IED12	IED11
1a	I>@5	I>@5	I>@5	I>@5	I>@5	I>@5
1b	32	275	477	675	879	1079

2a	32	258		459		655		872		1071	
2b	32	362		562		756		865		1066	
2c	32	212		412		612		830		1030	
3a	I>@5	I>@5		I>@5		I>@5		-			
3b	40	I>@5		I>@5		618					
→	4a	4b	4c	5a	5b	5c	5d	6a	6b	6c	6d
FuseZ	255	105	33	92.5	53	17.5	17	101	36	37	36
IEDZ	40*	ms = Millisecond, I>@5 = Overload stage operating in 5 s, → Fault cases in columns, IEDs in rows *IEDZ, IED14 and IED13 have same operating times in cases 4a-6d.									
IED14	240*										
IED13	440*										

Primary protection devices are highlighted in green color and backups are highlighted in blue color.

The summary of islanded mode fault cases presented in Table 14 and the results presented in Table 15 show that in the islanded mode fault cases 1a, 3a and 3b, neither are the adaptive OC protection settings avoided, nor is the definite-time protection coordination maintained. The islanded cases 1a, 3a and 3b are obvious islanded modes with either minimum magnitudes of fault current contributions from DERs or minimum number or capacity of DERs. Hence, the adaptive OC settings can only be avoided in islanded mode case 1a by increasing the fault current contributions of DERs as done in case 1b. The adaptive OC protection settings can be avoided in islanded mode cases 3a and 3b by adding 25 per cent extra MVA capacity. All of the remaining islanded mode fault cases avoid the adaptive OC protection settings.

The results in Table 15 indicate that the operating time of the primary IED or fuseZ is delayed in most of the islanded mode fault cases resulting in extended CTI delays between backup IEDs. The operating time of fuseZ is delayed up to 20 ms or less in islanded mode fault cases 4c, 6b, 6c and 6d. Hence, a revised CTI delay of 40 ms instead of the existing 20 ms between fuseZ and the first backup IEDZ may solve the coordination problem though with some compromise on backup IEDs' operations. The protection coordination between IEDs in islanded mode fault cases 1a, 3a and 3b can be improved by increasing the fault current contributions of DERs, using only the grid-forming control of all DERs and adding 25 per cent extra MVA capacity.

The avoidance of adaptive OC protection settings, the maintenance of definite-time protection coordination, and the operation of fuses within 20 ms are possible by using existing available DERs and battery storages as fault current sources in the islanded mode fault cases 2c, 5c and 5d. However, extra activated fault current sources need to be disconnected quickly after the fault removal to avoid the AC microgrid instability due to a subsequent overvoltage tripping of DERs.

4.5 Evaluation of active grid codes of DERs

This section presents the case study about the evaluation of dynamic reactive power capabilities of converter-based DERs according EN 50549-2-2019 grid code requirements, as reported in Publication V of this thesis. The reactive power capacity required to be provided by DERs connected at medium voltage has been evaluated during the unbalanced faults in both the grid-connected and islanded modes of AC microgrid operation. Dynamic reactive power is required during the short-circuit faults or sudden voltage steps either to support the local grid voltage for maintenance of voltage stability, or to raise the magnitude of fault current, particularly the magnitude of negative-sequence current in order to detect the faults. Due to the limited scope, the focus of this case study is only on the detection of unbalanced LL short-circuit faults during the grid-connected and islanded modes of AC microgrid with the help of extra dynamic reactive power (Q) injection.

For the evaluation of Q-injection requirements according to the EN 50549-2-2019 grid code, a generic model of converter-based DERs using the synchronous frame of reference or dq-control is developed. It is the same model of the converter-based DERs as used in the previous PSCAD-based case study of Section 4.2, however, for this case study it has been remodeled in MATLAB/Simulink. The generic model of converter-based DERs is capable of LVRT and provides 1.2 p.u. of fault current contribution during short-circuit faults or when the voltage of any phase falls below 0.8 p.u. The grid-following and grid-forming controls are incorporated in the generic model of converter-based DERs. With the grid-forming control, the DER model operates with an independent control of voltage and frequency in the islanded mode using a separate PLL-2 instead of PLL-1. Figure 63 (a) shows the dq-control of the developed generic model of converter-based DERs with a description of the outer power-control loop during the faults. The mentioned generic model of converter-based DERs represents both the WTG and PV systems.

The AC microgrid model used for this case study (Figure 63 b) applies the same capacity of the WTG and PV system with both sources equal in capacity in respect of their immediate loads, and thus represents configuration 3 of Figure 15. Therefore, it will be straightforward to use higher threshold settings of definite-time overcurrent function in the grid-connected mode and lower threshold settings of definite-time overcurrent function in the islanded mode for the detection of short-circuit faults. In Figure 63 (b), each CB is operated by the IED of the related number. For example, CB1 is operated by IED1, and so on. The tripping threshold settings for different protection functions used in this case study are presented in Table 16. The time delay settings of different protection IEDs and functions are given in Table 17.

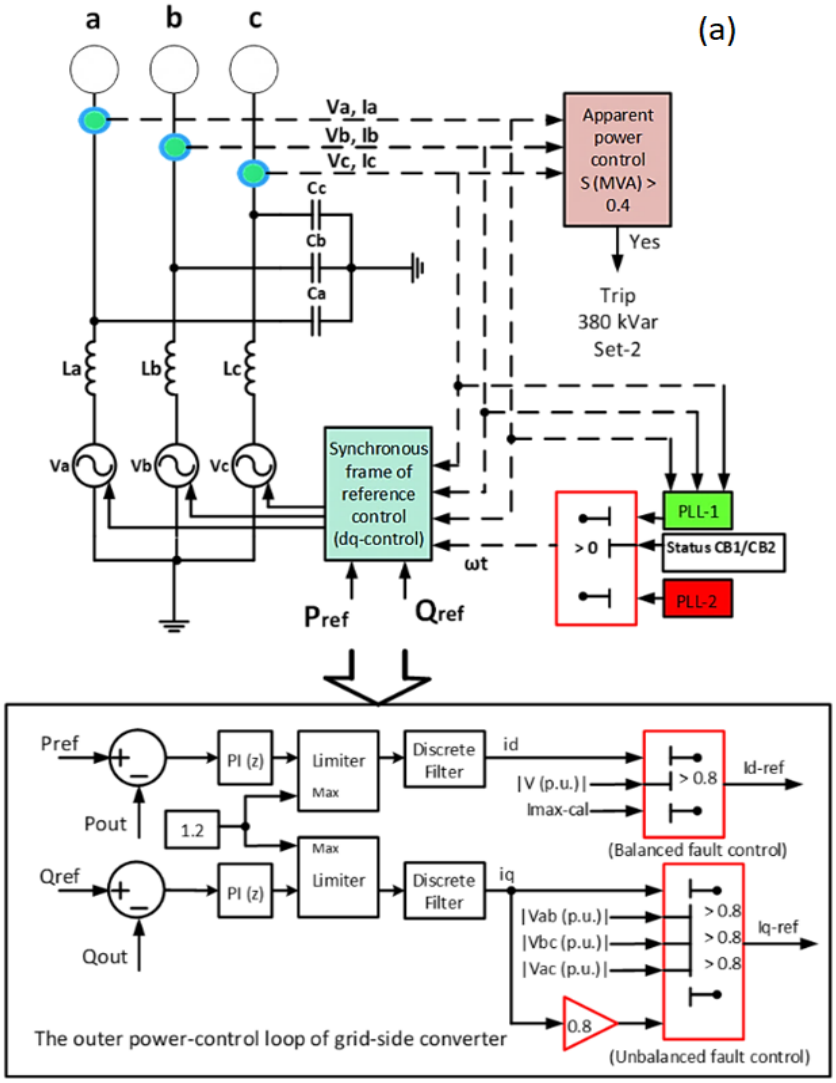
a
b
c
(a)
Va, Ia
Vb, Ib
Vc, Ic
Cc
Cb
Ca
La
Lb
Lc
Va
Vb
Vc
Apparent power control S (MVA) > 0.4
Yes
Trip 380 kVar Set-2
Synchronous frame of reference control (dq-control)
ωt
Pref
Qref
PLL-1
> 0
Status CB1/CB2
PLL-2
Pref
PI (z)
Limiter
Max
Discrete Filter
id
|V (p.u.)|
Imax-cal
> 0.8
Id-ref
(Balanced fault control)
Pout
1.2
Max
Qref
PI (z)
Limiter
Discrete Filter
iq
|Vab (p.u.)|
|Vbc (p.u.)|
|Vac (p.u.)|
> 0.8
> 0.8
> 0.8
Iq-ref
Qout
0.8
The outer power-control loop of grid-side converter
(Unbalanced fault control)

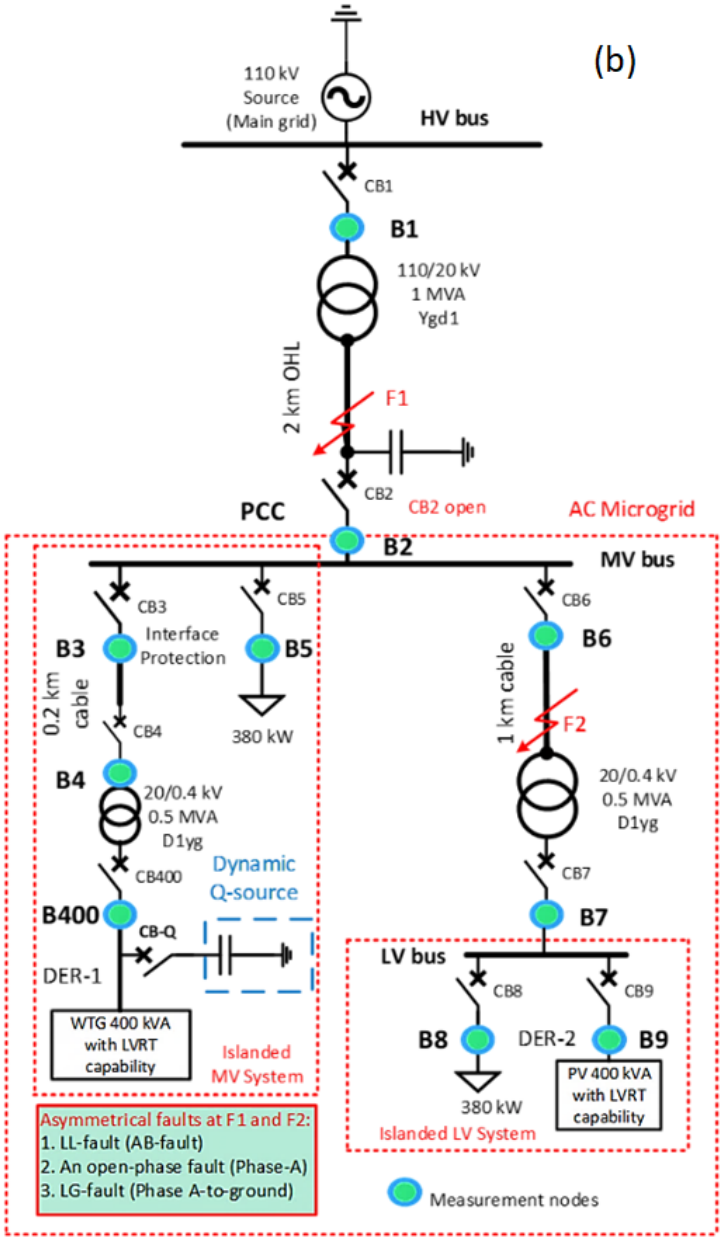

Figure 63. (a) the coupled DQ-control of the generic converter-based DER and (b) the Simulink model of a radial AC microgrid.

Table 16. Tripping thresholds of different protection functions.

Protection functions	Tripping thresholds	
	Grid-connected mode	Islanded mode
Positive-sequence overcurrent ($OC^1 = I_1$ = ANSI 51P)	2.25 p.u.	1.2 p.u.
Ratio of negative-sequence & positive-sequence overcurrent (I_2/I_1)	1.3	1.0-1.3
Zero-sequence overcurrent ($OC^0 = I_0 = I_G$ = ANSI 51G)	0.45-0.5 p.u.	0.45-0.5 p.u.
Negative-sequence overvoltage (OV^2 = ANSI 47)	0.5 p.u.	0.5 p.u.
Zero-sequence overvoltage (OV^0 = ANSI 59N)	0.5 p.u.	0.5 p.u.
Positive-sequence undervoltage (UV^1 = ANSI 27D)	0.85 p.u.	0.85 p.u.
Positive-sequence overvoltage (OV^1 = ANSI 59)	1.2 p.u.	1.2 p.u.
ANSI = American National Standards Institute		

Table 17. Time delay settings of different IEDs and functions.

Protection functions	Coordinated time delays (s)							
	IED1	IED2	IED3	IED6	IED5	IED7	IED8	IED9
$OC^1 = I_1$	0.8	0.6	0.9	0.4	0.9	0.2	0.02	0.25*
Ratio I_2/I_1	0.8	0.6	0.9	0.4	0.9	0.2	0.02	0.4
$OC^0 = I_0 = I_G$	0.8	0.6	0.9	0.4	0.9	0.2	0.02	0.4
OV^2	3.0	2.5	4.0	2.0	4.0	1.5	1.0	4.0
OV^0	3.0	2.5	4.0	2.0	4.0	1.5	1.0	4.0
UV^1/ OV^1	3.5	3.0	5.0	2.5	5.0	2.0	1.5	5.0
*This setting is modified/corrected in order to provide the mandatory low voltage ride-through up to 250 ms.								

Figure 64 shows the protection logic used at IEDs 1, 2, 3, 6, and 7 for the detection of unbalanced LL faults F1 and F2 in the grid-connected and islanded modes, respectively. The positive-sequence OC, zero-sequence OC, and the ratio of negative-sequence OC to the positive-sequence OC (I_2/I_1) are used as the primary protections. The negative-sequence OV and zero-sequence OV functions are used as the first local backup protections, whereas the positive-sequence UV and positive-sequence OV functions are used as the second local backup protections.

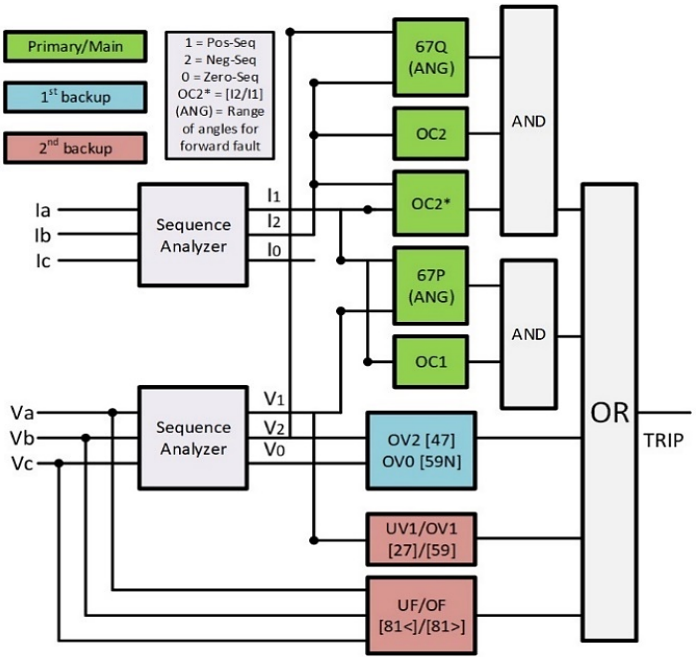

Figure 64. Protection logic with main and backup protection functions used at IEDs 1, 2, 3, 6, and 7 for the detection of LL faults.

The generic model of converter-based DERs is inherently incapable of meeting the Q-injection requirements of the grid code during faults due to the coupled sequence control and modelling limitations. Therefore, an additional dynamic Q-source (a thyristor-switched capacitor or equivalent) is connected at the LV terminals of the WTG behind the 20/0.4 kV transformer (Figure 63) to meet the Q-injection requirements. The full capacity of the additional dynamic Q-source is 760 kVar and it consists of two sets of thyristor-switched capacitors each with 380

kVar capacity. Both sets of the dynamic Q-source are quickly connected during faults or voltage steps. However, if the apparent power limit of the DER is exceeded, then one set is instantaneously disconnected. The activation of the dynamic Q-injection function happens when one or more phase-to-phase voltages are outside the static voltage range of 80–120% of the rated voltage at the connection point.

According to the grid code EN 50549-2-2019, the additional positive-sequence reactive current (ΔI_{Q1}) needs to be set by the gradient k_1 according to:

$$\Delta I_{Q1} = k_1 . \Delta U_1, \tag{2}$$

where ΔU_1 is the sudden jump or change of the positive-sequence voltage defined by equation (3):

$$\Delta U_1 = \frac{U_1 - U_{1\_1\text{min}}}{U_c}, \tag{3}$$

where U_1 is the actual positive-sequence voltage, $U_{1\_1\text{min}}$ is the 1-minute average of the pre-fault positive-sequence or RMS voltage, and U_c is the voltage at the connection point. The additional negative-sequence reactive current (ΔI_{Q2}) needs to be set by the gradient k_2 according to:

$$\Delta I_{Q2} = k_2 . \Delta U_2, \tag{4}$$

where ΔU_2 is the sudden jump or change of the negative-sequence voltage defined as:

$$\Delta U_2 = \frac{U_2 - U_{2\_1\text{min}}}{U_c}, \tag{5}$$

where U_2 is the actual negative-sequence voltage, and $U_{2\_1\text{min}}$ is the 1-minute average of the pre-fault negative-sequence voltage or zero. The gradients k_1 and k_2 have to be set in the range of 2–6 with a minimum step size of 0.5. The dynamic Q-injection has to be provided with a step response of 25 ms and a settling time of 50 ms. For a voltage below 15% of U_c no reactive current supply is required.

The results of LL fault detection and compliance check of EN 50549-2-2019 grid code requirements of the reactive current provision in grid-connected and islanded modes are presented in the following Sections 4.5.1–4.5.2.

4.5.1 Line-to-line fault F1 in the grid-connected mode

Figure 65 shows the derived symmetrical components of fault current and the ratio I_2 to I_1 (I_2/I_1) at IED1 during LL fault F1 in the grid-connected mode. It can be seen in Figure 65 (a) that both positive- and negative-sequence components of current at IED1 increase equally after LL fault F1 is applied at a simulation time of 2 s. However, after the activation of dynamic Q-source at 2.1 s, the positive-sequence current decreases and negative-sequence current increases. This results in the ratio I_2/I_1 at IED1 to increase from about 1.0 right after the fault to above 1.3 after the activation of the dynamic Q-source (Figure 65 (b)). This increased I_2/I_1 ratio can be used to detect LL fault F1 downstream to IED1. However, in the presented case, the positive-sequence overcurrent function of IED1 issues the tripping command to CB1 at 2.8 s according to threshold setting of Table 16 and the time delay setting or definite-time coordination of Table 17. The Q-source activation delay of 0.1 s prevents the tripping command by the I_2/I_1 ratio in this fault case. For the complete isolation of the LL fault F1, CB2 has been transfer-tripped by IED1 in this case. However, other local protection functions at IED2 like the negative-sequence overcurrent function with 0.45–0.5 p.u. tripping threshold can also be used for tripping CB2. Depending on the required tripping threshold of the protection function (Table 16) and the definite-time coordination setting (Table 17), CB2 may trip before CB1 in the absence of a communication link used for transfer-trip, resulting in a loss of protection coordination. Further details and additional results can be found in Publication V.

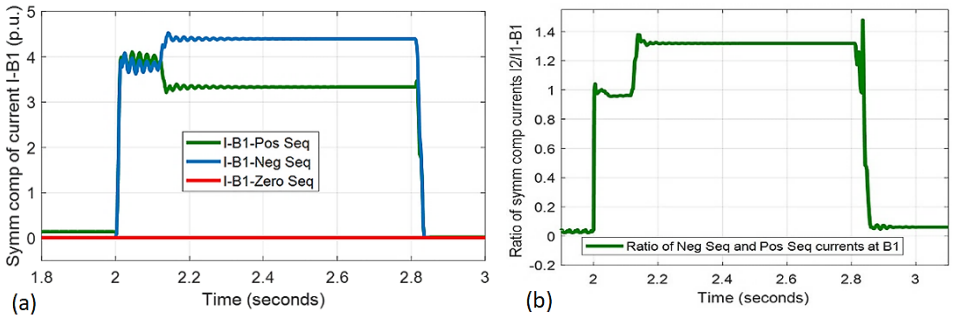

Figure 65. (a) symmetrical components of current and (b) the ratio I_2/I_1 at IED1 during LL fault F1 in the grid-connected mode.

For the Q-injection compliance check, according to the EN 50549-2-2019 grid code, the derived symmetrical components of current at B400 and symmetrical components of voltage at B3 during LL fault F1 in the grid-connected mode are shown in Figure 66. The measurement node B3 is the connection point of the WTG to the medium voltage bus (Figure 63) where the interface protection is installed, and the voltage is measured in order to calculate the required amount of additional reactive current. The measurement node B400 is the connection point of the

dynamic Q-source (Figure 63) where the additional amount of reactive current provided can be measured to verify the grid code compliance.

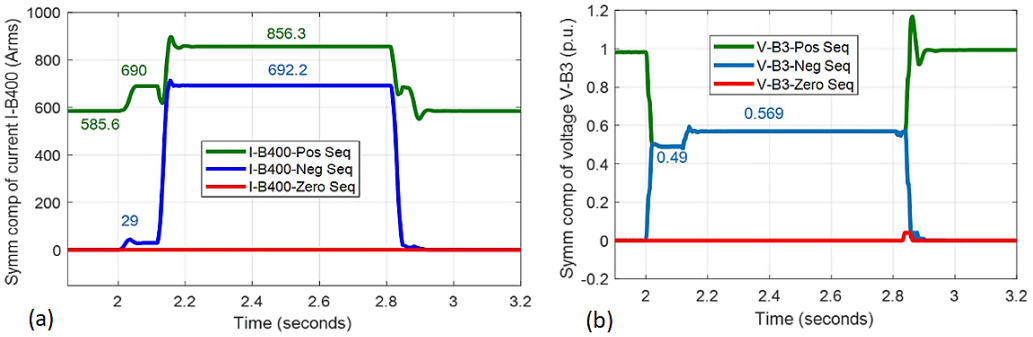

Figure 66. (a) symmetrical components of current at B400 and (b) symmetrical components of voltage at B3 during LL fault F1 in the grid-connected mode.

The required minimum and maximum magnitude of positive-sequence reactive current according to equations (2) and (3) based on voltage measurement at the interface protection bus B3 (Figure 66 (b)) will be as follows:

$$\Delta U_1 = \frac{U_1 - U_{1\_1\min}}{U_c} = \frac{0.49-1}{1} = -0.51\ p.u. \quad (6)$$

$$\Delta I_{Q1} = k_1.\Delta U_1 = 2\ (-0.51\ p.u.) = -1.02\ p.u.\ (MIN:) \quad (7)$$

$$\Delta I_{Q1} = k_1.\Delta U_1 = 6\ (-0.51\ p.u.) = -3.06\ p.u.\ (MAX:) \quad (8)$$

In equation (6), $U_1 = 0.49\ p.u.$ and $U_{1\_1\min} \approx 1.0\ p.u.$ according to the voltage measurement at bus B3 shown in Figure 66 (b). The minimum value of gradient $k_1 = 2$ and the maximum value of gradient $k_1 = 6$ in equations (7) and (8), respectively. The negative sign in equation (6) indicates a positive-sequence undervoltage, therefore the negative sign in equations (7) and (8) indicates the supply or generation of reactive power required. This is called the overexcited operation mode of DERs, used for providing voltage support to the main grid.

The required minimum and maximum magnitude of negative-sequence reactive current according to equations (4) and (5) based on voltage measurement at the interface protection bus B3 (Figure 66 (b)) will be as follows:

$$\Delta U_2 = \frac{U_2 - U_{2\_1\min}}{U_c} = \frac{0.49-0}{1} = 0.49\ p.u. \quad (9)$$

$$\Delta I_{Q2} = k_2.\Delta U_2 = 2\ (0.49\ p.u.) = 0.98\ p.u.\ (MIN:) \quad (10)$$

$$\Delta I_{Q2} = k_2.\Delta U_2 = 6\ (0.49\ p.u.) = 2.94\ p.u.\ (MAX:) \quad (11)$$

In equation (9), $U_2 = 0.49$ *p.u.*, $U_{2\_1min} = 0$ *p.u.* and $U_c = 1.0$ *p.u.* according to the voltage measurement at bus B3 shown in Figure 66 (b). The minimum value of gradient $k_2 = 2$ and the maximum value of gradient $k_2 = 6$ in equations (10) and (11), respectively. For the negative-sequence voltage change (ΔU_2) and the additional negative-sequence reactive current (ΔI_{Q2}), there will always be a positive sign due to the absence of negative-sequence voltage before the fault ($U_{2\_1min} = 0$ *p.u.*). Hence the additional negative-sequence current (ΔI_{Q2}) can only be provided in the underexcited mode.

After calculating the minimum and maximum magnitudes of required positive- and negative-sequence reactive currents, it is checked whether the additional Q-source connected at the LV terminals of the WTG injects the required amount of positive- and negative-sequence reactive currents during the LL fault F1 in the grid-connected mode. Figure 66 (a) shows the measured symmetrical components of current at bus B400 before, during and after the LL fault F1 in the grid-connected mode. The current at B400 is predominantly active current before the fault (up to the simulation time of 2 s), whereas it is predominantly reactive current during the fault (from the simulation time of 2 s to 2.8 s).

It can be observed from Figure 66 (a) that after the activation of Q-source at 2.1 s, the positive-sequence reactive current increases to 856.3 A, that corresponds to 1.46 p.u. of the current before the fault (585.6 A). This 1.46 p.u. magnitude of injected positive-sequence reactive current during the LL fault F1 lies within the required minimum and maximum values calculated using equations (7) and (8), respectively, and with $\Delta I_{Q1} = -1.46$ *p.u.*, and $\Delta U_1 = -0.51$ *p.u.*, the gradient $k_1 = 2.86$. This means that the minimum requirement of positive-sequence reactive current is met according to EN 50549-2-2019 grid code with the additional dynamic Q-source of 760 kVar.

It can also be observed from Figure 66 (a) that after the activation of Q-source at 2.1 s, the negative-sequence reactive current increases to 692.2 A, that corresponds to 1.18 p.u. of the current before the fault (585.6 A). This 1.18 p.u. magnitude of injected negative-sequence reactive current during the LL fault F1 lies within the required minimum and the maximum values calculated using equations (10) and (11), respectively. With $\Delta I_{Q2} = 1.18$ *p.u.*, and $\Delta U_2 = 0.49$ *p.u.*, the gradient $k_2 = 2.4$. This means that the minimum requirement of negative-sequence reactive current is met according to EN 50549-2-2019 grid code with the additional dynamic Q-source of 760 kVar.

4.5.2 Line-to-line fault F2 in the islanded mode

Figure 67 shows the derived symmetrical components of fault current and the ratio I_2/I_1 at IED6 during the LL fault F2 in the islanded mode. It can be observed from Figure 67 (a) that both positive- and negative-sequence components of current at IED6 increase equally after the LL fault F2 is applied at simulation time of 6 s. However, after the activation of dynamic Q-source at 6.1 s, the positive-sequence current decreases and negative-sequence current increases. This results in the ratio I_2/I_1 at IED6 to increase from about 1.0 right after the fault to above 1.3 after the activation of dynamic Q-source (Figure 67 (b)). This increased I_2/I_1 ratio can be used to detect LL fault F2 downstream of IED6. The ratio I_2/I_1 protection function at IED6 issues the tripping command to CB6 at 6.4 s according to threshold setting of Table 16 and the time delay setting or definite-time coordination of Table 17. For the complete isolation of the LL fault F2, CB7 has been transfer-tripped by IED6 in this case. Other local protection functions at IED7 like a negative-sequence overcurrent function with a 0.45–0.5 p.u. tripping threshold cannot be used for tripping CB7 because the negative-sequence overcurrent at IED7 is less than the tripping threshold. Similarly, the negative-sequence overvoltage at IED7 is also less than the tripping threshold of 0.5 p.u., particularly after the activation of Q-source. Therefore, in this fault case, only the positive-sequence undervoltage function at IED7 will provide backup for the transfer-trip failure from IED6 to CB7 according to the time delay setting or definite-time coordination of Table 17. Further details and additional results can be found in Publication V.

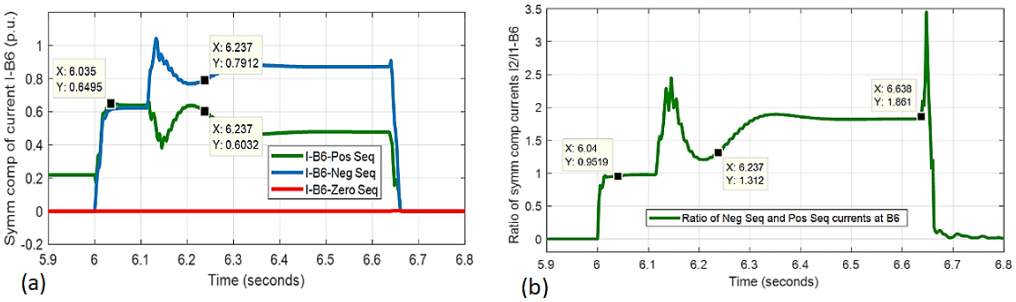

Figure 67. (a) symmetrical components of current and (b) the ratio I_2/I_1 at IED6 during LL fault F2 in the islanded mode.

For the Q-injection compliance check according to EN 50549-2-2019 grid code, the derived symmetrical components of current at B400 and symmetrical components of voltage at B3 during LL fault F2 in the islanded mode are shown Figure 68. The measurement node B3 is the connection point of the WTG to the medium voltage bus (Figure 63) where the interface protection is installed, and the voltage is measured in order to calculate the required amount of additional reactive

current. The measurement node B400 is the connection point of the dynamic Q-source (Figure 63) where the additional amount of reactive current provided can be measured to verify the grid code compliance.

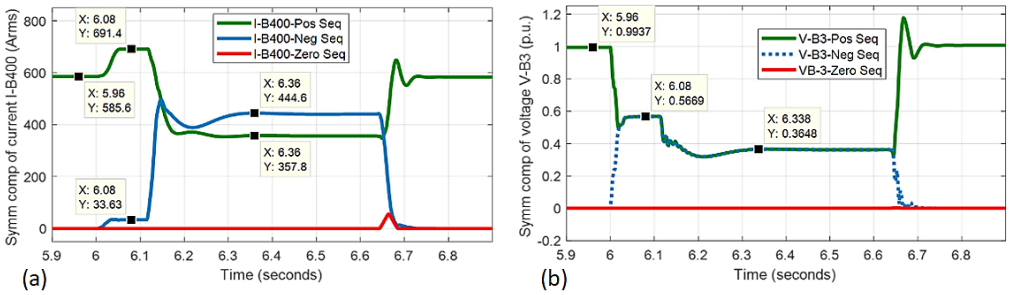

Figure 68. (a) symmetrical components of current at B400 and (b) symmetrical components of voltage at B3 during LL fault F2 in the islanded mode.

The required minimum and maximum magnitude of positive-sequence reactive current according to equations (2) and (3) based on voltage measurement at the interface protection bus B3 (Figure 68 (b)) will be as follows:

$$\Delta U_1 = \frac{U_1 - U_{1\_1\min}}{U_c} = \frac{0.5669 - 0.9937}{0.9937} = -0.4295\ p.u. \quad (12)$$

$$\Delta I_{Q1} = k_1 . \Delta U_1 = 2\ (-0.4295\ p.u.) = -0.859\ p.u.\ (MIN:) \quad (13)$$

$$\Delta I_{Q1} = k_1 . \Delta U_1 = 6\ (-0.4295\ p.u.) = -2.577\ p.u.\ (MAX:) \quad (14)$$

In equation (12), $U_1 = 0.5669\ p.u.$, and $U_{1\_1\min} = 0.9937\ p.u.$ according to the voltage measurement at bus B3 shown in Figure 68 (b). The minimum value of gradient $k_1 = 2$ and the maximum value of gradient $k_1 = 6$ in equations (13) and (14), respectively. The negative sign of ΔI_{Q1} means that reactive power supply is required for the voltage support as explained in the previous grid-connected fault case.

The required minimum and maximum magnitude of negative-sequence reactive current according to equations (4) and (5) based on voltage measurement at the interface protection bus B3 (Figure 68 (b)) will be as follows:

$$\Delta U_2 = \frac{U_2 - U_{2\_1\min}}{U_c} = \frac{0.5669 - 0}{0.9937} = 0.57\ p.u. \quad (15)$$

$$\Delta I_{Q2} = k_2 . \Delta U_2 = 2\ (0.57\ p.u.) = 1.14\ p.u.\ (MIN:) \quad (16)$$

$$\Delta I_{Q2} = k_2 . \Delta U_2 = 6\ (0.57\ p.u.) = 3.42\ p.u.\ (MAX:) \quad (17)$$

In equation (15), $U_2 = 0.5669\ p.u.$, $U_{2\_1\min} = 0\ p.u.$ and $U_c = 0.9937\ p.u.$ according to the voltage measurement at bus B3 shown in Figure 68 (b).

After calculating the minimum and maximum magnitudes of required positive- and negative-sequence reactive currents, it is checked whether the additional Q-source connected at the LV terminals of the WTG injects the required amount of positive- and negative-sequence reactive currents during the LL fault F2 in the islanded mode. Figure 68 (a) shows the measured symmetrical components of current at bus B400 before, during and after the LL fault F2 in the islanded mode. The current at B400 is predominantly active current before the fault (up to the simulation time of 6 s), whereas it is predominantly reactive current during the fault (from the simulation time of 6 s to 6.4 s).

It can be observed from Figure 68 (a) that after the activation of Q-source at 6.1 s, the positive-sequence reactive current decreases to 357.8 A, that corresponds to 0.61 p.u. of the current before the fault (585.6 A). This 0.61 p.u. magnitude of injected positive-sequence reactive current during the LL fault F2 is less than the required minimum and the maximum values calculated using equations (13) and (14), respectively. With $\Delta I_{Q1} = -0.61\ p.u.$, and $\Delta U_1 = -0.4295\ p.u.$, gradient $k_1 = 1.42$. This means that the minimum requirement of positive-sequence reactive current is not met according to the EN 50549-2-2019 grid code with the dynamic Q-source of 760 kVar during the LL fault F2 in the islanded mode.

It can also be observed from Figure 68 (a) that after the activation of Q-source at 6.1 s, the negative-sequence reactive current increases to 444.6 A, that corresponds to 0.759 p.u. of the current before the fault (585.6 A). This 0.759 p.u. magnitude of injected negative-sequence reactive current during the LL fault F2 is also less than the required minimum and the maximum values calculated using equations (16) and (17), respectively. With $\Delta I_{Q2} = 0.759\ p.u.$, and $\Delta U_2 = 0.57\ p.u.$, the gradient $k_2 = 1.33$. This means that the minimum requirement of negative-sequence reactive current is also not met according to the EN 50549-2-2019 grid code with the dynamic Q-source of 760 kVar during the LL fault F2 in the islanded mode.

This examination concludes that although the minimum requirements of dynamic positive- and negative-sequence reactive current are not met according to EN 50549-2-2019 grid code in the islanded mode, the injected reactive current with Q-source of 760 kVar is enough to detect LL fault F2. It is worth noting here that the EN 50549-2-2019 grid code requirement of reactive current is generally applicable for all types of balanced and unbalanced short-circuit faults at the defined voltage conditions, and specified only for the grid-connected mode. It is already checked in the previous Section 4.5.1 that the selected capacity of Q-source meets the grid code requirements of reactive current according to EN 50549-2-2019 during the grid-connected mode. For the islanded mode, even the reduced Q-injection requirement will also work, at least for the detection of LL faults.

Nevertheless, the main purpose of an additional Q-injection was to enhance the negative-sequence component of current to detect LL faults during grid-connected and islanded modes. That purpose is achieved in quite a successful manner, and further details can be found in Publication V.

4.6 Evaluation of a new directional protection scheme

Directional discrimination is also required for ring or loop networks and radial networks of AC microgrids with DERs on both sides of the fault point for proper coordination of IEDs in forward and reverse directions of faults. For this purpose, the directional overcurrent protection function (ANSI 67) with either definite-time or inverse-time characteristics is usually used. The design of directional element 67 is done using different principles which are usually different for balanced, unbalanced, and ground faults.

For balanced faults, the positive-sequence directional element (67P) can be designed using positive-sequence voltage as the reference, or polarizing quantity and positive-sequence current as the operating quantity. Depending on the set criteria, when the phase angle enters the operating area and the fault current magnitude exceeds the setting threshold, a forward or reverse fault is declared. If the positive-sequence voltage becomes zero during the fault, the stored magnitude of the voltage before the fault is used for the detection of fault direction.

For unbalanced faults, the negative-sequence directional element (67Q) can be designed using negative-sequence voltage as the reference, or polarizing quantity and negative-sequence current as the operating quantity. Similarly, the zero-sequence directional element (67G) can be designed using zero-sequence voltage as the reference, or the polarizing quantity and zero-sequence current as the operating quantity for the ground faults.

Sections 4.6.1–4.6.4 present design principles and evaluations of new 67P and 67Q directional elements for LL unbalanced faults in grid-connected and islanded modes of the AC microgrid model (Figure 63) as reported in Publication V.

4.6.1 Design principle of the 67P element

Three approaches have been considered for the design of the 67P element. The first approach assumes the maximum torque line to be at a relay characteristic angle (RCA) of 60° lagging from the measured angle of the reference voltage (positive-sequence voltage V_1). The second approach assumes the maximum torque line to

be at an RCA of 30° lagging from the measured angle of the reference voltage (V_1). The third approach assumes the maximum torque line to be at an RCA of 0° from the measured angle of the reference voltage (V_1). In all three approaches, the zero torque line is assumed to be at RCA±90°. The fault is considered to be in the forward direction if the measured angle of the positive-sequence current (I_1) lies in between RCA±90° or a maximum torque line±90°. Otherwise, the fault is considered in the reverse direction. The fault is declared in the forward or reverse direction only if the magnitude of I_1 is 2.25 p.u. or greater in the grid-connected mode and 1.2 p.u. or greater in the islanded mode. The considered thresholds of I_1 are made on the basis of the assumption that converter-based DERs provide a fault current contribution of 1.2 p.u.

4.6.2 Design principle of the 67Q element

The same principles as considered for the design of 67P element design are also considered for the design of the 67Q element, however, the negative-sequence voltage (V_2) is used as the reference quantity and the negative-sequence current (I_2) is used as the operating quantity. Moreover, the forward direction of fault is assumed in the opposite direction of the considered RCA or maximum torque line. With these assumptions, if the measured angle of the negative-sequence current (I_2) lies in between RCA±90° or a maximum torque line±90°, the fault is considered to be in the reverse direction, otherwise the fault is considered in the forward direction. The fault is declared in the forward direction or reverse direction only if the ratio of negative-sequence current (I_2) to positive-sequence current (I_1) is greater than 1.3 in both the grid-connected and islanded modes. The considered threshold of I_2/I_1 ratio is made on the basis of the assumption that an extra Q-source of twice the rated capacity of converter-based DER is activated quickly after the fault happens when the voltage criteria for its activation (according to IEC 50549-2-2019) are reached as explained in Section 4.5. Additionally, the magnitude of $I_2 \geq 0.5$ p.u. is used as the restraining quantity to avoid a false operation of the 67Q element during the load unbalance. Figure 69 shows the OR logic of the proposed 67P and 67Q directional elements.

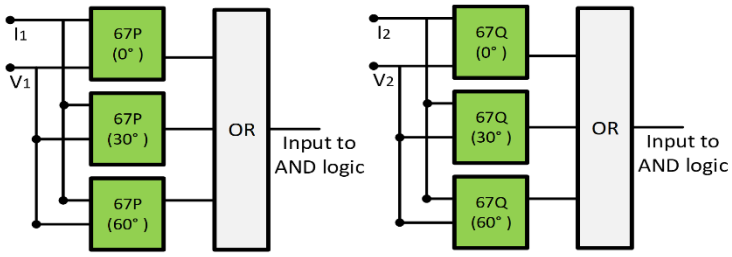

Figure 69. OR logic of the proposed directional elements.

4.6.3 Evaluation of the 67P element in the grid-connected mode

The positive-sequence and negative-sequence voltages and currents during the LL fault F1 in the grid-connected mode of the AC microgrid model (Figure 63) are given in Table 18. In Section 4.6.3, the evaluation of only the 67P directional element is presented for the LL fault F1 in the grid-connected mode using the principle of design as explained in Section 4.6.1, because the 67Q element at B1 will not work in this fault case.

Table 18. The symmetrical components of voltages and currents during LL fault F1 in the grid-connected mode.

Quantity	Before Q-injection	After Q-injection	Quantity	Before Q-injection	After Q-injection
V_1 at B1	1.0 ∠0° p.u.	1.0 ∠0° p.u.	V_1 at B2	0.49 ∠-29° p.u.	0.569 ∠-30.35° p.u.
I_1 at B1	3.9 ∠-87° p.u.	3.33 ∠-87.6° p.u.	I_1 at B2	0.725 ∠176° p.u.	0.6953∠-123.2° p.u.
V_2 at B1	0 ∠93° p.u.	0 ∠91.5° p.u.	V_2 at B2	0.49 ∠-149° p.u.	0.569 ∠-150.35° p.u.
I_2 at B1	3.8 ∠-88° p.u.	4.4 ∠-88.5° p.u.	I_2 at B2	0.525 ∠-146.7° p.u.	0.8784 ∠-106.3° p.u.

Figure 70 shows the plotting of V_1 and I_1 at buses B1 and B2 on the 360° plane during LL fault F1 in the grid-connected mode before and after the Q-injection, assuming an RCA of 60° and 30° lagging with respect to V_1 at B1 and B2. The shaded area on the 360° plane indicates the forward direction of the fault whereas the unshaded area indicates the reverse direction of the fault. This means that if the angle of the fault current (I_1) lies within the shaded area the fault is considered to be in the forward direction, otherwise it is considered in the reverse direction. The variable lengths of the radius along the 360° plane marked with blue color indicate the thresholds of the magnitudes of voltages and currents in per unit.

Figure 70 clearly reveals the indication of a forward direction of LL fault F1 at bus B1 because the angle of I_1 at B1 lies in the shaded area and the magnitude of I_1 at B1 is greater than the set threshold of 2.25 p.u. This is true for the fault current (I_1) before and after the additional Q-injection at DER-1. The angle of I_1 at B2 correctly indicates the reverse direction of LL fault F1 before the additional Q-injection at DER-1. However, after the additional Q-injection at DER-1, the angle of I_1 at B2 lies in the shaded area and therefore incorrectly indicates the forward direction of LL fault F1 at B2. Nevertheless the magnitude of I_1 at B2 is less than the set threshold of 2.25 p.u. before and after the additional Q-injection. Hence, the reverse or forward direction of LL fault F1 at B2 is not declared by the AND logic of the scheme.

In Figure 70, the characteristic of the 67P element marked with red lines is used for the direction of fault at bus B1, whereas the characteristic of the 67P element marked with purple lines is used for the direction of fault at bus B2.

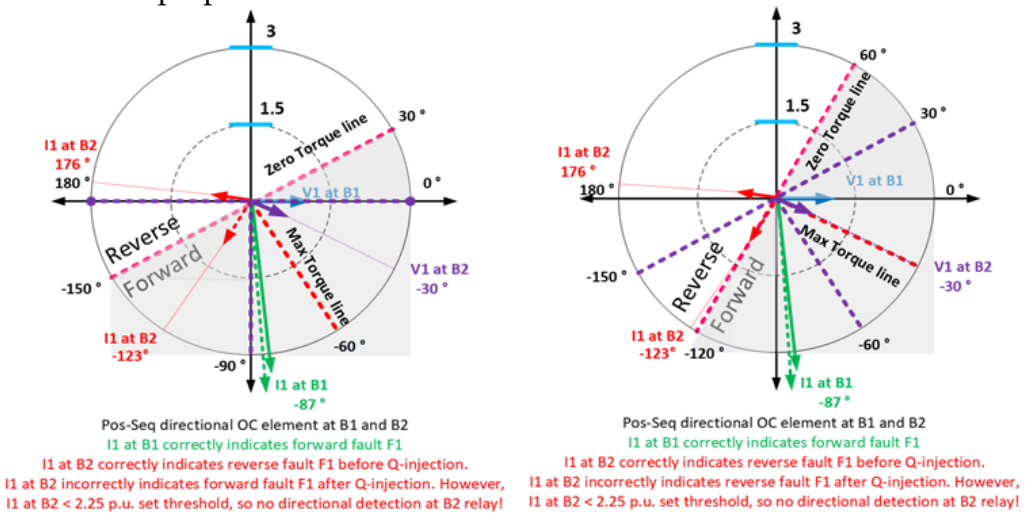

Figure 70. The operation of the 67P directional element at buses B1 and B2 during LL fault F1 in the grid-connected mode with an RCA of 60° and 30° lagging with respect to V_1 at B1 and B2.

4.6.4 Evaluation of the 67Q element in the islanded mode

The positive-sequence and negative-sequence voltages and currents during the LL fault F2 in the islanded mode of the AC microgrid model (Figure 63) are given in Table 19. In Section 4.6.4, the evaluation of only the 67Q directional element is presented for the LL fault F2 in islanded mode using the principle of design as explained in Section 4.6.2, because the 67P element will not work in this fault case.

Table 19. The symmetrical components of voltages and currents during LL fault F2 in the islanded mode.

Quantity	Before Q-injection	After Q-injection	Quantity	Before Q-injection	After Q-injection
V_1 at B6	0.58 ∠-9.89° p.u.	0.38 ∠-90.66° p.u.	V_1 at B7	0.58 ∠22.58° p.u.	0.38 ∠-55.14° p.u.
I_1 at B6	0.6495 ∠-28.45° p.u.	0.6 ∠-5.519° p.u.	I_1 at B7	0.372 ∠-134.8° p.u.	0.486∠139.3° p.u.
V_2 at B6	0.567 ∠-129.9° p.u.	0.364 ∠149.3° p.u.	V_2 at B7	0.54 ∠-162.3° p.u.	0.3653 ∠117.4° p.u.
I_2 at B6	0.6234 ∠52.32° p.u.	0.88 ∠30.56° p.u.	I_2 at B7	0.3334 ∠-160.9° p.u.	0.2122 ∠116.9° p.u.

Figure 71 shows the operation of the 67Q directional element during the LL fault F2 in the islanded mode, assuming an RCA of 60° lagging with respect to V_2 at B6 and B7 before and after Q-injection.

Figure 71 clearly reveals the indication of a forward direction of LL fault F2 at bus B6 in the islanded mode because the angle of I_2 at B6 lies in the shaded area and the magnitude of fault current I_2 at B6 is greater than the set threshold of 0.5 p.u. This is true for the fault current I_2 at B6 before and after the additional Q-injection at DER-1. However, the ratio of I_2/I_1 is less than the set threshold of 1.3 before the Q-injection activation and it only increases to a value greater than 1.3 after the Q-injection activation. This means that the 67Q element will declare a forward fault at B6 only after the Q-injection activation in the islanded mode. This is so because the ratio of I_2/I_1 is used as the tripping criterion, and the magnitude of I_2 is used as the constraining quantity.

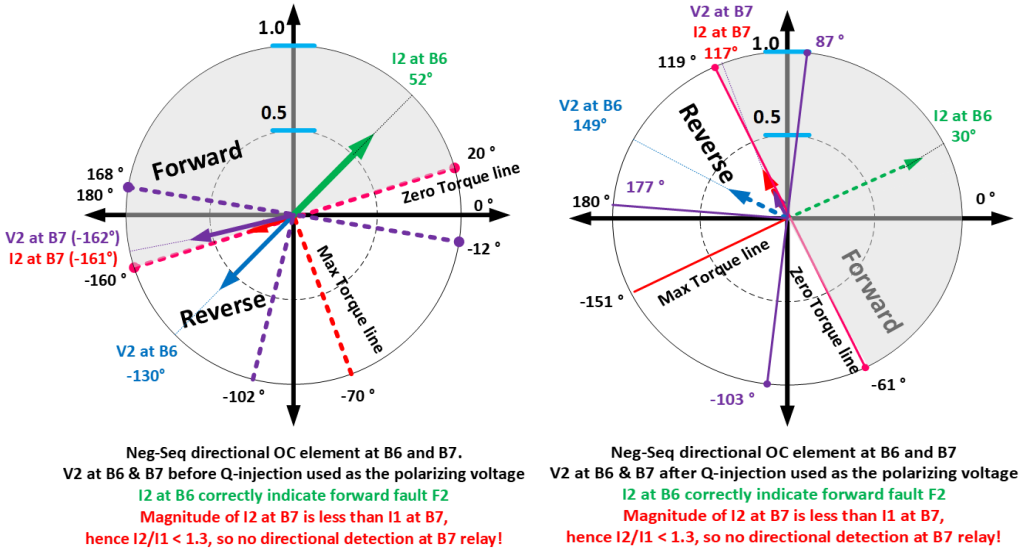

Figure 71. The operation of the 67Q directional element at buses B6 and B7 during LL fault F2 in the islanded mode with an RCA of 60° lagging with respect to V_2 at B6 and B7.

The angle of I_2 at B7 correctly indicates the reverse direction of LL fault F2 in the islanded mode before and after the additional Q-injection at DER-1 because the angle of I_2 at B7 lies in the unshaded area in both cases (Figure 71). Nevertheless, the magnitude of I_2 at B7 is less than the set threshold of 0.5 p.u. and the ratio of I_2/I_1 is also less than 1.3 before and after the additional Q-injection. Hence, the reverse direction of LL fault F2 at B7 in the islanded mode is not declared by the AND logic of the scheme.

It should be noted that in Figure 71, the characteristic of the 67Q element marked with red lines is used for the direction of fault at bus B6 whereas the characteristic of the 67Q element marked with purple lines is used for the direction of fault at bus B7. Further detailed information can be found in Publication V.

The evaluation of 67P and 67Q elements with Q-injection from both sides of the fault point will be covered in future publications. This will be useful for finding limitations and further applications of the proposed directional elements also in AC microgrids with looped or ring networks. It is assumed that the proposed 67P and 67Q elements may also work during other unbalanced types of faults like LLLG, LLG and LG. However, further study and simulations are required to confirm this. Also, a new 67G directional scheme using zero-sequence components could be developed on the basis of similar principles of operation as for 67P and 67Q.

4.7 Detection of open phase or series faults

The effective and potential schemes for the detection of open phase or series faults have been described in publication V of this thesis on the basis of a technical report (IEEE PES, 2020). Two of the potential schemes have been selected and analyzed in Publication V for the detection of phase-A open fault F1 in the grid-connected mode. The first potential scheme is based on the symmetrical components of currents, and the second potential scheme is based on the phase current unbalance for the detection of an open phase condition. The phase-A open fault F1 is created at the end of a 2 km line near PCC in the simulation model (Figure 63) at the simulation time of 2 s by opening the phase-A of CB2 in the grid-connected mode.

Figure 72 shows the rms instantaneous line currents and symmetrical components of current observed at bus B2 during open phase-A fault F1 in the grid-connected mode. Figure 72 (b) indicates an increasing negative-sequence current (I_2) after the opening of phase-A of CB2 from the simulation time of 2 s onwards. The magnitude of negative-sequence current (I_2) is equal to or greater than 50% of the pre-fault positive-sequence current (I_1). Therefore, the magnitude of I_2 or the ratio of I_2/I_1 can be used effectively for the detection of phase-A open fault F1 in the grid-connected mode. This scheme requires the magnitude of I_2 to be less than 50% of I_1 or the ratio of I_2/I_1 to be less than 0.5 during the maximum possible load unbalance in the network to avoid false tripping.

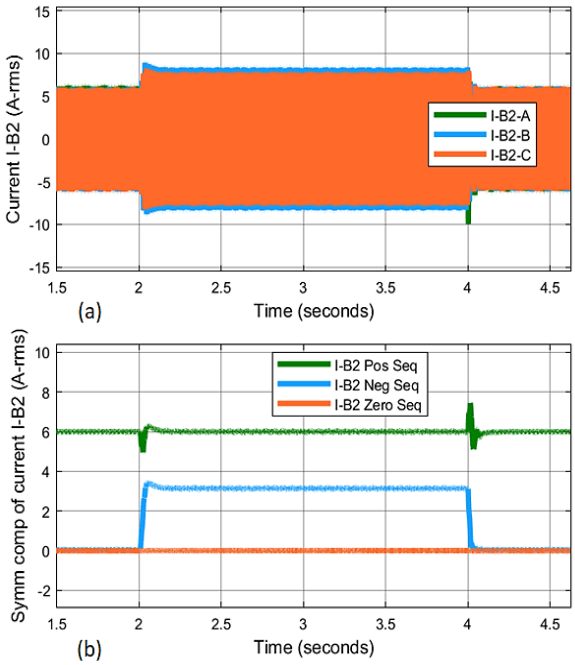

Figure 72. (a) the rms instantaneous line currents and (b) symmetrical components of current observed at bus B2 during an open phase-A fault F1 in the grid-connected mode.

Figure 73 indicates that the rms magnitude of line-A (*I-B2:A*) decreases whereas the rms magnitudes of line-B (*I-B2:B*) and line-C (*I-B2:C*) increase after the opening of phase-A of CB2 from the simulation time of 2 s onwards. Moreover, the line current *I-B2:A* of open phase-A is 50% or less than the line currents *I-B2:B* and *I-B2:C* of closed phases B and C. Therefore, the ratio of rms line currents can be a reliable indicator for the detection of phase-A open fault F1 in the grid-connected mode. Any ratio of rms line currents *(I-B2:A/I-B2:B) or (I-B2:A/I-B2:C)* equal to or less than 0.5 will indicate an open phase-A fault. Similarly, a phase-B open fault F1 and phase-C open fault F1 can also be detected. For the reliable detection of single-phase open faults, the load current unbalance or load current ratio between the phases needs to be maintained above 0.5 or 50% in normal operation.

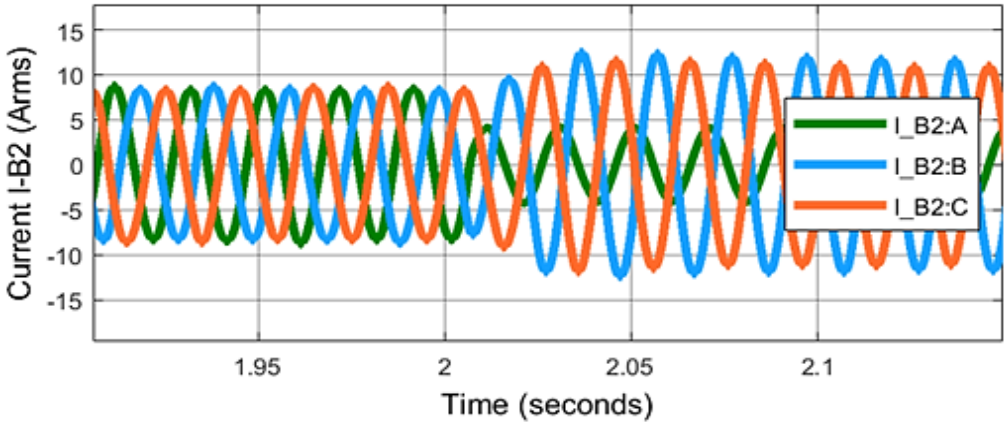

Figure 73. The rms instantaneous line currents observed at bus B2 during phase-A open fault F1 in the grid-connected mode.

The effectiveness of the above methods used for the detection of single-phase open faults needs to be further investigated for the detection of other types of open phase or series faults, like two-phase or three-phase open faults, particularly for the islanded mode of operation. This will be done in future publications. Additionally, other methods will also be simulated and tested in future for the sake of comparison.

4.8 New LVRT and HVRT curves for DERs

The new LVRT and HVRT (voltage vs time) curves of converter-based DERs are suggested in Publication II and Publication V of this thesis. The main objective of the new LVRT curve of the converter-based DERs is to ensure that each DER stays connected and also injects a fault current current according to its maximum capability for a duration of at least 2 s after the fault or voltage step so that primary and backup protection coordination is maintained. The main objective of the new HVRT curve of the converter-based DERs is to ensure that DERs ride through (stay connected) during times of overvoltage. The overvoltage is created by loading or unloading of transformers during switching operations when the AC microgrid transits from the grid-connected to the islanded mode and vice versa. The new HVRT curve will ensure a smooth transition from the grid-connected to the islanded mode and vice versa without the wide disconnections of DERs in the islanded AC microgrid. For achieving the HVRT capability, the DERs may need overvoltage protection devices, a high level of insulation, reactive power compensation, voltage regulation equipment, or another effective scheme. This all depends on the design of the converter, as well as the regulations and methods followed by the DER manufacturers. Some methods for reducing the transient

overvoltage at wind farm terminals are discussed in (Cai et al., 2016). The improved HVRT strategy for type-4 WTG with fully-rated converter is presented in (P. Liu et al., 2022). Also, for the LVRT capability of the converter-based DERs, some extra protection devices may be required like a crowbar switch at the DC link etc. Different LVRT strategies for WTGs are mentioned in (Howlader & Senjyu, 2016).

Considering the above factors, a new LVRT curve for converter-based DERs has been proposed and compared with other LVRT curves in Publication II as represented by the green line in Figure 74. According to the proposed LVRT curve, the DERs will stay connected and continue providing fault current from the inception of fault (or low voltage event) up to a duration of 2 s. After 2 s of the fault event, the DERs should raise their terminal voltage to 0.85 p.u. within the next 1 s or disconnect from the network. The voltage axis (from time axis 0 to 2 s) can be reduced to zero to cover even extreme short-circuit faults with zero voltage.

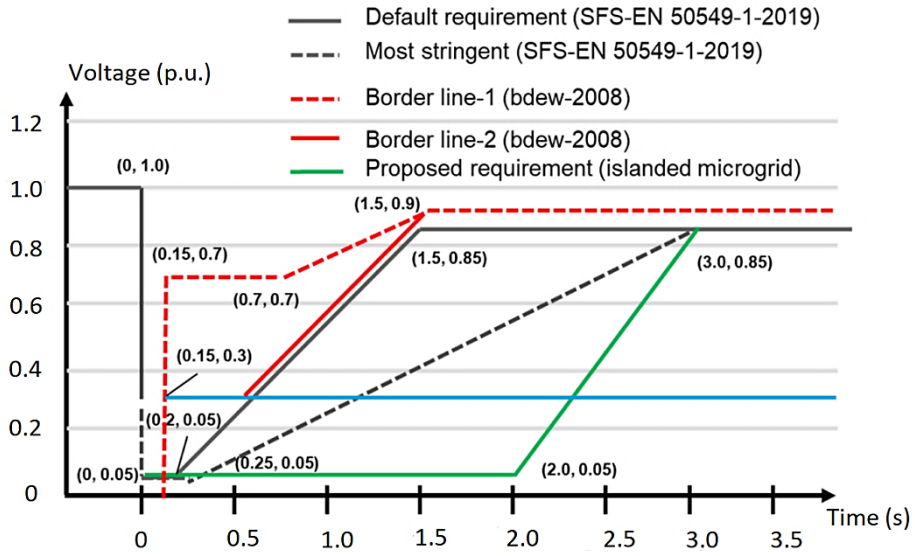

Figure 74. New LVRT curve for the converter-based DERs (green line) compared with other LVRT curves.

The new HVRT curve shown in Figure 75 is suggested based on the overvoltage observed in the simulation results of Publication IV during the transition of the AC microgrid from the grid-connected to the islanded mode. The new HVRT curve is applicable for the initial five cycles of the supply voltage frequency, that is, 0.1 s for a 50 Hz frequency. After the initial 0.1 s of the transition mode, the HVRT curve proposed by EN 50549-1-2019 and EN 50549-2-2019 grid codes will be applied.

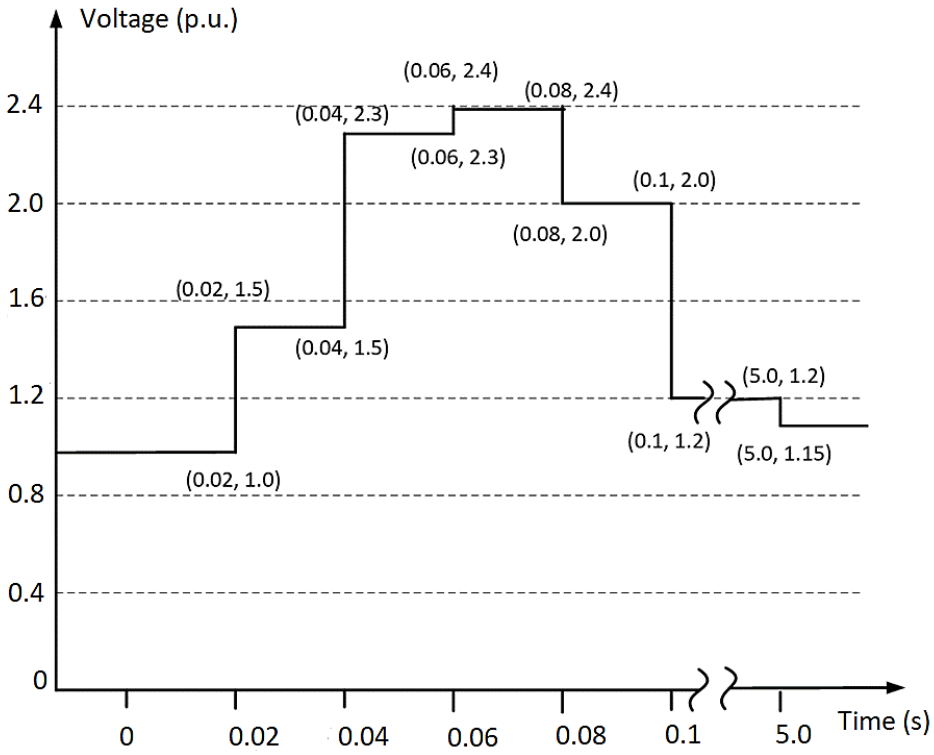

Figure 75. New five-cycle HVRT curve for converter-based DERs.

5 CONCLUSIONS AND FUTURE WORK SUGGESTIONS

5.1 Configurations of a radial AC microgrid

There can be various different configurations of an AC microgrid depending on the size, location, and control of DERs, BESS and related power electronic converters, in addition to network type and design. In the context of this thesis, four different types of radial AC microgrid configurations have been considered. These four radial AC microgrid configurations (configuration 1–configuration 4) are defined in Figure 76 in relation to the publications of this thesis. The first three configurations are step-down substation or feeder types of radial AC microgrids with MV and LV AC microgrids located at the respective MV and LV sides of the distribution transformer. The fourth configuration is a step-up substation or feeder type of radial AC microgrid with BESS connected at the LV side and load connected at the MV side.

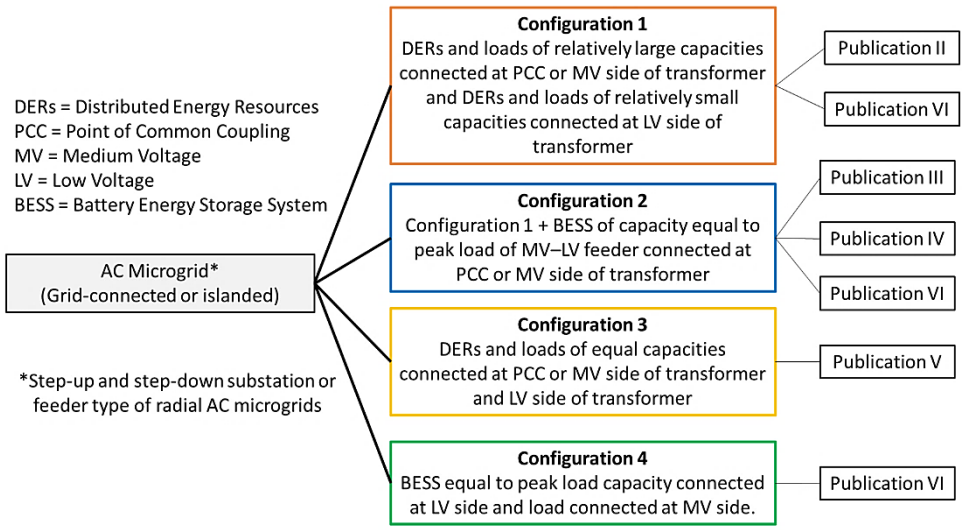

Figure 76. Configurations of a radial AC microgrid under consideration.

5.2 Conventional protection

In AC microgrids with configuration 1, at least one converter-based DER of a relatively large capacity is located at the MV side of the MV–LV distribution transformer. Therefore, for configuration 1 of AC microgrid with a limited fault current contribution up to 1.2 p.u. from all DERs, some definite-time overcurrent relays can use the same higher threshold settings as used in the grid-connected mode, while other relays use the adaptive lower threshold settings in the islanded mode depending on the availability of the relatively large converter-based DER.

However, the creation of further islands (MV system island and LV system island) within the islanded AC microgrid of configuration 1 separates the MV section with a large DER from the LV section with a small DER. Therefore, three-phase faults can only be detected by using the adaptive lower threshold settings of overcurrent relays in each section. The details of this phenomenon are discussed in Section 4.2 and Publication II. Publication VI also considers some islanded AC microgrids of configuration 1.

In AC microgrids with configuration 2, the BESS of capacity equal to the combined peak load of the MV–LV feeder is also located at the MV side of the MV–LV transformer, in addition to at least one converter-based DER of relatively large capacity. Therefore, the adaptive protection settings of definite-time overcurrent relays can be avoided if BESS provides a fault current contribution of 1.15–3.17 p.u. and other DERs provide fault current contributions of 1.2 p.u. However, the creation of islands within the islanded AC microgrid separates the section with a relatively large DER and BESS from the section with a relatively small DER. Therefore, adaptive lower threshold settings of definite-time overcurrent relays are required for the detection of three-phase faults inside the islanded LV section with a relatively small DER. The results show that the definite-time overcurrent function performs better than the inverse-time overcurrent function with the similar levels of fault current contributions of DERs. Further details can be found in Section 4.1 and Publication III. Publication IV also considers configuration 2 of the AC microgrid. Publication VI considers a slightly modified islanded version of configuration 2.

In AC microgrids with configuration 3, the converter-based DERs of equal capacity are located at both ends of the MV–LV distribution transformer and there is no large DER or BESS available in the islanded mode of operation. Therefore, for configuration 3 of the AC microgrid with a limited fault current contribution of DERs up to 1.2 p.u., three-phase faults can only be detected with adaptive lower threshold settings of overcurrent functions in the islanded mode. Configuration 3 of the AC microgrid is considered in Publication V.

For the harbor area AC microgrid with distributed DERs and BESS considered in Publication VI and presented in Section 4.4, different configurations of the islanding mode of operations are possible with the grid-forming control of converter-based DERs and BESS. Six configurations of islanded AC microgrids have been considered for the harbor area AC microgrid. Five of the considered islanded mode configurations are similar to configuration 1 and configuration 2 of Figure 76. Therefore, correct operations of definite-time overcurrent relays and fast fuse operations in the islanded modes are dependent on the fault current

contribution levels of DERs and BESS, and on the size or capacity of their converters. The fault current contribution up to 2.5–3 p.u. of the converter-based DERs and BESS is found to be enough for fast fuse operations within 20 ms and to avoid adaptive definite-time overcurrent settings of relays in the considered islanded modes.

The only exception for the islanded harbor area AC microgrid is configuration 3 of Figure 62, and that configuration is unique because the BESS of peak load capacity is connected at the LV side and the load is connected at the MV side of the distribution transformer. The configuration 3 of Figure 62 is referred to as configuration 4 in Figure 76. In AC microgrids with configuration 4, only adaptive protection will be able to detect faults and maintain protection coordination between OC relays even with a 3 p.u. limited fault current contribution of BESS. However, an additional BESS capacity of 25% will avoid adaptive protection settings and maintain proper protection coordination between definite-time OC relays in AC microgrids with configuration 4, according to the results presented in Publication VI.

For the operations of inverse-time overcurrent relays in the islanded harbor area AC microgrid, the fault current contribution of 2.5–3 p.u. is most probably not enough to avoid adaptive overcurrent settings. Nevertheless, the operations of inverse-time overcurrent relays in the islanded modes need to be checked further for different fault locations, and for different inverse-time characteristics to determine this phenomenon. This analysis will be useful for distribution networks in the U.S. and other countries using the inverse-time overcurrent function as the main protection scheme.

5.3 Adaptive protection

The adaptive overcurrent protection is the natural choice for the islanded mode of AC microgrids with configurations 1–4 (Figure 76), due to the limited magnitude of fault current contribution of converter-based DERs up to 1.2 p.u. The application of the adaptive overcurrent protection scheme using adaptive communication-based IEDs, and the centralized control architecture is the mainstream for AC microgrids. Different adaptive protection case studies and practical applications can be found in the literature review sections of Publications I–IV. The peer-to-peer Ethernet-based communication protocols offered by IEC 61850 standard, and particularly the GOOSE messages are suitable for implementing adaptive protection schemes with centralized as well as decentralized control architectures.

The results show that communication-based fault detection, isolation and adaptation of overcurrent protection settings in grid-connected and islanded modes is possible within 250 ms of the LVRT curve of DERs. The communication-based fault detection and isolation is independent of the fault location and the normal definite-time coordination of the relays. As long as the communication link is reliable and continuous, the fault detection, isolation, transition to islanded mode and change of adaptive protection settings could be completed faster using IEC 61850 standard based logical selectivity than by the usual methods. The monitoring of communication signal continuity, the redundancy of communication links, the check on quality and continuity of subscribed or received GOOSE messages by IEDs and cybersecurity need to be ensured for communication-based fault detection and isolation schemes.

The algorithms for adaptive protection schemes for AC microgrids using centralized and decentralized control architectures are proposed. In both cases, only two pre-defined reliable setting groups are changed adaptively, depending on the status of circuit breaker(s). The real-time simulation-based validation of adaptive protection algorithms and the estimation of round-trip time delay has been performed. The traditional definite-time coordination scheme between IEDs in parallel to the communication-based coordination is suggested for providing remote backup protection during communication failures. This will ensure the uninterrupted operations of the AC microgrid, though with delayed fault detection and isolation than seen in the communication-based coordination scheme. The transfer trip scheme and some directional protection is also required if DERs are located at both ends of the fault point. The simplest directional scheme is the current magnitude comparison scheme as proposed in Publication II for AC microgrids of configuration 1. Though the proposed directional scheme is also completely dependent on a communication link between relays.

The islanded LV system (encircled with green line in Figure 37) consisting of only PV system and LV load feeder will require an additional BESS in parallel with PV system to be used as a grid-forming source in order to continue power supply in that isolated or standalone LV section. If converters of both PV system and BESS provide a combined limited fault current contribution of 1.2 p.u. (as assumed in Publication II) then only adaptive lower setting group of definite-time overcurrent function will be able to detect three-phase short-circuit faults at LV load feeder. In this case, UV and symmetrical components based protection functions will provide local backup against high impedance and other unbalanced shunt faults. A local non-directional adaptive protection will be enough to protect LV load feeder assuming no fault current is being fed by other DERs installed along the LV feeder. Because of the limited scope, only substation type of LV AC microgrid (with

aggregated peak load of LV feeder supplied by a PV system connected at LV substation) is considered.

The performance of the proposed adaptive protection algorithms is independent of different types of control schemes used for converters as long as the converters are capable of providing a fault current contribution of 1.2 p.u. of the rated current or larger during faults. The proposed adaptive protection algorithms will also perform without problems if only an undervoltage measurement is available at an IED location. It means that high impedance faults causing an undervoltage of 0.5 p.u. or less could also be detected and isolated. However, only short-circuit faults are considered for the evaluation due to the limited scope of the thesis.

5.4 Grid codes

The EN 50549-2-2019 and IEEE 1547-2018 standards or grid codes for the connection requirements of DERs have been reviewed from the AC microgrid protection point of view. In this regard, the selected EN 50549-2-2019 grid code requirement of the dynamic reactive current injection by converter-based DERs has been evaluated during LL faults in the grid-connected and islanded modes of AC microgrid. The additional capacity of dynamic reactive power equal to twice the rated MVA capacity of converter-based DER is found to be enough to meet the minimum grid code requirements. Additionally, the new LVRT and HVRT curves of converter-based DERs are suggested for the islanded mode of operation. With the increasing penetration levels of renewable energy generation in distribution networks, the grid code requirements will keep changing, so it will be necessary to re-evaluate the new requirements. Moreover, further clarifications of the existing grid code requirements are also necessary, for example the discrimination of the provision of positive- and negative-sequence reactive current during different types of faults in the islanded mode. This type of discrimination will reduce the dynamic reactive power capacity required during faults in the islanded mode.

5.5 Directional protection

Directional protection is required in AC microgrids with loop networks or in AC microgrids with radial networks with DERs located at both ends of the fault point. The directional protection discriminates between the forward and reverse direction of the faults using some predefined principle of operation. The faults in the forward direction need to be isolated for the maintenance of protection coordination or selectivity between protection IEDs for an increased operational reliability of the distribution networks. This thesis proposes and evaluates new

directional protection schemes for AC microgrids based on the magnitudes and angles of symmetrical components of fault currents and voltages during LL faults in both grid-connected and islanded modes. The positive-sequence directional protection scheme 67P uses the magnitudes and angles of positive-sequence voltage and current during the LL fault. The negative-sequence directional protection scheme 67Q uses the magnitudes and angles of negative-sequence voltage and current during the LL fault. With few exceptions, the proposed directional schemes detect and isolate the LL fault by tripping a circuit breaker in the forward direction and prevent the tripping of a circuit breaker in the reverse direction of the fault. The reactive current injection needs to be avoided at the downstream of the network or LV side of the distribution network in the islanded mode of operation to avoid missing operation or causing a disturbance of the proposed directional schemes. The proposed directional schemes will also be tested for AC microgrids with loop networks in future publications.

5.6 Detection of open phase faults

Various effective and potential methods for the detection of the open phase or series faults are listed in Publication V. Two methods for the detection of open phase faults including symmetrical components and phase current unbalance have been analyzed and found to be effective for the detection of single-phase open faults. Further research in this regard is required to also detect two-phase and three-phase open faults. Additionally, HIL testing of these methods will provide the proof of concept for practical implementation.

5.7 Discussion

Communication-based adaptive protection schemes of radial AC microgrids with converter-based DERs are presented in this thesis. The IEC 61850 GOOSE protocol using Ethernet communication is selected for the implementation of centralized and decentralized adaptive protection schemes. A transfer time delay of 10–20 ms is assumed for one-way GOOSE message exchange between two IEDs and the assumed transfer time delay has been verified using real-time HIL testing. The listed six research questions addressed in this thesis are briefly answered in Section 5.7 based on considered assumptions and produced simulation results.

1) To what extent are conventional overcurrent protections suitable for the protection of an AC microgrid with converter-based DERs?

It is evident from results that conventional overcurrent protections using single setting group are not suitable for the protection of an AC microgrid with converter-based DERs. Although definite-time overcurrent relays using single setting group work without problems during three-phase short-circuit faults in the grid-connected mode, their operations become ineffective in the islanded mode of an AC microgrid. The inverse-time overcurrent relays using single setting group operate slower than definite-time overcurrent relays using single setting group during remote three-phase short-circuit faults in the grid-connected mode and during all considered three-phase short-circuit faults in the islanded mode. These conclusions are based on assumptions that only converter-based DERs are connected to an AC microgrid and fault current contributions of DERs are limited to 1.2 p.u. of the rated output current. The detailed answer to this question is given in Section 5.2 considering different configurations of a radial AC microgrid with and without an additional BESS.

2) What type of communication-based adaptive protection schemes will be required in radial AC microgrids with converter-based DERs?

The implementation of communication-based adaptive protection schemes can be done using centralized, decentralized or hybrid centralized and decentralized architectures depending on the reliability requirements of loads connected in radial AC microgrids. The hybrid centralized and decentralized adaptive protection scheme will provide benefits of both schemes by using an alternate scheme if one scheme fails. In any scheme, two pre-defined reliable setting groups, one for the grid-connected mode and other for the islanded mode, will be changed in an adaptive manner assuming all relays to be definite-time overcurrent relays. The detailed answer to this question is given in Section 5.3.

3) To what extent will the adaptivity of protection schemes in AC microgrids with converter-based DERs be affected or avoided when BESS are used as fault current sources?

The answer to this question depends on the particular case of an AC microgrid under study. In this thesis, the harbor area AC microgrid with converter-based DERs and BESS has been considered to check if adaptive overcurrent settings can be avoided. It has been found that adaptive definite-time overcurrent settings can be avoided if DERs and BESS provide fault current contribution of 2.5–3 p.u. This also ensures that fuse operates within 20 ms during three-phase short-circuit faults. The detailed answer to this question is given in Section 5.2 for the islanded modes of the harbor area AC microgrid.

4) What types of directional protection schemes are required for the grid-connected and islanded modes of operation of AC microgrids with converter-based DERs?

Different types of directional protection schemes have been reviewed in Publication V of this thesis. Considering the limited fault current contribution of converter-based DERs, symmetrical components based directional overcurrent elements (positive-sequence element [67P] and negative-sequence element [67Q]) have been suggested and evaluated in Section 4.6. These directional elements are briefly summarized in Section 5.5 to answer this question. Additionally, a simple current magnitude comparison based directional scheme is also proposed in Publication II for AC microgrids of configuration 1.

5) How can the IEC 61850 communication-based adaptive protection schemes of AC microgrids be tested and validated?

A wide range of testing methods of AC microgrids are discussed in Publication IV, Publication VII and Section 3.5 of this thesis. The IEC 61850 communication-based adaptive protection scheme of AC microgrids has been tested and validated using real-time HIL testing in this thesis. The details of the real-time HIL testing of adaptive protection are given in Publication IV and Section 4.3 of this thesis.

6) What kind of grid codes and communication standards will be required for future AC microgrids, particularly for the islanded mode of operation to ensure the proper protection of AC microgrids?

The operations of AC microgrids in both grid-connected and islanded modes require separate kind of grid codes for each mode of operation. It is found from the review done in Publication V that EN grid codes are only available for the grid-connected mode of operation in Europe. Section 3.1 shows that many IEC standards of AC microgrids are still in their earlier stages of the development. Considering these factors, new LVRT and HVRT curves of converter-based DERs are suggested for the islanded mode of AC microgrids in this thesis as explained in Section 4.8. Regarding communication standards, there are many SCADA communication protocols available as reviewed in Publication VII which can be used also for AC microgrids. However, IEC 61850 communication standard is getting more attention these days due to various advantages it offers as explained in Section 3.3.6. Therefore, IEC 61850 communication standard is selected for study in this thesis.

5.8 Limitations and applicability of the proposed solutions

Beside the limitations of the scope of this thesis mentioned in Section 1.6 the proposed solutions were developed and validated using only a limited number of various system models. Furthermore, the following additional limitations are applicable to the results presented:

- Only Edition 1 of IEC 61850 communication standard has been tested.
- Focus of HIL testing was only on "StVal" data attribute of XCBR logical node.
- The results of HIL testing are applicable only to the used hardware and software and the results are generated on the basis of "as available" laboratory setup and Ethernet communication.

Despite of these limitations the author believes that the proposed solutions are applicable to wide variety of radial AC microgrids. However, author acknowledges that considering some specific cases as indicated in Chapter 4, some further studies are required. In this regard, all the applied simulation models are available from the author on request.

5.9 Future work

The increasing applications of communication-based adaptive protection schemes for AC microgrids, the ever-increasing connections of converter-based DERs, the proposals of new grid codes, and the increasing levels of BESS applications for operational flexibility require a number of different kinds of detailed analyses and validation tests of the new approaches. In this regard, not only CHIL testing but also combined CHIL and PHIL simulations will be required for the practical implementation of new AC microgrid configurations in the future. The implementation and analysis of different grid-forming and decoupled sequence control using the detailed models of converter-based DERs, the development of more accurate RT simulation solutions using FPGAs, co-simulations of EMT and phasor models, and analyses of protection schemes for looped and hybrid AC–DC microgrids will be important and interesting research areas in the future.

Though Ethernet-based implementation of IEC 61850 tunneled-GOOSE protocol is reliable for communication between substations, it might not be a cost-effective solution. The application of IEC 61850 routable-GOOSE message using different wireless technologies like 4G, 5G etc. may provide an economical choice. The

applications of PMUs and Micro-PMUs using synchronized measurements and cloud based wide area control for adaptive and backup protection schemes, and other advanced protection solutions based on optimization methods and artificial intelligence techniques will be important topics of the future research.

Regarding LG or earth faults in AC microgrids, a separate detailed study is required that should include a comparison of all possible earthing systems used for MV and LV AC microgrids. This will also be an important topic of the future research.

REFERENCES

ABB. (2009). *Relion® 670 series Self supervision techniques, 670 series Principles and functions Document ID: 1MRK 580 172-XEN*. ABB AB Substation Automation Products, Västerås, Sweden. https://library.e.abb.com/public/9830608e2e48f75fc12576f10031debf/1MRK580172-XEN_A_en_670_series_self_supervision.pdf

ABB. (2011a). *Distribution Automation Handbook Section 8.2 Relay Coordination*. ABB Oy. https://library.e.abb.com/public/eccfd9ab4d23ca1dc125795f0042c8db/DAHandbook_Section_08p02_Relay_Coordination_757285_ENa.pdf

ABB. (2011b). *Relion® Protection and Control. 650 Series IEC 61850 Communication Protocol Manual, Revision: Product version: 1.1 Document ID: 1MRK 511 242-UEN*. ABB AB Substation Automation Products SE-721 59. https://search.abb.com/library/Download.aspx?DocumentID=1MRK511242-UEN&LanguageCode=en&DocumentPartId=&Action=Launch&DocumentRevisionId=-

ABB. (2014). *Relion® Protection and Control 670 series 2.0 IEC IEC 61850 Edition 1 Communication Protocol Manual Document ID: 1MRK 511 302-UEN*. ABB AB Substation Automation Products SE-721 59. https://library.e.abb.com/public/85dfdd305f314030c1257d940036249d/1MRK511302-UEN_-_en_Communication_protocol_manual__IEC_61850_Edition_1__670_series_2.0__IEC.pdf

Ackermann, T. (2005). *Wind Power in Power Systems*. John Wiley & Sons, Ltd.

Adamiak, M., Baigent, D., & Mackiewicz, R. (2009). IEC 61850 communication networks and systems in substations: An overview for users. *The Protection & Control Journal*, 61–68.

Aftab, M. A., Roostaee, S., Suhail Hussain, S. M., Ali, I., Thomas, M. S., & Mehfuz, S. (2018). Performance evaluation of IEC 61850 GOOSE-based inter-substation communication for accelerated distance protection scheme. *IET Gener Transm Dis*, *12*(18), 4089–4098. https://doi.org/10.1049/iet-gtd.2018.5481

Alam, M. N., Das, B., & Pant, V. (2015). A comparative study of metaheuristic optimization approaches for directional overcurrent relays coordination. *Electric Power Systems Research*, *128*, 39–52. https://doi.org/10.1016/j.epsr.2015.06.018

Alipoor, J., Miura, Y., & Ise, T. (2015). Power System Stabilization Using Virtual Synchronous Generator With Alternating Moment of Inertia. *IEEE Journal of Emerging and Selected Topics in Power Electronics*, *3*(2), 451–458. https://doi.org/10.1109/JESTPE.2014.2362530

Al-Nasseri, H., & Redfern, M. A. (2008). Harmonics content based protection scheme for Micro-grids dominated by solid state converters. *2008 12th*

International Middle-East Power System Conference, 50–56. https://doi.org/10.1109/MEPCON.2008.4562361

Al-Nasseri, H., Redfern, M. A., & Li, F. (2006). A voltage based protection for micro-grids containing power electronic converters. *2006 IEEE Power Engineering Society General Meeting*, 7 pp.-. https://doi.org/10.1109/PES.2006.1709423

Altuve, H. J., Zimmerman, K., & Tziouvaras, D. (2016). Maximizing line protection reliability, speed, and sensitivity. *2016 69th Annual Conference for Protective Relay Engineers (CPRE)*, 1–28. https://doi.org/10.1109/CPRE.2016.7914896

Amin, M. R., Negnevitsky, M., Franklin, E., Alam, K. S., Zicmane, I., Lomane, T., & Varfolomejeva, R. (2021). Frequency Control using Grid-forming and Grid-following Battery Energy Storage Systems. *2021 IEEE 62nd International Scientific Conference on Power and Electrical Engineering of Riga Technical University (RTUCON)*, 1–6. https://doi.org/10.1109/RTUCON53541.2021.9711699

Apostolov, A., & Vandiver, B. (2015, June). To GOOSE or not to GOOSE? that is the question. *Protection, Automation and Control Magazine, PAC World*, *18*(32), 18–25.

Atteya, A. I., El Zonkoly, A. M., & Ashour, Hamdy. A. (2017). Optimal relay coordination of an adaptive protection scheme using modified PSO algorithm. *2017 Nineteenth International Middle East Power Systems Conference (MEPCON)*, 689–694. https://doi.org/10.1109/MEPCON.2017.8301256

Australian Energy Market Operator, AEMO. (2013). *Wind Turbine Plant Capabilities Report 2013 Wind Integration Studies* [Technical Information Paper]. Australian Energy Market Operator, AEMO. https://aemo.com.au/-/media/files/electricity/nem/security_and_reliability/reports/wind_turbine_plant_capabilities_report.pdf

Baier, M., Bhavaraju, V., Murch, W., & Teleke, S. (2017). *Making microgrids work: Practical and technical considerations to advance power resiliency* (Thought Leadership White Paper WP027009EN / GG). Eaton. https://www.eaton.com/content/dam/eaton/services/eess/eess-documents/making-microgrids-work-wp027009en.pdf

Baran, M., & El-Markabi, I. (2004). Adaptive over current protection for distribution feeders with distributed generators. *IEEE PES Power Systems Conference and Exposition, 2004.*, 715–719 vol.2. https://doi.org/10.1109/PSCE.2004.1397672

Beheshtaein, S., Cuzner, R., Savaghebi, M., & Guerrero, J. M. (2019). Review on microgrids protection. *IET Generation, Transmission & Distribution*, *13*(6), 743–759. https://doi.org/10.1049/iet-gtd.2018.5212

Bekker, F., Nohe, S., & Echeverria, A. (2015, June). Non-Deterministic PAC Systems to Meet Deterministic Requirements. *Protection, Automation and Control Magazine, PAC World*, *18*(32), 54–59.

Bignucolo, F., Caldon, R., & Prandoni, V. (2008). Radial MV Networks voltage regulation with distribution management system coordinated controller. *Electric Power System Research*, *78*, 634–645.

Bintoudi, A. D., Zyglakis, L., Apostolos, T., Ioannidis, D., Al-Agtash, S., Martinez-Ramos, J. L., Onen, A., Azzopardi, B., Hadjidemetriou, L., Martensen, N., Demoulias, C., & Tzovaras, D. (2017). Novel hybrid design for microgrid control. *IEEE PES Asia-Pacific Power and Energy Engineering Conference (APPEEC), Bangalore, India*. https://doi.org/doi: 10.1109/APPEEC.2017.8308958

Bollen, M. H. J., & Häger, M. (2004). Power quality: Interactions between distributed energy resources, the grid and other customers. *In Proceedings of the 1st International Conference on Renewable Energy Sources and Distributed Energy Resources, Brussels, Belgium, 1-3 December*.

Bollen, M. H. J., & Rönnberg, S. K. (2017). Hosting Capacity of the Power Grid for Renewable Electricity Production and New Large Consumption Equipment. *Energies*, *10*(1325). https://doi.org/10.3390/en10091325

Bollen, M., & Hassan, F. (2011). *Integration of Distributed Generation in the Power System*. Wiley-IEEE Press.

Bonetti, A., Spitzenberg, K., Schottenius, L., & Larsson, S. (2020). *Technical Guide Testing self-powered relays with SVERKER 900* (Technical Guide CR036201AE V01). Megger Sweden AB. https://www.researchgate.net/publication/344340419

Brahma, S. M., & Girgis, A. A. (2004). Development of adaptive protection scheme for distribution systems with high penetration of distributed generation. *IEEE Transactions on Power Delivery*, *19*(1), 56–63. https://doi.org/10.1109/TPWRD.2003.820204

Brand, K.-P. (2004). The standard IEC 61850 as prerequisite for intelligent applications in substations. *IEEE Power Engineering Society General Meeting, 2004.*, 714-718 Vol.1. https://doi.org/10.1109/PES.2004.1372909

Brunner, C. (2015, December). IEC 61850 Update: Testing in IEC 61850. *Protection, Automation and Control Magazine, PAC World*, *18*(34), 27.

Bukhari, S. B. A., Haider, R., Zaman, M. S. U., Oh, Y.-S., Cho, G.-J., & Kim, C.-H. (2018). An interval type-2 fuzzy logic based strategy for microgrid protection. *International Journal of Electrical Power & Energy Systems*, *98*, 209–218. https://doi.org/10.1016/j.ijepes.2017.11.045

Cai, R., Andersson, M., & Xie, H. (2016). Methods for Transient AC Overvoltage Reduction at Wind Farm Terminal. *2016 China International Conference on Electricity Distribution (CICED 2016)*, Paper No. CP0154, pp. 1–6. https://library.e.abb.com/public/e3e31dabd0234053b4c637832cc6497c/Methods%20for%20Transient%20AC%20Overvoltage%20Reduction%20at%20Wind.pdf

Chandorkar, M. C., Divan, D. M., & Adapa, R. (1993). Control of parallel connected inverters in standalone AC supply systems. *IEEE Transactions on Industry Applications*, *29*(1), 136–143. https://doi.org/10.1109/28.195899

Che, L., Khodayar, M. E., & Shahidehpour, M. (2014). Adaptive Protection System for Microgrids: Protection practices of a functional microgrid system. *IEEE Electrification Magazine*, *2*(1), 66–80. https://doi.org/10.1109/MELE.2013.2297031

Chowdhury, S., Chowdhury, S. P., & Crossley, P. (2009). *Microgrids and Active Distribution Networks*. Institution of Engineering and Technology. https://digital-library.theiet.org/content/books/po/pbrn006e

Clarke, G. R., Reynders, D., & Wright, E. (2004). *Practical Modern SCADA Protocols: DNP3, 60870.5 and Related Systems*. Elsevier; Oxford, London.

Coffele, F., Booth, C., & Dyśko, A. (2015). An Adaptive Overcurrent Protection Scheme for Distribution Networks. *IEEE Transactions on Power Delivery*, *30*(2), 561–568. https://doi.org/10.1109/TPWRD.2013.2294879

Conti, S., Raffa, L., & Vagliasindi, U. (2009). Innovative solutions for protection schemes in autonomous MV micro-grids. *2009 International Conference on Clean Electrical Power*, 647–654. https://doi.org/10.1109/ICCEP.2009.5211985

Daehnick, C., Klinghoffer, I., Maritz, B., & Wiseman, B. (2020). *Aerospace & Defense Practice Large LEO satellite constellations: Will it be different this time?* McKinsey & Company. https://www.mckinsey.com/~/media/McKinsey/Industries/Aerospace%20and%20Defense/Our%20Insights/Large%20LEO%20satellite%20constellations%20Will%20it%20be%20different%20this%20time/Large-LEO-satellite-constellations-Will-it-be-different-this-time-VF.pdf

Dewadasa, J. M., Ghosh, A., & Ledwich, G. (2008). Distance protection solution for a converter controlled microgrid. *Fifteenth National Power Systems Conference (NPSC),* 586–591. https://www.iitk.ac.in/npsc/Papers/NPSC2008/oral/p69.pdf

Dewadasa, M., Ghosh, A., & Ledwich, G. (2009). An inverse time admittance relay for fault detection in distribution networks containing DGs. *TENCON 2009 - 2009 IEEE Region 10 Conference*, 1–6. https://doi.org/10.1109/TENCON.2009.5396204

Dewadasa, M., Ghosh, A., & Ledwich, G. (2011). Protection of microgrids using differential relays. *AUPEC 2011*, 1–6.

Dimeas, A., Tsikalakis, A., Kariniotakis, G., & Korres, G. (2013). Microgrids Control Issues. In *Microgrids* (pp. 25–80). John Wiley & Sons, Ltd. https://doi.org/10.1002/9781118720677.ch02

Doyle, M. T. (2002). Reviewing the impacts of distributed generation on distribution system protection. *IEEE Power Engineering Society Summer Meeting, 1*, 103–105 vol.1. https://doi.org/10.1109/PESS.2002.1043186

Du, W., Liu, Y., Huang, R., Tuffner, F. K., Xie, J., & Huang, Z. (2022). Positive-Sequence Phasor Modeling of Droop-Controlled, Grid-Forming Inverters with Fault Current Limiting Function. *2022 IEEE Power & Energy Society Innovative Smart Grid Technologies Conference (ISGT)*, 1–5. https://doi.org/10.1109/ISGT50606.2022.9817530

Du, W., Schneider, K. P., Tuffner, F. K., Chen, Z., & Lasseter, R. H. (2019). Modeling of Grid-Forming Inverters for Transient Stability Simulations of an all Inverter-based Distribution System. *2019 IEEE Power & Energy Society Innovative Smart Grid Technologies Conference (ISGT)*, 1–5. https://doi.org/10.1109/ISGT.2019.8791620

Du, W., Tuffner, F. K., Schneider, K. P., Lasseter, R. H., Xie, J., Chen, Z., & Bhattarai, B. (2021). Modeling of Grid-Forming and Grid-Following Inverters for Dynamic Simulation of Large-Scale Distribution Systems. *IEEE Transactions on Power Delivery*, *36*(4), 2035–2045. https://doi.org/10.1109/TPWRD.2020.3018647

Eissa, M. M. (2018a). A New Wide-Area Protection Scheme for Single- and Double-Circuit Lines Using 3-D-Phase Surface. *IEEE Transactions on Power Delivery*, *33*(6), 2613–2623. https://doi.org/10.1109/TPWRD.2018.2808288

Eissa, M. M. (2018b). Challenges and novel solution for wide-area protection due to renewable sources integration into smart grid: An extensive review. *IET Renewable Power Generation*, *12*(16), 1843–1853. https://doi.org/10.1049/iet-rpg.2018.5175

El Hariri, M., Harmon, E., Youssef, T., Saleh, M., Habib, H., & Mohammed, O. (2019). The IEC 61850 Sampled Measured Values Protocol: Analysis, Threat Identification, and Feasibility of Using NN Forecasters to Detect Spoofed Packets. *Energies*, *12*(19). https://doi.org/10.3390/en12193731

El Naily, N., Saad, Saad. M., Hussein, T., & Mohamed, F. A. (2017). Minimizing the impact of distributed generation of a weak distribution network with an artificial intelligence technique. *Applied Solar Energy*, *53*(2), 109–122. https://doi.org/10.3103/S0003701X17020128

Elbana, M. S., Abbasy, N., Meghed, A., & Shaker, N. (2019). MPMU-based smart adaptive protection scheme for microgrids. *Journal of Modern Power Systems and Clean Energy*, *7*(4), 887–898. https://doi.org/10.1007/s40565-019-0533-6

El-Khattam, W., & Sidhu, T. S. (2008). Restoration of Directional Overcurrent Relay Coordination in Distributed Generation Systems Utilizing Fault Current Limiter. *IEEE Transactions on Power Delivery*, *23*(2), 576–585. https://doi.org/10.1109/TPWRD.2008.915778

El-khattam, W., & Sidhu, T. S. (2009). Resolving the impact of distributed renewable generation on directional overcurrent relay coordination: A case study. *IET Renewable Power Generation*, *3*(4), 415-425(10).

Enayati, B., Bravo, R., Ropp, M., Higginson, M., Agüero, Key, T., Cleveland, F., Siira, M., Quint, R., Vartanian, C., & Zhang, L. (2018). *Impact of IEEE 1547*

Standard on Smart Inverters (Technical Report, White Paper PES-TR67). IEEE PES Industry Technical Support Task Force.

Erunkulu, O. O., Zungeru, A. M., Lebekwe, C. K., Mosalaosi, M., & Chuma, J. M. (2021). 5G Mobile Communication Applications: A Survey and Comparison of Use Cases. *IEEE Access*, *9*, 97251–97295. https://doi.org/10.1109/ACCESS.2021.3093213

Etherden, N. (2014). *Increasing the Hosting Capacity of Distributed Energy Resources Using Storage and Communication* [Doctoral Thesis, Luleå University of Technology, Sweden]. https://www.diva-portal.org/smash/get/diva2:991499/FULLTEXT01.pdf

European Commission. (n.d.-a). *2030 climate & energy framework* [An official website of the European Union]. European Commission. Retrieved April 5, 2021, from https://ec.europa.eu/clima/policies/strategies/2030_en

European Commission. (n.d.-b). *2050 long-term strategy* [An official website of the European Union]. European Commission. Retrieved April 5, 2021, from https://ec.europa.eu/clima/policies/strategies/2050_en

European Commission. (n.d.-c). *Sustainable Development Goals* [An official website of the European Union]. European Commission. Retrieved March 25, 2021, from https://ec.europa.eu/international-partnerships/sustainable-development-goals_en

Eurostat. (2020, December). *Renewable energy statistics* [Eurostat, European Commission]. Eurostat Statistics Explained. https://ec.europa.eu/eurostat/statistics-explained/index.php/Renewable_energy_statistics#Wind_and_water_provide_most_renewable_electricity.3B_solar_is_the_fastest-growing_energy_source

Finnish Government Valtioneuvosto. (2020, February 3). *Government roadmap to carbon neutral Finland-climate leadership means opportunities for the whole country* [Government Communications Department]. Finnish Government. https://valtioneuvosto.fi/en/-/10616/hallitus-laati-tiekartan-hiilineutraaliin-suomeen-edellakavijyys-ilmastotoimissa-luo-mahdollisuuksia-koko-suomeen

Fusero, M., Tuckey, A., Rosini, A., Serra, P., Procopio, R., & Bonfiglio, A. (2019). A Comprehensive Inverter-BESS Primary Control for AC Microgrids. *Energies*, *12*(20), 3810. https://doi.org/10.3390/en12203810

Gao, X., Zhou, D., Anvari-Moghaddam, A., & Blaabjerg, F. (2021). Grid-Following and Grid-Forming Control in Power Electronic Based Power Systems: A Comparative Study. *IECON 2021 – 47th Annual Conference of the IEEE Industrial Electronics Society*, 1–6. https://doi.org/10.1109/IECON48115.2021.9589432

Gers, J. M., & Holmes, E. J. (2004). *Protection of electricity distribution networks* (2nd ed.). The Institution of Electrical Engineers.

Ghadiri, S. M. E., & Mazlumi, K. (2020). Adaptive protection scheme for microgrids based on SOM clustering technique. *Applied Soft Computing*, *88*, 106062. https://doi.org/10.1016/j.asoc.2020.106062

Ghalei Monfared Zanjani, M., Mazlumi, K., & Kamwa, I. (2018). Application of μPMUs for adaptive protection of overcurrent relays in microgrids. *IET Generation, Transmission & Distribution*, *12*(18), 4061–4068. https://doi.org/10.1049/iet-gtd.2018.5898

Gore, R. N., & Valsan, S. P. (2018). Wireless communication technologies for smart grid (WAMS) deployment. *2018 IEEE International Conference on Industrial Technology (ICIT)*, 1326–1331. https://doi.org/10.1109/ICIT.2018.8352370

Gouveia, J., Moreira, C. L., & Lopes, J. A. P. (2019). Grid-Forming Inverters Sizing in Islanded Power Systems – a stability perspective. *International Conference on Smart Energy Systems and Technologies (SEST), 2019*, 1–6. https://doi.org/doi: 10.1109/SEST.2019.8849110.

Guerrero, J. M., Chandorkar, M., Lee, T.-L., & Loh, P. C. (2013). Advanced Control Architectures for Intelligent Microgrids—Part I: Decentralized and Hierarchical Control. *IEEE Transactions on Industrial Electronics*, *60*(4), 1254–1262. https://doi.org/10.1109/TIE.2012.2194969

Hatziargyriou, N. D., Jenkins, N., Strbac, G., Pecas Lopes, J. A., Ruela, Engler, A., Oyarzabal, J., Kariniotakis, G., & Amorim, A. (2006). Microgrids-Large Scale Integration of Microgeneration to Low Voltage Grids. *CIGRE 2006 Paris, France, Aug.,* C6-309.

Helinks LLC. (n.d.). *HELINKS System Tools For IEC 61850 Harness the power of IEC 61850*. Helinks LLC IEC61850 Expertise Engineering Substation Automation. Retrieved February 2, 2023, from https://www.helinks.com/

Heussen, K., Babazadeh, D., Degefa, M. Z., Taxt, H., Merino, J., Nguyen, V. H., Teimourzadeh Baboli, P., Moghim Khavari, A., Rikos, E., Pellegrino, L., Tran, Q. T., Jensen, T. V., Kotsampopoulos, P., & Strasser, T. I. (2020). Test Procedure and Description for System Testing. In T. I. Strasser, E. C. W. de Jong, & M. Sosnina (Eds.), *European Guide to Power System Testing: The ERIGrid Holistic Approach for Evaluating Complex Smart Grid Configurations* (pp. 13–33). Springer International Publishing. https://doi.org/10.1007/978-3-030-42274-5_2

Hirsch, A., Parag, Y., & Guerrero, J. (2018). Microgrids: A review of technologies, key drivers, and outstanding issues. *Renewable and Sustainable Energy Reviews*, *90*, 402–411. https://doi.org/10.1016/j.rser.2018.03.040

Horowitz, K. A. W., Ding, F., Mather, B., & Palmintier, B. (2018). *The Cost of Distribution System Upgrades to Accommodate Increasing Penetrations of Distributed Photovoltaic Systems on Real Feeders in the United States* (Technical Report NREL/TP-6A20-70710). National Renewable Energy Laboratory, NREL. https://www.nrel.gov/docs/fy18osti/70710.pdf

Horowitz, S. H., & Phadke, A. G. (2008). *Power System Relaying* (3rd ed.). John Wiley & Sons Ltd.

Hou, D., & Dolezilek, D. (2010). IEC 61850-What It Can and Cannot Offer to Traditional Protection Schemes. *Schweitzer Engineering Laboratories, Inc. SEL J. Reliab. Power*, *1*(2), 1–11.

Howlader, A. M., & Senjyu, T. (2016). A comprehensive review of low voltage ride through capability strategies for the wind energy conversion systems. *Renewable and Sustainable Energy Reviews*, *56*, 643–658. https://doi.org/10.1016/j.rser.2015.11.073

Ibrahim, R. A., & Zakzouk, N. E. (2022). A PMSG Wind Energy System Featuring Low-Voltage Ride-through via Mode-Shift Control. *Applied Sciences*, *12*(3), 964. https://doi.org/10.3390/app12030964

IEC 61850-5. (2003). *Communication Networks and Systems in Substations—Part 5: Communication Requirements for Functions and Device Models*. International Electrotechnical Commission, TC 57: Geneva, Switzerland, 2003.

IEC 61850-5. (2013). *Communication Networks and Systems in Substations—Part 5: Communication Requirements for Functions and Device Models*. International Electrotechnical Commission, TC 57: Geneva, Switzerland, 2013.

IEC 61850-9-2. (2011). *Communication networks and systems for power utility automation—Part 9-2: Specific communication service mapping (SCSM)—Sampled values over ISO/IEC 8802-3*. International Electrotechnical Commission, TC 57: Geneva, Switzerland, 2011.

IEEE PES. (2020). *Methods for detecting and analyzing an open phase condition of a power circuit to a nuclear plant station service or startup transformer* (Technical Report PES-TR75). IEEE PES Power Syst. Relay. Control Committee. Working Group K11.

IEEE Standards Association. (n.d.). *IEEE SA Standards Store IEEE Catalog Protective Relaying*. Retrieved November 21, 2022, from https://www.techstreet.com/subgroups/36815?sort_direction=desc+NULLS+LAST&sort_order=edition_date&action=show&controller=subgroups&gateway_code=ieee&id=36815&sort_direction=desc+NULLS+LAST&sort_order=edition_date&per_page=10

IEEE Std 242. (2001). IEEE Recommended Practice for Protection and Coordination of Industrial and Commercial Power Systems (IEEE Buff Book). *IEEE Std 242-2001 (Revision of IEEE Std 242-1986) [IEEE Buff Book]*, 1–710. https://doi.org/10.1109/IEEESTD.2001.93369

IEEE Std 1547.4. (2011). IEEE Guide for Design, Operation, and Integration of Distributed Resource Island Systems with Electric Power Systems. *IEEE Std 1547.4-2011*, 1–54. https://doi.org/10.1109/IEEESTD.2011.5960751

International Energy Agency, IEA. (n.d.). *Access to electricity* [Official Website of IEA]. IEA. Retrieved August 22, 2022, from https://www.iea.org/reports/sdg7-data-and-projections/access-to-electricity

IRENA. (2016). *Scaling up Variable Renewable Power: The Role of Grid Codes* (p. 98). International Renewable Energy Agency (IRENA). www.irena.org/publications

IRENA. (2020). *Global Renewables Outlook: Energy transformation 2050* (Outlook ISBN 978-92-9260-238-3; p. 291). International Renewable Energy Agency. www.irena.org/publications

ISO/IEC 7498-1. (1994). *Information technology-Open Systems Interconnection-Basic Reference Model: The Basic Model*. ISO/IEC Switzerland.

Jager, J., Keil, T., Shang, L., & Krebs, R. (2004). New protection co-ordination methods in the presence of distributed generation. *2004 Eighth IEE International Conference on Developments in Power System Protection*, *1*, 319-322 Vol.1. https://doi.org/10.1049/cp:20040127

Javadi, M. S., Esmaeel Nezhad, A., Anvari-Moghaddam, A., & Guerrero, J. M. (2018). Optimal Overcurrent Relay Coordination in Presence of Inverter-Based Wind Farms and Electrical Energy Storage Devices. *2018 IEEE International Conference on Environment and Electrical Engineering and 2018 IEEE Industrial and Commercial Power Systems Europe (EEEIC / I&CPS Europe)*, 1–5. https://doi.org/10.1109/EEEIC.2018.8494605

Jenkins, N., Wu, X., Jayawarna, N., Zhang, Y., Lopes, J. P., Moreira, C., Madureira, A., & Silva, J. P. da. (2005). *Large Scale Integration of Micro-Generation to Low Voltage Grids, Work Package E, Deliverable DE2, Protection Guidelines for a Microgrid* (ENK5-CT-2002–00610; pp. 1–370).

Jeong, Y., Lee, H., Lee, S., & Kim, Y. (2013). High-speed AC circuit breaker and high-speed OCR. *CIRED 22nd International Conference on Electricity Distribution Stockholm, 10–13 June 2013*, Paper No. 0608.

Jin, Y. T., Park, S. J., Lee, S. J., & Choi, M. S. (2011). Intelligent agent based protection for smart distribution systems. *CIRED 21st International Conference on Electricity Distribution, 6–9 June, 2011*, Paper No. 0383. http://www.cired.net/publications/cired2011/part1/papers/CIRED2011_0383_final.pdf

Jin, Z., & Wang, X. (2022). A DQ-Frame Asymmetrical Virtual Impedance Control for Enhancing Transient Stability of Grid-Forming Inverters. *IEEE Transactions on Power Electronics*, *37*(4), 4535–4544. https://doi.org/10.1109/TPEL.2021.3124286

Kannuppaiyan, S., & Chenniappan, V. (2015). Numerical inverse definite minimum time overcurrent relay for microgrid power system protection. *IEEJ Transactions on Electrical and Electronic Engineering*, *10*(1), 50–54. https://doi.org/10.1002/tee.22066

Kar, S., & Samantaray, S. R. (2014). Time-frequency transform-based differential scheme for microgrid protection. *IET Generation, Transmission & Distribution*, *8*(2), 310-320(10).

Keyhani, A., Marwali, M. N., & Dai, M. (2010). *Integration of green and renewable energy in electric power systems*. John Wiley & Sons, Inc.

Khaligh, A., & Dusmez, S. (2012). Comprehensive Topological Analysis of Conductive and Inductive Charging Solutions for Plug-In Electric Vehicles. *IEEE Transactions on Vehicular Technology*, *61*, 3475–3489. https://doi.org/doi: 10.1109/TVT.2012.2213104

Khavnekar, A., Wagh, S., & More, A. (2015). Comparative analysis of IEC 61850 Edition-I and II standards for substation automation. *2015 IEEE International Conference on Computational Intelligence and Computing Research (ICCIC)*, 1–6. https://doi.org/10.1109/ICCIC.2015.7435756

Khederzadeh, M. (2009). Application of TCSC to restore directional overcurrent relay coordination in systems with distributed generation. *CIRED 2009 - 20th International Conference and Exhibition on Electricity Distribution - Part 1*, 1–4. https://doi.org/10.1049/cp.2009.0515

Kim, H. S., & Lu, D. D. (2010). Review on wind turbine generators and power electronic converters with the grid-connection issues. *20th Australasian Universities Power Engineering Conference, Christchurch, New Zealand*, 1–6.

Koushki, B., Safaee, A., Jain, P., & Bakhshai, A. (2014). Review and comparison of bi-directional AC-DC converters with V2G capability for on-board EV and HEV. *IEEE Transportation Electrification Conference and Expo (ITEC)*, 1–6.

Krstic, S., Wellner, E. L., Bendre, A. R., & Semenov, B. (2007). Circuit Breaker Technologies for Advanced Ship Power Systems. *2007 IEEE Electric Ship Technologies Symposium*, 201–208. https://doi.org/10.1109/ESTS.2007.372086

Kumar, D. S., J.S., S., & S., B. S. (2020). Micro-synchrophasor based special protection scheme for distribution system automation in a smart city. *Protection and Control of Modern Power Systems*, *5*(1), 9. https://doi.org/10.1186/s41601-020-0153-1

Kumar, D. S., & Srinivasan, D. (2018). A Numerical Protection Strategy for Medium-Voltage Distribution Systems. *2018 IEEE Innovative Smart Grid Technologies - Asia (ISGT Asia)*, 1056–1061. https://doi.org/10.1109/ISGT-Asia.2018.8467835

Kumm, J. J., Schweitzer, E. O., & Hou, D. (1994). Assessing the Effectiveness of Self-Tests and Other Monitoring Means in Protective Relays. *30th Annual Minnesota Power Systems Conference, October 1994*. https://cdn.selinc.com/assets/Literature/Publications/Technical%20Papers/6004_AssessingEffectiveness_Web.pdf

Kuzlu, M., Pipattanasomporn, M., & Rahman, S. (2014). Communication network requirements for major smart grid applications in HAN, NAN and WAN. *Computer Networks*, *67*, 74–88. https://doi.org/10.1016/j.comnet.2014.03.029

Laaksonen, H. (2011). *Technical Solutions for Low-Voltage Microgrid Concept* [Doctoral Thesis, University of Vaasa, Finland.]. http://www.uva.fi/materiaali/pdf/isbn_978-952-476-345-5.pdf

Laaksonen, H., Ishchenko, D., & Oudalov, A. (2014). Adaptive Protection and Microgrid Control Design for Hailuoto Island. *IEEE Transactions on Smart Grid*, *5*(3), 1486–1493. https://doi.org/10.1109/TSG.2013.2287672

Laaksonen, H., Kauhaniemi, K., & Voima, S. (2011). Protection system for future LV Microgrids. *CIRED 21st International Conference on Electricity Distribution, 6–9 June,2011*, Paper No. 0431. http://www.cired.net/publications/cired2011/part1/papers/CIRED2011_0431_final.pdf

Lasseter, R., Akhil, A., Marnay, C., Stephens, J., Dagle, J., Guttromson, R., Meliopoulous, A. S., Yinger, R., & Eto, J. (2002). *Integration of Distributed Energy Resources. The CERTS microgrid concept* (White Paper LBNL-50829). Consortium for Electric Reliability Technology Solutions, CERTS. https://escholarship.org/uc/item/9w88z7z1

Lasseter, R. H., & Piagi, P. (2004). Microgrid: A Conceptual Solution. *IEEE 35th Annual Power Electronics Specialists Conference (IEEE Cat. No.04CH37551), 2004, Aachen, Germany, 20-25 June*, *6*, 4285–4290. https://doi.org/doi: 10.1109/PESC.2004.1354758

Leitloff, V., Brun, Ph., de Langle, S., Ilas, B., Darmony, R., Jobert, M., Bertheau, Ch., Ferret, P., Boucherit, M., Duverbecq, G., Cayuela, J. P., & Bouchet, R. (2016). Testing of IEC 61850 based functional protection chain using non-conventional instrument transformers and SAMU. *13th International Conference on Development in Power System Protection 2016 (DPSP)*, 1–6. https://doi.org/10.1049/cp.2016.0037

Leyva-Mayorga, I., Soret, B., Röper, M., Wübben, D., Matthiesen, B., Dekorsy, A., & Popovski, P. (2020). LEO Small-Satellite Constellations for 5G and Beyond-5G Communications. *IEEE Access*, *8*, 184955–184964. https://doi.org/10.1109/ACCESS.2020.3029620

Li, C., Huang, Y., Deng, H., & Zhang, X. (2022). Comparison on Frequency Stability of High Inverter Penetration Power System with Different Grid-forming Controls. *2022 International Conference on Power Energy Systems and Applications (ICoPESA)*, 374–380. https://doi.org/10.1109/ICoPESA54515.2022.9754388

Li, H., & Chen, Z. (2008). Overview of different wind generator systems and their comparisons. *IET Renewable Power Generation*, *2*(2), 123–138. https://doi.org/10.1049/iet-rpg:20070044

Li, M., Wang, Y., Hu, W., Shu, S., Yu, P., Zhang, Z., & Blaabjerg, F. (2022). Unified Modeling and Analysis of Dynamic Power Coupling for Grid-Forming Converters. *IEEE Transactions on Power Electronics*, *37*(2), 2321–2337. https://doi.org/10.1109/TPEL.2021.3107329

Li, X., Dyśko, A., & Burt, G. (2012). Enhanced protection for inverter dominated microgrid using transient fault information. *11th IET International Conference on Developments in Power Systems Protection (DPSP 2012)*, 1–5. https://doi.org/10.1049/cp.2012.0081

Lin, H., Guerrero, J. M., Jia, C., Tan, Z., Vasquez, J. C., & Liu, C. (2016). Adaptive overcurrent protection for microgrids in extensive distribution systems. *IECON 2016 - 42nd Annual Conference of the IEEE Industrial Electronics Society*, 4042–4047. https://doi.org/10.1109/IECON.2016.7793091

Lin, H., Sun, K., Tan, Z.-H., Liu, C., Guerrero, J. M., & Vasquez, J. C. (2019). Adaptive protection combined with machine learning for microgrids. *IET Generation, Transmission & Distribution*, *13*(6), 770–779. https://doi.org/10.1049/iet-gtd.2018.6230

Liu, J., Miura, Y., & Ise, T. (2016). Comparison of Dynamic Characteristics Between Virtual Synchronous Generator and Droop Control in Inverter-Based Distributed Generators. *IEEE Transactions on Power Electronics*, *31*(5), 3600–3611. https://doi.org/10.1109/TPEL.2015.2465852

Liu, P., Zhu, G., Ding, L., Gao, X., Jia, C., Ng, C., & Terzija, V. (2022). High-voltage ride-through strategy for wind turbine with fully-rated converter based on current operating range. *International Journal of Electrical Power & Energy Systems*, *141*, 108101. https://doi.org/10.1016/j.ijepes.2022.108101

Liu, S., Gao, Z., Wu, Y., Kwan Ng, D. W., Gao, X., Wong, K.-K., Chatzinotas, S., & Ottersten, B. (2021). LEO Satellite Constellations for 5G and Beyond: How Will They Reshape Vertical Domains? *IEEE Communications Magazine*, *59*(7), 30–36. https://doi.org/10.1109/MCOM.001.2001081

Luo, W., Hu, T., Ye, Y., Zhang, C., & Wei, Y. (2020). A hybrid predictive maintenance approach for CNC machine tool driven by Digital Twin. *Robotics and Computer-Integrated Manufacturing*, *65*, 101974. https://doi.org/10.1016/j.rcim.2020.101974

Mackiewicz, R. (n.d.). *Technical Overview and Benefits of the IEC 61850 Standard for Substation Automation*. Retrieved June 16, 2021, from https://library.e.abb.com/public/04519389e504d7ddc12576ff0070704d/3BUS095131_en_IEC61850_Overview_and_Benefits_Paper_General.pdf

Mackiewicz, R. E. (2006). Overview of IEC 61850 and Benefits. *2006 IEEE PES Power Systems Conference and Exposition*, 623–630. https://doi.org/10.1109/PSCE.2006.296392

Maneekorn, C., Premrudeepreechacharn, S., Supannon, A., & Puangsukra, R. (2020). Development of Distance Relay Based on Wide-Area Protection for Transmission Systems of Provincial Electricity Authority. *2020 International Conference on Smart Energy Systems and Technologies (SEST)*, 1–6. https://doi.org/10.1109/SEST48500.2020.9203406

Marnay, C., Chatzivasileiadis, S., Abbey, C., Iravani, R., Joos, G., Lombardi, P., Mancarella, P., & Appen, J. V. (2015). Microgrid Evolution Roadmap.

International Symposium on Smart Electric Distribution Systems and Technologies (EDST), Vienna, Austria, 139–144. https://doi.org/10.1109/SEDST.2015.7315197

Masters, C. L. (2000). Voltage-rise the big issue when connecting embedded generation to long 11 kV overhead lines. *Embedded Generation, IEE Power Engineering Journal,* 5–12.

Mechouma, R., Azoui, B., & Chaabane, M. (2012). Three-phase grid connected inverter for photovoltaic systems, a review. *First International Conference on Renewable Energies and Vehicular Technology, Nabeul, Tunisia, 26-28 March*, 37–42. https://doi.org/doi: 10.1109/REVET.2012.6195245.

Memon, A. A. (2013). *Analyses of reactive power compensation strategies in medium and low voltage electrical network systems in the wake of renewable energy infeed* [Master's Thesis]. Brandenburg University of Technology, Cottbus, Germany.

Meng, J., Liu, B., Guo, F., Ni, Q., Wang, Y., & Zhao, P. (2021). Current Limiting Strategy of Grid Forming Converter. *2021 IEEE Sustainable Power and Energy Conference (ISPEC)*, 626–631. https://doi.org/10.1109/iSPEC53008.2021.9736033

Metz, B., Davidson, O. R., Bosch, P. R., Dave, R., & Meyer, L. A. (2007). *Climate Change 2007 Mitigation of Climate Change* [Contribution of Working Group III to the Fourth Assessment Report of the Intergovernmental Panel on Climate Change]. IPCC. https://www.ipcc.ch/site/assets/uploads/2018/03/ar4_wg3_full_report-1.pdf

Meyer, C., Schroder, S., & De Doncker, R. W. (2003). Design of solid-state circuit breakers for medium-voltage systems. *2003 IEEE PES Transmission and Distribution Conference and Exposition (IEEE Cat. No.03CH37495)*, *2*, 798–803 vol.2. https://doi.org/10.1109/TDC.2003.1335377

Mishra, M., Panigrahi, R. R., & Rout, P. K. (2019). A combined mathematical morphology and extreme learning machine techniques based approach to micro-grid protection. *Ain Shams Engineering Journal*, *10*(2), 307–318. https://doi.org/10.1016/j.asej.2019.03.011

Mishra, M., & Rout, P. K. (2018). Detection and classification of micro-grid faults based on HHT and machine learning techniques. *IET Generation, Transmission & Distribution*, *12*(2), 388–397. https://doi.org/10.1049/iet-gtd.2017.0502

Mocanu, S., & Thiriet, J. (2021). Real-Time Performance and Security of IEC 61850 Process Bus Communications. *River Publishers*, *10*(2), 1–42. hal-03192264. https://doi.org/10.13052/jcsm2245-1439.1021

Momesso, A. E. C., Bernardes, W. M. S., & Asada, E. N. (2019). Fuzzy adaptive setting for time-current-voltage based overcurrent relays in distribution systems. *International Journal of Electrical Power & Energy Systems*, *108*, 135–144. https://doi.org/10.1016/j.ijepes.2018.12.035

Momesso, A. E. C., Bernardes, W. M. S., & Asada, E. N. (2020). Adaptive directional overcurrent protection considering stability constraint. *Electric Power Systems Research*, *181*, 106190. https://doi.org/10.1016/j.epsr.2019.106190

Moreno, N., Flores, M., Torres, L., Juarez, J., & Gonzalez, D. (2010, April). Case Study: IEC 61850 as Automation Standard for New Substations at CFE, Practical Experiences. *12th Annual Western Power Delivery Automation Conference*. https://selinc.com/api/download/7405?id=7405

Musavi, F., Edington, M., Eberle, W., & Dunford, W. G. (2012). Evaluation and Efficiency Comparison of Front End AC-DC Plug-in Hybrid Charger Topologies. *IEEE Transactions on Smart Grid*, *3*(1), 413–421. https://doi.org/doi: 10.1109/TSG.2011.2166413.

NERC. (n.d.). *Standard PRC-005-6 – Protection System, Automatic Reclosing, and Sudden Pressure Relaying Maintenance*. NERC. Retrieved October 10, 2022, from https://www.nerc.com/pa/Stand/Reliability%20Standards/PRC-005-6.pdf

NERC. (2017). *Distributed Energy Resources Connection Modeling and Reliability Considerations* [Technical Report]. North American Electric Reliability Corporation. https://www.nerc.com/comm/Other/essntlrlbltysrvcstskfrcDL/Distributed_Energy_Resources_Report.pdf

NERC. (2018). *Bulk Electric System Definition, Reference Document, Version 3*. North American Electric Reliability Corporation, NERC. https://www.nerc.com/pa/Stand/2018%20Bulk%20Electric%20System%20Definition%20Reference/BES_Reference_Doc_08_08_2018_Clean_for_Posting.pdf

Netsanet, S., Zhang, J., & Zheng, D. (2018). Bagged Decision Trees Based Scheme of Microgrid Protection Using Windowed Fast Fourier and Wavelet Transforms. *Electronics*, *7*(5). https://doi.org/10.3390/electronics7050061

Nikkhajoei, H., & Lasseter, R. H. (2007). Microgrid Protection. *2007 IEEE Power Engineering Society General Meeting*, 1–6. https://doi.org/10.1109/PES.2007.385805

Oudalov, A., & Fidigatti, A. (2009). Adaptive network protection in microgrids. *Int. J. Distrib. Energy Resour.*, *5*, 201–226.

Palizban, O. (2016). *Distributed Control Strategy for Energy Storage Systems in AC Microgrids: Towards a Standard Solution* [Doctoral Thesis]. University of Vaasa, Finland.

Palizban, O., Hafezi, H., Kauhaniemi, K., & Hämäläinen, M. (2020). Hardware-in-the-loop Testing of Line Differential Protection Relay Based on IEC 61850 Process Bus. *IET Conference Proceedings*, 5 pp.-5 pp.(1).

Papaspiliotopoulos, V. A., Korres, G. N., & Hatziargyriou, N. D. (2015). Protection coordination in modern distribution grids integrating optimization techniques

with adaptive relay setting. *2015 IEEE Eindhoven PowerTech*, 1–6. https://doi.org/10.1109/PTC.2015.7232558

Pattabiraman, D., Lasseter., R. H., & Jahns, T. M. (2018). Comparison of Grid Following and Grid Forming Control for a High Inverter Penetration Power System. *2018 IEEE Power & Energy Society General Meeting (PESGM)*, 1–5. https://doi.org/10.1109/PESGM.2018.8586162

Perera, N., & Rajapakse, A. D. (2006). Agent-based protection scheme for distribution networks with distributed generators. *2006 IEEE Power Engineering Society General Meeting*, 6 pp.-. https://doi.org/10.1109/PES.2006.1709528

Phadke, A. G., Wall, P., Ding, L., & Terzija, V. (2016). Improving the performance of power system protection using wide area monitoring systems. *Journal of Modern Power Systems and Clean Energy*, *4*(3), 319–331. https://doi.org/10.1007/s40565-016-0211-x

Piagi, P., & Lasseter, R. H. (2006). Autonomous control of microgrids. *IEEE Power Engineering Society General Meeting, Montreal, QC, Canada, 18-22 June*. https://doi.org/doi: 10.1109/PES.2006.1708993

Qu, Z., Zhang, G., Cao, H., & Xie, J. (2017). LEO Satellite Constellation for Internet of Things. *IEEE Access*, *5*, 18391–18401. https://doi.org/10.1109/ACCESS.2017.2735988

Rasheduzzaman, M., Mueller, J. A., & Kimball, J. W. (2014). An Accurate Small-Signal Model of Inverter- Dominated Islanded Microgrids Using dq Reference Frame. *IEEE Journal of Emerging and Selected Topics in Power Electronics*, *2*(4), 1070–1080. https://doi.org/10.1109/JESTPE.2014.2338131

Rathnayake, D. B., Akrami, M., Phurailatpam, C., Me, S. P., Hadavi, S., Jayasinghe, G., Zabihi, S., & Bahrani, B. (2021). Grid Forming Inverter Modeling, Control, and Applications. *IEEE Access*, *9*, 114781–114807. https://doi.org/10.1109/ACCESS.2021.3104617

Rechsteiner, R. (2008). *Wind Power in Context–A clean Revolution in the Energy Sector* (p. 17) [Executive summary]. Energy Watch Group / Ludwig-Boelkow-Foundation. https://www.energywatchgroup.org/wp-content/uploads/01b_Wind_Power_in_Context_exec_summary_2008-12-18.pdf

Ritchie, H., Roser, M., & Rosado, P. (2020). *Energy—Access to Electricity* [Online Resource]. Our World in Data. https://ourworldindata.org/energy

Rockefeller, G. D., Wagner, C. L., Linders, J. R., Hicks, K. L., & Rizy, D. T. (1988). Adaptive transmission relaying concepts for improved performance. *IEEE Transactions on Power Delivery*, *3*(4), 1446–1458. https://doi.org/10.1109/61.193943

Sadeghkhani, I., Hamedani Golshan, M. E., Guerrero, J. M., & Mehrizi-Sani, A. (2017). A Current Limiting Strategy to Improve Fault Ride-Through of Inverter

Interfaced Autonomous Microgrids. *IEEE Transactions on Smart Grid*, *8*(5), 2138–2148. https://doi.org/10.1109/TSG.2016.2517201

Sajadi, A., Kenyon, R. W., Bossart, M., & Hodge, B.-M. (2021). Dynamic Interaction of Grid-Forming and Grid-Following Inverters with Synchronous Generators in Hybrid Power Plants. *2021 IEEE Kansas Power and Energy Conference (KPEC)*, 1–6. https://doi.org/10.1109/KPEC51835.2021.9446204

Samadi, A., & Chabanloo, R. M. (2020). Adaptive coordination of overcurrent relays in active distribution networks based on independent change of relays' setting groups. *International Journal of Electrical Power & Energy Systems*, *120*, 106026. https://doi.org/10.1016/j.ijepes.2020.106026

Samantaray, S. R., Joos, G., & Kamwa, I. (2012). Differential energy based microgrid protection against fault conditions. *2012 IEEE PES Innovative Smart Grid Technologies (ISGT)*, 1–7. https://doi.org/10.1109/ISGT.2012.6175532

Sen, S., & Kumar, V. (2018). Microgrid control: A comprehensive survey. *Annual Reviews in Control*, *45*, 118–151. https://doi.org/10.1016/j.arcontrol.2018.04.012

Sharma, N. K., & Samantaray, S. R. (2020). PMU Assisted Integrated Impedance Angle-Based Microgrid Protection Scheme. *IEEE Transactions on Power Delivery*, *35*(1), 183–193. https://doi.org/10.1109/TPWRD.2019.2925887

Shi, Shenxing., Jiang, Bo., Dong, Xinzhou., & Bo, Zhiqian. (2010). Protection of microgrid. *10th IET International Conference on Developments in Power System Protection (DPSP 2010). Managing the Change*, 1–4. https://doi.org/10.1049/cp.2010.0209

Shih, M. Y., Castillo Salazar, C. A., & Conde Enríquez, A. (2015). Adaptive directional overcurrent relay coordination using ant colony optimisation. *IET Generation, Transmission & Distribution*, *9*(14), 2040–2049. https://doi.org/10.1049/iet-gtd.2015.0394

Shih, M. Y., Conde, A., Leonowicz, Z., & Martirano, L. (2017). An Adaptive Overcurrent Coordination Scheme to Improve Relay Sensitivity and Overcome Drawbacks due to Distributed Generation in Smart Grids. *IEEE Transactions on Industry Applications*, *53*(6), 5217–5228. https://doi.org/10.1109/TIA.2017.2717880

Siemens. (n.d.). *Engineering software for IEC 61850 systems–IEC 61850 System Configurator, Engineering tools for protection, Siemens Global*. Retrieved February 1, 2023, from https://new.siemens.com/global/en/products/energy/energy-automation-and-smart-grid/protection-relays-and-control/engineering-tools-for-protection/engineering-software-iec-61850-system-configurator.html

Singh, M., Vishnuvardhan, T., & Srivani, S. G. (2016). Adaptive protection coordination scheme for power networks under penetration of distributed energy resources. *IET Generation, Transmission & Distribution*, *10*(15), 3919–3929. https://doi.org/10.1049/iet-gtd.2016.0614

Sirviö, K., Kauhaniemi, K., Memon, A. A., Laaksonen, H., & Kumpulainen, L. (2020). Functional Analysis of the Microgrid Concept Applied to Case Studies of the Sundom Smart Grid. *Energies*, *13*(16). https://doi.org/10.3390/en13164223

Skendzic, V., Ender, I., & Zweigle, G. (2007). *IEC 61850-9-2 Process Bus and Its Impact on Power System Protection and Control Reliability*. 1–7. https://selinc.com/api/download/3479/

Song, S.-M., Kim, J.-Y., Choi, S.-S., Kim, I.-D., & Choi, S.-K. (2018). New Simple-Structured AC Solid-State Circuit Breaker. *IEEE Transactions on Industrial Electronics*, *65*(11), 8455–8463. https://doi.org/10.1109/TIE.2018.2809674

Sortomme, E., Venkata, M., & Mitra, J. (2010). Microgrid protection using communication-assisted digital relays. *IEEE PES General Meeting*, 1–1. https://doi.org/10.1109/PES.2010.5588146

Steinhauser, F., & Vandiver, B. (2015, June). How fast does the GOOSE fly? (Within the substation or intercontinental). *Protection, Automation and Control Magazine, PAC World*, *18*(32), 39–43.

Sun, Y., Chen, X., Yang, S., Rusli, Tseng, K. J., & Amaratunga, G. (2017). Micro PMU based monitoring system for active distribution networks. *2017 IEEE 12th International Conference on Power Electronics and Drive Systems (PEDS)*, 518–522. https://doi.org/10.1109/PEDS.2017.8289180

Tao, F., Zhang, H., Liu, A., & Nee, A. Y. C. (2019). Digital Twin in Industry: State-of-the-Art. *IEEE Transactions on Industrial Informatics*, *15*(4), 2405–2415. https://doi.org/10.1109/TII.2018.2873186

Teodorescu, R., Liserre, M., & Rodriguez, P. (2011). *Grid Converters for Photovoltaic and Wind Power Systems* (First). John Wiley & Sons.

Terwiesch, P., Rytoft, C., Meier, H. E., Bawa, H., Reinhardt, P., & Moglestue, A. (2010). *ABB Review Special Report IEC 61850* (pp. 1–64) [The corporate technical journal]. ABB Asea Brown Boveri Ltd.

Ton, D. T., & Smith, M. A. (2012). The U.S. Department of Energy's Microgrid Initiative. *The Electricity Journal*, *25*(8), 84–94. https://doi.org/10.1016/j.tej.2012.09.013.

Ton, D. T., & Wang, W. P. (2015). A More Resilient Grid: The U.S. Department of Energy Joins with Stakeholders in an R&D Plan. *IEEE Power and Energy Magazine*, *13*(3), 26–34. https://doi.org/doi: 10.1109/MPE.2015.2397337.

UCAIug. (n.d.). *About UCAIug*. UCA International Users Group. https://www.ucaiug.org/aboutUCAIug/default.aspx

United Nations (UN). (n.d.). *Take Action for the Sustainable Development Goals*. The United Nations. Retrieved March 25, 2021, from https://www.un.org/sustainabledevelopment/sustainable-development-goals/

United States Environmental Protection Agency (EPA). (n.d.-a). *Distributed Generation of Electricity and its Environmental Impacts* [An official website of

the United States government]. US EPA. Retrieved March 25, 2021, from https://www.epa.gov/energy/distributed-generation-electricity-and-its-environmental-impacts

United States Environmental Protection Agency (EPA). (n.d.-b). *Sources of Greenhouse Gas Emissions* [An official website of the United States government]. US EPA. Retrieved March 25, 2021, from https://www.epa.gov/ghgemissions/sources-greenhouse-gas-emissions

Urciuoli, D. P., Veliadis, V., Ha, H. C., & Lubomirsky, V. (2011). Demonstration of a 600-V, 60-A, bidirectional silicon carbide solid-state circuit breaker. *2011 Twenty-Sixth Annual IEEE Applied Power Electronics Conference and Exposition (APEC)*, 354–358. https://doi.org/10.1109/APEC.2011.5744620

Ustun, T. S., Ozansoy, C., & Zayegh, A. (2012). Modeling of a Centralized Microgrid Protection System and Distributed Energy Resources According to IEC 61850-7-420. *IEEE Transactions on Power Systems*, *27*(3), 1560–1567. https://doi.org/10.1109/TPWRS.2012.2185072

Velaga, Y. N., Prabakar, K., Singh, A., & Sen, P. K. (2021). Traveling Wave Relays for Distribution Feeder Protection with High Penetrations of Distributed Energy Resources. *2021 IEEE Rural Electric Power Conference (REPC)*, 59–66. https://doi.org/10.1109/REPC48665.2021.00016

Voima, S., Kauhaniemi, K., & Laaksonen, H. (2011). Novel protection approach for MV Microgrid. *CIRED 21st International Conference on Electricity Distribution, 6–9 June*, Paper 0430. http://www.cired.net/publications/cired2011/part1/papers/CIRED2011_0430_final.pdf

Wannous, K., Toman, P., Jurák, V., & Wasserbauer, V. (2019). Analysis of IEC 61850-9-2LE Measured Values Using a Neural Network. *Energies*, *12*(9). https://doi.org/10.3390/en12091618

Ward, S., Gwyn, B., Antonova, G., Apostolov, A., Austin, T., Beaumont, P., Beresh, B., Bradt, D., Brunello, G., Bui, D.-P., Carden, M., Cunico, R., Deronja, A., Elmore, W., Garcia, R., Haas, B., Hanbali, A., Harris, R., Heavey, P., … Udren, E. (2010). Redundancy considerations for protective relaying systems. *2010 63rd Annual Conference for Protective Relay Engineers*, 1–10. https://doi.org/10.1109/CPRE.2010.5469478

Wester, C., & Smith, T. (2011). Fully monitoring protection and control systems. *2011 64th Annual Conference for Protective Relay Engineers*, 215–221. https://doi.org/10.1109/CPRE.2011.6035622

Yang, C., Huang, L., Xin, H., & Ju, P. (2021). Placing Grid-Forming Converters to Enhance Small Signal Stability of PLL-Integrated Power Systems. *IEEE Transactions on Power Systems*, *36*(4), 3563–3573. https://doi.org/10.1109/TPWRS.2020.3042741

Yilmaz, M., & Krein, P. T. (2013). Review of Battery Charger Topologies, Charging Power Levels, and Infrastructure for Plug-In Electric and Hybrid Vehicles. *IEEE*

Transactions on Power Electronics, *28*(5), 2151–2169. https://doi.org/doi: 10.1109/TPEL.2012.2212917

You, Y., Chen, C., Hu, F., Liu, Y., & Ji, Z. (2022). Advances of Digital Twins for Predictive Maintenance. *Procedia Computer Science*, *200*, 1471–1480. https://doi.org/10.1016/j.procs.2022.01.348

Yu, J. J. Q., Hou, Y., Lam, A. Y. S., & Li, V. O. K. (2019). Intelligent Fault Detection Scheme for Microgrids With Wavelet-Based Deep Neural Networks. *IEEE Transactions on Smart Grid*, *10*(2), 1694–1703. https://doi.org/10.1109/TSG.2017.2776310

Zamani, M. A., Yazdani, A., & Sidhu, T. S. (2012). A Communication-Assisted Protection Strategy for Inverter-Based Medium-Voltage Microgrids. *IEEE Transactions on Smart Grid*, *3*(4), 2088–2099. https://doi.org/10.1109/TSG.2012.2211045

Zhang, F., & Mu, L. (2015). Wide-area protection scheme for active distribution networks based on phase comparison. *2015 5th International Conference on Electric Utility Deregulation and Restructuring and Power Technologies (DRPT)*, 927–932. https://doi.org/10.1109/DRPT.2015.7432360

Zhang, H., Xiang, W., Lin, W., & Wen, J. (2021). Grid Forming Converters in Renewable Energy Sources Dominated Power Grid: Control Strategy, Stability, Application, and Challenges. *Journal of Modern Power Systems and Clean Energy*, *9*(6), 1239–1256. https://doi.org/10.35833/MPCE.2021.000257

Zhong, Q.-C., Ma, Z., Ming, W.-L., & Konstantopoulos, G. C. (2015). Grid-friendly wind power systems based on the synchronverter technology. *Energy Conversion and Management*, *89*, 719–726. https://doi.org/10.1016/j.enconman.2014.10.027

Zhong, Q.-C., Nguyen, P.-L., Ma, Z., & Sheng, W. (2014). Self-Synchronized Synchronverters: Inverters Without a Dedicated Synchronization Unit. *IEEE Transactions on Power Electronics*, *29*(2), 617–630. https://doi.org/10.1109/TPEL.2013.2258684

Zhong, Q.-C., & Weiss, G. (2011). Synchronverters: Inverters That Mimic Synchronous Generators. *IEEE Transactions on Industrial Electronics*, *58*(4), 1259–1267. https://doi.org/doi: 10.1109/TIE.2010.2048839

Zhou, Z., Wang, W., Lan, T., & Huang, G. M. (2021). Dynamic Performance Evaluation of Grid-Following and Grid-Forming Inverters for Frequency Support in Low Inertia Transmission Grids. *2021 IEEE PES Innovative Smart Grid Technologies Europe (ISGT Europe)*, 01–05. https://doi.org/10.1109/ISGTEurope52324.2021.9640034

Zielinski, J. S. (2016). Microgrids and Resilience. *Rynek Energii*. https://www.cire.pl/pliki/2/16zielinskizet16.pdf

Electric Power Systems Research 129 (2015) 23–31

Contents lists available at ScienceDirect

Electric Power Systems Research

journal homepage: www.elsevier.com/locate/epsr

A critical review of AC Microgrid protection issues and available solutions

Aushiq Ali Memon*, Kimmo Kauhaniemi

Department of Electrical Engineering and Energy Technology, University of Vaasa, PO Box 700, FI-65101 Vaasa, Finland

ARTICLE INFO

Article history:
Received 8 December 2014
Received in revised form 27 May 2015
Accepted 9 July 2015
Available online 1 August 2015

Keywords:
AC Microgrid
Protection issues
Protection schemes
Islanded mode
Grid-connected mode

ABSTRACT

One of the main technical issues in the practical implementation of a Microgrid is the design of the proper protection scheme. The scheme must be capable to meet the basic protection requirements of selectivity, sensitivity and reliability not only in grid-connected mode but also in islanded mode of operation. Since the introduction of Microgrid concept, many researchers have introduced various new protection schemes to be incorporated in medium and low voltage Microgrids. Most of the researchers agree that the conventional protective devices usually based on overcurrent principle are inadequate to provide complete protection for Microgrids during both grid-connected and islanded mode of operation, hence new protection techniques based on other principles must be developed. The new protection schemes should be not only adaptable according to operational modes of Microgrid but also sensitive enough to detect and clear the lowest possible fault currents within Microgrid quickly ensuring minimum supply disruption to consumers. This paper briefly reviews protection issues in AC Microgrids and presents state of the art protection schemes for AC Microgrids developed and proposed so far. It also gives a critical analysis of each proposed method and categorizes the protection issues and schemes on the basis of operational modes of AC Microgrid. At the end, it has been concluded that more effort is still needed to overcome the limitations of proposed protection schemes and to improve reliability of communication system for adaptive protection schemes or provide alternate means to cope with communication failures. Moreover, protection against cyber-attacks is crucial for safe and secure operation of future Microgrids.

Contents

* Corresponding author. Tel.: +358 414744093; fax: +358 63175225.
E-mail addresses: Aushiq.Memon@uva.fi (A.A. Memon), kimmo.kauhaniemi@uva.fi (K. Kauhaniemi).

http://dx.doi.org/10.1016/j.epsr.2015.07.006
0378-7796/

1. Introduction

The low-carbon emitting kW-scale distributed generators (DGs) like reciprocating engine generators, gas turbines or fuel cells acting as combined heat and power (CHP) units close to consumer premises along with renewable energy sources (RES) like small wind turbines and solar photovoltaic (PV) modules collectively known as distributed energy resources (DERs) or microsources and heat and electricity storage technologies have to play an important role in future electric supply systems. The increased energy-efficiency, reduced carbon emissions, improved power quality and reliability, reduced line losses and deferral of grid expansion are the most prominent benefits offered by DERs installed near the load centres. These benefits cannot be fully exploited with traditional method of integrating a limited number of stand-alone DERs with distribution networks according to "fit and forget" rule in which DERs are bound to be disconnected from network whenever any disturbance occurs on electric grid as per IEEE Standard 1547. Moreover, the integration of individual DERs can cause variety of problems like local voltage rise, violations in thermal limits of certain lines and transformers, unintentional islanding etc. As the penetration level of DERs in developed countries will reach a significant level, it will create a number of new dynamic operational, control and safety challenges for medium and low voltage electric supply networks which were actually not designed to be connected with any type of generation. These new challenges could be better addressed by a properly designed, operated, controlled, managed and protected "Microgrid" [1–4].

The Microgrid is an alternative systematic approach to integrate small-scale DERs into LV ($\leq$1 kV) and MV (1–69 kV) distribution systems in order to facilitate the simultaneous generation of electricity and heat for local electric and heat loads; this approach allows for local control of distributed generation and thereby reduces or eliminates the need for central dispatch [1,5]. A Microgrid behaving like a single producer or load is not only capable of operating efficiently and safely with its local distribution network but it is also capable of islanding. After islanding, Microgrid continues to provide uninterruptible power supply to priority (or sensitive) loads according to its generation capacity within the agreed power quality level and thus increases the reliability of the system. From operational point of view, the DERs must be provided with power electronics interfaces and controls to offer the needed flexibility for ensuring operation of Microgrid as a single aggregated system and maintaining defined level of power quality and energy output [1–3]. There are at least three alternative control strategies for Microgrid operations: centralised control, distributed (decentralised) control and autonomous control as explained in [6].

Presently, an islanded operation is not allowed by the utilities, network operators and regulators and it is required to disconnect all DERs automatically from the network after both planned and unplanned switching operations (by anti-islanding protection incorporated in DERs) due to safety concerns and in compliance with existing control and protection constraints of distribution systems [1,7,8]. For realisation of maximum advantages of high DG penetration, the islanded operation of Microgrid must be considered which will obviously have strong consequences on the existing safety, control, protection and dispatch practices and strategies of electrical energy [9]. IEEE Standard 1547.4-2011 with title of "IEEE guide for design, operation and integration of distributed resource island systems with electric power systems" has been developed which covers the intentional islands in electric power systems that contain distributed resources (DR). In this guide Microgrid has been termed as "DR island system" and seven types of planned or intentional DR island system configurations have been presented [6]. This guide is a good effort to provide an introduction to design, operation and implementation issues of future Microgrids present on primary distribution systems with some limitations as explained in its sub-clause 1.3.

It is essential for a properly operating Microgrid that the interconnecting switch (connecting Microgrid with main grid) must open during any unacceptable power quality disturbance or fault on the main grid and the DERs must be capable to carry the load on the islanded section while maintaining the proper levels of voltage and frequency for the islanded loads. Suitable load-shedding schemes should be implemented if DER generation capacity does not meet the load demand of islanded system. Depending on the technology of switch, some momentary power disruptions may happen (DERs may seize to energise the islanded section for some short period of time) during transition from grid-connected to islanded mode; in this scenario the DERs in the islanded portion must be capable of quick restart and picking up the islanded load after opening of the switch. The DERs must be capable of supplying the real and reactive power requirements in the islanded mode and should sense a fault current downstream of the interconnecting switch. After the restoration of the main grid supply, the switch should not close unless both the grid and islanded system are properly synchronised, that is, voltage, frequency and phase angle of the both systems must be within acceptable limits [6,10]. For faults within the island system, there must be protection system which can sense the fault and quickly isolate the faulty portion from the rest of the system ensuring minimum loss of generation and load interruptions. The protection system of islanded system must be more sensitive because fault currents in islanded system will be of much lower magnitudes than those of the grid-connected system [1].

This paper is organised in a manner that Section 2 briefly describes the protection issues in Microgrid, Section 3 reviews the state of art protection schemes developed and proposed so far along with their comparison in tabular form and Section 4 presents discussion. In the end, the conclusion of the paper is presented in Section 5.

2. Protection issues

2.1. Protection coordination (selectivity) with DG

Protection coordination (selectivity) is adversely affected by DG penetration in distribution systems. Traditional overcurrent protection is designed for radial distribution systems with fault current flow in single direction; whereas the connection of DERs into distribution networks changes the singly fed radial networks into complicated ones having multiple sources and thus the flow of fault current is changed from unidirectional to bidirectional [1]. The protection system of a typical distribution system is traditionally based on time or current coordination principle, in which the protective device closest to the fault called main protection operates first and if it fails to operate then backup protection operates after a predetermined time delay. However, if main protection is a fuse and backup protection is the recloser then it is normal practice to coordinate the fast operating curve of the recloser to operate first followed by the fuse, if fault is not cleared; this is commonly known as fuse saving scheme which is usually applied for clearance of temporary faults [11]. The conventional distribution protection is comprised of low cost and simple protective devices like overcurrent (OC) relays, circuit breakers, reclosers and fuses. It is usual practice in USA to provide inverse OC relays at distribution sub-station, the reclosers at main feeder while the fuses on laterals, whereas in Finland and majority of other European countries, definite time OC relays are used at origin of primary distribution feeders and fuses at secondary sub-stations (this practice may vary from country to country). For radial networks, the protection coordination between relays, reclosers and fuses is well established, however, when DGs are connected the networks no longer remain radial and the coordination between protective devices is either altered or completely lost [12,13]. The extent to which protection coordination is affected by DGs depends on the capacity, type and location of DGs [14–16]. The different adverse effects of DG connection on distribution network protection include false tripping of feeders, nuisance tripping of protection devices, blinding of protection, increase/decrease in fault level with connection/disconnection of DERs affecting reach of OC relay, unwanted islanding, prevention of automatic reclosing and out-of-synchronism reclosing [1,17,18].

2.2. Protection issues in Microgrids

Microgrid protection issues can be broadly divided into two categories; protection issues when Microgrid operates in grid-connected mode and protection issues when Microgrid operates in islanded mode. In grid-connected mode (normal mode), the protection problems are related with the response time of Microgrid isolation device (circuit breaker) at the point of common coupling (PCC) for events on utility grid and Microgrid, prevention of spurious or false tripping by isolation device as well as re-synchronisation and reconnection speed of Microgrid with utility grid after the disappearance of an event. In grid-connected mode the response time of protection devices installed within Microgrid (line protection and DER protection) for events on Microgrid is also considered. For Microgrid operation in islanded mode, the response time of protective devices within Microgrid (line protection and DER protection) for events within Microgrid is taken into account which largely depends on the complexity of Microgrid. The main concern in islanded mode of operation is the reduced short-circuit current at which OC protection devices either do not respond or if they do respond, their operation time is much longer than the required time (seconds instead of milliseconds) [1,2].

2.2.1. Selection of protection device/switch

The choice of the protection device is dependent on the required speed of operation, voltage level as well as the availability of fault current; it may range from a moulded-case circuit breaker to a high speed solid-state switch. The required speed of response by Microgrid PCC switch (breaker) to an event on either side of utility transformer largely depends on the sensitivity of load connected within Microgrid [1,2]. Another consideration for high speed response of protective device is the potential loss of Microgrid stability due to faults on the utility grid or within Microgrid, especially when directly-coupled DGs are connected within Microgrid which are very sensitive to voltage dips due to faults and may endanger the Microgrid stability [19].

2.2.2. Spurious separations or false trips

Spurious separations or false trips may occur for example due to failure of PCC device to discriminate whether the fault is on the utility side or within the Microgrid. Spurious separations are not only caused by the inexpensive electromechanical relays and breakers but also by sophisticated microprocessor-based protection devices working only on information (voltage and frequency measurements) available at PCC. Presently, the only reliable method to avoid spurious separations and providing fast tripping of PCC breaker is to have “transfer trip” from utility sub-station breaker. The Microgrid and the utility operations are less affected due to spurious separations as long as the Microgrid has the capability to restore its normal operation after separation. However, spurious separations can result in increased cost due to more operations of PCC device thus decreasing its life time and increasing the labour for restoration of normal operations. Moreover, false trips can result in Microgrid exposure to power quality problems, unwarranted outage to non-priority loads (which are usually disconnected due to islanding) and loss of revenue as well as a period of over frequency operation for exporting Microgrids [1,2].

2.2.3. Re-synchronisation

The availability of re-synchronisation equipment at Microgrid PCC should also be considered so that Microgrid can be reconnected with utility grid as soon as utility is ready to connect all previously disconnected loads due to islanding. The process of re-synchronisation and reconnection may either be manual or automatic and it may need several seconds to several minutes depending on the characteristics of the system [2]. Various types of Microgrid synchronisation schemes have been reviewed in [20] and the schemes have been categorised into three main types: active, passive and open-transition transfer synchronisation. Both active and passive synchronisation schemes maintain high reliability as compared to open-transition transfer scheme but active synchronisation schemes are more complex and uneconomical. Moreover in [20], passive synchronisation scheme have been suggested using traditional synchrocheck relay and switched capacitor banks for Microgrid with both directly-coupled and converter-based DERs. However, the use of switched capacitor banks for voltage balancing after Microgrid islanding may result in slow re-synchronisation. Automatic re-synchronisation scheme incorporated through Microgrid central controller using communication network is suggested for complicated Microgrid structures in [1].

2.2.4. Events/faults during grid-connected mode

For a fault on the utility grid during normal operation, the response of the protection devices of individual DERs (anti-islanding protection) should be not to trip before the protection device at PCC trips and DERs should continue operation during sensing and switching of PCC device. To allow this all DERs should have fault ride through (FRT) capability [21]. For a fault within Microgrid during normal operation, the response of line/feeder

protection must be to disconnect the faulty portion from the rest of system as quick as possible and how it is done depends on the features and complexity of Microgrid and the protection strategy used [2]. There may be some non-fault cases resulting in low voltages at PCC like voltage unbalances and non-fault open phases which are difficult to be detected and may potentially create hazards for sensitive loads, microsources etc. Therefore, some protection mechanisms must be developed to avoid such situations [1].

2.2.5. Events/faults during islanded mode

When Microgrid operates in islanded mode, the nature of problems becomes completely different from that of grid-connected mode. In grid-connected mode, the fault currents of higher magnitudes (10–50 times the full load current) are available from the utility grid in order to activate conventional OC protection devices. On the contrary, for a stand-alone Microgrid the fault current of about five times the full load current is available [1]. When a large number of converter-based DERs are connected in Microgrid, the fault currents of only 2–3 times the full load current (or even less depending on control method of converter [22]) are available [23]. The conventional OC protection devices are usually set to operate at 2–10 times the full load current. Hence, due to this drastic reduction of fault level, the time-current coordination of OC protective devices is disturbed; the high-set instantaneous OC devices and OC devices with extremely inverse characteristics like fuses are most likely to be affected [1].

2.2.6. Anti-islanding protection

Another important consideration for islanding mode of operation is related with anti-islanding (or Loss-of-Mains) protection of DERs. The deactivation of anti-islanding protection is generally required if the amount of microsource generation within Microgrid is very high. If anti-islanding protection is kept activated then there is chance that it may cause uncontrolled islands within Microgrid due to its fast tripping. Hence, it will be desirable to deactivate anti-islanding protection instantly when an isolated Microgrid is detected to be formed, to do that, DERs must have FRT capability to cope with voltage and frequency transients caused by islanding [1,21]. As reported in [1], the most reliable and fast method to deactivate anti-islanding protection of DERs is to send a trip blocking signal through Microgrid central controller using communication link. The fast and reliable method for islanding detection is necessary for a stable operation of Microgrid. The islanding detection methods are generally divided into three categories: Passive, active and telecom-based [24]. Various passive and active Loss-of-Mains detection methods and algorithms have been reported in [25–27]. Passive islanding detection methods are preferred over active methods due to factors of speed, reliability and power quality, whereas, telecom-based methods are more complex and costly as compared with passive methods. However, some passive islanding detection methods based on measured electrical quantities like voltage and frequency may fail or take longer time to detect islanding when generation and loads in Microgrid are nearly equal [24,28]. To solve this problem, a new passive islanding detection method based on pattern recognition approach for the extracted current and voltage transient signals (at DG terminals) generated during disconnection of the main grid is proposed in [28]. The method uses discrete wavelet-transform and classification technique (decision-tree (DT) classifier) to extract current and voltage signal energies (detail coefficients) in various frequency bands. The transient detector is used to trigger the classifier after a delay of 0.01 s if the value of the detail coefficient exceeds a pre-set threshold value. The performance of the proposed method has been compared with other passive methods in [24]. The response time of the proposed DT relay is (30–48) ms for various islanding events and DG types. However, high level of noise in voltage/current signal may further degrade the performance of proposed relay and the setting of threshold values is not clearly mentioned. The potential application of synchronised phasor measurements using phasor measurement units (PMUs) and global positioning system (GPS) at either side of PCC for Loss-of-Mains detection is mentioned in [25]. The high capital cost of PMUs makes this scheme uneconomical [25]. Moreover, possibility of GPS signal loss or impairment causing clock drift consequently make PMUs less accurate (or function incorrectly) and less reliable, therefore PMUs with back-up clock functionality will be required [29].

2.2.7. Role of Microgrid control architecture in protection

Microgrid configuration may change due to various control actions like load-shedding in peak-hours or increase in local generation for export to grid for optimum and economical operation of Microgrid. Therefore, adaptive protection system will be required to change protection relay settings dynamically according to changing configuration of Microgrid. Adaptive protection scheme can be implemented with centralised or decentralised control approaches, but each approach requires different communication architecture. The centralised control architecture for adaptive protection is the conventional method. In this method, a central controller coordinates the protection settings. However, failure of central controller causes full loss of adaptive protection and therefore, redundancy in central controller is required. The centralised communication architecture is supported by various communication protocols like Modbus, DNP3, IEC 60870-5-101/104, IEC 61850 and it can be implemented with serial/bus communication, over PLC (power-line carrier) or via Ethernet network. The decentralised control architecture depends on information exchange between distributed intelligent electronic devices (IEDs). Each IED acts autonomously after receiving information from other IED to change its active setting group. The decentralised architecture is only feasible when the communication protocol allows direct communication between IEDs. Presently, the industry is focused on IEC 61850 as the standard protocol for decentralised communication. The decentralised architecture requires a bus or Ethernet network for implementation, though it can also be implemented with 4G wireless network or over PLC [30].

The earlier research shows that traditional protection devices with single setting are incompatible with Microgrid protection philosophy which ensures safe and secure operation of Microgrid in both the grid-connected and islanded mode of operation. Hence it becomes inevitable to look for alternate means and methods of faults detection and isolation which can work equally well in both grid-connected and islanded mode of operation, that is, new protection schemes must be adaptable [1,2,31,32]. The new protection schemes should not only consider the reduction in fault levels but also consider the chances of bidirectional fault current flow in some feeders [1]; besides, the new protection schemes should also use communication links to ensure fast and reliable operation.

3. Protection schemes for Microgrids

A critical review of some proposed protection schemes in the recent scientific literature is presented in this section. The protection schemes are divided into three main categories: the schemes for only grid-connected mode, the schemes for only islanded mode and the schemes for both grid-connected and islanded mode. Tables 1 and 2 summarise the protection schemes for only islanded mode and the protection schemes for both grid-connected and islanded mode respectively with advantages/limitations of each scheme.

Table 1
Protection schemes for only islanded mode.

No.	Protection scheme	Applied methods/functions	Test system features				Faults	Advantages/limitations
			DG	Load	Line	Volt. level		
1.	Harmonic content based protection scheme [39]	THD and frequency measurement of converter voltages, communication link between relays	C-DGs	Constant MVA	OHL radial	11/0.48 kV	LLG	Difficult to assess THD threshold values for different fault types, possibility of relay trip failure when more dynamic loads are connected or if some DGs with pure voltage output, sensitivity problems with varying fault impedances
2.	Voltage based protection scheme [40]	abc-dq0 transformation of DGs output voltages and communication link between relays.	C- DGs	Constant MVA	OHL radial	11/0.48 kV	LLL, LL, LG	Single-pole tripping and high impedance faults are not considered, trip decision depends on communication link
3.	Symmetrical component and residual current based scheme [41]	OC relays, static switch at PCC, zoning principle.	C- DGs	kW	-	0.48 kV	LG, LL	No use of communication link and provides full protection from LG and LL faults. However, three phase and high impedance faults and single pole tripping not considered
4.	Adaptive protection scheme [21]	IEDs (voltage, current, directional OC measurements with interlocking), high speed communication link, zoning.	C- DGs	Constant MVA	OHL radial	20 kV	–	Adaptable to operational modes of Microgrid but highly dependent on communication link, detailed simulation results for particular types of faults are not discussed

3.1. The protection schemes for only grid-connected mode

A protection coordination scheme based on OC principle and time dependent characteristics of current to prevent high fault clearing times and maximizing DG connection to MV distribution networks is presented in [33]. This strategy provides extra benefit of running extensive radial networks with directly-coupled DGs (D-DGs) or closed-loop networks with converter-based DGs (C-DGs). However, this scheme is unclear about high impedance faults (HIF) and is more effective with increased number of relays. An adaptive overcurrent pickup strategy for MV feeder with C-DGs and radial overhead line (OHL) has been proposed in [18]. This scheme updates the OC relay minimum pickup current on the basis of the fault analysis of the system. However, this scheme is more effective when some of DGs are disconnected. A protection strategy using conventional OC relays with definite time grading for a LV Microgrid with both D-DGs and C-DGs connected to OHL and cable network has been presented in [34]. The proposed scheme does not use any communication link and can be applied without any modification of existing protection system, hence it is economical.

An intelligent agent based protection scheme for radial OHL distribution system without DG and for closed loop system with DG is proposed in [35]. The scheme assumes peer to peer communication between IEDs. The scheme provides higher speed of back up protection as compared to conventional protection, autonomous system monitoring and adjustment of parameters, but needs high speed communication.

In [36,37], it has been proposed to use a fault current limiter (FCL) in series with DG unit in order to limit the fault current contribution from DG during fault and thus return the system to its original state as if no DG was connected. In this way original directional OC relay settings can be used without disconnection of DG. The use of TCSC (thyristor controlled series capacitor) as an FCL has been proposed in [38]. The FCLs offer many advantages like no DG disconnection, use of original relay settings, avoid upgrading of equipment for handling large currents. But impedance of FCL increases with increase in individual DG capacity hence its cost increases. Moreover transient response of FCL is another concern.

3.2. The protection schemes for only islanded mode

A protection scheme based on monitoring of harmonic content of C-DGs in an islanded Microgrid is proposed in [39]. In this scheme the total harmonic distortion (THD) of the voltage at the converter terminal of the DG is continuously monitored by the protection relay and when THD exceeds a threshold value during a fault, the converter gets a shutdown by the relay. The variation of the amplitude of fundamental frequency of the faulted phase is used to detect the fault type (the frequency of faulted phase is dropped as compared to sound phase) and comparison of THD of voltage between sound and faulted phase is used to identify the fault location (faulted phase has greater THD than sound phase). The relay with more THD is considered to be in fault zone or nearer to the fault location and has to trip in order to clear the fault. However, for correct relay to trip, relays must be synchronised using communication link.

A voltage based protection scheme for islanded Microgrids containing C-DGs is proposed in [40]. The scheme monitors the output voltages of DGs and transforms them into dc quantities using d–q frame of reference. Any type of disturbance in DGs output voltages due to network faults is reflected as a disturbance in d–q quantities. The scheme utilizes the concept of zones and uses communication link between relays in order to discriminate between the faults inside and outside of the zone. The considered scheme has been verified with the help of simulations for different types of faults at various locations. However, HIF and single-pole tripping have not been taken into account.

A protection scheme based on the principle of symmetrical components and residual current measurement for islanded operation of Microgrid is proposed in [41]. In the paper the term "differential current" is applied, but the principle is same as in the common residual current devices. The proposed scheme uses residual current devices as primary protection of LG faults for the zones upstream the faults and zero sequence current as primary protection of LG faults for the zones downstream of the fault. The negative sequence current is used as primary protection for LL faults. I^2t protection is used as primary backup for both LG and LL events and

Table 2
Protection schemes for both grid-connected and islanded mode.

No.	Protection scheme	Applied methods/functions	Test system features				Faults	Advantages/limitations
			DG	Load	Line	Volt. level		
1.	Adaptive directional overcurrent protection [42]	Numerical directional OC relays with directional interlocking capability	D-DGs	Constant MVA	Cable radial	6/0.4 kV	LLL, LL, LG	High implementation cost, simulation results only for D-DGs, HIF not considered, Centralized control is used for protection settings, needs communication
2.	Differential protection scheme[47]	OC relays and communication link	C-DGs and D-DGs	–	OHL and cable, radial	MV	LG, LLL	Economical (traditional OC relays and existing communication link), but ineffective when loads are unbalanced
3.	Current travelling waves based scheme [54]	Bus bar voltages for faults detection and current travelling waves for fault location	–	–	–	10/0.4 kV	–	Unaffected by power flow, fault current, load unbalance, plug-and-play generators and independent of Microgrid operational mode but no simulation results
4.	Multi-agent protection schemes [43]	Network zoning, IEDs, communication link, wavelet coefficients of transient current for fault location	D-DGs	Constant MVA	OHL radial	24.9 kV	LG, LLG-HIF	No central data processor, no voltage transformers, no time synchronized measurements, less computation, effective for all types of faults including HIF, but requires means to differentiate between fault and switching transients to avoid false trips, needs high speed communication
5.	Inverse-time admittance- based protection scheme [51]	Inverse–time admittance relay, directional element, zoning	C-DGs	Constant MVA	OHL radial and closed loop	11 kV	LLL, LL, LG, LLG	No use of communication link, slow tripping for high impedance faults and higher DG infeed, measurement errors due to fundamental extraction because of harmonics, transients and decaying dc components
6.	Pattern recognition based scheme [52,53]	Time-frequency transform (S-transform), spectral energy contours, calculation of differential energy	C-DGs and D-DGs	Constant MVA	OHL radial and closed loop	25 kV	LLL, LL, LG, LLG, LLLG HIF	More robust than current differential scheme, immune to noise and less sensitive to synchronisation error, uses both time and frequency information (more data for decision making), proposed for wide area protection

under-voltage as secondary protection if I^2t protection fails due to insufficient current levels.

An adaptive protection scheme based on telecommunication and modern protection relays or IEDs for Microgrid with C-DGs is presented in [21]. The scheme has been applied to MV feeder divided into four protection zones and between each zone a circuit breaker is installed which is controlled by an IED, the DG units are also provided with IEDs. The IEDs are provided with voltage and currents measurements as well as directional OC protection function and are connected with each other through high speed communication links. The proposed method uses voltage measurements for fault detection and current direction for fault location. In the proposed method, complete system selectivity and speed is obtained through transfer of fault direction and interlocking information between IEDs using communication based on IEC 61850.

3.3. The protection schemes for both grid-connected and islanded mode

3.3.1. Adaptive protection schemes

An adaptive protection scheme based on the principle of network zoning is presented in [13]. Zoning of the feeders is done in a way that each zone has appropriate balance DG and load with DG capacity slightly larger than load. Moreover, in each zone at least the largest DG is equipped with load frequency control capability. After zoning, some fast operating switches equipped with synchronisation-check relays and having capability to receive remote signals from sub-station breaker are placed between each of two zones. A computer-based relay having high processing power, large storage capacity and capability to communicate with zone breakers and DG relays is installed at sub-transmission sub-station. This computer-based relay has to perform the functions of online fault detection and isolation of faulted zone by tripping the appropriate zone breaker and DG connected to that zone. In addition, sub-station relay has to perform the reclosing in case of temporary faults in any of the zones. The scheme is not suitable for systems with low DG penetration and to a great extent depends on centralised relay and communication links. The need of continuous synchronised current measurements at each circuit breaker and DG location with the help of GPS and PMU make this scheme quite expensive.

An adaptive protection scheme employing numerical directional OC relays with directional interlocking capability for Microgrid with both D-DGs and C-DGs is proposed in [42]. The scheme is based on Microgrid central controller which updates the protection settings according to Microgrid operational mode using advanced communication link ensuring fast tripping.

A multi-agent based protection scheme using a wavelet transform technique is presented in [43] for distribution system with DGs. The scheme divides the network into several segments and relay agents are installed at interconnection points between these segments. The relay agents detect and isolate the fault through communication with neighbouring agents. The faulted zone is determined through feedback signals from current transformers (CTs) installed at interconnected branches which measure the current leaving the node. From the measurement of transient currents, wavelet transform coefficients are calculated and on the basis of the sign of the wavelet transform coefficients a fault is assigned to be internal or external. If the wavelet transform coefficients of the currents measured at all points have the same sign, the fault is categorised as internal fault, otherwise considered as an external fault. A relay agent diagnoses a fault on its bus bar as an internal fault and immediately trips all circuit breakers connected to the bus bar to clear the fault and communicates its decision to other relay agents. In [44], a new adaptive relay protection concept based on multi-agent approach has been proposed for MV smart grid. The proposed method is adaptable and is based on distributed intelligence but can be made adaptable through centralised intelligence.

A comparison between directional OC protection and distance protection with the help of PSCAD simulations has been presented in [45]. It is concluded that distance protection performs better than directional OC protection. Therefore, an adaptive protection based on directional OC protection for the grid-connected and distance protection for the islanded mode of Microgrid has been suggested.

3.3.2. Differential protection schemes

One differential protection scheme using communication-assisted digital relays working on the principle of synchronised phasor measurements has been suggested in [46] for MV Microgrids embedded with both D-DGs and C-DGs. Instantaneous differential protection is used as the primary protection and adjacent relays are used as backup in case of breaker failure. Comparative voltage protection is used as tertiary protection in case of relay or communication failure. The suggested scheme is also capable of detecting HIF. However, the proposed scheme is uneconomical to implement and assumes advanced technical features that are still not available in the present state-of-the-art equipment like high performance relays and breakers as well as high sensitive current transformers.

In [47], a protection strategy based on the principle of differential current and utilizing traditional OC relays and communication link has been advised for MV Microgrids having both D-DGs and C-DGs. This scheme offers economical implementation, but not effective during unbalanced load.

A differential protection scheme is suggested in [48] as a means of primary protection for MV Microgrid with C-DGs and closed loop OHL for both the grid-connected and islanded mode of operation. The scheme uses OC and under voltage based protection schemes as backup protection in case of breaker or communication link failure. Current differential relays are used for feeder and bus protection while DGs are protected using under voltage, reverse power flow, over voltage and synchronism check relays. This scheme may suffer problems due to switching transients and unbalanced loads.

3.3.3. Distance protection schemes

A distance protection scheme has been presented in [49] for Microgrid with C-DGs. The performance of distance relays with Mho characteristic has been evaluated in a radial feeder system for unbalanced (LG, LL, LLG) faults using PSCAD simulations and MATLAB calculations. A method of converter control is proposed to limit the converter current by reducing the voltage in the faulty phase(s) while keeping the voltage of healthy phases unaltered. The effects of fault resistance and load are considered on the Mho characteristic. It has been observed that the relay downstream to the fault operates unnecessarily for ground faults when a star-connected load is connected downstream to the fault and low fault impedance appears at the fault point. To alleviate this problem the addition of a directional feature to the distance relay has been suggested. To solve the same problem, a negative sequence impedance analysis has been done at each distance relay location in [50]. It has been found that reactive part of negative sequence impedance can be used to discriminate forward and reverse faults effectively for radial networks with C-DGs.

An inverse time admittance-based relay is proposed in [51] for radial distribution system with several C-DGs. The proposed scheme is capable of detecting fault currents even with lower magnitudes. In this scheme, first of all a normalized admittance is obtained, then this normalized admittance is used to obtain an inverse time tripping characteristic of relay. The relay trips when the normalized admittance becomes greater than 1.0 or the measured admittance becomes greater than total admittance

of protected line segment. In the proposed scheme, each relay has two protection zones (Zone-1 and Zone-2) and the unique inverse time characteristic for each zone depending on the value of admittance in that zone. Thus each upstream relay provides backup for the immediate downstream relay. The scheme recommends the use of directional feature in order to differentiate between forward and reverse faults. Moreover, a third zone (Zone-3) for each relay is also introduced in order to detect the high impedance/resistance faults. For Zone-3, each relay has two tripping characteristics, one for forward faults and other for reverse faults.

3.3.4. Pattern recognition schemes

A differential energy based protection scheme using time–frequency transform technique S-transform has been proposed in [52,53] for MV Microgrid with radial/loop network and C-DGs. In the proposed protection scheme, first of all the currents at both ends of faulted line are obtained from the respective buses which are then processed through a modified S-transform and their time–frequency contours are generated. The spectral energy content of time–frequency contours of fault current signals is calculated and then the differential energy is computed. The differential energy of time–frequency contours of fault currents at both ends of faulted line is the key indicator for recognition of fault patterns in Microgrid. The trip signal is issued on the basis of a set threshold on the differential energy for different fault situations in Microgrid. The simulation results show that the differential energy varies considerably in the faulted phase as compared with healthy phase and therefore faulted phase can easily be identified.

3.3.5. Other miscellaneous schemes

A new protection strategy based on the principle of current travelling waves is introduced in [54]. The scheme uses the local bus bar voltages to detect a fault and current travelling waves to find the fault location. The occurrence of fault at any feeder will cause the change in power frequency voltages of the bus connected to that feeder depending on the type of fault. Current transformers are used for the measurement of travelling waves and wavelet multiresolution analysis is used for decomposition of travelling waves. With the comparison of magnitude and polarity of initial travelling waves the faulted feeder is determined.

A protection scheme utilizing new programmable microprocessor-based relays with directional elements has been proposed in [55] for LV Microgrid containing C-DGs, D-DGs and unbalanced loads. The fault detection functions used for the islanded mode of operation are comprised of instantaneous OC relay and voltage based relay for detection of solid faults, negative and zero sequence components of fault current for detection of medium impedance faults and energy level method as proposed in [56] for detection of HIF. In addition to three directional elements (one for each phase), a negative sequence directional element is also utilized to avoid false trips due to low magnitude fault currents. A current-magnitude comparison technique is also suggested to avoid false tripping by directional element. A neutral voltage displacement function has also been suggested to detect ground faults of MV side of transformer in an islanded mode. For grid-connected mode, the conventional OC protection devices (fuses and relays) with inverse time characteristics and microprocessor-based relays without communication link are suggested. The proposed scheme requires no communication or adaptive protection devices and to a great extent is independent of fault current magnitude, operational mode of Microgrid as well as type and size of DERs. It also enables single-pole tripping.

4. Discussion

In order to protect a particular type of AC Microgrid in both grid-connected and islanded mode of operation, an adaptive protection is necessarily required. Most of the proposed adaptive protection methods are completely dependent on exchange or transfer of data/information in the shape of measured system parameters (voltage, current, phase angle, etc.) and direction and interlocking signals between different protection agents (IEDs) via some kind of communication link. Therefore, for an effective adaptive protection scheme, the reliability of communication link is critical. The factors like high risks of communication link failures and cyber security threats as well as the high costs involved to avoid them are the major challenges for implementation of economical adaptive protection schemes. Wider application of the most advanced standard IEC 61850 basing on modern Ethernet technologies in relay protection results in increased level of susceptibility to cyber-attacks as already reported in [57]. More information about cyber security and other potential threats to modern digital relay protection can be found in [58–60]. These challenges should be addressed properly in order to fully exploit the benefits of adaptive protection schemes. Considering the above factors, the future protection schemes for AC Microgrids, in general, are most likely to be hybrid in nature comprised of optimum combination of traditional effective protection schemes (directional OC, differential, distance etc.) and new adaptive communication-based protection schemes using pattern recognition approaches, synchrophasors, fault current limiters and energy storages. The choice will depend on the type of Microgrid structure, reliability needs of consumers and the type and control of DERs. Additionally, redundant protection and communication systems will be required for Microgrid providing higher level of reliability.

5. Conclusion

Main protection issues of AC Microgrid and available solutions proposed in the most recent scientific literature have been reviewed and a critical analysis of suggested protection schemes for AC Microgrid has been produced. The critical analysis is based on basic protection philosophy of Microgrid to have a safe and secure operation in both grid-connected and islanded mode of operation. Moreover, the available protection schemes have been categorized according to their effectiveness for particular operational modes of Microgrid and network topology. Various protection functions as well as advantages/limitations of each proposed protection scheme have also been mentioned. It is concluded that more effort is still needed to overcome the limitations of proposed protection schemes in order to make them effective for all types of fault events including high impedance faults in a selective, sensitive, reliable and cost-effective way ensuring minimum supply disruption to consumers. Most of the proposed adaptive protection schemes that are able to work in both grid-connected and islanded mode of Microgrid require communication links. Therefore, improvement of communication system reliability through redundancy or other means, provision of alternate methods to cope with communication failures (if no reliable communication) and protection against cyber attacks are inevitable for safe and secure operation of future Microgrids.

Acknowledgement

The financial support provided by the Finnish Funding Agency for Technology and Innovation (Tekes) through the Smart Grid and Energy Markets (SGEM) project (Grant No. 1031/09) is greatly acknowledged.

References

[1] S. Chowdhury, S.P. Chowdhury, P. Crossley, Microgrids and active distribution networks, in: IET Renewable Energy Series 6, The Institution of Engineering and Technology, London, United Kingdom, 2009.
[2] R. Lasseter, et al., Integration of distributed energy resources, in: The CERTS Microgrid Concept, Lawrence Berkeley National Lab, 2002.
[3] N. Hatziargyriou, H. Asano, R. Iravani, C. Marnay, Microgrids, IEEE Power Energy Mag. 5 (2007) 78–94.
[4] D. Infield, F. Li, Integrating micro-generation into distribution systems—a review of recent research, in: IEEE Power and Energy Society General Meeting—Conversion and Delivery of Electrical Energy in the 21st Century, 2008, pp. 1–4.
[5] R.H. Lasseter, P. Paigi, Microgrid: a conceptual solution, in: IEEE 35th Annual Power Electronics Specialists Conference, PESC 04, 2004, pp. 4285–4290, 6.
[6] IEEE, IEEE Guide for Design, Operation, and Integration of Distributed Resource Island Systems with Electric Power Systems, IEEE Std 1547. 4-2011, 2011, pp. 1–54.
[7] A.P.S. Meliopoulos, Challenges in simulation and design of μGrids, in: IEEE Power Engineering Society Winter Meeting, 2002, pp. 309–314, 1.
[8] R.C. Dugan, Distributed resources and reliability of distribution systems, in: IEEE Power Engineering Society Summer Meeting, 2002, pp. 105–108, 1.
[9] F. Katiraei, M.R. Iravani, P.W. Lehn, Micro-grid autonomous operation during and subsequent to islanding process, IEEE Trans. Power Delivery 20 (1) (2005) 248–257.
[10] B. Kroposki, R. Lasseter, T. Ise, S. Morozumi, S. Papatlianassiou, N. Hatziargyriou, Making microgrids work, IEEE Power Energy Mag. 6 (2008) 40–53.
[11] J. Gers, T. Holmes, Protection of Electricity Distribution Networks, second ed., Peter Peregrinus Ltd, London, 2005.
[12] M.H. Aslinezhad, S.M. Sadeghzadeh, J. Olamaei, Overcurrent relays protective coordination in distribution systems in presence of distributed generation, Int. J. Tech. Phys. Prob. Eng. (IJTPE) 3 (June) (2011) 40–46.
[13] S.M. Brahma, A.A. Girgis, Development of adaptive protection scheme for distribution systems with high penetration of distributed generation, IEEE Trans. Power Delivery 19 (2004) 56–63.
[14] M.T. Doyle, Reviewing the impacts of distributed generation on distribution system protection, in: IEEE Power Engineering Society Summer Meeting, 2002, pp. 103–105, vol. 1.
[15] L.K. Kumpulainen, K.T. Kauhaniemi, Analysis of the impact of distributed generation on automatic reclosing, in: IEEE PES Power Systems Conference and Exposition, 2004, pp. 603–608, 1.
[16] J.J. Burke, Power Distribution Engineering: Fundamentals and Applications, CRC Press (MARCEL DEKKER, INC.), New York, 1994, pp. 374.
[17] H. Zayandehroodi, A. Mohamed, H. Shareef, M. Mohammadjafari, A Comprehensive review of protection coordination methods in power distribution systems in the presence of DG, Przegląd Elektrotechniczny 8 (2011) 142–148.
[18] M. Baran, I. El-Markabi, Adaptive over current protection for distribution feeders with distributed generators, in: IEEE PES Power Systems Conference and Exposition, 2004, pp. 715–719, 2.
[19] H. Laaksonen, K. Kauhaniemi, S. Voima, Protection system for future LV Microgrids, in: CIRED 21st International Conference on Electricity Distribution, 6–9 June, 2011, Frankfurt, 2011 (Paper 0431).
[20] N.W.A. Lidula, A.D. Rajapakse, Voltage balancing and synchronization of microgrids with highly unbalanced loads, Renewable Sustainable Energy Rev. 31 (2014) 907–920.
[21] S. Voima, K. Kauhaniemi, H. Laaksonen, Novel protection approach for MV Microgrid, in: CIRED 21st International Conference on Electricity Distribution, 6–9 June, 2011, Frankfurt, 2011 (Paper 0430).
[22] H. Laaksonen, K. Kauhaniemi, Fault type and location detection in islanded Microgrid with different control methods based converters, in: CIRED 19th International Conference on Electricity Distribution, 21–24 May, Vienna, 2007, pp. 1–4 (Paper 0372).
[23] T. Loix, T. Wijnhoven, G. Deconinck, Protection of microgrids with a high penetration of inverter-coupled energy sources, in: Integration of Wide-Scale Renewable Resources into the Power Delivery System, 2009 CIGRE/IEEE PES Joint Symposium, 2009, pp. 1–6.
[24] N.W.A. Lidula, A.D. Rajapakse, A pattern recognition approach for detecting power islands using transient signals—Part II: Performance evaluation, in: IEEE Trans. Power Delivery. July, 2012, pp. 1071–1080, 27.
[25] M. Geidl, Protection of power systems with distributed generation: state of art, in: Technical Rep., ETH, Zurich, Switz., 2005.
[26] P. Naisani, D. Tholomier, T. Yip, G.J. Lloyd, Protection of distributed generation (DG) interconnection, in: 63rd Annual Conference for Protective Relay Engineers, 2010, pp. 1–17.
[27] P. Crolla, A.J. Roscoe, A. Dysko, G.M. Burt, Methodology for testing loss of mains detection algorithms for microgrids and distributed generation using real-time power hardware-in-the-loop based technique, in: IEEE Eighth International Conference on Power Electronics and ECCE Asia (ICPE & ECCE), 2011, pp. 833–838.
[28] N.W.A. Lidula, A.D. Rajapakse, A pattern recognition approach for detecting power islands using transient signals—Part I: Design and implementation, IEEE Trans. Power Delivery 25 (December) (2010) 3070–3077.
[29] www.nerc.com, Extended loss of GPS Impact on Reliability, Preliminary Special Reliability Assessment Whitepaper, 2014, available at: http://www.nerc.com/docs/escc/PNT%20-%20Power%20Systems%20V19.pdf (accessed on 19.5.2015) 1–8.
[30] N. Hatziargyriou, Microgrids: Architectures and Control, John Wiley & Sons, West Sussex, UK, 2013.
[31] A.R. Haron, A. Mohamed, H. Shareef, A review on protection schemes and coordination techniques in Microgrid systems, J. Appl. Sci. 12 (2) (2012) 101–112 (Asian Netw. for Scientific Inf.).
[32] H.J. Laaksonen, Protection principles for future microgrids, IEEE Trans. Power Electron. 25 (2010) 2910–2918.
[33] J. Jager, T. Keil, L. Shang, R. Krebs, New protection co-ordination methods in the presence of distributed generation, in: Eighth IEE International Conference on Developments in Power System Protection. 1, 2004, pp. 319–322, 2004.
[34] N. Jenkins, et al., Large Scale Integration of Micro-Generation to Low Voltage Grids, Work Package E, Deliverable DE2, Protection Guidelines for a Microgrid, 2005, pp. 1–370, ⟨http://www.microgrids.eu/micro2000/delivarables/deliverable_de2.pdf⟩. (Contract no: ENK5-CT-2002-00610).
[35] Y.T. Jin, S.J. Park, S.J. Lee, M.S. Choi, Intelligent agent based protection for smart distribution systems, in: CIRED 21st International Conference on Electricity Distribution, 6–9 June, 2011, Frankfurt, 2011 (Paper No. 0383).
[36] W. El-Khattam, T.S. Sidhu, Restoration of directional overcurrent relay coordination in distributed generation systems utilizing fault current limiter, IEEE Trans. Power Delivery 23 (2008) 576–585.
[37] W. El-Khattam, T.S. Sidhu, Resolving the impact of distributed renewable generation on directional overcurrent relay coordination: a case study, IET Renew. Power Gener. 3 (2009) 415–425.
[38] M. Khederzadeh, Application of TCSC to restore directional overcurrent relay coordination in systems with distributed generation, in: CIRED 20th International Conference on Electricity Distribution, 8–11 June, 2009, Prague, 2009 (Paper 0041).
[39] H. Al-Nasseri, M.A. Redfern, Harmonics content based protection scheme for Micro-grids dominated by solid state converters, in: Power System Conference, 2008. MEPCON 2008. 12th International Middle-East, 2008, pp. 50–56.
[40] H. Al-Nasseri, M.A. Redfern, F. Li, A voltage based protection for micro-grids containing power electronic converters, in: IEEE Power Engineering Society General Meeting, 2006, p. 7.
[41] H. Nikkhajoei, R.H. Lasseter, Microgrid protection, in: IEEE Power Engineering Society General Meeting, 2007, pp. 1–6.
[42] A. Oudalov, A. Fidigatti, Adaptive network protection in microgrids, Int. J. Distrib. Energy Resour. 5 (2009) 201–226.
[43] N. Perera, A.D. Rajapakse, Agent-based protection scheme for distribution networks with distributed generators, in: IEEE Power Engineering Society General Meeting, 2006, p. 6.
[44] K. Kauhaniemi, S. Voima, Adaptive relay protection concept for smart grids, in: Renewable Efficient Energy II Conference, 21–22 March, 2012, Vaasa, Finland, 2012.
[45] S. Voima, H. Laaksonen, K. Kauhaniemi, Adaptive protection scheme for smart grids, in: 12th IET International Conference on Developments in Power System Protection (DPSP 2014), 2014, pp. 1–6.
[46] E. Sortomme, S.S. Venkata, J. Mitra, Microgrid protection using communication-assisted digital relays, IEEE Trans. Power Delivery 25 (2010) 2789–2796.
[47] S. Conti, L. Raffa, U. Vagliasindi, Innovative solutions for protection schemes in autonomous MV micro-grids, in: International Conference on Clean Electrical Power, 2009, pp. 647–654.
[48] M. Dewadasa, A. Ghosh, G. Ledwich, Protection of microgrids using differential relays, in: Universities Power Engineering Conference (AUPEC), 2011 21st Australasian, 2011, pp. 1–6.
[49] J.M. Dewadasa, A. Ghosh, G. Ledwich, Distance protection solution for a converter controlled microgrid, in: Fifteenth National Power Systems Conference (NPSC), December, IIT Bombay, 2008, pp. 586–591.
[50] M. Dewadasa, A. Ghosh, G. Ledwich, Line protection in inverter supplied networks, in: Australasian Universities Power Engineering Conference (AUPEC'08), 2008, pp. 1–6 (Paper P-053).
[51] M. Dewadasa, A. Ghosh, G. Ledwich, An inverse time admittance relay for fault detection in distribution networks containing DGs, in: TENCON 2009—2009 IEEE Region 10 Conference, 2009, pp. 1–6.
[52] S.R. Samantaray, G. Joos, I. Kamwa, Differential energy based Microgrid protection against fault conditions, in: IEEE PES Innovative Smart Grid Technologies (ISGT), 2012, pp. 1–7.
[53] S. Kar, S.R. Samantaray, Time-frequency transform-based differential scheme for Microgrid protection, IET Gener. Transm. Distrib. 8 (2014) 310–320.
[54] Shenxing Shi, Bo Jiang, Xinzhou Dong, Zhiqian Bo, Protection of microgrid, in: 10th IET International Conference on Developments in Power System Protection (DPSP 2010), Managing the Change, 2010, pp. 1–4.
[55] M.A. Zamani, T.S. Sidhu, A. Yazdani, A protection strategy and microprocessor-based relay for low-voltage microgrids, IEEE Trans. Power Delivery 26 (2011) 1873–1883.
[56] R.D. Christie, H. Zadehgol, M.M. Habib, High impedance fault detection in low voltage networks, IEEE Trans. Power Delivery 8 (1993) 1829–1836.
[57] CIGRE Working Group B5.38, The Impact of Implementing Cyber Security Requirements using IEC 61850, Technical Brochure 427, Paris, Aug. (2010).
[58] V. Gurevich, Cyber and Electromagnetic Threats in Modern Relay Protection, CRC Press, Taylor and Francis Group, FL, 2015.
[59] V. Gurevich, Susceptibility of modern relay protection: will protection from cyber attacks help? Serb. J. Electr. Eng. 11 (2014) 233–241.
[60] N. Kush, E. Ahmed, M. Branagan, E. Foo, Poisoned GOOSE: exploiting the GOOSE protocol, in: Proceedings of the Twelfth Australasian Information Security Conference (AISC 2014), Auckland, New Zealand, 2014, pp. 17–22, 149.

energies

MDPI

Article

An Adaptive Protection for Radial AC Microgrid Using IEC 61850 Communication Standard: Algorithm Proposal Using Offline Simulations

Aushiq Ali Memon * and Kimmo Kauhaniemi

School of Technology and Innovations, University of Vaasa, Wolffintie 34, FI-65200 Vaasa, Finland; Kimmo.Kauhaniemi@univaasa.fi

* Correspondence: aushiq.memon@univaasa.fi or aushiq_37@yahoo.com; Tel.: +358-414-744-093

Received: 23 August 2020; Accepted: 9 October 2020; Published: 13 October 2020

Abstract: The IEC 61850 communication standard is getting popular for application in electric power substation automation. This paper focuses on the potential application of the IEC 61850 generic object-oriented substation event (GOOSE) protocol in the AC microgrid for adaptive protection. The focus of the paper is to utilize the existing low-voltage ride through characteristic of distributed generators (DGs) with a reactive power supply during faults and communication between intelligent electronic devices (IEDs) at different locations for adaptive overcurrent protection. The adaptive overcurrent IEDs detect the faults with two different preplanned settings groups: lower settings for the islanded mode and higher settings for the grid-connected mode considering limited fault contributions from the converter-based DGs. Setting groups are changed to lower values quickly using the circuit breaker status signal (XCBR) after loss-of-mains, loss-of-DG or islanding is detected. The methods of fault detection and isolation for two different kinds of communication-based IEDs (adaptive/nonadaptive) are explained for three-phase faults at two different locations. The communication-based IEDs take decisions in a decentralized manner, using information about the circuit breaker status, fault detection and current magnitude comparison signals obtained from other IEDs. However, the developed algorithm can also be implemented with the centralized system. An adaptive overcurrent protection algorithm was evaluated with PSCAD (Power Systems Computer Aided Design) simulations, and results were found to be effective for the considered fault cases.

Keywords: AC microgrid; adaptive protection; IEC 61850 GOOSE protocol; substation automation

1. Introduction

According to the CIGRE C6.22 working group definition, microgrids are electrical distribution systems containing loads and distributed energy resources (DERs) like distributed generators (DGs) (renewable/nonrenewable), energy storage devices or controlled loads that can be operated in a controlled and coordinated way either while connected to the main power network or while islanded [1]. Microgrids can be classified as either AC microgrids, DC microgrids or AC/DC hybrid microgrids, each having their own advantages, limitations and challenges, as described in [2]. The technical challenges of AC microgrids can be broadly divided into two main categories: control challenges and protection challenges. The protection challenges can be further divided into two categories according to operational modes of the AC microgrid: grid-connected mode and islanded mode protection challenges.

When the AC microgrid is operated in the grid-connected mode, a large magnitude of fault current (ten times the full-load current or more) is available from the main grid in order to activate the overcurrent protection devices within the AC microgrid. When the AC microgrid is operated in the islanded mode, a very low magnitude of fault current is available from DGs within the AC

microgrid, and hence, overcurrent devices with a single setting become insensitive. The consequences are the miscoordination of overcurrent devices, longer tripping delays and even no trips at all during different fault situations. The magnitude and duration of the fault current is mainly limited by the control of the converter-based DGs within the AC microgrid, which can be overcome by an additional fault-current source (FCS), like an energy storage device with high short-circuit capacity, and thus, single-setting overcurrent devices will become effective. However, the connection of an additional FCS will make the protection scheme unreliable due to dependence upon the single energy storage device. Moreover, the connection of many such FCSs will make the scheme quite expensive [3]. Another alternative approach for using only single-setting overcurrent devices can be the limitation of the fault current from the main grid or directly coupled DGs using fault-current limiters (FCLs) in grid-connected mode and using lower fault-current trip settings, which can also work in islanded mode with reduced short-circuit currents. This approach causes overcurrent devices to be more sensitive in grid-connected mode and prone to nuisance tripping during transient events [4]. The huge difference of the fault-current magnitude and duration in grid-connected and islanded mode calls for adaptive protection schemes for the AC microgrid.

The adaptive protection schemes can be only overcurrent-based [5] or a combination of overcurrent-based and unit type (current differential) or based on other new protection methods like traveling waves-based [3]. The adaptive overcurrent protection necessarily requires such overcurrent devices that provide the flexibility for changing the tripping settings like numerical overcurrent (OC) relays with several setting groups [5]. The overcurrent schemes can be used more effectively in AC microgrids with the majority of directly coupled DGs (synchronous generators) compared with only the converter-based DGs, since the latter provide very limited fault currents for a very limited duration of time. Another reasonable adaptive approach is to use only the overcurrent protection scheme in the grid-connected mode and other protection schemes like directional overcurrent, harmonic content-based, voltage-based, symmetrical component-based, etc. in islanded mode for the AC microgrid with the converter-based DGs, with all functions included in a single protection device called the IED (intelligent electronic device). However, the protection schemes proposed for the islanded mode are not effective in every fault situation, and the majority of them need high-speed communication to remain effective [4]. Finding a suitable and cost-effective combination of different effective protection schemes for the islanded mode with the converter-based DGs to work as primary and backup protection in a coordinated manner is still a huge challenge. An adaptive protection can be implemented either in a centralized manner by using a microgrid central controller to change the active-group settings [5] or in a decentralized manner in which IEDs in the microgrid change their own active-settings groups by receiving a trip-signal/breaker status from another IED or circuit breaker. The centralized adaptive protection scheme necessarily requires a redundant microgrid central controller to maintain a certain level of reliability. For a decentralized adaptive protection scheme, the IEDs must be equipped with the required intelligent agents and logics in order to perform various functions in an autonomous manner using the available information (data/measurements/signals) both locally and remotely.

Previously, the adaptive protection for the AC microgrid using centralized protection and communication architecture was proposed in [5–7]. An adaptive overcurrent protection for microgrids using inverse-time directional overcurrent relays (DOCRs) was presented in [8]. In this paper, artificial neural networks (ANNs) at the central human machine interface (HMI) or data concentrator are implemented for the detection and location of the faults. The protection coordination of OC relays using the linear programming approach is presented for the radial and looped configurations of microgrids in both the grid-connected and islanded modes. An adaptive protection combined with machine learning for medium voltage (MV) microgrids was reported in [9]. The proposed methodology requires a database available beforehand, which has been obtained through simulation in this research. Then, using the data mining methodology, the meaningful information is extracted quantitatively from the database. The ANN is used for fault detection and support vector machine (SVM) for fault location.

The proposed method also requires relay settings calculations and recordings in the control center or relays beforehand. Moreover, the proposed scheme may generate inaccuracies in the case of data corruption, and therefore, additional countermeasures will be required. A new adaptive protection coordination scheme based on the Kohonen map or self-organizing map (SOM) clustering algorithm was proposed recently in [10] for the inverse-time OC relays. In this paper, the protection coordination is improved gradually in the three phases of the proposed algorithm, namely conventional, clustering and sub-clustering phases. The proposed method uses digital OC relays with four setting groups. The performance of the method was presented in terms of the total miscoordination time (TMT) index using a modified IEEE 33-bus network with two synchronous generators and two electric vehicle (EV) charging stations. A decentralized adaptive protection scheme using DOCRs, teleprotection and a fuzzy system in real time was proposed in [11] for the transmission system. In this paper, the transient stability constraint satisfying the maximum operating time of DOCRs was considered. Due to the dynamic adaption of the fuzzy system to the changing system conditions, the actuation time of relays was decreased, keeping the stability and coordination intact. An optimal overcurrent relay coordination in the presence of inverter-based wind farms and electrical energy storage devices was presented in [12]. In this paper, the optimal protection coordination of inverse-time DOCRs with varying load demands and changing unit commitments of DGs is presented using mixed integer nonlinear programming. A hybrid particle swarm optimization-integer linear programming (PSO-ILP) algorithm was suggested recently in [13] for the proper coordination of OC relays by suggesting proper settings groups for the changing network states. The adaptive differential protections for wind farm-integrated networks were reported in [14,15]. However, the differential protection inherently cannot provide the backup protection, and usually, the time-coordinated overcurrent protection is used as the backup protection.

The modeling of the inter-substation communication based on the IEC 61850 standard was presented in [16] for the differential protection (Sampled Values (SV) messages) and in [17] for the distance protection (generic object-oriented substation event (GOOSE) messages). In both [16] and [17], the virtual simulated communication networks were used based on a non-real-time tool called the riverbed modeler network software. In both references [16] and [17], the tunneling communication mechanism between substations was used for the differential and the distance protection functions, respectively. In [16], it was evaluated that the dedicated fiber optic network link had better performance in terms of the end-to-end delay of SV and GOOSE messages compared with an asynchronous transfer mode (ATM) link and synchronous optical networking (SONET) links. It was concluded in [17] that the links with lower bandwidths were not suitable for long distances; however, a more accelerated distance protection can be implemented, even with lower bandwidth links, compared with the conventional distance protection scheme. An adaptive protection system based on the IEC 61850 for MV smart grids was presented in [18]. In this paper, the dynamic publisher/subscriber reconfiguration of the protection devices for the implementation of the advanced fault location, isolation and service restoration (FLISR) was suggested. Since, the remote changes of the IED settings are not supported by the current versions of the IEC 61850 standard, therefore, the change of the operational settings after the network reconfiguration was suggested using the exchange of MMS (manufacturing message specification) messages with IEDs. Additionally, the logic selectivity was proposed to support remote changes of GOOSE communication schema without interrupting the FLISR operation. A mixed-layer 2/3 approach was also suggested in the paper to support both the MMS and the GOOSE implementations for the field demo of an Italian MV network. A detailed survey of different adaptive protections of microgrids was presented recently in [19]. For a further detailed review of different microgrid protection schemes, their challenges and developments, the recent review articles [20–23] are suggested, in addition to the previous review article [4] by the authors. For further information related to IEC 61850-based substation automation systems and related issues, the recent literature survey done in [24] is also recommended.

Based on the recent literature review presented above, it was found that less literature is available for the role of IEC 61850 standard-based communication in the protection coordination of the AC microgrids with decentralized protection and communication architecture. Moreover, a low-voltage

ride through (LVRT) capability with reactive power support from the converter-based DGs in the case of AC microgrid faults has rarely been used for adaptive protection. The high risks of communication link failures and unacceptable and unpredictable communication delays are still the limiting factors to use communication links for high-speed protection functions. However, the use of a communication link is inevitable for protection functions like transfer trips from the breaker/IED at the point of common coupling (PCC) to another breaker/IED within the AC microgrid for loss of mains detection and changing preplanned active-groups settings/functions during the transition from the grid-connected to island mode for deactivating sensitive anti-islanding protection during faults and for reverse interlocking schemes. In this paper, the main focus is to discuss how an IEC 61850 communication can be applied for a decentralized preplanned adaptive overcurrent protection in a radial AC microgrid. Additionally, the DGs with LVRT capability and reactive power support in islanded mode are considered in order to implement the adaptive overcurrent protection.

The rest of the paper is organized in a manner that Section 2 presents adaptive protection based on the IEC 61850 communication standard by explaining a generalized architecture of the adaptive AC microgrid. Section 3 gives a case study background of the adaptive protection of a radial AC microgrid, explaining GOOSE (generic object-oriented substation event) message delays (transfer time) for IED to IED communication for different functions, the schematic diagram of radial the AC microgrid and adaptive protection settings of different IEDs. Section 4 explains the details of the proposed adaptive protection methods and results for both the grid-connected and islanded modes of operation. Additionally, the control of DGs and the LVRT capability of DGs are also explained in this section. Section 5 gives a brief discussion about the previous methods, the contribution of the research presented in this paper and what is needed for the practical implementation of the proposed method in the future. Section 6 provides the conclusion of the paper.

2. Adaptive Protection Based on IEC 61850 Communication Standard

An adaptive protection is necessarily required for AC microgrids due to changing operational modes (grid-connected and islanded), due to the formation of controlled islands due to faults within the AC microgrid, due to intermittent DGs and periodic load variations and due to the economical operations of the AC microgrid [4,25]. An adaptive protection is defined as an online activity that changes to the preferable protection device response for modified system conditions or requirements. An adaptive protection is normally automated, but some timely human interventions may also be included. Adaptive relay is a relay that includes various settings, characteristics or logic functions capable of speedy online modifications by means of externally generated signals or control actions [26]. The modern intelligent electronic devices (IEDs) not only provide various protection functions (overcurrent, over/under voltage, etc.) integrated in a single physical device but, also, offer various setting groups for each of the available protection functions. The various setting groups of the protection functions can be modified or altered in an adaptive manner using the communication link between IEDs and IEDs and circuit breakers (CBs). Recently, the popularity of the IEC 61850 communication standard for application in electric power substation automation has increased considerably due to its promise of interoperations among IEDs from different manufacturers. The initial focus of the standard is on communication between IEDs within a single substation, but its extension for communication between several substations in the future is possible. The IEC 61850 standard explains the standardized structures for the data model and definitions of rules for the exchange of these data. IEDs from different manufacturers that comply with these standard data model definitions can then communicate, understand and interact with each other [26]. The IEC 61850 standard as a common protocol enables the integration of all protection, control, measurement and monitoring functions [27].

The generalized architecture for adaptive AC microgrid protection based on the IEC 61850 communication standard is depicted in Figure 1. The IEC 61850 communication architecture for adaptive AC microgrid protection can be subdivided into three levels: process level, bay level and substation level. At the process level, the electrical parameters measurement data (MMXU) from the

voltage and current sensors (VTs and CTs) and status of the circuit breakers (XCBR) inside the AC microgrid will be collected and digitized by merging units (MUs). At the bay level, the IEDs for lines, DGs and loads of the AC microgrid will collect the digitized measurement data (MMXU) and circuit breaker status signals (XCBR) from the process bus. Each MU will publish data to process the bus, and each IED will subscribe to the respective published data from the process bus. Each of the line, DG and load IED will use measurement data (MMXU) from their respective MU for performing the active protection function like overcurrent protection in the case of faults. The status signal of the circuit breakers inside the AC microgrid (XCBR) will be used by each adaptive IED to change the active setting groups of the protection function in the case of a fault inside the AC microgrid in islanded mode. Moreover, a XCBR signal can also be used for the transfer trip of nonadaptive IEDs that are unable to detect the faults within the islanded AC microgrid. All IEDs at the bay level will also receive the status signal (XCBR_pcc) from the circuit breaker at the point of common coupling through the station bus at the substation level. The status signal from the PCC breaker (XCBR_pcc) will be used by each adaptive IED within the AC microgrid to change the active setting group of the protection function from grid-connected mode settings to islanded-mode settings and vice versa. The signal (XCBR_pcc) can also be used for the detection of the loss-of-mains event by DG IEDs and to deactivate the sensitive loss-of-mains protection functions in order to maintain stability and reliability of supply within the AC microgrid during the transition from the grid-connected to islanded mode. The station bus at the substation level will provide primary communication between the various logical nodes of IEDs. In other words, all IEDs at the bay level will communicate and share data/information (MMXU, XCBR, and XCBR_pcc) with each other using the station bus. At the station bus, a remote access point will also exist to share data with remote clients (for wide-area measurement and protection, etc.) through a wide-area network (WAN). This remote access point will implement security functions like data encryption and authentication for all data transfers and, thus, will unburden the individual IEDs to perform these tasks.

For an adaptive OC protection, the coordination between the control and protection of the AC microgrid will also be required, and control action will be required first, followed by protection action. In the grid-connected mode, a high fault current from the grid will be available, so depending on the protection settings of IEDs, it may be required to limit the magnitude of the fault current by the activation of FCLs, and in the islanded-mode with converter-based DGs, the enhancement of the fault current magnitude may be required by the activation of additional FCSs. The numerical results presented in [28] indicate that a majority of the photovoltaic (PV) inverters contribute a fault current of 200% or less for a duration of only an initial half-cycle and 110% of the rated current for an additional duration of 10 cycles or less. It is mentioned in [29] that the grid-connected converters can feed fault currents of 1.1–1.5 p.u. of their nominal currents. It should here be noted that extra FCSs like batteries, flywheels or supercapacitors with quick response times (≤10 ms) [30] will either be necessarily required to support some type of DGs like photovoltaic DGs for providing standard LVRT capability or extending the LVRT duration of other types of DGs like wind turbine generators (WTGs) for proper protection coordination if the WTG is not capable of providing LVRT. The results presented in [31] show that a wind turbine of 1 MW can provide a fault current of magnitude equal to 120% of the rated current for seven cycles of supply frequency. This duration of seven cycles with a 50-Hz supply frequency is approximately equal to the initial duration of 150 ms after fault in the LVRT characteristic of the German BDEW-2008 standard [32]. Although the duration of 150 ms looks sufficient for the maintenance of proper protection coordination between two successive IEDs within the AC microgrid, assuming high speed communication with 3–10-ms one-way fast trip message transfer as per the IEC 61850 standard and high-speed circuit breakers (one-cycle operation). However, in some cases like data loss in the transmission channel, the retransmission of the message is required, which will result in an additional delay. Moreover, the coordination between various IEDs for breaker failure protection may be required. In such situations, the extension of the initial duration after the fault in the LVRT curve beyond 150 ms will be required, and hence, additional FCSs (flywheels or supercapacitors) will

be required. In addition to that, a redundant communication and redundant synchronization clock architecture will be required to cover the communication link and synchronization clock failures as recommended in [33].

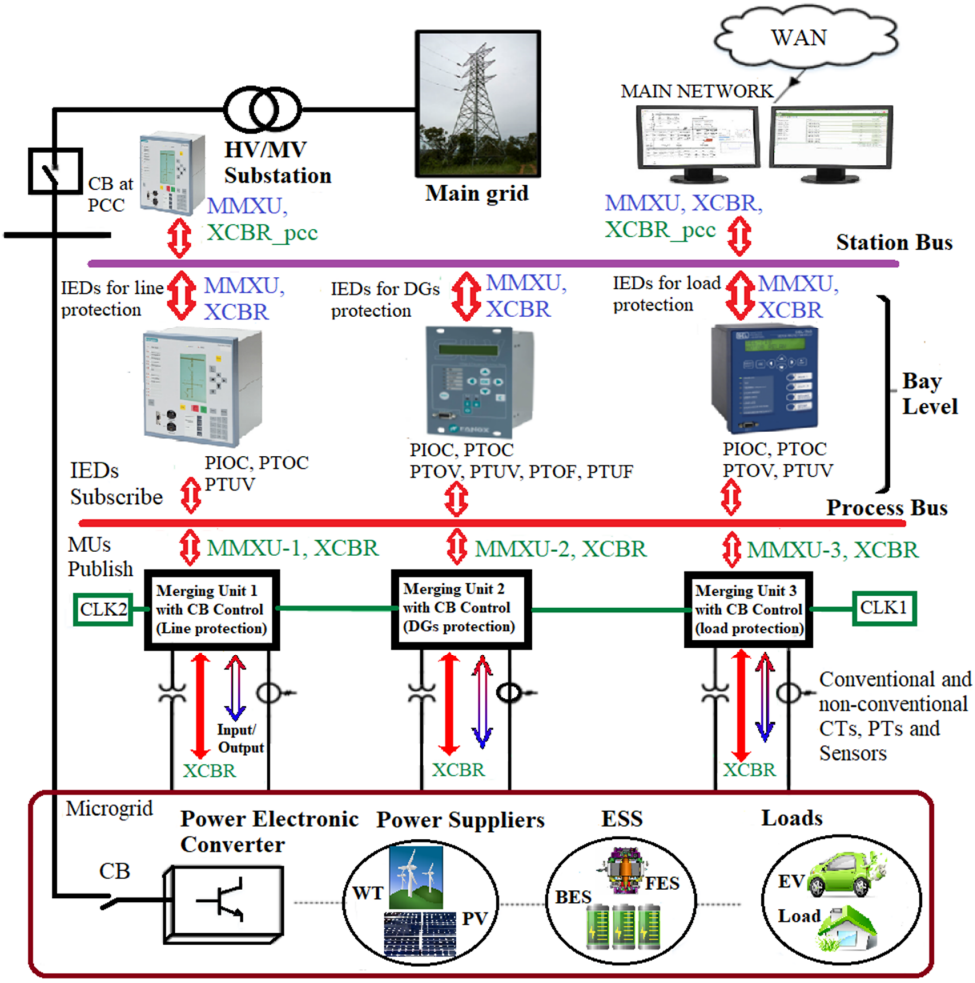

Figure 1. Adaptive AC microgrid protection based on the IEC 61850 communication standard. HV: High Voltage, WT: Wind Turbine, ESS: Energy Storage System, BES: Battery Energy Storage, FES: Flywheel Energy Storage, MMXU: Measurement, XCBR: Circuit Breaker, CT: Current Transformer, PT: Potential Transformer (VT: Voltage Transformer), CLK: Clock, PIOC: Instantaneous Overcurrent Protection, PTOC: AC Time Overcurrent Protection, PTOV: (Time) Overvoltage Protection, PTUV: (Time) Undervoltage Protection, PTOF: Overfrequency Protection, PTUF: Underfrequency Protection.

In this paper, the main focus was given to the adaptive OC protection using fault contributions from DGs with LVRT capability, particularly in the islanded mode of the AC microgrid. Hence, the control of DGs is not discussed in detail, except a few control actions for maintaining the voltage and frequency at the islanded sections, as explained in Section 4. Moreover, the loads and generation are considered balanced in islanded mode of the AC microgrid. The same is true even for the islanded MV and LV (low voltage) sections of the AC microgrid. The paper is limited to single fault events (three-phase short-circuit faults only) during the grid-connected and islanded modes with smooth transitions to islands. However, the method presented can be extended to other types of faults. In this paper, it is not considered how the islanded AC microgrid is reconnected back to the main grid after

the removal of the fault events, which is mainly related to resynchronization procedures and not directly related to AC microgrid protection. Considering the previous research, the fault contributions from DGs (both PV and WTG) are taken as 1.2 p.u. or 120% of their rated nominal currents for a duration of 150 ms after the fault. During the initial fault duration of 150 ms, the active, passive and other islanding detection and protection schemes are considered normally interlocked and can be activated quickly after the loss of communication. This means that the anti-islanding protections like under-voltage protection at DG locations can be set by default to only detect fault conditions but not trip, and DGs start providing fault currents instantaneously according to the LVRT characteristics. The trip-blocking signal to anti-islanding protection can be sent additionally from an IED at PCC after a fault is detected on the main grid side; it should be done as fast as possible and within 3 ms after fault detection, as per the IEC 61850 standard. In this paper, the term "adaptive IED" mainly refers to the communication-assisted definite time overcurrent (DTOC) relay with two preplanned setting groups: higher setting group for the grid-connected mode and lower setting group for the islanded mode of operation. The case study of a typical radial AC microgrid equipped with adaptive DTOC relays and DGs with LVRT capability is presented in the next section.

3. Case Study

An IED-to-IED GOOSE message exchange within a substation is required for fast bus tripping in the case of bus faults and the interlocking of bus-IED in the case of feeder/line faults, the protection scheme traditionally known as the reverse interlocking scheme. The IED-to-IED GOOSE messages can also be used in the case of breaker failure to trip the adjacent breaker(s). This can be done by sending a trip command message to adjacent breakers from a protection IED with a built-in breaker failure function or from a dedicated IED performing only the breaker failure function. The transfer trip may also be required between two substations. The transfer time requirement of 10 ms was set in IEC 61850 for fast trip messages (releases and status changes) between substations (transfer time class TT5) and 3 ms for fast trips and blocking messages between IEDs within a substation (transfer time class TT6) [33,34]. The transfer time requirement also varies with respect to the specific protection function. The transfer times required for various protection functions are given Table 1.

Although very strict time requirements have been demanded in IEC 61850 for type 1A fast trip messages, in this study, an average transfer time of 10–20 ms was considered for the one-way GOOSE message to cover the limitations (the limited failures of LAN within a maximum allowed transfer time of 18 ms), safety margins (errors in the time-stamp accuracy) and redundant GOOSE messages for communication between substations, as explained in [35]. IEC 61850-90-1 [36] recommends a maximum time delay of 5 to 10 ms on the communication channel depending on the voltage level [37]. However, in order to meet the requirements of security, reliability and dependability according to the IEC 60834 standard, the communication system should meet the 3-ms transfer time requirement for 99.9999 percent of the time and should have a delay no longer than 18 ms for the remainder of the time [38]. A fixed transfer time of 20 ms is thus used for both IED-to-IED communication within a substation and IED-to-IED communication between different substations in this study to cover even the worst time delay of 18 ms for the type 1A messages. In practical cases, generally, the transfer time for communication between IEDs at different substations is longer than the transfer time within the same substation. Measuring the one-way communication latency by a round-trip time between two remote substations was discussed in [39]. The selected one-way transfer time of 20 ms for producing results corresponded to the fast messages of type 1B (the ideal case) with performance class P2/P3 (transfer time class TT4) [33,35], and it covers the worst-case delay of 18 ms of type 1A fast messages according to the IEC 60834 mentioned above. The considered transfer time was also within the range of practical observed time delays in the light-weight implementation of the IEC 61850 standard-based GOOSE messages done in [40]. Although GOOSE messages apply the heartbeat messages and an IED will issue a so-called burst of GOOSE messages right after the detection of the fault, for the final trip decision, the IED necessarily needs to know the updated status at the downstream IED after the fault

to ensure proper coordination. The selected 20-ms communication delay between IEDs ensures that even the type 1A GOOSE messages with the maximum delay of 18 ms are also subscribed by IED for the trip decision. Another reason of selecting a 20-ms delay between IEDs is the potential requirement to use GOOSE messages to transfer analog data between IEDs for trip decision criterion like vectors of measured values (RMS values), which need to be transmitted only once per cycle of 50-Hz frequency. It means a new analog measurement data is required to be transmitted in just every 20 ms [37]. In the earlier publication [33], it was mentioned that there were two types of GSE (generic substation event) messages: GSSE (generic substation state event) message and GOOSE message. The GSSE message is the old binary-only message type. All the modern systems use the more flexible GOOSE message, which transfers both binary and analog data. Both GSSE and GOOSE can coexist but are not compatible with each other. The proposed protection algorithm in this paper not only uses the binary data but, also, uses the analog data (RMS magnitude of currents) for the trip decision.

Table 1. Protection functions, logical nodes and performance requirements as per IEC 61850-5:2003 (Annex G) [34].

Function	Performance Transfer Time (ms)	Corresponding LNs (Decomposition)	Starting Criteria/Remarks
Distance protection (PDIS)	5–20	IHMI, ITCI, ITMI, PDIS, TCTR, TVTR, XCBR, other primary equipment-related LNs	The monitoring part of the function is set into operation if the function is started. The function issues a start (pickup) signal in the case of an alert situation (impedance crosses boundary 1) and a trip in case of an emergency situation (impedance crosses boundary 2).
Bay interlocking	10	IHMI, ITCI, CILO, CSWI, XCBR, XSWI, (PTUV)—if applicable	The recalculation of interlocking conditions starts by any position change of the switchgear (circuit breaker, isolator, and grounding switch). Depending on the implementation, the recalculation may start not before switchgear selection.
Station-wide interlocking	-Blocking and release: 10 -Reservation: 100	IHMI, ITCI, CILO, CSWI, XCBR, XSWI, (PTUV)—if applicable	Position change of a switching device or request of the command function.
Breaker failure	5 (Delay settable ≤ 100)	IHMI, ITCI, ITMI, P . . . , RBRF, TCTR, CSWI	If a breaker gets a trip signal by some protection (for example, line protection) but does not open because of an internal failure, the fault has to be cleared by the adjacent breakers. The adjacent breakers may include breakers at remote substations (remote line ends). For this purpose, the breaker failure protection is started by the protection trip and supervises if the fault current disappears or not. If not, a trip signal is sent to all adjacent breakers after a preset delay.
Automatic protection adaptation (generic)	1–100 (Depending on the considered function)	IHMI, ITCI, ITMI, P . . .	-The protection trip makes the breaker failure protection alert, and the fault is cleared by adjacent breakers. The protection specialist may change the protection parameters (settings) if needed by static or slow predictable power system reconfiguration. -If the conditions for protection change dynamically during operation, the parameters of the protection may be changed by local or remote functions. Very often, complete pretested sets of parameters are changed rather than single parameters. -Changes in conditions are detected and communicated by some other functions, and the protection function is adapted to the changed power system condition.
Reverse blocking function (OC relays)	5	IHMI, ITCI, ITMI, P . . . (more than one)	- When a protection is triggered by OC: it sends blocking signal to upstream protections. it trips/opens its associated breaker if it does not receive a blocking signal issued by downstream protection.

In this paper, the conventional GOOSE (tunneled-GOOSE) messages in layer 2 (horizontal communication) with an Ethernet link are considered, because the short distances (a few km) between substations are considered. However, for the longer distances between substations where an Ethernet link is not possible, the routable-GOOSE (R-GOOSE) messages in layer 3 (vertical communication) for wide-area or system protection applications could be used, especially with wireless communication technologies using synchrophasors in compliance with IEC TR 61850-90-5. Some applications of R-GOOSE were reported in [41]. The normal predefined fixed GOOSE message transfer delay of 40 ms

(2 cycles of 50-Hz power system) was assumed previously for the adaptive protection of the microgrid using communication over a WiMAX network in [42], and the actual latency observed was within 35 ms with no data packet loss. However, due to packet loss and, consequently, retransmissions, the overall delay could further increase, thus limiting the application of WiMAX (R-GOOSE) to comparatively slower control and protection actions like status updates and protection settings during scheduled maintenance and load management. The adaptive protection methodology presented in this paper is concerned with primary and backup protections of the microgrid during faults in predefined operational modes: grid-connected or islanded modes. With this regard, a communication-dependent coordination methodology is proposed in Section 4 for the cases when the fault happens between two defined IEDs in grid-connected and islanded modes. The proposed methodology is very generic in nature and can be implemented in any protection IED.

The schematic diagram of a radial AC microgrid under study is shown in Figure 2. The considered AC microgrid consists of one MV bus of 20 kV (Substation Bus-2) and one LV bus of 0.4 kV (Substation Bus-3). A load of 2 MW at Substation Bus-2 is supplied by a wind turbine generator (WTG) of 2-MVA capacity, whereas a load of 0.4 MW at Substation Bus-3 is supplied by a photovoltaic (PV) generator of 0.4 MVA. The MV bus (Substation Bus-2) of the AC microgrid is connected with the LV bus (Substation Bus-3) of the AC microgrid through a 1-km-long, 20-kV cable line and 0.5-MVA, 20/0.4-kV transformer. The AC microgrid is connected with the main grid through a 2-km-long, 20-kV overhead line and an intermediate 20-kV Substation Bus-1. The WTG is connected to Substation Bus-2 through a 0.2-km-long 20-kV cable and a 2-MVA, 0.69/20-kV transformer (inside the WTG model). A 2-km overhead line between Substation Bus-1 and Substation Bus-2 is protected by two circuit breakers, CB1 and CB2, with the related protection IEDs. The protection IED1 is considered to be a nonadaptive IED due to its direct connection with the main grid, whereas the protection IED2 is considered as an adaptive IED. In the grid-connected mode, IED2 operates with settings that enable the tripping of CB2 in the case of bus fault F8 at Substation Bus-2 and facilitates the transfer trips of CB2 after receiving the CB1 open-state signal in the case of short-circuit fault F1. However, if IED2 fails to receive a CB1 open-state signal in the case of short-circuit fault F1 after the opening of CB1 and the AC microgrid already changed to islanded mode with a trip-block signal to all IEDs, this will be the failure of the transfer trip. In this case IED2 can provide a backup operation by opening CB2 with the fault current still coming from the DGs within the AC microgrid. This can be performed by IED2 either with the islanded mode settings or using the current magnitude comparison and the direct transfer trip failure logic, as explained later in Section 4. The IED2 may take quite some time to change its active group settings from the grid-connected mode settings to the islanded mode settings, and this will require DGs to remain online for additional time beyond the standard LVRT curve until the IED2 settings are changed and the tripping of CB2 is executed. However, the backup operation of CB2 by the direct transfer trip failure logic implemented at IED2 could be performed within the standard LVRT curve. In the islanded mode, the IED2 settings are adapted so that the fault F1 is detected when the CB1 is open. The 1-km cable line between Substation Bus-2 and Substation Bus-3 is protected by CB6 and CB7 with the related protection IEDs. The protection IED6 and IED7 are also considered to be adaptive.

The adaptive IED6 primarily protects both the cable line and the 20/0.4-kV transformer from short-circuit fault F2 during both the grid-connected and islanded mode of operations. In the islanded mode, after sensing the fault current at its location, the adaptive IED6 trips CB6 and transfer trips circuit breaker CB7. Additionally, IED6 and IED7 can compare the post-fault magnitude of currents at their locations with a 1.2-p.u. threshold and determine the location and direction of the fault between IED6 and IED7, as explained in the coming section. The adaptive IED7 can also provide backup protection in case of transfer trip failure (like the adaptive IED2 does, as explained earlier) in the case of the fault F2 in the grid-connected mode, in addition to the normal protection against bus fault F4 at Substation Bus-3 in both the grid-connected and islanded modes by direct tripping CB7 and transfer tripping CB9. The IED7 can only provide an "adaptive trip" to CB7 for the transfer trip failure from IED6 in the case of short-circuit fault F2 in the grid-connected mode if sufficient fault current contribution

from PV is available beyond the standard LVRT characteristic curve. This is because the IED7 may need quite some time to change its active group settings from the grid-connected mode settings to the islanded mode settings, and PV must remain online until IED7 settings are changed and CB7 tripping is executed. For this purpose, a new LVRT curve proposed later in this paper can be used. The 0.2-km cable connecting WTG with Substation Bus-2 is protected by CB3 with an adaptive IED3. Both MV and LV loads are also provided with adaptive IEDs (IED5 and IED8), which trip CB5 and CB8 adaptively in the case of load-side short-circuit faults F3 and F9 in both grid-connected and islanded modes of the AC microgrid.

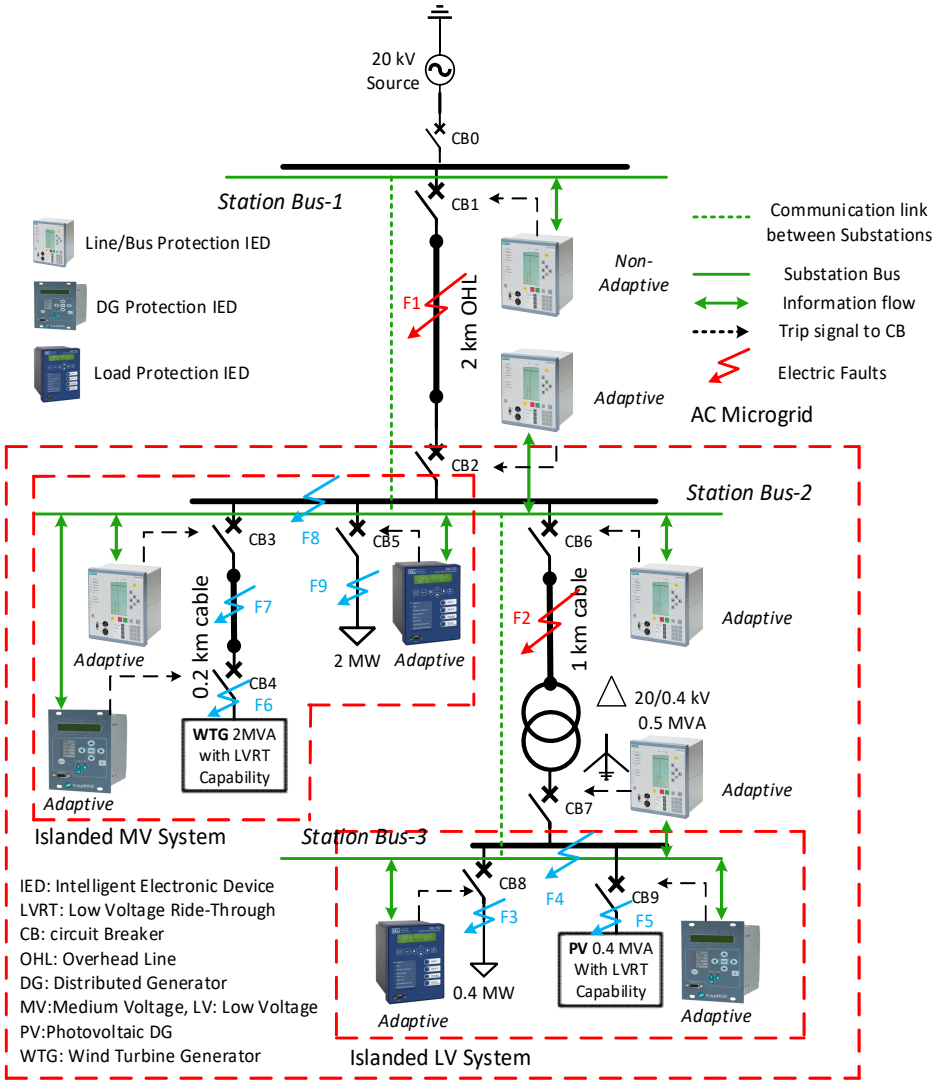

Figure 2. The radial MV/LV AC microgrid model for adaptive protection study.

The adaptive IEDs with two preplanned setting groups for AC microgrid lines are provided with only under-voltage (UV) local backup protection (Figure 3a) and adaptive IEDs with two preplanned setting groups for loads with both under and over-voltage (UV/OV) backup protection (Figure 3b). The DG protection IEDs (IED4 and IED9) are also considered to be adaptive in order to differentiate between the grid-connected and islanded mode operations. Moreover, DG protection IEDs should not trip instantaneously in the case of all external faults and allow DGs to provide fault current

contributions according to predefined standard LVRT characteristics. A multifunctional adaptive IED for the protection of converter-based DGs is shown in Figure 4, which consists of adaptive OC and anti-islanding protection functions. In practice, DGs may be provided with unit protection and IEDs with several fault protection and anti-islanding protection functions. In this study, the anti-islanding protection functions (passive/active methods) of DG protection IEDs are assumed normally "disabled" if the communication link is continuous and enabled quickly when the communication link is lost. Thus, communication-based loss-of-mains detection with no nondetection zone can be used as a primary means of anti-islanding protection and passive/active methods as backup in the case of communication link failure. All the sensitive protections within the islanded AC microgrid need to be disabled/interlocked during the starting of DGs, motor loads and during the transient period when changing from the grid-connected to islanded mode and vice versa.

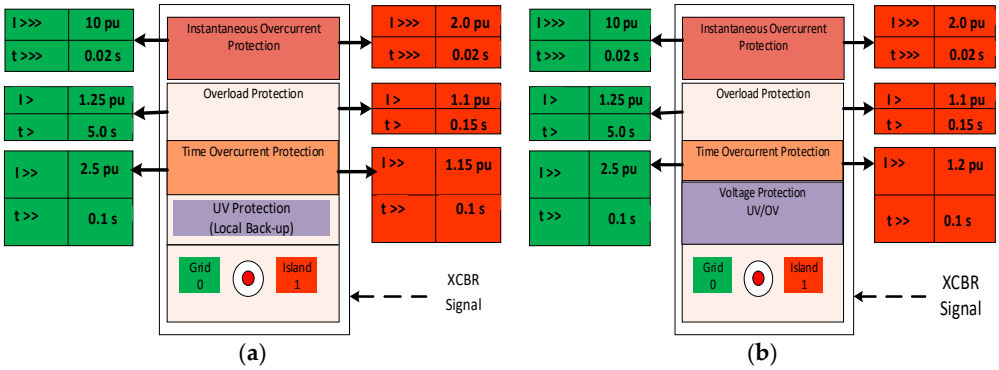

Figure 3. Adaptive definite time overcurrent (DTOC) relays with two preplanned setting groups: (**a**) for lines with local undervoltage (UV) backup protection and (**b**) for loads with local voltage protection (UV/over-voltage (OV)).

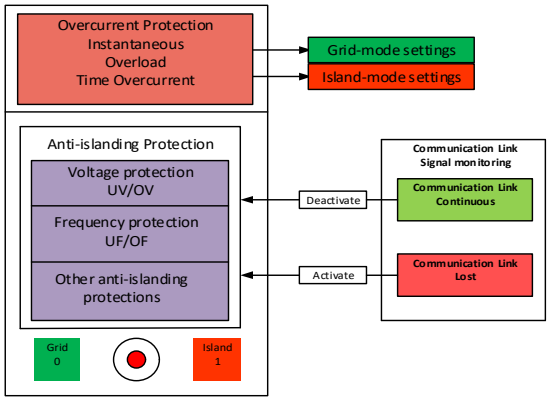

Figure 4. A multifunctional adaptive intelligent electronic device (IED) for the protection of converter-based distributed generators (DGs).

4. Adaptive Protection Methods and Results

Although several faults may happen in the presented AC microgrid, only adaptive protection methods and results of three-phase ungrounded short circuit faults with 0.01-Ohm fault resistance at locations F1 and F2 are presented. Moreover, for the sake of simplicity, it is assumed that three-phase fault F2 occurs only in the islanded mode. Nevertheless, the adaptive protection method for fault F2 also considers the protection option in the case of F2 in the grid-connected mode, as explained in the following text. Figure 5 shows the flowchart of communication-based nonadaptive IED1 for protection

during fault F1. IED1 provides primary protection for fault F1 and the backup protection with definite time delay for all other downstream faults using OC relay and UV protection works as backup of the OC relay. The IED1 normally uses the redundant communication link to get information about downstream faults and use this information for trip decisions. If the fault is downstream, it waits for the CB2 to trip first. On receiving a CB2 failure signal, it trips CB1 and sends a CB1 status "open" GOOSE message (XCBR signal) to all IEDs to change their settings to the islanded mode. Even if CB1 fails, it can transfer the trip incoming breaker CB0 of substation-1 to initiate the islanding. If no communication link is available, IED1 will simply trip CB1 using definite time delays depending on the magnitude of the current. Figure 6 shows the steps for the clearance of fault F1 using GOOSE messages with different transmission delays. In both cases, at step 7, IED2 can be used in an adaptive manner for tripping CB2 to clear F1 completely, if not directly tripped by the CB1 status transfer trip, as mentioned in step 7 of Figure 6. If CB2 is not tripped with the CB1 status transfer trip or the adaptive trip by IED2, then fault F1 will not clear due to fault energization by DGs in the AC microgrid, and DGs will trip after LVRT time is elapsed.

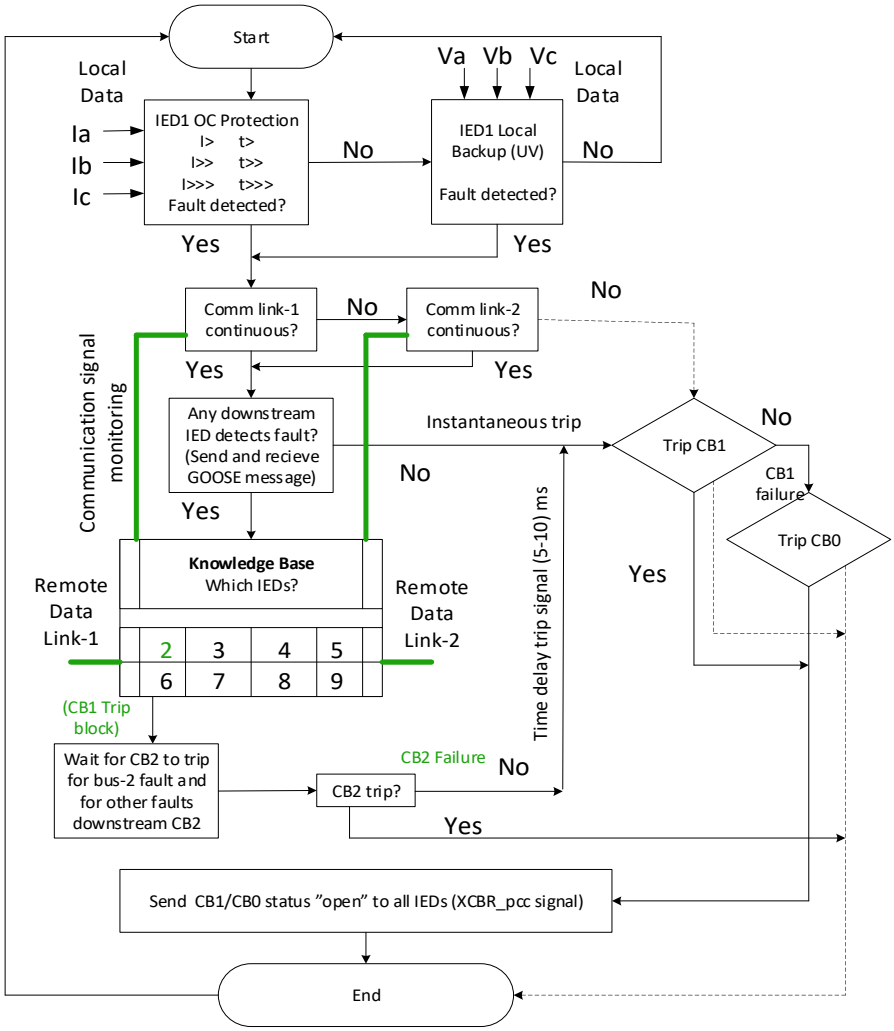

Figure 5. Flowchart for communication-based nonadaptive IED1 providing primary protection for fault F1 and remote backup for all downstream faults in the grid-connected mode. UV: Undervoltage protection.

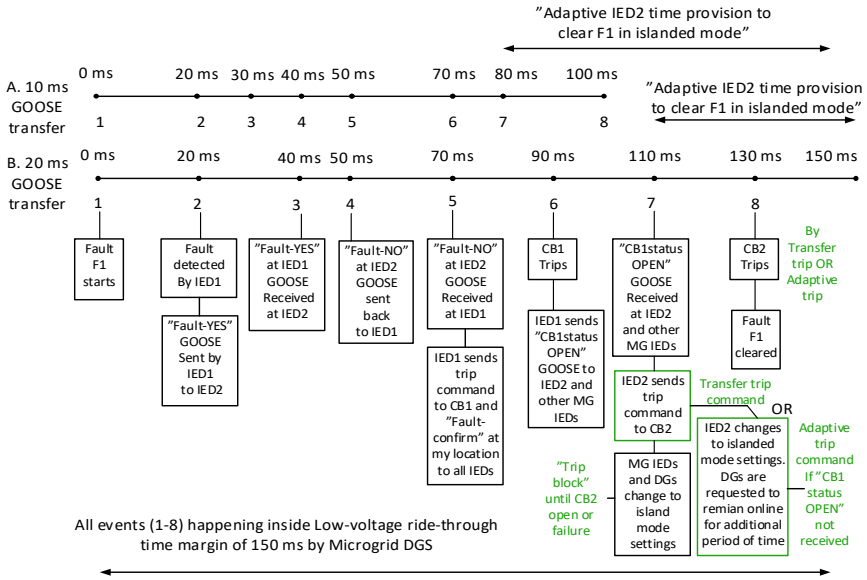

Figure 6. Fault F1 clearance time with 10-ms and 20-ms GOOSE message transfer delays (CB2 can trip by transfer trip GOOSE from IED1 or by adaptive IED2 using islanded mode settings).

Figure 7 shows the flowchart for the clearance of fault F2 in both grid-connected and islanded modes by adaptive IED6 by tripping CB6 and sending trip signal XCBR "open" to IED7 for tripping CB7. With CB6 and CB7 open, two separate islands were created within the islanded AC microgrid, one supplied by only PV (LV microgrid) and other supplied by only WTG (MV microgrid). If fault F2 occurs in the grid-connected mode, then only the LV microgrid will be isolated, and the MV microgrid will operate in the grid-connected mode. IED7 will also need the current flow direction in the case of fault F2, since this fault will be energized by both PV and WTG in islanded mode, which will avoid nuisance tripping by IED6 in the case of bus-3 fault or fault F3 at the LV load. IED7 can easily know if the fault is upstream or downstream of its location after receiving "YES fault GOOSE" from IED6 by simply calculating the RMS magnitude of the current at its location. If the magnitude of current at IED7 is ≤1.2 p.u. of the normal set current, the fault is considered to be upstream of IED7, since the fault contribution at IED7 will come from downstream PV only. In this case, IED7 will send "NO fault GOOSE" to IED6. If the magnitude of the current at IED7 is >1.2 p.u. of the normal set current, the fault is considered to be downstream of IED7. In this case, IED7 will send "YES fault GOOSE" to IED6, and IED6 will wait until the next GOOSE from IED7. The red and green colors in Figure 7 differentiate between the grid-connected and islanded mode features. On the failure of CB6, IED6 will trip CB2, CB3 and CB7 to clear F2 in the grid connected mode, whereas CB7 and CB3 will be tripped in the islanded mode to clear fault F2 completely. Hence, CB6 failure during fault F2 in both grid-connected and islanded modes will cause complete power interruptions to MV microgrid loads. Figure 8 shows the steps for the clearance of fault F2 using GOOSE messages with different transmission delays. It should be noted that, in steps 5 and 6 and 7 and 8 of Figures 6 and 8, the time delay for circuit breaker operation is considered 20 ms, which is one cycle of 50-Hz supply. This means high-speed AC circuit breakers operating in one cycle [43] will be required for the implementation of the proposed adaptive OC protection scheme.

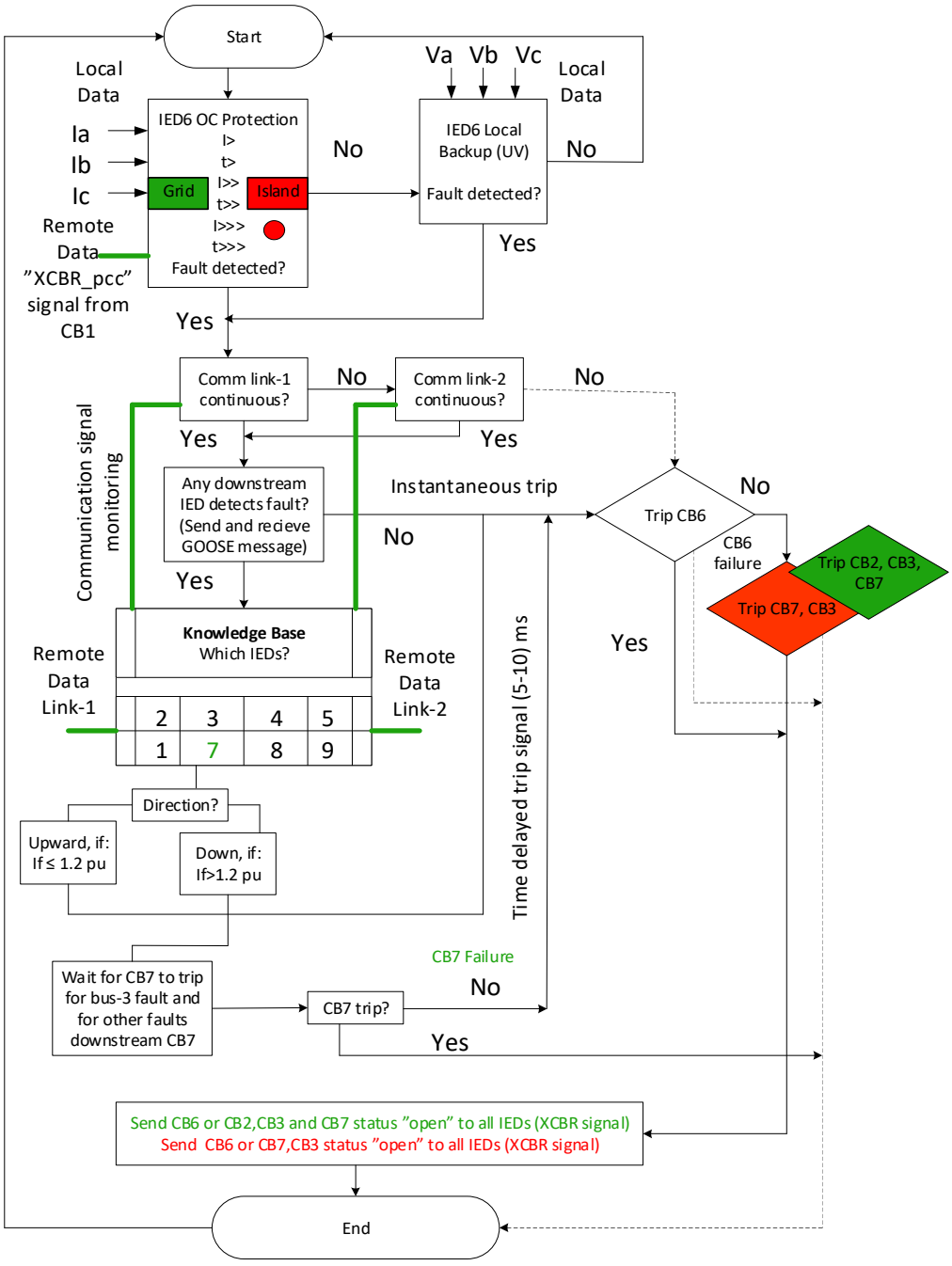

Figure 7. Flowchart for communication-based adaptive IED6 providing primary protection for fault F2 and remote backup for all downstream faults in both grid-connected and islanded modes.

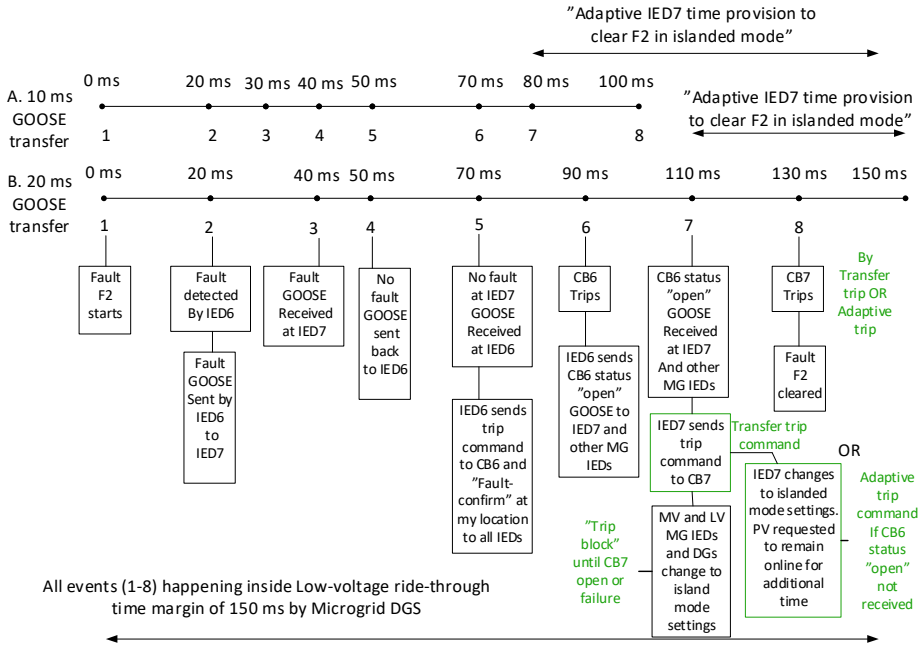

Figure 8. Fault F2 clearance time with 10-ms and 20-ms GOOSE message transfer delays (CB7 can trip by transfer trip GOOSE from IED6 or by adaptive IED7 using islanded mode settings).

Table 2 shows the normal flow of currents measured at the IED1, IED2, IED6 and IED7 locations during four different DG scenarios in the grid-connected mode. The maximum currents used for the adaptive DTOC settings are also indicated in Table 2. The fault current magnitudes at the concerned IEDs during the short-circuit fault F1 in the grid-connected mode and the short-circuit fault F2 in the islanded mode are shown in Table 3. Table 4 shows the DTOC settings and time grading of the IEDs 1, 2, 6 and 7 in the grid-connected and islanded modes. In this study, only the high-stage setting group (I>>) of Table 4 was used for the detection of the three-phase short circuit faults, and the isolation of the fault (tripping) is totally dependent on the GOOSE message transfer, according to Figures 6 and 8. However, in the case of complete communication failure, the time grading of Table 4 ensures selective operation. Table 5 explains the adaptivity and current magnitude comparison (CMC) requirements at IEDs of Figure 2 for three-phase faults (F1–F9) at different locations in different modes of operation. In the grid-connected mode, the higher setting group like that given in column two of Table 4 will be applied for all IEDs irrespective of the connection and disconnection status of DGs. This higher setting group is denoted by SG_{GM} in Table 5 to represent the active settings in the grid-connected mode. For all IEDs except IED1, IED5 and IED8, a separate local current magnitude comparison function/logic is proposed for the operation in both the grid-connected and islanded modes when DGs are actively participating in load sharing with the connection status "YES". The CMC function in the IEDs will logically work in parallel with the communication-based DTOC protection and would act quickly with the "transfer trip communication failure" signal to trip the local downstream IED during the upstream fault if it does not receive the transfer trip signal (CB status "OPEN") from the upstream IED after a predefined time period (time period between step 6 and 7 in Figure 6). The CMC function will continuously receive the analog value of the current from the local MU and compare it with the current threshold of 1.2 p.u. of the max current; if the current is less than the threshold and the upstream IED also sends a fault detection GOOSE "YES", the fault is assumed to be the upstream fault. Then, if no transfer trip GOOSE is received from the upstream IED within 110 ms of the fault (event 7 in Figure 6), the IED will trip the local circuit breaker to clear the fault completely. In this way, the CMC function implemented in the communication-based adaptive protection (Figure 7) could not only detect the direction of the fault,

but it could also act as a backup for direct transfer trip (DTT) communication failure. The proposed CMC function can only work for the feeder with a strong DG source on one side and a comparatively weaker DG source with a predefined fault current contribution on the other side. For example, during the fault F1 in the grid-connected mode when the connection status of both the WTG and PV is "YES", the IED2-IED4, IED6-IED7 and IED9 all will need the CMC function to determine if the fault is at the downstream or the upstream location. However, only IED2 will activate the CMC trip function after the transfer trip GOOSE message from IED1 is found undetected (not received). In the same way, during the fault F2 in the islanded mode of operation when the connection status of both the WTG and PV is "YES", the IED6-IED7 and IED9 need the CMC function to know if the fault is upstream or downstream of these relays. IED6 using the CMC function will detect the fault F2 to be downstream, while IED7 and IED9 will detect the fault to be upstream of their locations. Then, when the transfer trip GOOSE from IED6 is not received by the IED7, it will initiate the backup using CMC logic to trip CB7 in order to clear the fault F2 completely, while IED9 will continue following the LVRT curve. The topmost AND logic in Figure 9a,b presents the backup for DTT failure from IED6 during the fault F2 using the CMC function/logic. It should be noted that, in the islanded mode, when the connection status of both the WTG and PV is "YES"(the scenario of Table 5, column 3), then the WTG of 2 MW acts as a comparatively stronger source than the PV of 0.4 MW. Therefore, the grid-connected mode settings "SG_{GM}" for IED6-IED9 will remain effective and unchanged in this islanded mode scenario, and only IED3-IED5 need to change to the islanded mode settings (SG_{IM}). This way, the minimum number of IEDs will need to adapt to the islanded mode settings, and simple logics for the primary and backup protections, for example, at IED7 (Figure 9a), could be used. This will also prevent the OC function of IED7 and IED9 to start pickup for the "out of zone" fault F2 in the islanded mode scenario of Table 5, column 3.

Table 2. Normal RMS (Root mean square) currents at considered intelligent electronic device (IED) locations with four different distributed generator (DG) scenarios in grid-connected mode. WTG: wind turbine generators and PV: photovoltaic.

IED No.	Current (A) Only Grid Scenario-1	Current (A) WTG + Grid Scenario-2	Current (A) PV + Grid Scenario-3	Current (A) WTG + PV + Grid Scenario-4
IED1	69.1 [1]	12.476	58.39	1.098
IED2	69 [1]	12.43	58.34	1.05
IED6	11.571	11.572 [1]	2.873	2.876
IED7	573.8	575 [1]	182.81	182.84

[1] The maximum currents used for adaptive overcurrent (OC) settings.

Table 3. Fault currents (RMS) at considered IED locations with DG scenario-4 (F1 in grid-connected mode and F2 in islanded mode).

IED No.	Current (A) during Fault F1 in Grid-Connected Mode	Current (A) during Fault F2 in Islanded Mode
IED1	28,000	-
IED2	67 [2]–82.8 [3]	-
IED6	-	70
IED7	-	700

[2] Before CB1 tripping (grid-connected mode). [3] After CB1 tripping (used for IED2 adaptive tripping).

Table 4. Settings of overcurrent IEDs for grid-connected and islanded modes as per DG scenarios 1–4 in Table 2 considering the max normal magnitude of current through IEDs in these scenarios.

IED No.	DTOC Relay Settings for Grid-Connected Mode (SG_{GM})	DTOC Relay Settings for Islanded Mode (SG_{IM})
IED1	I>> 2.5 × 69.1 = 172.75 [4] A t>> 0.8 [6] s	-
IED2	I>> 2.5 × 69 = 172.5 [4] A t>> 0.6 [6] s	I>> 1.15 × 69 = 79.35 [5] A t>> 0.6 [6] s
IED6	I>> 2.5 × 11.572 = 28.93 [4] A t>> 0.4 [6] s	I>> 1.15 × 11.572 = 13.31 [5] A t>> 0.4 [6] s
IED7	I>> 2.5 × 575 = 1437.5 [4] A t>> 0.2 [6] s	I>> 1.15 × 575 = 661 [5] A t>> 0.2 [6] s

[4] Definite time overcurrent (DTOC) setting group for the grid-connected mode (SG_{GM}). [5] DTOC setting group for the islanded mode (SG_{IM}). [6] Conventional time-coordination only used in the case of communication failure.

Table 5. The adaptivity of SG_{GM} or SG_{IM} settings and CMC [8] requirements at various IEDs (Figure 2) during different faults in grid-connected and islanded mode scenarios with predefined fixed fault current contributions from DGs.

IED No.	Grid-Connected Mode (WTG + PV)-Yes	Islanded Mode (WTG + PV)-Yes	Islanded Mode WTG-No, PV-Yes PV-Export Mode	Islanded Mode WTG-No, PV-Yes PV Island
IED1	SG_{GM} (F1–F9) [8]	-	-	-
IED2	SG_{GM} + CMC [7] (F1)	-	-	-
IED3	SG_{GM} + CMC (F1, F8 and F9)	SG_{IM} + CMC (F8 and F9)	-	-
IED4	SG_{GM} + CMC (F1, F7–F9)	SG_{IM} + CMC (F7–F9)	-	-
IED5	SG_{GM} (F1–F9)	SG_{IM}	SG_{IM}	-
IED6	SG_{GM} + CMC (F1, F8 and F9)	SG_{GM} + CMC (F2, F8 and F9)	SG_{IM}	-
IED7	SG_{GM} + CMC (F1–F2, F7–F9)	SG_{GM} + CMC (F2, F7–F9)	SG_{IM}	-
IED8	SG_{GM} (F1–F9)	SG_{GM}	SG_{IM}	SG_{IM}
IED9	SG_{GM} + CMC (F1–F4, F8 and F9)	SG_{GM} + CMC (F2 and F3, F8 and F9)	SG_{IM}	SG_{IM}

[7] Current magnitude comparison: $I_{IED} \leq 1.2$ p.u. of max possible normal current at a location, then fault is upstream; $I_{IED} > 1.2$ p.u. of max possible normal current at a location, then fault is downstream. [8] Fault locations (F1 to F9) for which the CMC feature is required at the corresponding IED. Note: Table 5 considers the minimum required settings of the main (primary) protection for the detection of the faults, and the final successful islanded scenarios are considered.

If, during the islanded mode (Table 5, column 3 mode), the settings of IED6, IED7 and IED9 are changed to the islanded mode settings (SG_{IM}), then OC function of all the three IEDs will start picking up not only during the downward fault F5 but, also, during the upward faults F4 and F2. Hence, the protection logic for the detection of the "in-zone" fault direction and location will become more complex with the islanded mode settings (Figure 9b) compared with the protection logic with the grid-connected mode settings (Figure 9a). The bottom AND logic of Figure 9a represents the protection logic of IED7 with the grid-connected mode settings (SG_{GM}) for "in-zone" fault F4, where only "NO fault" detection signals at downward IED8 and IED9 are sufficient to activate the primary and time-delayed backup protection at IED7, in addition to the local IED7 and upward IED6 "fault YES" signals and the CMC function outputs for "downward" fault. The bottom AND logic (black) of Figure 9b represents the protection logic of IED7 with the islanded mode settings (SG_{IM}) for the "in-zone" fault F4, where not only "NO fault" detection at downward IED8 and IED9 are required, but also, the CMC function output at IED9 for "upward" and "downward" faults will also be required to activate the primary and time-delayed backup protection at IED7, respectively, in addition to the local IED7 and upward IED6 "fault YES" signals and the CMC function outputs for the "downward" fault. The protection logics presented in Figure 9 will be necessary in order to quickly detect the fault and isolate the faulty section within 150 ms, keeping the stability of the remaining system intact if the communication system performance is according to the predefined boundaries. In the case of communication failure, the normal communicationless time coordination described in Table 4 will be applied.

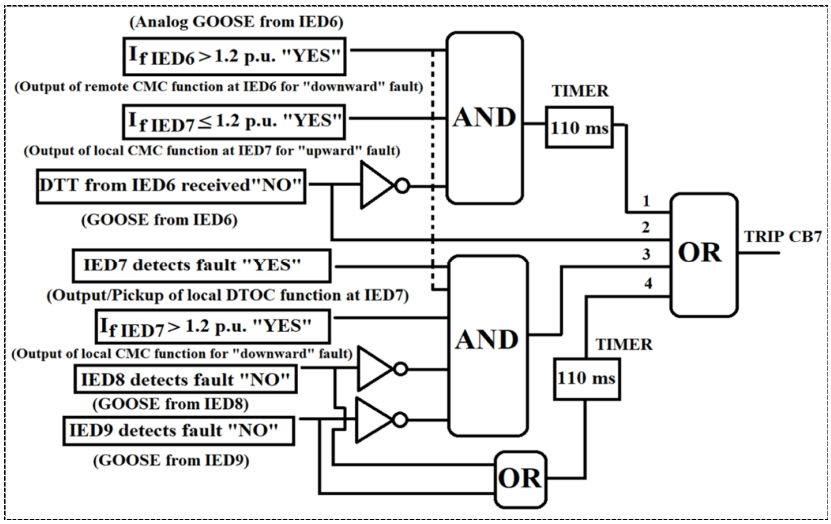

(**a**)

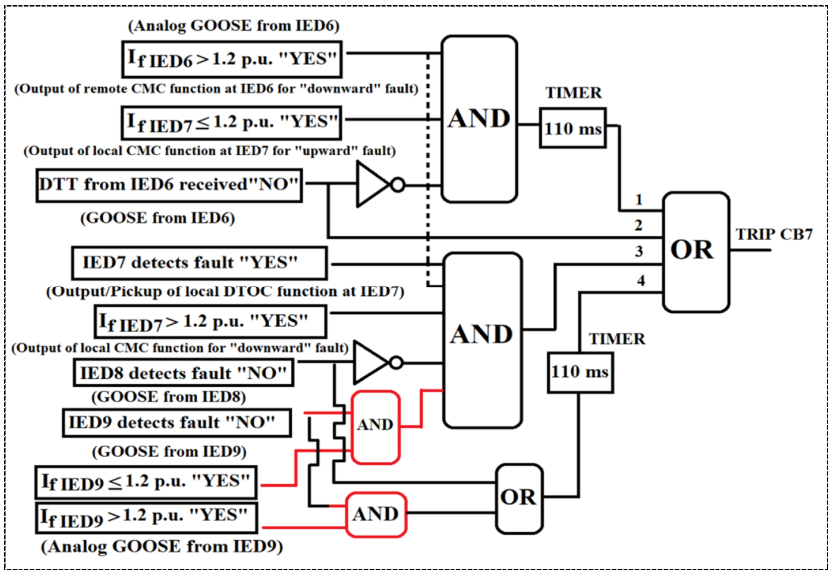

(**b**)

Figure 9. The application of the current magnitude comparison (CMC) function as GOOSE logic at communication-based IED7 to provide backup for the delayed/missing direct transfer trip (DTT) from the IED6 at a remote station bus when: (**a**) SG $_{GM}$ settings are used and (**b**) SG $_{IM}$ settings are used. (1) Backup for DTT from IED6, (2) normal DTT, (3) in-zone primary OC protection of IED7 and (4) time-delayed backup OC protection for IED8 and IED9.

4.1. Results for Fault F1 in Grid-Connected Mode and Transition to Islanded Mode

For three-phase fault F1, the adaptive OC relay logics are implemented in PSCAD (Power Systems Computer Aided Design) simulation software according to Figure 6 and settings according to Figure 3 and Table 4. The fault starts at 1.2 s and ends at 5 s; this fault duration is small, but it is assumed to be a permanent fault. The fault current magnitude at IED1 and IED2 before and after the fault F1 is shown in Figure 10. It shows that fault current magnitude is enough at IED1 location and can be detected easily with higher OC settings (SG $_{GM}$). However, the fault current magnitude at IED2 is not enough

to detect the fault with its higher settings, since at IED2, the fault contribution mainly comes from DGs, which are set to provide a fault current up to 1.2 p.u. of rated DG current. Hence, to remove fault F1 completely, either CB2 should be remotely direct transfer-tripped by IED1 using "CB1statusOpen" signal communication or IED2 should adapt to lower settings (SG_{IM}) and issue an "adaptive trip" command to CB2 if "CB1statusOpen" is not received at IED2 within the predefined delay. Figure 11 shows the tripping of CB1 at about 1.29 s with a delay of 90 ms after the fault at 1.2 s and CB2 tripping at 1.334 s with a delay of about 134 ms after the fault at 1.2 s, as per method-B steps 6-8 in Figure 6; in this case, CB2 is successfully transfer-tripped. Figure 12 shows the RMS magnitude of the current of DGs before, during and after the fault F1 with the successful CB2 transfer trip method. Figure 13 shows the detection of fault F1 by lower settings of adaptive IED2 in islanded mode (CB1 already open, and transfer trip from IED1 to IED2 failed) and subsequent tripping of CB2 to clear F1 completely. The CB1 is tripped at 1.29 s according to method-B step 6 in Figure 6, and IED1 sends the circuit breaker status "Open" to all IEDs within next 20 ms. The DGs and IEDs except IED2 within the islanded AC microgrid receive the circuit breaker status "Open" from IED1 and change their mode/settings at 1.31 s; all IEDs (except IED2) remain in a "trip block" state until a "CB2 open" or "CB2 breaker failure" signal from IED2 is received. Meanwhile, an adaptive IED2 changes to lower settings due to transfer trip failure; it detects the fault, sends an "adaptive trip" command to CB2 at 1.345 s and CB2 finally trips at 1.37s. On receiving the "CB2 open" signal, all IEDs within the AC microgrid may issue "block release" to their CBs after the terminal voltage of DGs will reach a value >50% of its normal value. This will ensure no IED tripping during transition to the normal islanded mode, because DGs will continue LVRT and fault contribution until 50% terminal voltage is reached after the fault clearance recovery.

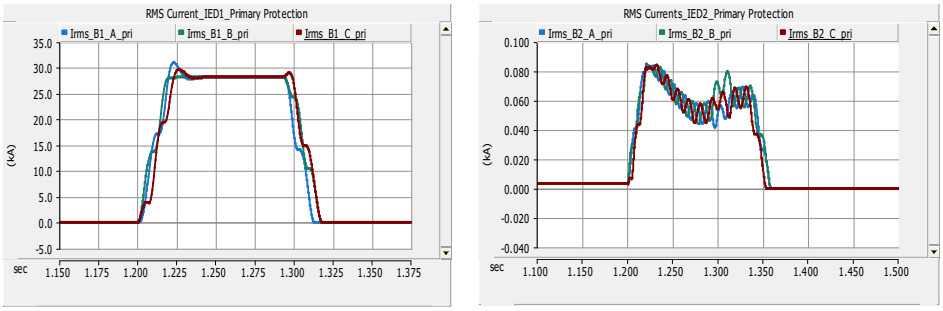

(**a**) (**b**)

Figure 10. RMS magnitude of the current before, during and after fault F1 at: (**a**) IED1 and (**b**) IED2 (CB2 transfer trip).

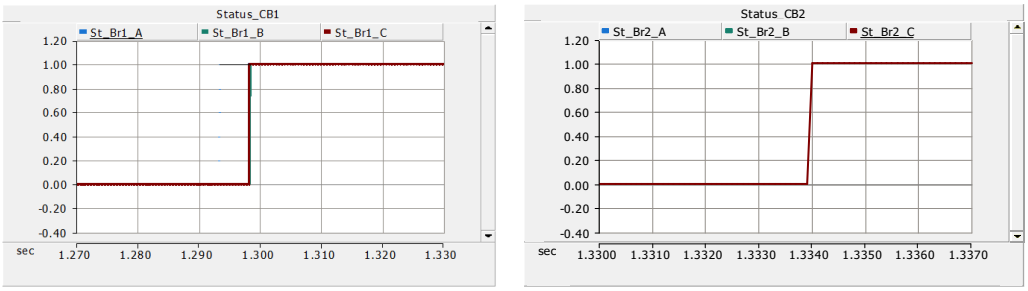

(**a**) (**b**)

Figure 11. Operating time and status of breakers before, during and after the clearance of fault F1: (**a**) CB1 (main protection trip) and (**b**) CB2 (direct transfer trip). CB Status: 0 = False (NO trip/Close) and 1 = True (YES trip/Open).

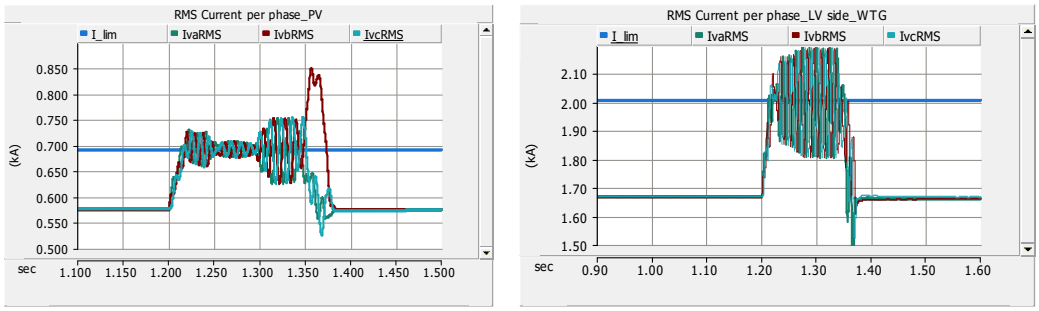

(**a**) (**b**)

Figure 12. RMS magnitude of current per phase of DGs before, during and after fault F1 (CB2 transfer trip): (**a**) LV side of the PV system and (**b**) LV side of WTG. Note: I_lim is the preset limit of the fault current contribution of DGs.

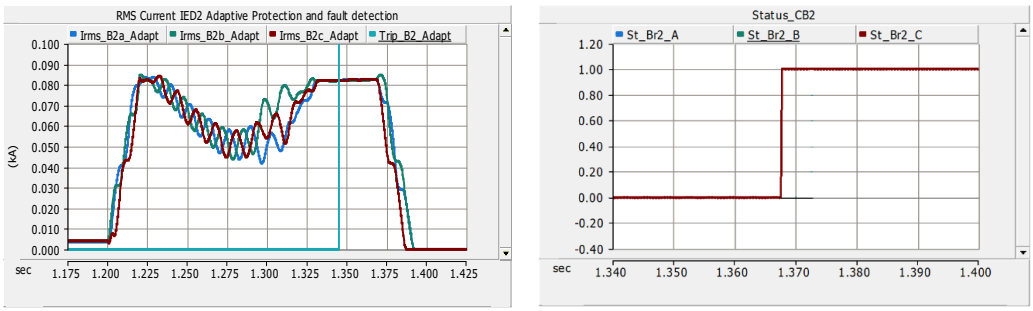

(**a**) (**b**)

Figure 13. Adaptive IED2 trip after the unsuccessful direct transfer trip from IED1: (**a**) RMS magnitude of the current at adaptive IED2 and relay operating time and (**b**) CB2 status and operating time during an IED2 adaptive trip.

Figure 14 shows the RMS magnitude of the current of DGs before, during and after the fault F1 with an adaptive IED2 trip. The results in Figure 13 show that it takes 20 ms more than the required 150 ms time for clearance of the fault with adaptive IED2 settings. This is because the DG output current takes an extra 10 ms to stabilize and reach the threshold setting of adaptive IED2. Moreover, both IED2 and CB2 take 5 ms more than the set time of 20 ms for fault detection and tripping. Figure 13 also shows that it will take 15 ms extra for DGs to restore to normal operations (normal currents) in the islanded AC microgrid after the removal of fault F2 completely at 1.37 s. These types of extra delays highlight the demand of faster communication with less than 20 ms one-way transfer delay or extension of the initial time after the fault inception in the LVRT characteristic curve for effective adaptive protection in order to maintain the supply in islanded mode. Otherwise, it will cause the complete loss of DGs within the AC microgrid during fault F1 due to the tripping by anti-islanding (e.g., UV) protection at 150 ms after the fault. This, of course, will decrease the reliability of supply for AC microgrid loads due to extra time for the black start of DGs in the islanded mode, then removal of fault F1 by adaptive IED2 and, finally, the restoration of the normal load. In the presented cases by using a 20-ms delay of one-way GOOSE transfer for the complete removal of fault F1, the transfer trip method is faster than using adaptive IED2 tripping in the islanded mode: a direct transfer trip takes about 150 ms after the fault, and the second backup procedure (adaptive tripping) takes about 190 ms after the fault. However, if the delay of 10 ms for one-way GOOSE transfer is used (Method-A in Figure 6), then even the backup adaptive tripping after the failure of the direct transfer trip could be accomplished within 150 ms after the fault, and the present LVRT curve of the DGs will remain valid.

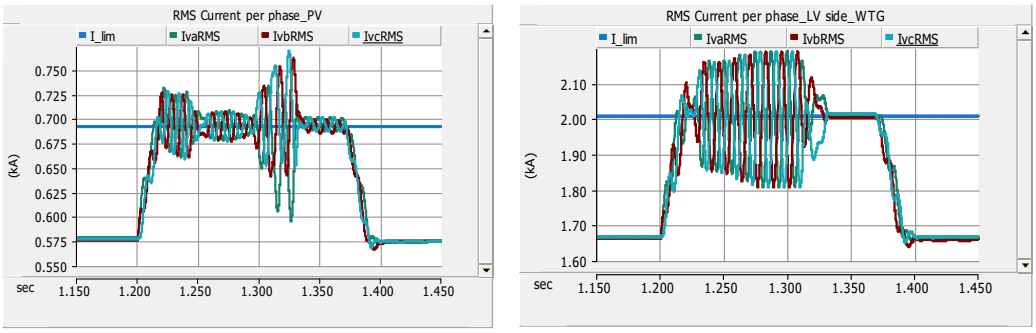

(**a**) (**b**)

Figure 14. RMS magnitude of the current per phase of DGs before, during and after fault F1 (adaptive IED2 trip): (**a**) LV side of the PV system and (**b**) LV side of the WTG. Note: At 1.29–1.3 s, CB1 trips (Figure 10a), and at 1.37 s, CB2 adaptively trips (Figure 12b).

Control of DGs

Both DGs (WTG and PV) are operated in fixed P-Q (active power-reactive power) control near the unity power factor operation; their active and reactive power supply before, during and after the fault F1 are shown in Figure 15. In grid-connected mode, the current-controlled voltage source converters (VSCs) of both the WTG and the PV models operate in the grid-imposed frequency mode (the grid-following mode) using the PLL (phase locked loop). However, after receiving the CB1 "open" signal, the current-controlled VSCs of both DGs use the reference voltage angle from the free-running VCO (voltage controlled oscillator) and operate in the controlled-frequency mode (the grid-forming mode), since the PLL loses its synchronism after the loss of grid voltage. The variation of the LV side currents of DGs observed during the fault F1 in the grid-connected mode before the tripping of CB1 and before the activation of VCO (Figures 12 and 14) are due to PLL errors in the simulation model during the fault, but this does not cause errors in the OC function operations. Some additional resistances (0.39 ohm per phase) are connected in the series with the output terminal inductors of the PV system to maintain a terminal voltage constant in islanded mode. These types of grid-following and grid-forming VSC controls are explained in more detail in [44]. Previously, the conventional f/P (frequency/active power) and V/Q (voltage/reactive power) droop is applied to at least one grid-side converter of a WTG from the group of WTGs connected to the same bus to act as the voltage and frequency control sources in the islanded mode. The converters of the remaining WTGs follow the controlled system frequency. In this way, the response of the islanded system due to the sudden large changes of the load is kept smoother compared with the controls where the voltage and frequency droops are applied to converters of all WTGs [45,46]. The results in Figures 16 and 17 indicate how the AC microgrid is smoothly transitioned to the islanded mode with the applied controls of DGs after the fault F1 is cleared. Figure 16 indicates the variation of frequency during the clearance of fault F1; therefore, the frequency immunity of DGs is also required in addition to the standard LVRT characteristics.

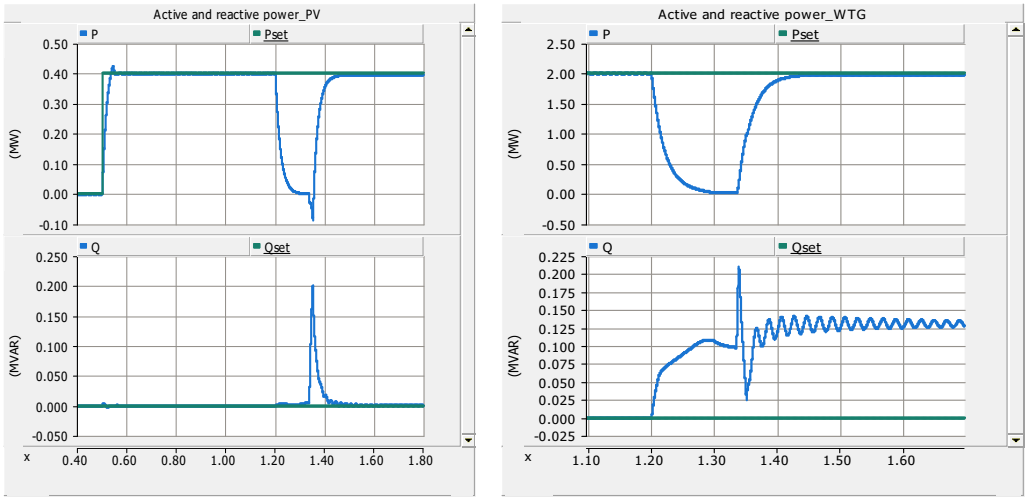

(**a**) (**b**)

Figure 15. T Active power (P) and reactive power (Q) supply from DGs before, during and after fault F1: (**a**) P and Q from the PV system and (**b**) P and Q from the WTG. Note: WTG supplies the entire Q demand in islanded mode.

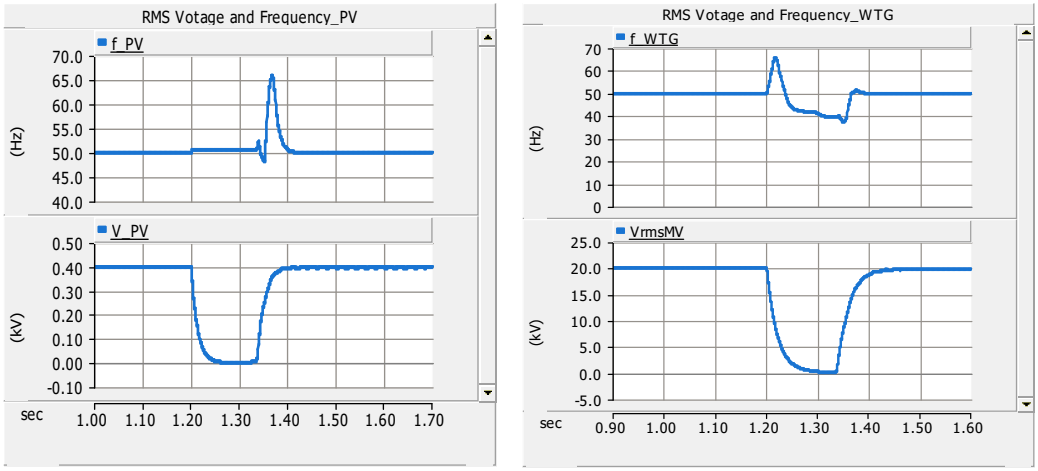

(**a**) (**b**)

Figure 16. Three-phase RMS voltage and frequency of DGs before, during and after fault F1 (**a**) low-voltage (LV) side of the PV system and (**b**) medium voltage (MV) side of the WTG.

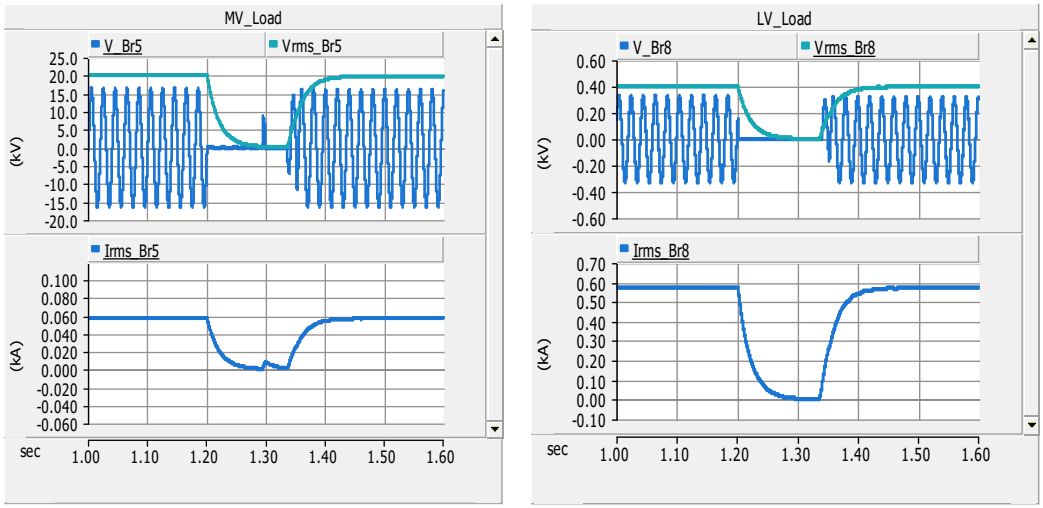

(**a**) (**b**)

Figure 17. Three-phase RMS voltage and current and single-phase instantaneous voltage at loads before, during and after fault F1: (**a**) MV load and (**b**) LV load.

4.2. Results for Fault F2 in Islanded Mode and the Creation of Two Islands within the Islanded AC Microgrid

For three-phase fault F2 in the islanded mode (CB1 and CB2 open in Figure 2), the adaptive OC relay logics are implemented in PSCAD according to Figure 8 and settings according to Figure 3 and Table 4. The fault starts at 1.2 s and ends at 5 s; this fault duration is small, but it is assumed to be a permanent fault. The fault current magnitude at IED6 and IED7 before, during and after fault F2 in the islanded mode is shown in Figure 18. It shows that the fault current magnitude is enough at the IED6 location, which is supplied by the WTG that is set to supply 1.2 p.u. of its rated current during the fault. The fault current at IED6, which is supplied by the WTG, is considerably higher than the maximum current at IED6 during any DG scenario, and therefore, the fault can be detected easily even with the grid-connected mode higher OC settings (SG_{GM}) of IED6 (Table 4). Hence, IED6 can be a nonadaptive IED for this fault case. The fault current magnitude is limited at the IED7 location during F2, which is supplied only by the PV system; therefore, the fault F2 can only be detected by IED7 with islanded mode lower settings (SG_{IM}). The IED7 should be necessarily adaptive in order to work even when the transfer trip from IED6 fails. Since the AC microgrid in this case is islanded, the settings of IED7 are already changed to islanded mode settings; hence, both IED6 and IED7 can detect the fault and trip simultaneously to remove the fault F2 after checking the magnitude of the current at downstream IED8. Alternatively, the trip block signal can be issued to IED7 from IED6, and IED7 can later be transfer-tripped after the opening of CB6. The results shown in this section are based on IED6 with one setting group (SG_{GM}) that can detect the fault F2 in both the grid-connected and islanded modes. Although IED7 is adaptive, it has been transfer-tripped by IED6 in these results (Figure 19), according to method-B (20-ms GOOSE transfer) of Figure 8. Figure 20 shows the RMS currents of DGs before, during and after the fault F2 in islanded mode with fault clearance using CB2 direct transfer trip. Figure 21 shows the active and reactive power supply from DGs before, during and after the fault F2. Additionally, it is shown in Figures 22 and 23 how smoothly two islands are formed within the islanded AC microgrid after the clearance of the fault F2 at 1.34 s. The results of adaptive IED7 tripping after transfer trip failure from IED6 during the fault F2 are not included to avoid repetition, in which case the adaptive IED7 may detect the fault with the lower settings (SG_{IM}) just like the adaptive IED2, as explained in Section 4.1. In that case, the adaptive IED7 will wait until the time of direct transfer trip is elapsed; this is considered as a transfer trip failure from IED6. The adaptive IED7 will then decide to trip CB7 with the lower settings for the complete clearance of the fault F2 during transfer trip failure.

It should also be noted that the WTG is comparatively stronger source than the PV system. Therefore, for faults F3, F4 or F5 in islanded AC microgrid (CB1 and CB2 open in Figure 2), the WTG may still provide sufficient fault current, and the higher current settings (SG $_{GM}$) for IED7, IED8 and IED9 may still work for any of the faults F3–F5 downstream of the WTG. For these faults (F3–F5), the current comparison method to find the location of the faults (upstream or downstream faults) will also be valid for the islanded mode with the WTG in operation. However, after the removal of the fault F2 (CB6 and CB7 open), two further islands will be created: the islanded MV system and the islanded LV system (Figure 2). The islanded MV system will be supplied by only the WTG, and the islanded LV system will be supplied by only the PV system. In this situation, only the adaptive lower settings (SG $_{IM}$) of IED8 and IED9 will work. For any islanded scenario, IED3, IED4 and IED5 will always require lower adaptive settings (SG $_{IM}$).

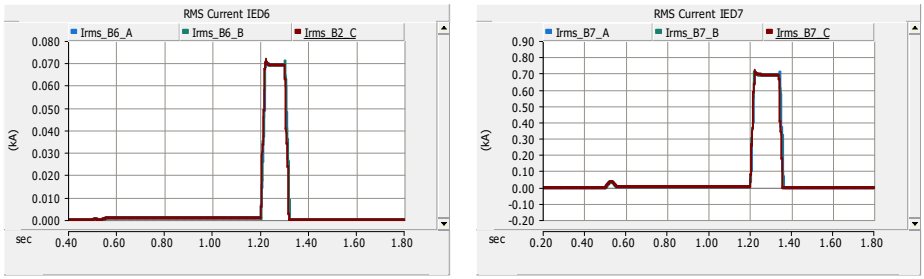

(**a**) (**b**)

Figure 18. RMS current magnitude before, during and after fault F2 in the islanded mode at: (**a**) IED6 and (**b**) IED7 (IED7 direct transfer trip).

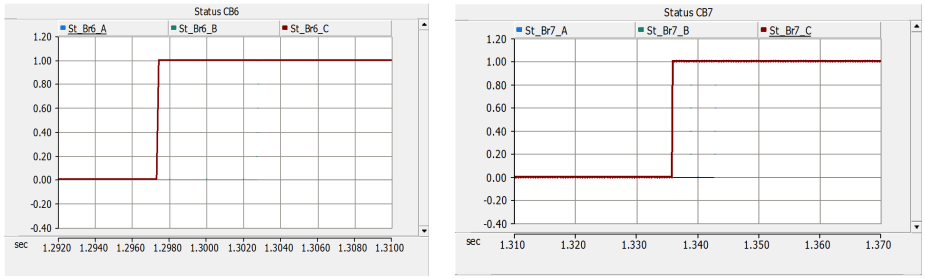

(**a**) (**b**)

Figure 19. The operating times and status of breakers before, during and after the clearance of fault F2 in the islanded mode: (**a**) CB6 (main protection trip) and (**b**) CB7 (direct transfer trip).

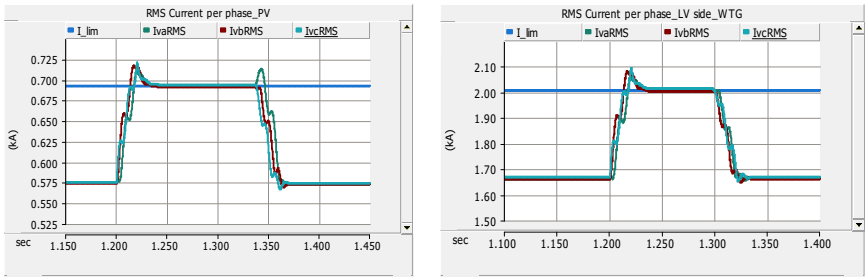

(**a**) (**b**)

Figure 20. RMS current magnitude per phase of DGs before, during and after fault F2 in the islanded mode (CB7 transfer trip): (**a**) LV side of the PV system and (**b**) LV side of the WTG.

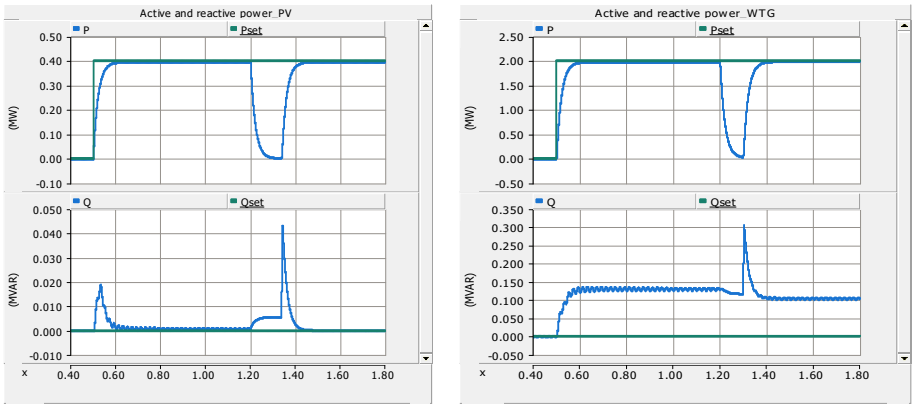

(**a**) (**b**)

Figure 21. Active (P) and reactive (Q) power supply from DGs before, during and after fault F2 in the islanded mode: (**a**) P and Q from the PV system and (**b**) P and Q from the WTG.

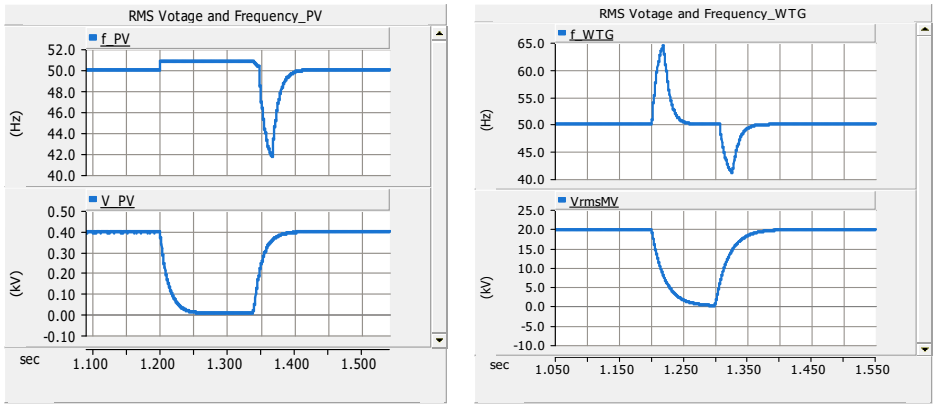

(**a**) (**b**)

Figure 22. Three-phase RMS voltage and the frequency of DGs before, during and after fault F2 in islanded mode at: (**a**) the LV side of the PV system and (**b**) MV side of the WTG.

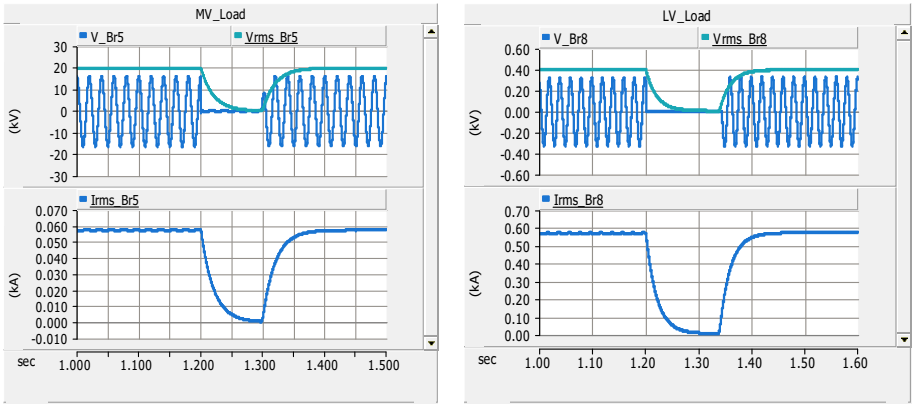

(**a**) (**b**)

Figure 23. Three-phase RMS voltage, current and single-phase instantaneous voltage at loads before, during and after the fault F2 in the islanded mode at: (**a**) the MV load and (**b**) LV load.

The LVRT Capability of DGs

The DGs are required to remain connected to the network during the voltage dips or faults, and depending on the requirements, the DGs may be requested to feed-in short-circuit fault currents up to the agreed value (or according to the limits of DGs) in order to support the detection of faults. This is called the low-voltage ride through (LVRT), under-voltage ride through (UVRT) or fault ride through (FRT) requirement. In the grid-connected mode, the LVRT capability of DGs is usually required to maintain the stability of the system, since the disconnection of many DGs even for a fraction of a second may result in large voltage or frequency fluctuations, causing the voltage or frequency instability of the entire system. The synchronous generators are more sensitive to voltage dips, and hence, their LVRT requirements are considerably less stringent in comparison with the nonsynchronous generators, including the converter-based generators, which can remain connected for the extended durations. In the islanded mode of operation, not only the system stability is important, but also, the quick detection and isolation of the fault is equally important. Additionally, the protection coordination or selectivity between the main and backup protection has to be ensured. Figure 24 shows the comparison of different LVRT requirements of nonsynchronous generators, including the converter-based generators, according to the previous German BDEW-2008 standard [32] and the latest European Standard EN 50549-1:2019 adopted as the Finnish National Standard SFS-EN 50549-1:2019 [47]. The DGs are required to remain connected in parallel with the LV or MV networks if the voltage at the connection point is above the voltage-time curves of Figure 24 (red and black curves). Although, the LVRT requirements are expectedly limited to the most stringent curves, however, the network operators may define their own LVRT characteristics. These standards do not define the LVRT requirements for the islanded mode of operation. Therefore, a new LVRT characteristic was proposed in this paper for the islanded mode operation of the nonsynchronous DGs, including the converter-based DGs shown as a green voltage-time curve in Figure 24. According to this new proposed LVRT characteristic, the DGs will remain connected to the islanded MV/LV microgrid for at least 2 s after the voltage dip or the fault and feed-in short-circuit current of at least 1.2 p.u. of the rated current. With the proposed LVRT characteristic, not only the stability of the islanded microgrid will be maintained, but also, a good protection coordination between adaptive IEDs will be ensured. The WTG and BESS (battery energy storage systems) with full-scale converters are capable of providing this requirement. Normally, in the presence of high-speed communication, the standard grid-connected LVRT curves will be used; however, in case of communication failure, the definite-time coordination of IEDs with the proposed LVRT curve will be applied.

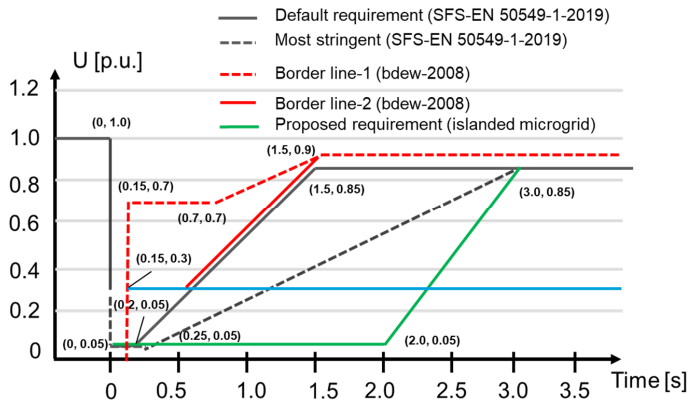

Figure 24. The low-voltage ride through (LVRT) capability of the nonsynchronous generators, including the converter-based generators: The red and blue voltage-time curves according to [32] and the black voltage-time curves according to [47]; the green voltage-time curve is the new proposed LVRT curve for the islanded mode of operation.

5. Discussion

An adaptive OC protection for the AC microgrid using the IEC 61850 communication standard and LVRT capability of DGs is presented in this paper. Previously, an adaptive OC protection was presented in [48]; the scheme updated the inverse-time OC relay curve by changing the pick-up current with respect to DG infeed, but the focus was mainly on medium impedance faults at the end of the radial distribution network detected by a single-substation relay. The similar type of adaptive OC protection was proposed in [49] for distribution networks with DGs using local data and two-setting groups for the inverse-time OC relay. However, the scheme does not use remote data by communication systems and is prone to nuisance and slow trips, resulting in DG loss. A directional adaptive inverse-time relay was presented more recently for HIL (Hardware-In-Loop) testing, and real-time simulations in [50,51]. In these papers, an FCL was used for limiting the wind turbine generator fault contribution, and its effects on relay settings were observed. This directional adaptive inverse-time relay using a multiagent system does not consider/mention the effects of communication delays on protection coordination. Moreover, it involves tedious calculations to generate various inverse time setting groups for changing the network configurations and those for all relays in the networks. Although, traditionally, inverse-time OC performs better than definite-time OC in terms of the minimum operation time close to the power source, but in the AC microgrid environment with many DG sources, this may not be completely true. The inverse-time OC relays are affected the most with the increased penetration level of DGs [4], and it is the usual practice to limit the fault contribution from DGs to overcome the adverse effects, as it was also done in [51]. An adaptive OC protection for distribution networks was proposed in [52] that calculated and applied the new settings of OC relays directly whenever any significant change in the network occurred. The algorithm presented did not use precalculated settings and was initiated either by the monitoring block in the coordination layer or energy management system during topology changes using the communication link. The scheme was verified using the real-time digital simulator (RTDS) and IEC 61850 GOOSE messaging. However, the adaptive OC scheme was implemented using a centralized approach; the type of DG unit was not specifically described, and higher coordination delays were used. Moreover, the proposed adaptive OC scheme also gave slower tripping times compared with the traditional OC relay in some cases. In this paper, the communication-based definite-time OC relays with only two predefined setting groups are suggested. These two setting groups can be changed adaptively and quickly by each IED autonomously after receiving the status of DGs (on/off), CB status change (open/close), fault current magnitude and fault detection GOOSE signal from other IEDs. Moreover, the simple method of calculating the magnitude of the current at their locations, comparing it with the predefined threshold 1.2 p.u. of the max current and sharing this information with other IEDs will be useful for quick detection of the fault location after knowing the status of each DG. The nuisance tripping can also be avoided with fault current magnitude sharing between IEDs and with the careful use of trip block/release signals. The proposed current magnitude comparison method also avoids the additional measurement of voltage for the detection of the fault current direction. However, a voltage magnitude measurement can be used as a local backup protection for OC function. The proposed scheme in this paper can also be extended to low impedance single-phase ground faults and other asymmetrical faults. The method proposed in this paper will be evaluated with a real-time digital simulator of OPAL-RT for hardware-in-the-loop (HIL) simulations using actual Ethernet-based GOOSE communication between IEC 61850-based IEDs from different vendors for its practical implementation, and this will be presented in a separate research article in the future.

6. Conclusions

The adaptive OC protection utilizing the LVRT characteristic of DGs and using circuit breaker status signals transmission by IEC 61850 communication standard were presented for the grid-connected and the islanded mode of the radial AC microgrid. Moreover, a new LVRT curve for the islanded mode of operation is proposed. The fixed delays for GOOSE message communication between IEDs are assumed

according to IEC 61850 and the practical values. According to the considered assumptions, the results look promising, as per the evaluation by PSCAD simulations. The general methodology presented in this paper for three-phase faults can also be extended to other types of faults. The effectiveness of the considered adaptive OC protection for single-phase and high impedance faults for AC microgrids with different grounding schemes will be an important and interesting topic of the future study. Moreover, HIL simulations using actual IEDs and Ethernet-based IEC 61850 communication will also be performed for the practical implementation of the proposed methods.

Author Contributions: Conceptualization, A.A.M.; methodology, A.A.M.; software, A.A.M.; validation, A.A.M.; formal analysis, A.A.M.; investigation, A.A.M.; data curation, A.A.M.; writing—original draft preparation, A.A.M.; writing—review and editing, K.K.; visualization, A.A.M.; supervision, K.K.; project administration, K.K. and funding acquisition, K.K. All authors have read and agreed to the published version of the manuscript.

Funding: This work was carried out mainly in the Protect-DG research project with the financial support provided by the European Regional Development Fund (ERDF) through Business Finland with Grant No.4332/31/2014. Some parts of this work were done in the SolarX research project with the financial support provided by the Business Finland with Grant No. 6844/31/2018. The financial support provided through these research projects is highly acknowledged.

Acknowledgments: The corresponding author is very thankful to his colleague Sampo Voima for useful discussion and collaboration about the topic during the earlier stage work of the paper in the Protect-DG research project.

Conflicts of Interest: The authors declare no conflict of interest.

References

1. Microgrids at Berkeley Lab, Grid Integration Group. Energy Storage and Distributed Resources Division, Microgrids, Microgrid Definitions. Available online: https://building-microgrid.lbl.gov/microgrid-definitions (accessed on 30 June 2020).
2. Justo, J.J.; Mwasilu, F.; Lee, J.; Jung, J.W. AC-microgrids versus DC-microgrids with distributed energy resources: A review. *Renew. Sustain. Energy Rev.* **2013**, *24*, 387–405. [CrossRef]
3. Li, X.; Dyśko, A.; Burt, G. Enhanced protection for inverter dominated microgrid using transient fault information. In Proceedings of the 11th IET International Conference on Developments in Power Systems Protection (DPSP 2012), Birmingham, UK, 23–26 April 2012; pp. 1–5.
4. Memon, A.A.; Kauhaniemi, K. A critical review of AC Microgrid protection issues and available solutions. *Electr. Power Syst. Res.* **2015**, *129*, 23–31. [CrossRef]
5. Oudalova, A.; Fidigatti, A. Adaptive Network Protection in Microgrids. *Int. J. Distrib. Energy Resour.* **2009**, *5*, 201–226. Available online: https://www.researchgate.net/publication/228344453_Adaptive_network_protection_in_microgrids (accessed on 6 April 2017).
6. Ustun, T.S.; Ozansoy, C.; Zayegh, A. Modeling of a Centralized Microgrid Protection System and Distributed Energy Resources According to IEC 61850-7-420. *IEEE Trans. Power Syst.* **2012**, *27*, 1560–1567. [CrossRef]
7. Zamani, M.A.; Yazdani, A.; Sidhu, T.S. A Communication-Assisted Protection Strategy for Inverter-Based Medium-Voltage Microgrids. *IEEE Trans. Smart Grid* **2012**, *3*, 2088–2099. [CrossRef]
8. Lin, H.; Guerrero, J.M.; Jia, C.; Tan, Z.H.; Vasquez, J.C.; Liu, C. Adaptive overcurrent protection for microgrids in extensive distribution systems. In Proceedings of the IECON 2016, 42nd Annual Conference of the IEEE Industrial Electronics Society, Florence, Italy, 23–26 October 2016; pp. 4042–4047. [CrossRef]
9. Lin, H.; Sun, K.; Tan, Z.; Liu, C.; Guerrero, J.M.; Vasquez, J.C. Adaptive protection combined with machine learning for microgrids. *IET Gener. Transm. Distrib.* **2019**, *13*, 770–779. [CrossRef]
10. Ghadiri, S.M.E.; Mazlumi, K. Adaptive protection scheme for microgrids based on SOM clustering technique. *Appl. Soft Comput.* **2020**, *88*, 106062. [CrossRef]
11. Momesso, A.E.C.; Bernardes, W.M.S.; Asada, E.N. Adaptive directional overcurrent protection considering stability constraint. *Electr. Power Syst. Res.* **2020**, *181*, 106190. [CrossRef]

12. Javadi, M.S.; Nezhad, A.E.; Anvari-Moghaddam, A.; Guerrero, J.M. Optimal Overcurrent Relay Coordination in Presence of Inverter-Based Wind Farms and Electrical Energy Storage Devices. In Proceedings of the 2018 IEEE International Conference on Environment and Electrical Engineering and 2018 IEEE Industrial and Commercial Power Systems Europe (EEEIC/I&CPS Europe), Palermo, Italy, 12–15 June 2018; pp. 1–5. [CrossRef]
13. Samadi, A.; Chabanloo, R.M. Adaptive coordination of overcurrent relays in active distribution networks based on independent change of relays' setting groups. *In. J. Electr. Power Energy Syst.* **2020**, *120*, 106026. [CrossRef]
14. George, S.P.; Ashok, S. Adaptive differential protection for transformers in grid-connected wind farms. *Int. Trans. Electr. Energy Syst.* **2018**, *28*, e2594. [CrossRef]
15. Prasad, C.D.; Biswal, M.; Abdelaziz, A.Y. Adaptive differential protection scheme for wind farm integrated power network. *Electr. Power Syst. Res.* **2020**, *187*, 106452. [CrossRef]
16. Ali, I.; Hussain, S.M.S.; Tak, A.; Ustun, T.S. Communication Modeling for Differential Protection in IEC-61850-Based Substations. *IEEE Trans. Ind. Appl.* **2018**, *54*, 135–142. [CrossRef]
17. Aftab, M.A.; Roostaee, S.; Hussain, S.M.S.; Ali, I.; Thomas, M.S.; Mehfuz, S. Performance evaluation of IEC 61850 GOOSE-based inter-substation communication for accelerated distance protection scheme. *IET Gener. Transm. Distrib.* **2018**, *12*, 4089–4098. [CrossRef]
18. de Sotomayor, A.A.; della Giustina, D.; Massa, G.; Dedè, A.; Ramos, F.; Barbato, A. IEC 61850-based adaptive protection system for the MV distribution smart grid. *Sustain. Energy Grids Netw.* **2018**, *15*, 26–33. [CrossRef]
19. Barra, P.H.A.; Coury, D.V.; Fernandes, R.A.S. A survey on adaptive protection of microgrids and distribution systems with distributed generators. *Renew. Sustain. Energy Rev.* **2020**, *118*, 109524. [CrossRef]
20. Beheshtaein, S.; Cuzner, R.; Savaghebi, M.; Guerrero, J.M. Review on microgrids protection. *IET Gener. Transm. Distrib.* **2019**, *13*, 743–759. [CrossRef]
21. Mahamedi, B.; Fletcher, J.E. Trends in the protection of inverter-based microgrids. *IET Gener. Transm. Distrib.* **2019**, *13*, 4511–4522. [CrossRef]
22. Hussain, N.; Nasir, M.; Vasquez, J.C.; Guerrero, J.M. Recent Developments and Challenges on AC Microgrids Fault Detection and Protection Systems–A Review. *Energies* **2020**, *13*, 2149. [CrossRef]
23. Patnaik, B.; Mishra, M.; Bansal, R.C.; Jena, R.K. AC microgrid protection—A review: Current and future prospective. *Appl. Energy* **2020**, *271*, 115210. [CrossRef]
24. Aftab, M.A.; Hussain, S.M.S.; Ali, I.; Ustun, T.S. IEC 61850 based substation automation system: A survey. *Int. J. Electr. Power Energy Syst.* **2020**, *120*, 106008. [CrossRef]
25. Hatziargyriou, N. *Microgrids: Architectures and Control*; John Wiley & Sons: West Sussex, UK, 2013.
26. Rockefeller, G.D.; Wagner, C.L.; Linders, J.R.; Hicks, K.L.; Rizy, D.T. Adaptive transmission relaying concepts for improved performance. *IEEE Trans. Power Deliv.* **1988**, *3*, 1446–1458. [CrossRef]
27. Relion Protection and Control. *650 Series IEC 61850 Communication Protocol Manual*, Revision: Product version: 1.1; ABB AB Substation Automation Products SE-721 59: Västerås, Sweden, 2011. Available online: https://search.abb.com/library/Download.aspx?DocumentID=1MRK511242-UEN&LanguageCode=en&DocumentPartId=&Action=Launch&DocumentRevisionId=- (accessed on 15 May 2015).
28. Katiraei, F.; Holbach, J.; Chang, T.; Johnson, W.; Wills, D.; Young, B.; Marti, L.; Yan, A.; Baroutis, P.; Thompson, G.; et al. Investigation of Solar PV Inverters Current Contributions during Faults on Distribution and Transmission Systems Interruption Capacity. In Proceedings of the Western Protective Relay Conference, Washington, DC, USA, 16–18 October 2012.
29. Turcotte, D.; Katiraei, F. Fault Contribution of Grid-Connected Inverters. In Proceedings of the 2009 IEEE Electrical Power Conference, Montreal, QC, Canada, 22–23 October 2009.
30. Palizban, O.; Kauhaniemi, K. Energy storage systems in modern grids—Matrix of technologies and applications. *J. Energy Storage* **2016**, *6*, 248–259. [CrossRef]
31. Keller, J.; Kroposki, B. *Understanding Fault Characteristics of Inverter-Based Distributed Energy Resources*; National Renewable Energy Laboratory: Golden, CO, USA, 2010.
32. *Technical Guideline Generating Plants Connected to the Medium-Voltage Network Guideline for Generating Plants' Connection to and Parallel Operation with the Medium-Voltage Network*; German Association of Energy and Water Industries (BDEW): Berlin, Germany, 2008.

33. Hou, D.; Dolezilek, D. IEC 61850-What It Can and Cannot Offer to traditional Protection Schemes, Schweitzer Engineering Laboratories, Inc. *SEL J. Reliab. Power* **2010**, *1*, 20080912.
34. IEC 61850-5:2013. *Communication Networks and Systems in Substations—Part 5: Communication Requirements for Functions and Device Models*; International Electrotechnical Commission, TC 57: Geneva, Switzerland, 2013.
35. Van Rensburg, M.; Dolezilek, D.; Dearien, J. Case Study: Lessons Learned Using IEC 61850 Network Engineering Guideline Test Procedures to Troubleshoot Faulty Ethernet Network Installations, Schweitzer Engineering Laboratories, Inc. In Proceedings of the Power and Energy Automation Conference, Spokane, Washington, DC, USA, 21–23 March 2017. Available online: https://www.eiseverywhere.com/file_uploads/0fca13690b4579341cf53b62d22a0647_Dolezilek1.pdf (accessed on 5 June 2020).
36. IEC/TR 61850-90-1:2010. *Communication Networks and Systems for Power Utility Automation—Part 90-1: Use of IEC 61850 for the Communication between Substations*; International Electrotechnical Commission, TC 57: Geneva, Switzerland, 2010.
37. Aichhorn, A.; Etzlinger, B.; Unterweger, A.; Mayrhofer, R.; Springer, A. Design, implementation, and evaluation of secure communication for line current differential protection systems over packet switched networks. *Int. J. Crit. Infrastruc. Prot.* **2018**, *23*, 68–78. [CrossRef]
38. Chelluri, S.; Dolezilek, D.; Dearien, J.; Kalra, A. Understanding and Validating Ethernet Networks for Mission-Critical Protection, Automation, and Control Applications. March 2014. Available online: https://pdfs.semanticscholar.org/ef57/a6a7655bed807bdd301e7c009d0f2dda4965.pdf (accessed on 2 September 2020).
39. Fred Steinhauser, Lessons Learned Time Related Issues Latency Measurements in Digital Grids, PAC World #Issue 052. June 2020. Available online: https://www.pacw.org/latency-measurements-in-digital-grids (accessed on 28 September 2020).
40. Mekkanen, M.; Kauhaniemi, K.; Kumpulainen, L.; Memon, A.A. Light-Weight IEC 61850 GOOSE Based LOM Protection for Smart Grid. In Proceedings of the CIRED 2018 Ljubljana Workshop on Microgrids and Local Energy Communities, Ljubljana, Slovenia, 7–8 June 2018; p. 0031.
41. Apostolov, A. R-GOOSE: What it is and its application in distribution automation. *CIRED—Open Access Proc. J.* **2017**, *2017*, 1438–1441. [CrossRef]
42. Ustun, T.S.; Khan, R.H.; Hadbah, A.; Kalam, A. An adaptive microgrid protection scheme based on a wide-area smart grid communications network. In Proceedings of the 2013 IEEE Latin-America Conference on Communications, Santiago, Chile, 24–26 November 2013; pp. 1–5.
43. Jeong, Y.W.; Lee, H.W.; Kim, Y.G.; Lee, S.W. High-speed AC circuit breaker and high-speed OCR. In Proceedings of the 22nd International Conference and Exhibition on Electricity Distribution (CIRED 2013), Stockholm, Sweden, 10–13 June 2013; pp. 1–4.
44. Yazdani, A.; Iravani, R. Chapter 9 Controlled-Frequency VSC System. In *Voltage-Sourced Converters in Power Systems: Modeling, Control, and Applications*; John Wiley and Sons, Inc.: Hoboken, NJ, USA, 2010.
45. Kanellos, F.D.; Hatziargyriou, N.D. Control of Variable Speed Wind Turbines in Islanded Mode of Operation. *IEEE Trans. Energy Convers.* **2008**, *23*, 535–543. [CrossRef]
46. Kanellos, F.D.; Hatziargyriou, N.D. Control of variable speed wind turbines equipped with synchronous or doubly fed induction generators supplying islanded power systems. *IET Renew. Power Gener.* **2009**, *3*, 96–108. [CrossRef]
47. SFS-EN 50549-1. Part1: Connection to a LV distribution network. Generating plants up to and including Type B. In *Requirements for Generating Plants to Be Connected in Parallel with Distribution Networks*; European Committee for Standardization: Brussels, Belgium, 2019.
48. Baran, M.; El-Markabi, I. Adaptive over current protection for distribution feeders with distributed generators. In Proceedings of the IEEE PES Power Systems Conference and Exposition, New York, NY, USA, 10–13 October 2004; pp. 715–719.
49. Mahat, P.; Chen, Z.; Bak-Jensen, B.; Bak, C.L. A Simple Adaptive Overcurrent Protection of Distribution Systems with Distributed Generation. *IEEE Trans. Smart Grid* **2011**, *2*, 428–437. [CrossRef]
50. Liu, Z.; Hoidalen, H.K. An adaptive inverse time overcurrent relay model implementation for real time simulation and hardware-in-the-loop testing. In Proceedings of the 13th International Conference on Development in Power System Protection 2016 (DPSP), Edinburgh, UK, 7–10 March 2016. [CrossRef]

51. Liu, Z.; Høidalen, H.K. A simple multi agent system based adaptive relay setting strategy for distribution system with wind generation integration. In Proceedings of the 13th International Conference on Development in Power System Protection 2016 (DPSP), Edinburgh, UK, 7–10 March 2016. [CrossRef]
52. Coffele, F.; Booth, C.; Dyśko, A. An Adaptive Overcurrent Protection Scheme for Distribution Networks. *IEEE Trans. Power Deliv.* **2015**, *30*, 561–568. [CrossRef]

Microgrid protection with conventional and adaptive protection schemes

Aushiq Ali Memon*, Hannu Laaksonen, Kimmo Kauhaniemi

*Corresponding author: aushiq.memon@uva.fi

School of Technology and Innovations, University of Vaasa, Vaasa, Finland.

A. Anvari-Moghaddam et al. (eds.) *Microgrids*, Power Systems, https://doi.org/10.1007/978-3-030-59750-4_19

Introduction

Microgrid is considered as the building block for the future smart grids, therefore a properly designed microgrid is essential for the proper functioning of the entire smart grid. Microgrid has many definitions but in general it is a well-designed local distribution system of electricity which facilitates the local integration of many small-scale renewable energy sources and energy storage systems to meet the local energy demand of consumers in a smart, secure, efficient, controlled, protected and managed environment. Unlike the traditional distribution systems of electricity, microgrids can operate in islanded mode when the main grid is disconnected due to faults. The islanded mode operation of microgrid will enhance the reliability level of existing distribution system if some sections of distribution networks are planned as microgrids. However, the islanded mode operation of microgrid has many challenges and one important challenge is related to the design of protection scheme. This chapter addresses the issues related to protection schemes in microgrid, gives an overview of the existing and new requirements of protection schemes and analyses the potential of the existing and adaptive protection schemes of microgrid.

19.1 Microgrid protection issues

Microgrid protection issues can be classified into two broad categories depending on its operational modes [1]: (1) Microgrid protection issues in grid-connected mode (2) Microgrid protection issues in islanded mode.

For the grid-connected mode of microgrid the faults inside microgrid as well as faults outside microgrid are considered. In the grid-connected mode protection schemes of microgrids should not operate unnecessarily for faults outside the microgrid for example faults upstream of the circuit breaker (CB) at point of common coupling (PCC). All faults insides the microgrid should be detected and selectively isolated for minimum interruption to other parts. During external faults at the main grid, microgrid should be able to disconnect quickly to protect its loads and start operating in islanded mode and as soon as the external fault is removed it should be reconnected to the main grid. The external faults at the main grid could be close-in faults or other far-end faults resulting in the loss of mains, hence both types of faults should be differentiated. In the grid-connected mode fault contribution from both the main grid and microgrid sources is considered. If microgrid has the majority of synchronous generator-based distributed energy resources (DERs), then fault contribution from the main grid could be reduced and overcurrent relays may experience selectivity issues like more time to issue a trip command. On the other hand, if the majority of converter-based DERs are connected inside the microgrid, then it will not have significant issues during the grid-connected mode since fault contribution from the converter-based DERs could be limited to twice the rated current capacity or even less depending on converter settings or rating.

For the islanded mode of operation the faults inside the microgrid are only considered and fault contribution from local DERs and energy storage systems is taken into account. Microgrid protection should detect and isolated the faults selectively even in islanded mode of operation. During island operation, for example in low-voltage (LV) microgrids, large fault currents from the upstream power system grid are not available. In addition, a large share from the DER units in LV microgrids will be inverter-based with low fault currents. Therefore, traditional one-directional protection schemes, assuming large difference between fault and load currents, are not applicable during island operation. These traditional protection methods could also have slower fault clearing time and reduced sensitivity and selectivity. This means that the system reliability is expected to decrease if the protection schemes are not adapted [2]. For these reasons, conventional over-current (OC) protection based of fuses and one setting group will not be able to guarantee selectivity during different types of possible faults. Therefore, LV network conventional protection will not be compatible with island operated LV microgrids and new protection schemes with adaptivity must be created. On the other hand, new LV microgrid protection scheme needs to be economical

and simple [3], [4]. For medium-voltage (MV) microgrids after isolation from the utility grid, local DERs are the only fault current sources in the electric island and the fault current level depends on the types, sizes and locations of the DER. However, it is generally lower than the fault current from the utility grid [5]. The reduced fault current contributions from microgrid DERs require revised protection settings with the reduced pickup or threshold values of currents for islanded mode or protection schemes based on other protection principles like differential current [6], symmetrical components and residual current based [7], voltage based [8], harmonic content based [9] or suitable combination of them should be employed to detect and clear the fault in islanded mode. An adaptive protection scheme [10] using high speed communication links and numerical directional overcurrent protection relays could also be a suitable protection scheme to change protection settings adaptively according to grid-connected mode or islanded mode operations.

In the creation of new protection system for microgrids, multiple issues need to be taken into account, like

- The number of zones for protection,
- Operation speed specifications for the different operation modes and configurations of microgrid and
- Protection methods for microgrid normal grid-connected and islanded operation [4].

The created microgrid protection system also needs to be compatible with the microgrid operation and control solutions. Some key issues related to the LV microgrid protection are briefly reviewed based on [11] from which more detailed information can be found. The extent and number of microgrid protection zones will determine the required number of protective devices (PDs) for microgrid protection. However, the protection system simultaneously needs to fulfil the customer requirements and be economically feasible [4].

The essential structural choices will define the operation speed needs and principles for the protection of LV microgrid and correspondingly the operation speed requirements will determine some of the structural choices required to fulfil the operation speed needs. Main reasons for the operation speed requirements of LV microgrid protection are stability and customer sensitivity. The stability needs to be maintained after fast disturbances like after islanding due to fault in the upstream network during normal grid-connected operation or after fault in LV microgrid during islanded operation. One important issue related to the operation principles of LV microgrid protection is the fault behaviour of the converter-based DER units. The fault behaviour needs to be compatible with the developed microgrid protection scheme [4].

As stated in [12], the microgrid protection issues cannot be solved without a complete understanding about microgrid dynamics before, during and after islanding or fault. Related to this, for example, directly connected rotating generators or motors are very sensitive from the stability viewpoint in voltage dips caused by faults during microgrid island operation, and so they may endanger the stability of the microgrid. Therefore, if directly connected rotating machines are connected to microgrid, protection should operate rapidly during all kind of faults. For example, if microgrid customers have fuses with high nominal currents, there can be a risk that customer protection may operate too slowly during island operation due to small fault currents and that may lead to instability after clearance of the fault [4].

In cases where overcurrent based protection is utilized during island operation, the protection and control functions of IEDs in microgrids may need real-time information about network topology, the status of DER units (on or off), the state of charge of storage systems, and also number and size of loads connected to the microgrid. These conditions have to be updated and checked continuously in order to guarantee that protection settings are suitable for the actual configuration [3], [4].

Based on the above and as mentioned in [12], the high-speed operation of the protection devices is very crucial for a reliable operation of the microgrid protection system. Utilization of high-speed telecommunication is expected to be an essential part of future smart grid protection systems to achieve fast and selective protection both in grid connected and islanded modes of operation. The same communication protocols and standards used in HV/MV network can be applied directly to the LV microgrids. However, due to the smaller scale of LV microgrids, the costs of protection devices must also be lower than the cost of devices used in the HV/MV network [4].

One important issue, which is required to enable stable transition from the normal grid-connected operation to island operation, is coordination of IED protection settings with DER unit fault-ride-through (FRT) requirements (especially low-voltage-ride-through, LVRT). In order to avoid unwanted tripping, faulty lines must be

disconnected first by the protection system and after that the DER units should be disconnected according to their FRT or LVRT functionality. Rapid protection operation is needed especially if there are many protection zones. Therefore, communication-based protection methods and schemes are often required to achieve selectivity [13]. Some further discussion about issues related to the protection of microgrids can be also found in [2], [4].

19.1.1 DER unit fault behaviour and effect on microgrid protection

In the future proper co-ordination between distributed generation (DG) unit grid codes and distribution network protection schemes will be increasingly important during the both grid-connected and islanded operation of microgrids. The operation time settings of short-circuit and earth-fault protection must be selective with DER unit fault-ride-through settings during normal operation**.** In MV network short-circuit protection operation time delays have traditionally been dependent on fault-current magnitude or measured impedance with fixed time delays or inverse time curves. In the future, MV networks will be increasingly divided into multiple protection zones in order to improve supply reliability. Therefore, short-circuit protection operation times may become too long if high-speed communication based and e.g. IEC 61850 GOOSE signals-based interlocking/blocking schemes are not utilized. On the other hand, the communication may fail or is not available and therefore also grid code compatible protection schemes which are not based on high-speed communication are needed in the future at least as a back-up for communication-based schemes.

Regarding the fault behaviour required from DER units during faults, it is important to ensure that the fault behaviour is compatible with the developed LV microgrid protection scheme and considers also the including FRT needs. This means that when the protection for an island operated microgrid is determined, one of the most important considerations is related to the fault current contribution of the converter-based DER units [4], [14].

Fault behaviour and fault current feeding capability of a DER unit is also highly dependent on the type of the DER unit. For example, a synchronous generator is usually able to feed prolonged fault current (about 200 to 400% of nominal current). An induction generator, in the initial stage, feeds almost as big a fault current as a synchronous generator, but the feeding is reduced quickly. Fault current fed by the inverter-connected generating unit is typically limited to 1.2–1.3 p.u. and highly dependent on the control system and control principles as well as grid code requirements regarding fault-ride-through and reactive current feeding requirements.

During normal grid-connected operation of microgrid with different types of DER units the grid codes can require FRT capability from the DER units in terms of frequency (*f*), rate-of-change-of-frequency (*df/dt*), voltage (*U*) and voltage support. Traditionally, in grid-connected operation, larger DER units have more FRT and frequency as well as voltage support related requirements in the grid codes. For example, regarding voltage support the FRT capability of DER units is defined with a voltage-against-time-profile (LVRT curve). In addition, also additional voltage support by capacitive/reactive, positive sequence, current injection during faults is required from MV and HV network connected converter-/doubly-fed-induction-generator (DFIG) -based DER units during grid-connected operation. Synchronous generator DER units naturally provide a voltage support during faults by feeding reactive current. Required dynamic response of the reactive current feeding is usually also defined in the grid codes for the converter-based DER units. However, LVRT capability and additional reactive current feeding of the converter-based DER units, like wind turbines, is not just a control issue. It also requires suitable technology to be applied in the DC-link of the converter, like for example, DC-link chopper or supercapacitor and crowbar possibly as a back-up.

Most grid codes for the grid-connected operation of DER units do not include any special requirements for the supply of negative sequence current. In synchronous generators, the negative sequence current is fed naturally and there are no effective measures to influence it. In contrast, with voltage source converters (VSCs) it is possible to individually control positive and negative sequence quantities. The main reason for the minimization of negative sequence current has been the impact of asymmetrical voltages on the DER unit (e.g. wind turbine) without considering the impact of it on the network voltages or network protection. The negative sequence may be controlled to mitigate twice the fundamental frequency oscillations appearing in the converter/inverter DC-link during asymmetrical faults. Therefore, in many applications the negative sequence component injection has been reduced partially or fully. However, full negative sequence current reduction control also reduces the line-to-line (2-phase) short circuit current to the level of the load current or even to zero which means that it may

prevent the correct operation of network protection in 2-phase short-circuit faults. To overcome this problem, extensions to grid code have been proposed, which would require DG to inject a clearly defined level of negative sequence current. This is also a requirement already in Germany. From the network voltages point of view the effect of negative sequence fault current feeding during asymmetrical faults is beneficial because it reduces the negative sequence voltage, improves the voltage phase symmetry and reduces the overvoltages in the healthy phases during 2-phase short-circuits. However, negative sequence current injection will limit the control capability of the DG in the positive sequence. It can be expected that the future grid codes will increasingly specify requirements for asymmetrical / imbalanced negative sequence current injection during asymmetrical faults.

Usually the control mode change of one or more DER units connected to the distribution network is required after changing from the normal grid-connected operation to island mode. Traditionally, this means that under normal operation the DER unit uses active(*P*)/reactive(*Q*) power control and after islanding the control mode is changed to voltage(*U*)/frequency(*f*) control (or voltage/speed control). However, control schemes which do not require changing after transition to/from island operation have also been proposed. For example, in [15], an enhanced control strategy was proposed which improves the performance of a DER unit under network faults and transient disturbances, in a multi-unit microgrid setting. The proposed control strategy does not require the detection of the mode of operation and switching between different controllers (for grid-connected and islanded) modes, and it enables the adopted DER units to ride through network faults, irrespective of whether they take place within the host microgrid or impact the upstream grid [15].

LVRT, high voltage ride-through (HVRT) as well as *f* and *df/dt* related FRT capabilities are required during LV microgrid island operation also from the small-scale DER units which typically is not the case during grid-connected operation. Typically, in grid-connected operation the small-scale DER units, like PV units, are only required to support frequency stability during over-frequency situations by their active power-frequency (*Pf*)-droop control. From the island operated LV microgrid protection viewpoint, it is important to know exactly how the converter-based DER units behave during the faults and what kind of fault current (active, reactive, positive sequence, negative sequence etc.) they will feed. Therefore, so called 'microgrid grid codes' for island operated networks are necessary for the development of future smart grid protection solutions to reduce complexity and to avoid the need for too many case specific alternatives [4], [14].

Based on the simulations done in [14], the increased reactive power feeding with the converter-based DER units, was found to be beneficial for the possible overcurrent-based protection in LV microgrid. However, it did not significantly reduce the usability of undervoltage-based protection either due to resistive characteristics of LV lines. On the other hand, the reactive power feeding during the fault did not significantly reduce the magnitude of the voltage dip, i.e. support microgrid voltage during the fault. In the end, the excessive reactive power feeding of the converter-based DER units during the fault in island operated LV microgrid was not justified based on the simulations in [14]. Therefore, it was suggested that during faults in LV island operated microgrid the fault current fed by the converter-based DER units is recommended to be active instead of reactive if possible. In addition, the control of the converters during possible faults was not recommended to change due to the increased possibility of instabilities after fault clearance.

19.1.2 Example – Microgrid transition to islanded operation

In following, the example from [16] is used to define the protection needs (functions, time selectivity) when intentional island operation and especially successful transition to island operation is considered.

From island operation perspective (in addition to grid code FRT requirements from DG units during the normal grid-connected operation) it is required that the wind farm (green) in Fig. 19.1 as well as DER ① and ② have sufficient FRT capabilities. Figure 19.1 shows possible intended islands and MV feeder short-circuit protection at CB1-CB4 which is assumed to be directional like the earth-fault protection. In the following, the time selectivity issues (Figure 19.2) are discussed, with different fault scenarios (faults A-E in Figure 19.1), regarding successful transition to island operation.

In Figure 19.2 protection time selectivity issues, general time delay setting principles and the role of high-speed communication is shown when a) islanding is not allowed and b) islanding is possible. Figure 19.2 also illustrates the role of high-speed communication based interlockings/blockings (as well as transfer trip-based islanding detection) in the reliable and selective operation of future distribution networks with many sequential protection

zones and the possibility for intended island operation. In Figures 19.1 and 19.2 the idea is that the possible operation principles of directional short-circuit protection in forward direction can be

1) Directional overcurrent protection with fixed time delay (and high-stage / low-stage settings)
2) Distance protection with fixed time delay (in forward direction)

Similarly, in Figures 19.1 and 19.2 the possible operation principles of directional protection in the reverse direction (for intentional islanding) can be

1) Under-voltage with fixed time delay (and high-stage/low-stage settings) AND current direction detection in the reverse direction. Function pick-up/start is only based on undervoltage (i.e. not in overcurrent, because fault current levels of inverter-based DER units can be fairly low as discussed in previous chapters)
2) Distance protection with fixed time delay (in the reverse direction)

From Figures 19.1 and 19.2 it can be seen that selectivity problems are possible if communication based interlockings/blockings for example are NOT used (Figure 19.2a)), because coordination between LVRT curve of DG units (defined by grid codes) and required time differences between CB2 and CB3 in forward direction may be hard to achieve. This naturally depends on the number of consecutive protection zones and the allowed time difference between the operation time delays of CB2 and CB3.

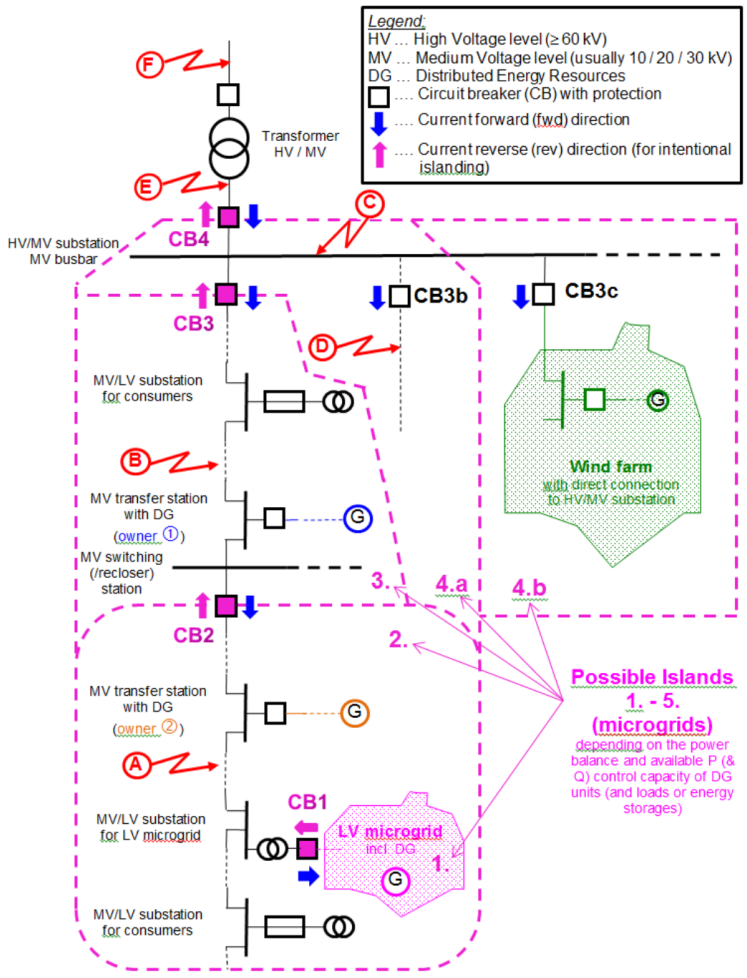

Figure 19.1. Possible intended islands 1.–4. b (see also Figure 19.2) [16].

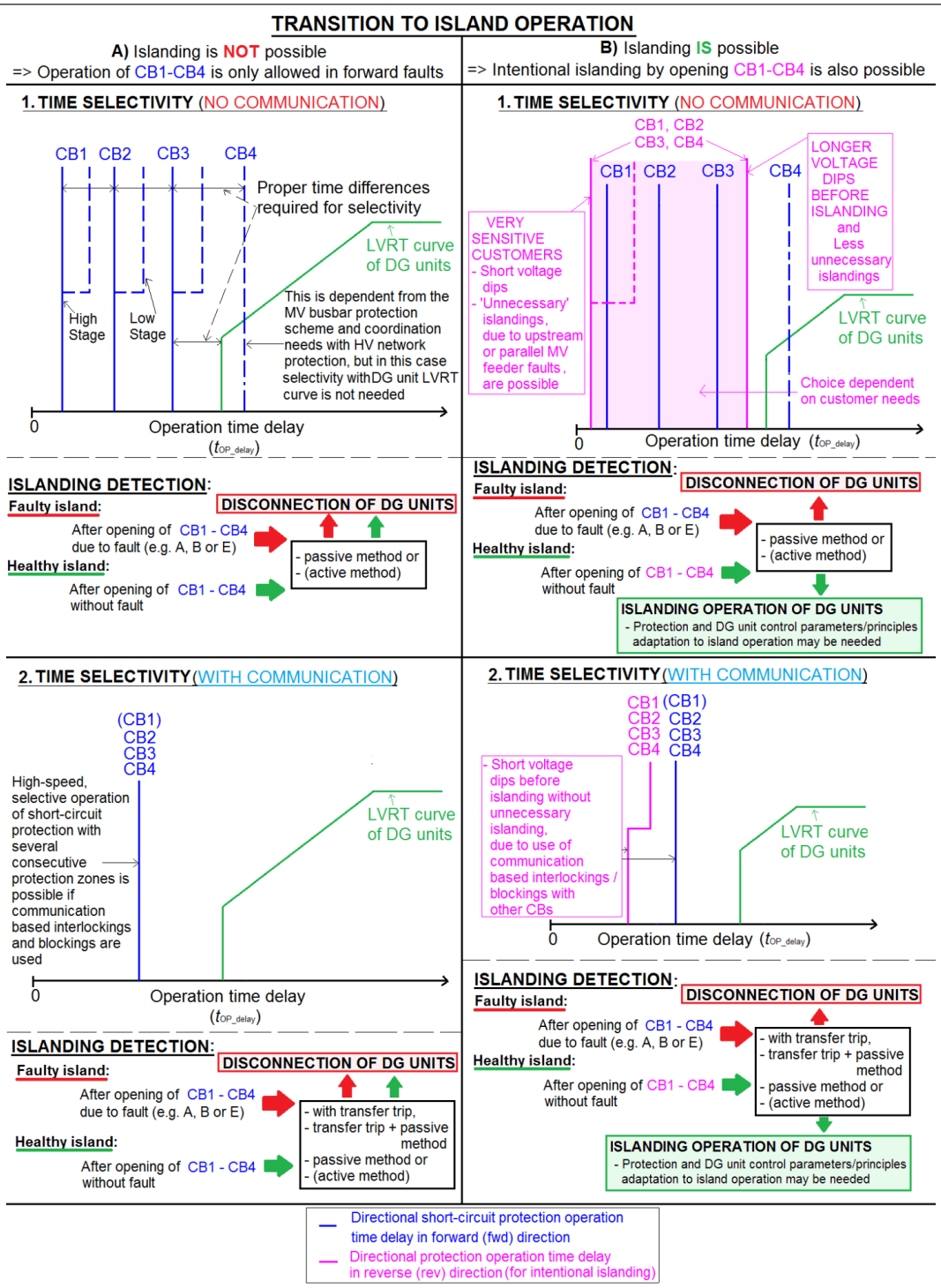

Figure 19.2. Protection time selectivity issues, setting principles and the role of high-speed communication when a) islanding is NOT allowed and b) islanding IS possible (see also Figure 19.1) [16].

Transition to intentional island operation IS only possible (Figure 19.2b) if active and reactive power unbalance at CB1, CB2, CB3 or CB4 is small enough (or enough, rapidly controllable active and reactive power units exist in the possible island (1.-4.b in Figure 19.1) before the protection start/operation of CB1-CB4 in the reverse direction). If this is not the case transition to island operation should not be allowed. Here it is worth mentioning that the recent grid codes enable/support transition to intentional island operation because of the *P/f*-droop control requirements

of DER units during over-frequency situations (under-frequency based load shedding schemes could have similar kind of effect) and possibly also due to voltage control (Q/U-control) requirements.

In the above discussion and in Figure 19.2, only short-circuit protection has been considered, but naturally also earth-fault protection principles and settings must be proper during both normal and island operation. Therefore, it should be noted here that after opening CB2, CB3 or CB4, the MV network neutral earthing method may change e.g. from compensated to isolated and MV feeder IEDs earth-fault protection settings and protection principles also needs to adapt to these changes.

In the following, the protection operation principles during different faults A-E in the example network shown in Figure 19.1 are described. It is assumed that high-speed communication is available/possible, and islanding IS possible (Figure 19.2b) using time selectivity (with communication) if power generation and consumption are close to each other behind the possible island connection point CB.

In case of fault A in Figure 19.1 (see also Figure 19.2):

- CB1 will operate in reverse direction and disconnect the LV microgrid intentionally from the utility network:
  - If active and reactive power unbalance at CB1 is small enough (i.e. stable transition to island operation is possible) as stated above.
  - CB1 could also send signals to the LV microgrid DER units to change their control mode etc. after operation.
- CB2 will operate in forward direction
  - CB2 sends simultaneously interlocking signal to CB3 (and CB4) to prevent their false operation and
  - CB2 can also send a communication-based transfer trip (faulty island) disconnection signal to DER unit ②

Wind farm and DER unit ① will remain connected according to the LVRT curve of DG units (Figure 19.2).

In case of fault B in Figure 19.1 (see also Figure 19.2):

- CB1 will operate in reverse direction and disconnect the LV microgrid intentionally from the utility network:
  - If active and reactive power unbalance at CB1 is small enough.
  - CB1 could also send signals to the LV microgrid DER units to change their control mode etc. after operation.
- CB2 may also operate in reverse direction and disconnect part of the MV feeder intentionally from the utility network to island operation:
  - If active and reactive power unbalance at CB2 is small enough.
  - CB2 could also send signal to DER unit ② to change the control mode etc. after operation.

  CB3 will operate in forward direction
  - CB3 sends simultaneously interlocking signal to CB4 to prevent false operation and
  - CB3 can also send a communication-based transfer trip (faulty island) disconnection signal to DER unit ①

Wind farm will remain connected according to the LVRT curve (Figure 19.2).

In case of fault C in Figure 19.1 (see also Figure 19.2):

- MV busbar fault
- CB1 will operate in reverse direction and disconnect the LV microgrid intentionally from the utility network:
  - If active and reactive power unbalance at CB1 is small enough.
  - CB1 could also send signals to the LV microgrid DER units to change their control mode etc. after operation.
- CB2 may also operate in reverse direction and disconnect part of the MV feeder intentionally from the utility network to island operation:
  - If active and reactive power unbalance at CB2 is small enough.
  - CB2 could also send a signal to DER unit ② to change the control mode etc. after operation.
- CB3 may also operate in reverse direction and disconnect either part of the MV feeder (beginning of the feeder, 3. in Figure 19.1) OR the whole MV feeder (2. &3. in Figure 19.1) to island operation:
  - Depending on the active and reactive power unbalance at CB3 and CB2.
  - Co-ordination with islanding of part of MV feeder by opening CB2 may be beneficial/required.

- CB3 could also send a signal to DER unit ① (AND/OR DER unit ② depending on the power balance situation) to change control mode etc. or to disconnect

- CB4 will operate in forward direction.

The wind farm will be disconnected according to LVRT curve (Figure 19.2). Also, directional short-circuit protection in the reverse direction could be included in CB3c in order to disconnect the wind farm more rapidly in case of busbar faults like fault C (Figure 19.1). However, in case of upstream faults (like fault E and F in Figure 19.1) this reverse direction protection at CB3c should be blocked by communication to enable fault-ride-through support from the wind farm according to grid codes (e.g. LVRT curve).

In case of fault D in Figure 19.1 (see also Figure 19.2):

- Parallel MV feeder fault
- CB3b will operate in forward direction (Figure 19.1) and simultaneously send the interlocking signal to other CBs (e.g.) to avoid unnecessary islandings and to ensure selectivity.

DER units ① and ② as well as the wind farm will remain connected according to the LVRT curve (Figure 19.2).

In case of fault E in Figure 19.1 (see also Figure 19.2):

- HV/MV transformer fault => intentional islanding can take place:
  - Possible indication about intentional islanding possibility from HV/MV transformer protection IED to MV feeder IEDs.
- CB1 will operate in reverse direction and disconnect the LV microgrid intentionally from the utility network:
  - If active and reactive power unbalance at CB1 is small enough.
  - CB1 could also send signals to the LV micro-grid DER units to change their control mode etc. after operation.
- CB2 may also operate in reverse direction and disconnect part of the MV feeder intentionally from the utility network to island operation:
  - If active and reactive power unbalance at CB2 is small enough
  - CB2 could also send a signal to DER unit ② to change the control mode etc.
- CB3 may also operate in reverse direction and disconnect either part of the MV feeder (beginning of the feeder, 3. in Figure 19.1) OR the whole MV feeder (2. &3. in Figure 19.1) to island operation:
  - Depending on the active and reactive power unbalance at CB3 and CB2
  - Co-ordination with islanding of part of MV feeder by opening CB2 may be beneficial/required
  - CB3 could also send a signal to DG unit ① (AND/OR DER unit ② depending on the power balance situation) to change the control mode etc. or to disconnect
- Alternatively, CB4 may also operate in reverse direction and disconnect:
  1) All MV feeders (4.b in Figure 19.1) to island operation.
  2) Some of the MV feeders (e.g. (4.a in Figure 19.1)) to island operation:
     - Simultaneously the disconnection signal from CB4 is send to MV feeder CBs (e.g. (CB3c in Figure 19.1)) which cannot be included into intentional island.
     - Wind farm remains connected according to the LVRT curve (Figure 19.2) unless disconnection signal to CB3c (Figure 19.1) is send by CB4.
  - This intentional island scheme is somewhat more complex due to the increased number of possible island sizes.
  - Size of the island depends on the active and reactive power unbalance at CB4, CB3 and CB2 and
    - Needs (central) co-ordination with islanding of part of or whole MV feeder by opening CB3 or CB2.
    - Signals to DER unit ① and ② to change the control mode etc. after operation or to disconnect will be sent based on the planned island size (which depends from the power balance situation before fault C).

In case of fault F in Figure 19.1 (see also Figure 19.2):

- HV network fault => intentional islanding should not take place (if there is an alternative HV network supply route available), MV and LV network connected DER units should ride-through HV network faults and possibly also support the HV network according to grid code requirements (for example by reactive power injection)
  - Possible indication about HV network fault could be sent from the HV/MV transformer protection IED to MV feeder IEDs to indicate that in this case intentional islanding is not possible/allowed

- Instead FRT and HV network support of DER units is preferred
  - However, if very sensitive customers (sensitive to voltage dips) are connected to MV or LV network then similar actions could take place as described above for the other faults.

19.2 Protection requirements

The traditional protection scheme requirements include sensitivity, selectivity, and reliability. However, the capability of microgrid to work in islanded mode demands the additional requirement of adaptivity for the protection scheme. Moreover, microgrid transition from the islanded mode to the grid-connected mode or even from the isolated mode to the islanded mode require re-synchronization function in order to avoid wrong protection tripping during transition periods. Since, the transitions from the grid-connected to the islanded mode and vice versa are mainly dependent on the connection and disconnection status of microgrid switches/breakers, therefore selection of proper switching technology is also important. In this section, the existing and new protection requirements of microgrid are discussed.

19.2.1 Sensitivity

Sensitivity is one of the essential requirements of a protection scheme. Any protection scheme should be sensitive enough to sense and detect the abnormality or fault in the power system components and respond to clear the fault as soon as possible. Sensitivity can be defined as "the ability of the protection system to detect even the smallest faults within the protected zone" [17]. Sensitivity is related to the minimum pickup or threshold value of measured or sensed quantity which is by some margin above or below the boundary of normal operating value. Different protection methods have different sensitivity levels depending on operational characteristics or settings and the magnitude of electrical or physical quantity on which protection scheme is working. Fuses for example are the traditional and simple overcurrent protection devices which depend on the magnitude of current flowing through the fusible element which blows or melts due to thermal effects produced by the current. Fuses are both sensing and interrupting devices with inverse operational characteristics, which means less time of fusing operation at high magnitude of current and more time of fusing operation at low or minimum magnitude of current flowing through the fusible element. The operational characteristics of fuses greatly depend on the material of fusible element through which electric current flows during the fault. Therefore, operational characteristics of fuses can be changed only by changing the material of fusible element, but once fuse type is selected and installed the operational characteristics can no longer be changed, this makes fuse a non-resettable device. Different types of fuses have different time-current characteristics and therefore different levels of operating sensitivities. The other protection device working on overcurrent principle is the overcurrent relay. The sensitivity of definite time overcurrent relay depends on its capability or settings to detect the lowest possible magnitude of current flowing through the circuit during a fault. Usually, the lowest possible magnitude of current is observed in case of single-line to ground (SLG) short circuit fault with high fault impedance and the maximum current is observed during three-phase (LLL) short circuit fault. In conventional radial distribution systems with power flow in one direction, overcurrent protection schemes for the detection of SLG faults need to be more sensitive in comparison with overcurrent protection schemes for the detection of three-phase faults. However, with the increasing connection of small-scale DER units particularly the converter-based DERs result in very reduced three-phase fault current levels which greatly affect the sensitivities of existing overcurrent relays and both definite-time and inverse-time overcurrent relays may experience the blinding of overcurrent protection. The blinding of protection scheme occurs when a fault exists but the protection scheme is unable to detect the fault due to wrong or less sensitive settings. Moreover, transient events like starting of motor loads, the energization of transformers and switching of capacitor banks may affect the sensitivity of overcurrent protection and result in wrong or unnecessary trips due to more sensitive settings. Additional filtering, signal processing algorithms or even changed protection philosophies or functions can be employed to avoid these situations. Microgrids require different levels of sensitivities in overcurrent protection schemes to differentiate between faults in the grid-connected and islanded mode of operation. In the grid-connected mode less sensitive settings are required in order to avoid the unnecessary trips of protection schemes and in the islanded mode more sensitive settings are necessary in order to avoid the blinding of protection scheme. Other protection functions based on the measurement of voltage, frequency or impedance may have different levels of sensitivities in different operational modes and different fault categories and these functions should be carefully selected and configured. For example, the measurement of fault resistance (R_F) coverage is used as a means of evaluating sensitivity of directional overcurrent, distance and differential protections for SLG faults [17].

19.2.2 Selectivity

Selectivity or coordination is an important requirement of the traditional protection system which ensures that only the section of power system close to the fault is isolated and the minimum portion of power system is interrupted. For a complete selective or a coordinated protection scheme primary protection operates first after fault detection inside the protection zone and backup protection operates only after primary protection fails to detect and isolate the fault after a predetermined time delay. For definite time OC relays definite time based coordination is done which starts for example from the extreme load end of the feeder towards the source side of the feeder or substation. It means for faults at the extreme end of the feeder on the load side, OC relay near the load operates first and then a coordination interval of 0.2 s or so is used between each upstream OC relay towards the substation end for the backup protection of downstream relays. Usually fast acting relays and breakers or instantaneous adjustable devices like miniature circuit breaker (MCB) or moulded case circuit breakers (MCCB) are used on the load side for short circuit protection. If due to any problem, load side primary protection fails, the first upstream relay near the load will operate as backup after a coordination interval of 0.2 s, the same is valid for all subsequent upstream faults. This definite time based coordination is commonly used for three-phase faults in radial distribution feeders. Definite time relay coordination is simple, independent of fault current magnitude and it provides complete coordination as long as each relay is able to detect the fault. The only drawback for definite time coordination is longer tripping times for faults near the source or substation side of the feeder. The inverse-time OC relays, commonly known as inverse definite minimum time (IDMT) relays have operating times which are inversely proportional to the magnitude of current, the higher the fault current magnitude, the faster the IDMT relay operates. The IDMT relays have several families of inverse characteristic curves with different degrees of inversity like standard inverse, very inverse and extremely inverse characteristics. For a given pickup current above the minimum pickup value and an identical time-dial setting, an extremely inverse IDMT relay operates faster than a very inverse relay and a very inverse relay operates faster than the standard inverse. The IDMT relays with an inverse or very inverse characteristics are most commonly used types and ideally the relays with the same inverse characteristics are used throughout the system [18]. The IDMT relays operate faster for faults near the source or substation and slower for faults away from the substation. Compared with the coordination of definite time relays, the coordination of IDMT relays is much complicated and a time intensive job, however it all depends on the method used. The general methods used for the coordination of IDMT relays include trial and error, curve fitting and optimization techniques using different algorithms [19]. In traditional radial distribution systems with power flow in one direction the coordination of OC relays may not be affected, however when considerable amount of DERs are connected the coordination is either altered or completely lost depending on the capacity, type and location of DERs [20] [21]. For microgrids with nearly 100% DER supply with the majority of the converter-based DERs, the loss of protection coordination will result in the reduced security of supply to consumers due to the disconnection of large portions which is not in line with the very fundamental purpose of microgrids. Therefore, microgrid protection must be coordinated in both the grid-connected and islanded mode of operation. This could be done by the separate coordination study and settings of grid-connected and islanded mode protections or by providing sources of high fault current also in islanded mode. A case study of protection coordination in the grid-connected and islanded mode of microgrid using definite-time and inverse-time OC relays is presented in Section 19.3 for further understanding about selectivity issues.

19.2.3 Reliability

Reliability is the ability of protection scheme to operate correctly and it is usually defined in terms of dependability and security of relay operations. Dependability is defined as the measure of certainty that protection relay will operate and trip for all faults for which it is designed and security is the measure of certainty that protection relay will not operate and trip incorrectly. Traditionally, protection schemes have been designed to provide high dependability at some degree of compromise of security which may increase the false operations of protection schemes resulting in the unwanted trippings of power system elements. Traditional large interconnected power systems provide some degree of redundancy due to many alternative paths of power flow and therefore the loss of a generator or a line (n-1 criterion) due to a false trip is less objectionable in comparison with the sustained fault which may damage the faulty component [17][22] [23]. But, the false trips of a distribution line due to the unsecure protection scheme in radial, grid-connected microgrids is less acceptable because it may jeopardize the stability of microgrid. The false trips of breaker at microgrid connection point to the main grid may result in unwanted islanding, increased re-synchronization operations for the restoration of grid-connected operations, unwarranted outage to non-priority loads and microgrid exposure to power quality problems [12][24]. In islanded mode of operation, a false trip of a grid-forming generator may result in complete blackout due to consequent tripping of grid-following generators. The reliability of modern multifunction numerical relays using communication links is not only dependent on hardware and software based failures but also on the

dependability and security of the communication system. In order to analyse the dependability and security of protection scheme different fault trees can be used. Fault tree analysis is a useful tool for the comparison of relative reliability of protection schemes. The construction of a fault tree starts with the identification of component failures which may cause a failure to trip (a dependability problem) or an unwanted trip (a security problem). The AND, OR or other gates are used to represent the combinations of failure rates. The idea behind using the OR gate is that any of several failures can cause the protection scheme to fail, whereas, the AND gate expresses the idea that all component failures happen simultaneously to cause a protection scheme to fail. Various combinations of protection schemes using fiber-optic channels have been analysed for dependability and security using fault trees [17]. Such type of reliability analysis will be useful for protection schemes in microgrids.

19.2.4 Adaptivity

The adaptivity of microgrid protection scheme is the new requirement which is the ability of protection scheme to adapt its settings according to changing operational modes from the grid-connected to islanded mode and vice versa. An adaptive protection is defined as an on-line activity that changes the preferable response of protection device according to changing states of system or its requirements. Adaptive protection is usually automated, but some necessary human interventions can also be included. An adaptive relay is a protection device or relay that includes different setting groups, characteristics or logic functions which can be altered or changed on-line very quickly by using external signals or control commands [25]. The modern numerical relays, also called intelligent electronic devices (IEDs), not only provide various protection functions (overcurrent, over/under voltage etc.) integrated in a single physical device, but also offer various settings groups for each of the available protection functions. These setting groups can be changed in an adaptive manner using the communication link between IEDs and IEDs and circuit breakers (CBs). Adaptivity of protection scheme in microgrid is mainly required due to different magnitudes of fault current sensed by OC relays in grid-connected and islanded modes and due to the connection and disconnection of DERs. Further detailed discussion on adaptive protection is given in Section 19.4.

19.2.5 Re-synchronization

Re-synchronization is the ability of a well-planned microgrid to reconnect back to the main grid soon after the clearance of faults on the main grid side. The availability of re-synchronization means at the microgrid point of connection to the main grid is necessary for the smooth transition of microgrid from the islanded mode to the grid-connected mode. Re-synchronization is the process of connecting islanded microgrid back to the main grid after checking or measuring voltage, frequency and phase angle of both systems and closing the breaker contacts for parallel operation only if these parameters are within acceptable limits as per table 5 of IEEE Std 1547-2003 [26]. Three types of synchronization schemes have been mentioned in [27]: active, passive and open transition synchronization. In active synchronization there is a control mechanism which can be used to match voltage, frequency and phase angle of islanded microgrid to the main grid before closing the breaker contacts. Active synchronization requires collection or sensing of conditions for both the main grid and islanded microgrid and then communicating this information to the control mechanism. Passive synchronization uses traditional synchrocheck relay for closing breaker contacts if voltage, frequency and phase angle of both the main grid and islanded microgrid reach within specified limits. Passive technique also requires sensing of conditions for both the main grid and islanded microgrid, however it is slower than active synchronization. Open transition synchronization requires the disconnection of loads and DGs inside microgrid before reconnection and does not require any sensing or measurement of conditions. Both active and passive synchronization methods maintain high reliability of microgrid as no load or DG disconnection is required. The same procedure of synchronization is applicable for the reconnection of any synchronous DG, the converter-based DG or isolated zones with one or more DGs back to the large portion of islanded microgrid in islanded mode.

19.2.5.1 LV microgrid synchronized re-connection

One important issue in enabling future Smart LV Grids with island operation capability is that challenges related to the synchronized reconnection (i.e. re-synchronization) of island operated microgrid are solved. Islanded microgrid may be synchronized with utility system directly after islanding, but later the synchronism is lost due to generation and load variations inside the microgrid. This means that the voltage phase angle difference across microgrid interconnection switch or circuit-breaker will change. Microgrid re-synchronization or synchronized re-connection of microgrid means that the voltage angle difference between utility grid and microgrid needs to be minimized before reconnection [4].

In the HV network where line reactance X is much larger than line resistance R the active power P depends mainly on load angle δ and reactive power Q depends mainly on voltage difference. This means that the active power P control directly controls the load angle δ and frequency f. Generators in HV network are typically directly connected with synchronous generators (SGs) which can be controlled, for example, during synchronization of separate power system areas. In HV network synchronism check relays have typically such settings that frequency difference over open CB needs to be less than 55 mHz and phase difference 20°–45° before CB connection [28].

On the other hand, in LV microgrids a large share of the DER units are connected through the inverter- or converter-based interfaces and microgrid synchronized re-connection can be done by the control of these DER units. In LV networks the line resistance R is much larger than the line reactance X and therefore, the active power P depends mainly on voltage difference, while the load angle δ and frequency is mainly dependent on reactive power Q. This means that one possibility to manage the phase difference across microgrid interconnection CB could be coordinated reactive power control of the DER units.

The chosen strategy is dependent on the chosen microgrid concept. In [29], it was proposed that the control of grid-forming energy storage unit (master unit) could slowly shift the microgrid frequency reference closer to the utility grid frequency before reconnection. However, for example with P/f -droop controlled DER units re-synchronization requires the coordinated control of all DER units. This coordination should be done by an external central controller, e.g. microgrid management system or controller, which manages all the DG units during the synchronization process [30] [31].

Voltage imbalance due to asymmetrical loads and single-phase DG units affects the voltage phase difference across open microgrid interconnection CB so that the phase difference deviation can be different in phases A, B and C. This asymmetry between phases may also require to be reduced before microgrid re-synchronization.

Active components in the connection point of microgrid, such as microgrid interconnection switch, central energy storage unit and microgrid management system, are responsible for microgrid synchronized re-connection. In [32] it was proposed that synchronous island operation could be done using a reference signal with phase and frequency information to the microgrid master unit. The phase difference before re-synchronization should be within acceptable levels, e.g. less than 60° [32]. Based on [33], microgrid re-synchronizing function has to meet a more stringent requirement than the one defined by IEEE 1547 which requires that the phase difference between a microgrid and the utility grid needs to be smaller than 20° before closing the interconnection CB. In [34], LV microgrid re-synchronization was studied and different synchronized reconnection enabling functionalities were developed and simulated.

In the simulations [34] either

1. Master unit voltage phase angle or
2. Reactive power output of DG units was modified to enable synchronized reconnection and in addition also
3. Controllable single-phase loads were used in for phase asymmetry compensation at MV/LV distribution substation.

The simulation results in [34] showed that both re-synchronization functions

1) Voltage phase angle adjustment by master unit control and
2) DER unit reactive power feeding can be utilized to enable successful LV microgrid re-synchronization.

However, the voltage phase difference deviation or asymmetry between phases A, B and C across microgrid interconnection switch still existed with these re-synchronization functions. If this phase difference deviation is too large, it must be compensated before LV microgrid re-synchronization. In simulations of [34] this phase difference deviation was well corrected by the connection of resistive or capacitive single-phase loads at MV/LV distribution substation. However, quite large frequency and voltage oscillations after the connection of single-phase capacitive loads were detected when compared to the connection of purely resistive loads.

In general, the simulation results of [34] clearly showed that re-synchronization is not necessarily a significant issue with small, e.g. less than 10°, phase difference across microgrid interconnection CB when only the converter-based

DER units are connected to microgrid. Reason for this was that phase-locked-loop (PLL) component will draw grid-following/-supporting converters into phase with the utility grid frequency after re-connection. On the other hand, with directly connected synchronous generators even small phase difference across interconnection CB during re-synchronization was found to be challenging. Therefore, re-synchronization functions for minimizing phase angle difference and possibly also voltage unbalance before LV microgrid reconnection will be needed and in practice these functions should be coordinated by microgrid central controller or management system [4].

19.2.6 Circuit breaker technology

The circuit breaker (CB) technology for AC power systems has been well-developed over years and variety of CB and switching technologies are available nowadays. AC circuit breakers range from miniature circuit breakers (MCB), moulded case circuit breakers (MCCB) and air circuit breaker (ACB) for low voltage levels up to 600 V, these devices include relays and CBs combined in one physical device. For medium voltage (MV) applications mechanical CBs are available using mostly vacuum and SF6 as arc extinguishing medium and spring, pneumatic, hydraulic, and electromagnetic mechanisms for electrode separation to interrupt the circuit. Most of the MV mechanical circuit breakers operate within 3−5 cycles of supply voltage after getting trip command from protection relays. However, some efforts have been made to still decrease the time of MV mechanical circuit breaker operation by developing new breaker prototypes using combination of Thomson coil actuator and permanent magnet actuators which give one cycle interruption for the largest current duty of T100a, but it is expensive solution. The other prototype using Thomson coil actuator and spring mechanism reduced the normal trip time delay of vacuum circuit breaker (VCB) from 15 ms to 13.5−14 ms [35]. AC solid state circuit breakers (AC-SSCB) provide the faster tripping response compared with mechanical circuit breakers. AC-SSCB can be classified into two broad categories: Non-current-limiting and current limiting types. Non-current limiting AC-SSCBs are constructed using inverse parallel SCRs (Silicon controlled rectifiers) and current limiting AC-SSCBs are constructed using faster power semiconductors switches like IGBTs (insulated gate bipolar transistors) and IGCTs (integrated gate-commutated thyristors). Non-current limiting SCR based AC-SSCBs can be compatible with traditional protection coordination with downstream breakers or fuses and offer advantages like silent operations, long life and half-cycle tripping response. However, for the worst case asymmetrical fault currents of 200kA peak for 85kA rms current, SCRs should be protected by fuses. On the other hand, current limiting AC-SSCBs result in higher power losses than non-current limiting AC-SSCBs and can be problematic for the protection coordination of traditional systems even if a few of these breakers are connected in the system. Therefore, entire protection schemes need to be designed based on only current limiting AC-SSCBs, this may be well suited to microgrids with only the converter-based DERs. Current limiting AC-SSCBs have many design challenges like employing suitable snubbers, metal-oxide varistors (MOVs) and dynamic breaking resistors for energy dissipation and voltage limiting during interruption as well as capability to differentiate between a fault current and load transients to avoid false trips [36].

19.3 Conventional protections for AC microgrids

Conventional protection of microgrids is usually based on overcurrent principle using either definite-time or inverse definite OC relays. In addition, voltage-based (over/under voltage) and frequency-based (over/under frequency) protections are also used for the protection of DERs, for detection of islanding situation or for load-frequency control in microgrids. However, only overcurrent protection schemes are discussed is this section.

19.3.1 Overcurrent protection (Definite-time vs Inverse time)

The most common protection scheme used in traditional distribution systems is based on overcurrent principle. Both definite-time and inverse-time (IDMT) OC relays are used in a coordinated manner so that interruption should be limited to only faulty section. For both static and microprocessor-based relays the working time of OC relays is decided based on two details: CB opening time (0.04-0.1 s) and security factor (0.12-0.22 s). In this way total time of OC relay operations is in the range of 0.2-0.4 s [18]. For definite-time OC relays only pickup current (I_P), CB opening time and security factor are required to decide the total operating time of primary and backup relays. However, for IDMT OC relays the relay operating time is decided based on different relay characteristics defined by Eq.1 according to IEC 255-3 [37]:

$$t = \frac{k\,a}{(\frac{I}{I_P})^{b-1}} \qquad (1)$$

where t is the relay operating time, k is the time dial setting (TDS), I is the current detected by relay, I_P is the pickup current and a, b are the constants defining relay characteristics.

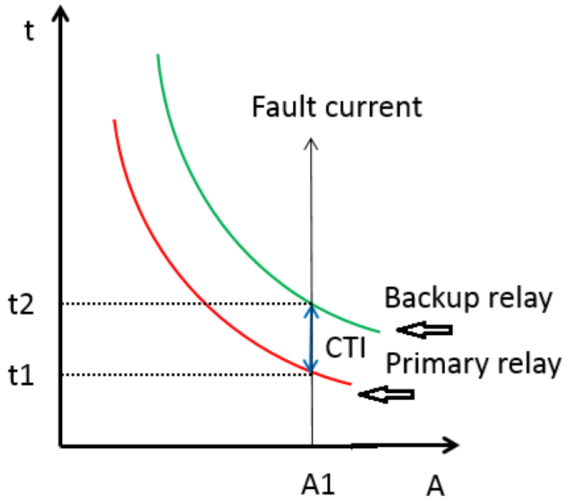

Figure 19.3 Time current characteristics curve of primary and backup inverse-time OC relays

Mainly two sets of standard inverse-time relay characteristics are applied, IEC and ANSI (in USA). Additionally, relays may include options to have some manufacturer specific characteristics or even freely programmable characteristics. It means based on types of characteristics curve (inverse, very inverse, extremely inverse etc.) different relay manufacturers may have different/additional constants for inverse-time OC relay characteristics [38] in addition to the standard IEC or ANSI constants. Generally, the settings of inverse-time OC relays should be adjusted so that there is always some coordination time interval (CTI) between primary and backup relay to ensure correct selective operation. Fig. 19.3 shows the time current characteristic curves for primary and backup inverse-time OC relays. For fault current of magnitude A1 (Fig. 19.3) primary relay will operate first at time t1 and if primary relay fails to operate than backup relay will operate at time t2 which is equal to t1+CTI. If adequate CTI (0.2-0.3 s) is not ensured, then nuisance trips may happen. For a given current, the higher the TDS is the greater the time to tripping contact closure is. Since TDS provides up and down adjustment of inverse-time OC relay characteristics and pickup current provides left and right adjustment of characteristics on the coordination plots, therefore proper CTI can be established through proper selection of TDS and I_P values [18].

The coordination practice of using definite-time characteristics or inverse-time characteristics vary between Europe/Japan and North America. In Europe and Japan it is common that primary distribution systems are operated as impedance grounded or ungrounded three-wire systems and hence no presence of single-phase laterals protected by fuses. Therefore, relay coordination can be achieved using definite-time characteristics. In North America, the usual practice is to operate grounded four-wire distribution systems with loads served by single-phase laterals protected by fuses. Therefore, coordination is done using inverse-time current characteristics which is suitable for fuse coordination [39]. However, in this section both definite-time and inverse-time coordination characteristics are used and the performance of both is compared for traditional three-phase distribution system operation without DERs, for grid-connected operation of AC microgrid with DERs and for islanded mode operation of AC microgrid with DERs and central battery energy storage system (BESS). The single-line diagrams of the grid-connected AC microgrid (Fig. 19.4) and islanded AC microgrid (Fig. 19.5) are used to verify the coordination of OC relays at CB1, CB2, CB6, CB7 and CB8 locations for three-phase short-circuit faults F1, F6 and F8 as explained in the following subsections.

The circuit breakers CB1-CB9 in Fig. 19.4 are operated by corresponding OC relays (OCR1-9) for faults in corresponding zones (zone1-9), and therefore OC relay-1 (OCR-1) means the relay at CB1 location and so on. Definite-time coordination starts from the relay OCR-8 at the extreme load end which is set to trip instantaneously after 0.04 s of the fault. OCR-7 is set to trip after 0.2 s of the fault, OCR-6 is set to trip after 0.4 s of the fault, OCR-2 is set to trip after 0.6 s of the fault and OCR-1 is set to trip after 0.8 s of the fault. The pickup current setting of each relay (OCR1-2 and OCR6-8) is set at 2.25 p.u. of maximum current a relay can experience during normal operation without DERs (Wind turbine and photovoltaic). For inverse-time current coordination, the same type of relay characteristic is chosen for all inverse-time OCRs (inverse-time OCR1-2, OCR6-8) which is very inverse characteristic with constants of relays a =13.5 and b = 1 (Eq. (1)).

The selected values of TDS for inverse-time OCRs are 0.05, 0.15, 0.25, 0.28 and 0.29 for OCR8, OCR7, OCR6, OCR2 and OCR1 respectively, in order to ensure a proper coordination of relays. The pickup current for each inverse-time OCR is chosen to be the same as chosen for definite-time OCRs which is 2.25 p.u. of maximum current a relay can experience during normal operation without DERs. The performance of definite-time and inverse-time OCRs with regard to the speed of operation and selectivity for three different operational modes is analysed in the following subsections. It is worth here mentioning that the settings of both definite-time and inverse-time OCRs is kept the same in all three modes to observe the issues in different modes when single-settings OCRs are used. The real-time modelling of relays and other components is done by using Matlab/Simulink and RT-Lab software of OPAL-RT.

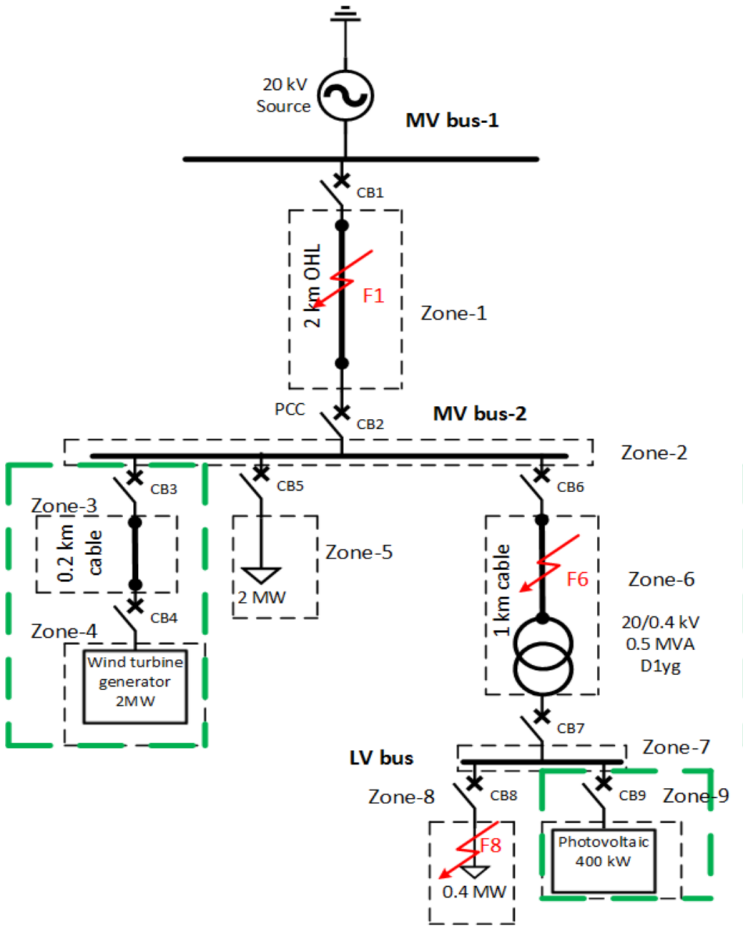

Figure 19.4 Grid-connected mode of AC Microgrid with single setting OC relay protection

19.3.1.1 Protection coordination in grid-connected mode without DERs

In this subsection, the protection coordination of definite-time OCRs and inverse-time OCRs with very inverse characteristic is analysed for the grid-connected mode of AC microgrid without DERs. It means, in this subsection the coordination of OCRs in path CB1-2-6-7-8 is observed without considering green zones in Fig. 19.4. This makes the system of Fig. 19.4 a traditional MV/LV distribution system protected by OCRs. A three-phase permanent short-circuit fault is applied separately at locations F1, F6 and F8 ($R_{F1} = R_{F6} = 5.001$ Ohm, $R_{F8} = 0.001$ Ohm) for a duration of 18 s (starting from 2s to 20 s in simulations) and tripping time of primary and backup OCRs was noted for both very inverse-time and definite-time characteristics. During fault F1 only tripping time of primary protection can be observed. Tab- 19.1 presents the tripping time durations (t_{op}) for primary and backup relays for the faults F1, F6 and F8. The CTI values in Tab- 19.1 (given in brackets) in columns 4 and 5 indicate the coordination time intervals between primary and backup-1 OCRs, between backup-1 and backup-2 OCRs and between backup-2 and backup-3 OCRs. Also, fault currents in per unit (p.u.) of rated current at corresponding OCRs in every fault case is given. During three-phase short-circuit fault F1, the tripping of primary inverse-time OCR1 is much faster than definite-time OCR1 because inverse-time OCR1 trips after 0.6843 s of the fault F1 whereas definite-time OCR1 trips after 0.8 s of the fault F1. During fault F6 also, primary inverse-time OCR6 trips

faster in 0.0732 s compared with primary definite-time OCR6 which trips in 0.4 s. In order to observe the tripping times of backup-1 OCR2 and backup-2 OCR1 protections of primary OCR6 during fault F6, the tripping of CB6 and CB2 was disabled to simulate breaker failures. It is observed that backup-1 inverse-time OCR2 and backup-2 inverse-time OCR1 of inverse-time OCR6 also trip faster than backup-1 definite-time OCR2 and backup-2 definite-time OCR1 of definite-time OCR6 while maintaining a good CTI of 0.2638 s between primary and backup-1 and CTI of 0.428 s between backup-1 and backup-2 during fault F6. However, during fault F8 not only the primary inverse-time OCR8 is slower than the primary definite-time OCR8, but also all backup inverse-time OCRs are slower than backup definite-time OCRs. The CTI between primary inverse-time OCR8 and backup-1 inverse-time OCR7 is 0.2757 s and CTI between backup-1 inverse-time OCR7 and backup-2 inverse-time OCR6 is 0.3062 s which are longer than the corresponding CTIs of 0.16s and 0.2 s of definite-time OCRs during fault F8. It can be observed from Tab-19.1, that backup-3 inverse-time OCR2 operates considerably slower (t_{op} =6.9592 s) than backup-3 definite-time OCR2 (t_{op} =0.6 s) due to reduced fault current of 3.45 p.u. at OCR2 during the fault F8. It is also observed that due to very low fault current (1.65 p.u.) at OCR1 during 18 s of fault F8, neither inverse-time OCR1 nor definite-time OCR1 provide backup-4 for OCR8 due to higher pickup current settings. Therefore, during fault F8 limited selective coordination only up to OCR2 is possible. In conclusion for this case, inverse-time OCRs provide faster tripping times while maintaining good coordination between primary and backup relays during faults F1 and F6. However, during fault F8 inverse-time OCRs are much slower and provide lesser coordination compared with definite-time OCRs during fault F8. So during fault F8 only definite-time OCRs provide faster tripping times and good selective coordination.

TABLE-19.1 Protection coordination in grid-connected mode without DERs (No green zones, 3,4 and 9)

Fault (duration)	Relay No.	Primary/Backup	Very inverse-time t_{op} (CTI)	Definite-time t_{op} (CTI)	Fault current at relay (p.u.)
F1 (18 s)	OCR1	Primary	0.6843	0.8	19.9
F6 (18 s)	OCR6	Primary	0.0732	0.4	159
	OCR2	Backup-1	0.337 (CTI_{6-2} = 0.2638 s)	0.6 (CTI_{6-2} = 0.2 s)	27.48
	OCR1	Backup-2	0.765 (CTI_{2-1} = 0.428 s)	0.8 (CTI_{2-1} = 0.2 s)	18.11
F8 (18 s)	OCR8	Primary	0.1368	0.04	19.72
	OCR7	Backup-1	0.4125 (CTI_{8-7} = 0.2757 s)	0.2 (CTI_{8-7} = 0.16 s)	19.72
	OCR6	Backup-2	0.7187 (CTI_{7-6} = 0.3062 s)	0.4 (CTI_{7-6} = 0.2 s)	19.05
	OCR2	Backup-3	6.9592 (CTI_{6-2} = 6.2405 s)	0.6 (CTI_{6-2} = 0.2 s)	3.45
	OCR1	Backup-4	No trip in 18 s	No trip in 18 s	1.65

19.3.1.2 Protection coordination in grid-connected mode with DERs

In this subsection, the protection coordination of definite-time OCRs and inverse-time OCRs with very inverse characteristic is analysed for the grid-connected mode of AC microgrid with the converter-based DERs. It means in this section the coordination of OCRs in path CB1-2-6-7-8 is observed with green zones of DERs (Zones 3,4 and 9) also included (Fig 19.4). This makes the section below PCC breaker CB2 in Fig 19.4 as a grid-connected AC microgrid with DERs (when CB1-2 closed) where a wind turbine DER is connected at 20 kV MV bus-2 and photovoltaic DER is connected at 0.4 kV LV bus. The main purpose of this case study is to observe how the speed and selectivity of inverse-time OCRs are affected after the connection of DERs. It should be noted here that both DERs (wind turbine and photovoltaic systems) provide FRT capability, means no trip until fault is cleared and provide 1.2 p.u. of rated current during faults when voltage is below 0.5 p.u. Fault types and durations in this case are the same as mentioned in previous subsection 19.3.1.1 and performance of inverse-time and definite-time OCRs is observed in terms of speed and selectivity. In addition to tripping times, CTI and fault currents of OCRs, DERs fault contribution and DERs terminal voltage at connection point are also noted in this case (Tab- 19.2). During fault F1 primary inverse-time OCR1 operates faster at t_{op} = 0.7068 s than primary definite-time OCR1 which operates at t_{op} = 0.8 s. However, due to reduced fault current experienced by inverse-time OCR1 in this case, its tripping time is 22.5 ms slower than it was in the previous case without DERs (Subsection 19.3.1.1). During fault F6, primary inverse-time OCR6 operates at the same time (t_{op} = 0.0732 s) as it operated during the same fault in the previous case without DERs (Subsection 19.3.1.1) even if the fault current at OCR6 has been reduced by 10 p.u.(from 159 p.u. to 149 p.u.) after the connection of DERs. However, backup-1 inverse-time OCR2 and backup-2 inverse-time OCR-1 are observed with 11 ms and 26.7 ms slower tripping responses respectively during fault F6 compared with the same fault in the previous case without DERs (Subsection 19.3.1.1) due to comparatively reduced fault currents. However, still faster tripping times and good CTI is observed for primary and backup inverse-time OCRs compared with definite-time OCRs during faults F1 and F6. During fault F8, primary inverse-time OCR8 operates slower than primary definite-time OCR8, but its tripping time is faster compared with inverse-time OCR8 in the previous case without DERs (Subsection 19.3.1.1) due to increased fault current observed at OCR8 because some fault current contribution comes from photovoltaic DER in this case.

Whereas backup-1 inverse-time OCR7, backup-2 inverse-time OCR6 and backup-3 inverse-time OCR2 are slower compared with backup-1 definite-time OCR7, backup-2 definite-time OCR6 and backup-3 definite-time OCR3 during fault F8 in this case. However, backup-1 inverse-time OCR7 and backup-2 inverse-time OCR6 have nearly the same tripping times during fault F8 in this case (Tab-19.2) compared with tripping times during the same fault in the previous case without DERs (Tab-19.1) even if the fault current seen at both OCRs is somehow reduced in this case after DER connections (Tab. 19.2). The tripping time of backup-3 inverse-time OCR2 during fault F8 has also increased from t_{op} = 6.9592 s in the previous case without DERs (Tab-19.1) to t_{op} = 8.5675 s in this case due to comparatively reduced fault current seen by OCR2 (Tab-19.2). It is also observed that due to very low fault current of 1.0851 p.u. at OCR1 during fault F8 (Tab-19.2), neither inverse-time OCR1 nor definite-time OCR1 provide backup-4 for OCR8 during fault F8 in this case with DER connections. Therefore, like the previous case (Subsection 19.3.1.1) in this case also a limited selective coordination only up to OCR2 is possible during fault F8. In conclusion for this case, inverse-time OCRs provide faster tripping times compared with definite-time OCRs while maintaining good coordination between primary and backup relays during faults F1 and F6. However, during fault F8 inverse-time OCRs are much slower and provide lesser coordination compared with definite-time OCRs during fault F8. So during fault F8 only definite-time OCRs provide faster tripping times and good selective coordination. Comparing this case with DERs to previous case without DERs, it can be said that the inclusion of DERs somehow make inverse-time OCRs slower due to reduced fault current contribution from the main grid. Some inverse-time relays e.g., OCR8 sense increased fault current due to DER connection and operate faster as compared to their operation without DERs. Definite-time OCRs show the same performance for the grid-connected mode with DERs and without DERs.

TABLE-19.2 Protection coordination in grid-connected mode with DERs (Green zones included)

Fault (duration)	Relay No.	Primary/Backup zone	Very inverse-time t_{op} (CTI)	Definite-time t_{op} (CTI)	Fault current at relay (p.u.)	DERs fault contribution
F1 (18 s)	OCR1	Primary	0.7068	0.8	14.6	$I_{F,\,pv,\,wtg} \leq 1.0$ p.u. ($U_{pv,wtg} = 0.9$ p.u.)
F6 (18 s)	OCR6	Primary	0.0732	0.4	149	$I_{F,wtg} \leq 1.04$ p.u. $I_{F,pv} \leq 1.01$ p.u. ($U_{wtg} = 0.872$ p.u.) ($U_{pv} = 0.837$ p.u.)
	OCR2	Backup-1	0.348 ($CTI_{6\text{-}2}$ =0.2748 s)	0.6 ($CTI_{6\text{-}2}$ = 0.2 s)	26.74	
	OCR1	Backup-2	0.7917 ($CTI_{2\text{-}1}$ =0.4437 s)	0.8 ($CTI_{2\text{-}1}$ = 0.2 s)	13.31	
F8 (18 s)	OCR8	Primary	0.1277	0.04	20.89	$I_{F,pv} = 1.17$ p.u., ($U_{pv} < 0.5$ p.u.) $I_{F,wtg} \leq 1.0$ p.u. ($U_{wtg} \leq 1.0$ p.u.)
	OCR7	Backup-1	0.412 ($CTI_{8\text{-}7}$ = 0.2843 s)	0.2 ($CTI_{8\text{-}7}$ = 0.16 s)	18.095	
	OCR6	Backup-2	0.7175 ($CTI_{7\text{-}6}$ = 0.3055 s)	0.4 ($CTI_{7\text{-}6}$ = 0.2 s)	17.806	
	OCR2	Backup-3	8.5675 ($CTI_{6\text{-}2}$ = 7.85 s)	0.6 ($CTI_{6\text{-}2}$ = 0.2 s)	3.215	
	OCR1	Backup-4	No trip in 18 s	No trip in 18 s	1.0851	

19.3.1.3 Protection coordination in islanded mode with DERs and BESS

In this subsection, the protection coordination of definite-time OCRs and inverse-time OCRs with very inverse characteristic is analysed for the islanded mode of AC microgrid with DERs and BESS (battery energy storage system). In this case islanding is created by opening CB2 assuming that fault F1 had happened earlier in time and OCR1 had tripped CB1 and transfer tripped CB2 within next 0.5-0.8 s. Then 2.4 MW BESS has been activated quickly as a grid-forming DER after closing CB10. An islanded AC microgrid with BESS, DERs and single-settings OCRs is shown in Fig. 19.5. It is assumed that BESS is provided with a converter of higher current rating (≥ 3 p.u.) and BESS can act as fault current source during any fault in islanded mode. Such battery converters are installed in Bronsbergen microgrid, Netherlands which have the continuous current of 290 A and provide fault current of 1100 A [40] Such fault current sources can provide fault current up to 5 s [41]. A fault current source using energy storage devices like a flywheel, a battery or ultracapacitor is proposed in [40][41] which is a modular system and multiple units can be connected in parallel to suit the local fault level. In this case it is studied that if such type of fault current source is provided at PCC then how it serves the purpose of achieving faster tripping times and maintaining protection coordination in the islanded mode.

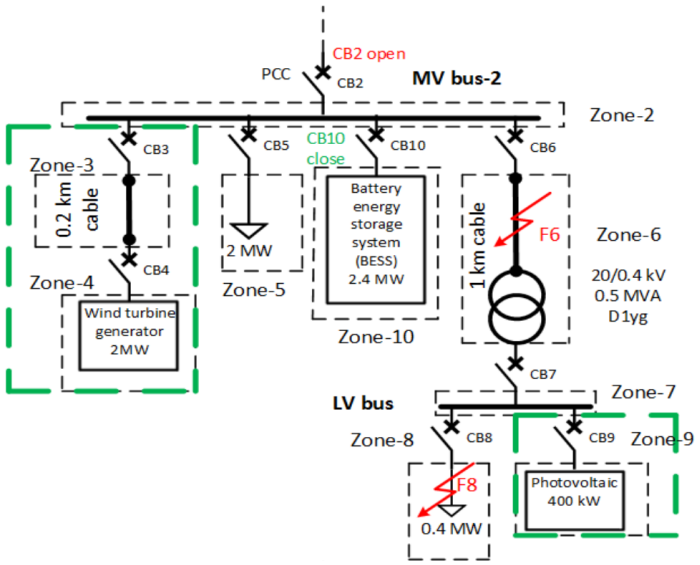

Figure 19.5 Islanded mode of AC Microgrid with single setting OC relay protection

In this subsection, the coordination of OCRs in path CB6-7-8 is observed with the green zones of DERs (Zone 3,4 and 9) and BESS zone (Zone10) included (Fig. 19.5). In this case the performance of OCRs has been observed for three-phase permanent short-circuit faults F6 and F8 (R_{F6} = 5.001 Ohm, R_{F8} = 0.001 Ohm) applied separately for a duration of 14 s (starting from 6s to 20 s) and relay tripping times are noted for different primary and backup OCRs in path CB6-7-8. All DERs and BESS have FRT capability during faults, and they provide fault current until the fault is cleared. During fault F6 in islanded mode, primary inverse-time OCR6 trips after 0.6163 s of fault which is 0.2163 s slower than primary definite-time OCR-6 which trips after 0.4 s of the fault F6. The OCR6 experiences 20.3 p.u. of fault current during fault F6 and all DERs including BESS provide maximum fault current contribution during this fault (Tab- 19.3). As compared to trip times in previous two grid-connected mode cases (Subsections 19.3.1.1 and 19.3.1.2), tripping time of primary inverse-time OCR6 during fault F6 in this case is 0.5431 s slower than tripping time of the same inverse-time OCR6 in previous two grid-connected cases (Tab-19.1 and 19.2). However, tripping time of primary definite-time OCR6 during fault F6 in this case is the same as in previous two grid-connected mode cases. During fault F8 in islanded mode, primary inverse-time OCR8 trips at 0.1977 s which is much slower than the tripping time of 0.04 s of primary definite-time OCR8. It means primary inverse-time OCR8 is 0.1577 s slower than primary definite-time OCR8 during fault F8 in islanded mode. Compared with trip times of primary inverse-time OCR8 in previous grid-connected mode cases (Subsections 19.3.1.1 and 19.3.1.2) tripping time of primary inverse-time OCR8 is 0.061-0.07 s slower during fault F8 in islanded mode. The tripping times of backup-1 inverse-time OCR7 and backup-2 inverse-time OCR6 are also slower than tripping times of backup-1 definite-time OCR7 and backup-2 definite-time OCR6, respectively during fault F8 in this case. Compared with the previous grid-connected case without DERs (Subsection 19.3.1.1), the tripping times of backup-1 inverse-time OCR7 and backup-2 inverse-time OCR6 are 0.3485-0.6423 s slower during fault F8 in islanded mode. When compared with the previous grid-connected case with DERs (Subsection 19.3.1.2), the tripping times of backup-1 inverse-time OCR7 and backup-2 inverse-time OCR6 in islanded mode are also 0.349-0.6435 s slower during fault F8 in islanded mode. In conclusion to this islanded mode case, primary and backup definite-time OCRs provide faster tripping times and maintain good protection coordination during faults F6 and F8 compared with primary and backup inverse-time OCRs during the same faults. The primary inverse-time OCR8 tripping time during fault F8 in islanded mode is acceptable. However, tripping times of primary inverse-time OCR6 during fault F6, and backup-1 inverse-time OCR7 and backup-2 inverse-time OCR6 during fault F8 in islanded mode are quite slow. Therefore, slower fault clearance at LV load with inverse-time OCRs can potentially damage the load if a fault current source is connected in islanded mode. Hence, for the islanded mode of operation definite-time OCRs perform better with faster tripping times and good CTI between primary and backup protection as compared to inverse-time OCRs which become slower to operate with increased CTI between primary and backup protection.

It should be noted here that in both the grid-connected mode with DERs and the islanded mode of AC microgrid (cases 19.3.1.2 and 19.3.1.3) during fault F6 if primary OCR6 trips CB6 then it should transfer trip CB7 for complete F6 fault clearance, otherwise photovoltaic DER may still feed the fault in the reverse direction. The second method is to trip photovoltaic DER after fault F6 is cleared by OCR6 by anti-islanding protection. The

conventional method is to trip all DERs immediately after the fault is detected inside the microgrid. This conventional method reduces the reliability of supply to load. The other case of islanding can be the creation of islands within islanded mode after fault F6 is cleared by tripping CB6 and CB7. In this case both LV bus and MV bus-2 sections will be isolated and in this case it will be very difficult to clear the fault F8 in the islanded LV bus section with only fault contribution from photovoltaic DER. In this situation, lower adaptive trip settings will be required even for definite-time OCR8. Adaptive protection of microgrid is discussed in Section 19. 4.

TABLE-19.3 Protection coordination in islanded mode with DERs (Green zones included) and BESS as grid-forming source

Fault (duration)	Relay No.	Primary/Back up zone	Very inverse-time t_{op} (CTI)	Definite-time t_{op} (CTI)	Fault current at relay (p.u.)	DERs fault contribution
F6 (14 s)	OCR6	Primary	0.6163	0.4	20.3	$I_{F,wtg}$ = 1.2 p.u., $I_{F,pv}$ =1.17 p.u. $U_{pv,\ wtg}$ < 0.12 p.u. $I_{F,BESS}$ = 3.17 p.u. U_{BESS} < 0.12 p.u.
F8 (14 s)	OCR8	Primary	0.1977	0.04	13.45	$I_{F,wtg}$ = 1.2 p.u. $I_{F,pv}$ = 1.17 p.u., U_{pv} < 0.1 p.u., U_{wtg} < 0.45 p.u. $I_{F,BESS}$=1.15p.u.,U_{BESS}≤0.5 p.u.
	OCR7	Backup-1	0.761(CTI_{8-7}=0.563 s)	0.2 (CTI_{8-7} = 0.16 s)	11.25	
	OCR6	Backup-2	1.361 (CTI_{7-6} = 0.6 s)	0.4 (CTI_{7-6} = 0.2 s)	11.12	

19.4 Adaptive protection for AC microgrids

As discussed in previous sections microgrids can operate in both the grid-connected and islanded mode. For the grid-connected mode, sufficient fault current is available from the main grid in order to trip OCRs in case of any fault inside microgrid. However, in islanded mode of operation only limited fault current contribution from local DERs is available which is not sufficient for the proper operation of OCRs inside microgrid. The reduction of fault current contributions from DERs in islanded mode requires lower pickup currents for OCRs. If the OCRs designed with lower pickup values are used in both the grid-connected and islanded modes, then false operations will increase, and OCRs may even trip during switching transients and momentary overloads in the grid-connected mode. To overcome this OCR sensitivity problem two general solutions are available: (1) Connect some high fault current providing DERs inside microgrid in islanded mode and use OCRs with only grid-connected mode pickup settings in both modes (2) Use two different OCRs with different pickup settings, one for the grid-connected and other for the islanded mode. First solutions can be useful at some degree if a large number of synchronous generators are available inside microgrid. If a large number of the converter-based DERs inside microgrid are available, then the second solution is the most favourite choice. However, in order to implement different OCRs with different settings for the grid-connected and islanded modes, OCRs will need to be alternatively activated and deactivated or their logic or settings changed after knowing the present mode of operation for the correct detection of the faults and avoiding false operations. The information about microgrid mode is usually in terms of open or close status signals from circuit breakers, particularly breakers at connection point of the main grid and microgrid. The adaptive protection can be implemented with a central controller or in an autonomous/decentralized manner after getting microgrid mode information. It is obvious that communication based adaptive protections will be quick and dynamic, however delays in data transmission, reception and processing and failures of communication links also require non-communication based adaptive protections.

19.4.1 Communication-based adaptive protection

Communication-based adaptive protections can be broadly classified into two categories: (1) Centralized adaptive protections (2) Decentralized (autonomous) adaptive protections. Centralized and decentralized adaptive protections are explained separately in the following subsections.

19.4.1.1 Centralized adaptive protection

The centralized communication-based adaptive protection is the conventional approach in which centralized control architecture is used. In this method, a central controller adapts the protection settings in a coordinated manner after collecting information about the system changes at one central location. This method requires a very powerful central controller which can save, process and communicate data with other components or systems. The centralized controller reduces the computation burden on individual devices and therefore simple devices can be installed for protection and control purposes. However, this method has one drawback that if the central controller fails, it causes a complete loss of adaptive protection and hence a redundant central controller is must for increased reliability. Various communication protocols like Modbus, DNP3, IEC 60870-5-101/104, IEC 61850 support the

centralized communication architecture and its implementation can be done using serial/bus communication, over PLC (power-line carrier) or via Ethernet network [42].

19.4.1.2 Decentralized adaptive protection

The decentralized communication-based adaptive protection uses distributed intelligent electronic devices (IEDs) or multi-agent systems. Each IED acts in an autonomous way after getting information from other IED to modify its active setting group. The decentralized adaptive protection reduces the burden on the central controller, however IEDs with increased data storage capacity, more computational and processing power will be needed in addition to fast and reliable communication links between IEDs. The feasibility of decentralized architecture is only possible if direct communication between IEDs is allowed by the communication protocol. Presently, the focus of industry is mainly on IEC 61850 as the standard protocol for horizontal communication between IEDs. Although a bus or Ethernet network is required to implement the decentralized architecture, but 4G/5G wireless network or PLC can be the other useful options for its implementation [42]. The IEC 61850 communication standard is getting popular for application in electric power substation automation. The IEC 61850 standard offers the possibility that IEDs of different manufacturers can interoperate or interact with each other. This standard is initially focused on communication between IEDs within single substation but can be extended for communication between various substations in the future. The IEC 61850 standard provides a set of standard model structures for data and rules defining how to exchange these data. The IEDs from different manufacturers that comply with these model definitions can then communicate, understand, and interact with each other [43]. The IEC 61850 communication standard, by one common protocol, enables the integration of several functions including protection, control, measurement, and monitoring etc. [44].

19.4.2 Review of communication-based protection schemes for AC microgrids

In the literature, several solutions have been suggested for the protection of islanded microgrids. Some main solutions are reviewed in the following.

19.4.2.1 Directional overcurrent protection

Directional overcurrent protection can be used to protect the distribution system with bi-directional current flow. One problem with the overcurrent protection is that faults closer to the source might take a longer time to clear. However, this problem can be overcome with modern microprocessor-based devices, by having shorter coordination margin, and instantaneous over-current protection. Still, there could be protection co-ordination issues because of changing fault current due to DER or change in the network configuration. An advanced solution could be adaptive directional over-current protection based on the status of the generators and networks' topology.

Adaptive Directional Overcurrent Protection

In adaptive protection, relays still carry out the protection function using local measurements. However, their settings are updated locally or remotely via communication links. Apart from the additional voltage transformer (VT) and microprocessor-based relays, this scheme may also require a central controller and a communication link to the relays; but this communication does not need to be very fast nor very reliable.

In the solution of [45], relays detect the islanding condition themselves and reconfigure their neighbours if they detect a topology change [46]. Paper [45] suggests local information utilizing adaptive protection to handle the overcurrent protection challenges in the distribution network with DG. The settings of the relays are updated based on monitoring the operating states (grid connected or island) and detected faulted section. In [45] it is proposed that the faulted section detection could be done by using time overcurrent characteristics of the protective relays. The adaptive feature was also proposed in [3] for the protection of microgrids; where directional overcurrent relays are reconfigured by a remote central unit in case of grid separation (islanding) or grid reconnection to consider for the change of short-circuit level. The central unit is constantly aware of the network topology and the connected generators [46]. Paper [47] has also presented an adaptive protection scheme for distribution networks which consists of multiple DG units. According to real-time monitoring of the state and topology of the distribution network, the active setting groups (Figure 19.6) of the protection relays are adjusted. A programmable logic application is called at central controller to perform adjustments after changes in circuit breaker (CB) status (Figure 19.6). A controller which is centralized is integrated to the substation with IEC 61850 based communications to

execute the control functions. The programmable logic in this central controller (substation computer or RTU) is used to modify the settings with IEC 61131-3 compatible programming languages. The adaptive protection scheme presented in paper [47] together with microgrid control system has also been developed and adapted for a real demonstration at Hailuoto island in Finland [48].

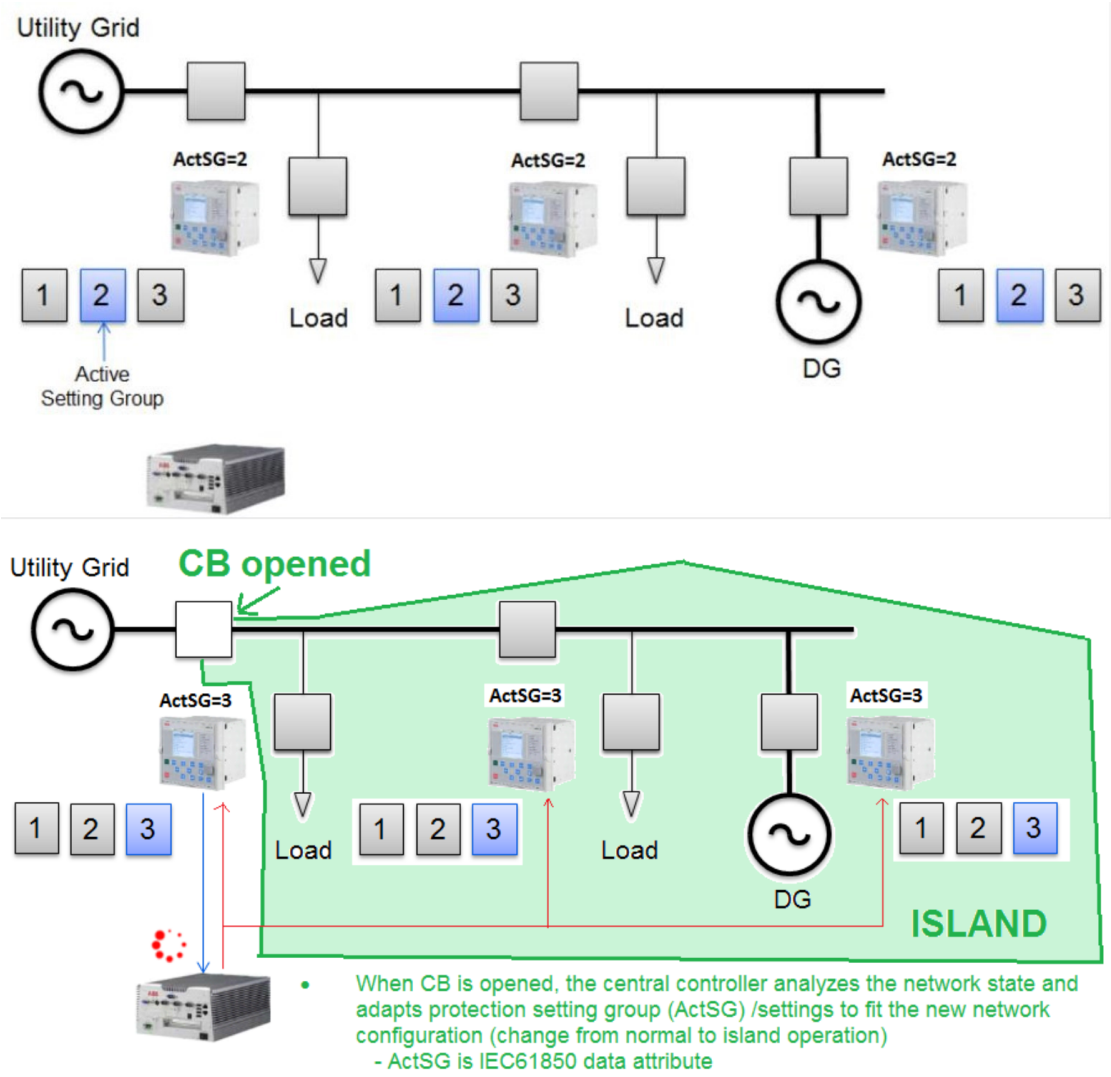

Figure 19.6. Adaptive protection by change of IED setting group.

Based on the literature, it has been stated in [49] that the major challenges related to the implementation of an adaptive protection system can be:

- The requirement for communication infrastructure
- The requirement for previous knowledge about all possible microgrid configurations
- The requirement to update or upgrade large amount of protection devices (e.g. fuses) which are currently used in the distribution networks (especially on LV network)

19.4.2.2 Current symmetrical components based protection

Protection scheme proposals based on current symmetrical components try to enhance the performance of traditional overcurrent protection [49]. For example, in [50], it was suggested that fault detection in islanded

microgrids could be based on current symmetrical components. In [50] it was proposed to utilize in the event of an upstream phase-to-earth fault zero-sequence current detection (coordinated with unbalanced loads) and negative sequence current for phase-to-phase faults. In [51], a pilot instantaneous overcurrent protection scheme was briefly presented to perform instantaneous protection of a local line and remote bus-bar independent of the DG unit location. In [52], a three-level, communication-based protection selectivity scheme was proposed to be applied with voltage-restrained directional overcurrent protection. In [53], a fault current magnitude independent strategy for protection in LV microgrids with microprocessor-based overcurrent relays and directional elements, was suggested considering both operation modes (grid-connected and islanded).

19.4.2.3 Distance protection

Distance protection uses measured impedance or admittance values to detect the fault. In reference [54], it has been stated that distance protection seems to be a potential protection scheme for island operated MV networks. On the other hand, papers [55]–[57] have proposed directional inverse time-based admittance protection (Inverse Time Admittance, ITA), for grid-connected and islanded operation. This means that it can operate both in forward and reverse faults, but the reach settings should be different in forward and reverse directions. In the paper [13], comparison of distance and directional overcurrent protection was done considering only 3-phase short circuit faults. It was concluded that distance protection could selectively separate faults in MV and LV networks. Further, based on the simulations and the analysis, it was stated that overcurrent protection cannot be used if fault current levels within the island are close to the maximum load current. Based on this distance protection could be more suitable for being used in island operation. However, when also two phase and earth faults are considered the viability of distance protection must be further studied [13].

19.4.2.4 Voltage based protection schemes

Due to lack of high fault currents, it has been proposed by [58], [59] that voltages could be used for protection of an islanded microgrid. For example, paper [59] proposed a method which was based on a voltage measurement comparison: the location where the lowest voltage level is measured is tripped [46]. However, it is difficult to realize selective microgrid protection during island operation with voltage or current relays alone [60]. In [9] the same authors as in [59] also proposed to use the total harmonic distortion (THD) of voltage to enhance the protection of microgrids with the inverter-based DG units during earth faults. After detection fault type based on the variation of the fundamental frequency (50 Hz), the voltage THD seen by different feeder protection relays was analysed to determine the faulted part of the network. To prevent the challenges of previous methods related to detecting the oscillation waveform of the voltage variation, instead of voltage magnitude, [61] suggested to use only the positive sequence voltage. In [62], it was stated that a distinction between three fault types is possible by only considering the positive/direct and negative/inverse sequence voltage components, without using the zero sequence/homopolar information. Reference [63] proposed the same type of method to detect the fault and faulted network part, based on a voltage measurement at busbar and its transformation from abc coordinates to dq coordinates. In [64], the reduction in system voltage has been also used to implement an under-voltage back-up protection scheme for current differential protection.

Main problems with voltage-based methodologies during island operation, based on [49], are:

- Small differences in voltage drop seen by the relays at both ends of short lines can lead to protection maloperation, due to reduced voltage gradient.
- Challenges with practical application of some of these methods and also with potentially required communication system, when large amount of DG units are present.
- Solution can be highly dependent on the network architecture as well as on the defined relay protection zone related to every DG unit.
- Challenges in high-impedance-fault (HIF) detection.

19.4.2.5 Current differential

In [64], line differential protection based on current measurements was chosen for the microgrid because it is non-sensitive to bidirectional power flows, changing fault current levels and amount of DG units. It is also stated that current differential protection offers the needed protection during both grid-connected and islanded operation and it

is not affected by a weak infeed. This means that current line differential protection is able to detect internal faults even without having any DG units connected. The use of differential protection for microgrids with low fault current level has been suggested also in [65]–[69] to protect inverter-dominated microgrids. However, differential protection might be expensive since protective devices must be placed on every line segment of the network. Therefore, [69] proposes to form protection zones consisting of several line segments.

In addition, it is worth mentioning that the topology of the sample network i.e., schematic diagram in [64] is chosen to be very well suited for differential protection also during island operation. In general, current differential protection is not very suitable for the protection of islanded part of the distribution network having a radial topology and many protection zones (i.e. for protection of 'last' protection zones with an open end/CB).

19.4.2.6 Protection based on voltage and directional overcurrent

In [62], a microgrid protection strategy based on voltage and current measurements was proposed in addition to a voltage-based protection scheme. Also, in [70]–[71], the use of voltage measurement based fault detection has been considered and a potential solution for small microgrids is presented in the form of voltage controlled overcurrent devices to enable the use of lower current threshold settings.

In addition, in references [54], [4], [11], [72]–[73] microgrid protection schemes based on the use of both voltage and directional overcurrent are analysed. However, these schemes are based on the utilization of high-speed communication for interlocking/blocking purposes to ensure selective operation of protection during island operation. In the following, these proposed schemes for LV and MV microgrids are presented.

19.4.3 Protection of LV AC microgrids

Different kind of protection methods and principles for microgrids have been proposed. One problem in some proposed solutions for LV microgrid protection is that their applicability is limited to microgrids with only converter-based DG units. Therefore, these solutions may overlook others e.g. requirements on the operational speed of protection to maintain the stability of LV microgrid with directly connected rotating machines after fault clearance. According to [4] key fundamental properties required from the future LV microgrid protection systems include,

i. Adaptivity,
ii. Utilization of fast standard-based communication (IEC 61850),
iii. Fast operation in deep voltage dips due to faults to maintain stability in healthy part of LV microgrid,
iv. Fast operation to fulfil needs of very sensitive customers,
v. Selective operation in faults of every kind and
vi. Unnecessary operation of protection devices (PDs) and disconnection of DER units must be avoided.

In the following, two different proposed protection schemes for LV microgrids based on the utilization of both voltage and current (with direction detection) are shortly presented and more details can be found from the references. The main difference of the proposed protection schemes is that the first one (Proposed LV Scheme 1) relies on the extensive use of high-speed communication and the other (Proposed LV Scheme 2) is not based on the use of communication.

19.4.3.1 Proposed LV microgrid protection scheme 1

In references [4], [11], [72]–[73], the following scheme for the protection of LV microgrids has been proposed. The main structural choices of the proposed LV microgrid protection system are summarized in Figure 19.7 showing the type of protection devices (PD 1-4). When the measurements of active and reactive power flow between the utility grid and the LV microgrid are needed during normal operation, then also current measurements need to be included in PD 1. However, from the proposed protection system point of view the current measurement at PD 1 is not necessarily needed. Properties of the examined LV microgrid e.g. type, number and location of fault current feeding DER units made it difficult to realize selective protection for PD 2s during island operation, which is only based on current or voltage relays. Therefore, the protection algorithm of PD 2s during the island operation of LV microgrid was chosen to be multi-criteria based where both voltage and current measurements have been utilized (Figure 19.7).

The protection of PD 2s should also be able to adapt to the present network configuration as well as to the current states of the DG units during island operation. This adaptation of settings and pick-up limits of PD 2s could be realized, for example, by microgrid management system (MMS) when the microgrid configuration changes. During island operation PD 1 is changed to be ready for re-synchronization of microgrid back to the utility grid which requires that phase voltages be measured from both sides of PD 1. The protection settings of PD 2s are changed to the ones needed in island operation. To avoid the malfunction of PD 2s, the protection settings of PD 2s are not changed from normal to island operation settings before all possible transients and oscillations in voltages, currents and frequency are stabilized after transition to island operation. MMS will also send the state changed from island to normal operation signals to PD 2s and PD 4s after successful re-connection back to the utility grid. From island operated microgrid power balance viewpoint, the role of MMS is also important. For example, after fault F2 at LV feeder the MMS must immediately, after operation of LV feeder protection (PD 2), send new set point values for those DGs or DER units which still are connected to the healthy part of the microgrid or disconnect the less critical customer loads.

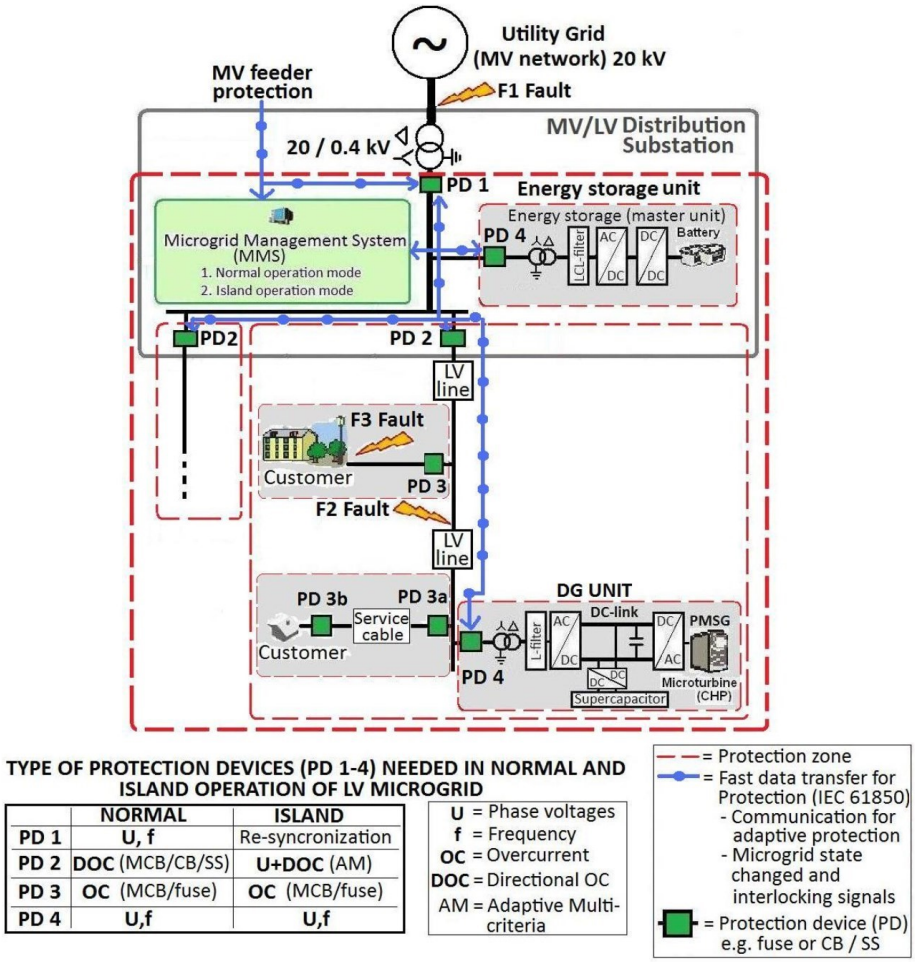

TYPE OF PROTECTION DEVICES (PD 1-4) NEEDED IN NORMAL AND ISLAND OPERATION OF LV MICROGRID

	NORMAL	ISLAND
PD 1	U, f	Re-syncronization
PD 2	DOC (MCB/CB/SS)	U+DOC (AM)
PD 3	OC (MCB/fuse)	OC (MCB/fuse)
PD 4	U,f	U,f

U = Phase voltages
f = Frequency
OC = Overcurrent
DOC = Directional OC
AM = Adaptive Multi-criteria

= Protection zone
= Fast data transfer for Protection (IEC 61850)
- Communication for adaptive protection
- Microgrid state changed and interlocking signals
= Protection device (PD) e.g. fuse or CB / SS

Figure 19.7. Number of protection zones and type of protection devices (PD 1-4) needed in normal and island operation of LV microgrid. [4], [11], [72]–[73].

During the islanded operation of a microgrid, possible oscillations due to sudden changes in the microgrid configuration need to be taken into account for the protection concept to achieve selective protection and to avoid the unnecessary tripping of protection. This could be done by using communication based interlocking signals. During islanded operation rapid communication is required for microgrid protection needs between protection devices (PD 1 and 2) as well as between master unit and DER units. MMS must also be able to communicate with all the other components and customer loads in the microgrid. Communication should preferably be based on commonly used standards like IEC 61850. Active microgrid components at the connection point of the microgrid (PD 1, master unit and MMS) are also responsible for microgrid re-synchronization. More information for example

about the functions needed for LV microgrid protection in the proposed scheme as well as details about the operation curves of PDs in the proposed LV microgrid protection system during grid-connected and islanded operation can be found in [4], [11]. It is enough from the proposed LV microgrid protection system point of view that the converter-based DER units will feed 2xI_n active current (I_n is nominal current) during faults in LV microgrid for the required FRT time defined by the operation curves of different PDs.

19.4.3.2 Proposed LV microgrid protection scheme 2

In [15] and [74], strategies for the coordination of protective devices, in typical radial distribution networks with DER, were proposed. Expanding on the idea presented in [15], in [53] and [74] protection strategies based on microprocessor-based relays for LV microgrids has been proposed. One of the salient features of this protection scheme is that it does not require communications or adaptive protective devices. In addition, it is stated in [53] that the proposed scheme is to a large extent independent of the fault current magnitude, the microgrid operational mode, and the type and size of the DER, subject to the modified relay setting for the grid-connected mode of operation [15].

19.4.4 Protection of MV AC microgrids

In [15] and [75], communication-based protection methods have been suggested, which should be implementable by commercially available protection relays, for the protection of inverter-based medium-voltage (MV) microgrids. Proposed scheme also includes a backup protection method to handle the failure of the communication network. In [15] it was also stated that the suggested protection method is independent of the operation mode of the microgrid as well as of the fault current level, type, size, and location of the DER units.

19.4.4.1 Proposed MV microgrid protection scheme 1

In [76] one potential protection scheme without communication was proposed for short-circuit and earth-fault protection of an island operated medium-voltage (MV) microgrid with many protection zones. The suggested protection method was not dependent on the fault current level fed by the DER units and was compatible and selective with DG unit low-voltage-ride-through (LVRT) curves. However, the LVRT curve of the inverter- and synchronous generator-based DER units may be different. Because rotating generators typically cannot have as long fault-ride-through (FRT)/LVRT capability as the inverter-based DER units may have, and the islanded MV microgrid with synchronous generators can be divided into fewer protection zones than with inverter-based DERs. The suggested protection strategy is only for islanded microgrid operation, but there are some similarities with previously, in [77]–[80], presented short-circuit protection strategies for the grid-connected operation.

The short-circuit and earth-fault protection operation speed in the proposed scheme are not dependent on fault-current level or measured impedance. In contrast, they are based on voltage measurements from that network point (also considering the direction of the current). This means that it is easier to achieve selectivity with DER units LVRT requirements especially without fast communication and when there are many protections zones in the MV feeder. The suggested protection method could be also used as a back-up method for communication assisted strategies. It can also be mentioned that the earth-fault protection part of the proposed protection scheme is only applicable to neutral isolated MV microgrids. The main principles of this proposed protection scheme are presented broadly in Figures 19.8, 19.9 and 19.10. From [76], a more detailed descriptions with case examples can be found.

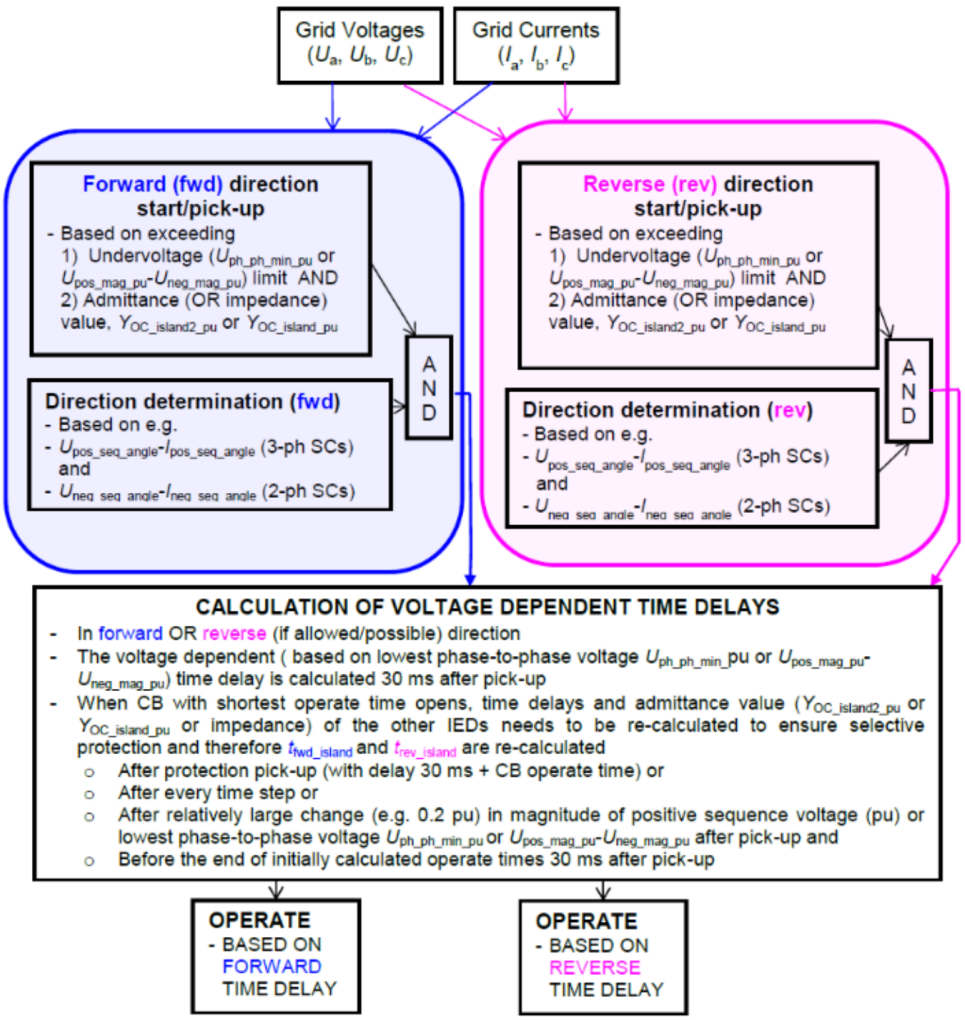

Figure 19.8. Suggested directional short-circuit protection strategy for island operated MV networks [76].

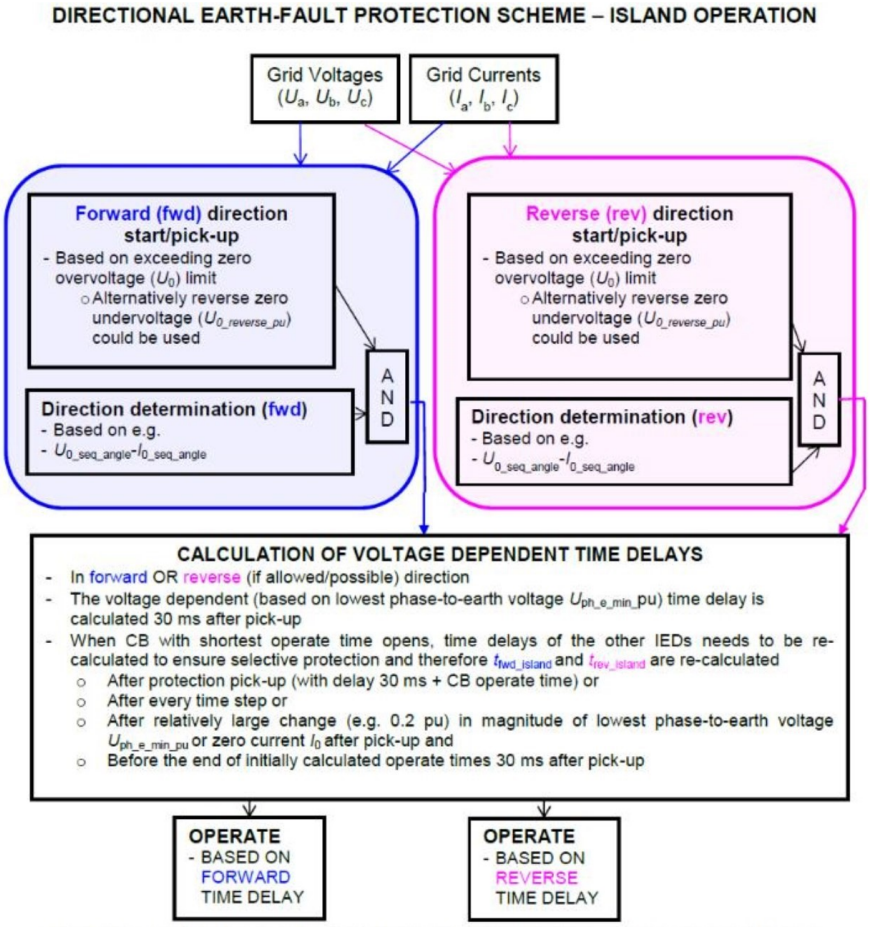

Figure 19.9. Suggested directional earth-fault protection strategy for island operated (earthing isolated) MV networks [76].

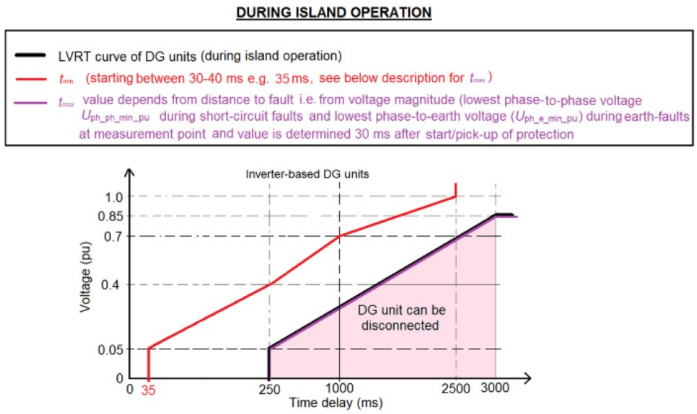

Figure 19.10. Protection voltage dependent operation time delay curve during island operation with inverter-based DG units [76].

Table 19.4 summarizes the differences between the proposed protection strategy [76] and few other previously proposed protection methods for island operated microgrids. From Table 19.4 one can see that the key advantage of the proposed strategy (6. in Table 19.4), when compared with other previously proposed methods (1.–5. in Table 19.4), is that it is selective with DG unit LVRT curves/FRT requirements. In addition, it can be applied to microgrids with many protection zones without the requirement for fast communication.

TABLE 19.4 [76]
DIFFERENCES OF PROTECTION SCHEMES FOR ISLAND OPERATED MICROGRIDS

Protection Scheme	Sensitivity / Applicability also to microgrids with only the converter-based DER units	Selectivity of MV and LV faults	Requirement for fast communication to achieve selectivity in microgrids with DER unit FRT curves and with many protection zones
1. Directional Over-Current (DOC)	NO	NO/YES*)	YES
2. Distance	YES	YES	YES
3. Current Differential**)	YES	YES	YES
4. Voltage + DOC	YES	YES	YES
5. ITA [57], [81]	YES	YES	YES
6. Proposed Scheme [76]	YES	YES	NO

*) Case dependent, but not if only the converter-based DER units and low pick-up settings, **) Network topology dependent, not suited for microgrids with radial feeders without DER units at the end of the feeders

19.4.4.2 Enhanced MV microgrid protection scheme 1 – HIF detection included

In [76] (Subsection 19.3.8.1) a new protection strategy was suggested including short-circuit and earth-fault protection for island operated, neutral isolated MV microgrid. In [82], the MV microgrid protection strategy, with mainly OH lines and the inverter-based DER units, was enhanced so that it also included high-impedance-fault (HIF) detection (Figure 19.11). Additionally, other improvement possibilities were suggested in [82], like, DER unit high-voltage-ride-through (HVRT) curve compatibility and use of adaptive start/pick-up setting. More details can be found in [82].

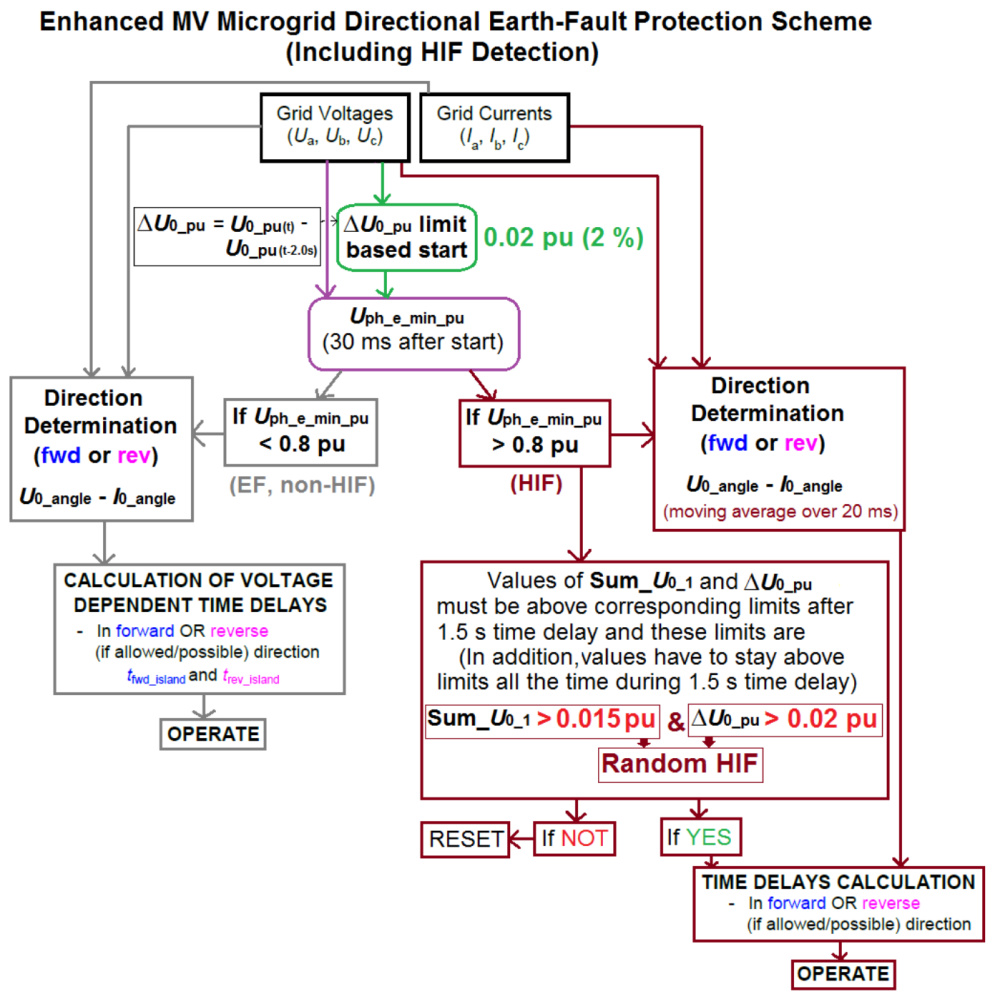

Figure 19.11. Improved MV microgrid protection strategy [82].

19.4.5 Communication-less adaptive protection

The communication-based adaptive protections may become ineffective due to communication system failure. In this situation protection settings cannot be changed according to changing network configurations. Therefore, some communication-less adaptive protections should be developed to takeover in case of communication failures. A method for knowing the present condition or state of grid operation (grid-connected or islanded) has been proposed in [83] which uses some local schemes installed near the protection devices. The proposed scheme uses the thyristor which is fired during a short waveform interval of voltage, then thyristor voltage and currents are monitored. The monitored voltage and currents are then used to calculate the grid equivalent impedance. From the value of grid equivalent impedance it is determined whether the main grid is connected or not. After determining the grid operating condition, a command is sent locally to the protection device to change its active group settings. The scheme can be used as communication-less adaptive protection scheme or can be used as a backup of communication-based schemes to provide resiliency during communication failures. However, the proposed scheme may not be effective for weak grids. The use of energy storage systems as fault current sources like batteries, flywheels, supercapacitors etc. for providing increased fault current by deactivating the fault current limiters of DERs locally or activating extra energy storage devices during the events of communication failures or cyber-attacks is proposed in [84]. However, this scheme will require over-rated converters of energy storage systems to sustain increased fault currents.

19.4.6 Islanding detection during island operation of nested microgrid

Functionalities like islanding detection should also operate during the islanded operation of (MV+MV or MV+LV) nested microgrids. In [85], islanding detection of LV network connected generation unit during nested (MV+LV) microgrid islanded operation was studied by simulations with PSCAD model from real-life smart grid pilot (Fig. 19.12). The main focus of the simulations was on the study and comparison of the usage possibilities of combined (high-speed communication based transfer trip & fault detection/direction + voltage vector shift) (Fig. 19.13) and multi-criteria (voltage total harmonic distortion U_{THD} & voltage unbalance VU) based islanding detection schemes in nested microgrid consisting only of converter-based DER units [85] (Fig. 19.14).

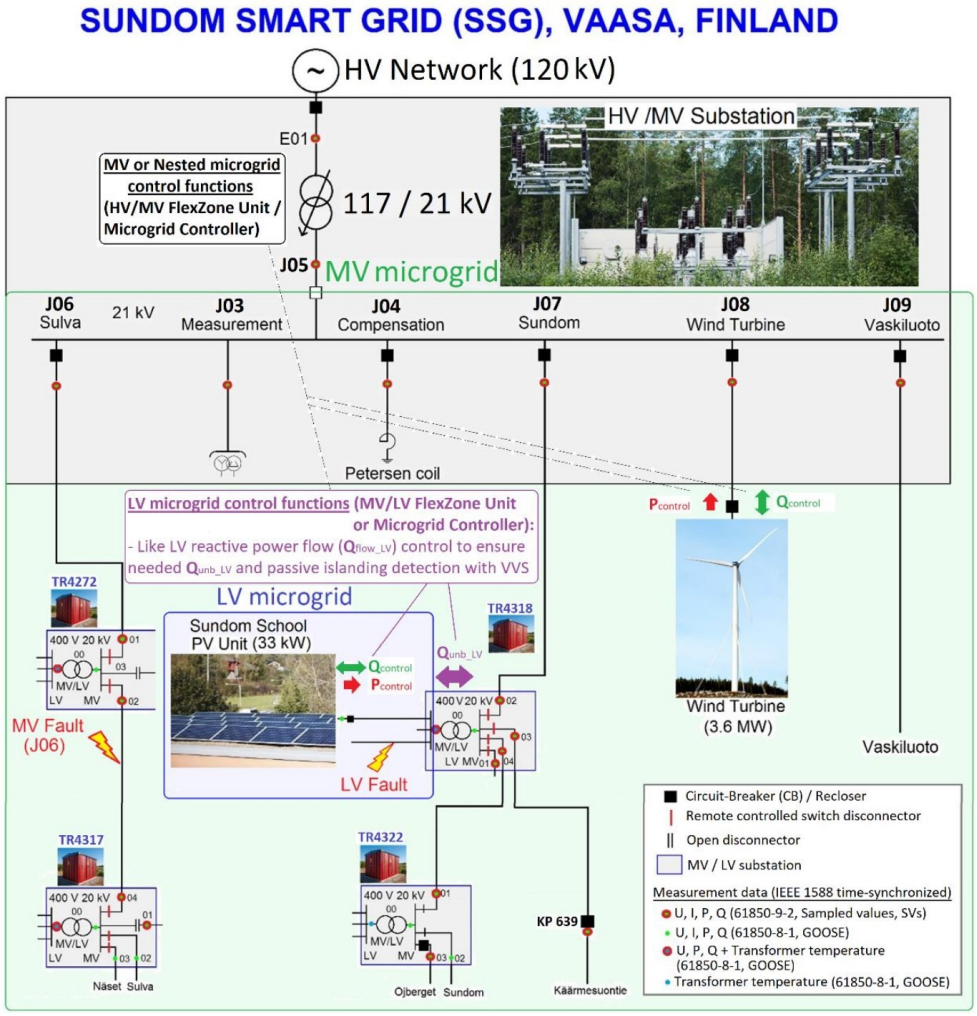

Figure 19.12. Sundom Smart Grid (SSG) to study islanding detection of LV network connected DER unit during nested (MV+LV) microgrid islanded operation [85].

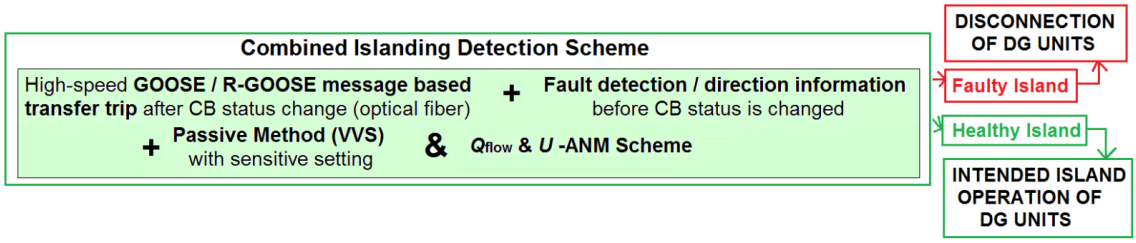

Figure 19.13. Combined islanding detection scheme [85].

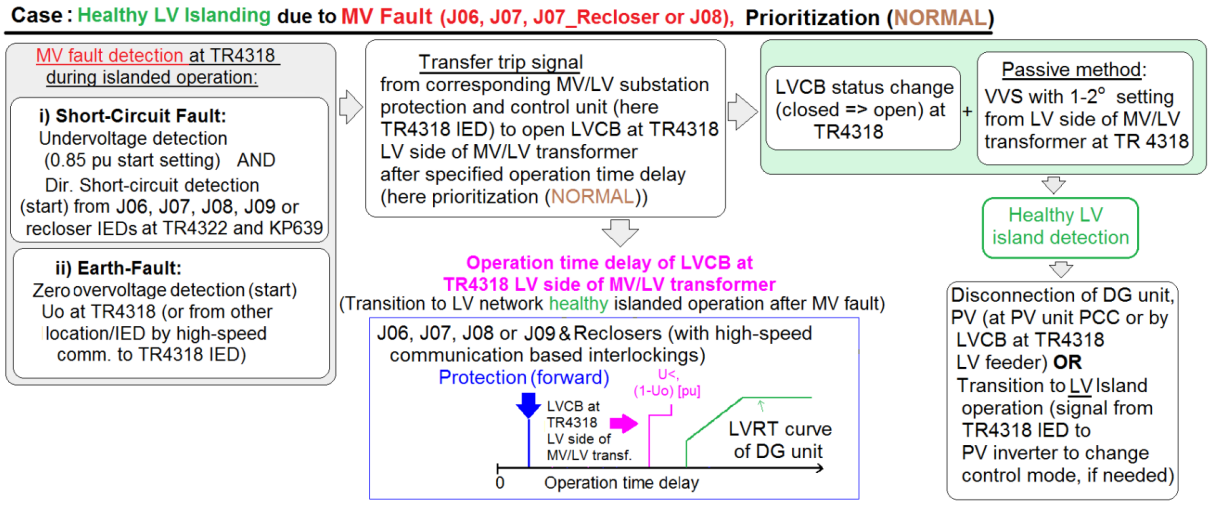

Figure 19.14. LV network DG unit (PV) primary islanding detection scheme example case (healthy LV islanding after MV fault) during islanded operation of SSG (Fig. 19.12) [85].

Based on the simulations it was concluded that combined islanding detection scheme (Fig. 19.13) seems to be very feasible for the islanding detection with LV network connected inverter-based DG units in nested (MV+LV) microgrids. However, the detection logic for faults must be adapted. In the future, nested microgrid control and protection functionality could be centralized/de-centralized in control and protection units at HV/MV and MV/LV substations. For example, the fault detection and location determination could be coordinated between these units by using high-speed communication, real-time synchronized measurements from multiple locations simultaneously as well as knowledge about the type, status and location of different DER units in order to always ensure selective islanding detection.

19.4.7 Need for microgrid grid codes

As stated in Subsection 19.1.1 from the islanded microgrid (LV or MV) protection viewpoint, the FRT capabilities and requirements as well as fault current contribution of the converter-based DER units during the faults is of importance. Microgrid grid codes for the island operated networks could 'standardize' the requirements more specifically for LV and MV microgrid by considering their typical features etc. in more detailed manner. This would also reduce complexity and the need for many case specific alternatives could be avoided. Compatibility of the DER unit FRT requirements, fault behaviour and island operated microgrid protection principles as well as operation speed requirements are naturally very critical from microgrid frequency and voltage stability viewpoint and these could be also defined as part of the microgrid grid codes.

For example, in LV microgrids the fault current fed by converter-based DER units could be required to be active and less than $2xI_n$ active current (I_n is nominal current) during faults in LV microgrid for the required FRT time defined by the operation curves of different PDs (Fig. 19.7, 19.15, 19.16).

On the other hand, in MV microgrids the HVRT curve during island operation for converter-based DER units could be defined in microgrid grid codes as shown in Fig. 19.17. It must be always simultaneously confirmed that the HVRT curve requirement of the DER unit, as part of the protection scheme during islanded microgrid operation, is compatible with safety regulations (e.g. touch voltages during earth-faults). Otherwise, faster MV microgrid protection schemes e.g. based on the use of high-speed communication may need to be utilized.

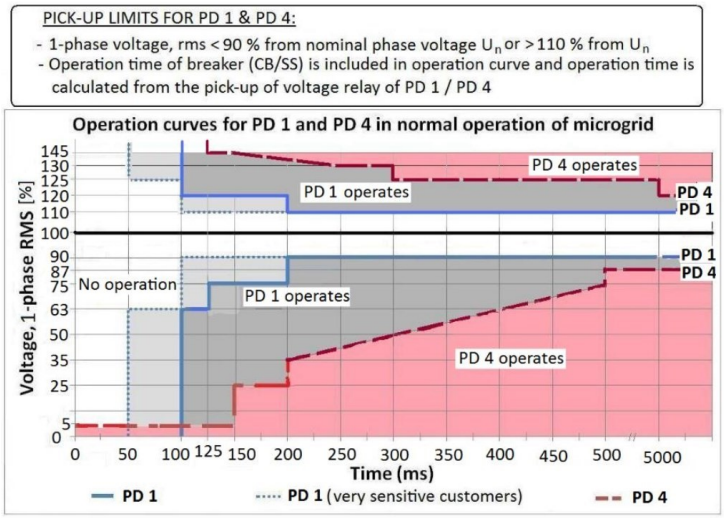

Figure 19.15. Operation curves for voltage relays (PD 1 in normal operation and PD 4 in normal and island operation) (see Fig. 19.7) [4], [11], [72]–[73].

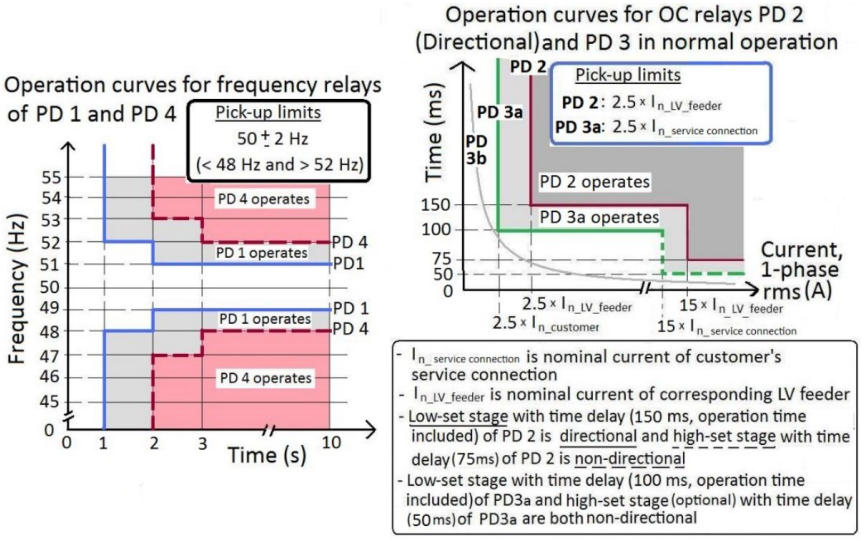

Figure 19.16. Operation curves frequency relays of PD 1 and PD 4 in normal and island operation of microgrid and operation curves for OC relays of PD 2 (directional low-set stage and non-directional high-set stage) in normal operation and PD 3 in normal and island operation (see Fig. 19.7) [4], [11], [72]–[73].

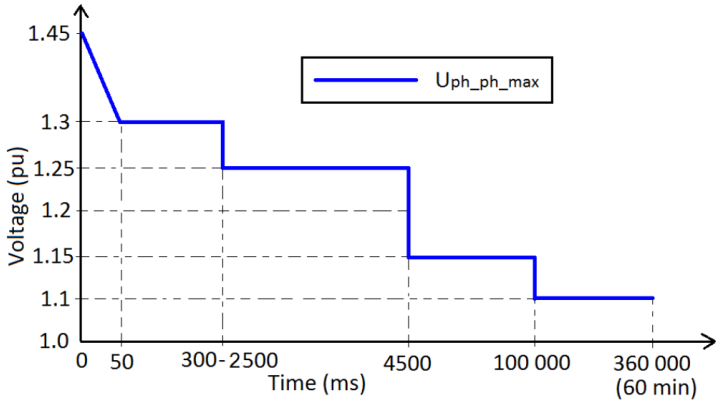

Figure 19.17. Proposed HVRT curve during MV microgrid island operation for converter-based DER units [82].

19.5 Protection of DC microgrids

In DC microgrids, all DERs and loads are connected to a common DC bus. The DERs generating AC power (wind turbine, micro-turbine) are interfaced to the DC bus by using AC-DC converters and AC loads are interfaced by using DC-AC converters. On the other hand, all DGs generating DC power inherently (PVs, fuel cells, batteries) and DC loads are connected to the DC bus using DC-DC converters. Typically, DC microgrids are categorized into different topological configurations, like multi-terminal, zonal and DC looped. The chosen topology of DC microgrid is dependent on application, reliability level, and voltage level. Independent of the topology, there are two types of DC bus architectures i.e., (1) unipolar DC bus topology using two-level voltage source converters (VSCs) and (2) bipolar bus topology using three-level neutral-point-clamped VSCs. The DC microgrid protection schemes are typically divided into a) unit based and b) non-unit based i.e. protective device/breaker based. For example, in ships and DC homes the most typical protection scheme has been unit-based protection. A unit-based protection scheme means that protection functionality exists within the DER units and tries to either limit the DC-side fault current or drive it to zero.

The common DC bus can be interfaced to the main AC distribution grid via a bidirectional AC-DC converter. Depending on the voltage level of DC bus, DC microgrids can be classified as low voltage DC (LVDC) or medium voltage DC (MVDC) microgrids. Protective devices of DC microgrid with non-unit-based protection scheme are represented by a generic block "PD" representing protective device as these are different from conventional CBs operated by protective relays [86]. The main requirements of selectivity, sensitivity and speed of an effective AC protection system are also expected from a DC protection system. However, DC protection cannot meet all requirements of AC protection in a very straightforward way. Because in AC system sufficient protection speed is required to maintain the stability of synchronous generators while allowing a combined relay and breaker operating times for several cycles of fundamental frequency. For DC systems, in contrast, the protection system should be substantially faster because a contribution to the fault current by a voltage source converter (VSC) even for a duration of more than few milliseconds can damage the converter unless some DC fault current limiting/blocking mechanism is available to protect the converter. Additionally, DC protection should isolate the fault before the blockage of IGBT switches of the converter happens because due to the blockage of IGBTs, the converter control will be lost, and more time will be required for the post fault restoration process. The requirement to prevent IGBTs blocking imposes strict requirements for the protection of DC microgrids. The technology of DC breakers and off-the-shelf digital DC relays is at a very low advancement level. Therefore, it is common practice to trip the breakers on the AC side of all converters during a DC fault in a DC system and then the fault is isolated using DC disconnectors This approach is fast enough to protect the converter, but it is not selective because the loss of the complete DC system happens during any fault. Overcurrent protection is not the optimum selection for DC microgrid protection because the relay should be capable of differentiating between in-zone and out-of-zone well before the fault current reaches its final value. Moreover, the fault resistance also severely affects the selectivity and sensitivity of DC overcurrent relays [87]. The common method used for the location of DC fault is based on the travelling-waves principle [88] which uses a communication link to find the arrival times of fault-induced travelling waves at two ends of a line. Using the difference between two arrival times and wave propagation velocity, the location of fault can be identified. Due to the presence of noise and short lines in DC microgrids, this method faces problems. Moreover, travelling-waves relays are very costly for implementation in DC microgrids [87]. The other protection methods proposed for DC microgrids as reported in [19] include overcurrent, current derivative, directional overcurrent, distance and differential protections. The common protective/interrupting devices for DC microgrids are fuses, moulded case circuit breakers, no load switches and SSCBs [19] [86]. DC microgrids are evolving and so are DC protection systems. Until adequate DC protection devices are available the applications of DC microgrids will be limited to only special applications like avionics, automotive, marine, the international space station (ISS), spacecraft, aircraft, electronic computers, and servers in data centres.

Acknowledgements

This work has been carried out as part of SolarX project at the University of Vaasa, Finland. SolarX project is mainly funded by Business Finland (grant No. 6844/31/2018). Some part of this work has been done in VINPOWER project and main funding for VINPOWER project came from European Regional Development Fund, ERDF (project No. A73094). The financial support provided through these projects is greatly acknowledged.

References:

[1] Aushiq Ali Memon, Kimmo Kauhaniemi, A critical review of AC Microgrid protection issues and available Solutions, Electric Power Systems Research 129 (2015) 23–31.

[2] Pierre Janssen, Monitoring, protection and fault location in power distribution networks using system-wide measurements, PhD thesis, 2013, available at: http://theses.ulb.ac.be/ETD-db/collection/available/ULBetd-10152013-111608/unrestricted/PhD_thesis_Pierre_Janssen_final.pdf

[3] Oudalov, A., Fidigatti, A., Degner, T., Valov, B., Hardt, C., Yarza, J. M., Li, R., Jenkins, N., Awad, B., Van Overbeeke, F., Hatziargyriou, N. & Lorentzou, M., Novel protection systems for microgrids, Final version of partial report for WORK PACKAGE C (TC2: Technical requirements for network protection) on More MicroGrids EU-project, 2009.

[4] Laaksonen, H., Technical Solutions for Low-Voltage Microgrid Concept, Ph.D. thesis, Dept. of Electrical and Energy Engineering, University of Vaasa, Acta Wasaensia, 241, Vaasa 2011. 271 pages. Available at: http://www.uva.fi/materiaali/pdf/isbn_978-952-476-345-5.pdf

[5] A. Oudalov, New Technologies for Microgrid Protection, Santiago 2013 Symposium on Microgrids, 2013, Available at: http://der.lbl.gov/sites/der.lbl.gov/files/santiago_oudalov.pdf.

[6] S. Conti, L. Raffa, U. Vagliasindi, Innovative solutions for protection schemes in autonomous MV micro-grids, in: International Conference on Clean Electrical Power, 2009, pp. 647–654.

[7] H. Nikkhajoei, R.H. Lasseter, Microgrid protection, in: IEEE Power Engineering Society General Meeting, 2007, pp. 1–6.

[8] H. Al-Nasseri, M.A. Redfern, F. Li, A voltage based protection for micro-grids containing power electronic converters, in: IEEE Power Engineering Society General Meeting, 2006, p. 7.

[9] H. Al-Nasseri, M.A. Redfern, Harmonics content based protection scheme for Micro-grids dominated by solid state converters, in: Power System Conference, 2008. MEPCON 2008. 12th International Middle-East, 2008, pp. 50–56.

[10] A. Oudalov, A. Fidigatti, Adaptive network protection in microgrids, Int. J. Distrib. Energy Resour. 5 (2009) 201–226.

[11] Laaksonen, H. & Kauhaniemi, K., Smart Protection Concept for LV Microgrid, International Review of Electrical Engineering (IREE), Vol. 5 No. 2, March–April 2010.

[12] Chowdhury, S., Chowdhury, S.P. & Crossley, P., Microgrids and Active Distribution Networks, Published by The Institution of Engineering and Technology, London, United Kingdom: Athenaeum Press Ltd, Gateshead, Tyne & Wear, 2009.

[13] Voima, S., Laaksonen, H. & Kauhaniemi, K., Adaptive Protection Scheme for Smart Grids. The IET 12th International Conference on Developments in Power System Protection (DPSP) 2014, Copenhagen, Denmark, March 31 - April 3, 2014.

[14] Laaksonen, H. & Kauhaniemi, K. & Voima, S., DG Unit Fault Behavior and Protection of LV Microgrid, International Review on Modelling and Simulations (IREMOS), Vol. 3 No. 3, June 2010.

[15] Zamani, M. A., Protection and control of active distribution networks and microgrids, PhD thesis, The University of Western Ontario, London, Ontario, Canada, 2012.

[16] CIGRE (Joint Working Group B5/C6.26/CIRED). Protection of Distribution Systems with Distributed Energy Resources. Final Report. March 2015.

[17] H. J. Altuve, K. Zimmerman and D. Tziouvaras, "Maximizing line protection reliability, speed, and sensitivity," 2016 69th Annual Conference for Protective Relay Engineers (CPRE), College Station, TX, 2016, pp. 1-28.

[18] IEEE Std-242-2001 Recommended Practice for Protection and Coordination of Industrial and Commercial Power Systems (IEEE Buff Book).

[19] Siavash Beheshtaein, Robert Cuzner, Mehdi Savaghebi, Josep M. Guerrero, Review on microgrid protection, IET Gener. Transm. Distrib., 2019, Vol. 13 Iss. 6, pp. 743-759

[20] S.M. Brahma, A.A. Girgis, Development of adaptive protection scheme for distribution systems with high penetration of distributed generation, IEEE Trans. Power Delivery 19 (2004) 56–63.

[21] M.T. Doyle, Reviewing the impacts of distributed generation on distribution system protection, in: IEEE Power Engineering Society Summer Meeting, 2002,pp. 103–105, vol. 1.

[22] Stanley H . Horowitz, Arun G . Phadke, Power System Relaying, Third Edition, John Wiley & Sons Ltd, West Sussex, 2008.

[23] Juan M. Gers, Edward J. Holmes, Protection of electricity distribution networks - 2nd ed, The Institution of Electrical Engineers, London, 2004.

[24] R. Lasseter, et al., Integration of distributed energy resources, in: The CERTS Microgrid Concept, Lawrence Berkeley National Lab, 2002.

[25] G. D. Rockefeller, C. L. Wagner, J. R. Linders, K. L. Hicks and D. T. Rizy, "Adaptive transmission relaying concepts for improved performance," in IEEE Transactions on Power Delivery, vol. 3, no. 4, pp. 1446-1458, Oct 1988

[26] IEEE Std 1547-2003 IEEE Standard for Interconnecting Distributed Resources with Electric Power Systems

[27] IEEE, IEEE Guide for Design, Operation, and Integration of Distributed Resource Island Systems with Electric Power Systems, IEEE Std 1547. 4-2011, 2011, pp.1–54.

[28] AREVA T&D. (2002). Network Protection & Automation Guide. First edition.

[29] Arulampalam, A., Barnes, M., Engler, A., Goodwin, A. & Jenkins, N. (2004). Control of power electronic interfaces in distributed generation microgrids. International Journal of Electronics 91: 9, 503–523.

[30] Nuñez, J., Gil de Muro, A. & Oyarzabal, J. (2010). Development and evaluation of innovative local controls to improve stability and islanding detection. WPA: Design of Microsource and Load Controllers for Efficient Integration, TA1: Requirements for various DGs in supporting MicroGrid operation, Advanced Architectures and Control Concepts for More MicroGrids, STREP project funded by the EC under 6FP, SES6-019864, Labein Tecnalia, Derio, Spain.

[31] Van Overbeeke, F. & Cobben, S. (2010). Operational aspects of a microgrid with battery storage. In Proceedings of IEEE PES Conference on Innovative Smart Grid Technologies Europe. Gothenburg, Sweden.

[32] Oyarzabal, J., Jimeno, J., Agnostos, D., Arnold, G., Berg, A., Mustermann, E., Agnostos, T., Mustermann, H. & Yarza, J. M. (2009). Report on applied data structures and mapping to communication means. Report as part of WORK PACKAGE E (Standardization of technical and commercial protocols and hardware) on More MicroGrids EU-project.

[33] Eto, J., Lasseter, R., Schenkman, B., Stevens, J., Klapp, D., Volkommer, H., Linton, E., Hurtado, H. & Roy, J. (2009). Overview of the CERTS Microgrid Laboratory Test Bed. In Proceedings of Integration of Wide-Scale Renewable Resources into the Power Delivery System, 2009 CIGRE/IEEE PES Joint Symposium. Calgary, Canada.

[34] Laaksonen, H. & Kauhaniemi, K. Synchronized Re-Connection of Island Operated LV Microgrid Back to Utility Grid. Proc. IEEE PES ISGT Europe, Gothenburg, Sweden. October 2010.

[35] Young-woo JEONG, Hyun-wook LEE, Seok-won LEE, Young-geun KIM, HIGH-SPEED AC CIRCUIT BREAKER AND HIGH-SPEED OCR, CIRED 22nd International Conference on Electricity Distribution Stockholm, 10-13 June 2013, Paper 0608.

[36] S. Krstic, E. L. Wellner, A. R. Bendre and B. Semenov, "Circuit Breaker Technologies for Advanced Ship Power Systems," 2007 IEEE Electric Ship Technologies Symposium, Arlington, VA, 2007, pp. 201-208

[37] Sekar Kannuppaiyan, Vivekanandan Chenniappan, Numerical Inverse Definite Minimum Time Overcurrent Relay for Microgrid Power System Protection, IEEJ Trans 2015; 10: 50–54.

[38] M. Pujiantara, D. C. Riawan, A. Indrasaputra, T. P. Sari and V. Raki Mahindara, "The Automation of Time Dial Setting Calculation and Inverse Type Curve Selection for Over Current Relay Based on Numerical Computation in Real Industrial Electrical System," 2018 Conference on Power Engineering and Renewable Energy (ICPERE), Solo, Indonesia, 2018, pp. 1-6.

[39] IEEE Std C37.112-1996, IEEE Standard Inverse-Time Characteristic Equations for Overcurrent Relays

[40] F. van Overbeeke, "Fault current source to ensure the fault level in inverter dominated networks," CIRED 2009 - The 20th International Conference and Exhibition on Electricity Distribution - Part 2, Prague, 2009, pp. 1-13.

[41] F. van Overbeeke, "Fault current source to ensure the fault level in inverter-dominated networks," CIRED 2009 - 20th International Conference and Exhibition on Electricity Distribution - Part 1, Prague, Czech Republic, 2009, pp. 1-4

[42] N. Hatziargyriou, Microgrids: Architectures and Control, John Wiley & Sons, West Sussex, UK, 2013.

[43] Daqing Hou, Dave Dolezilek (2010), IEC 61850-What It Can and Cannot Offer to traditional Protection Schemes, Schweitzer Engineering Laboratories, Inc., SEL Journal of Reliable Power, Vol. 1, No. 2, Oct.

[44] Relion Protection and Control, 650 Series IEC 61850 Communication Protocol Manual, Document ID: 1MRK 511 242-UEN, Issued: February 2011, Revision: - Product version: 1.1, ABB 2011.

[45] P. Mahat, Z. Chen, B. Bak-Jensen, and C.L. Bak, A Simple Adaptive Overcurrent Protection of Distribution Systems with Distributed Generation, IEEE TRANSACTIONS ON SMART GRID, VOL. 2, NO. 3, SEPTEMBER 2011.

[46] Pierre Janssen, Monitoring, protection and fault location in power distribution networks using system-wide measurements, PhD thesis 2013, available at: http://theses.ulb.ac.be/ETD-db/collection/available/ULBetd-10152013-111608/unrestricted/PhD_thesis_Pierre_Janssen_final.pdf

[47] D. Ishchenko, A. Oudalov, and J. Stoupis, Protection Coordination in Active Distribution Grids with IEC 61850, IEEE 2012.

[48] Laaksonen, H. & Ishchenko, D. & Oudalov, A., Adaptive Protection and Microgrid Control Design for Hailuoto Island, IEEE Transactions on Smart Grid, 6.3.2014

[49] G. Buigues, A. Dyśko, V. Valverde, I. Zamora, and E. Fernández Microgrid Protection: Technical challenges and existing techniques, , International Conference on Renewable Energies and Power Quality (ICREPQ'13), Bilbao (Spain), 20-22 March, 2013: http://www.icrepq.com/icrepq'13/262-buigues.pdf

[50] H. Nikkhajoei, et al., Microgrid fault protection based on symmetrical and differential current components, 2006.

[51] L. Bin, et al., Design of protection and control scheme for microgrid systems, in Universities Power Engineering Conference (UPEC), 2009 Proceedings of the 44th International, 2009, pp. 1-5.

[52] R. J. Best, et al., Communication assisted protection selectivity for reconfigurable and islanded power networks, in Universities Power Engineering Conference (UPEC), 2009 Proceedings of the 44th International, 2009, pp. 1-5.

[53] M. A. Zamani, T. S. Sidhu and A. Yazdani, A protection strategy and microprocessor-based relay for low-voltage microgrids, IEEE Trans. on Power Delivery, vol. 26, no. 3, pp. 1873-1883, Jul. 2011.

[54] Voima, S., Kauhaniemi, K. & Laaksonen, H., Novel Protection Approach for MV Microgrid, CIRED 2011, Frankfurt, Germany, June 6–9, 2011.

[55] M. Dewadasa, Protection for distributed generation interfaced networks, Electrical Engineering, Faculty of Built Environment and Engineering, Queensland University of Technology, Queensland (Australia), 2010.

[56] M. Dewadasa, et al., Control and protection of a microgrid with converter interfaced micro sources, in Power Systems, 2009. ICPS '09. International Conference on, 2009, pp. 1-6.

[57] Dewadasa, M. Protection of distributed generation interfaced networks, Thesis, Queensland University of Technology, Queensland, Australia, 2010.

[58] Laaksonen, H. & Kauhaniemi, K., Fault Type and Location Detection in Islanded Microgrid with Different Control Methods Based Converters, In Proceedings of 19th International Conference and Exhibition on Electricity Distribution. Vienna, Austria, 2007.

[59] Al-Nasseri, H. & Redfern, M. A., A New Voltage based Relay Scheme to Protect Micro-Grids dominated by Embedded Generation using Solid State Converters, In Proceedings of 19th International Conference on Electricity Distribution. Vienna, Austria, 2007.

[60] Oudalov, A. & Fidigatti, A., Microgrid protection and modern protection Devices, Final report as part of WORK PACKAGE C (TC2: Technical requirements for network protection) on More MicroGrids EU-project, 2008.

[61] C. Hou, et al., A study of voltage detection based fault judgement method in micro-grid with inverter interfaced power source, in The International Conference on Electrical Engineering, Shenyang (China), 2009, pp. 1-5.

[62] T. Loix, et al., Protection of microgrids with a high penetration of inverter-coupled energy sources, in Integration of Wide-Scale Renewable Resources into the Power Delivery System, 2009 CIGRE/IEEE PES Joint Symposium, 2009, pp. 1-6.

[63] W. Xiao-ping, et al., Research on the relay protection system for a small laboratory-scale microgrid system, in Industrial Electronics and Applications (ICIEA), 2011 6th IEEE Conference on, 2011, pp. 2712-2716.

[64] M. Dewadasa, Member, A. Ghosh, and G. Ledwich, Protection of Microgrids Using Differential Relays, (2011) Protection of microgrids using differential relays. In Proceedings from AUPEC 2011. https://eprints.qut.edu.au/47434/1/2011011990.ePrints.Dewadasa.pdf

[65] Conti Stefania, Raffa Lorenzo and Vagliasindi Umberto, Analysis of protection issues in autonomous MV micro-grids, 20th International Conference on Electricity Distribution. CIRED 2009. - pp. 1-5.

[66] Casagrande, E., Woon, W.L., Zeineldin, H.H., Svetinovic, D., A Differential Sequence Component Protection Scheme for Microgrids With Inverter-Based Distributed Generators, IEEE Transactions on Smart Grid (Volume: 5 , Issue: 1 , Jan. 2014) https://ieeexplore.ieee.org/abstract/document/6678658

[67] Sortomme E., Venkata S.S. and Mitra J., Microgrid protection using communication assisted digital relays, IEEE Transactions on Power Delivery. - 2010. - pp. 2789-2796.

[68] Brahma S.M., Fault location in power distribution system with penetration of distributed generation, IEEE Transactions on Power Delivery. - 2011. - 99: Vol. 1.

[69] Venkata S.S. et al., Advanced and adaptive protection for active distribution grid, 22nd International Conference on Electricity Distribution (CIRED 2013). – Stockholm, Sweden, 2013.

[70] R. M. Tumilty, et al., Approaches to Network Protection for Inverter Dominated Electrical Distribution Systems, in Power Electronics, Machines and Drives, 2006. The 3rd IET International Conference on, 2006, pp. 622-626.

[71] Tumilty, R. M., Elders, I. M., Burt, G. M. & McDonald, J. R., Coordinated Protection, Control & Automation Schemes for Microgrids, International Journal of Distributed Energy Resources 3: 3, 225–241, 2007.

[72] Laaksonen, H., Protection Principles for Future Microgrids, IEEE Transactions on Power Electronics, Vol. 25, No. 12, December 2010.

[73] Laaksonen, H., Kauhaniemi, K. & Voima, S., Protection System for Future LV Microgrids, CIRED 2011, Frankfurt, Germany, June 6–9, 2011.

[74] M. A. Zamani, T. S. Sidhu and A. Yazdani, A strategy for protection coordination in radial distribution networks with distributed generators, in Proc. IEEE Power and Energy Society General Meeting, 8 pages, Jul. 2010.

[75] M. A. Zamani, A. Yazdani and T. S. Sidhu, A communication-assisted protection strategy for inverter-based medium-voltage microgrids, in IEEE Trans. on Smart Grid, 12 pages, Vol 3, No. 4. Dec. 2012.

[76] Laaksonen, H. Protection Scheme for Island Operated Medium-Voltage Microgrid, International Review of Electrical Engineering (IREE), Vol. 10 No. 4, August 2015.

[77] H. Laaksonen, Future-proof MV Distribution Network Short-Circuit Protection Scheme, International Review of Electrical Engineering (IREE), vol. 10, February 2015, pp. 98 – 108.

[78] H. Laaksonen, Protection of Future Active Distribution Networks with Distributed Generation, CIGRE Conference ~SEAPAC 2015~, 2015, Sydney, Australia.

[79] H. Laaksonen, Grid Code Compatible Protection Scheme for Smart Grids, The 23rd International Conference on Electricity Distribution ~CIRED 2015~, 2015, Lyon, France.

[80] H. Laaksonen, Comparison of New LVRT Compatible MV Network Short-Circuit Protection Schemes, International Review on Modelling and Simulations (IREMOS), vol. 8, April 2015, pp. 122 – 131.

[81] M. Dewadasa, A. Ghosh, Microgrid Operation and Control: DELIVERABLE 6: Protection of Meshed Microgrids, CSIRO Intelligent Grid Research Cluster- Project 7, Queensland Univ. of Technology, Queensland, Australia. [Online]. Available: http://igrid.net.au/resources/downloads/project7/P7%20M6%20Meshed%20Microgrid%20Protection.pdf

[82] Laaksonen, H., Hovila, P. Enhanced MV Microgrid Protection Scheme for Detecting High-Impedance Faults. 12th IEEE PES PowerTech Conference, PowerTech Manchester 2017, Manchester, UK, June 18-22, 2017.

[83] Roberta R. Ferreira, Patry J. Colorado, Ahda P. Grilo, Julio C. Teixeira, Ricardo C. Santos, Method for identification of grid operating conditions for adaptive overcurrent protection during intentional islanding operation, International Journal of Electrical Power & Energy Systems, Volume 105, 2019,Pages 632-641

[84] H. F. Habib, C. R. Lashway and O. A. Mohammed, "On the adaptive protection of microgrids: A review on how to mitigate cyber-attacks and communication failures," 2017 IEEE Industry Applications Society Annual Meeting, Cincinnati, OH, 2017, pp. 1-8.

[85] H. Laaksonen and P. Hovila, "Islanding Detection During Intended Island Operation of Nested Microgrid," 2018 IEEE PES Innovative Smart Grid Technologies Conference Europe (ISGT-Europe), Sarajevo, 2018, pp. 1-6.

[86] R. M. Cuzner and G. Venkataramanan, "The Status of DC Micro-Grid Protection," 2008 IEEE Industry Applications Society Annual Meeting, Edmonton, AB, 2008, pp. 1-8.

[87] A. Hooshyar and R. Iravani, "Microgrid Protection," in Proceedings of the IEEE, vol. 105, no. 7, pp. 1332-1353, July 2017.

[88] M. M. Saha, J. J. Izykowski, and E. Rosolowski, Fault Location on Power Networks. London, U.K.: Springer-Verlag, 2010, ch.1.

IEEE Access
Multidisciplinary ⋮ Rapid Review ⋮ Open Access Journal

Received October 9, 2021, accepted October 29, 2021, date of publication November 15, 2021, date of current version November 24, 2021.

Digital Object Identifier 10.1109/ACCESS.2021.3128370

Real-Time Hardware-in-the-Loop Testing of IEC 61850 GOOSE-Based Logically Selective Adaptive Protection of AC Microgrid

AUSHIQ ALI MEMON, (Member, IEEE), AND KIMMO KAUHANIEMI, (Member, IEEE)
School of Technology and Innovations, University of Vaasa, 65200 Vaasa, Finland

Corresponding author: Aushiq Ali Memon (amemon@uwasa.fi)

This work was supported in part by Business Finland through the SolarX Research Project under Grant 6844/31/2018, and in part by the European Regional Development Fund (ERDF) through the VINPOWER Research Project under Grant A73094.

ABSTRACT The real-time (RT) hardware-in-the-loop (HIL) simulation-based testing is getting popular for power systems and power electronics applications. The HIL testing provides the interactive environment between the actual power system components like control and protection devices and simulated power system networks including different communication protocols. Therefore, the results of the RT simulation and HIL testing before the actual implementation in the field are generally more acceptable than offline simulations. This paper reviews the HIL testing methods and applications in the recent literature and presents a step-by-step documentation of a new HIL testing setup for a specific case study. The case study evaluates real-time implementation of previously proposed communication-dependent logically selective adaptive protection algorithm of AC microgrids using HIL testing of IEC 61850 generic object-oriented substation event (GOOSE) protocol. The RT model of AC microgrid including the converter-based distributed energy resources and battery storage along with IEC 61850 GOOSE protocol implementation is created in MATLAB/Simulink and RT-LAB software using OPAL-RT simulator platform. Local area network (LAN) at the laboratory acts as IEC 61850 station bus for exchanging GOOSE Boolean signals between the RT target and the actual digital relay. The evaluation of the round-trip delay using the RT simulation has been performed. It is found that the whole process of fault detection, isolation and adaptive setting using Ethernet communication is possible within the standard low voltage ride through curve maintaining the seamless transition to the islanded mode. The signal monitoring inside the relay is suggested to avoid false tripping of the relay.

INDEX TERMS Adaptive protection, AC microgrid, logic selectivity, IEC 61850 GOOSE, real-time simulation, HIL testing, converter-based DERs, battery storage.

I. INTRODUCTION

Microgrids are the local distribution systems connected with many local distributed energy resources (DERs) and controllable/non-controllable loads with the capability of operating in both the grid-connected and intentional or unintentional islanding modes. The DERs or generators in microgrids include the small-scale variable or non-dispatchable renewable energy sources (VRES) like the wind turbine generators (WTGs) and solar photovoltaic (PV) systems and non-variable or dispatchable RES (NVRES) like mini-hydropower, biomass, geothermal and other combined heat and power (CHP) generators. The VRES usually require some form of energy storage systems (ESS) like battery energy storage systems (BESS), superconducting magnetic energy storage (SMES), supercapacitors (SC), flywheel energy storage systems (FESS) and pumped hydroelectric energy storage (PHES) to smooth out the short, medium and long term operational and weather-related power fluctuations. The ESS including BESS, FESS, and electric vehicles (EVs) may behave like controllable loads when working in the charging mode and as controllable generators when working in the discharging mode. So, depending on the availability of power generation resources measured in terms of

The associate editor coordinating the review of this manuscript and approving it for publication was Siqi Bu.

the active power generation capability of DERs, the state of charge (SOC) of BESS and EVs and their mode of operation (charging or discharging), the microgrid will behave as a net producer or consumer to the main distribution network in the grid-connected operation. However, ideally in the islanded mode of operation the availability of power generation resources including the active and reactive power should be equal to the demand of the local load plus microgrid losses and thus the microgrid should behave as a self-sufficient system [1], [2]. Microgrids can be AC microgrids, DC microgrids or hybrid AC/DC microgrids but in this paper only utility-scale AC microgrids are considered due to their potential for the large-scale adoption in distribution systems.

The AC microgrid is essentially an aggregated system comprised of many parallel operating complex systems like dispatchable and non-dispatchable DERs, ESSs, controllable and uncontrollable loads, hence its operation, management, control, and protection are equally complex in nature [3]. One of the complexities involved in the AC microgrid is its operation also in the islanded mode with the extensive share of the converter-based DERs. In this paper the term ''extensive share'' refers to the 100% share of the converter-based DERs. The operation of microgrid in the islanded mode enhances the reliability of the distribution system but requires different adaptive approaches in terms of operation, management, control and protection compared with the grid-connected mode, particularly, when a large number of converter-based DERs are connected in the islanded microgrid. The converter-based DERs on the one hand offer the quick response times and the possibility of controlling system variables like voltage, current, active power and reactive power smoothly, but on the other hand they lack the inertial response and provide the limited fault contribution. This creates challenges for the traditional control and protection equipment to keep the system intact during different operational and contingency events. Therefore, the need is increased to revise the traditional control and protection schemes, adapt them according to new evolving scenarios or put forward the new control and protection schemes to tackle these challenges [4]. For example, the hybrid centralized and decentralized [5] or distributed hierarchical control systems [6], [7] and adaptive protection schemes using high speed communication links [8]–[11] could be the options to meet new challenges if these schemes are well-designed, prototyped and validated through reliable tests before the actual deployment in the field.

The digital real-time simulations (DRTS) offer the interactive platforms for different complex components of smart grids and microgrids including control, protection and communication devices for testing, validation and prototyping different microgrid design concepts and operations with much reduced costs and risks compared with the fully physical experiments. The real-time (RT) interaction of simulations with individual physical components is not possible with the traditional computer-based offline simulation platforms. Therefore, the popularity of RT simulations has increased in the new era of power system evolution with the increasing penetration levels of DERs connected to transmission and distribution systems. Many designing, testing, prototyping and training studies based on RT simulations are being conducted in the fields of power systems, power electronics, control and communication systems in the broad context of smart grid developments [12]. An overview of RT simulation and testing methods along with the related literature review of the latest studies using RT simulations is presented separately in the next section of this paper.

From the protection point of view, all types of faults inside the microgrid both in the grid-connected and islanded modes should be detected, located, and selectively isolated to prevent the possible damage to the property and equipment without causing supply interruption to the healthy parts of the microgrid [2]. From the control point of view in the grid-connected mode, DERs in microgrid should be operated in a manner to utilize as much renewable energy as locally available and surplus energy should be exported to other parts of the local distribution networks through market participation for net profitability. In the islanded mode of operation, the surplus energy should be stored and the loss of any load or generator due to faults should be equally compensated by generation control/curtailment or load shedding respectively to maintain the voltage and frequency stability of the remaining healthy system inside the microgrid. The microgrid management system (MMS) can achieve power balance through ESS in the primary control level, provide unit commitment and economic dispatch functions through an energy management system (EMS) implemented in the secondary control level and ancillary services to the main grid like voltage and frequency support by tertiary control [3]. A survey of the microgrid EMS is presented in [13] which is based on four categories including non-renewables, ESS, demand side management (DSM) and hybrid systems. The latest literature reviews on microgrid protection and related challenges can be found in [14]–[19].

To ensure the uninterrupted power to the healthy parts of the microgrid, the ESS resources inside the microgrid should be allocated according to the reliability demand of the priority and non-priority load categories and located near the non-dispatchable VRES to avoid the load flow complexities. The larger capacities of ESS equal in capacities to the peak demand of the microgrid loads should, however, be located at the point of common coupling (PCC) so that these could be used as local centralized grid-forming DERs during the islanded mode. For example, in [20] a grid-forming centralized BESS of a minimum 12 MW capacity is selected for a peak load of 31 MW to meet N-1 criterion and replace one diesel generator operation in an islanded power system operating in parallel with another diesel generator of 12 MW and two WTGs of 9 MW and 5.5 MW. The results show that the selected 12 MW capacity of BESS also successfully maintained the stability of the islanded power system. The connection of the peak load capacities of ESS at PCC will provide significant help for the seamless transition of microgrid to the islanded mode. In case of the faults or accidental opening of

the main grid breaker, the rest of the microgrid will be able to operate in the islanded mode by the quick connection of the grid-forming converter of the centralized ESS or changing its control mode from the normal grid-following mode to the grid-forming mode [21], [22]. This way a single stronger source compared with the individual DERs in the microgrid although weaker than the main grid, will still provide enough frequency and voltage stability in the islanded mode. Moreover, the fault detection in the islanded mode will be easier with a stronger centralized ESS providing an additional fault current contribution compared with the case when all the individual fault-current-limiting converter-based DERs are operating in the grid-forming mode with no centralized ESS. However, the individual converter-based DERs should also be capable of operating in both the grid-forming and grid-following modes so that the loss of the centralized ESS due to faults, the accidental opening of the breaker or the cyberattack, etc. should not result in a complete blackout of the islanded microgrid. Even if the blackout occurs inside the islanded AC microgrid, then with a centralized BESS available, the black start or the transient-free resynchronization to the main grid could easily be facilitated [23]–[26].

The grid-following or grid-forming control modes of the converter-based DERs in the grid-connected mode, transition mode, islanded mode and isolated mode (facility island) should therefore in principle be according to the division shown in Table 1. This will ensure the smooth transition from one mode to the other without the loss of voltage and frequency stability as it is evident from the results of this paper. The change of the control mode from the grid-following mode to the grid-forming mode for some or all DERs of the microgrid during the islanded mode operation is recommended in IEEE 1547.4-2011 [27].

In Table 1, the grid-connected mode indicates the operation of the microgrid when DERs, ESS and the loads of the microgrid are completely connected to the main grid synchronously and the microgrid is behaving like a net consumer or producer of the active and reactive power at the PCC. In the grid-connected mode, all the centralized as well as the decentralized DERs/ESS should operate with the grid-following control (Table 1, column 2).

The transition mode indicates the operation of the microgrid when it is partly connected to the main grid or network during the faults or other events which have resulted in the opening of the grid-side breaker but the breaker at PCC is still closed. In the transition mode, the main grid voltage is not available due to the open circuit condition. Therefore, the centralized DER(s)/ESS at PCC of the microgrid should immediately change to the grid-forming control to provide the reference rotating frequency signal (ωt) for the decentralized DERs/ESS during the transition mode (Table 1, column 3). This way the decentralized DER(s)/ESS would not need change their control and keep operating smoothly with the same grid-following control even during the transition mode.

The islanded mode (Table 1, column 4) indicates the situation when the breaker at PCC is also opened and the microgrid is completely isolated from the main grid. In the islanded mode, the centralized DER(s)/ESS should continue operation with the grid-forming control and the decentralized DERs/ESS should continue operation with the grid-following control unless the centralized DER(s)/ESS are also disconnected due to faults or other events. In case the centralized DER(s)/ESS are disconnected, then all the decentralized DERs/ESS should immediately change to the grid-forming control to provide the uninterrupted power for the loads in the islanded mode. It is obvious that the loss the centralized DER(s)/ESS would require other control actions like load shedding or power curtailment for maintaining the voltage and frequency stability of the microgrid in the islanded mode.

TABLE 1. Control modes of DERs according to size/location and operational modes of microgrid.

DER location/size	DERs control in different operational modes of microgrid			
	Grid-connected Mode	Transition Mode	Islanded Mode	Isolated Mode
Centralized[1] *ESS/DER*	Grid-following control	Grid-forming control	Grid-forming control	-
Decentralized[2] *DERs*	Grid-following control	Grid-following control	Grid-following control	Grid-forming control

[1]The DER and/or ESS capacity installed at microgrid PCC equal to combined peak load of microgrid.[2]The capacity of individual DER and/or ESS at downstream of microgrid PCC equal to peak load of the vicinity.

The isolated mode or facility island according to IEEE 1547.4-2011 (Table 1, column 5) refers to the operation of any individual DER/ESS of the declared microgrid facility which is disconnected from the microgrid during the grid-connected or the islanded mode but can fully or partially supply the local load in its immediate vicinity. In the isolated mode, the individual DER/ESS should only operate with the grid-forming control unless it is possible to operate the isolated individual DER and its related ESS with the combined grid-forming and grid-following control. In the combined grid-forming and grid-following control in the isolated mode, the ESS should operate with the grid-forming control while the individual DER should operate in grid-following mode.

The grid-following control mode of DERs is the usual control method in the grid-connected mode operation of the AC microgrids. In the grid-following control mode the voltage (V) and the frequency (f) of the AC microgrid are controlled only by the main grid. The reference rotating frequency signal (ωt) is derived from the measured three-phase grid-side voltage to generate the power of the same frequency as the main grid. A phase-locked loop (PLL) is usually used to extract the rotating frequency signal (ωt) from the measured three-phase grid-side voltage. However, in the islanded, isolated, or even the transition mode after the loss of the

grid connection, the measured three-phase grid-side voltage is not available. Therefore, DERs need to change their control mode from the normal grid-following mode to the local independent voltage and frequency control mode called the grid-forming control of DERs. The grid-forming and the grid-following control of the BESS inverter for AC microgrid is presented in [28]. An overview of the different methods of the grid-forming inverter control is given in [29]. The droop-free distributed secondary control of the grid-forming and grid-following converters in AC microgrids is proposed in [30].

The grid-following or the grid-forming controls of the converter-based DERs can be changed using the trip signal of the circuit breakers (CBs) and/or the local voltage measurements during the fault. When the operation of microgrid is stabilized after the transition mode, the settings of digital relays or the intelligent electronic devices (IEDs) should also be changed adaptively according to the new operational mode (grid-connected, islanded, or isolated mode) to detect and isolate the possible faults in the future. In this paper, the IEC 61850 generic object-oriented substation event (GOOSE) message containing the data of a Boolean signal representing the fault detection/pickup signal of an overcurrent (OC) relay is used for the estimation of the round-trip communication delay. The tripping status of circuit breaker (CB) at PCC is used both for changing the control mode or activation of the centralized BESS and for changing the active setting group of IEDs for an adaptive protection in AC microgrid. However, the magnitude of the local voltage at the connection points of DERs is used to provide the fault ride through (FRT)/low voltage ride through (LVRT) behavior and fault current contribution during the fault.

This paper provides a comprehensive review of the hardware-in-the-loop (HIL) testing methods and applications in the recent literature and presents a step-by-step documentation of a new HIL testing setup for a specific case study. The presented case study evaluates the real-time implementation of previously proposed communication-dependent logically selective adaptive protection algorithm of AC microgrids [11] using the HIL testing of IEC 61850 GOOSE protocol. It is found that the whole process of fault detection, isolation and adaptive setting using Ethernet communication is possible within the standard 150 ms/250 ms LVRT curve. The results look promising for the dynamic voltage and frequency stability and the seamless transition of the AC microgrid to the islanded mode. The real-time HIL testing also detects the intermittent loss of the Boolean signal data using the GOOSE protocol which could result in false tripping of the protection relay. Therefore, the monitoring of the status 0 of the subscribed Boolean signal inside the protection relay is suggested to improve the security of the relay.

The rest of the paper is organized in a way that Section II presents a comprehensive review on the RT simulation and testing methods, and Section III explains the adaptive protection schemes in the AC microgrids. Section IV presents the methodology and results of the real-time HIL testing of the communication-dependent logically selective adaptive protection using IEC 61850 GOOSE protocol. Section V gives a short discussion on the proposed RT testing and its applications and Section VI gives conclusions.

II. REAL-TIME SIMULATION AND TESTING METHODS

The RT simulators for the electrical networks have evolved from the earlier analog simulators or the transient network analyzers using the physical hardwired components of reduced sizes to the hybrid analog and digital simulators. Nowadays the complete digital simulators using the digital signal processor (DSP) and microprocessor technologies are the mainstream. The first commercially available real-time digital simulator (RTDS) was developed and demonstrated by RTDS Technologies using DSP-based proprietary technology. The development of low-cost multi-core processors and commercial off-the-shelf (COTS) computer components from Intel Corporation and Advanced Micro Devices (AMD) paved the way for the development of low-cost and easily scalable fully digital standard computer-based RT simulators. The fully digital computer-based RT simulators have been in use since the end of the 1990s for power system analysis, design, testing, planning and operations. For example, ARENE developed by Electricite de France, NETOMAC developed by Siemens, the general-purpose processor-based RT simulator developed by OPAL-RT Technologies and the dSPACE RT simulation and control. Both the OPAL-RT and the dSPACE RT simulators use MATLAB/Simulink as the main modelling tool for the simulation [31]–[34].

The main difference between the non-RT or offline simulation platforms and the RT simulation platforms is the time required to solve a system of complex equations and produce the output result, called "the execution time" of the simulation (Fig. 1). The RT simulators use a fixed-time step, T_s (for example, 50 microsecond (μs)) for the execution of the simulation with the same rate as the real-world clock. This means the RT simulator solves the system of equations and gives output after a fixed-time interval (step-size T_s) of RT simulation and continues to do so at regular equal time intervals. Therefore, the output voltage and current waveforms are produced using data points at discrete time intervals. Hence,

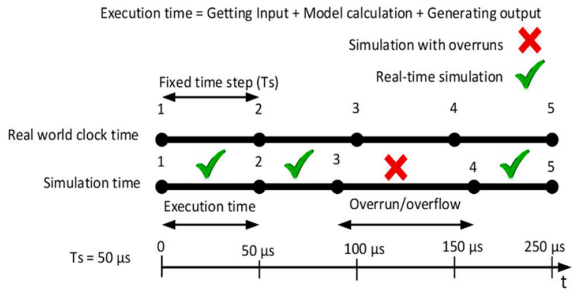

FIGURE 1. The comparison of simulation time with real world clock time for a discrete real-time EMT simulation with and without overruns.

RT simulators are inherently the discrete time electromagnetic transient (EMT) simulators using only the fixed-step solvers. The resolution of the voltage and current waveforms, the accuracy of the results and the speed of RT simulation is greatly dependent on the selection of step-size. The smaller the step-size, the better the resolution and accuracy. If the execution time of the RT simulation is shorter or equal to the selected step-size, the simulation is considered as the real-time. If the execution time is greater than the step-size for one or more time-steps then overruns will occur, and simulation is considered as the non-RT or offline. Fig. 1 explains the RT simulation with and without overruns. In case of overruns during RT simulation, either step-size should be increased, or the system model should be simplified to run the simulation in real-time without overruns. The typical step-size in RT simulators is in the range of 20-100 μs, however by using dedicated field-programmable gate array (FPGA) a step-size of as low as 1 μs can be achieved [32], [35].

A. CLASSIFICATION OF THE DIGITAL REAL-TIME SIMULATION

The DRTS can be classified into two main categories based on the simulation setup and field specific applications: 1) fully digital real-time simulation, and 2) hardware-in-the-loop or HIL simulation. A fully DRTS is the category of simulation in which the entire system including control, protection and other auxiliary devices are modelled inside the simulator and no external devices or inputs/outputs (I/Os) are involved in any case. The model-in-the-loop (MIL), software-in-the-loop (SIL) or processor-in-the-loop (PIL) are considered as the fully digital RT simulation types. The HIL simulation is the type of DRTS in which a part or some parts of the fully DRTS are replaced with physical components like protection relays, converters, controllers etc. In the HIL simulation the device or the hardware-under-test (HUT) is connected to the RT simulator via input/output interfaces like filters, digital-to-analog (DA) and analog-to-digital (AD) converters, signal conditioning devices (power amplifiers and sensors etc.) or communication links. The limited RT simulation controls can be executed with HIL simulations with user-defined inputs like closing and opening of the switches for the connection and disconnection of the components inside the simulated power system [31].

If the HIL simulation employs the external control hardware that interacts with the virtual simulated power system, then the simulation is called the controller hardware-in-the-loop (CHIL) simulation. The CHIL simulation is usually used for rapid controller prototyping (RCP) or testing of a newly developed or designed controllers. In the CHIL simulation, the external controller gets the feedback signals from the RT simulator, processes these feedback signals to generate the required outputs and then sends back these outputs to the simulated system inside the RT simulator. In the CHIL simulation no real power exchange happens to or from the HUT but only the control signals are exchanged. However, if the HUT in the HIL simulation is an actual power source or a sink that can generate or absorb electric power and it is interfaced to the RT simulator using the power amplifiers, then this type of HIL setup is called power hardware-in-the-loop (PHIL) simulation. In the PHIL simulation, the reference signals are generated based on the solution of the virtual simulated system, scaled down inside the model and sent to the power amplifier which produces the appropriate voltages and currents to be applied to the power HUT. In the same way, the feedback signals of the measured voltages and currents from the power HUT are appropriately scaled and sent back to the RT simulator via power amplifiers or sensors for a complete simulation loop [31].

The HIL testing of protection relays does not fall under the category of the PHIL simulation even if the voltage and current amplifiers are used for sensing the actual voltages and currents in relay testing because the protection relays as the HUT do not generate or consume power. The HIL testing of electrical machines, DERs, power electronics converters (EVs and charging equipment etc.), fault current limiters (FCLs) etc. fall under the PHIL simulation category [31]. Whereas the HIL testing of the DER controllers, power electronic converter controllers, phasor measurement units (PMUs), protection relays etc. is considered as the CHIL simulation [36].

In the SIL testing, the basic concern is the compatibility of the power and control simulation software platforms with different communication interface protocols used between them in addition to the synchronization and initial condition mismatch problem. In the CHIL testing, the operating voltage mismatches of analog and digital ports, the noise and delay in the transmitted signal as well as packet loss of the data are the potential challenges. In the PHIL testing, the basic challenge is the use of power amplifiers between the RT simulator and the HUT for voltage scaling and feeding back current to the simulator via an analog port thus forming a closed-loop system. In the PHIL testing, the loss of stability may damage the equipment and in order to achieve stability the accuracy of testing may be compromised. Therefore, fine-tuning is necessary in the PHIL testing to achieve the acceptable level of accuracy without the loss of stability [37]. Fig. 2 presents the generalized categories of the real-time digital simulation used for power system testing.

More recently, the idea of the PHIL simulation which is limited for testing only single devices has been extended for testing the whole microgrids or distribution systems and a new term of Power System-in-the-loop (PSIL) is introduced. The PSIL testing offers the future perspective of hybrid experiments involving power hardware, power network configurations and control hardware and software (combined CHIL and PHIL simulations) but with the increased level of complexity and challenges. These challenges include the complexity of implementing RT compliant interfaces between different components and domains like RT simulations, controllers, electrical components, SCADA (supervisory control and data acquisition) system, etc. Additionally, the issues like communication latency and interface stability

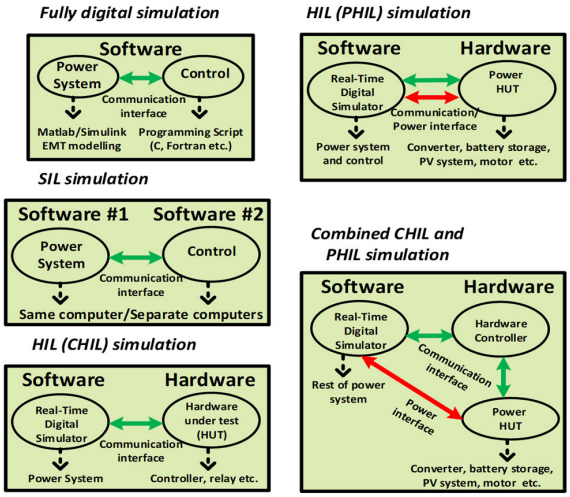

FIGURE 2. The generalized categories of digital real-time simulations for power system testing [36].

need to be assessed properly for ensuring the safety of equipment and the users. The PSIL testing concept can also be adopted for the remote connections of laboratories for the research, development and training purposes [36]. The details of the cyber-physical energy system (CPES) level testing and the validation approach of the European research infrastructure ERIGrid project for a holistic approach of the smart grid can be found in [38]. The fundamentals, challenges and solutions of joint PHIL and co-simulation experiments for the holistic validation of CPES are discussed in [39].

B. REVIEW OF TESTING APPLICATIONS OF RT SIMULATIONS

The applications of RT simulators can be classified into four high-level categories: functional applications, field specific applications, simulation fidelity-based applications and Multiphysics applications. The functional applications of RT simulators include designing, RCP, testing, teaching and training etc. The field specific applications of RT simulators may include but not limited to power systems, power electronics and control systems. The simulation fidelity-based applications of RT simulators include EMT simulations, phasor simulations and hybrid phasor and EMT simulations. Whereas the Multiphysics applications of RT simulators include thermoelectric, electromechanical, power systems with integrated communication and gas networks, etc. [32].

Mainly, there are two types of power disturbances or transients which need to be simulated in power systems: electromagnetic transients (EMTs) and electromechanical transients. The EMTs are very fast occurring disturbances in the time range of μs to milliseconds (ms). The EMTs may happen due to sudden modifications in power system configurations like the opening and closing of the CBs or power electronics switches during the faults or equipment failures. The study and analysis of EMT phenomena require the accurate modelling of power system components.

The electromechanical transients are comparatively slower than the EMTs happening in the time range of milliseconds to seconds. Usually, the oscillations of rotating machines produced by the mismatch of power generation and consumption are related to electromechanical transients. The electromechanical simulations utilize the quasi-steady-state phasor technique for modelling the power system components. The phasors are allowed to vary in order to produce the dynamic response related with rotating machines. The mathematical models in phasor simulations are simplified or averaged versions of EMT models [35], [40].

The use of RT simulations for the analysis of electromechanical transients in phasor domain is not common in scientific research except in dispatcher training simulators [41]. The hybrid or co-simulation of EMT and phasor type RT simulations may be of interest for large transmission and distribution system operators with many DERs for the interactive and interdependent type of studies. Due to the lack of computational ability to perform RT simulations of large-scale power systems in the pure EMT domain only a small part of interest can be modelled in EMT for the HIL testing and the remainder of the power system is modelled in phasor domain. However, the hybrid simulations have the main challenges of using the EMT-to-phasor and phasor-to-EMT converters between two different types of simulations for updating the equivalent circuits in both domains of the hybrid simulation and exchanging the data that should be error-free. Due to the operation of EMT and phasor simulations with different simulation time-steps such as 50 μs and 10 milliseconds, respectively, large errors may happen in case of fast transients in EMT domain. The accuracy of hybrid EMT and phasor type of RT simulations can be at acceptable level in most cases of only AC systems but not for the hybrid AC/DC power systems. For those, additional techniques are required for accuracy improvement [32], [35]. Various case studies of co-simulation of EMT and phasor models are presented in [42]. In this paper, only the fixed-step EMT type of RT simulations are used and discussed for performing the HIL testing of protection relays in the following sections. A brief literature review of recent microgrid and smart grid studies conducted with the help of RT simulations is presented in this section to present the big picture and latest trends in this regard.

A combined CHIL and PHIL simulation for the testing of smart grid control algorithms has been proposed in [37]. In this regard, a four-stage testing chain of the smart grid control algorithm (SGCA) is suggested before the field implementation. These four stages include pure software simulation (offline simulation), SIL testing, CHIL testing and the combined CHIL and PHIL testing. The interface options and the challenges of SIL, CHIL, PHIL and combined CHIL and PHIL tests are also discussed. The combined CHIL and PHIL simulation is applied to a case study of an optimal centralized coordinated voltage control (CVC). The testing is done using

a modified benchmark low-voltage (LV) microgrid presented in [43] assuming a three-phase balanced network.

The CHIL simulation for peak shaving and optimized voltage control using a centralized control scheme and BESS has been presented in [44]. In the same paper PHIL simulation is also presented using a single-phase hardware PV inverter along with PV simulator as HUT.

The development and validation case study of a system-integrated smart PV inverter has been presented in [45]. The case study demonstrated comprises three stages of testing including SIL and CHIL testing, PHIL testing and the cyber-physical PHIL testing with communication network co-simulation. The SIL testing is performed using MATLAB/Simulink models. The controller and its communication interface are implemented using IEC 61499 and the framework for industrial automation and control (4DIAC) based simulation model. For the CHIL testing the real-time models of the power system and PV inverter have been simulated using the Typhoon HIL RT simulator and the smart inverter controller is embedded onto a physical DSP. The PHIL testing is performed using physical hardware comprised of a three-phase PV inverter as HUT which is interfaced to PV emulator via the DC bus and to the grid emulator via the AC bus. The physical hardware is interfaced to the OPAL-RT simulator using AD and DA converters interface. Several tests for different load profiles and microgrid configurations have been performed for the observation of the effects of channel and router delays on the controller and the PHIL distribution network model.

The CHIL testing framework for the validation of microgrid ancillary services is presented in [46] for the verification of the control algorithm and its further improvement. The issues of real-time simulation related to modelling, circuit partitioning and multi-rate design are also discussed in this paper. The advantages of the CHIL testing particularly for the grid-compliance testing of generators and network voltage stability studies have been discussed in [47]. This paper indicates that the CHIL testing has the potential to be considered as a requirement for future standardization procedures.

The HIL co-simulation setup for the RT simulation of the smart grid including the communication network is presented in [48] for testing the coordination between the breakers during a three-phase line fault and the resulting behavior of microgrid after the fault clearance. The test setup consists of Simulink desktop real-time (SLDRT) kernel to generate C-code and National Instruments NI cRIO FPGA hardware. These two simulator platforms are connected and synchronized with each other over Ethernet network using UDP (User Datagram Protocol) protocol. The test setup also includes physical low voltage CB units coordinated using IEC 61850 communication protocols. The setup is able to measure the delays of 31-36 ms due to communication and internal processing of the real devices (relays and CBs). The similar co-simulation setup is also used in [49] for a case study of frequency control of a synchronous generator and PV system microgrid during the reduction in irradiation level of PV system and a load increase at the connection point.

The HIL testing for the control of a battery-less microgrid consisting of a diesel-driven synchronous generator and PV system is presented in [50]. The primary control of the microgrid related to the PV curtailment of the active power based on droop control for the frequency control and meeting the minimum load ratio of the diesel generator is tested using pure digital RT simulation with RTDS simulator. For testing the secondary control algorithm of the microgrid, a combined CHIL and PHIL setup has been used.

The HIL testing platform consisting of three voltage source converters (VSCs), one dSPACE control card, one DC network cabinet, three grid simulators and two RTDS cubicles is presented in [51] for the hybrid AC and DC systems interaction studies. The testing setup can be used for the small and large disturbance studies, testing and validation of ancillary services, grid synchronization, power quality assessment and power system protection. Two case studies one for the subsynchronous resonance damping and the other for the fast frequency support have been demonstrated using the HIL setup.

The details about the application of HIL simulation for the upgradation of the protective relays or IEDs in a large industrial facility are discussed in [52]. The investment of the cost and time in HIL testing technology provided the net saving and increased overall value in terms of many benefits in the development, testing, training and execution of the IEDs upgradation project. The HIL simulation of a hybrid smart inverter is presented in [53]. With this setup of power electronics implemented in Typhoon HIL both the hardware topology and microcontroller unit including the firmware have been tested and improved at different operating scenarios.

The CHIL simulation of a multi-functional inverter operating in AC microgrid has been presented in [54]. The testing setup uses RTDS simulator for the inverter and the AC microgrid modelling and dSPACE hardware for the control implementation. The CHIL simulation-based validation of the ancillary functionalities of the inverter are tested. These tests include the active filtration of harmonic currents in the grid-connected mode, the control of voltage and frequency at the point of connection during the time of islanding (transition mode) and the power flow control of BESS according to the demand and power generation of the PV system.

The PHIL test-bench for hybrid EMT and phasor co-simulation has been developed in [55] to simulate a LV distribution grid and test the dynamic behavior of the power components. The hybrid co-simulation model is developed using MATLAB/Simulink and executed in real-time using a Speedgoat RT target machine. The problems associated with the use of a switched-mode current-controlled power amplifier as a power HUT are highlighted.

The applications of PHIL simulation for laboratory education and understanding the important topics of power system operations including the increased integration of DERs,

power sharing between synchronous generators and DERs, voltage control with on load tap changer (OLTC) and DERs, short circuits with inverter-based DERs and microgrid operation have been discussed in [56]. The positive feedback from students about the use the PHIL simulation for hands-on laboratory exercises and diploma dissertations is also discussed.

The multi-site framework for the RT co-simulation of transmission and distribution systems and the architecture of virtual integration of digital RT simulator laboratories located at four sites in three different countries across Europe connected via pan-European data networks (public Internet) is presented in [57]. Two kinds of interfaces are required for the presented virtual interconnected laboratories for large systems simulation/emulation (VILLAS) architecture: lab-to-lab interface and lab-to-cloud interface. The lab-to-lab interface at each laboratory manages data exchange between the local and remote simulators and acts as a gateway of communication. The data exchange between the lab-to-lab interfaces is done using the UDP protocol due to its lower delay variation compared with the TCP (Transmission Control Protocol). The lab-to-cloud interface manages the data exchange between the laboratory and the cloud platform for the on-demand services. The ideal transformer model interface algorithm (IA) is used for the PHIL co-simulation. The setup uses the time-domain (TD) inside the simulators for EMT simulations and the dynamic phasor (DP) domain for the co-simulation algorithm and data exchange.

The idea presented in [36] is further advanced to establish a global RT Superlab across Europe and the United States (U.S.) by connecting eight laboratories with ten digital RT simulators from three major vendors (OPAL-RT, RTDS and Typhoon HIL) [58]. Another setup of the remote connections of RT simulators located in the laboratories of the U.S. and Australia for performing the geographically-dispersed PHIL co-simulation studies is presented in [59]. The connection of the remote labs is done using a centralized entity in the form of a web application called the simulation whiteboard. In addition to providing the remote interconnections and acting as a watchdog, the simulation whiteboard also performs other functions like simulation coordination, time synchronization and data logging. A case study of smoothing the combined output of PV/battery inverter and PV-only inverter under intermittent solar irradiation is investigated using coordinated control. The power network models are implemented using the GRIDLAB-D software and the PV controller algorithm is implemented in Simulink for this case study.

An analytical approach for the mitigation of communication delays in multiple remotely connected HIL testing experiments has been proposed in [60]. The proposed method includes the procedure of the observer delay compensation approach for the communication delay compensation along with the required computational and communication architecture. The suggested method is validated using the HIL testing between two remotely connected laboratories each having an OPAL-RT simulator separated by a distance of 115 km with a sample mean communication delay of 30 ms per round trip. However, the results are based on perfect knowledge of the model systems and further studies are required for the imperfect and variable knowledge of systems.

The detailed reviews on RT testing and simulation methods for microgrids in different areas of application presented in [61] and [62] are recommended for further in-depth study. For the detailed review on the RT modelling and the simulation methods of power electronics and related challenges, the references [63] and [64] are suggested. The application of RT simulations using FPGA based accurate solutions particularly for different power electronics applications have recently been reported in many references. Related to this the references [65]–[79] are suggested for further reading. Table 2 presents the summary of the latest HIL testing applications.

III. ADAPTIVE PROTECTION WITH IEC 61850

The adaptivity of the protection schemes is the new requirement for the detection and isolation of faults in both the grid-connected and islanded mode operation of AC microgrids. The main reason behind the requirement of the adaptivity is the variation in magnitude of fault current in the grid-connected and the islanded mode. Due to the absence of the main grid in the islanded mode the magnitude of fault current is expected to be lower than the pickup current value of the grid-connected mode particularly if the large number of the converter-based DERs are connected in AC microgrid. This may cause the blinding of the OC relays which are usually used for fault detection in medium voltage (MV) and LV networks. The adaptivity of protection scheme can be implemented either using the same principle of fault detection and isolation or using the separate principles in both modes of operation. For example, the first option could mean using OC relays with different settings in the grid-connected and the islanded mode while the other option means using OC relays only in the grid-connected mode and differential current, directional OC or symmetrical components in the islanded mode. Moreover, the adaptive protection can be implemented using either the centralized or decentralized control and communication architecture. The IEC 61850 communication standard including GOOSE and SV (sampled values) protocols using Ethernet network could facilitate the implementation of successful adaptive protection schemes. Several adaptive protection schemes have been suggested in the scientific literature as previously reviewed and reported in [2], [4], [11], [80]. The most practical and latest adaptive protection schemes are reviewed in this section.

An adaptive protection using the centralized control and communication architecture has been demonstrated and practically installed at a 20 kV feeder pilot of the largest geographical island in Finland called the Hailuoto island. The islanded mode operation on the Hailuoto island is supported by a 0.5 MW WTG and a 1.5 MW diesel generator for a peak load of 1144 kW. The centralized adaptive protection is

TABLE 2. Summary of different HIL testing applications.

HIL type	Simulator	App field	Case study	Benchmark system
CHIL [46]	-	MGC[2]	Ancillary services	Generic MG[1] system
CHIL [47]	-	Grid code	Voltage stability, LVRT, anti-islanding.	Generic test setup
CHIL [48][49]	SLDRT + NI cRIO FPGA	MGCP[3]	Coordination, frequency control.	Generic MG system
CHIL [51]	RTDS + dSPACE	Hybrid AC/DC power	Subsynchronous resonance, fast frequency support.	Generic lab setup
CHIL [52]	-	Relay upgrade	IEC 61850, protection & metering.	Industrial substation
CHIL [53]	Typhoon HIL	Power electron.	Control of hybrid smart inverter.	Experimental prototype
CHIL [54]	RTDS + dSPACE	MGC	Power control, harmonic filter.	Generic MG system
PHIL [55]	Speedgoat	Power distribution	EMT-phasor co-simulation, power amplifier as HUT.	LV distribution grid
PHIL [57]	RTDS + OPAL-RT	Remote lab connections	Lab-to-lab co-simulation, PV generation and EV charging impact on voltage & freq.	Italian transmission & distribution grid
PHIL [59]	GRIDLAB-D + PNSS	Remote lab connections	Smoothing of PV output power during intermittent solar irradiation.	US & Australian distribution networks
CHIL, PHIL [37]	RTDS	SGC[4]	Optimal centralized voltage control.	Modified 3-Ph CIGRE LV network [43]
CHIL, PHIL [44]	-	SGC	Peak shaving, voltage control.	1-Ph CIGRE LV network
SIL, CHIL, PHIL [45]	Typhoon HIL + OPAL RT	MGC	Intentional islanding, the effects of channel and router delays on controllers.	Generic MG system
CHIL, PHIL [50]	RTDS	MGC	Primary & secondary control, demand response, active power curtailment.	Generic lab setup
CHIL, PHIL [58]	RTDS + OPAL-RT + Typhoon HIL	Global RT Superlab	Co-simulation, active & reactive power control at AC/DC transmission & distribution.	CIGRE HV & MV networks, CERT MG, IEEE 13 bus feeder, PV test bed.

[1]MG = Microgrid, [2]MGC = Microgrid control, [3]MGCP = Microgrid control and protection, [4]SGC = Smart grid control.

applied using IEC 61850 communication standard for changing the directional OC relays settings [10].

The centralized communication-assisted protection for MV microgrids with the converter-based DERs proposed in [81] uses symmetrical current components based directional module and OC relays in the grid-connected mode and the under-voltage, the symmetrical current components based high-impedance fault detection and the directional module for the islanded mode of operation. The scheme uses the definite time coordination in combination with fault detection modules as a backup if the communication fails. The proposed scheme does not use the adaptive settings, however the separate methods for fault detection in the grid-connected and islanded modes. To activate and deactivate different methods of the variable sensitivities in the grid-connected and islanded modes, the scheme necessarily requires the communication signal which makes the scheme fall under the category of adaptive protection schemes. The adaptive protection schemes using the centralized communication architecture have also been suggested previously in [82]–[84].

An adaptive protection for a campus microgrid presented in [85] uses the directional OC relays with adaptive settings for the detection of load-side faults and for the implementation of the localized differential protection to detect faults in the loop sections. The islanding mode operation is supported by a gas turbine synchronous generator operating in parallel to the WTGs, PVs and BESS to service a load of 8 MW. The adaptive scheme proposed uses the transfer trip or the permissive overreaching transfer trip (POTT) as the backup for the primary protection failures and the non-directional substation OC relay as the backup of the transfer trip failures in the grid-connected mode. A high speed (2 ms) optical fiber communication link with highly reliable communication capability is used for the adaptive protection. The scheme prefers the localized differential protection over the centralized differential protection due to the fact that the centralized scheme results in unacceptable computational time delays by the central controller.

The other adaptive and IEC 61850 communication-based protection schemes have been suggested recently for microgrids and distribution networks with DERs in [86]–[93]. Our previous paper [11] proposed an adaptive protection algorithm using IEC 61850 GOOSE communication for a radial AC microgrid to operate within the standard LVRT time period of DERs.

The proposed method provides the natural coordination in terms of the standard time delays of 10 ms or 20 ms between the publication and the subscription of a Boolean GOOSE signal. Thus, the process of fault detection and isolation is accomplished within the standard LVRT curve of DERs after the fault if the communication is reasonably reliable. In this paper, the reliability of the proposed method is practically checked using the real-time HIL simulation of IEC 61850 GOOSE protocol implemented in the RT target and the actual digital relay. However, the previously proposed algorithm for the detection and isolation of a three-phase (3Ph) close-in short-circuit fault F1 near the microgrid PCC (Fig. 5) is slightly modified in this paper. The only modification is that DER control and adaptive settings are changed with respect to CB2 status change rather than CB1 status change. Further improvements have been suggested to increase the reliability of the proposed communication-dependent logically selective adaptive protection. The scheme is capable of being extended also to the looped microgrids and can be implemented with the centralized or the decentralized communication architecture.

IV. HIL TESTING METHODOLOGY AND RESULTS

Fig. 3 presents the modified version of the previously proposed communication-dependent adaptive and logically

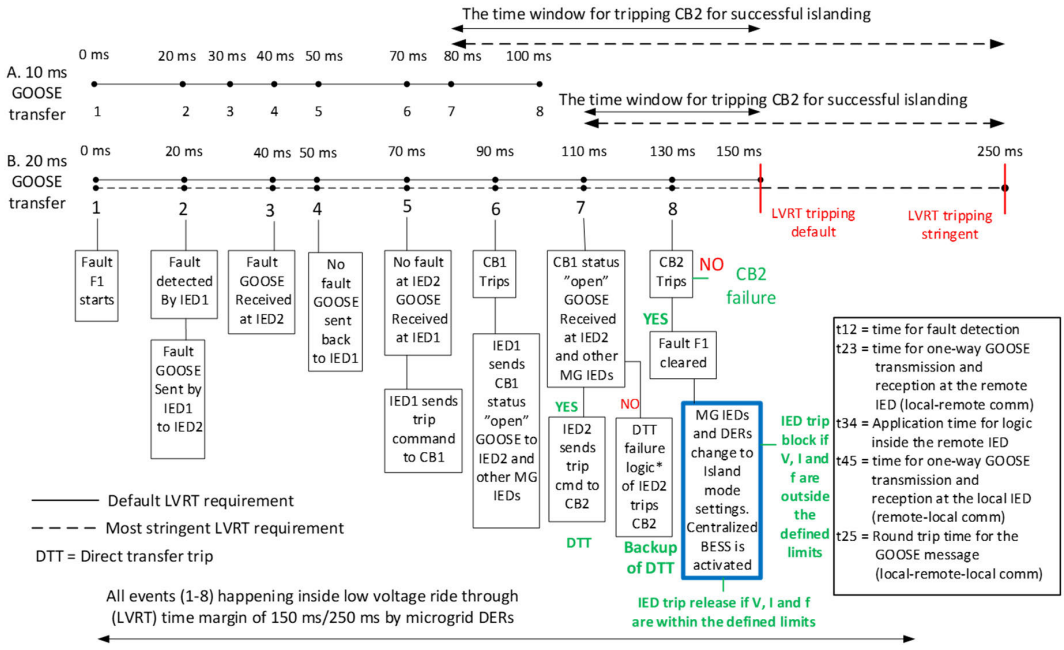

FIGURE 3. The communication-dependent logically selective protection algorithm for the detection and isolation of fault F1 using the centralized control architecture and aligned with EN 50549-1-2019 and EN 50549-2-2019 LVRT standards.

selective fault detection and isolation algorithm for the grid-side fault F1 in [11]. The main modification is that in the modified algorithm the control of DERs and the setting groups of IEDs are changed after the opening of the CB2 at the PCC of the microgrid which was done previously after the opening of the grid-side circuit breaker CB1. The algorithm assumes that the fault F1 happens in the grid-connected mode between the CB1 and CB2 locations and only the grid-side relay at CB1 location detects the fault F1. Additionally, the modified algorithm also includes the most stringent LVRT requirement for the converter-based DERs according to the new European grid code standards EN 50549-1:2019 and EN 50549-2:2019.

Fig. 3 and Fig. 4 show the implementation of the proposed algorithm with the centralized and the decentralized control architecture, respectively. With the centralized control architecture, if the fault F1 happens then the central relay at CB1 collects the fault information and then decides to open the circuit breaker CB1 and sends transfer trip command to the remote circuit breaker CB2. With the decentralized control architecture, if the fault happens then each relay at CB1 and CB2 locations collects the fault information and decides to open the corresponding circuit breaker independently. In this paper, only the protection algorithm using the centralized control architecture (Fig. 3) is evaluated.

The main objective behind the HIL testing is to estimate the round-trip time of a fault detection Boolean signal using the real-time simulation. It means the estimation of time delay from the event 2 to event 5 (t_{25}) of the protection algorithm of Fig. 3 which is actually the round-trip time between relays at CB1 and CB2 locations. The other objective is to check if the "10 ms GOOSE transfer" timeline is more practical than the "20 ms GOOSE transfer" timeline (Fig. 3). In the HIL testing CB1 is opened instantaneously after collecting "No fault" information of the IED at CB2 using the IEC 61850 GOOSE protocol and CB2 is opened using the transfer trip command from the IED at CB1 location.

This section explains the steps taken to carry out the IEC 61850 GOOSE communication-based HIL testing of VAMP digital relay using the RTDS of OPAL-RT and Ethernet link communication. Both the VAMP digital relay and the OPAL-RT simulator were capable of publishing and subscribing at least one Boolean signal using IEC 61850 GOOSE protocol. The testing of VAMP digital relay not only involved the successful publication and subscription, but it also included the recording of the real-time Boolean signal (fault detection signal) during the publication and the subscription by both the real-time digital simulator and the VAMP relay. The real-time GOOSE signal data was recorded using OpWriteFile block of the OPAL-RT simulator which saves the real-time data in a MATLAB file (.mat) format. The subscription of the real-time GOOSE signal by the VAMP relay, however, involved only the time stamp-based subscription of GOOSE message visible from the "Event Buffer" memory of the VAMP relay. In other words, it was not possible to record the subscribed GOOSE signal of the VAMP relay

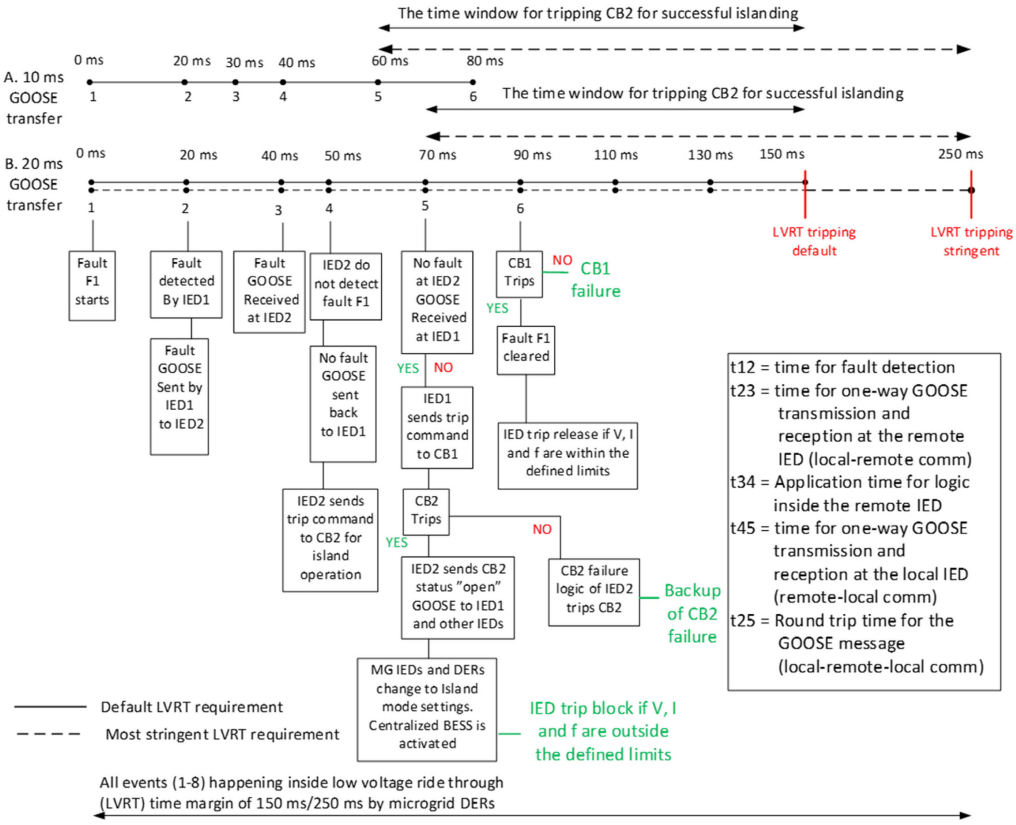

FIGURE 4. The communication-dependent logically selective protection algorithm for the detection and isolation of fault F1 using the decentralized control architecture and aligned with EN 50549-1-2019 and EN 50549-2-2019 LVRT standards.

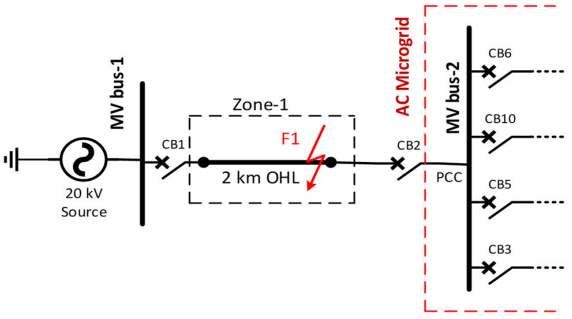

FIGURE 5. The 3Ph close-in short-circuit fault F1 near microgrid PCC.

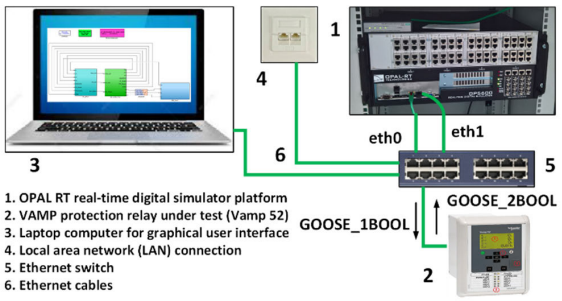

FIGURE 6. The HIL testing setup at the FREESI Laboratory.

by the OPAL-RT simulator at the receiving-end Ethernet link adapter of the VAMP relay. This means the OPAL-RT simulator could only record the Boolean signal in real-time at three instances: 1. When the GOOSE signal is published by the OPAL-RT simulator, 2. When the GOOSE signal is subscribed by the OPAL-RT simulator, and 3. When the GOOSE signal is published by the VAMP relay and subscribed by the OPAL-RT simulator. Fig. 6 presents the IEC 61850 GOOSE HIL testing setup at the FREESI (Future Reliable Electrical and Energy Systems Integration) laboratory of the University of Vaasa, Finland.

The HIL testing setup hardware in Fig. 6 includes the OPAL-RT simulator platform, VAMP relay, the laptop computer for the graphical user interface (GUI) for commands and the visualization of the results, the Ethernet switch and the Ethernet cables for connections. The software involved

in this HIL testing includes the RT-LAB of OPAL-RT, MATLAB/Simulink toolbox Simscape (the previous SimPowerSystems), VAMPSET relay configuration software and the Wireshark network protocol analyzer to capture the published GOOSE message packets from the local Ethernet. The description of the hardware involved in the IEC 61850 GOOSE protocol testing is given in the following subsections.

A. REAL-TIME HIL TESTING HARDWARE

1) OPAL-RT SIMULATOR PLATFORM

The OPAL-RT simulator platform used for the HIL testing case study is OP5600 HIL Box (Fig. 6, number 1) with four 3.2 GHz INTEL processor cores with Redhat Linux operating system and six Ethernet network ports. Two Ethernet network ports are available at the front while the rest of the Ethernet network ports are located at the back of the chassis. The OP5600 simulator is available in different configurations operating with either Spartan 3 or Virtex 6 FPGA platforms with the target computer having minimum four to maximum thirty-two 2.4 or 3.3 GHz cores or without any target computer. In general, the front of the OP5600 HIL Box chassis consists of the monitoring interfaces and connectors whereas the back of the chassis consists of all I/O connectors, power cable, main power switch and the FPGA monitoring connections. The main housing architecture of the OP5600 HIL Box is divided into two sections: The upper section and the lower section. Both the upper and the lower sections are connected by a DC power cable and a PCIe (Peripheral Component Interconnect Express) cable, a high-speed serial computer expansion bus [94], [95]. The signal conditioning modules in the used platform include the OP5330 DA converter module with 16 single-ended output channels [96], the OP5340 AD converter module with up to 16 differential channels [97], the OP5353 digital input signal conditioning module with 32 opto-isolated digital inputs (4-50 Vdc input voltage) [98] and the OP5360 digital output module with 32 digital output channels (5-30 Vdc output voltage) [99].

2) THE VAMP RELAY UNDER TEST

The device or the hardware-under-test called HUT used in the HIL testing is VAMP 52 feeder and motor protection relay of the Schneider Electric (Fig. 6, number 2). The Vamp 52 is a numerical protection relay or IED with signal filtering, protection and control functions fully implemented through digital processing. The VAMP 52 protection relay uses an adapted Fast Fourier Transformation (FFT) numerical technique. By using the synchronized sampling of the measured signal (voltage or current) with 32 samples per cycle, the FFT solution is realized with just a 16-bit micro controller without the help of a separate DSP.

The protection functions of the VAMP 52 relay include a three-stage OC protection (IEC: I>, I≫, I≫> or IEEE: 50/51), thermal overload protection (IEC: T> or IEEE: 49), current unbalance protection (IEC: I_2/I_1 > or IEEE: 46), CB failure protection (IEC: CBFP or IEEE: 50BF) and several other feeder and motor specific functions. The VAMP 52 relay has also eight independent programmable stages (IEC: Prg1-8 or IEEE: 99) for special applications. The user can select the supervised signal and the comparison mode to build custom programmable protection stages. The VAMP 52 relay has four setting groups available and the switching between setting groups can be controlled manually or by using the digital and virtual inputs including mimic display, communication and logic inputs.

The VAMP 52 relay is capable of communicating with other systems using the most common protocols including Modbus RTU (Remote Terminal Unit), Modbus TCP, Profibus DP (Decentralized Periphery), IEC 60870-5-101, IEC 60870-5-103, IEC 61850, SPA (Strömberg Protection Acquisition) bus, Ethernet/IP and DNP (Distributed Network Protocol) 3.0. [100].

3) OTHER HARDWARE

The laptop computer used is equipped with Intel(R) Core (TM) i7-6600U CPU (central processing unit) @ 2.60GHz, 2.81 GHz processor and 16 GB (gigabyte) of installed RAM. The computer is connected to the same Ethernet network switch where the OPAL-RT simulator and the VAMP relay are connected (see Fig. 6). One port of the Ethernet switch at the lab is connected to the local area network (LAN) which acts as IEC 61850 station bus with all devices connected to it.

B. THE CREATION OF RT SIMULATION MODEL

In this section the description about the general benchmark model of a radial AC microgrid used for the HIL simulation is given along with the modelling steps to create the MATLAB/Simulink Simscape and RT-LAB real-time versions of the described AC microgrid model. Additionally, the implementation of IEC 61850 communication inside the RT model of the AC microgrid is also described in this section.

1) THE RADIAL AC MICROGRID MODEL IN SIMULINK/SIMSCAPE

The schematic diagram of a general benchmark model of a radial AC microgrid used for the HIL testing is shown in Fig. 7. The AC microgrid is connected to the 20 kV main grid MV bus-1 at CB2 location via a 2 km overhead line. CB2 location is therefore the PCC for the main grid and the AC microgrid. The normal downstream connections at MV bus-2 in the AC microgrid consist of a WTG of 2 MW capacity, a load of 2 MW and a 1 km MV cable feeder connecting MV bus-2 with LV bus through a 0.5 MVA, 20/0.4 kV transformer. Additionally, a BESS of 2.1 MW capacity is also connected at MV bus-2. The BESS is assumed as a charging load in the grid-connected mode, while it can be used as a grid-forming source only during the islanded mode of operation when CB2 is open due to fault F1. The LV bus of the AC microgrid consists of a PV system of 400 kW capacity and a load of 400 kW.

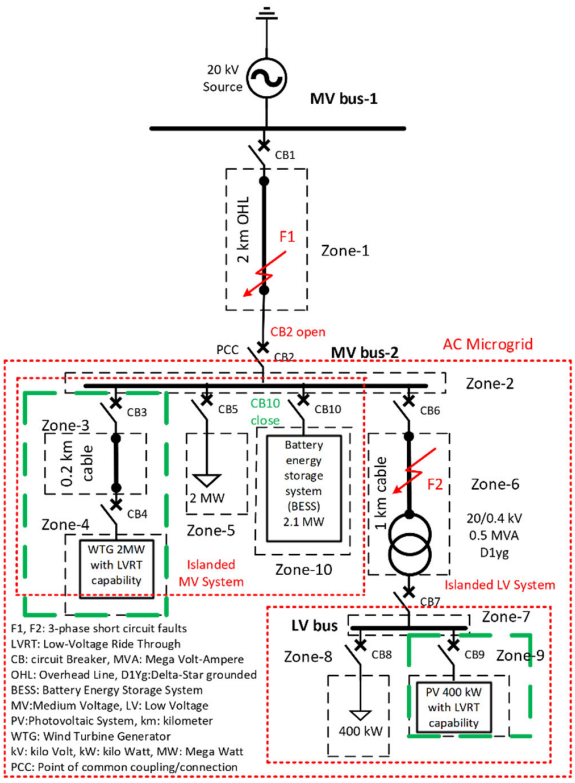

FIGURE 7. The general benchmark model of a radial AC microgrid used for HIL testing.

The radial AC microgrid model (Fig. 7) was previously modelled and analyzed using offline simulations in PSCAD software for the development of an adaptive protection algorithm using the IEC 61850 communication standard but without the connection of a BESS (Zone 10 in Fig. 7). The details about the developed adaptive protection algorithm and the fault analysis with the earlier PSCAD model can be found in [11]. The AC microgrid model has been further developed using MATLAB/Simulink modelling environment with an additional BESS of 2.1 MW_{peak} connected at MV bus-2 to be used as grid-forming source for the islanded mode of operation.

The WTG, PV and BESS models are the average type models developed in MATLAB/Simulink; their details are given in the next subsection. The overhead line and cables are represented by 3Ph pi-section lines, the transformers are 3Ph two-winding transformers, and the main grid is represented by a 3Ph 20 kV 50 Hz programmable voltage source. The results of the protection coordination of the definite-time and the inverse-definite minimum time (IDMT) OC relays in the grid-connected mode without and with DERs and in the islanded mode with DERs and the central grid-forming BESS have already been presented in the previous paper [4] using MATLAB/Simulink and RT-LAB version of the model.

In this paper, the HIL simulation testing of the actual VAMP relay is performed after the real-time implementation

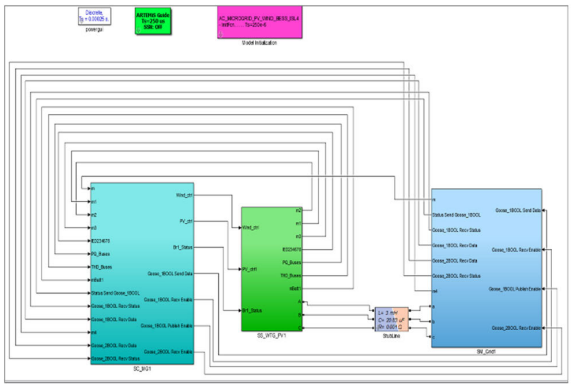

FIGURE 8. The topmost view of the RT model of AC microgrid developed in Simulink/RT-LAB with IEC 61850 GOOSE protocol implemented.

of the IEC 61850 publisher and subscriber blocks in the RT-LAB model using the Ethernet communication link. The main objectives are to find the expected round-trip communication delays of a Boolean signal exchanged between two relays at different substations (the centralized and distributed relays), the seamless transition from the grid-connected to the islanded mode with the exchange of Boolean logical signals and the implementation of an adaptive protection during the grid-connected and the islanded mode. In this way, the realization extent of the earlier proposed adaptive protection algorithm [11] can be found with HIL simulation testing for its practical implementation. Additionally, the dynamic behavior of DER models in real-time simulation is also compared.

2) THE RT COUNTERPART OF THE RADIAL AC MICROGRID MODEL

After the complete offline modelling and simulation of the AC microgrid model (Fig. 7), the model was converted to the real-time version using the RT-LAB software of OPAL-RT. The topmost level of the AC microgrid model developed in Simulink and RT-LAB is presented in Fig. 8.

The developed RT-LAB model (Fig. 8) consists of total three subsystems, two of them are computational subsystems named as SM_Grid1 and SS_WTG_PV1 and one is a console subsystem named as SC_MG1. The data between two computation subsystems (SM_Grid1 and SS_WTG_PV1) is exchanged synchronously through shared memory. The data between any computational subsystems (SM_Grid1 or SS_WTG_PV1) and the console subsystem (SC_MG1) is exchanged asynchronously through TCP/IP link.

The SM_Grid1 and SS_WTG_PV1 subsystems are connected with each other using an ARTEMiS stubline which provides the decoupling of the state space matrices of two subsystems thus reducing the memory overflow and increasing the simulation speed. The details of the SM_Grid1 subsystem are shown in Fig. 9.

The SM_Grid1 subsystem consists of the main grid components up to zone-1 of Fig. 7 including 20-kV 3Ph

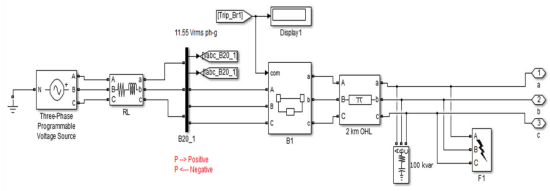

FIGURE 9. The details of the SM_Grid1 subsystem of the developed Simulink/RT-LAB model.

programmable voltage source, MV-bus1, CB1 and overhead line of 2 km. Additionally, a 3Ph capacitor bank of 100 kvar is also connected in this subsystem for the proper voltage regulation. A 3Ph short-circuit fault F1 with $R_f = 5.001$ Ohm at the end of 2 km overhead line is also located in SM_Grid1 subsystem. The rest of the components of AC microgrid of Fig. 7 including the components in protection zones 2-10 and circuit breakers CB2-CB10 along with 3Ph short circuit fault F2 with $R_f = 0.001$ Ohm are located in SS_WTG_PV1 subsystem. The details of SS_WTG_PV1 subsystem are given in Fig. 10. The details of the PV_system1 and the BESS inside the SS_WTG_PV1 subsystem are given in Fig. 11 and Fig. 12, respectively.

The WTG model (Fig. 10, green) is adopted from the example model [101]. However, the parameters of the WTG model like voltage, power capacity, frequency etc. have been changed according to the AC microgrid model of Fig. 7. The WTG average model is able to run correctly with fixed time-step discrete solver suitable for RT simulation. The time-step of 250 μs is used to avoid overruns during RT simulation. The WTG model is also capable of providing the LVRT during the faults with an optional fault current contribution of 1.2-2 times the full rated current during the short circuit fault by setting the maximum output current limit of its full-scale converter.

The PV model (Fig. 11) is adopted from the "Active Distribution Grid" model developed in [102], [103]. However, the parameters (voltage, power capacity etc.), the control and the protection of the PV model have been modified according to the AC microgrid model (Fig. 7). The LVRT behavior is also added to the PV model to provide 1.2-2 times the full rated current during the short circuit faults when the grid-side voltage drops below 50%.

The BESS model (Fig. 12) has been developed on the basis of the PV model given in [104]. The 2.1 MW_{peak}, (600 V_{dc} (nominal), 698 V_{dc} (fully charged), 3000 AH (nominal)) battery is connected at the input of DC-DC boost converter to raise its voltage to 1100 V_{dc} at the DC-link. The 1100 V_{dc} at the DC-link was used as input to a 3Ph inverter for getting 690 V_{ac} at the output RLC-filter which is then step up to 20 kV by a 2.5 MVA, 0.69/20 kV 3Ph transformer for the connection to the MV bus-2.

After the creation of subsystems, the next step is to take measurement signals out from the computation subsystems to the console subsystem for the real-time observation of the model behavior. The measurements from

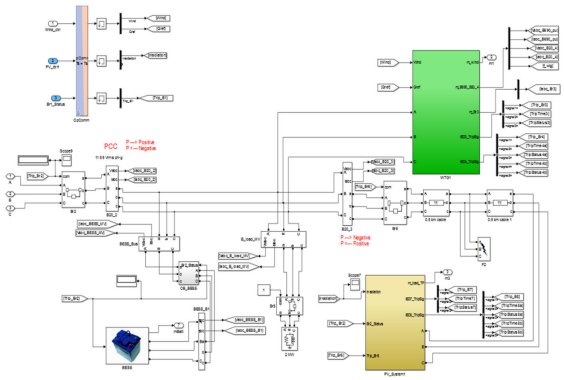

FIGURE 10. The details of the SS_WTG_PV1 subsystem of the developed Simulink/RT-LAB model.

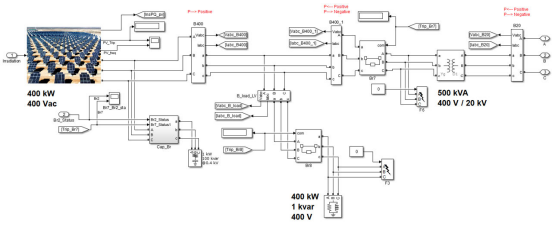

FIGURE 11. The details of the PV_System1 of the SS_WTG_PV1 subsystem of the developed RT-LAB model.

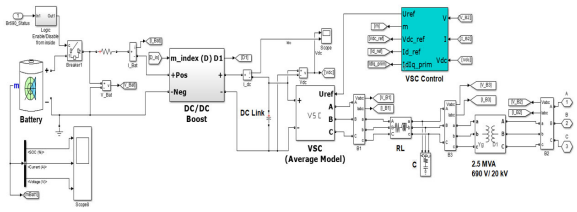

FIGURE 12. The details of the BESS of the SS_WTG_PV1 subsystem of the developed RT-LAB model.

the output ports (Outports) of one subsystem to the input ports (Inports) of the other subsystem have to be transferred through OpComm blocks of the RT-LAB/ARTEMiS. Fig. 10 shows three input ports with different control signals transferred from SC_MG1 subsystem to the SS_WTG_PV1 subsystem through OpComm block located in SS_WTG_PV1 subsystem. In the same way, different measurements have been transferred from the SM_Grid1 subsystem and SS_WTG_PV1 subsystem to the SC_MG1 (Fig. 8) using the individual OpComm blocks with unique "Acquisition Group" numbers for each measurement inside the SC_MG1 subsystem. If everything is correctly connected and the settings of the model are saved using Simulink, the model is ready for the real-time software-in-the-loop or fully digital RT simulation using the RT-LAB software. However, for the implementation of IEC 61850 protocol, extra

publisher and subscriber blocks are required as explained in the next subsection.

With the addition of the RT target in RT-LAB and the availability of the RT-LAB model in the project explorer, the model can be opened in RT-LAB editor for the compilation or code generation. The C code can be generated and transferred to the target using the ''Build the model'' command. Any errors generated during ''Build the model'' process have to be removed first before proceeding to the next step of ''Load the model.''

After the successful completion of the ''Build the model'' process without any error messages, the next step is to ''Load the model.'' After ''Load the model'' command from the RT-LAB editor, the model will be loaded on the target and a message will appear in the ''view'' section of the RT-LAB under the ''Display'' tab indicating a pause mode with ''zero (0)'' overruns.

The final step is the real-time running of the RT-LAB model by ''Execute the model'' command from the model editor. This will open the console subsystem ''SC_MG1'' replica created automatically by RT-LAB. From this console, the real-time measurements can be seen and controlled by changing the controller inputs on-the-fly. The display view of the model will show the new message indicating the run mode along with synchronized time step of the simulation.

From the monitoring view of the RT-LAB model (the last Fig. in Appendix), it can be seen if the model is running with any overruns or not and how much is the minimum, maximum and average timing jitter of each subsystem of the model. A timing jitter can be defined as the difference between the expected execution time (Ts) and the actual execution time (dt) of the simulation. A timing jitter around 7 μs is considered as a good jitter according to OPAL-RT. As mentioned in the earlier chapters, too little time-step of simulation may give overruns and too large a time-step will give erroneous results. If the jitter is too close to the time-step of simulation, it will cause overruns. In most cases, the overruns will vanish after increasing the time-step of simulation. The accuracy of the results should be carefully checked by saving the results in MAT-file format using the OpWriteFile block of ARTEMiS by carefully setting its mask parameters.

3) THE IMPLEMENTATION OF IEC 61850 GOOSE PROTOCOL IN THE RT MODEL FOR HIL TESTING

For the Ethernet network transmission of the Boolean signals represented by logical states of 0 and 1 for the YES/NO fault detection or open/close states of the CBs of the model, the IEC 61850 GOOSE protocol needs to be implemented inside the error free RT-LAB model. The implementation of the IEC 61850 GOOSE protocol in RT-LAB model can be done through ''Opal IEC 61850 GOOSE Publisher'' and ''Opal IEC 61850 GOOSE Subscriber'' blocks of IEC 61850 library of the RT-LAB. Although, the GOOSE publisher and subscriber blocks can be located in any computation subsystems like SM_Grid1 or SS_WTG_PV1, but these have been placed only in SM_Grid1 subsystem of the RT-LAB model.

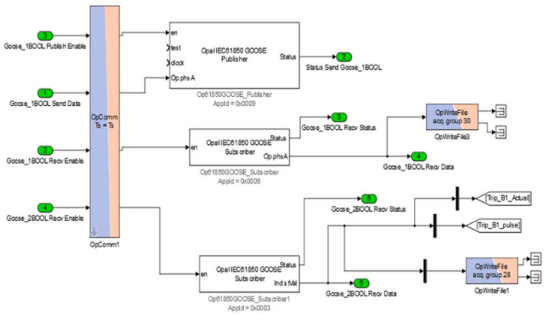

FIGURE 13. The Opal IEC 61850 GOOSE publisher and subscriber blocks placed inside SM_Grid1 subsystem.

TABLE 3. Inputs and outputs of goose publisher and subscriber blocks.

Input/ Output	Description (signal name)	From/To subsystem
GOOSE PUBLISHER BLOCK (AppId = 0x0009)		
en	Enable or disable GOOSE publication (Goose-1BOOL Publish Enable)	From SC-MG1
test	-	-
clock	-	-
Op phsA	Data of the signal to be published (Goose-1BOOL Send Data)	From SC-MG1
Status	True/False status of published signal (Status Send Goose-1BOOL)	To SC-MG1
GOOSE SUBSCRIBER BLOCK (AppId = 0x0009)		
en	Enable or disable GOOSE subscription (Goose-1BOOL Recv Enable)	From SC-MG1
Status	True/False status of subscribed signal (Goose-1BOOL Recv Status)	To SC-MG1
Op phsA	Data of the subscribed signal (Goose-1BOOL Recv Data)	To SC-MG1
GOOSE SUBSCRIBER BLOCK (AppId = 0x0003)		
en	Enable or disable GOOSE subscription (Goose-2BOOL Recv Enable)	From SC-MG1
Status	True/False status of subscribed signal (Goose-2BOOL Recv Status)	To SC-MG1
Ind stVal	Data of the subscribed signal (Goose-2BOOL Recv Data)	To SC-MG1

The Opal IEC 61850 GOOSE Publisher and Subscriber blocks inside the SM_Grid1 subsystem and their inputs and outputs are shown in Fig. 13 and described in Table 3. There is only one GOOSE publisher block with application ID AppId = 0 × 0009 used for sending the fault detection Boolean signal represented by GOOSE message name ''Goose_1BOOL'' from the OC relay inside the SM_Grid1 subsystem to the station bus/Ethernet switch (Fig. 6, number 5) for the IED under test (VAMP relay) to subscribe.

The GOOSE publisher block (Fig. 13, Table 3) receives two input signals from the console subsystem SC_MG1 namely ''Goose_1BOOL Publish Enable'' and ''Goose_1BOOL Send Data'' and sends one output signal ''Status Send Goose_1BOOL'' to the console subsystem SC_MG1. The output of the GOOSE publisher block named as ''Status Send Goose_1BOOL'' is sent to the console subsystem SC_MG1 for the real-time monitoring. A simple

two-way control switch with input 1 to enable and input 0 to disable the publishing of the GOOSE message is used inside the SC_MG1 subsystem for controlling the ''Status'' output of the published signal in real-time. The output of the two-way control switch is directed back to the SM_Grid1 subsystem as the signal ''Goose_1BOOL Publish Enable'' connected to the input ''en'' of the GOOSE publisher block. The GOOSE publisher block will publish the GOOSE_1BOOL signal to the station bus/Ethernet switch only if the status of its input ''en'' is logical ''TRUE''. The second input signal to the GOOSE publisher block is the actual GOOSE data signal named as ''Goose_1BOOL Send Data'', here it is the fault detection signal of OC relay inside SM_Grid1. The fault detection data signal is already transferred to the console system SC_MG1 from the SM_Grid1 subsystem for the real-time monitoring. Now the fault detection signal is directed back from the console subsystem SC_MG1 back to the SM_Grid1 as input ''Goose_1BOOL Send Data'' to the GOOSE publisher block connected to its input ''*Op phsA*'' for publishing to the Ethernet switch.

The first GOOSE subscriber block with AppId $= 0 \times 0009$ (Fig. 13, Table 3) receives the only input control signal ''en'' from the console subsystem SC_MG1. A simple two-way switch with input 1 to enable and input 0 to disable the subscription of the GOOSE message is used inside the console subsystem SC_MG1 for the real-time control of input ''en''. The GOOSE subscriber block will subscribe to the GOOSE signal from the station bus/Ethernet switch only if the status of its input ''en'' is logical ''TRUE''. The real-time status of the subscribed signal can be monitored from the first output ''Status'' of the GOOSE subscriber block. The second output ''*Op phsA*'' of the GOOSE subscriber block contains the actual data of the Goose_1BOOL signal subscribed from the Ethernet switch that is sent to the console subsystem SC_MG1 for the real-time monitoring. The real-time subscribed signal ''Goose_1BOOL Recv Data'' can also be saved in MAT-file using the OpWriteFile block (Fig. 13) for offline data analysis later to check the quality/performance of the subscribed data signal.

The second GOOSE subscriber block with AppId $= 0 \times 0003$ (Fig. 13, Table 3) also receives the only input signal ''en'' from the console subsystem SC_MG1. This GOOSE subscriber block is used to subscribe to the Goose_2BOOL signal published by the VAMP relay to the Ethernet switch. The real-time subscribed signal ''Goose_2BOOL Recv Data'' is sent to the console subsystem SC_MG1 for the real-time monitoring. This signal can also be saved in MAT-file using the OpWriteFile block (Fig. 13) for offline data analysis later to check the quality of the subscribed signal. The real-time monitoring and saving of the data of the published and subscribed GOOSE messages establishes a closed-loop two-way communication link between the OPAL-RT target and the actual VAMP relay through the Ethernet switch.

The real-time subscribed signal ''Goose_2BOOL Recv Data'' published by the VAMP relay has been used to trip CB1 in real-time inside the SM_Grid1 subsystem. The same data signal sent from the SM_Grid1 subsystem to SS_WTG_PV1 subsystem via the console subsystem SC_MG1 is also used for tripping CB2. The results are explained in the following sections. The control and data inputs connected to the GOOSE publisher and subscriber blocks have to pass through the OpComm block first as it is done in Fig. 13.

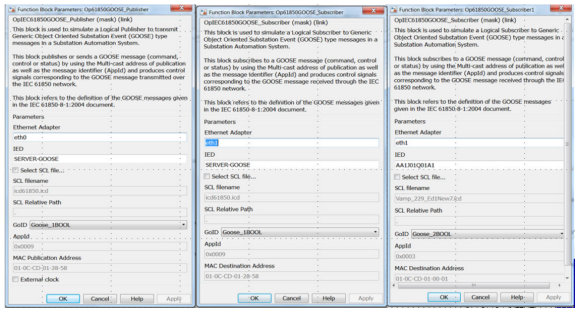

FIGURE 14. The parameter settings of the GOOSE publisher and subscriber blocks of Fig. 13.

The mask parameter settings of the Opal IEC 61850 GOOSE publisher and GOOSE subscriber blocks of Fig. 13 are described in Fig. 14. The names of the Ethernet Adapter and IED have to be written manually in the related masks of the publisher and subscriber blocks. The rest of the parameters are automatically read from the SCL (Substation Configuration description Language) file which is actually an ICD (IED capability description) file of the protection relay or OPAL-RT target. The OPAL-RT target may have many Ethernet adapters named as eth0, eth1, eth2 and so on. It is recommended to publish the GOOSE message via the one Ethernet adapter and subscribed the same GOOSE message via the other Ethernet adapter. It means both the GOOSE publisher and the GOOSE subscriber blocks should have different Ethernet adapters. Therefore, the Ethernet adapter eth0 is used for the GOOSE publisher block and the Ethernet adapter eth1 is used for the GOOSE subscriber blocks (Fig. 14). The IED names manually entered in the GOOSE publisher and GOOSE subscriber masks should match the IED names written in the ICD files. The IED name ''SERVER-GOOSE'' is the name of the virtual IED of OPAL-RT target which is written in the ICD file named ''iec61850.icd'' provided in the IEC 61850 demo of OPAL-RT. The IED name ''AA1J01Q01A1'' is the name of the actual VAMP relay which is written in the ICD file named ''Vamp_229_Ed1New7.icd'' created after the final configuration of IEC 61850 GOOSE protocol of the VAMP relay using the VAMPSET relay configuration software.

The GOOSE publisher and the GOOSE subscriber blocks should use the same ICD file in order to communicate with each other successfully. The same GOOSE message ''Goose_1BOOL'' should be selected from the GoID (GOOSE ID) drop-down boxes of the masks of the GOOSE

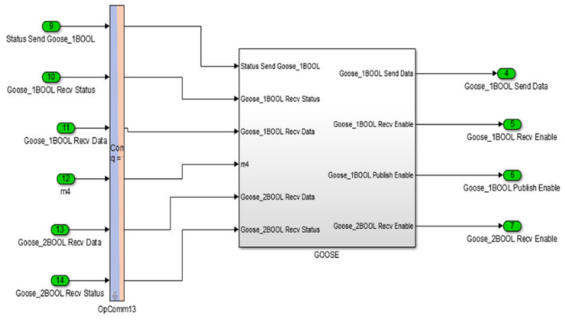

FIGURE 15. The real-time monitoring and control of the GOOSE messages in SC_MG1 subsystem.

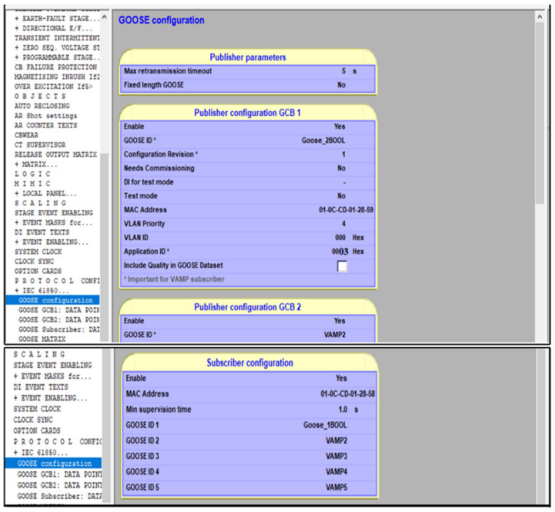

FIGURE 16. The GOOSE configuration menu of the VAMPSET software.

publisher and the subscriber blocks. The OPAL-RT subscriber block accepts the ICD file of the external test device with the same GoID messages as included the ICD file ''iec61850.icd'' provided by OPAL-RT even with the different IED name, AppId and MAC (media access control) destination address. Therefore, during the configuration of the external relay the same GoIDs should be used as in the ICD file ''iec61850.icd'' but with different AppId and MAC destination address to distinguish between the two different IEDs. Fig. 15 shows how GOOSE message inputs received from the SM_Grid1 are used for the real-time monitoring and control of the published and subscribed GOOSE messages inside SC_MG1 console subsystem.

C. THE CONFIGURATION OF THE IEC 61850 GOOSE PROTOCOL IN VAMP RELAY

After the opening of the VAMPSET relay configuration software and after the proper communication settings and establishment of the communication link with the VAMP relay, the IEC 61850 protocol can be configured. The detailed guide about the configuration of IEC 61850 protocol of VAMP relays can be found in [105]. Only the main points of the configuration of IEC 61850 protocol are discussed here based on the application note AN61850.EN005 [105].

The activation of the IEC 61850 protocol will enable the ''IEC 61850 main config'' to be selectable in the group list to the left side of the VAMPSET window. In the ''IEC 61850 main config'' menu only the IED name should be set differently for each device connected to the same network. This IED name will appear in the final ICD file to be used in GOOSE subscriber block of the OPAL-RT. Additionally, ''Dataset 1'' is selected in the ''LLN0 and LPHD DOs in datasets'' section of the ''IEC 61850 main config,'' where LLN0 stands for the logical node device, LPHD stands for the logical physical device and DOs stands for the data objects.

The most important part in this study is the configuration of the GOOSE messages to be published and subscribed by the VAMP relay. The GOOSE configuration menu (Fig. 16) can be opened from the VAMPSET left side group list where the GOOSE messages published and subscribed by the VAMP relay under test can be configured. The maximum retransmission timeout and fixed length GOOSE (Yes/No) can be defined in publisher parameters. The fixed GOOSE message feature is only defined by Edition 2 of IEC 61850, hence ''No'' should be selected for testing Edition 1 of IEC 61850. The VAMP relay under test is capable of publishing only two GOOSE messages each containing 8 bits of data packets, one GOOSE message is configured in ''Publisher configuration GCB1'' section and other configured in ''Publisher configuration GCB2'' section. The GCB1 and GCB2 stand for GOOSE control block 1 and 2, respectively. In addition to enabling the GOOSE message publication by selecting ''Yes'' in the ''Publisher configuration GCB1'' section, the other important parameters marked with $*$ include the GOOSE ID, configuration revision and the application ID along with the multi-cast MAC address.

The GCB1 and GCB2 are used to control the sending of data packets of two GOOSE messages. The data to be sent is defined/selected in the ''GOOSE GCB1: Data Points'' and ''GOOSE GCB2: Data Points'' configuration menus for data points in group 1 and group 2, respectively. For example, the GOOSE message to be published by the VAMP relay is defined with GOOSE ID of ''Goose_2BOOL,'' MAC address of 01-0C-CD-01-28-59 and AppId of 0003 Hex (Hexadecimal). The data to be sent by Goose_2BOOL message is defined in ''GOOSE GCB1: Data Points'' as the ''Logic1'' signal which is the ''Logic output 1'' of the ''OR'' logic defined in the LOGIC configuration section (Fig. 17). The status of all signals in the list of GOOSE GCB Data Points should indicate OK, otherwise the data is not sent.

In the ''Subscriber configuration'' sections, the incoming GOOSE messages subscribed by the VAMP relay are configured. As can be seen from Fig. 16, VAMP relay can subscribe to multiple GOOSE messages (maximum five) but all

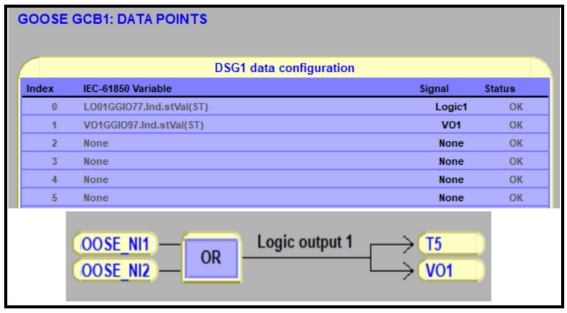

FIGURE 17. The GOOSE publisher data in "GOOSE GCB1: DATA POINTS" and related OR Logic output 1.

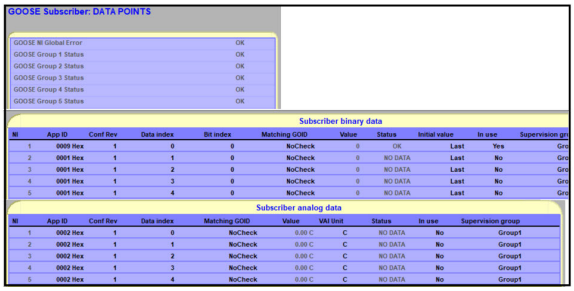

FIGURE 18. The GOOSE subscriber data in "GOOSE Subscriber: DATA POINTs" menu.

from one defined MAC Destination Address. The subscribed GOOSE message in this study is the first GOOSE message in the list which has the Goose ID of "Goose_1BOOL" and it is coming from the MAC Adress "01-0C-CD-01-28-58" of the RT target. The "Enable" should be changed to "Yes" in order to subscribe to the GOOSE message by the VAMP relay. The GOOSE data bits to be received by VAMP relay are defined in the "GOOSE Subscriber: DATA POINTS" menu. The binary/Boolean signals in the "Subscriber binary data" and analog signals in the "Subscriber analog data" sections of the "GOOSE Subscriber: DATA POINTS" menu (Fig. 18). The most important setting in the GOOSE Subscriber: DATA POINTS menu is the entry of the "App ID" of the incoming GOOSE message in Hexadecimal format. The App ID of each GOOSE message sent to the VAMP relay should be different because it is the main criteria of receiving GOOSE message in the VAMP relay. The other important settings in the "GOOSE Subscriber: DATA POINTS" menu include the "In use" and "Supervision Group" settings.

For the to be subscribed GOOSE message Goose_1BOOL which is a binary signal coming from RT target, the App ID of "0009 Hex," "In use" selection of "Yes" and "Group Supervision" of "Group1" have been entered into the "Subscriber binary data" section in row 1, with the network input index (NI) 1 in column 1 of row 1 (Fig. 18). The GOOSE_NI1 is connected to the NI in the GOOSE matrix so that the subscribed Goose_1BOOL message from the RT target can be used as binary input to the OR logic presented in Fig. 17.

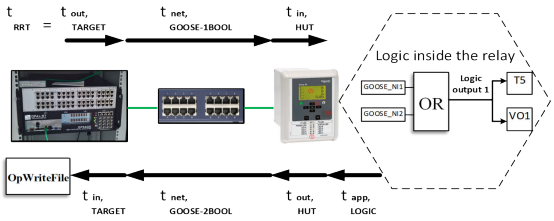

FIGURE 19. The round-trip time delay (t_{RTT}) estimation with real-time testing.

After completing the configuration of the IEC 61850 GOOSE protocol with the VAMPSET software, all new configured settings can be written to the VAMP relay using the "Communication > Write All Settings to Device" command. The configuration settings can be saved in "AnyName.vf2" file for future use. Moreover, ICD file can be created for use inside the GOOSE Subscriber block of the RT-LAB as discussed earlier. Using the VAMPSET interface, the real-time Goose_1BOOL subscription by the VAMP relay can also be monitored from the "GOOSE Subscriber: Data Points," "Logic" and the "Output Matrix" menus with a successful Ethernet link connection. For real-time monitoring "Enable continuous updating" and "Sync time and date from computer" should be activated. The time stamp information about the subscribed GOOSE messages can be observed in the "Event Buffer" menu of the VAMPSET interface.

D. THE REAL-TIME HIL TESTING OF THE IEC 61850 GOOSE PROTOCOL

In this subsection, the testing of the VAMP relay performed using a Boolean signal representing the actual fault detection/pickup signal "Yes" (signal status = 0) of the OC relay at CB1 location (Fig. 7) is described. During this test, the VAMP relay was time synchronized with the computer time and date using VAMPSET interface. The fault detection signal "status = 0" is published by the OPAL-RT target as GOOSE_1BOOL message from its Ethernet port eth0 which is subscribed by the VAMP relay and used for OR logic (Fig. 17) created inside the VAMP relay. The logic output 1 of the OR logic is published back as GOOSE_2BOOL message by the VAMP relay which is then subscribed by the OPAL-RT target through its Ethernet port eth1 and saved in OpWriteFile. It means the testing procedure of Fig. 19 is followed assuming OPAL-RT located at CB1, and the VAMP relay located at CB2.

The round-trip time delay ($t_{RTT} = t_{25}$) for the status change consists of seven individual delays according to (1) [106]:

$$t_{RTT} = t_{25} = t_{23} + t_{34} + t_{45} \quad (1)$$

$$t_{23} = t_{outTARGET} + t_{net\ Goose\_1BOOL} + t_{inHUT} \quad (2)$$

$$t_{34} = t_{appLOGIC} \quad (3)$$

$$t_{45} = t_{outHUT} + t_{net\ Goose\_2BOOL} + t_{inTARGET} \quad (4)$$

where, t_{25} is the round-trip time delay between events 2 and 5 (Fig. 3), t_{23} is the time delay between events 2 and 3, t_{34} is the time delay between events 3 and 4 and t_{45} is the time delay between events 4 and 5 in Fig. 3, $t_{out\ TARGET}$ is the delay by RT target to publish Goose_1BOOL on the Ethernet network, $t_{net\ Goose-1BOOL}$ is the delay of the Ethernet network until Goose_1BOOL message is available at the HUT (VAMP relay), $t_{in\ HUT}$ is the delay by the HUT to subscribe to Goose_1BOOL message as GOOSE_NI1, $t_{app\ LOGIC}$ is the delay of the OR logic to generate Logic output1 using GOOSE_NI1, $t_{out\ HUT}$ is the delay by the HUT to publish the Logic output1 via Goose_2BOOL message, $t_{net\ Goose-2BOOL}$ is the delay of the Ethernet network until Goose_2BOOL message is available at RT target and $t_{in\ TARGET}$ is the time taken by RT target to subscribe to Goose_2BOOL message, extract the information and write it on OpWriteFile for recording (Fig. 19).

It is a hard task to estimate each of the seven individual non-deterministic time delays mentioned in (1)-(4) because the time stamp information at the individual input and output stage of each device including the RT target, the Ethernet switch, HUT and even at the logic implemented inside the HUT is required for it. However, the time stamp information is only available at the HUT, and it is available during the GOOSE subscription stage just to indicate at which clock time this signal has been updated in the ''event buffer.'' The only exception is the estimation of time delay t_{TARGET} for one way GOOSE publication and subscription by the OPAL-RT target which includes three delays $t_{out,TARGET}$, $t_{net\ Goose-1BOOL}$ and $t_{in\ TARGET}$ and can be estimated by publishing the GOOSE signal from one Ethernet port (eth0) of the target and subscribing to the same GOOSE signal from other Ethernet port (eth1) of the same target. By recording both the published and subscribed GOOSE messages on OpWriteFile and matching the signals will give the estimation of t_{TARGET}. The similar estimation technique has been used for the estimation of t_{RTT} of the GOOSE message as shown in Fig. 19.

The actual fault detection signal at CB1 location does not repeat its status change multiple times but only once from the initial status of ''No'' (signal status = 1) to the final status of ''Yes'' (status signal = 0). Here, it should be noted that the ''final status = 0'' is the output of ''NOT'' gate implemented at the output of the OC relay at CB1 inside the RT model to trip the circuit breaker CB1 in case the fault is not detected by the OC relay at CB2. The final inverted status 0 of OC relay at CB1 acts as a trip command ''Yes'' for the CB, since in MATLAB/Simulink the CB trips with a ''zero'' input signal.

It has been conventionally assumed through ''OR Logic'' implemented inside VAMP relay that if ''No'' fault is detected at the CB2 location then the Goose_2BOOL published by the VAMP relay will have the same final status 0 as that of the Goose_1BOOL at CB1 location (OPAL-RT target). Fig. 20 presents the published and subscribed fault detection Boolean GOOSE signals saved in OpWriteFile and plotted with MATLAB commands. In this test, a three-phase short-circuit fault is applied for a duration of 1s from the simulation time of 3 s

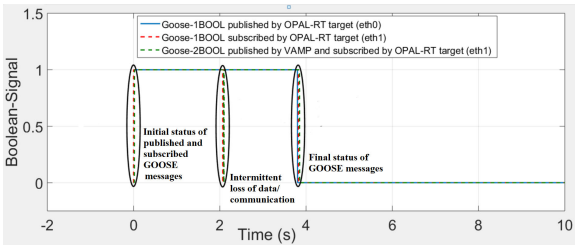

FIGURE 20. The published and subscribed fault detection Boolean GOOSE signals saved in OpWriteFile.

to 4 s and the OC relay at CB1 is set to detect the fault at 3.8 s. This means the status of fault detection signal changes only at simulation time of 3.8 s. The fault detection status signal is published by OPAL-RT target via Ethernet adapter eth0 as Goose_1BOOL message (blue color) and subscribed by OPAL-RT target via Ethernet adapter eth1 as Goose_1BOOL message (red color) for the estimation of the delay t_{TARGET}. The subscribed Goose_1BOOL message is published back by the VAMP relay and subscribed by the OPAL-RT target as Goose_2BOOL (green color) for the estimation of the round-trip time (t_{RTT}). The initial status 1 of the Boolean signal, indicates ''No fault detection'' and the final status 0 of the Boolean signal indicates ''Yes fault detection.''

The initial status 1 for the ''No fault detection'' signal from the start of the RT simulation at Time = 0 s till the round-trip back from the VAMP relay to the OPAL-RT target at Time = 0.021 s is zoomed out as shown in Fig. 21. The time from 0 to 0.021 s is the round-trip time (t_{RTT}) of the initial status 1 of the ''No fault detection'' signal. The delay $t_{TARGET\ St1}$ of the initial status 1 (red color) is very small and hardly distinguishable from the original published signal (blue color). The OPAL-RT target continuously publishes the current status of the Boolean signal after every time step (Ts) of the simulation and after the publication and subscription the signal is being recorded on OpWriteFile blocks. The status of the Goose_2BOOL signal (green color) from the time 0 to 0.021 s (Fig. 21) does not indicate the status changed to status 0. It, however, means that during the time 0 to 0.021 s, Goose_2BOOL published by VAMP relay is absent (not yet subscribed) at the OPAL-RT target, which by default is recorded as the ''0'' inside the MAT file of the OpWriteFile block. Therefore, by setting the initial delayed conditions starting after 0.021 s at the input of CBs, the false tripping of CB1 and CB2 during the initial simulation time up to 0.021 s can be avoided during the simulation.

The initial status 1 of the published and subscribed Boolean signals, starting from the simulation time of 0.021 s to onwards, should ideally remain the same till 3.8 s when the fault is detected by the OC relay at CB1. However, it can be seen from the Fig. 20 and more closely from Fig. 22 that there is some intermittency of the subscribed signals for about 10 ms. The data recording of both the subscribed signals Goose_1BOOL (red color) and Goose_2BOOL

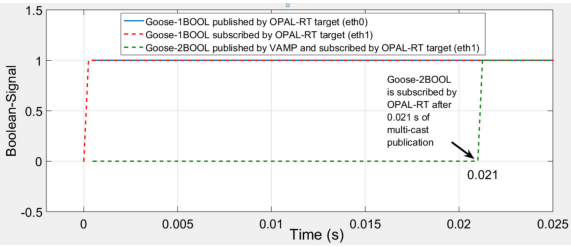

FIGURE 21. The initial status 1 of published and subscribed fault detection Boolean GOOSE signals.

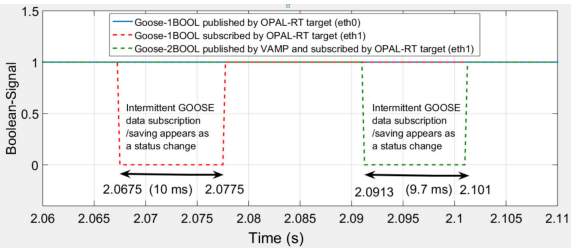

FIGURE 22. The intermittent/missing data recording of the subscribed Boolean GOOSE signals during the initial status 1.

(green color) is missing and appearing as a changed signal status 0 at 2.0675 s of the simulation time. The intermittency of the initial status 1 of the subscribed Boolean signal happens only once but at different times of simulation during three tests and for different lengths of duration in each case. This has happened most probably due to the software bug in the OPAL-RT target or some loss of data packets but not from the relay model as the published signal in blue color is always continuous. The consequent false tripping of the CBs could be avoided in one way by introducing the monitoring of the continuity of the signal status for 15 ms or 20 ms at the inputs of the CBs inside the model and the signal should be assumed continuous if it is continuous for a duration of 15 ms or 20 ms. However, if the CBs are capable of resetting quickly with the status change during the simulation and the final results of the simulation are not affected then this intermittency can be easily ignored as done in this case.

After ignoring the intermediate discontinuity of the initial fault detection signal with status 1, the most important thing to observe is the behavior of the final status 0 of the signal after 3.8 s which is the actual fault detection event. The continuous behavior of the final status 0 of the Boolean signal, at simulation time 3.8 s onwards, is evident from the results of Fig. 23. The status change inside the model happens at 3.8 s, it is published as Goose_1BOOL message by the OPAL-RT target at 3.8027 s (blue color) and subscribed by the OPAL-RT target at 3.8223 s (red color), resulting in $t_{TARGET} = 19.6$ ms. The VAMP relay publishes Goose_2BOOL after subscribing to Goose_1BOOL and performing the OR logic which is ultimately subscribed by OPAL-RT target at 3.8510 s resulting in $t_{RTT} = 48.3$ ms.

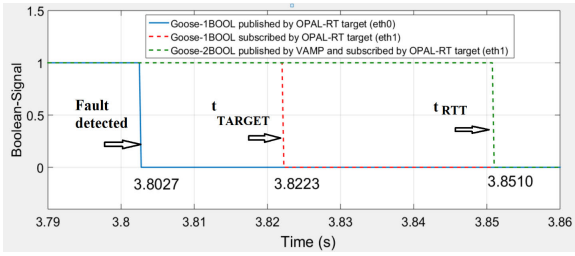

FIGURE 23. The final status 0 of published and subscribed fault detection Boolean GOOSE signals.

TABLE 4. The time delays of the final status 0 of the published and subscribed GOOSE Boolean signals in three tests.

Signal (Time delay)	Test-1	Test-2	Test-3	Average
Goose-1BOOL pub[2] by OPAL ($t_{out\ TARGET\ St0}$[4])	2.5 ms[1]	2.7 ms	2.7 ms	2.63 ms
Goose-1BOOL sub[3] by OPAL ($t_{TARGET\ St0}$)	19.5 ms	37.7 ms	17.3 ms	24.83 ms
Goose-2BOOL pub by VAMP sub by OPAL ($t_{RTT\ St0} = t_{25}$)	48.3 ms	52.5 ms	39.5 ms	46.76 ms

[1]ms = millisecond, 1 ms = 0.001 s, [2]pub = published, [3]sub = subscribed, [4]St0 = Status 0.

In this way, many tests were performed for the estimation of the round-trip time, Table 4 shows three selected best-case scenario testing results. The worst-case maximum round-trip time of $t_{RTT} = 90$ ms was observed for the same test case at another time of testing. The estimation of the round-trip time using the real-time HIL-testing will help to implement the IEC 61850 communication-dependent logically selective adaptive protection algorithm for AC microgrids proposed in [11].

E. THE RESULTS FOR IEC 61850 GOOSE PROTOCOL DEPENDENT ADAPTIVE PROTECTION

In this section, the results are presented for the IEC 61850 GOOSE protocol dependent adaptive protection of a radial AC microgrid (Fig. 7) and smooth transition to islanded mode operation using the centralized BESS after the short-circuit fault F1 at 2 km overhead line near the CB2 location. Additionally, the results also include the detection and the isolation of the short-circuit fault F2 at mid-point of a 1 km cable inside the islanded AC microgrid. Due to the inherent limitation of both the VAMP relay and the OPAL-RT target (IEC 61850 ICD file) to publish and/or subscribe to a maximum of two Boolean signals at a time, only the results of fault F1 are dependent IEC 61850 GOOSE communication protocol. However, the test can be repeated, and very similar results can also be obtained for the fault F2. The inclusion

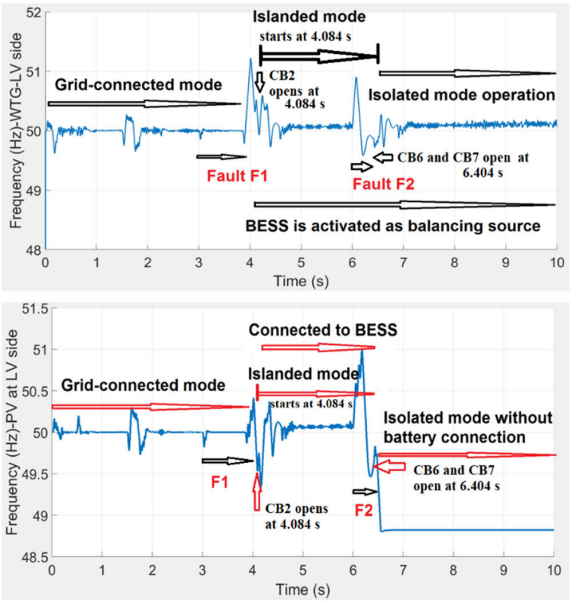

FIGURE 24. The frequency (Hz) of DERs before and after the fault F1 in grid-connected mode and before and after the fault F2 in the islanded mode: WTG (top), PV system (bottom).

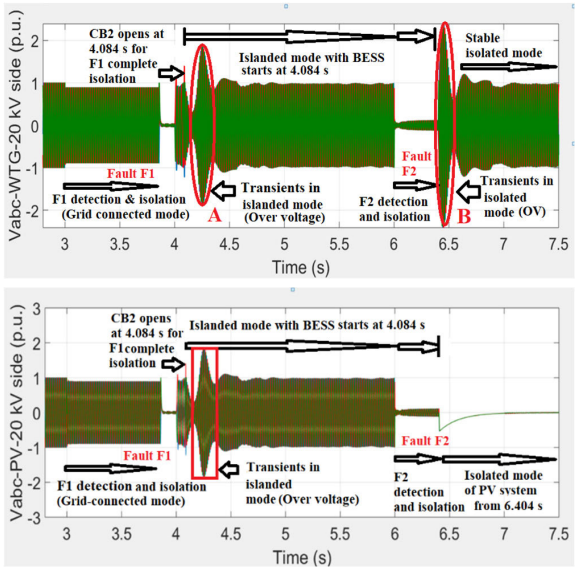

FIGURE 25. Three-phase voltage (p.u.) of DERs before and after the fault F1 in grid-connected mode and before and after the fault F2 in the islanded mode: 20 kV side of WTG (top) 20 kV side of PV system (bottom).

of the fault F2 results is particularly important to present the behavior of DERs during the islanded mode with centralized BESS and during the facility island mode of the PV system without BESS.

The estimation of the round-trip time (t_{RTT}) in the previous section was important because using the subscribed Goose_2BOOL signal the centralized BESS is activated as well as CB1 and CB2 are also tripped to isolate the AC microgrid from fault F1 completely and start the islanded mode. The behavior of the frequency at the LV-side of the WTG and the PV system during the faults F1 and F2 and during the different operational modes is presented in Fig. 24. As it is evident that the frequency at DERs is well maintained around 50 Hz during the grid-connected mode and in the islanded mode with the centralized BESS after the fault F1. During the isolated mode of operation after the fault F2 when the islanded MV system and the islanded LV system (Fig. 7) are isolated, the frequency of the WTG remains well maintained around 50 Hz due to the presence of the centralized BESS. However, the frequency of the PV system is dropped below 49 Hz in the isolated mode of operation either due to the absence of any BESS in the islanded LV system or some control problem with the PV model or the PLL block, however, it remains well above 48.5 Hz. The PV system can operate up to 90 minutes for the frequency range of 48.5-49 Hz according to the European grid code EN 50549-1-2019.

The behavior of the voltage on 20 kV side of the WTG and the PV system during the faults F1 and F2 and during the different operational modes is presented in Fig. 25. As it can be seen that during the 3Ph short-circuit fault F1 with $R_f = 5.001$ Ohm in the grid-connected mode, the voltage at the connection points of DERs is decreased to only 0.9 p.u. until the fault F1 is isolated by CB1 tripping at 3.851 s. From the simulation time of 3.851 s to 4s the voltage at the connection points of DERs is consequently decreased to the minimum (near to zero) value due to the CB1 tripping indicating the loss of the main grid. This minimum voltage for a duration of 149 ms has happened due to the delayed CB2 transfer trip implementation in the RT simulation discussed later in the following paragraph. At the simulation time of 4 s, the fault naturally disappears and the voltage at the connection points of DERs is restored to the normal range of 0.9 p.u. because the active fault duration of only 1 s from the simulation time of 3 s to 4 s is considered for the fault F1. The CB2 trips at simulation time of 4.084 s to completely isolate the fault F1. The activation of the centralized BESS is implemented with the opening status signal of the CB2. Therefore, the BESS also starts as the grid-forming source at 4.084 s to support the seamless transition to the islanded mode without the disconnection of DERs.

At the start of the islanded mode with centralized BESS, there is some undervoltage followed by a transient overvoltage region marked as area A (Fig. 25) which may result in the unstability of the islanded mode in case the overvoltage protection of DERs is activated in this region. Therefore, DERs should have high voltage ride through (HVRT) or overvoltage ride through (OVRT) capability to remain stable and not disconnect due to overvoltage during this short transition period of about 5 cycles (100 ms) in the islanded mode. The same HVRT is required during the isolated mode

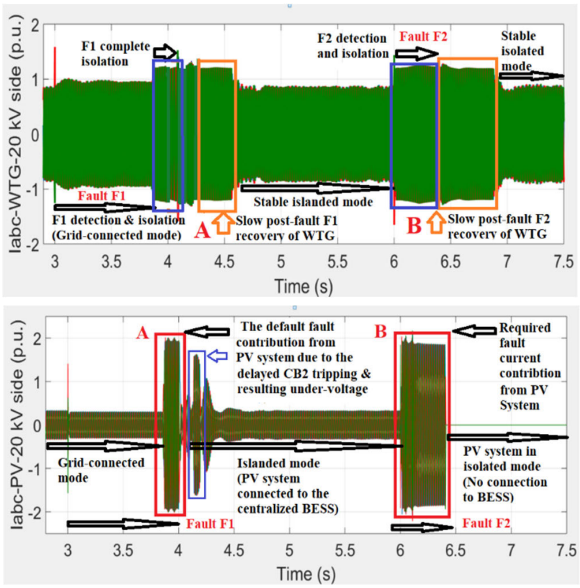

FIGURE 26. Three-phase current (p.u.) of the DERs before and after the fault F1 in grid-connected mode and before and after the fault F2 in the islanded mode: 20 kV side of WTG (top) 20 kV side of PV system (bottom).

after the fault F2 in the islanded mode marked as area B in Fig. 25 (top). From the simulation time of 4.25 s to onwards, a very stable voltage at the connection points of DERs is achieved in the islanded mode. During the islanded mode, a three-phase short-circuit fault F2 with $R_f = 0.001$ Ohm is applied at simulation time of 6 s. As can be seen from Fig. 25, that the voltage at the connection points of DERs is decreased to minimum (near to zero) due to the lower fault resistance during F2 compared with the same during F1.

The fault F2 is detected by OC relay at CB6 and isolated at 6.404 s by tripping CB6 and transfer tripping CB7. This will result in two island systems within the islanded AC microgrid: MV island system with the WTG, the BESS and 2 MW load; LV island system with only the PV system and 0.4 MW load operating without BESS. At the simulation time of 6.5 s, MV island system achieves a stable isolated mode of operation while LV island system lost the voltage of the centralized BESS at its 20 kV connection point (Fig. 25 (bottom)). The PV system in the LV island which is a facility island can only operate with the grid-forming control for the continuity of supply to the LV load. The voltage and current at the LV load before, during and after the faults F1 and F2 can be observed from the figures given in the Appendix.

The behavior of the current on 20 kV side of the WTG and the PV system during the faults F1 and F2 and during different operational modes is presented in Fig. 26. As it is evident from Fig. 25 that during the fault F1, the voltage at the connection point of DERs is only decreased to 0.9 p.u., hence both the WTG and the PV do not provide the fault current contribution of 1.2 p.u. and 2 p.u. respectively until CB1 is opened. This means the grid-side voltage does not decrease to 0.5 p.u. or less in order to trigger the fault current contribution or LVRT of DERs during the fault F1. However, after the communication-dependent detection and isolation of the fault F1 and opening of CB1 at simulation time of 3.851 s, the grid-side voltage is lost at the connection points of DERs. This consequently triggers the fault current contribution from DERs (LVRT capability), and both the WTG and the PV system provide a default maximum fault current contribution until CB2 is also opened at 4.084 s for a complete F1 isolation (area A, Fig. 26).

The default fault current contributions from the WTG (area A in blue color) in Fig. 26 (top) and from the PV system (area A in red color) in Fig. 26 (bottom) for a duration of 233 ms during the time 3.851 s to 4.084 s is the result of the delayed transfer trip of CB2. Actually, the CB2 transfer trip is implemented in a way that the subscribed Goose_2BOOL signal from the SM_Grid1 is first transferred to the console subsystem SC_MG1 and then from the console subsystem SC_MG1 transferred to the SS_WTG_PV1 subsystem where CB2 is connected. Doing this results in a delayed CB2 transfer trip due to the asynchronous connection between the console subsystem SC_MG1 and the computation subsystem SS_WTG_PV1. But, if the transfer trip of CB2 is implemented like CB1 tripping using a separate Goose_2BOOL subscriber block (Fig. 13) also in the SS_WTG_PV1 subsystem of the RT model then the extended CB2 opening delay will not happen and both CB1 and CB2 would trip simultaneously at 3.8510 s in the RT simulation. Consequently, the undervoltage and fault contribution time between 3.851 s and 4 s in Fig. 25 and Fig. 26, respectively could be decreased or avoided.

During the initial voltage dip period from the simulation time 4.084 s and 4.25 s after the successful islanding, both the WTG and the PV system also provide the LVRT and fault contributions (the area between the blue and orange area A rectangles in Fig. 26 (top) and area A in blue color in Fig. 26 (bottom)). By comparing the fault current contribution and dynamics of the WTG and the PV system models during the fault F1 and F2, it can be seen from Fig. 26 (top) that the WTG continues providing fault current for an additional time even after the voltage is restored to the normal value (area A and area B in orange color). The PV system, on the other hand, provides the fault current contribution only when it is required (Fig. 26 (bottom) area A, area B in red color) and immediately gives the normal current after the voltage is restored above 50% of the nominal value. The WTG model has a very slow post-fault current recovery compared with the PV system. Therefore, the change of adaptive lower setting group of OC relays will be delayed in the islanded mode by sometime after the successful islanding. The generic model of the WTG with good dynamic behavior would, however, avoid the delay to the change of adaptive lower setting group as observed previously in [11].

The three-phase current in p.u. at the CB2 location during the grid-side fault F1 is presented in Fig. 27. This will help

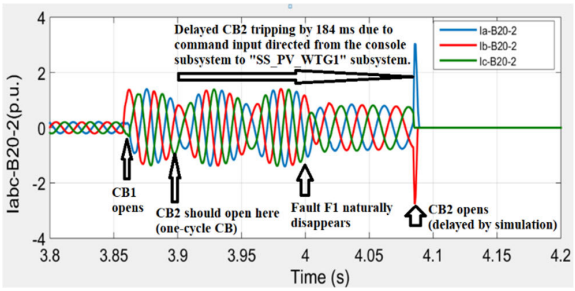

FIGURE 27. Three-phase current (p.u.) at CB2 location during the grid-side fault F1.

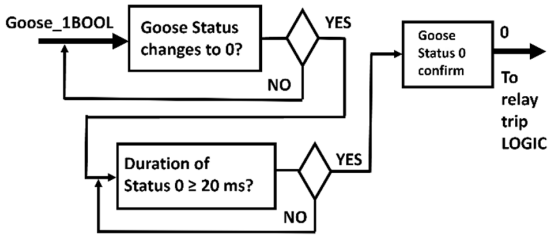

FIGURE 28. Boolean signal continuity check of status 0.

understand the complete fault F1 isolation. Fig. 27 shows that after the opening of CB1 at 3.851 s, CB2 will still carry a current fed by the WTG and the PV system and the fault F1 will remain charged by this current until either the fault disappears or CB2 is also opened. After the opening of CB2 at 4.084 s, the fault current disappears from the CB2 location indicating complete fault isolation. The persistence magnitude of current although lower than the fault current after the disappearance of the fault F1 and before the opening of CB2 appearing between simulation time of 4 s and 4.084 s in Fig. 27 is there because of the fault current contribution from DERs which is fed to the 100 kvar capacitor bank (Fig. 9). In the practical situation considering the centralized relay at CB1, if CB1 opens at 3.851 s, then with the one-way GOOSE transfer delay of 10 ms CB2 will open at 3.881 s assuming CB2 as one cycle CB. Thus, the completion of the IEC 61850 GOOSE communication dependent selective fault detection and isolation within 100 ms is possible after adding 20 ms of fault detection which closely matches with the "10 ms GOOSE message algorithm" proposed in [11] and reproduced in Fig. 3.

Considering the relays at CB1 and CB2 as decentralized relays, then CB2 will trip first after receiving "YES" fault detection Goose_1BOOL from the OC relay at CB1 as there is "NO" fault signal readily available at CB2 location because with the higher setting group the OC relay at CB2 does not pickup. So, the OC relay at CB2 will receive Goose_1BOOL, perform the OR logic and send trip command to CB2 meanwhile publish the Goose_2BOOL "NO" fault signal. This procedure will open CB2 completely at 3.851 s which also includes the one cycle duration (20 ms) of CB2 opening (Fig. 3). The OC relay at CB1 will issue trip command to CB1 at 3.851 s after receiving Goose_2BOOL "NO" fault signal and CB1 will open completely within 20 ms at 3.871 s resulting in complete fault detection and isolation in just 91 ms after adding 20 ms of fault detection, which is even faster than the "10 ms GOOSE message algorithm."

However, with a round-trip time (t_{25}) of 90 ms, the worst-case scenario, the "20 ms GOOSE message algorithm" looks more suitable and with the decentralized/centralized architecture, complete detection and isolation of fault F1 will happen around simulation time of 3.92-3.93 s, in just about 120-130 ms after the fault detection at 3.8 s. Again, it confirms the practical implementation of the "20 ms GOOSE message algorithm" which also assumes 130 ms for complete fault detection and isolation. The rest of the results are presented in the Appendix of the paper.

V. DISCUSSION

The communication will be a necessary and integral part of the future smart electric grids and microgrids. The IEC 61850 communication provides the standardized protocol for the exchange of the digital as well as analog type of data among IEDs of different vendors using the Ethernet link as the most reliable and fast medium. The implementation of different control and protection functions through logic selectivity implemented inside IEDs will be a more common trend. To prove the reliability and dependability extent of communication-dependent control and protection functions for example, adaptive protection [11], the HIL simulation testing of actual IEDs in real-time is necessary. The adaptive protection is the new requirement for microgrids which can be implemented with the centralized communication architecture, the distributed communication architecture or even with the hybrid communication architecture using both the centralized and the distributed architecture.

The round-trip testing of communication is generally used for the estimation of the one-way communication delay and can be carried out using different methods for example [106]. However, the dependency on the round-trip delay which involves various inherent delays has rarely been considered for a communication-dependent logically selective adaptive protection. Previously, the estimation of the round-trip delay was done in [106] for the loss of mains detection and transfer trip of DERs using IEC 61850 protocol. However, the method neither considered LVRT of DERs nor provided the complete interactive environment close to the reality in which the consequences of the delayed or missing tripping like the behavior of DERs including the frequency and voltage stability can be found. The HIL simulation testing provides the results close to the actual implementation and therefore can be widely acceptable as a "proof of concept" within its own limitations and additional challenges. This paper provides the results for the implementation extent of the communication-dependent logically selective adaptive

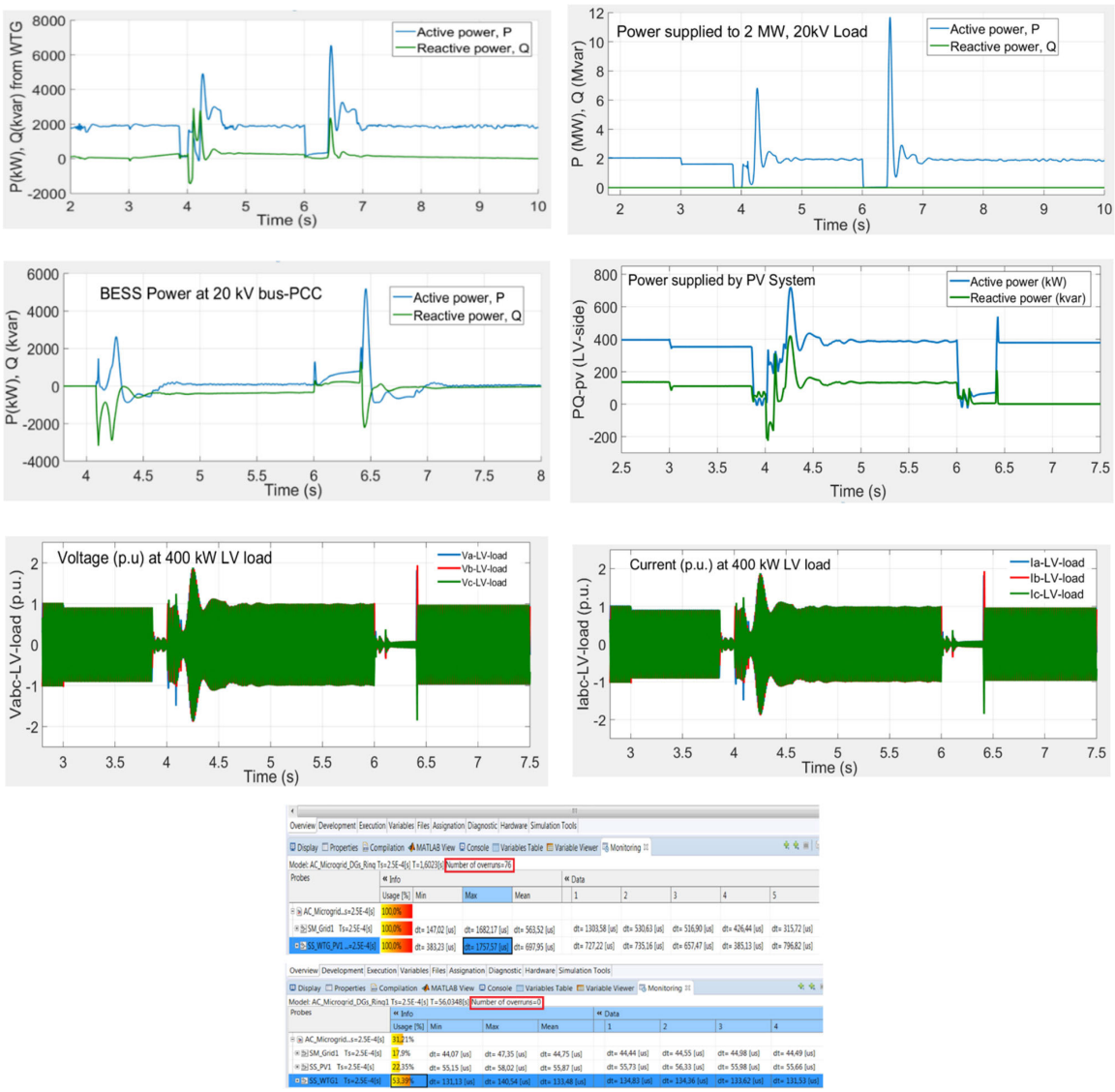

FIGURE 29. The active and reactive power supplied by DERs/BESS and consumed by MV load (top-4 figures), voltage and current at LV load (green figures) and the monitoring view of the RT-LAB model (bottom figure).

protection proposed in [11] using the HIL simulation testing. The results reveal that the previously proposed adaptive protection algorithm with the assumed conditions in the offline simulations is also giving the similar results in real-time HIL testing environment. Therefore, it can be implemented in the practical microgrids irrespective of the radial or looped network configuration. The method is capable of being extended to other types of signals like analog signals for other types of protection functions/applications with the similar or comparative results.

It should here be noted that the communication-dependent logically selective adaptive protection algorithms presented in Fig. 3 and Fig. 4 includes both the variable and fixed time delays. In this paper, only the variable time delays for a two-way communication (t_{25}) for the centralized architecture (Fig. 3) are estimated using the real-time HIL testing. The fixed time delays include the delays for the fault detection and opening times of the CBs which greatly depend on the method of fault detection and the type of CB used. In this paper, the instantaneous tripping of CB1 (ideal-case) is used and CB2 tripping is delayed only due to RT simulation model arrangements (worst-case). The fixed time delays of CB tripping can however easily be adjusted according to Fig. 3 by introducing 20 ms time delay at CB1 and 60 ms time delay at CB2 with the subscription of Goose_2BOOL message (event 5) independently in SM_Grid1 and SS_WTG_PV1 subsystems

in the RT model as explained previously. This is somewhat confusing due to the fact that only one and the same GOOSE message (Goose_2BOOL) is used for tripping both the CB1 and CB2 in the RT model. In practical situations, the OC relay at CB1 will subscribe to the updated Goose_2BOOL published by the OC relay at CB2 and publish Goose_1BOOL after tripping CB1. In the same way, the OC relay at CB2 will subscribe to the updated Goose_1BOOL published by the OC relay at CB1 and publish Goose_2BOOL after tripping CB2. Each relay may even publish two independent and the unique Boolean GOOSE messages one for the fault detection information and the other for CB tripping. This all depends on the capability of the relays to publish and subscribe to multiple GOOSE messages. Moreover, the fault detection signal (Goose_1BOOL) could be published right after 20 ms of the fault F1 at 3.02 s instead of 3.8 s as done in the HIL testing of this paper to get the results more aligned with the algorithm presented in Fig. 3.

The adaptive lower setting group-based fault detection and isolation although not used in this HIL testing case, but it is an integral part of the algorithm. For example, the algorithm can be repeated for the first fault to be F2 between CB6 and CB7 and the second fault to be F3 at LV load where F3 can only be detected with the lower setting groups assuming the PV provides the fault current contribution of 1.2 p.u. and the grid-connected or BESS-connected islanding pickup setting of the OC relay at LV load (CB8) is 2.25 p.u. In this situation, OC relay at CB8 of LV load (Fig. 7) will change its pickup settings after CB7 tripping (event 8 in Fig. 3). The HIL testing verifies that the seamless transition to the islanded and isolated modes is possible using the reliable, fast and dedicated communication link and the BESS in the islanded sections. However, the Boolean signal integrity should be maintained and the intermittent loss of data for a duration longer than 10-20 ms need to be avoided.

The Boolean signal continuity check of ''status 0'' (Fig. 28) for a duration longer than 20 ms after the GOOSE subscription will ensure the prevention of wrong tripping by the relays due to intermittent data loss. This signal continuity check delay when added as security delay in the events 3, 5 and 7 of Fig. 3 will obviously extend the overall duration of the proposed algorithm and therefore the stringent LVRT curve of DERs with 250 ms will be required. Due to the use of LAN connection in this HIL testing with a lot of other data traffic in the network, the results produced are close to the realistic substation automation environment with many IEDs and a lot of GOOSE data traffic. This paper will be a good reference for further applications and improvements of the communication-dependent logically selective adaptive protection.

VI. CONCLUSION

The real-time HIL testing has been carried out using the actual digital relay and the RT target for the verification of the adaptive protection using the IEC 61850 GOOSE protocol which was previously proposed in [11] using the offline simulations. The results look promising, and the previously assumed conditions are very close to RT simulation results. A dedicated, fast and reliable Ethernet link will ensure the implementation of the proposed adaptive protection and seamless transition to the islanded and isolated mode could be realized with a centralized or distributed control and communication architecture. A centralized BESS will help maintain the voltage and frequency stability for the seamless transition within 150 ms or 250 ms LVRT curve of DERs. The monitoring of status 0 of the Boolean signal will add security to the relay and avoid the unnecessary tripping of the relay during the brief communication discontinuity or loss of data. The similar data handling and monitoring concept inside the relay can also be applied for the analog type of signals. The proposed method can be readily applied to other control and protection applications e.g., in AC microgrids with looped networks.

APPENDIX

Additional results. See Figure 29.

ACKNOWLEDGMENT

The authors are very much thankful to their colleague Dr. Mike Mekkanen for the discussion and support in the preparation of the IEC 61850 testing platform at the FREESI Laboratory.

REFERENCES

[1] C. Marnay, S. Chatzivasileiadis, C. Abbey, R. Iravani, G. Joos, P. Lombardi, P. Mancarella, and J. von Appen, ''Microgrid evolution roadmap,'' in *Proc. Int. Symp. Smart Electr. Distrib. Syst. Technol. (EDST)*, Sep. 2015, pp. 139–144.

[2] A. A. Memon and K. Kauhaniemi, ''A critical review of AC microgrid protection issues and available solutions,'' *Electr. Power Syst. Res.*, vol. 129, pp. 23–31, Dec. 2015.

[3] K. Sirviö, K. Kauhaniemi, A. Ali Memon, H. Laaksonen, and L. Kumpulainen, ''Functional analysis of the microgrid concept applied to case studies of the Sundom smart grid,'' *Energies*, vol. 13, no. 16, p. 4223, Aug. 2020.

[4] A. A. Memon, H. Laaksonen, and K. Kauhaniemi, ''Microgrid protection with conventional and adaptive protection schemes,'' in *Microgrids*, A. Anvari-Moghaddam, H. Abdi, B. Mohammadi-Ivatloo, and N. Hatziargyriou, Eds. Cham, Switzerland: Springer, 2021, ch. 19, pp. 523–579, doi: 10.1007/978-3-030-59750-4_19.

[5] A. D. Bintoudi, L. Zyglakis, T. Apostolos, D. Ioannidis, S. Al-Agtash, J. L. Martinez-Ramos, A. Onen, B. Azzopardi, L. Hadjidemetriou, N. Martensen, C. Demoulias, and D. Tzovaras, ''Novel hybrid design for microgrid control,'' in *Proc. IEEE PES Asia–Pacific Power Energy Eng. Conf. (APPEEC)*, Nov. 2017, pp. 1–6, doi: 10.1109/APPEEC.2017.8308958.

[6] M. Yazdanian and A. Mehrizi-Sani, ''Distributed control techniques in microgrids,'' *IEEE Trans. Smart Grid*, vol. 5, no. 6, pp. 2901–2909, Nov. 2014, doi: 10.1109/TSG.2014.2337838.

[7] C. X. Dou and B. Liu, ''Multi-agent based hierarchical hybrid control for smart microgrid,'' *IEEE Trans. Smart Grid*, vol. 4, no. 2, pp. 771–778, Jun. 2013, doi: 10.1109/TSG.2012.2230197.

[8] P. Mahat, Z. Chen, B. Bak-Jensen, and C. L. Bak, ''A simple adaptive overcurrent protection of distribution systems with distributed generation,'' *IEEE Trans. Smart Grid*, vol. 2, no. 3, pp. 428–437, Sep. 2011, doi: 10.1109/TSG.2011.2149550.

[9] D. Ishchenko, A. Oudalov, and J. Stoupis, ''Protection coordination in active distribution grids with IEC 61850,'' in *Proc. IEEE PES TD*, May 2012, pp. 1–6, doi: 10.1109/TDC.2012.6281478.

[10] H. Laaksonen, D. Ishchenko, and A. Oudalov, "Adaptive protection and microgrid control design for Hailuoto island," *IEEE Trans. Smart Grid*, vol. 5, no. 3, pp. 1486–1493, May 2014, doi: 10.1109/TSG.2013.2287672.

[11] A. A. Memon and K. Kauhaniemi, "An adaptive protection for radial AC microgrid using IEC 61850 communication standard: Algorithm proposal using offline simulations," *Energies*, vol. 13, no. 20, p. 5316, Oct. 2020.

[12] A. Benigni, T. Strasser, G. De Carne, M. Liserre, M. Cupelli, and A. Monti, "Real-time simulation-based testing of modern energy systems: A review and discussion," *IEEE Ind. Electron. Mag.*, vol. 14, no. 2, pp. 28–39, Jun. 2020, doi: 10.1109/MIE.2019.2957996.

[13] H. Shayeghi, E. Shahryari, M. Moradzadeh, and P. Siano, "A survey on microgrid energy management considering flexible energy sources," *Energies*, vol. 12, no. 11, p. 2156, Jun. 2019.

[14] S. Beheshtaein, R. Cuzner, M. Savaghebi, and J. M. Guerrero, "Review on microgrids protection," *IET Gener., Transmiss. Distrib.*, vol. 13, no. 6, pp. 743–759, Mar. 2019.

[15] B. Mahamedi and J. E. Fletcher, "Trends in the protection of inverter-based microgrids," *IET Gener. Transm. Distrib.*, vol. 13, pp. 4511–4522, Oct. 2019.

[16] N. Hussain, M. Nasir, J. C. Vasquez, and J. M. Guerrero, "Recent developments and challenges on AC microgrids fault detection and protection systems—A review," *Energies*, vol. 13, no. 9, p. 2149, May 2020.

[17] B. Patnaik, M. Mishra, R. C. Bansal, and R. K. Jena, "AC microgrid protection—A review: Current and future prospective," *Appl. Energy*, vol. 271, Aug. 2020, Art. no. 115210.

[18] M. A. Aftab, S. M. S. Hussain, I. Ali, and T. S. Ustun, "IEC 61850 based substation automation system: A survey," *Int. J. Electr. Power Energy Syst.*, vol. 120, Sep. 2020, Art. no. 106008.

[19] A. Hirsch, Y. Parag, and J. Guerrero, "Microgrids: A review of technologies, key drivers, and outstanding issues," *Renew. Sustain. Energy Rev.*, vol. 90, pp. 402–411, Jul. 2018.

[20] J. Gouveia, C. L. Moreira, and J. A. P. Lopes, "Grid-forming inverters sizing in islanded power systems—A stability perspective," in *Proc. Int. Conf. Smart Energy Syst. Technol. (SEST)*, Porto, Portugal, Sep. 2019, pp. 1–6.

[21] J. Wang, C. Zhao, A. Pratt, and M. Baggu, "Design of an advanced energy management system for microgrid control using a state machine," *Appl. Energy*, vol. 228, pp. 2407–2421, Oct. 2018.

[22] J. Wang, A. Pratt, and M. Baggu, "Integrated synchronization control of grid-forming inverters for smooth microgrid transition," NREL, Atlanta, GA, USA, Tech. Rep. NREL/CP-5D00-72756, Aug. 2019.

[23] J. Rocabert, A. Luna, F. Blaabjerg, and P. Rodríguez, "Control of power converters in AC microgrids," *IEEE Trans. Power Electron.*, vol. 27, no. 11, pp. 4734–4749, Nov. 2012, doi: 10.1109/TPEL.2012.2199334.

[24] I. J. Balaguer, Q. Lei, S. Yang, U. Supatti, and F. Z. Peng, "Control for grid-connected and intentional islanding operations of distributed power generation," *IEEE Trans. Ind. Electron.*, vol. 58, no. 1, pp. 147–157, Jan. 2011, doi: 10.1109/TIE.2010.2049709.

[25] C. Cho, J.-H. Jeon, J.-Y. Kim, S. Kwon, K. Park, and S. Kim, "Active synchronizing control of a microgrid," *IEEE Trans. Power Electron.*, vol. 26, no. 12, pp. 3707–3719, Dec. 2011, doi: 10.1109/TPEL.2011.2162532.

[26] A. Micallef, M. Apap, C. Spiteri-Staines, and J. M. Guerrero, "Single-phase microgrid with seamless transition capabilities between modes of operation," *IEEE Trans. Smart Grid*, vol. 6, no. 6, pp. 2736–2745, Nov. 2015, doi: 10.1109/TSG.2015.2444912.

[27] *IEEE Guide for Design, Operation and Integration of Distributed Resource Island Systems With Electric Power Systems*, IEEE Standard 1547.4-2011, 2011, pp. 1–54.

[28] M. Fusero, A. Tuckey, A. Rosini, P. Serra, R. Procopio, and A. Bonfiglio, "A comprehensive inverter-BESS primary control for AC microgrids," *Energies*, vol. 12, no. 20, p. 3810, Oct. 2019.

[29] P. Unruh, M. Nuschke, P. Strauß, and F. Welck, "Overview on grid-forming inverter control methods," *Energies*, vol. 13, no. 10, p. 2589, May 2020.

[30] S. M. Mohiuddin and J. Qi, "A unified droop-free distributed secondary control for grid-following and grid-forming inverters in AC microgrids," in *Proc. IEEE PES Gen. Meeting (PESGM)*, Montreal, QC, Canada, Aug. 2020, pp. 1–5.

[31] M. D. O. Faruque, T. Strasser, G. Lauss, V. Jalili-Marandi, P. Forsyth, C. Dufour, V. Dinavahi, A. Monti, P. Kotsampopoulos, J. A. Martinez, K. Strunz, M. Saeedifard, X. Wang, D. Shearer, and M. Paolone, "Real-time simulation technologies for power systems design, testing, and analysis," *IEEE Power Energy Technol. Syst. J.*, vol. 2, no. 2, pp. 63–73, Jun. 2015, doi: 10.1109/JPETS.2015.2427370.

[32] X. Guillaud, O. Faruque, A. Teninge, A. H. Hariri, L. Vanfretti, M. Paolone, V. Dinavahi, P. Mitra, G. Lauss, C. Dufour, P. Forsyth, A. K. Srivastava, K. Strunz, T. Strasser, and A. Davoudi, "Applications of real-time simulation technologies in power and energy systems," *IEEE Power Energy Technol. Syst. J.*, vol. 2, no. 3, pp. 103–115, Sep. 2015, doi: 10.1109/JPETS.2015.2445296.

[33] J. Bélanger, P. Venne, and J. N. Paquin, "The what, where and why of real-time simulation," Opal-RT Technol., Montreal, QC, Canada, Tech. Rep., Jan. 2010. Accessed: Apr. 23, 2021. [Online]. Available: https://blob.opal-rt.com/medias/L00161_0436.pdf

[34] R. Kuffel, J. Giesbrecht, T. Maguire, R. P. Wierckx, and P. McLaren, "RTDS—A fully digital power system simulator operating in real time," in *Proc. Int. Conf. Energy Manag. Power Del. (EMPD)*, Singapore, Nov. 1995, pp. 498–503.

[35] S. Abourida, J. Bélanger, and V. Jalili-Marandi, "Real-time power system simulation: EMT vs. phasor," OPAL-RT Technol., Montreal, QC, Canada, Tech. Rep. opWP150620-sa-revA, Sep. 2016.

[36] V. H. Nguyen, Q. T. Tran, E. Guillo-Sansano, P. Kotsampopoulos, C. Gavriluta, G. Lauss, T. I. Strasser, T. V. Jensen, K. Heussen, O. Gehrke, Y. Besanger, T. L. Nguyen, M. H. Syed, R. Brandl, and G. Arnold, "Hardware-in-the-loop assessment methods," in *European Guide to Power System Testing*, T. Strasser, E. de Jong, and M. Sosnina, Eds. Cham, Switzerland: Springer, 2020, pp. 51–66.

[37] M. Maniatopoulos, D. Lagos, P. Kotsampopoulos, and N. Hatziargyriou, "Combined control and power hardware in-the-loop simulation for testing smart grid control algorithms," *IET Gener., Transmiss. Distrib.*, vol. 11, no. 12, pp. 3009–3018, May 2017.

[38] T. Strasser, E. de Jong, and M. Sosnina, Eds., *European Guide to Power System Testing*. Cham, Switzerland: Springer, 2020. [Online]. Available: https://link.springer.com/book/10.1007/978-3-030-42274-5

[39] V. H. Nguyen, Y. Besanger, Q. T. Tran, C. Boudinnet, T. L. Nguyen, R. Brandl, and T. I. Strasser, "Using power-hardware-in-the-loop experiments together with co-simulation for the holistic validation of cyber-physical energy systems," in *Proc. IEEE PES Innov. Smart Grid Technol. Conf. Eur. (ISGT-Europe)*, Sep. 2017, pp. 1–6, doi: 10.1109/ISGTEurope.2017.8260122.

[40] S. Henschel, "Analysis of electromagnetic and electromechanical power system transients with dynamic phasors," Ph.D. dissertation, Dept. Elect. Comput. Eng., Univ. British Columbia, Vancouver, BC, Canada, 1999.

[41] S. Gissinger, P. Chaumes, J.-P. Antoine, A. Bihain, and M. Stubbe, "Advanced dispatcher training simulator," *IEEE Comput. Appl. Power*, vol. 13, no. 2, pp. 25–30, Apr. 2000, doi: 10.1109/67.831425.

[42] F. Plumier, P. Aristidou, C. Geuzaine, and T. Van Cutsem, "Co-simulation of electromagnetic transients and phasor models: A relaxation approach," *IEEE Trans. Power Del.*, vol. 31, no. 5, pp. 2360–2369, Oct. 2016, doi: 10.1109/TPWRD.2016.2537927.

[43] S. Papathanassiou, N. Hatziargyriou, and K. Strunz, "A benchmark low voltage microgrid network," in *Proc. CIGRE Symp. Power Syst. Dispersed Gener.*, Athens, Greece, Apr. 2005, pp. 1–8.

[44] P. Kotsampopoulos, D. Lagos, N. Hatziargyriou, M. O. Faruque, G. Lauss, O. Nzimako, P. Forsyth, M. Steurer, F. Ponci, A. Monti, V. Dinavahi, and K. Strunz, "A benchmark system for hardware-in-the-loop testing of distributed energy resources," *IEEE Power Energy Technol. Syst. J.*, vol. 5, no. 3, pp. 94–103, Sep. 2018, doi: 10.1109/JPETS.2018.2861559.

[45] B. Lundstrom, S. Chakraborty, G. Lauss, R. Brundlinger, and R. Conklin, "Evaluation of system-integrated smart grid devices using software- and hardware-in-the-loop," in *Proc. IEEE Power Energy Soc. Innov. Smart Grid Technol. Conf. (ISGT)*, Sep. 2016, pp. 1–5, doi: 10.1109/ISGT.2016.7781181.

[46] Y. Huo and G. Gruosso, "Hardware-in-the-loop framework for validation of ancillary service in microgrids: Feasibility, problems and improvement," *IEEE Access*, vol. 7, pp. 58104–58112, 2019, doi: 10.1109/ACCESS.2019.2914346.

[47] G. Lauss, F. P. Andren, F. Leimgruber, and T. I. Strasser, "Analyzing standardization needs for CHIL-based testing of power systems and components," in *Proc. IEEE Int. Conf. Ind. Electron. Sustain. Energy Syst. (IESES)*, Jan. 2018, pp. 523–528, doi: 10.1109/IESES.2018.8349932.

[48] H. Palahalli, E. Ragaini, and G. Gruosso, "Smart grid simulation including communication network: A hardware in the loop approach," *IEEE Access*, vol. 7, pp. 90171–90179, 2019, doi: 10.1109/ACCESS.2019.2927821.

[49] H. Palahalli, Y. Huo, and G. Gruosso, "Implementation overview of a novel approach to smart microgrid real time simulation," in *Proc. IEEE Milan PowerTech*, Jun. 2019, pp. 1–6, doi: 10.1109/PTC.2019.8810602.

[50] N. Ntavarinos, P. Kotsampopoulos, D. T. Lagos, and N. Hatziargyriou, "Hardware in the loop testing of battery-less hybrid systems for off-grid power supply," in *Proc. IEEE Milan PowerTech*, Jun. 2019, pp. 1–6, doi: 10.1109/PTC.2019.8810591.

[51] T. Joseph, K. Jose, C. E. Ugalde-Loo, G. Li, and J. Liang, "Real-time hardware-in-the-loop platform for hybrid AC/DC power system studies," in *Proc. IEEE Milan PowerTech*, Jun. 2019, pp. 1–6, doi: 10.1109/PTC.2019.8810905.

[52] E. Tremblay, A. Kachurowski, D. Leschert, and K. Busby, "Protective relay upgrade utilizing real-time simulator technology," in *Proc. IEEE Petroleum Chem. Ind. Committee Conf. (PCIC)*, Sep. 2019, pp. 167–178, doi: 10.1109/PCIC30934.2019.9074529.

[53] V. S. Zeni, L. Munaretto, H. Chaves, N. C. Dal Pont, V. F. Gruner, and G. Finamor, "Hardware-in-the-loop simulation of smart hybrid inverter: A comparison of online simulation and practical results," in *Proc. 47th IEEE Photovolt. Spec. Conf. (PVSC)*, Jun. 2020, pp. 2005–2009, doi: 10.1109/PVSC45281.2020.9300809.

[54] D. C. S. Júnior, J. G. Oliveira, P. M. de Almeida, and C. Boström, "Control of a multi-functional inverter in an AC microgrid—Real-time simulation with control hardware in the loop," *Electr. Power Syst. Res.*, vol. 172, p. 201, Jul. 2019, doi: 10.1016/j.epsr.2019.03.016.

[55] M. Muhammad, H. Behrends, S. Geißendörfer, K. V. Maydell, and C. Agert, "Power hardware-in-the-loop: Response of power components in real-time grid simulation environment," *Energies*, vol. 14, no. 3, p. 593, Jan. 2021.

[56] P. C. Kotsampopoulos, V. A. Kleftakis, and N. D. Hatziargyriou, "Laboratory education of modern power systems using PHIL simulation," *IEEE Trans. Power Syst.*, vol. 32, no. 5, pp. 3992–4001, Sep. 2017, doi: 10.1109/TPWRS.2016.2633201.

[57] M. Stevic, A. Estebsari, S. Vogel, E. Pons, E. Bompard, M. Masera, and A. Monti, "Multi-site European framework for real-time co-simulation of power systems," *IET Gener., Transmiss. Distrib.*, vol. 11, no. 17, pp. 4126–4135, Nov. 2017.

[58] A. Monti, M. Stevic, S. Vogel, R. W. De Doncker, E. Bompard, A. Estebsari, F. Profumo, R. Hovsapian, M. Mohanpurkar, J. D. Flicker, V. Gevorgian, S. Suryanarayanan, A. K. Srivastava, and A. Benigni, "A global real-time superlab: Enabling high penetration of power electronics in the electric grid," *IEEE Power Electron. Mag.*, vol. 5, no. 3, pp. 35–44, Sep. 2018, doi: 10.1109/MPEL.2018.2850698.

[59] B. Lundstrom, B. Palmintier, D. Rowe, J. Ward, and T. Moore, "Trans-oceanic remote power hardware-in-the-loop: Multi-site hardware, integrated controller, and electric network co-simulation," *IET Gener., Transmiss. Distrib.*, vol. 11, no. 18, pp. 4688–4701, Nov. 2017.

[60] J. L. Cale, B. B. Johnson, E. Dall'Anese, P. M. Young, G. Duggan, P. A. Bedge, D. Zimmerle, and L. Holton, "Mitigating communication delays in remotely connected hardware-in-the-loop experiments," *IEEE Trans. Ind. Electron.*, vol. 65, no. 12, pp. 9739–9748, Dec. 2018, doi: 10.1109/TIE.2018.2821618.

[61] A. S. Vijay, S. Doolla, and M. C. Chandorkar, "Real-time testing approaches for microgrids," *IEEE J. Emerg. Sel. Topics Power Electron.*, vol. 5, no. 3, pp. 1356–1376, Sep. 2017, doi: 10.1109/JESTPE.2017.2695486.

[62] R. Ahmadiahangar, A. Rosin, A. N. Niaki, I. Palu, and T. Korõtko, "A review on real-time simulation and analysis methods of microgrids," *Int. Trans. Electr. Energy Syst.*, vol. 29, no. 11, Jun. 2019, Art. no. e12106.

[63] F. Li, Y. Wang, F. Wu, Y. Huang, Y. Liu, X. Zhang, and M. Ma, "Review of real-time simulation of power electronics," *J. Mod. Power Syst. Clean Energy*, vol. 8, no. 4, pp. 796–808, 2020, doi: 10.35833/MPCE.2018.000560.

[64] G. De Carne, M. Liserre, M. Langwasser, M. Ndreko, R. Bachmann, R. W. De Doncker, R. Dimitrovski, B. J. Mortimer, A. Neufeld, and F. Rojas, "Which deepness class is suited for modeling power electronics? A guide for choosing the right model for grid-integration studies," *IEEE Ind. Electron. Mag.*, vol. 13, no. 2, pp. 41–55, Jun. 2019, doi: 10.1109/MIE.2019.2909799.

[65] J. Zhu, G. Teng, Y. Qin, D. Lu, H. Hu, and Y. Xing, "A fully FPGA-based real-time simulator for the cascaded STATCOM," in *Proc. IEEE Energy Convers. Congr. Expo. (ECCE)*, Sep. 2016, pp. 1–6, doi: 10.1109/ECCE.2016.7854682.

[66] F. Montano, T. Ould-Bachir, and J. P. David, "An evaluation of a high-level synthesis approach to the FPGA-based submicrosecond real-time simulation of power converters," *IEEE Trans. Ind. Electron*, vol. 65, no. 1, pp. 636–644, Jan. 2018, doi: 10.1109/TIE.2017.2716880.

[67] C. Yang, Y. Xue, X.-P. Zhang, Y. Zhang, and Y. Chen, "Real-time FPGA-RTDS co-simulator for power systems," *IEEE Access*, vol. 6, pp. 44917–44926, 2018, doi: 10.1109/ACCESS.2018.2862893.

[68] Z. Shen, T. Duan, and V. Dinavahi, "Design and implementation of real-time MPSoC-FPGA-based electromagnetic transient emulator of CIGRÉ DC grid for HIL application," *IEEE Power Energy Technol. Syst. J.*, vol. 5, no. 3, pp. 104–116, Sep. 2018, doi: 10.1109/JPETS.2018.2866589.

[69] A. Hadizadeh, M. Hashemi, M. Labbaf, and M. Parniani, "A matrix-inversion technique for FPGA-based real-time EMT simulation of power converters," *IEEE Trans. Ind. Electron.*, vol. 66, no. 2, pp. 1224–1234, Feb. 2019, doi: 10.1109/TIE.2018.2833058.

[70] M. S. R. Leal, L. D. Simoes, R. L. S. Franca, M. M. Leal, F. B. Costa, and F. E. Taveiros, "Methodology to perform real-time simulation of power systems using a FPGA-based platform," in *Proc. Workshop Commun. Netw. Power Syst. (WCNPS)*, Nov. 2018, pp. 1–5, doi: 10.1109/WCNPS.2018.8604373.

[71] C. Liu, R. Ma, H. Bai, Z. Li, F. Gechter, and F. Gao, "FPGA-based real-time simulation of high-power electronic system with nonlinear IGBT characteristics," *IEEE J. Emerg. Sel. Topics Power Electron.*, vol. 7, no. 1, pp. 41–51, Mar. 2019, doi: 10.1109/JESTPE.2018.2873157.

[72] S. S. Sheikh, S. Iqbal, M. Kazim, and A. Ulasyar, "Real-time simulation of microgrid and load behavior analysis using FPGA," in *Proc. 2nd Int. Conf. Comput., Math. Eng. Technol. (iCoMET)*, Jan. 2019, pp. 1–5, doi: 10.1109/ICOMET.2019.8673431.

[73] R. Mirzahosseini and R. Iravani, "Small time-step FPGA-based real-time simulation of power systems including multiple converters," *IEEE Trans. Power Del.*, vol. 34, no. 6, pp. 2089–2099, Dec. 2019, doi: 10.1109/TPWRD.2019.2933610.

[74] A. Parizad, M. E. Iranian, A. Yazdani, H. R. Baghaee, and G. B. Gharehpetian, "Real-time implementation of asynchronous machine using LabVIEW RTX and FPGA module," in *Proc. IEEE Electr. Power Energy Conf. (EPEC)*, Oct. 2018, pp. 1–6, doi: 10.1109/EPEC.2018.8598390.

[75] B. R. Gama, W. C. Sant'ana, G. Lambert-Torres, C. P. Salomon, E. L. Bonaldi, L. E. Borges-Da-Silva, R. B. B. Carvalho, and F. M. Steiner, "FPGA prototyping using the STEMlab board with application on frequency response analysis of electric machinery," *IEEE Access*, vol. 9, pp. 26822–26838, 2021, doi: 10.1109/ACCESS.2021.3058059.

[76] R. Razzaghi, M. Mitjans, F. Rachidi, and M. Paolone, "An automated FPGA real-time simulator for power electronics and power systems electromagnetic transient applications," *Electr. Power Syst. Res.*, vol. 141, pp. 147–156, Dec. 2016.

[77] B. Zhang, Y. Wang, S. Tu, and Z. Jin, "FPGA-based real-time digital solver for electro-mechanical transient simulation," *Energies*, vol. 11, no. 10, p. 2650, Oct. 2018.

[78] B. Zhang, X. Jin, S. Tu, Z. Jin, and J. Zhang, "A new FPGA-based real-time digital solver for power system simulation," *Energies*, vol. 12, no. 24, p. 4666, Dec. 2019.

[79] L. Estrada, N. Vázquez, J. Vaquero, Á. de Castro, and J. Arau, "Real-time hardware in the loop simulation methodology for power converters using LabVIEW FPGA," *Energies*, vol. 13, no. 2, p. 373, Jan. 2020.

[80] P. H. A. Barra, D. V. Coury, and R. A. S. Fernandes, "A survey on adaptive protection of microgrids and distribution systems with distributed generators," *Renew. Sustain. Energy Rev.*, vol. 118, Feb. 2020, Art. no. 109524.

[81] M. A. Zamani, A. Yazdani, and T. S. Sidhu, "A communication-assisted protection strategy for inverter-based medium-voltage microgrids," *IEEE Trans. Smart Grid*, vol. 3, no. 4, pp. 2088–2099, Dec. 2012, doi: 10.1109/TSG.2012.2211045.

[82] A. Oudalov and A. Fidigatti, "Adaptive network protection in microgrids," *Int. J. Distrib. Energy Resour.*, vol. 5, no. 3, pp. 201–226, 2009. [Online]. Available: https://www.researchgate.net/publication/228344453_Adaptive_network_protection_in_microgrids

[83] T. S. Ustun, C. Ozansoy, and A. Zayegh, "Modeling of a centralized microgrid protection system and distributed energy resources according to IEC 61850-7-420," *IEEE Trans. Power Syst.*, vol. 27, no. 3, pp. 1560–1567, Aug. 2012, doi: 10.1109/TPWRS.2012.2185072.
[84] F. Coffele, C. Booth, and A. Dysko, "An adaptive overcurrent protection scheme for distribution networks," *IEEE Trans. Power Del.*, vol. 30, no. 2, pp. 561–568, Apr. 2015, doi: 10.1109/TPWRD.2013.2294879.
[85] L. Che, M. E. Khodayar, and M. Shahidehpour, "Adaptive protection system for microgrids: Protection practices of a functional microgrid system," *IEEE Electrific. Mag.*, vol. 2, no. 1, pp. 66–80, Mar. 2014, doi: 10.1109/MELE.2013.2297031.
[86] H. Lin, K. Sun, Z. Tan, C. Liu, J. M. Guerrero, and J. C. Vasquez, "Adaptive protection combined with machine learning for microgrids," *IET Gener., Transmiss. Distrib.*, vol. 13, no. 6, pp. 770–779, Mar. 2019.
[87] S. M. E. Ghadiri and K. Mazlumi, "Adaptive protection scheme for microgrids based on SOM clustering technique," *Appl. Soft Comput.*, vol. 88, Mar. 2020, Art. no. 106062.
[88] A. E. C. Momesso, W. M. S. Bernardes, and E. N. Asada, "Adaptive directional overcurrent protection considering stability constraint," *Electr. Power Syst. Res.*, vol. 181, Apr. 2020, Art. no. 106190.
[89] M. S. Javadi, A. E. Nezhad, A. Anvari-Moghaddam, and J. M. Guerrero, "Optimal overcurrent relay coordination in presence of inverter-based wind farms and electrical energy storage devices," in *Proc. IEEE Int. Conf. Environ. Electr. Eng. IEEE Ind. Commercial Power Syst. Eur. (EEEIC/ICPS Europe)*, Palermo, Italy, Jun. 2018, pp. 1–5.
[90] A. Samadi and R. M. Chabanloo, "Adaptive coordination of overcurrent relays in active distribution networks based on independent change of relays' setting groups," *Int. J. Electr. Power Energy Syst.*, vol. 120, Sep. 2020, Art. no. 106026.
[91] I. Ali, S. M. S. Hussain, A. Tak, and T. S. Ustun, "Communication modeling for differential protection in IEC-61850-based substations," *IEEE Trans. Ind. Appl.*, vol. 54, no. 1, pp. 135–142, Jan./Feb. 2018, doi: 10.1109/TIA.2017.2740301.
[92] M. A. Aftab, S. Roostaee, S. M. S. Hussain, I. Ali, M. S. Thomas, and S. Mehfuz, "Performance evaluation of IEC 61850 GOOSE-based inter-substation communication for accelerated distance protection scheme," *IET Gener., Transmiss. Distrib.*, vol. 12, no. 18, pp. 4089–4098, Oct. 2018.
[93] A. A. de Sotomayor, D. D. Giustina, G. Massa, A. Dedè, F. Ramos, and A. Barbato, "IEC 61850-based adaptive protection system for the MV distribution smart grid," *Sustain. Energy, Grids Netw.*, vol. 15, pp. 26–33, Sep. 2018.
[94] *OP5600 HILBOX User Guide Real-Time Simulator*, OPAL-RT Technol., Montreal, QC, Canada, 2011.
[95] OPAL-RT Technologies. *OP5600 Simulator, Versatile Real-Time Digital Simulator*. Accessed: May 14, 2021. [Online]. Available: https://www.opal-rt.com/simulator-platform-op5600/
[96] *OP5330 User Guide Digital to Analog Converter Module*, OPAL-RT Technol., Montreal, QC, Canada, 2014.
[97] *OP5340-1/OP5340-2 User Guide Analog to Digital Converter Module*, OPAL-RT Technol., Montreal, QC, Canada, 2014.
[98] *OP5353 16/32 Digital Inputs User Guide*, OPAL-RT Technol., Montreal, QC, Canada, 2011.
[99] *OP5360-2 User Manual 5 to 30V 32 Digital Output Module*, OPAL-RT Technol., Montreal, QC, Canada, 2010.
[100] *VAMP 50, VAMP 52, VAMP 50 Overcurrent and Earth Fault Protection Relay VAMP 52 Feeder and Motor Protection Relay Publication Version: V50/en M/A017, User Manual*, Schneider Electr., Rueil-Malmaison, France, 2016.
[101] *Wind Farm-Synchronous Generator and Full-Scale Converter (Type 4) Average Model*. Accessed: Sep. 9, 2017. [Online]. Available: https://www.mathworks.com/help/physmod/sps/ug/wind-farm-synchronous-generator-and-full-scale-converter-type-4-average-model.html
[102] H. Hooshyar, F. Mahmood, L. Vanfretti, and M. Baudette, "Specification, implementation, and hardware-in-the-loop real-time simulation of an active distribution grid," *Sustain. Energy, Grids Netw.*, vol. 3, pp. 36–51, Sep. 2015.
[103] H. Hooshyar, L. Vanfretti, and C. Dufour, "Delay-free parallelization for real-time simulation of a large active distribution grid model," in *Proc. 42nd Annu. Conf. IEEE Ind. Electron. SoC. (IECON)*, Oct. 2016, pp. 6278–6284, doi: 10.1109/IECON.2016.7793885.
[104] *400-kW Grid-Connected PV Farm (Average Model)*. Accessed: Dec. 7, 2017. [Online]. Available: https://www.mathworks.com/help/physmod/sps/ug/400-kw-grid-connected-pv-farm-average-model.html
[105] "IEC 61850 interface configuration for VAMP products and WIMO," Schneider Electr. Ind. SAS, Rueil-Malmaison, France, Appl. Note AN61850.EN005, 2012.
[106] M. Mekkanen, K. Kauhaniemi, L. Kumpulainen, and A. A. Memon, "Light-Weight IEC 61850 GOOSE based LOM protection for smart grid," in *Proc. CIRED Ljubljana Workshop Microgrids Local Energy Commun.*, Ljubljana, Slovenia, Jun. 2018, p. 31.

AUSHIQ ALI MEMON (Member, IEEE) received the B.E. degree in electrical engineering from the Quaid-e-Awam University of Engineering, Science and Technology, Nawabshah, Pakistan, in 2006, and the M.Sc. (Power Engineering) degree in electrical power engineering from the Brandenburg University of Technology, Cottbus, Germany, in 2013. He is currently pursuing the Ph.D. degree with the Department of Electrical Engineering, University of Vaasa, Finland. Previously, he was a Lecturer with the Quaid-e-Awam University of Engineering, Science and Technology, from 2007 to 2009. He was a Project Researcher with the University of Vaasa, from 2014 to 2020. His research interests include power system protection, microgrids, power system transient simulations, smart grids, and power electronics applications.

KIMMO KAUHANIEMI (Member, IEEE) received the M.S. and Ph.D. degrees in electrical engineering from the Tampere University of Technology, Finland, in 1987 and 1993, respectively. He has been previously employed by ABB Corporate Research Center and VTT Technical Research Centre of Finland. He is currently with the University of Vaasa, where he is a Professor of electrical engineering and also leads the Smart Electric Systems Research Group. His special research interests include power system transient simulation, protection of power systems, grid integration of distributed generation, and microgrids.

IEEE Access
Multidisciplinary ⋮ Rapid Review ⋮ Open Access Journal

Received 13 November 2022, accepted 26 November 2022, date of publication 2 December 2022,
date of current version 8 December 2022.

Digital Object Identifier 10.1109/ACCESS.2022.3226653

RESEARCH ARTICLE

Evaluation of New Grid Codes for Converter-Based DERs From the Perspective of AC Microgrid Protection

AUSHIQ ALI MEMON, (Member, IEEE), MAZAHER KARIMI, (Senior Member, IEEE), AND KIMMO KAUHANIEMI, (Member, IEEE)
School of Technology and Innovations, University of Vaasa, 65200 Vaasa, Finland
Corresponding author: Aushiq Ali Memon (amemon@uwasa.fi)

This work was supported by the SolarX Research Project funded by the Business Finland under Grant 6844/31/2018.

ABSTRACT The ever-increasing penetration levels of converter-based distributed energy resources (DERs) in medium and low voltage (MV/LV) distribution networks necessitate new and revised standards or connection requirements of generating units. These standardized connection requirements to be met by DERs are called grid codes. This paper reviews new European and IEEE grid codes of MV/LV converter-based DERs and presents an evaluation of selected grid codes applicable for AC microgrid protection. The selected grid codes are evaluated for both grid-connected and islanded modes of AC microgrid operation. The standardized settings of different protection schemes including symmetrical components-based protection schemes are evaluated for quick fault detection and isolation during the most challenging unbalanced faults in grid-connected and islanded modes. The extent of dynamic reactive power (Q) injection by DERs according to European grid codes is evaluated and the effect of Q-injection on fault detection and protection coordination is observed. The generic grid-forming DER model with coupled dq-control has been enabled to provide enough reactive current during the unbalanced faults with the help of an additional Q-source. It is concluded that the grid code requirement of dynamic Q-injection can be met by converter-based DERs with an additional Q-source of minimum capacity equal to twice the apparent power of individual DER in the grid-connected mode. The same extent of Q-injection is also useful for fault detection and reliable directional element design in the islanded mode. A new five-cycle overvoltage ride-through (OVRT) curve is also suggested for smooth transition to the islanded mode.

INDEX TERMS Grid codes, converter-based DERs, AC microgrid protection, symmetrical components.

I. INTRODUCTION

The strong desire to reduce carbon emissions and exploit the benefits of sustainable renewable energy sources (RES), the integration of distributed energy resources (DERs) in the distribution networks has been accelerated during the last decade. The DERs include wind turbine generators (WTGs), photovoltaic (PV) systems and other small-scale combined heat and power (CHP) micro-sources and energy storage systems (ESS). The integration of the DERs close to the load centers offers multiple advantages like the deferral of grid expansion, the reduction of distribution losses, the increased reliability and the continuity of uninterrupted power supply during grid outages. However, the connection of different individual DERs close to the load centers may cause some adverse operational problems like protection coordination and sensitivity problems, local voltage-rise, reduced power quality, over frequency, over loading of lines and transformers, and reactive power unbalance in the local distribution systems. Therefore, new mitigation measures are required to overcome these new challenges. One promising way to tackle these challenges is to plan the future smart distribution networks comprised of multiple individual self-managed and controlled building

The associate editor coordinating the review of this manuscript and approving it for publication was Nagesh Prabhu.

blocks called microgrids. A microgrid with different DERs, loads and ESS could be controlled locally using a microgrid management system (MMS) and thus could interact with the local distribution grid in an acceptable manner either as a net producer or a net consumer of the electrical energy. A microgrid can operate in the islanded mode during main grid outages, thus increasing the reliability of supply to the consumers [1], [2].

The grid-connected mode of operation of the DERs is the usual practice around the world except on distant geographical islands with no connection to the transmission and distribution grids. The diesel and gas generators are usually used there as the main energy sources along with WTGs, PVs and CHP units. For example, the Hailuoto island in Finland uses the diesel generator along with the WTGs and PVs systems for the islanded mode of operation during the grid outages [3]. The extensive use of the diesel and gas generators in this new era of clean and renewable generators is not much accepted and they are likely to be replaced with the BESS or operated only as a final resort when the rest of energy resources are completely depleted.

Currently, the islanded mode of operation of the DERs and microgrids is usually prohibited in the distribution networks due to technical limitations and safety concerns. The islanded mode of operation will, however, enhance the reliability level of the existing distribution networks if planned well with suitable grid-forming DERs and ESS [1], [2].

The behavior of the converter-based DERs is usually different from the behavior of the conventional synchronous generators. On the one hand, the converter-based DERs lack the inertia of rotating machines due to their decoupling with the electric grid through the frequency converters. On the other hand, the converter-based DERs provide the limited short-circuit current contribution due to the limited current ratings of the converters because of the economic reasons to employ highly over-rated converters. However, the converter-based DERs are very quick to operate and control within milliseconds (ms) thanks to the fast power electronic switches. Therefore, the behavior of the converter-based DERs can be easily and quickly controlled in any mode of operation, grid-connected or islanded mode [2].

The grid-connected and the islanded modes of operation of AC microgrid require adaptive overcurrent (OC) protection schemes with at least two setting groups of different current thresholds or sensitivities. This is required due to the increased fault current contribution from the main grid in the grid-connected mode and the reduced or limited fault current contribution from the converter-based DERs in the islanded mode even during the balanced three-phase (3Ph) or LLL faults. The most challenging unbalanced shunt faults like line-to-line (LL) and single-line-to-ground (SLG) faults and the series or open circuit faults result in fault current of less than or equal to load current. Therefore, symmetrical components-based protection schemes may also be required for detection of these faults. Additionally, the distribution lines with DERs on both sides and the ring or looped network topology require the reliable directional schemes for the maintenance of protection selectivity.

The symmetrical components analysis is usually used to find the magnitude of positive-, negative- and zero-sequence components of fault currents and voltages in a three-phase power system. During the normal operation of three-phase distribution system and a balanced ungrounded short-circuit fault (LLL-fault), only the positive-sequence (Pos-Seq) current flows from the sources or generators to the loads which is identical to the rms current. The occurrence of an unbalanced shunt fault like LL-fault between any two live conductors of a distribution line gives rise to both the Pos-Seq and negative-sequence (Neg-Seq) current. The zero-sequence (Zero-Seq) current only increases when there is a shunt fault to the ground, like the SLG, double-line-to-ground (LLG) or three-phase-to-ground (LLLG) faults. The Zero-Seq current may only be available locally depending on the transformer connection type of delta and star (grounded/grounded) at its primary and secondary side. A series fault also known as an open circuit fault generates both the Neg-Seq and Zero-Seq components. The Neg-Seq component is present in all fault types except the balanced LLL-fault and can be used for the detection of broken conductors on transmission or distribution lines and open/close failure of breaker on one or two poles. Any presence of the Neg-Seq and Zero-Seq components during the normal fault-free operation is an indication of unbalanced line impedances, source voltages or load currents [4], [5].

Traditionally, the phase OC or Pos-Seq OC function (51P) clears the most short-circuit faults within the preset coordinated tripping time intervals. The Neg-Seq OC function (51Q) and Zero-Seq OC function (51G) can be used as backup for the detection of those faults which are difficult to be detected by using only 51P protection function (e.g., LL, LG, LLG faults) [6]. The coordination of Neg-Seq and Zero-Seq OC functions can also be done in definite-time or inverse-time just like the Pos-Seq OC function [5], [7] and at least for a local backup to 51P function.

The setting of thresholds and tripping time intervals of the Neg-Seq and Zero-Seq OC functions (51Q and 51G) for the protection of distribution networks with lines and cables may vary depending on the type of grounding schemes, the type of faults and the resistance or impedance of the faults to be detected. These issues are usually addressed separately.

The setting of the tripping threshold of the Pos-Seq or phase OC function (51P) is usually selected above the maximum expected magnitude of load current or inrush current whichever is applicable. The setting of the tripping threshold of the Zero-Seq or ground OC function (51G) is usually selected above the value observed during the highest possible load unbalance [4]. The tripping threshold of 51Q function should be set above any standing load unbalance observed at the relay. For 3Ph motor loads a good level of sensitivity of 51Q function is achieved due to the balanced nature of loads. However, a large 1Ph load on transformer may compromise the sensitivity of 51Q function [8].

Directional discrimination is also required for proper selectivity or coordination of forward and reverse faults in ring-networks or networks with generators on both sides. This can be accomplished with the directional OC function (ANSI 67) with either definite-time or inverse-time characteristic.

The directional OC function not only requires the tripping threshold of the current but also requires the direction of the fault if the fault is in front of the relay (forward fault) or behind it (reverse fault). The directional coordination or discrimination of forward faults in the tripping direction and reverse faults in the non-tripping direction is done using different methods or principles which are usually different for balanced and unbalanced faults.

The directional element (67P) for the balanced fault is usually designed based on phase comparison of Pos-Seq voltage and Pos-Seq current using voltage as the reference or polarizing quantity and the current as the operating quantity. Depending on the set criteria if the phase angle enters the operating area, the fault direction is declared as the forward or the reverse. This scheme may fail due to close-in three-phase short-circuit fault which causes voltage of all phases to fall to a zero magnitude, therefore the magnitude of Pos-Seq voltage is also zero [9]. Hence, the stored memory of the voltage before the fault is usually required for this scheme to work properly for the detection of fault direction [10]. There are also other methods reported in [10], [11], [12], and [13] that use the current-only polarization for the estimation of fault current direction. These schemes can be useful in situations when either the voltage transformer (VT) is not available, or the extra cost of VT is to be avoided.

Using the Neg-Seq voltage and current, it is possible to design a reliable directional element (67Q) for all unbalanced faults in traditional distribution networks. For the ground faults, the Zero-Seq voltage and current can be used to design a ground directional element (67G). The principle of finding the direction can be based on traditional phase comparison of voltage and current or impedance-based directional element [4]. The details about the directional element design and evaluation can be found in [14]. The traditional Neg-Seq directional element and Neg-Seq impedance directional element are discussed in more details in [15].

The converter-based DERs behave as sources of the limited constant current of 1-2 p.u. during the faults irrespective of the design and control of their converters as voltage source converters or current source converters. The converter-based DERs typically provide negligible magnitude of Neg-Seq or Zero-Seq current. Most controllers of the converter-based DERs are usually designed to regulate Pos-Seq current and suppress the Neg-Seq current partially or entirely during the faults [16], [17]. The results from [18], [19], and [20] show the mis-operation of the Neg-Seq directional relays due to the different Neg-Seq fault current characteristics of the converter-based DERs (including type-4 WTG) compared with synchronous generators. However, this impact will be reduced in future as new grid codes require the converter-based DERs to supply a certain amount of Neg-Seq reactive current during the voltage steps or faults. The injection of Neg-Seq short-circuit current by the WTGs proportional to the Neg-Seq voltage is proposed in [17] particularly for the detection of LL-faults.

This requirement may vary according to different national and regional grid codes as reported in [21]. The reactive current support during the short-circuit faults up to the rated current of the DER is required by the latest EN grid code [22] as reviewed in the section II of this paper.

Different regions and countries of the world with increasing penetration levels of the DERs in transmission and distribution networks have set rules and regulations for the connection of DERs, called as ''grid standards'' or ''grid codes'' of DERs. These grid codes define the operational behavior of different types of DERs during the steady-state and fault conditions in order to avoid the adverse effects to the grid assets as well as to the local consumers in the grid-connected operation.

This paper reviews and evaluates the latest active IEEE standards and the common European standards/grid codes (abbreviated as EN) for the converter-based DERs connected at medium voltage (MV) and low voltage (LV) distribution networks for the grid-connected and islanded mode of operation. Particularly, the latest approved European standards EN 50549-1:2019 [23] and EN 50549-2:2019 [22] for generating plants to be connected in parallel with the LV and the MV distribution networks, respectively. The IEEE standard closely related to these European standards is the IEEE standard 1547-2018 [24] which deals with the interconnection and interoperability of the DERs with the associated electric power system (EPS). The impact of the IEEE standard 1547-2018 on the smart inverters is already evaluated in the technical report PES-TR67 of the IEEE power and energy society [25] which is considered as a guide in this review.

The IEEE standard 1547.4-2011 [26], which deals with the DER island system, has also been reviewed briefly to cover the islanded mode operation of the AC microgrid. Related to the different modes of AC microgrid operation like grid-connected, islanded and transition modes the change of DER controls are necessarily required to maintain the stability of the AC microgrid. Therefore, the IEEE standard 2030.7-2017 [27] which defines the specification of microgrid controllers has also been reviewed.

In this paper, the evaluation of EN 50549-1-2019 and EN 50549-2-2019 grid codes have been investigated from the perspective of the protection of AC microgrid. In this regard, symmetrical current- and voltage-based protection schemes have been evaluated for fault detection and protection coordination with a certain amount of reactive current injection by the grid-forming DER during the LL unbalanced faults. The additional amount of reactive current at DER terminals is injected only during the LL unbalanced faults to enhance the Neg-Seq component of fault current. For this purpose, an additional fast acting thyristor switched capacitor (TSC) has been suggested at LV terminals of DER. The TSC is

TABLE 1. Limits for thresholds for type B, C and D power generating modules [28].

Synchronous area	Limit for max capacity threshold from which on a power gen module is of type-B	Limit for max capacity threshold from which on a power gen module is of type-C	Limit for max capacity threshold from which on a power gen module is of type-D
CE	1 MW	50 MW	75 MW
GB	1 MW	10 MW	30 MW
Nordic	1.5 MW	10 MW	30 MW
IE and NI	0.1 MW	5 MW	10 MW
Baltic	0.5 MW	10 MW	15 MW

gen = generating, MW = Megawatt, CE = Continental Europe, GB = Great Britain, IE = Ireland, NI = Northern Ireland.

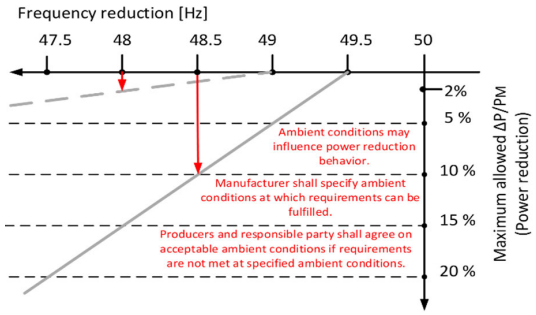

FIGURE 1. Maximum allowable power-reduction in case of UF [22].

switched only in continuous ON or OFF states when the fault condition becomes activated or deactivated by the control.

The use of additional TSC helps to detect the unbalanced shunt and series (open phase) faults using Neg-Seq OC and ratio of Neg-Seq OC and Pos-Seq OC protection functions particularly in the islanded mode of operation. The additional reactive current is evaluated at the DER terminals according to the EN 50549-2-2019 grid code. The DERs are modelled in MATLAB/Simulink using the synchronous frame of reference or dq-control with a limited amount of Neg-Seq current provision capability in the absence of TSC. The symmetrical components-based directional elements are also designed and evaluated during the LL unbalanced faults for the maintenance of protection selectivity before and after Q-injection.

The rest of the paper is organized in a way that Section 2 presents the review of the European EN grid codes for the converter-based DERs, and Section 3 gives review of the IEEE grid codes/standards for the converter-based DERs. Section 4 evaluates the protection related grid codes using the simulations performed with MATLAB/Simulink. Section 5 gives the discussion and Section 6 concludes the paper.

II. EN GRID CODES FOR CONVERTER-BASED DERS

This section reviews the two recently approved EN grid codes i.e., EN 50549-1:2019 [23] and EN 50549 2:2019 [22] for generating plants to be connected in parallel with the LV and MV distribution networks, respectively. Both of these grid codes cover the generating plants up to and including type-B. In conformance to the network code on requirements for grid connection of generators (NC RfG), type-A category of power generating modules have connection point below 110 kV and the maximum capacity of 0.8 kW or more. The type-B, type-C and type-D generating plants/modules are defined in Table 1 [28]. For example, in the Nordic synchronous area type-B generating plants have the active power (P) capacity range of 1.5-10 MW, type-C generating plants have the active power capacity range of 10-30 MW and type-D generating plants have the active power capacity range of 30 MW or more. From the context of this paper, the converter-based generating plants are referred to as DER plants or simply DERs.

A. CONTINUOUS OPERATING FREQUENCY AND VOLTAGE LIMITS

The considered EN grid codes of the DERs in general are comprised of two main parts, one-part deals with the steady-state operating conditions of the DERs and the second-part deals with the operating conditions of DERs during the fault events and other contingency or disturbance conditions. For the steady-state operating conditions, the normal or continuous operating ranges of voltage and frequency of the DERs are defined with respect to the different operational time durations to avoid the possible voltage and frequency instability of the well synchronized power system.

The continuous operating frequency range for the DERs connected to the LV and MV networks is defined as 49-51 Hz [22], [23]. The operation of DERs below the frequency of 49 Hz is considered as underfrequency (UF) operation and over the frequency of 51 Hz the operation is considered as the overfrequency (OF) operation.

During the operation below 49.5 Hz frequency in the grid-connected mode of operation, a maximum active power reduction (ΔP) of 10% of the maximum active power (P_M) per 1 Hz reduction of the frequency is allowed by default for the DER plants connected to the LV or MV networks. However, the most stringent requirement is to reduce only 2% of the maximum active power per 1 Hz reduction of the frequency (see Fig. 1) [22], [23]. Fig. 2 gives the minimum and stringent time periods for the DER operation during the UF and OF situations. The same operating ranges are applicable for the DERs connected to the LV and MV networks.

The continuous operating voltage range capability of the DER plants connected to LV networks is 85–110% of U_n where U_n is the nominal voltage [23] and the continuous operating voltage range capability of the DER plants connected to MV networks is 90–110% of U_c where U_c is the voltage at the connection point [22].

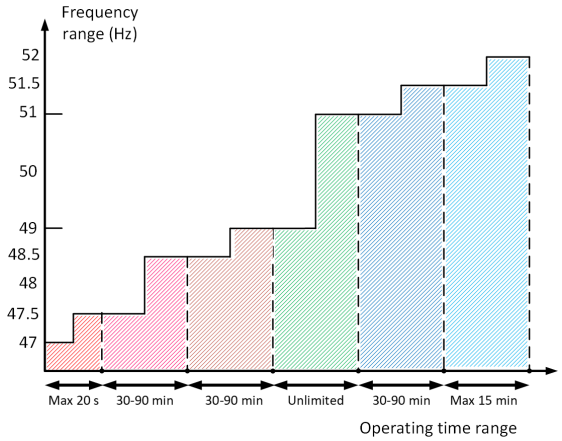

FIGURE 2. Operating time range vs frequency range [22], [23].

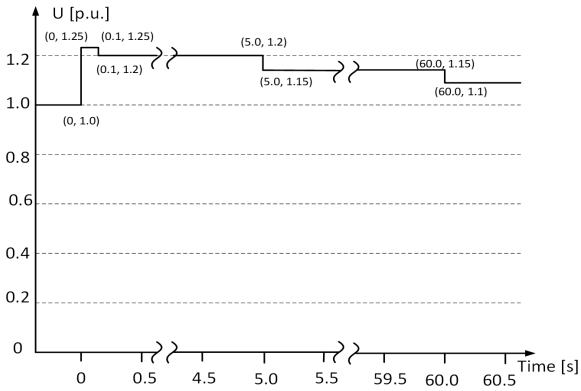

FIGURE 3. The OVRT curve of the DER plants for connection to the LV and MV networks [22], [23].

B. IMMUNITY TO THE FREQUENCY AND VOLTAGE DISTURBANCES

Beyond the continuous allowable voltage and frequency ranges the variations of the voltage and frequency are considered as *the disturbance operating conditions*. The immunity to disturbance operating conditions is required by the DER plants to prevent their unnecessary disconnection for maintaining the stability of the network, particularly with the high penetration level of the DERs in LV and MV networks. Three types of the immunities to disturbance are defined in both standards EN 50549-1-2019 [23] and EN 50549-2-2019 [22]: The first immunity is the rate-of-change-of-frequency (ROCOF) immunity, the second one is the undervoltage (UV) or LV ride-through (UVRT/LVRT) also called fault ride-through (FRT) immunity and the third one is the overvoltage (OV) or high voltage ride-through (OVRT/HVRT) immunity.

The ROCOF immunity means that the DER plant shall stay connected with the distribution network if the frequency of the distribution network changes with a specified ROCOF threshold. For a ROCOF equal to or greater than the specified value, the DER plant modules shall have ROCOF immunity. If the ROCOF threshold value is not specified, then 2 Hz/s for the non-synchronous DER plants including the converter-based DERs and 1 Hz/s for the synchronous DER plants shall apply. A sliding measurement window of 500 ms is considered for defining the ROCOF immunity. However, for the control action dependent on frequency measurement shorter than 500 ms measurement periods and for the small isolated distributed networks on islands higher than the specified ROCOF immunity values may be necessary. The ROCOF is used as a method for the detection of loss of mains condition in some European countries [22], [23]. Related to the ROCOF is the previous technical report [29] prepared by the U.S National Renewable Energy Laboratory (NREL) which suggests that the ROCOF method is fairly effective for the synchronous generators and not effective for the converter-based DERs. For the converter-based DERs it is recommended to use the active loss of mains detection methods.

The UVRT immunity means that during times of low voltages or faults (1ph, 2ph, 3ph) causing the low voltages, the DER plants should stay connected to the distribution network and not tripped. The DER plants should behave according to the defined UVRT voltage-time curve. The DER plants shall stay connected if the minimum voltage, phase-to-neutral (ph-N) or phase-to-phase (ph-ph), at the point of connection remains above the voltage-time curve. The default and the most stringent voltage-time curves of the UVRT requirement for the converter-based DER plants as defined in [22] and [23] are reproduced and compared in [34], hence not mentioned more in this section.

The OVRT immunity means that the DER plants shall stay connected to the LV and MV distribution networks if the highest voltage (ph-N or ph-ph) at the point of connection stays below the defined voltage-time curve of the OVRT capability (Fig. 3).

The grid code EN 50549-1-2019 [23] for the connection requirements of the LV distribution networks, excludes the micro-generating DERs with nominal current not exceeding 16 A per phase from OVRT requirement. Like the previous ROCOF and UVRT immunities, the OVRT immunity is also independent of the interface protection settings which always overrule the technical capabilities and decides about the connection or disconnection of the DER plant [22], [23].

C. THE SHORT-CIRCUIT CURRENT REQUIREMENT FOR THE CONVERTER-BASED DER PLANTS

The DER plants are required to have the capability of providing an additional amount of the reactive current for voltage support during the network faults and sudden voltage steps. This requirement is in addition to the default reactive power (Q) requirement of 33% of the design active power (P_D) and the stringent reactive power requirement of 48.4% of P_D when active power is above 20% of P_D during the normal continuous operating voltage and frequency limits [22]. For the DER plants connected to the LV networks, the additional amount of reactive current for voltage support is not required due to the potential interference with the grid

protection equipment [23]. However, if the reactive power during the network faults is required for the type-B DER plants connected to LV networks by the distribution system operator (DSO) then it will be according to the requirements defined in [22] for the DER plants connected to the MV networks which are reviewed in this section. For the voltage below 15% of U_c, no reactive current supply is required even for the DER plants connected to the MV networks.

The additional reactive current (I_Q) has to be supplied by the DER plants when there is sudden voltage change or jump and this requirement applies to voltage steps in both the Pos-Seq and the Neg-Seq components of the fundamental voltage. It means the voltage steps in Pos-Seq voltage will require additional reactive current in Pos-Seq and the voltage steps in Neg-Seq voltage will require additional current in Neg-Seq. The requirement of providing the additional reactive current should in principle be according to Fig. 4 up to the current limitation of the DER plant and at least up to the rated current (I_r). The additional reactive current in the Pos-Seq (ΔI_{Q1}) is set by the gradient k_1 according to equation (1):

$$\Delta I_{Q1} = k_1 \cdot \Delta U_1 \tag{1}$$

ΔU_1 in (1) is the sudden voltage jump or change for the Pos-Seq defined by equation (2):

$$\Delta U_1 = (U_1 - U_{11min})/U_c \tag{2}$$

U_1 in (2) is the actual voltage of the Pos-Seq and U_{11min} is the 1-minute average of the pre-fault voltage of the Pos-Seq or the RMS value. During the normal operation the Pos-Seq is almost identical to the RMS value. The additional reactive current in the Neg-Seq (ΔI_{Q2}) is set by the gradient k_2 according to equation (3):

$$\Delta I_{Q2} = k_2 \cdot \Delta U_2 \tag{3}$$

ΔU_2 in (3) is the sudden voltage jump or change for the Neg-Seq defined by equation (4):

$$\Delta U_2 = (U_2 - U_{2\_1min})/U_c \tag{4}$$

U_2 in (4) is the actual voltage of the Neg-Seq and U_{21min} is the 1-minute average of the pre-fault voltage of the Neg-Seq or zero. During the normal operation the Neg-Seq current is equivalent to zero. The gradients k_1 and k_2 shall be set in the range of 2-6 with a minimum step size of 0.5. The insensitivity range (Fig. 4) defined in terms of the sudden voltage jump can be in the range of ΔU_{1min} = 0-15% for both the Pos-Seq and the Neg-Seq components.

The step response of the additional reactive current should be "no greater than 30 ms" and the settling time of the additional reactive current should be "no greater than 60 ms." The same values of the step response and settling time are also valid for the inception of the fault and the fault clearance or any voltage step in the duration of the fault but apply only to the controlled reactive current. For the provision of an additional reactive current, the Pos-Seq and Neg-Seq components are limited to the same extent such that the asymmetry of the

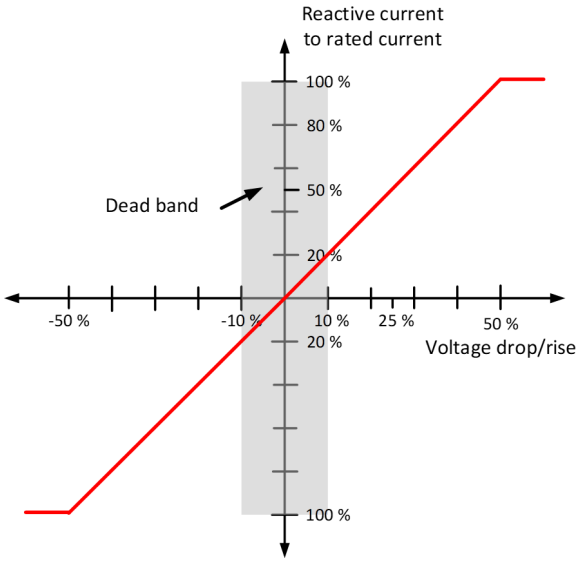

FIGURE 4. Principle of voltage support during faults and voltage steps [22].

support is maintained in case of an asymmetrical fault. Moreover, it is allowed to reduce the active current component to maximize the reactive current, but the reduction should be as small as possible.

The short-circuit current requirement could either be implemented in DER units or in an additional equipment in the DER plant. In this regard, the accuracy of the injected current and the response and settling time is evaluated at the clamps of the DER unit or at the clamps of the additional equipment if applicable due to high dynamic of the requirement. The function of the dynamic reactive current provision can be activated when one or more ph-ph voltages are outside the static voltage range (80-100% of U_c for UV and 100-120% of U_c for OV) or a sudden change in voltage occurs. This function can be deactivated after the re-entry of all ph-ph voltages into static range and after 5 s if the sudden voltage change does not result in any voltage exceeding the static voltage range [22].

D. THE INTERFACE PROTECTION REQUIREMENTS

There are three main objectives of the interface protection mentioned in [22] and [23] which include the prevention of an OV situation due to the power production of the DER plant, the detection of an unintentional island situation and disconnecting the DER plant in this case and providing the assistance to the distribution network in the restoration of the controlled state in case of voltage and frequency deviations beyond the regulated values. It is neither the primary objective of the interface protection to disconnect the DER plant from the distribution network in case of any short-circuit faults internal to the DER plant nor to prevent damages to the DER plant due to short-circuit faults on the distribution network. However, the interface protection may help preventing the

TABLE 2. Voltage and frequency functions for the interface protection [22], [23].

Protection function	Threshold	Operating time
UV[1] [27]	Stage 1: [27 <] (0.2-1) U_n adjustable by steps of 0.01 U_n Stage 2: [27 <<] (0.2-1) U_n adjustable by steps of 0.01 U_n	0.1-100 s adjustable in steps of 0.1 s 0.1-5 s adjustable in steps of 0.05 s
OV[1] [59]	Stage 1: [59 >] (1.0-1.2) U_n adjustable by steps of 0.01 U_n Stage 2: [59 >>] (1.0-1.3) U_n adjustable by steps of 0.01 U_n	0.1-100 s adjustable in steps of 0.1 s 0.1-5 s adjustable in steps of 0.05 s
OV 10 min mean[2]	(1.0-1.15) U_n adjustable by steps of 0.01 U_n	Start time ≤ 3 s not adjustable Time delay setting = 0 ms
UF[3] [81<]	Stage 1: [81 <] (47.0-50.0) Hz adjustable by steps of 0.1 Hz Stage 2: [81 <<] (47.0-50.0) Hz adjustable by steps of 0.1 Hz	0.1-100 s adjustable in steps of 0.1 s 0.1-5 s adjustable in steps of 0.05 s
OF[3] [81>]	Stage 1: [81 >] (50.0-52.0) Hz adjustable by steps of 0.1 Hz Stage 2: [81 >>] (50.0-52.0) Hz adjustable by steps of 0.1 Hz	0.1-100 s adjustable in steps of 0.1 s 0.1-5 s adjustable in steps of 0.05 s
Pos-Seq[4] UV [27D]	(20-100 %) U_n adjustable by steps of 1 % U_n	0.2-100 s adjustable in steps of 0.1 s
Neg-Seq[4] OV [47]	(1-100 %) U_n adjustable by steps of 1 % U_n	0.2-100 s adjustable in steps of 0.1 s
Zero-Seq[4] OV [59N]	(1-100 %) U_n adjustable by steps of 1 % U_n	0.2-100 s adjustable in steps of 0.1 s

[1]Protection shall comply with EN 60255-127 and evaluation of the fundamental or the rms value is allowed. [2]The calculation shall comply with 10 min aggregation of EN 61000-4-30 Class S and calculation of a new 10 min value at least every 3 s is sufficient which is then compared with threshold value. [3]The frequency protection shall function correctly for the input voltage range between 20%U_n and 120%U_n and inhibited for input voltages of less than 20%U_n. [4]Only for DER plants connected to MV networks.

damage to the DER units during the out-of-phase reclosing of the automatic recloser happening after some hundreds of milliseconds (ms). In some countries it is required that some technologies of DER units should have an appropriate immunity level against the consequences of the out-of-phase reclosing.

For the DER plants connected to the LV networks with nominal current above 16 A, the interface protection shall be provided with a dedicated device at the point of connection as defined by the DSO. For the micro-generating DERs with nominal current less than the defined threshold, the interface protection may be integrated into the DER unit. However, the integrated interface protection provision may not be possible either due to the placement of the protection system as near to the point of connection as possible for avoiding the nuisance OV tripping due to the voltage rise within the producer's network or due to the requirement of periodic field tests [23]. For the DER plants connected to the MV networks, the interface protection shall be realized only as a dedicated device and not integrated into the DER unit [22].

The interface protection relay shall act primarily on the interface switch or breaker. However, the DSO may require that the interface relay may act on another switch or breaker with a proper delay setting if the failure of interface switch happens. If the power supply of the interface protection fails, it shall trigger the interface switch without any delay. The DSO may require UPS in case of UVRT capability and delay in protection etc. [22], [23].

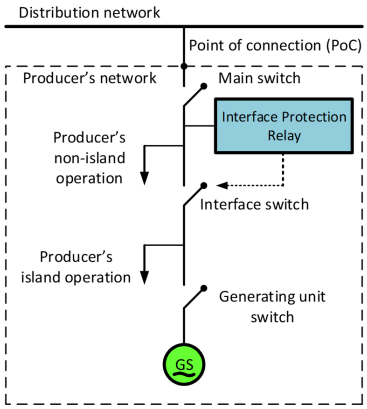

FIGURE 5. Schematic diagram of DER plant with dedicated interface protection relay and view of switches [22].

The different voltage and frequency functions for the interface protection and their settings for the DER plants connected to the LV and MV networks are summarized in Table 2.

The general requirement of the voltage protection is that all ph-ph (preferred) and ph-N voltages need to be evaluated with minimum measurement accuracy of ± 1% of U_n. The general requirement of the frequency protection is that the frequency shall be evaluated on at least one of the voltages (ph-ph or ph-N) with minimum measurement accuracy of ± 0.05 Hz. The reset time of protection is ≤ 50 ms. Fig. 5 shows the schematic diagram of the DER plant connected to the distribution network with different switches and a dedicated interface protection relay.

III. IEEE GRID CODES FOR CONVERTER-BASED DERS

The IEEE 1547-2018 standard [24] provides the technical specifications and requirements for the interconnection of DERs with electric power systems and associated interfaces at primary or secondary radial distribution systems with a nominal system frequency of 60 Hz. The IEEE 1547-2018 standard is closely related to the above reviewed European standards EN 50549-1:2019 [23] and EN 50549-2:2019 [22] for the LV and MV distribution networks with a nominal system frequency of 50 Hz. However, IEEE 1547-2018 divides the technical specifications and performance requirements of DERs into different categories based on low or high penetration levels of DERs. For example, the reactive power capability and voltage regulation requirements are divided into two categories: Category A for the low penetration levels and less frequent overall power output variations of DERs and Category B for the high penetration levels and large overall power output variations of DERs. Similarly, the abnormal operating performance of DERs depending on the stability/reliability of the bulk power system (BPS) is subdivided into three categories: category I, category II and category III operating performance. The category I abnormal operating performance requirements are related to the

essential BPS stability/reliability needs attainable by all DER technologies. The category II requirements deal with all BPS stability/reliability needs required for avoiding tripping for a wider range of disturbances coordinated with existing reliability standards. The category III requirements are recommended for both BPS stability/reliability and distribution system reliability/power quality needs coordinated with existing interconnection requirements for very high penetration level of DERs.

The IEEE 1547-2018 standard is applicable based on the name plate rating of all DER units within the local EPS. It does not define the maximum DER capacity for a specific installation interconnected to a single point of common coupling (PCC) or to a given feeder. The IEEE 1547-2018 standard allows the use of the supplement DER devices to meet the requirements of this standard. The supplement devices are not required to be co-located with the DER units but located within the Local EPS. The reference point of applicability (RPA) of this standard shall be at the PCC for all performance requirements except those otherwise stated in the standard. Only the IEEE 1547-2018 standard requirements for the high penetration levels of DERs (category III requirements) are considered and reviewed in this paper.

A. CONTINUOUS OPERATING FREQUENCY AND VOLTAGE LIMITS

The continuous operating frequency for the DERs connected at primary/MV or secondary/LV system is defined in the range of 58.8-61.2 Hz irrespective of the penetration level of DERs. The continuous operating voltage range for the DERs connected at primary or secondary distribution networks is defined as 0.88-1.10 per unit (p.u.) of nominal system voltage (RMS) at the PCC. The applicable voltages determining the performance of DERs can be measured as an individual ph-N, phase-to-ground (ph-g), or ph-ph combination and time resolution. It all depends on the location of the PCC at MV or LV system and the winding arrangements/configurations of transformers.

B. IMMUNITY AND RESPONSE TO THE ABNORMAL OPERATING CONDITIONS

The abnormal operation conditions include the short-circuit faults, open phase conditions and the unacceptable variations of voltage and frequency values. The stability of the Area EPS, the safety of the maintenance workers and general public and the avoidance of equipment damage are the main factors requiring appropriate DER response during the abnormal conditions. For short-circuit faults, the DERs are required to seize to energize and trip for all faults detected by the protection system of the Area EPS. The parameter adjustment of the DERs or the protection system may be required to ensure proper fault detection and protection coordination. The DERs shall seize to energize and trip all phases to which they are connected within 2.0 s of the open phase condition.

For the DER response to the unacceptable voltage variations, the IEEE 1547-2018 standard defines the mandatory

TABLE 3. DER response to the abnormal voltages (for abnormal operating performance category III) [24].

Shall trip-Category III				
Tripping function	Default settings		Ranges of allowable settings	
	Voltage (p.u. of nominal voltage)	Clearing time (s)	Voltage (p.u. of nominal voltage)	Clearing time (s)
OV2	1.20	0.16	Fixed at 1.20	Fixed at 0.16
OV1	1.10	13	1.10-1.20	1-13
UV1	0.88	21	0.0-0.88	21-50
UV2	0.50	2	0.0-0.50	2-21

TABLE 4. DER response to the abnormal frequencies (for abnormal operating performance category I, II And III) [24].

Tripping function	Default settings		Ranges of allowable settings	
	Frequency (Hz)	Clearing time (s)	Frequency (Hz)	Clearing time (s)
OF2	62.0	0.16	61.8-66.0	0.16-1000
OF1	61.2	300	61.0-66.0	180-1000
UF1	58.5	300	50.0-59.0	180-1000
UF2	56.5	0.16	50.0-57.0	0.16-1000

OV/UV trip settings separately for the category I, II and III abnormal performance categories. The default and the allowable settings of the two-stage OV and UV protection functions (OV1, OV2 and UV1, UV2) of the DERs and the corresponding clearing/tripping times for the performance category III are given in Table 3. For the OV and UV trip functions clearing time ranges and for the OV trip functions voltage ranges, the lower value is a limiting requirement, and the upper value is a minimum requirement. For the UV trip functions voltage ranges, the upper value is a limiting requirement, and the lower value is a minimum requirement. The limiting requirements values in Table 3 cannot be increased or decreased but the minimum requirements values can be increased and decreased, as necessary.

For the DER response to the unacceptable frequency variations, the IEEE 1547-2018 standard defines the mandatory OF/UF trip settings, the same settings for the abnormal performance categories I, II and III. The default and the allowable settings of the two-stage OF and UF protection functions (OF1, OF2 and UF1, UF2) of the DERs and the corresponding clearing/tripping times are given in Table 4.

For the OF and UF trip functions clearing time ranges and for the OF trip functions frequency ranges, the lower value is a limiting requirement, and the upper value is a minimum requirement. For the UF trip functions frequency ranges, the upper value is a limiting requirement, and the lower value is a minimum requirement. The limiting requirements values in Table 4 cannot be increased or decreased but the minimum requirements values can be increased and decreased, as necessary.

The settings outside the ranges of allowable settings in Table 3 and Table 4 shall only be allowed if necessary for the DER equipment protection, but these should not

TABLE 5. Voltage ride-through[1] requirements for DERs of abnormal operating performance category III [24].

Voltage range (p.u.)	Operating mode/response	Min ride-through time (s) (design criteria)	Max response time (s) (design criteria)
V>1.20	Cease to Energize	N/A	0.16
1.10 < V ≤ 1.20	Momentary Cessation	12	0.083
0.88 ≤ V ≤ 1.10	Continuous operation	Infinite	N/A
0.70 ≤ V < 0.88	Mandatory Operation	20	N/A
0.50 ≤ V < 0.70	Mandatory Operation	10	N/A
V < 0.50	Momentary Cessation	1	0.083

[1]HVRT in blue and LVRT in red color.

TABLE 6. Frequency ride-through* requirements for DERs of abnormal operating performance category I, II And III [24].

Frequency range (Hz)	Operating mode	Min time (s) (design criteria)
f > 62.0	No ride-through requirements apply to this range	
61.2 < f ≤ 61.8	Mandatory operation	299
58.8 ≤ f ≤ 61.2	Continuous operation	Infinite
57.0 ≤ f < 58.8	Mandatory operation	299
f < 57.0	No ride-through requirements apply to this range	

*HFRT in blue and LFRT in red color.

conflict with the disturbance voltage and frequency ride-through requirements. The voltage ride-through requirements including LVRT below the minimum continuous operating voltage and HVRT above the maximum continuous operating voltage for DERs of abnormal operating performance category III are given in Table 5. The DERs shall be designed to provide the voltage disturbance ride-through capability without exceeding DER capabilities.

Additionally, the DERs have to ride-through during multiple consecutive voltage disturbances in the ride-through operating region. The unsuccessful reclosing during the short-circuit faults, various faults during storms and dynamic voltage swings may be the causes of these consecutive temporary voltage disturbances. For the DERs of category-III, the maximum number of consecutive voltage ride-through disturbance sets is 3 with 5 s minimum time between successive disturbance sets. The time window for the new count of the disturbance sets is 20 minutes for the DERs of category-III. However, the DERs in general should ride-through as many voltage-disturbance sets as they are capable.

The frequency ride-through requirements including low-frequency ride-through (LFRT) below the minimum continuous operating frequency and the high-frequency ride-through (HFRT) above the maximum continuous operating frequency for DERs of abnormal operating performance categories I, II and III are given in Table 6. For the frequency of less than 57.0 Hz and above the 62.0 Hz, no ride-through requirements are applied. The DERs of category III shall have the capability of mandatory operation with frequency-droop (frequency-power) during the LFRT and HFRT. The IEEE 1547-2018 standard defines the ROCOF ride-through requirement for DERs of category III as 3.0 Hz/s. The ROCOF shall be the average rate of change of frequency over an averaging window of at least 0.1 s.

For both the voltage and frequency ride-through requirements, any tripping of DER or other failure to provide the specified ride-through capability, due to the DER self-protection as a direct or indirect result of voltage disturbance within the ride-through region shall constitute non-compliance with the IEEE 1547-2018 standard.

The exceptional conditions during which ride-through requirements shall not apply and the DER may cease to energize and trip without limitations include: 1) The net active power exported across the PCC into the Area EPS is maintained at a value less than the 10% of the aggregate rating of the DER connected to the Local EPS prior to any voltage disturbance. In this case, the Local EPS may intentionally disconnect from the Area EPS and form a Local EPS island, or 2) An active power demand of the Local EPS load equal to or greater than 90% of the pre-disturbance aggregate DER active power output is shed within 0.1 s of when the DER ceases to energize the Area EPS and trips.

The IEEE 1547-2018 also defines the voltage phase angle changes ride-through requirements for multi-phase DERs and single-phase DERs. According to these requirements, multi-phase DER shall ride-through for Pos-Seq phase angle changes within a sub-cycle-to-cycle period of the applicable voltage of less than or equal to 20 electrical degrees. Additionally, multi-phase DER shall remain in operation for change in the phase angle of individual phases less than 60 electrical degrees, provided that the Pos-Seq angle change does not exceeds the required criteria. Single-phase DER shall remain in operation for phase angle changes within a sub-cycle-to-cycle period of the applicable voltage of less than or equal to 60 electrical degrees [24].

C. ENTER SERVICE AND SYNCHRONIZATION PARAMETERS

The DERs shall not energize the area EPS until the applicable voltage and system frequency are within the ranges specified in Table 7 and permit service is set to ''Enabled''. The specified ranges in Table 7 do not mandate any DER to enter service and stay in operation but only permit to enter service.

The DER shall parallel with the area EPS without causing step changes in the RMS voltage at the PCC exceeding 3% of the nominal voltage at MV and 5% of the nominal voltage at LV point of connection.

The synchronization parameter limits for a synchronous connection to an EPS (or an energized Local EPS to an Area EPS) are defined in Table 8. These synchronization limits may be waived by the Area EPS operator if paralleling does not exceed the limitation of voltage fluctuations of 3-5% of the nominal voltage mentioned above.

D. THE DYNAMIC VOLTAGE SUPPORT DURING THE SHORT-CIRCUIT FAULTS

According to IEEE 1547-2018 standard, any DER may have the capability of dynamic voltage support during the LVRT

TABLE 7. Enter service criteria for DERs of category I, II, and III [24].

Enter service criteria		Default settings	Ranges of allowable settings
Permit service		Enabled	Enabled/Disabled
Applicable voltage within range	Minimum value	≥ 0.917 p.u.	0.88 p.u. to 0.95 p.u.
	Maximum value	≤ 1.05 p.u.	1.05 p.u. to 1.06 p.u.
Frequency within range	Minimum value	≥ 59.5 Hz	59.0 Hz to 59.9 Hz
	Maximum value	≤ 60.1 Hz	60.1 Hz to 61.0 Hz

TABLE 8. Synchronization parameter limits for synchronous connection to EPS [24].

Aggregate rating of DER units (kVA)	Frequency difference Δf (Hz)	Voltage difference ΔV (%)	Phase angle difference $\Delta\Phi$ (°)
0–500	0.3	10	20
> 500–1 500	0.2	5	15
> 1 500	0.1	3	10

and HVRT. The dynamic voltage support means rapid reactive power exchanges during voltage excursions to provide better voltage stability in distribution system during transient events. However, the dynamic voltage support shall not cause the DER to seize to energize in situations where the DER would not cease to energize without the dynamic voltage support. The dynamic voltage support may be utilized during the mandatory or permissive operation. The Area EPS operator may consider the impact of the dynamic voltage support from DER on the Area EPS protection. It is recommended that the dynamic voltage support implementation should have the capability of preventing the overvoltage in any phases of the applicable voltage when providing the dynamic voltage support for any types of faults (balanced or unbalanced).

E. ISLANDING

The IEEE 1547-2018 standard defines the islanding condition in distribution systems as: ''Island is a condition in which a portion of an Area EPS is energized solely by one or more Local EPSs through the associated PCCs while that portion of the Area EPS is electrically separated from the rest of the Area EPS on all phases to which the DER is connected. When an island exists, the DER energizing the island may be said to be ''islanding'' [24].

Two types of islands are defined in IEEE 1547-2018 standard: (1) An unintentional island and (2) An intentional island. An *intentional island* is a planned island whereas an *unintentional island* is an unplanned island. An intentional island is further defined as: ''A planned electrical island that is capable of being energized by one or more Local EPSs. These (1) have DERs and loads, (2) have the ability to disconnect from and to parallel with the Area EPS, (3) include one or more Local EPS(s), and (4) are intentionally planned'' [24].

The intentional island may be an ''intentional Area EPS island'' or an ''intentional Local EPS island'', the latter is also called facility island. An intentional Area EPS island is an intentional island that includes portions of the Area EPS, and an intentional Local EPS island is an intentional island that is totally within the bounds of a Local EPS. Here, the Local EPS means an EPS that is contained entirely within a single premises or group of premises. The Area EPS is usually comprised of different Local EPSs that has primary access to public rights-of-way and is subject to the regulatory oversight (see Fig. 6).

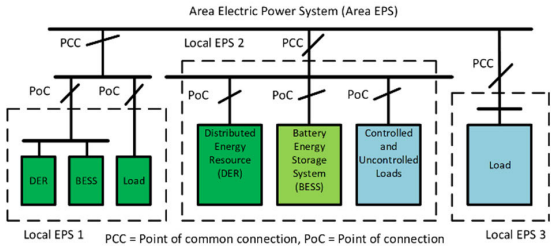

FIGURE 6. An area EPS with different local EPS categories.

1) DER CATEGORIES FOR OPERATION IN AN INTENTIONAL AREA EPS ISLAND

The IEEE 1547-2018 standard defines four categories of the participant DERs for operation in an intentional Area EPS island: *Uncategorized DERs* (not designed for intentional island), *intentional island-capable DERs*, *black start-capable DERs* and *isochronous-capable DERs* (can regulate voltage and frequency independently). These categories shall be stated by the DER operator, but the utilization shall be by mutual agreement between the DER operator and the operator of the intentional Area EPS island.

2) EXEMPTIONS FOR THE EMERGENCY SYSTEMS AND STANDBY DERS

The DER systems designated as emergency or critical operations power systems providing backup power for the hospitals, fire stations or other emergency facilities are exempt from the voltage and frequency disturbance ride-through requirements, intentional islanding requirements and interoperability, information exchange, information models and protocol requirements. The standby DERs used for infrequent testing purpose or used during load transfer to or from the Area EPS in a period of less than 300 s are also exempt from the above-mentioned requirements.

F. MICROGRID CONTROLLERS

The IEEE standard 1547.4-2011 [26] mentions different load categories and their requirements and sensitivities for the islanded mode of operation. The inrush current problems during motor starting and transformer energization need to be solved using soft-starter and series reactance respectively to avoid nuisance tripping of overcurrent (OC)/overload protection devices during cold load pickup and transition periods. An acceptable degree of load balance should be achieved by load monitoring on each phase and necessary corrective

actions should be taken like load reconfiguration and load shedding. The maximum active and reactive power requirements of the loads in the islanded mode should be known in advance and sources of active and reactive power should be available when required.

The area EPS grounding schemes/configurations (ungrounded, effectively grounded or impedance grounded) should be maintained even in the islanded mode. To do this the ground sources may require switching operations. An effectively grounded distribution system should maintain an adequate ground source at all times. Connecting multiple ground sources such as ground source transformer banks on the feeder may desensitize upstream protection devices by acting as a sink of unbalanced ground-fault currents and creating protection coordination problems during ground faults. This should be considered for the coordination of protection schemes [26].

A multifunctional communication-based microgrid management system (MMS) or microgrid control system (MCS) can be used to perform different management and control functions mentioned above for the proper operation of the microgrid in different modes of operation. The detailed functions of MMS are discussed in [30]. The physical implementation of control strategies consisting of software, hardware or a combination of software and hardware can be done in a centralized, decentralized/distributed or hybrid centralized and decentralized manner. A suitable combination of communication protocols like IEC 61850, DNP3, Modbus, IEC 60870-5 etc. can be used for this purpose. An autonomous communication-less control (droop-control) defined in [26] may be used for the basic and local control capabilities.

The IEEE standard 2030.7-2017 [27] defines the technical specifications and requirements of a generic microgrid controller or more specifically microgrid control system. The standard defines the core functions and their interactions allowing modularity and interoperability in physical implementations.

Two core functions of the MCS (Level-2 control) which supervise the lower-level functions (Level-1 control) are specified and defined in IEEE 2030.7-2017 [27]: The dispatch function and the transition function.

The dispatch function generates/calculates the dispatch order and sends it to the microgrid components as often as necessary based on the received or estimated state of microgrid and its components. It receives the dispatch mode information including the unplanned islanding (T1), planned islanding (T2), reconnect (T3), black start (T4), steady state grid-connected (SS1) and steady state islanded (SS2) modes from the transition function. The dispatch function operates on a longer timeframe compared with the transition function typically in the range of minutes.

The transition function provides the logic to switch the dispatch function between one of the relevant dispatch modes including the four transition modes (T1 to T4) and two steady state modes, SS1 and SS2. The transition function operates on a shorter timeframe compared with the dispatch function typically in the range of milliseconds.

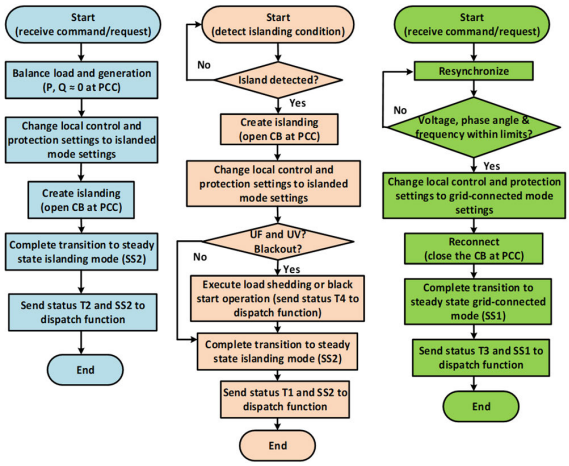

FIGURE 7. Flow charts for T2, T1 and T3 transition modes.

The process and steps of the transition function logic required for switching the dispatch function to the planned islanding mode (T2), the unplanned islanding mode (T1) and the reconnection to the main grid mode (T3) are mentioned in Fig. 7 with blue, red and green color flow charts, respectively.

IV. EVALUATION OF THE SELECTED GRID CODES FOR THE CONVERTER-BASED DERS

This section presents the evaluation of the dynamic reactive power injection capability of the converter-based DERs according to EN 50549-2-2019 grid code requirements from the perspective of AC microgrid protection in the grid-connected and the islanded modes. The standardized settings of the interface protection functions are evaluated during the unbalanced faults.

A. THE DYNAMIC REACTIVE POWER INJECTION DURING THE SHORT-CIRCUIT FAULTS

In this section the dynamic reactive power capability of a generic converter-based DER model connected to MV distribution network during unbalanced faults is evaluated using a MATLAB/Simulink model of AC microgrid (Fig. 8). The generic DER model is capable of LVRT and provides 1.2 p.u. of short-circuit current during the fault or when the voltage of any phase falls below 0.8 p.u. of the nominal voltage. The DER is also capable of operating as the grid-forming source with independent voltage and frequency control capability in the islanded mode using phase-locked loop PLL-2 (Fig. 9). The settings of the interface protection functions used in this study are done according the European standard EN 50549-2:2019 [22] and according to the ranges defined for the second-stages of the UV/OV and UF/OF protection functions (Table 2).

Two types of controls of the grid-side converter of DERs are discussed in [31]: The coupled sequence control (CSC)

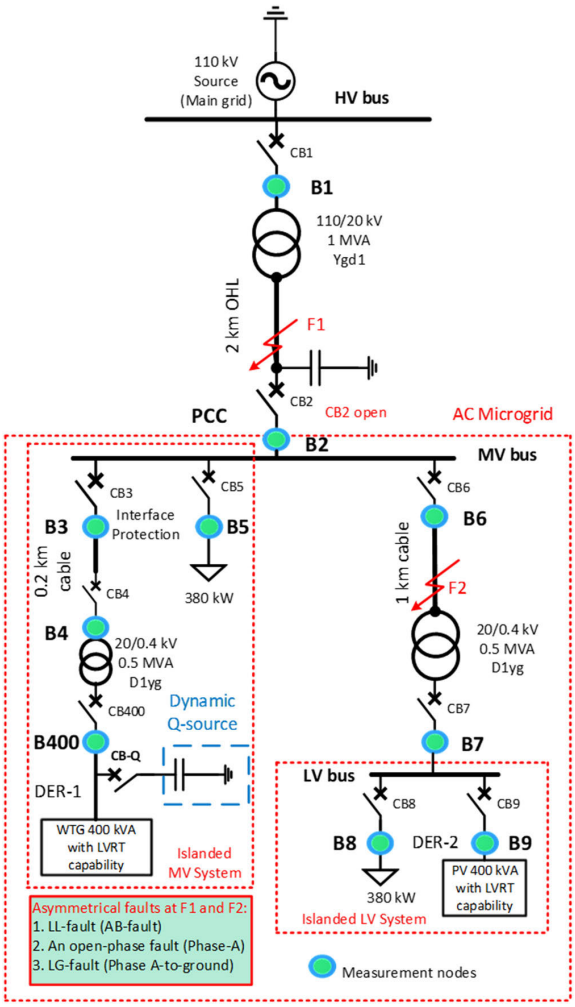

FIGURE 8. Simulink model of AC Microgrid used for the grid code evaluation of converter-based DERs.

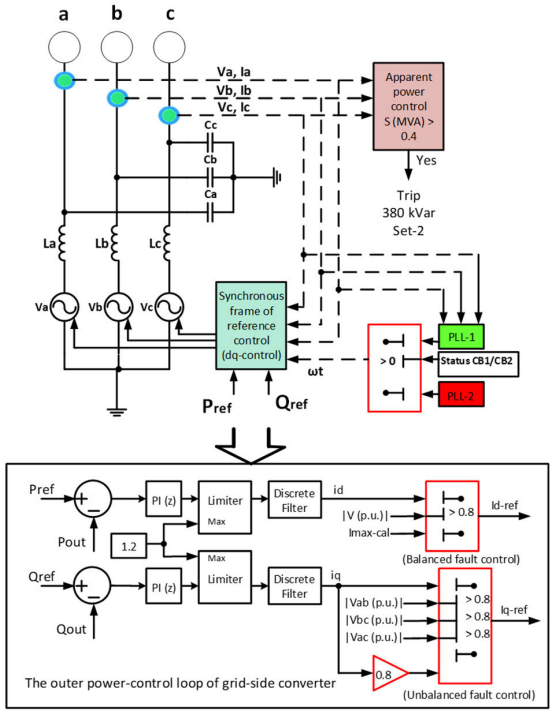

FIGURE 9. The synchronous frame of reference control (dq-control) of a generic grid-forming DER with description of the outer power-control loop during faults. The phase-locked loop PLL-1 is for the grid-connected mode and PLL-2 for the islanded mode.

and the decoupled sequence control (DSC). The CSC control method gives priority to the Pos-Seq current and provides very less amount of the Neg-Seq current. With the DSC control method, the Pos-Seq and Neg-Seq currents can be controlled independently, and enough magnitude of Neg-Seq current injection can be obtained. However, the DSC control also gives priority to the Pos-Seq current, and the remaining capacity of the converter is utilized for providing the Neg-Seq current. The output current of the most grid-side converters or inverters is primarily Pos-Seq with a small Neg-Seq current. Majority of the inverters do not produce Zero-Seq current [25]. In this paper, the dq-control in the synchronous frame of reference is used for the DERs which is a CSC control providing a limited amount of Neg-Seq current during the faults. Therefore, an additional Q-source (a thyristor-switched capacitor or equivalent) is used as an enabler to meet the grid code requirements during the faults.

An extra source of reactive power (dynamic Q-source in Fig. 8) is connected at LV terminals of the DER-1 to enable it to inject the reactive current during an external unbalanced short-circuit fault. This location of an extra Q-source connection is behind the generating unit switch in Fig. 5.

The dynamic Q-source consist of two sets of thyristor-switched capacitors of total 760 kVar capacity with each having 380 kVar capacity. The apparent power of the DER-1 is monitored during the reactive power injection so that its extent should be controlled within the rated MVA capacity of the DER-1. Normally, both sets of the dynamic Q-source are activated after the condition of reactive power injection is reached during the faults. However, if the apparent power limit of DER-1 is violated then one set of the dynamic Q-source is switched off instantly to avoid any overloading or overvoltage at the DER-1 terminals. The outer power-control loop of DER-1 and DER-2 by default reduces the q-axis current to 0.8 p.u. of the pre-fault value if the UV condition of 0.8 p.u. or less is reached during the faults (Fig. 9). The applied control of DERs is not enough to meet the grid code requirement of Neg-Seq current during faults. Hence, an additional Q-source is required to meet the stringent grid code requirements. The current during short-circuit faults is assumed as predominantly reactive current.

Table 9 shows the time delay settings of different protection functions of protection devices at different locations.

TABLE 9. The time delay settings of different protection relays and functions.

Functions	Coordinated time-delay (s)							
	CB1	CB2	CB3	CB6	CB5	CB7	CB8	CB9
OC^1	0.8	0.6	0.9	0.4	0.9	0.2	0.02	0.02
OC^{2*}	0.8	0.6	0.9	0.4	0.9	0.2	0.02	0.4
OC^0	0.8	0.6	0.9	0.4	0.9	0.2	0.02	0.4
OV^2	3.0	2.5	4.0	2.0	4.0	1.5	1.0	4.0
OV^0	3.0	2.5	4.0	2.0	4.0	1.5	1.0	4.0
UV^1/OV^1	3.5	3.0	5.0	2.5	5.0	2.0	1.5	5.0

*The ratio of I_2/I_1 during the fault is used as the main tripping criteria, the magnitude of I_2 during the fault is used as the restraining criteria, it means the tripping is allowed only if $I_2 > 0.35$ p.u. Only the coordination of the enabled protection relays in green columns is evaluated in this study. OC^1 = 51P, OC^2 = 51Q, OC^0 = 51G, $OC^{2*} = I_2/I_1$.

TABLE 10. The potential tripping thresholds of different protection functions.

Protection functions	Tripping thresholds**	
	Grid-connected mode	Islanded mode
OC^1	2.25 p.u.	1.2 p.u.
OC^{2*}	1.3	1.0-1.3
OC^0	0.45-0.5 p.u.	0.45-0.5 p.u.
OV^2	0.5 p.u.	0.5 p.u.
OV^0	0.5 p.u.	0.5 p.u.
UV^1/OV^1	0.85/1.2 p.u.	0.85/1.2 p.u.

** The maximum inrush current magnitude and the maximum load unbalance need to be evaluated for the final reliable thresholds of these protection functions. The settings of OC functions in the islanded mode are in general more sensitive than the grid-connected mode settings.

Table 10 shows the potential tripping threshold settings of different protection functions for the grid-connected and islanded modes. In addition to the Pos-Seq OC function (OC^1), a protection function based on the ratio of the Neg-Seq current (I_2) to the Pos-Seq current (I_1) or I_2/I_1 protection function (OC^{2*}) is also provided for the detection of unbalanced faults. The default tripping threshold setting of I_2/I_1 protection function is 1.3, however, it could be set well below this threshold depending on the magnitude of I_2 during different unbalanced faults. The idea behind selecting the tripping threshold of 1.3 is to trigger I_2/I_1 protection function only after the activation of the Q-injection function. The magnitude of I_2 during the fault is used as a restraining criterion, it means the tripping of I_2/I_1 protection function is only allowed if $I_2 > 0.35$-0.5 p.u.

At each relay location in Table 9, the symmetrical components of current or OC functions OC^1, OC^{2*} and OC^0 are used as the primary protections to detect the balanced and unbalanced short-circuit faults including the ground faults. The obvious symmetrical components of voltage during the faults like OV^2 and OV^0 functions are used as the first local backup protections at each relay location. The normal Pos-Seq UV^1 and OV^1 functions are used as the second local backup to all the symmetrical component-based OC and OV protection functions. All the local protection functions at each location are also coordinated with the corresponding protection functions at remote locations to cover the local malfunction of the protection relays for the maximum protection coverage.

1) UNBALANCED FAULTS IN THE GRID-CONNECTED MODE

a: CASE-1: LL-FAULT F1

The LL-fault F1 between phase A and phase B (AB-fault) with a fault resistance of 0.001 Ohm is applied at simulation time of 2 s and for a duration of 2 s from 2 s to 4 s at the end of 2 km line near the PCC of AC microgrid (Fig. 8) in the grid-connected mode. As mentioned previously, the LL-fault is an asymmetrical or unbalanced short-circuit fault which not only increases the short-circuit current in the Pos-Seq but also in the Neg-Seq component. Fig. 10 shows the instantaneous and symmetrical components of fault current observed at bus B1.

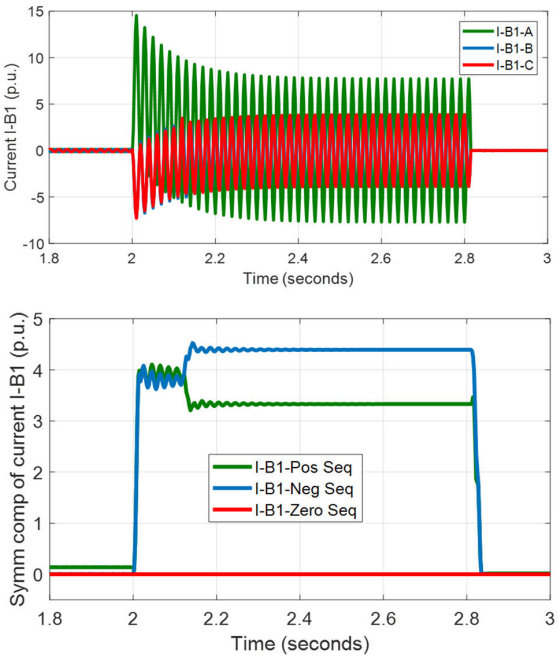

FIGURE 10. The instantaneous line current (top) and the derived symmetrical components of current (bottom) in p.u. observed at bus B1 during the LL-fault F1.

Fig. 10 (bottom) shows that the magnitudes of both the Pos-Seq and Neg-Seq components of current at B1 are increasing equally after the LL-fault F1 is triggered at 2s. However, after the injection of reactive current at 2.1 s, the magnitude of Neg-Seq current (I_2) is increased, whereas the magnitude of Pos-Seq current (I_1) is decreased at bus B1. This causes the ratio I_2/I_1 to increase from about 1.0 right after the fault to above 1.3 after the reactive power support (Fig. 11). This increased ratio of I_2/I_1 can be used as a means of detecting LL-faults downstream of bus B1. The I_2/I_1 protection function can be triggered, for example, when I_2/I_1 ratio becomes 1.3 to open CB1 after an intentional time delay of 0.8 s and to transfer trip CB2 after an additional delay of 0.02 s. However, in this study the Pos-Seq OC (OC^1) function is able to detect AB-fault F1 at 2.8 s due to enough magnitude of I_1 available from the main grid.

It should be noted that extra Q-source is activated within 0.1 s in this study after the fundamental voltage magnitude of any phase at the PCC (measured at interface protection B3) is decreased below the 0.8 p.u. according to EN 50549-2-2019 [22]. The Q-source activation function

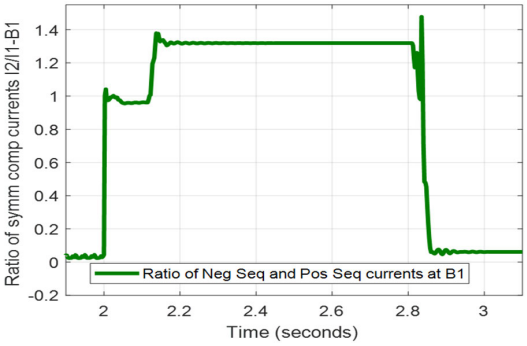

FIGURE 11. I_2/I_1 ratio at B1 after the AB-fault F1 (2-2.1 s) and after the 670 kVar Q-injection (2.1-2.8 s) during the LL-fault F1 in grid-connected mode.

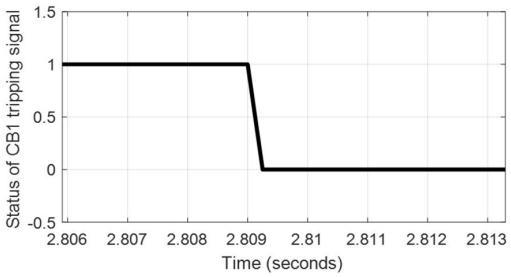

FIGURE 12. Tripping signal of the OC^1 function to trip CB1 after the LL-fault F1 in grid-connected mode.

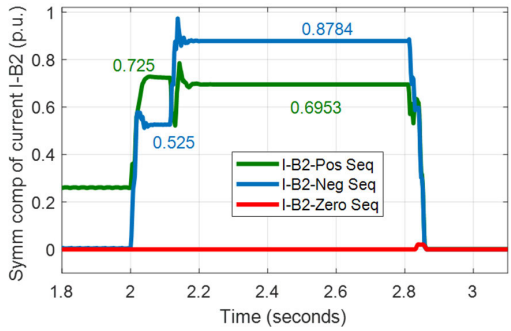

FIGURE 13. The derived symmetrical components of rms current in p.u. observed at bus B2 during the LL-fault F1 in grid-connected mode.

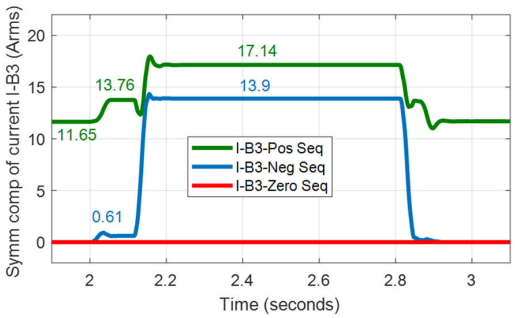

FIGURE 14. Fault current contribution from the DER-1 at PCC/MV side: The derived symmetrical components of rms current (A) observed at bus B3 during the LL-fault F1 in grid-connected mode.

also checks the connection status of CB2 and CB3 and the additional Q-source is activated only if both CB2 and CB3 are closed in the grid-connected mode. Although, the set tripping time delay of both the OC^1 and I_2/I_1 protection functions is same according to Table 9, but used switching delay of 0.1 s, that can be 40 ms in actual case, for the activation of Q-source causes OC^1 function to trip first after the threshold value of I_1 is reached at 2.8 s (Fig. 12). In this case, I_2/I_1 function will provide local backup if OC^1 function fails to detect the LL-fault due to any reason like low magnitude of I_1.

Fig 13 shows the symmetrical components of current observed at bus B2. The measurements at bus B2 are used for the protection functions acting on CB2. It should be noted that it is bus B2 which indicates the active and reactive power flow to and from the main grid or microgrid. In this case, the MV and LV loads are fully supplied by the local DERs of AC microgrid. Therefore, a low magnitude of load current flows at bus B2 before the fault. After the fault is applied, the fault current contribution comes from both the DER-1 connected at MV-bus B3 (Fig. 14) and DER-2 connected at LV-bus B9 (Fig. 16). The combined Pos-Seq fault current contribution from the DERs observed at B2 is less than the maximum normal Pos-Seq load current (about 22 A-rms) at B2 without the DERs. Therefore, the Pos-Seq overload or OC^1 function at B2 will not trip for the grid-side LL-fault F1. Only the Neg-Seq current at B2 can be used to detect this fault condition. But as the fault happens behind the relay of CB2 so some directional discrimination is required at CB2 to prevent the reverse fault tripping by the Neg-Seq OC (OC^{2*}) or I_2/I_1 protection function at B2.

If the Neg-Seq directional discrimination is not used at B2, then there is a high chance that the OC^{2*} or I_2/I_1 protection function may trip CB2 before the CB1. This is true because the time-coordination of the OC^{2*} is done just like the OC^1 starting from the LV load at CB8 towards the main grid or HV/MV transformer substation (Table 9). In this fault case, the set tripping threshold of 1.3 for the OC^{2*} or I_2/I_1 protection at B2 prevents the reverse fault tripping of CB2 before the tripping of CB1 by default without the use of 67Q directional element. Since, the DER-2 provides a low magnitude of I_2, therefore I_2/I_1 ratio of lower than 1.3 is achieved at B2.

The directional discrimination may also be required at CB6 and CB7 locations to prevent the reverse fault tripping by the Neg-Seq OC functions (OC^{2*} or I_2/I_1) at these locations during a LL-fault between CB6 and CB7 in the grid-connected mode. Particularly, if the DER-2 connected at LV-bus B9 is also required to provide the Neg-Seq current up to same extent of DER-1 during the faults. The directional element design is considered and evaluated for the selected cases in the next subsection.

Fig. 14 shows the symmetrical components of current observed at bus B3. The bus B3 is the PCC bus of the

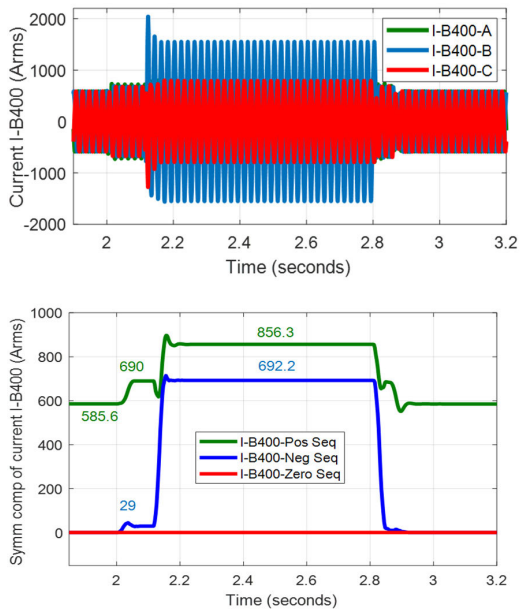

FIGURE 15. Fault current contribution from the DER-1 at LV side: The rms instantaneous line currents (top) and the derived symmetrical components of rms current (bottom) observed at bus B400 during the LL-fault F1 in grid-connected mode.

DER-1 where the interface protection is also installed with the required functions as per EN 50549-2-2019 grid code.

Fig. 14 shows that the magnitude of Neg-Seq current at B3 after the fault is quite lower compared with the Pos-Seq current during the fault from the simulation time of 2 s to 2.1 s. However, after the activation of additional Q-source at 2.1 s the magnitude of the Neg-Seq current is significantly increased to the level of Pos-Seq current after the fault. The activation of additional Q-source during the fault also increases the magnitude of the Pos-Seq current at B3 from 1.18 p.u. to 1.47 p.u. The variation of the Pos-Seq and Neg-Seq current up to the same extent is also be observed at LV side of DER-1 (Fig. 15).

A proper time-coordination and direction discrimination of OC^{2*} functions of CB3, CB2 and CB1 may be required to prevent the earlier tripping of the CB3 for the upstream grid-side faults if sensitive OC^{2*} tripping thresholds ($\leq$ 0.5 p.u.) are used. However, a higher tripping threshold of 1.3 of OC^{2*} or I_2/I_1 function and maximum time-delay at CB3 maintains the proper coordination. It can be observed from Fig. 15 (bottom) that the Q-source at DER-1 is activated with a step response of 25 ms and settling time of 50 ms which meet the EN 50549-2-2019 grid code requirements mentioned earlier in Section II part C.

Fig. 16 shows that the grid-side LL-fault F1 causes some current unbalance at DER-2, which causes some magnitude of the Neg-Seq current injected by the DER-2 during this fault. However, the magnitude of the Neg-Seq current injected by DER-2 is very much lower than the Pos-Seq load current ($\leq$ 6 % of the load current).

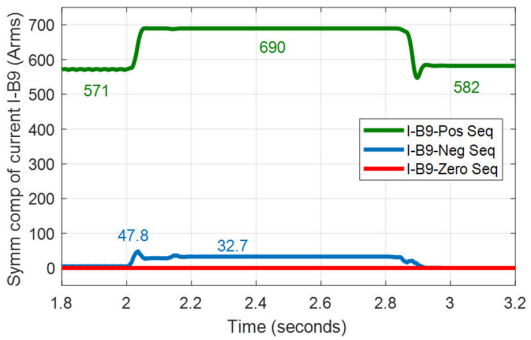

FIGURE 16. Fault current contribution from the DER-2: The derived symmetrical components of rms current (A) observed at bus B9 during the LL-fault F1 in the grid-connected mode.

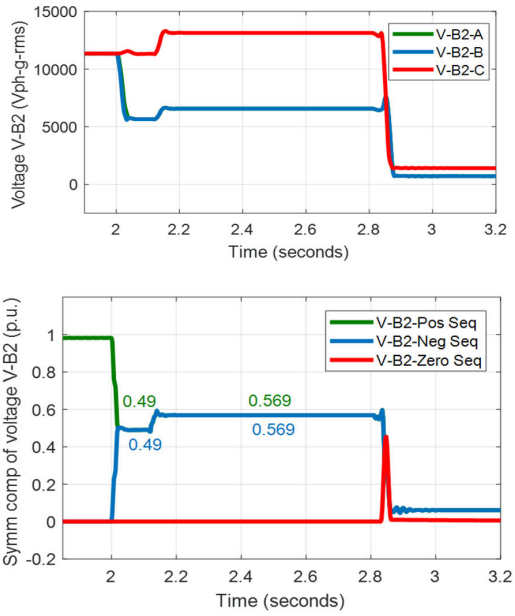

FIGURE 17. The rms phase-to-ground voltage (V) observed at bus B2 (top) and derived symmetrical components of voltage (bottom) in p.u. at bus B2 during the LL-fault F1 in grid-connected mode.

From Fig. 17 (V-B2) to Fig. 22 (V-B9) it can be seen that after the activation of Q-source during the grid-side LL-fault F1 the voltages at all buses particularly the bus B3 of PCC, bus B5 of MV-load and bus B8 of LV-load are improved. It means Q-injection during the fault provides voltage stability particularly for the single-phase loads. The only exceptions are the phase-A voltages of LV bus B400 of DER-1 (Fig. 19), LV-load bus B8 (Fig. 21) and LV bus B9 of DER-2 (Fig. 22). At these buses, the voltage of phase-A during the LL-fault F1 remains the same ($<$ 50 V) even after the Q-injection.

From Fig. 18 it can be observed that the magnitude of Neg-Seq and Pos-Seq voltage at bus B3 increases from 0.49 p.u. to about 0.57 p.u. after the Q-injection. It means according to settings of interface protection at CB3 (Table 9),

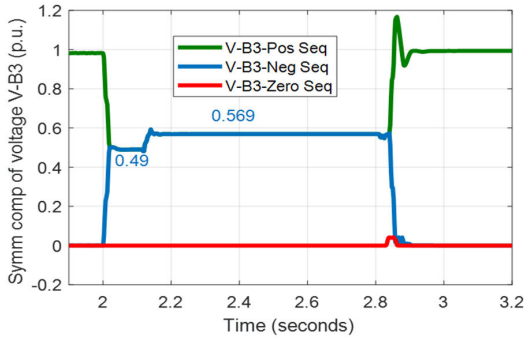

FIGURE 18. The instantaneous voltage (top) and the derived symmetrical components of voltage (bottom) in p.u. observed at bus B3 during the LL-fault F1 in grid-connected mode.

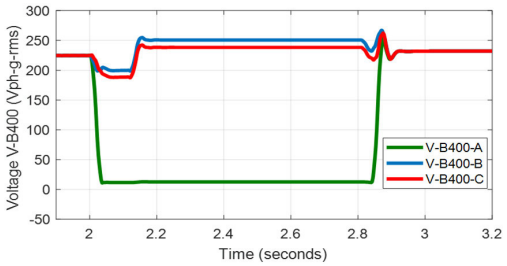

FIGURE 19. The rms phase-to-ground voltage (V) at the LV-side of DER-1 observed at bus B400 during the LL-fault F1 in grid-connected mode.

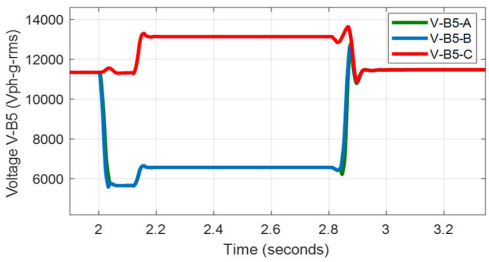

FIGURE 20. The rms phase-to-ground voltage (V) at the MV-load observed at bus B5 during the LL-fault F1 in grid-connected mode.

the Neg-Seq OV function (OV^2) will trip CB3 within 4.0 s after the Q-injection if other protection functions do not clear the grid-side LL-fault F1. From the results it can be observed that after the fault clearance at 2.82 s, the additional reactive power is deactivated, hence no Neg-Seq current (Fig. 15) or Neg-Seq voltage (Fig. 18) appear after the smooth transition of AC microgrid to the islanded mode. Fig. 23 shows the frequency of MV-load and LV-load before, during and after the LL-fault F1. Since the three-phase loads are closely balanced, therefore the frequency remains inside the continuous operating range.

b: GRID CODE COMPLIANCE CHECK FOR CASE-1:

The required minimum and maximum magnitude of Pos-Seq reactive current according to (1) and (2) based on voltage

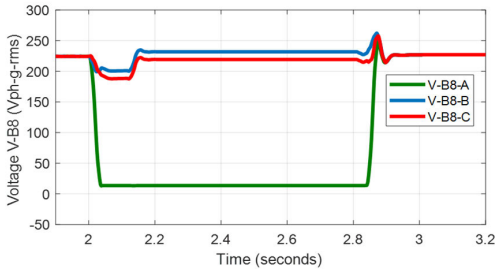

FIGURE 21. The rms phase-to-ground voltage (V) at the LV-load observed at bus B8 during the LL-fault F1 in grid-connected mode.

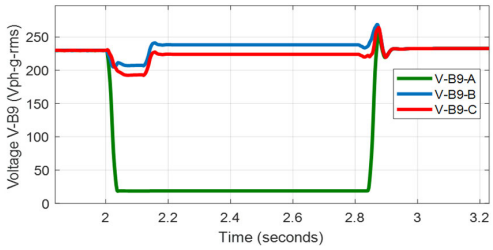

FIGURE 22. The rms phase-to-ground voltage (V) at the DER-2 observed at bus B9 during the LL-fault F1 in grid-connected mode.

measurement at the interface protection bus B3 (Fig. 18) will be as follows:

$$\Delta U_1 = (0.49 - 1)/1 = -0.51\text{p.u.}$$
$$\Delta I_{Q1} = 2\text{x}\,(-0.51\ \text{p.u.}) = -1.02\text{p.u. (MIN)} \quad (5)$$
$$= 6\text{x}\,(-0.51\ \text{p.u.}) = -3.06\ \text{p.u. (MAX)} \quad (6)$$

The required minimum and maximum magnitude of Neg-Seq reactive current according to (3) and (4) based on voltage measurement at the interface protection bus B3 (Fig. 18) will be as follows:

$$\Delta U_2 = (0.49 - 0)/1 = 0.49\ \text{p.u.}$$
$$\Delta I_{Q2} = 2\text{x}\,(0.49\ \text{p.u.}) = 0.98\text{p.u. (MIN)} \quad (7)$$
$$= 6\text{x}\,(0.49\ \text{p.u.}) = 2.94\ \text{p.u. (MAX)} \quad (8)$$

It should be noted that the negative sign of Pos-Seq voltage change (ΔU_1) indicates the voltage reduction or undervoltage, hence the negative sign of the additional Pos-Seq reactive current (ΔI_{Q1}) indicates the supply or generation of reactive power required. This is called as the overexcited operation mode of the DER (Fig. 4) used for providing voltage support to the grid. For the Neg-Seq voltage change (ΔU_2) and the additional Neg-Seq reactive current (ΔI_{Q2}), there will always be a positive sign due to the absence of Neg-Seq voltage before the fault. Hence the additional Neg-Seq current (ΔI_{Q2}) can only be provided in the underexcited mode.

Fig. 15 (bottom) shows that the normal Pos-Seq current (green color) provided by DER-1 at LV-side is 585.6 A that is purely active current. After the inception of the LL-fault F1 the current becomes 690 A that is purely reactive current.

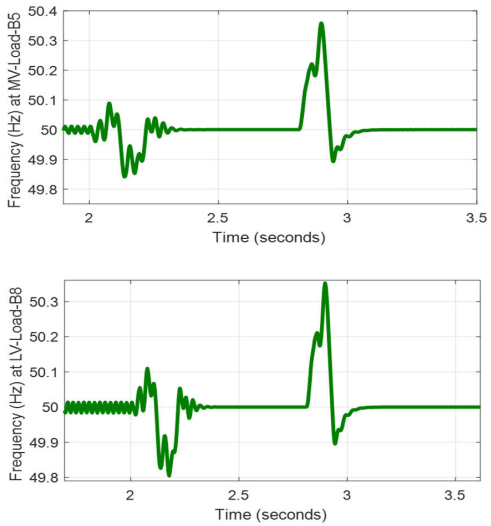

FIGURE 23. The frequency (Hz) at MV-load (top) and LV-load (bottom) during the LL-fault F1 in grid-connected mode.

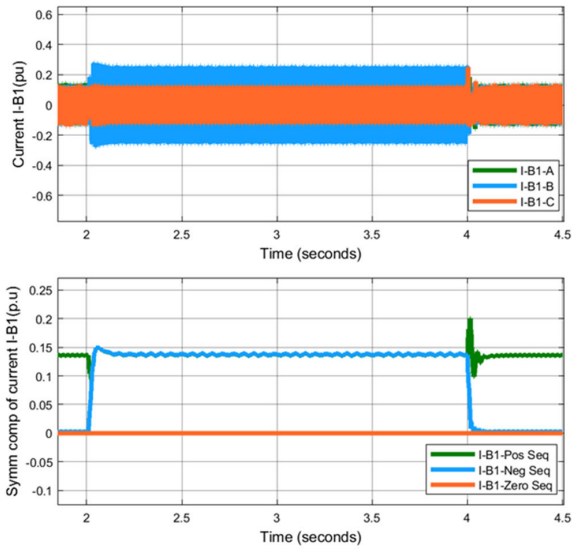

FIGURE 24. The instantaneous line current (top) and the derived symmetrical components of current (bottom) in p.u. observed at bus B1 during phase-A open fault F1 in grid-connected mode.

It means the DER-1 provides a default Pos-Seq reactive current of 1.18 p.u. during the LL-fault F1. However, after the activation of Q-source, the Pos-Seq reactive current increases to 856.3 A, which is1.46 p.u. of the normal Pos-Seq current. The Pos-Seq reactive current value of 1.46 p.u. lies in between the minimum and the maximum value as calculated in (5) and (6), respectively. With $\Delta I_{Q1} = -1.46$ p.u. and $\Delta U_1 = -0.51$, the gradient k_1 becomes equal to 2.86 (between 2 and 6) using (1). Hence, it can be said that the provision of the Pos-Seq reactive current by DER-1 during the LL-fault F1 before and after the activation of Q-source complies with the EN 50549-2-2019 grid code.

Fig. 15 (bottom) shows that the normal Neg-Seq current (blue color) provided by DER-1 at LV-side is equal to zero before the fault which becomes 29 A after the inception of the LL-fault F1. It means the DER-1 provides a default Neg-Seq reactive current of 0.049 p.u. during the LL-fault F1 which is far less than the minimum required value of 0.99 p.u. according to (7). Hence, DER-1 does not comply with EN 50549-2-2019 grid code for the Neg-Seq reactive current provision during the LL-fault F1 with the default setting/control. However, after the activation of Q-source, the Neg-Seq reactive current increases to 692.2 A which is about 1.18 p.u. of the normal Pos-Seq current. The Neg-Seq current value of 1.18 p.u. lies in between the minimum and the maximum value as calculated in (7) and (8), respectively. With $\Delta I_{Q2} = 1.18$ p.u. and $\Delta U_2 = 0.49$ p.u., the gradient k_2 becomes equal to 2.4 using (3). Hence, it can be said that the provision of the Neg-Seq reactive current by DER-1 during the LL-fault F1 complies with the EN 50549-2-2019 grid code after the activation of the dynamic Q-source.

c: CASE-2: PHASE-A OPEN FAULT F1

The phase-A open fault F1 is applied at simulation time of 2 s and for a duration of 2 s from simulation time of 2s to 4 s at the end of 2 km line near the PCC of AC microgrid (Fig. 8). The phase-A open fault is created by opening the pole-A of CB2 in the grid-connected mode.

Fig. 24 shows the instantaneous current and the derived symmetrical components of the current observed at bus B1. It can be seen from the Fig. 24 (bottom) that the Neg-Seq current at B1 increases after the creation of the phase-A open condition. Therefore, the Neg-Seq current can be used for the detection of phase-A open fault condition provided that the magnitude of the Neg-Seq current is well above the Neg-Seq current observed during the normal maximum possible unbalanced load condition. This is also true for the Neg-Seq current observed at bus B2 (Fig. 25 bottom). Otherwise, it will be difficult to detect phase-A open fault condition with only the Neg-Seq current. Fig. 26 (V-B3) shows that the voltage at the PCC remains within the static operating voltage range of 0.8-1.2 p.u., therefore Q-source is not activated. It also shows that the magnitude of the Neg-Seq voltage is also lower than the set threshold of 0.5 p.u. at the interface protection of the PCC. Hence, this fault condition is even not detected by the interface protection. The voltages and currents at all other buses remain within the normal operating ranges.

The other method to detect the phase-A open fault condition at F1 location is to observe the flow of current at phase-A/line-A of the secondary side of the HV/MV substation transformer. This will of course increase the number of measurement points and the related equipment (CTs or sensors). A negligible or lower current flow from phase-A of the secondary side of HV/MV transformer will indicate phase-A open condition.

Fig. 27 shows the RMS current at secondary side of the HV/MV transformer at bus B2. It clearly shows the current

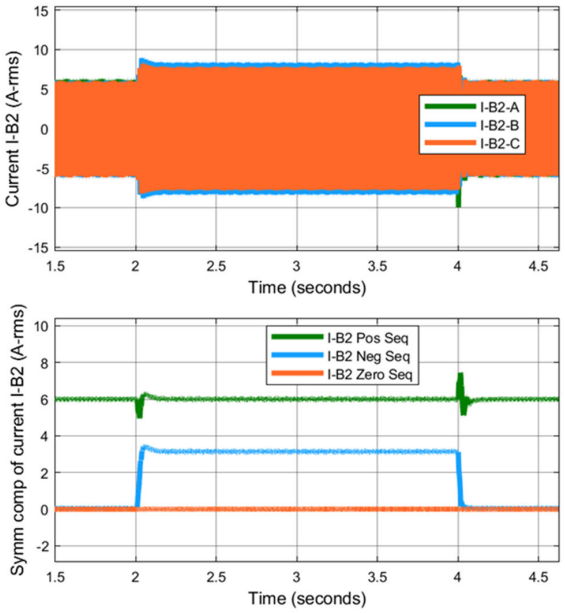

FIGURE 25. The rms instantaneous line currents (top) and the derived symmetrical components of rms current (bottom) observed at bus B2 during phase-A open fault F1 in grid-connected mode.

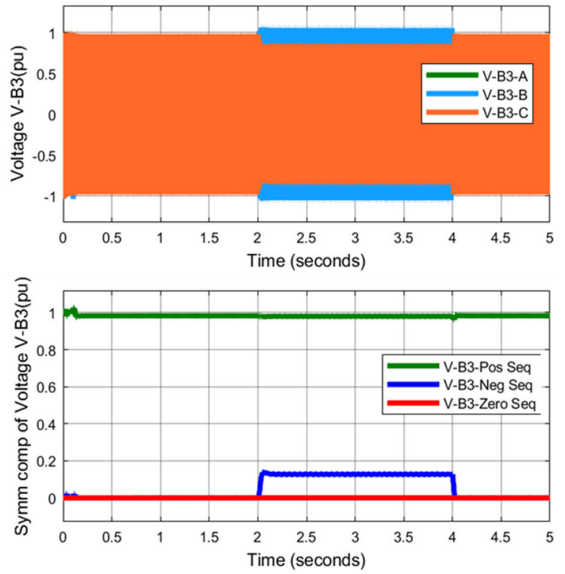

FIGURE 26. The instantaneous voltage (top) and the derived symmetrical components of voltage (bottom) in p.u. observed at bus B3 during phase-A open fault F1 in grid-connected mode.

in phase-A is less than the current in phase-B and phase-C from simulation time of 2 s to onwards. Various methods for the detection of open phase condition are discussed in [32]. Table 11 includes some of the effective and potential open phase detection schemes.

For the LL short-circuit fault and phase-A open fault at F1 in the grid-connected mode, the extent of dynamic

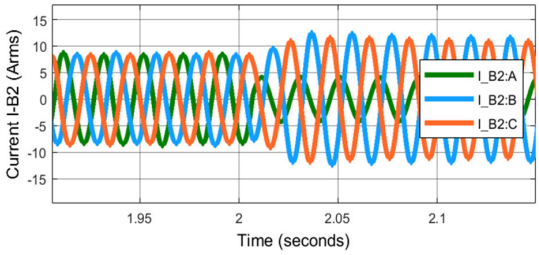

FIGURE 27. The rms instantaneous line currents observed at bus B2 during phase-A open fault F1 in grid-connected mode.

TABLE 11. The effective and potential open phase detection schemes [32].

Schemes	Description
Effective schemes	
Optical CT	Monitoring of magnetization and capacitive current. A reciprocal interferometer sensor and modulator mounted on each phase of transformer and signal processing circuit in the control room, connection via fiber optic and modulator trunk cable. IEC 61850-9-2LE process bus compliant relay.
Active neutral signal injection	Injection source, CT and controller. 100 mA, 45-90 Hz current injection. Monitoring of zero-sequence impedance and neutral OC.
Specially designed window-type CTs/sensors	Sensors installed on transformer HV bushings. Monitoring of current magnitude, phase angles, Symm Comp and waveforms. Specific relay algorithm used.
Potential schemes	
Phase current unbalance	Open phase current will be less than the healthy/closed phases. Chance of false detection during grid unbalances, therefore Symm Comp monitoring is also required.
Sequence voltage & current comparison	Magnitude and phase comparisons of Symm comp of currents and voltages.
Rogowski coils	Measurement of line currents, A/D conversion and fiber optic cable transmission.
CT open circuiting	Voltage measurement at CT secondary during intentional open circuit when measured current threshold is less than normal. No voltage at CT secondary indicates open phase at primary.
Microprocessor relays	Multiple methods: Ratio of 2nd harmonics to fundamental currents, comparison of measured current with digital filter response, zero-crossing detection, I_0/I_1 ratio, I_2/I_1 ratio.
Communication aided hybrid schemes	IEC 61850, DNP3 etc. communication protocols for information/measurement sharing between microprocessor relays and logics.

Q-injection has been found through simulation. The Q-injection of 760 kVar is required during the LL-fault F1 in order to meet the EN 50549-2-2019 grid code requirement. The extent of Q-injection during the LG-fault F1 is found to be half of that required during the LL-fault F1 in order to meet the EN 50549-2-2019 grid code requirement. The lower Q-injection during the LG-fault F1 is due to comparatively higher voltage of healthy phases during this fault.

The results for the LG-fault F1 are not included for the sake of brevity. For the effectively grounded AC microgrid, the LL-fault F1 in the grid-connected mode is correctly detected by the I_2/I_1 protection function at B1 after the Q-injection by DER-1. However, the LG-fault F1 is not detected by the I_2/I_1 protection function at B1 due to higher tripping threshold of

1.3. It means I_2/I_1 protection function at B1 requires different tripping thresholds for the LL-fault and LG-fault at the same location in the grid-connected mode. A lower ratio of I_2/I_1, for example 0.5, that is less than 1.3 can be used at B1 in order to detect both the LL-fault F1 and LG-fault F1 in the grid-connected mode. In that case, the magnitude of I_2 should be used as a restraining quantity. It means I_2/I_1 protection should only trip after reaching a threshold of 0.5 if the magnitude of I_2 is 0.35 p.u. or more. This will prevent the false tripping of I_2/I_1 protection during the times of off-peak load with some fair degree of unbalance loading.

2) UNBALANCED FAULTS IN THE ISLANDED MODE

a: CASE-3: LL-FAULT F2

The LL-fault F2 between phase A and phase B (AB-fault) is applied at simulation time of 6 s for a duration of 2 s from 6-8 s at the end of 1 km cable (Fig. 8) during the islanded mode of operation. Fig. 28 shows the instantaneous and symmetrical components of fault current observed at bus B6. Fig. 28 (bottom) shows that the magnitudes of both the Pos-Seq and Neg-Seq components of current at B6 are increasing equally after the LL-fault F2 is triggered at simulation time of 6 s. However, after the injection of reactive current at 6.1 s, the magnitude of Neg-Seq current is increased, whereas the magnitude of Pos-Seq current is decreased at bus B6. This causes the ratio I_2/I_1 to increase from about 0.95 right after the fault to above 1.3 after the Q-injection at simulation time of 6.237 s (Fig. 29). This increased ratio of I_2/I_1 has been used as a means of detecting LL-fault F2 downstream of bus B6. Therefore, I_2/I_1 protection trips CB6 at 6.637 s (Fig. 30) after the set definite time tripping delay of 0.4 s. The CB7 is transfer tripped from the CB6 after a delay of 0.02 s.

Fig. 31 shows the magnitude of the instantaneous and the symmetrical components of current observed at bus B7. Fig. 31 (bottom) shows that the magnitude of the Neg-Seq current at B7 is less than 0.35 p.u. after the inception of the LL-fault F2 at 6 s which is further decreased after the Q-injection of 760 kVar by the DER-1 at simulation time of 6.1 s. This means that I_2/I_1 protection at B7 will not trip for this upstream fault and a natural magnitude-based directional discrimination is maintained in the reverse direction due to very less Neg-Seq current infeed by the DER-2 (Fig. 32). Only the Pos-Seq UV at B6 will be able to provide the local backup to I_2/I_1 protection at B6 because Neg-Seq OV protection cannot trigger due to less than 0.5 p.u. of the Neg-Seq voltage at B6 during LL-fault F2 (Fig. 33). The reduction of the Neg-Seq voltage at B6 is mainly due to the Q-injection effect.

b: GRID CODE COMPLIANCE CHECK FOR CASE-3:

The required minimum and maximum magnitude of Pos-Seq reactive current according to (1) and (2) based on voltage measurement at the interface protection bus B3 (Fig. 34) will be as follows:

$$\Delta U_1 = (0.5669 - 0.9937)/0.9937 = -0.4295 \text{ p.u.}$$

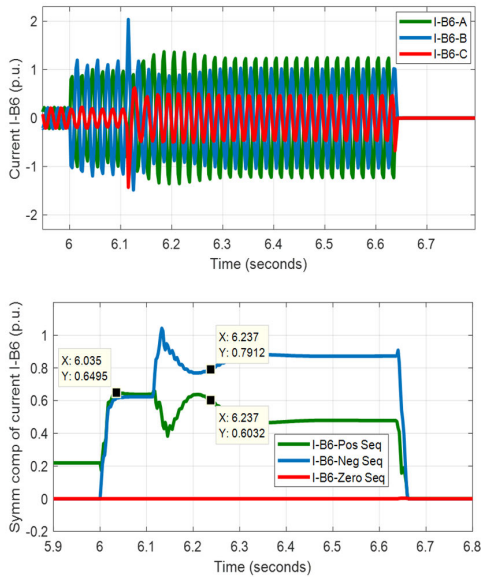

FIGURE 28. The instantaneous line currents (top) and the derived symmetrical components of current (bottom) in p.u. observed at bus B6 during LL-fault F2 in islanded mode.

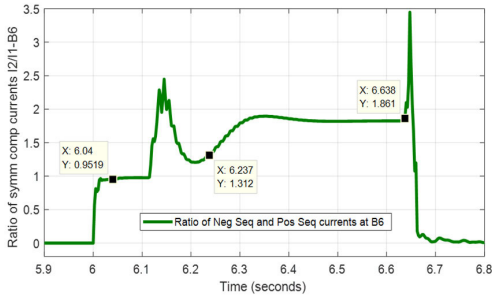

FIGURE 29. I_2/I_1 ratio at B6 after LL-fault F2 (from 6 s to 6.1 s) and after the Q-injection (from 6.1 s to 6.638 s) during LL-fault F2 in islanded mode.

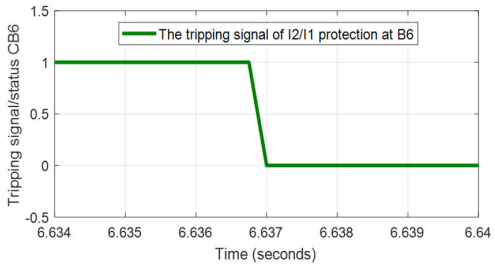

FIGURE 30. Tripping signal of the I_2/I_1 protection function at B6 to trip CB1 after the LL-fault F2 in islanded mode.

$$\Delta I_{Q1} = 2x\,(-0.4295 \text{ p.u.}) = -0.859 \text{ p.u. (MIN)} \quad (9)$$

$$= 6x\,(-0.4295 \text{ p.u.}) = -2.577 \text{ p.u. (MAX)} \quad (10)$$

The required minimum and maximum magnitude of Neg-Seq reactive current according to (3) and (4) based on voltage

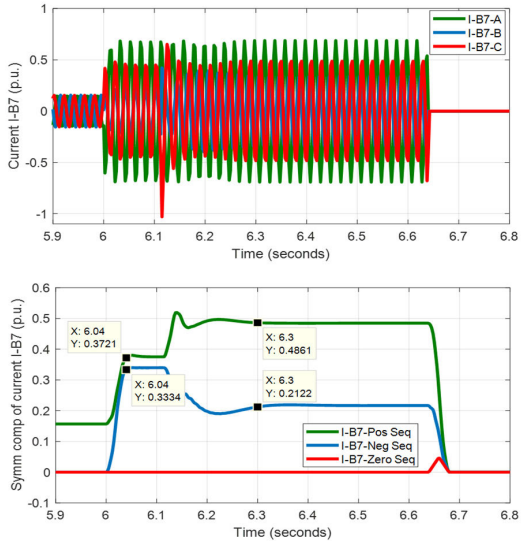

FIGURE 31. The instantaneous line currents (top) and the derived symmetrical components of current (bottom) in p.u. observed at bus B7 during LL-fault F2 in islanded mode.

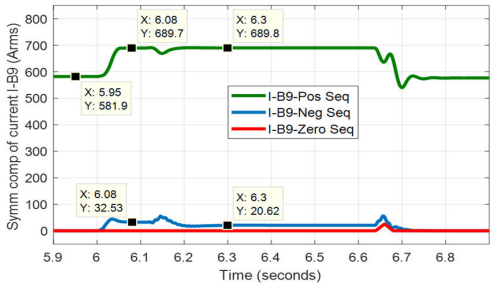

FIGURE 32. Fault current contribution from the DER-2: The derived symmetrical components of current in p.u. observed at bus B9 during LL-fault F2 in islanded mode.

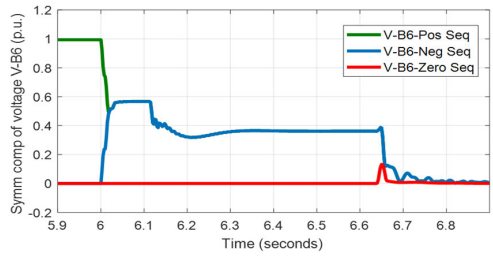

FIGURE 33. The derived symmetrical components of voltage in p.u. observed at bus B6 during LL-fault F2 in islanded mode.

measurement at the interface protection bus B3 (Fig. 34) will be as follows:

$$\Delta U_2 = (0.5669 - 0)/0.9937 = 0.57 \text{ p.u.}$$

$$\Delta I_{Q2} = 2\text{x}\,(0.57 \text{ p.u.}) = 1.14\text{p.u. (MIN)} \quad (11)$$

$$= 6\text{x}\,(0.57 \text{ p.u.}) = 3.42 \text{ p.u. (MAX)} \quad (12)$$

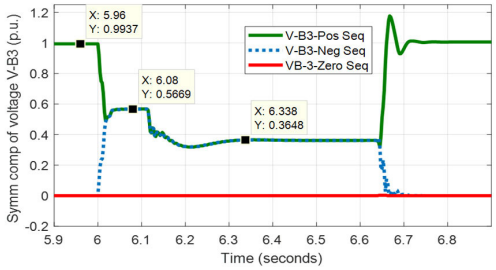

FIGURE 34. The derived symmetrical components of voltage in p.u. observed at bus B3 during LL-fault F2 in islanded mode.

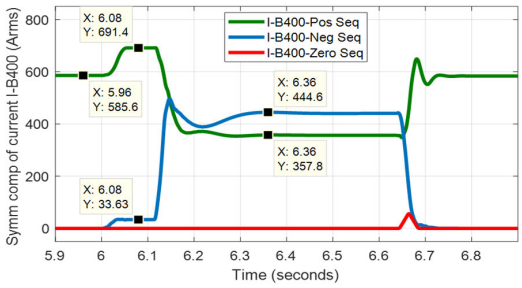

FIGURE 35. Fault current contribution from the DER-1 at LV side: The derived symmetrical components of rms current (A) observed at bus B400 during LL-fault F2 in islanded mode.

The negative sign of the Pos-Seq voltage change indicates the undervoltage situation at bus B3. Therefore, the negative sign of the additional Pos-Seq reactive current in (9)-(10) indicates that additional Pos-Seq current of 0.859-2.577 p.u. needs to be provided in overexcited operation (Fig. 4) to support the voltage at bus B3. Fig. 35 shows that the DER-1 reaches the Pos-Seq reactive current requirement of 0.61 p.u. (357.8 A) that is less than that calculated in (9). Fig. 35 also shows that DER-1 also reaches the Neg-Seq current requirement of 0.759 p.u. (444.6 A) against the minimum of 1.14 p.u. (667.6 A) of the Neg-Seq reactive current required according to (11). This means that in the islanded mode of operation more reactive power is required to meet the minimum Pos-Seq and Neg-Seq current requirements compared with the grid-connected mode requirement. Although, the minimum grid code requirements are not met by Q-injection of 760 kVar, but it is still enough capacity for the detection of the LL-fault F2 in the islanded mode of operation.

B. DIRECTIONAL ELEMENT

The indication of the direction of the fault (forward/reverse) discussed in this subsection is based on comparison of phase angle of operating (fault) current with respect to the reference or polarizing voltage. The Pos-Seq voltage (V_1) is used as the reference or polarizing quantity and the Pos-Seq current (I_1) during the fault is used as the operating quantity for the design of the Pos-Seq directional OC element 67P. Similarly, the Neg-Seq voltage (V_2) is used as the reference or polarizing quantity and the Neg-Seq current (I_2) during the fault is

TABLE 12. The Pos-Seq and Neg-Seq voltages and currents during LL-Faults.

Quantity	Before Q-injection	After Q-injection
LL-fault F1 in the grid-connected mode		
V_1 at B1	1.0∠0° p.u.	1.0∠0° p.u.
I_1 at B1	3.9∠-87° p.u.	3.33∠-87.6° p.u.
V_2 at B1 is zero	0∠93° p.u.	0∠91.5° p.u.
I_2 at B1	3.8∠-88° p.u.	4.4∠-88.5° p.u.
V_1 at B2	0.49∠-29° p.u.	0.569∠-30.35° p.u.
I_1 at B2	0.725∠176° p.u.	0.6953∠-123.2° p.u.
V_2 at B2	0.49∠-149° p.u.	0.569∠-150.35° p.u.
I_2 at B2	0.525∠-146.7° p.u.	0.8784∠-106.3° p.u.
LL-fault F2 in the islanded mode		
V_1 at B6	0.58 ∠-9.89° p.u	0.38 ∠-90.66° p.u
I_1 at B6	0.6495 ∠-28.45° p.u	0.6 ∠-5.519° p.u
V_2 at B6	0.567∠-129.9° p.u.	0.364∠149.3° p.u.
I_2 at B6	0.6234∠52.32° p.u.	0.88∠30.56° p.u.
V_1 at B7	0.58∠22.58° p.u.	0.38∠-55.14° p.u.
I_1 at B7	0.372∠-134.8° p.u.	0.486∠139.3° p.u.
V_2 at B7	0.54∠-162.3° p.u.	0.3653∠117.4° p.u.
I_2 at B7	0.3334∠-160.9° p.u.	0.2122∠116.9° p.u.

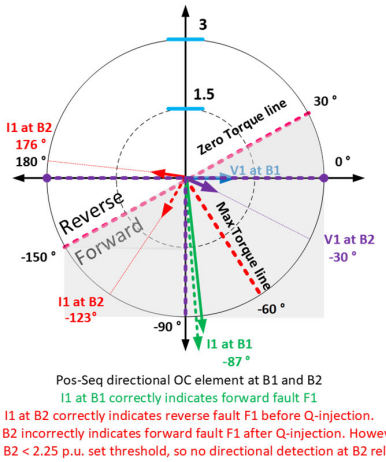

FIGURE 36. The 67P directional element operation at B1 and B2 during the LL-fault F1 in the grid-connected mode with RCA of 60° lagging with respect to V1 at B1 and B2.

used as the operating quantity for the design of the Neg-Seq directional OC element 67Q. The Pos-Seq and the Neg-Seq voltages and currents during the LL-fault F1 in the grid-connected mode and LL-fault F2 in the islanded mode are presented in Table 12.

a: 67P ELEMENT DESIGN PRINCIPLE

The maximum torque line is assumed to be at a relay characteristic angle (RCA) of 60° or 30° lagging from the measured angle of the reference voltage (V_1) and the zero torque line is assumed at ±90° from the RCA. If the measured phase angle of Pos-Seq current I_1 during the fault lies in between RCA ± 90°, the fault is classified as the forward fault by the 67P element. Otherwise, the fault is classified as the reverse fault. The third approach is to use RCA of 0 degrees with respect to the polarizing voltage (V_1) and assuming zero torque line at RCA ± 90°. This means the fault is considered in the forward direction if the Pos-Seq current I_1 during the fault is lagging or leading the reference voltage V_1 by 90°. These directional principles are adopted from [33] but with different polarizing and operating quantities. The forward/reverse fault is declared only if the magnitude of I_1 during the fault is 2.25 p.u. or greater in the grid-connected mode and 1.2 p.u. or greater in the islanded mode.

b: 67Q ELEMENT DESIGN PRINCIPLE

The same principles as discussed for the 67P element design are also considered for the 67Q element design but the Neg-Seq voltage V_2 is used as the polarizing quantity and the Neg-Seq current I_2 is used as the operating quantity. Additionally, the forward direction is considered in the opposite direction of the considered RCA. This means if the measured phase angle of Neg-Seq current I_2 during the fault lies in between RCA ± 90°, the fault is classified as the reverse fault by the 67Q element. Otherwise, it is classified as the forward fault. The forward/reverse fault is declared only if the ratio of I_2/I_1 during the fault is 1.3 or greater in both the grid-connected and the islanded modes. Moreover, the magnitude of $I_2 \geq 0.5$ p.u. is used as the restraining quantity to avoid the false operation of 67Q element during the load unbalance.

The above mentioned design principles of 67P and 67Q elements are applied for the forward/reverse fault directional discrimination during LL-fault F1 in the grid-connected mode and LL-fault F2 in the islanded mode. For the demonstration purpose, the operation of 67P directional element with RCA of 60° lagging is shown in Fig 36. Similarly, the operation of 67P directional element with RCA of 30° lagging is shown in Fig 37. The shaded area on the 360° planes of Fig 36 and Fig. 37 indicates the forward direction of the fault whereas the unshaded area indicates the reverse direction of the fault. The zero torque line is the boundary or threshold line for angles of the Pos-Seq fault current between the forward and the reverse direction regions. It means if the angle of the Pos-Seq fault current I_1 lies in the shaded area, the fault is considered in the forward direction otherwise it is considered in the reverse direction. The variable lengths of radius along the 360° plane marked with blue lines indicate the thresholds of the magnitudes of voltages and currents. The current threshold should be 2.25 p.u. or greater for the grid-connected mode and 1.2 p.u. or greater for the islanded mode.

The results (Table 12) show that only the 67P element could be reliable for LL-fault F1 in the grid-connected mode. This is clearly evident from the Fig. 36 and Fig. 37 that I_1 at B1 correctly indicate the fault to be in forward direction with its angle located in the shaded area and its magnitude greater than 2.25 p.u. set threshold. Fig. 36 and Fig. 37 also reveal that I_1 at B2 correctly indicate the reverse fault direction before Q-injection as its angle lies in the unshaded area. However, I_1 at B2 incorrectly indicate forward direction after Q-injection as its angle lies in the shaded area instead of unshaded area. The characteristic of 67P element at B2 with V_1 at B2 used as the polarizing quantity is drawn with purple lines

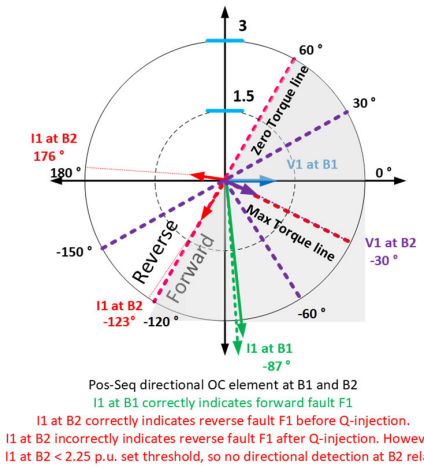

FIGURE 37. The 67P directional element operation at B1 and B2 during the LL-fault F1 in the grid connected mode with RCA of 30° lagging with respect to V1 at B1 and B2.

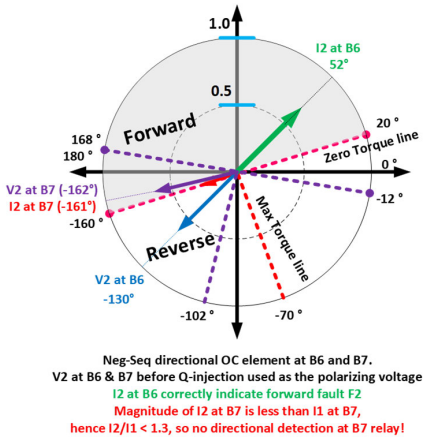

FIGURE 38. The 67Q directional element operation at B6 and B7 during the LL-fault F2 in the islanded mode before Q-injection with RCA of 60° lagging with respect to V2 at B6 and B7.

(see Fig. 36 and Fig. 37). The magnitude of I_1 at B2 is less than set threshold of 2.25 p.u., therefore the AND logic of 67P element at B2 will not indicate the presence of the reverse fault even if the angle indicates the fault to be in the forward or reverse direction. The 67P element would not be reliable during the LL-fault F2 in the islanded mode due to less than 1.2 p.u. magnitude of Pos-Seq current I_1 in both the forward direction (bus B6) and the reverse direction (bus B7).

The results (Table 12) reveal that the 67Q element would not work during the LL-fault F1 in the grid-connected mode due to nearly zero magnitude of Neg-Seq voltage V_2 in the forward direction (bus B1) and the ratio I_2/I_1 of less than 1.3 in both the forward direction (bus B1) and the reverse direction (bus B2) before Q-injection. Although the ratio I_2/I_1 of greater than 1.3 is obtained in the forward direction (bus B1) after Q-injection but the persistent zero magnitude

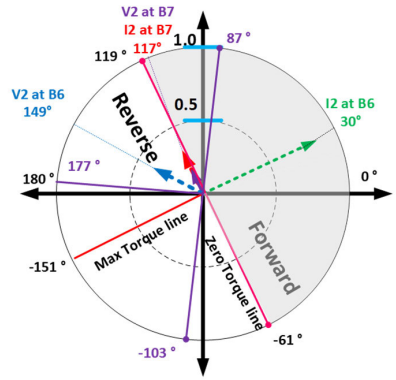

FIGURE 39. The 67Q directional element operation at B6 and B7 during the LL-fault F2 in the islanded mode after Q-injection with RCA of 60° lagging with respect to V2 at B6 and B7.

of V_2 even after Q-injection makes it inapplicable for the 67Q element operation. The 67Q element could be reliable during the LL-fault F2 in the islanded mode particularly in the forward direction (bus B6) after the activation of Q-injection function which results in the ratio I_2/I_1 of greater than 1.3.

The operation of 67Q directional element during the LL-fault F2 in the islanded mode with RCA of 60° lagging before and after Q-injection is shown in Fig. 38 and Fig. 39, respectively. It can be seen in Fig. 38 and Fig. 39 that I_2 at B6 correctly indicate the fault to be in forward direction with its angle located in the shaded area (green line), its magnitude greater than 0.5 p.u. and the ratio of I_2/I_1 during the fault is greater than the set threshold of 1.3. Fig. 38 and Fig. 39 also reveal that I_2 at B7 will correctly indicate the reverse fault direction before and after Q-injection as its angle lies in the unshaded area (red line). However, the magnitude of I_2 at B7 is less than set threshold of 0.5 p.u. and the ratio of I_2/I_1 is also less than 1.3 due to limited Q-injection by DER-2, therefore the AND logic of 67Q element at B7 will not indicate the presence of the reverse fault. The characteristic of 67Q element at B7 with V_2 at B7 used as the polarizing quantity is drawn with purple lines (see Fig. 38 and Fig. 39).

Similar results will be obtained for the 67Q element with the RCA of 0° and 30°. The RCA of 0° in particular would make the directional detection straightforward in the forward or the reverse direction for both 67P and 67Q directional elements even after Q-injection. The three directional characteristics with RCA of 0°, 30° and 60° can be used simultaneously with OR logic to cover the wide range of angle variations of the symmetrical component quantities. Fig. 40 shows the OR logic inputs/outputs of 67P and 67Q elements. Fig. 41 shows the standardized protection logic for the unbalanced faults used at the interface protection bus B3 and other buses (B1, B2, B6, B7). Fig. 40 explains the details of 67P (ANG) and 67Q (ANG) of Fig. 41.

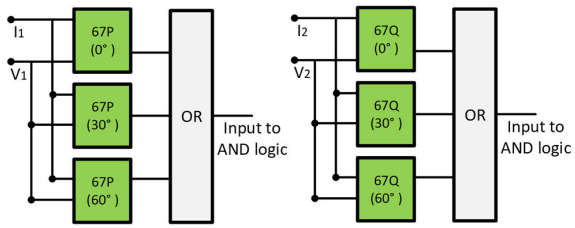

FIGURE 40. The OR logic of 67P and 67Q directional elements with RCA of 0°, 30° and 60°.

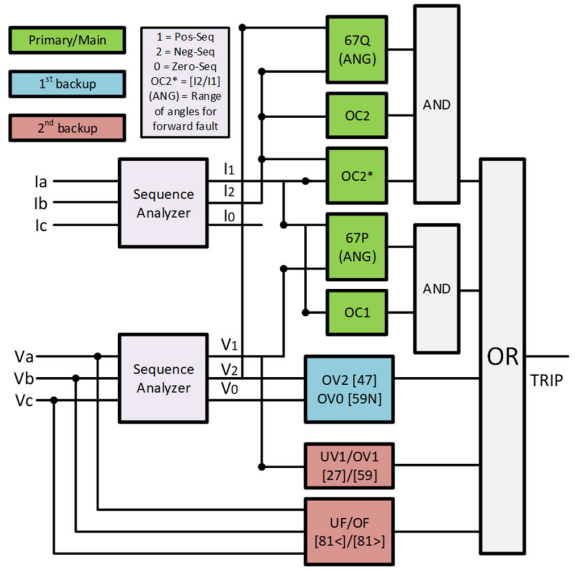

FIGURE 41. Standardized protection logic for the unbalanced faults used at the interface protection bus B3 and other buses (B1, B2, B6, B7).

C. GRID CODES PROPOSAL FOR ISLANDED MODE

From the review of European and IEEE grid codes for the DERs in MV/LV networks it is found that the grid codes for islanded mode of operation are still lacking. Although IEEE grid codes cover the transition and synchronization rules between the grid-connected and islanded modes during the intentional islanded mode in addition to few changes in OV, OF, UF ride-through and adaptive settings. However, particular UVRT, OVRT, LFRT and HFRT requirements for the islanded mode are still not mentioned. In our previous paper [34], we proposed a new UVRT curve for the islanded mode operation of AC microgrids. In this paper, we propose a new five-cycle OVRT curve for the islanded mode operation of AC microgrids (Fig. 42). The new OVRT curve is developed on the basis of overvoltage observed during the transition of AC microgrid to the islanded mode operation in our previous paper [35]. After the initial five cycles of the fundamental frequency during the transition mode, the normal OVRT curve (Fig. 3) will be applied. It means the new OVRT curve is similar to the OVRT curve for the grid-connected mode after the initial five cycles of the fundamental frequency during the transition to the islanded mode.

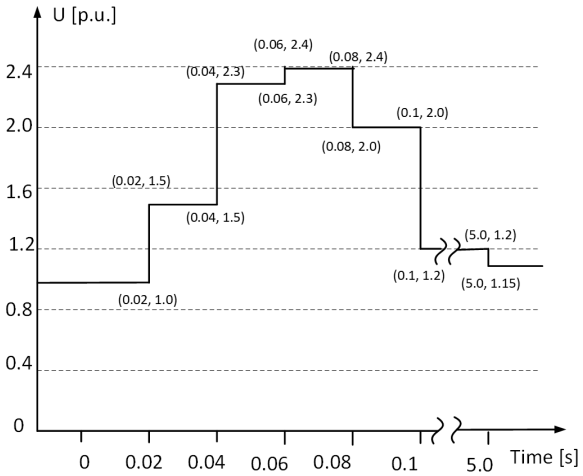

FIGURE 42. The new proposed five-cycle HVRT curve for smooth transition to the islanded mode operation.

TABLE 13. The Comparison of EN 50549 and IEEE 1547 grid codes of DERs.

EN Grid codes [22] [23]	IEEE Grid codes [24] [26] [27]
Applicable for only the grid-connected mode.	Applicable for both grid-connected and islanded modes. However, islanding mode requirements are defined generally and not specifically.
Limits of capacities of DERs specified (type-A & B)	Limits of capacities of DERs not specified
Requirements are applicable irrespective of penetration levels of DERs.	Requirements depend on penetration levels of DERs (categories I, II, III)
Applicable for 50 Hz distribution systems	Applicable for 60 Hz distribution systems
ROCOF immunity of 2 Hz/s	ROCOF immunity of 3 Hz/s
Specific limits for short-circuit current or reactive current by DERs during faults are defined.	Specific limits are not defined but DERs are required to have capability of exchanging reactive power during short-circuit faults for dynamic voltage stability during LVRT and HVRT events.
DERs have to ride-through only one voltage disturbance according to the defined LVRT curve.	DERs have to ride-through multiple voltage disturbances with specified short-time interval between two consecutive voltage disturbances.
No exemptions to UVRT, OVRT and frequency disturbance requirements for DERs.	Exemption to UVRT, OVRT and frequency disturbance requirements for emergency systems and standby DERs.
No voltage phase angle changes ride-through requirements for DERs are specified.	Voltage phase angle changes ride-through requirements for DERs are specified.
Interface protection settings of DERs overrule the technical capabilities and the ride-through requirements.	Any tripping of DERs for the self-protection and failure to provide ride-through requirements is considered as the non-compliance of the grid code.

The suggested five-cycle OVRT curve (Fig. 42) means that the DERs need to either ride-through during this time or a voltage regulation should be provided to avoid the DER tripping during the transition period by the OV protection.

V. DISCUSSION

The most relevant European and IEEE grid codes for the connection of the converter-based DERs to MV/LV networks have been reviewed and the selected grid code requirements have been evaluated. Table 13 presents a comparison between EN and IEEE grid codes of DERs.

One important requirement of the grid codes is the provision of the reactive current by the converter-based DERs during the voltage changes at the PCC. The certain amount of reactive current up to the rated current limit of individual DER has to be provided by the DERs both in the Pos-Seq and Neg-Seq components. The control of the converter-based DERs is usually designed to provide the Pos-Seq current during the voltage steps or faults and the Neg-Seq current is usually limited. Even if the DERs are controlled to provide the Neg-Seq reactive current as the priority, its magnitude may not be enough to meet the stringent grid code requirements. Therefore, extra Q-sources have to be installed in MV/LV networks to meet the new/revised grid code requirements.

In this study, the extent of Q-injection during the unbalanced faults has been found according to the minimum grid code requirements. Moreover, the effect of Q-injection on the unbalanced short-circuit faults detection, and protection coordination using different symmetrical components-based protection functions has been observed. It is found that Q-injection at LV terminals of DER equal to twice the MVA rating of the individual DER is enough to meet the minimum grid code requirements of EN 50549-2-2019 [22] during the unbalanced faults in the grid-connected mode. The extent of Q-injection higher than twice the MVA rating of individual DER is required during the unbalanced faults in the islanded mode. However, Q-injection of twice the MVA rating of the individual DER is also effective for the detection of the unbalanced short-circuit faults in the islanded mode.

It should be noted that the reactive current requirement mentioned in subsection C of section II is generally applicable for 3Ph balanced and unbalanced faults. It means the Pos-Seq current requirement during the LLL-faults and the Neg-Seq current requirement during the LLLG-faults and other unbalanced faults. For other types of unbalanced faults, the Q-injection requirement of EN 50549-2-2019 is open for future developments. In [36], a distinction is made between the fault types for the requirement of Q-injection. It states that a WTG unit must be able to provide a reactive current of at least 100% of the rated current during the 3-pole faults and at least 40% of the rated current during 1-pole and 2-pole faults. Moreover, the relevant reactive current requirements only consider voltage and reactive current changes ascertained from Pos-Seq system components of the basic harmonic component. However, maximum possible reactive current is allowed during the 1-pole and 2-pole faults with simultaneous flow of Neg-Seq current as permitted by WTG size. With the mentioned limits of reactive current during faults in [36], the selected capacity of Q-injection meets the grid code requirement. It is further clarified that the main purpose of an additional Q-injection in this study is the enhancement of short-circuit current level during the unbalanced faults particularly the Neg-Seq current. This has been achieved in quite successful manner. The proposed Q-injection method is also valid for the average WTG model.

It is recommended that the outer control of DERs (Fig. 9) should discriminate between the balanced and unbalanced short-circuit faults and give priority to Pos-Seq current during the balanced faults and Neg-Seq current during the unbalanced fault. From the context of DER control presented in this paper, this means that the Pos-Seq current should not be reduced during the balanced LLL-fault. The AND logic can be used for the detection of simultaneous voltage magnitude drop of three-phases to prioritize Pos-Seq current during the balanced LLL-fault. The protection of AC microgrids during the balanced LLL-fault is discussed in detail in our previous papers [34], [35]. In this study, only the symmetrical Q-injection has been used in order to maintain the asymmetry of voltage and current during the unbalanced faults. According to the previous study [37], an asymmetrical Q-injection may provide better performance in terms of voltage support at PCC. However, it may require separate control for each phase. Moreover, asymmetrical Q-injection may raise the voltage of individual phases to the extent of OV protection tripping threshold causing nuisance tripping.

The natural magnitude-based directional coordination is available due to extremely limited amount of the Neg-Seq current provision by the DER-2. Therefore, the AC microgrid can be protected against unbalanced short-circuit faults even without the 67P or 67Q directional elements. However, directional elements will be required if DER-2 also injects the Neg-Seq current up to the same extent of DER-1. This is a typical case for DERs in the ring networks which will be covered in future publications. Nevertheless, the 67Q directional element is also designed and evaluated for the discrimination of forward/reverse fault direction during the selected unbalanced LL-fault in the islanded mode. The Pos-Seq directional element 67P and Neg-Seq directional element 67Q can correctly indicate the forward AB-fault during the grid-connected and the islanded mode, respectively. The directional elements also detect the reverse faults reliably with few exceptions. During these exceptions, though the reverse fault is falsely detected by the directional elements, but its operation is restrained by the threshold settings. In this way a desired operational performance is achieved. During inrush conditions, the blocking of the 67Q directional element is recommended [7]. The protection coordination between the primary/main and backup protections of Fig. 41 at various locations (buses 1, 2, 3, 6 and 7) was also observed according to the settings of Table 9 during the considered faults with and without Q-injection and it was found quite satisfactory.

VI. CONCLUSION

The latest grid codes of DERs connected to the MV/LV networks have been reviewed and the evaluation of selected grid codes applicable for AC microgrid protection is presented. The extent of Q-injection during the unbalanced faults in the grid-connected and islanded modes is determined through simulations. The determined amount of Q-injection meets the minimum grid code requirements and helps detect the unbalanced faults in both the grid-connected and islanded

modes. A new five-cycle OVRT curve is also suggested for smooth transition to the islanded mode operation. The standardized protection settings maintain the proper protection coordination. In future, this work will be further extended for the AC microgrids with the ring-network topology. This means the 67P and 67Q directional elements will be used to distinguish between the forward and reverse faults due to Q-injection of the same extent from both sides of the fault point.

ACKNOWLEDGMENT

The authors would like to thank their colleague Prof. Hannu Laaksonen for sharing useful literary material.

REFERENCES

[1] A. A. Memon and K. Kauhaniemi, "A critical review of AC microgrid protection issues and available solutions," *Electr. Power Syst. Res.*, vol. 129, pp. 23–31, Dec. 2015.

[2] A. A. Memon, H. Laaksonen, and K. Kauhaniemi, "Microgrid protection with conventional and adaptive protection schemes," in *MicroGrids*, A. Anvari-Moghaddam, H. Abdi, B. Mohammadi-Ivatloo, and N. Hatziargyriou, Eds. Cham, Switzerland: Springer, 2021, ch. 19, pp. 523–579, doi: 10.1007/978-3-030-59750-4_19.

[3] H. Laaksonen, D. Ishchenko, and A. Oudalov, "Adaptive protection and microgrid control design for Hailuoto island," *IEEE Trans. Smart Grid*, vol. 5, no. 3, pp. 1486–1493, May 2014, doi: 10.1109/TSG.2013.2287672.

[4] F. Calero, "Rebirth of negative-sequence quantities in protective relaying with microprocessor-based relays," in *Proc. 57th Annu. Conf. Protective Relay Eng.*, Mar. 2004, pp. 1–30.

[5] *ABB, Negative Sequence Overcurrent Relay and Protection Assemblies RXIIK 4 and RAIIK 400, 1MRK 509 045-BEN Revision: B*, ABB AB Substation Automat. Products, Västerås, Sweden, 2013.

[6] A. F. Elneweihi, E. O. Schweitzer, and M. W. Feltis, "Negative-sequence overcurrent element application and coordination in distribution protection," in *Proc. IEEE Power Eng. Soc. Summer Meet.*, Seattle, WA, USA, Jul. 1992, pp. 1–9.

[7] Z. Xin, H. Wang, X. Dong, and X. Ren, "Inverse time zero sequence protection based on traveling wave startup information," in *Proc. 3rd Asia Energy Electr. Eng. Symp. (AEEES)*, Mar. 2021, pp. 772–775, doi: 10.1109/AEEES51875.2021.9403052.

[8] M. Dupuis, N. Mahoney, A. Padmanabhan, and K. Bhuvaneshwaran, "Negative-sequence overcurrent considerations for induction motor loads," in *Proc. 70th Annu. Conf. Protective Relay Eng. (CPRE)*, Apr. 2017, pp. 1–8, doi: 10.1109/CPRE.2017.8090039.

[9] M. M. Eissa and O. P. Malik, "A new digital directional transverse differential current protection technique," *IEEE Trans. Power Del.*, vol. 11, no. 3, pp. 1285–1291, Jul. 1996, doi: 10.1109/61.517482.

[10] M. M. Eissa, "Current directional protection technique based on polarizing current," *Int. J. Electr. Power Energy Syst.*, vol. 44, no. 1, pp. 488–494, Jan. 2013, doi: 10.1016/j.ijepes.2012.07.043.

[11] A. Ukil, B. Deck, and V. H. Shah, "Current-only directional overcurrent protection for distribution automation: Challenges and solutions," *IEEE Trans. Smart Grid*, vol. 3, no. 4, pp. 1687–1694, Dec. 2012, doi: 10.1109/TSG.2012.2208127.

[12] A. Jalilian, M. T. Hagh, and S. M. Hashemi, "An innovative directional relaying scheme based on postfault current," *IEEE Trans. Power Del.*, vol. 29, no. 6, pp. 2640–2647, Dec. 2014, doi: 10.1109/TPWRD.2014.2312019.

[13] I. Kiaei, S. Lotfifard, and M. Ghanaatian, "Current-only directional overcurrent protection using postfault current," in *Proc. IEEE Texas Power Energy Conf. (TPEC)*, Feb. 2019, pp. 1–5, doi: 10.1109/TPEC.2019.8662199.

[14] J. Roberts and A. Guzman, "Directional element design and evaluation," in *Proc. 21st Annu. West. Protect. Rel. Conf.*, Oct. 1994, pp. 1–27. Accessed: Jan. 10, 2022. [Online]. Available: https://cdn.selinc.com/assets/Literature/Publications/Technical%20Papers/6009_DirectionalElement_JBR-AG_20060803_Web.pdf

[15] B. Fleming, "Negative-sequence impedance directional element," in *Proc. 10th Annu. ProTest User Group Meet.*, Pasadena, CA, USA, Feb. 1998, pp. 1–11. Accessed: Jan. 10, 2022. [Online]. Available: https://cms-cdn.selinc.com/assets/Literature/Publications/Technical%20Papers/6072_NegSeq_Web.pdf?v=20180724-151349

[16] IEEE PES, "Impact of inverter based generation on bulk power system dynamics and short-circuit performance," IEEE PES. Ind. Tech. Support Task Force, Piscataway, NJ, USA, Tech. Rep. PES-TR68, Jul. 2018.

[17] I. Erlich, T. Neumann, F. Shewarega, P. Schegner, and J. Meyer, "Wind turbine negative sequence current control and its effect on power system protection," in *Proc. IEEE Power Energy Soc. Gen. Meeting*, Dec. 2013, pp. 1–5, doi: 10.1109/PESMG.2013.6672880.

[18] M. Nagpal and C. Henville, "Impact of power-electronic sources on transmission line ground fault protection," *IEEE Trans. Power Del.*, vol. 33, no. 1, pp. 62–70, Feb. 2018.

[19] B. Chen, A. Shrestha, F. A. Ituzaro, and N. Fischer, "Addressing protection challenges associated with type 3 and type 4 wind turbine generators," in *Proc. 68th Annu. Conf. Protective Relay Eng.*, College Station, TX, USA, Mar. 2015, pp. 335–344.

[20] A. Haddadi, I. Kocar, E. Farantatos, and J. Mahseredjian, "System protection guidelines for systems with high levels of renewables: Impact of wind & solar generation on negative sequence and power swing protection," EPRI, Palo Alto, CA, USA, EPRI Tech. Rep. 3002010937, 2017.

[21] W. Zhang, J. Rocabert, J. I. Candela, and P. Rodriguez, "Synchronous power control of grid-connected power converters under asymmetrical grid fault," *Energies*, vol. 10, no. 7, p. 950, Jul. 2017, doi: 10.3390/en10070950.

[22] *Requirements for Generating Plants to be Connected in Parallel With Distribution Networks. Part 2: Connection to a MV Distribution Network. Generating Plants up to and Including Type B*, Standard SFS-EN 50549-2:2019, Eur. Committee Electrotechnical Standardization, Brussels, Belgium, Feb. 2019, pp. 1–80.

[23] *Requirements for Generating Plants to be Connected in Parallel With distribution Networks. Part 1: Connection to a LV Distribution Network. Generating Plants up to and Including Type B*, Standard SFS-EN 50549-1:2019, Eur. Committee for Electrotechnical Standardization, Brussels, Belgium, Feb. 2019, pp. 1–71.

[24] *IEEE Standard for Interconnection and Interoperability of Distributed Energy Resources With Associated Electric Power Systems Interfaces*, Standard IEEE 1547-2018, IEEE Standards Association, IEEE Standards Coordinating Committee 21, Feb. 2018, pp. 1–136.

[25] IEEE PES, "Impact of IEEE 1547 standard on smart inverters," IEEE Power Energy Soc., Piscataway, NJ, USA, Tech. Rep. PES-TR67, May 2018, pp. 1–64.

[26] *IEEE Guide for Design, Operation, and Integration of Distributed Resource Island Systems with Electric Power Systems*, IEEE Standard 1547. 4-2011, IEEE Standards Association, IEEE Standards Coordinating Committee 21, Jul. 2011, pp. 1–42.

[27] *IEEE Standard for the Specification of Microgrid Controllers*, IEEE Standard 2030.7-2017, IEEE Standards Association, IEEE Standards Coordinating Committee 21, Dec. 2017, pp. 1–41.

[28] (Nov. 25, 2016). *European Union Emissions Trading Scheme—Legal Point of View, Type A Power Generating Module, Category: European Union Electricity Market Glossary*. Accessed: Aug. 19, 2020. [Online]. Available: https://www.emissions-euets.com/internal-electricity-market-glossary/1032-type-a-power-generating-module

[29] Z. Ye, D. Finney, R. Zhou, M. Dame, B. Premerlani, B. Kroposki, and S. Englebretson, "Testing of GE universal interconnection device," NREL, Golden, CO, USA, Tech. Rep. NREL/TP-560-34676, Aug. 2003. Accessed: Jun. 27, 2021. [Online]. Available: https://www.nrel.gov/docs/fy03osti/34676.pdf

[30] K. Sirviö, K. Kauhaniemi, A. A. Memon, H. Laaksonen, and L. Kumpulainen, "Functional analysis of the microgrid concept applied to case studies of the Sundom smart grid," *Energies*, vol. 13, no. 16, p. 4223, Aug. 2020, doi: 10.3390/en13164223.

[31] *Impact of Inverter-Based Resources on Protection Schemes Based on Negative Sequence Components*, EPRI, Washington, DC, USA, Jul. 2019.

[32] IEEE PES, "Methods for detecting and analyzing an open phase condition of a power circuit to a nuclear plant station service or startup transformer," IEEE PES Power Syst. Relay. Control Committee. Working Group K11, Piscataway, NJ, USA, Tech. Rep. PES-TR75, Jan. 2020.

[33] J. L. Blackburn and T. J. Domin, *Protective Relaying: Principles and Applications*, 3rd ed. Boca Raton, FL, USA: CRC Press, 2007.

[34] A. A. Memon and K. Kauhaniemi, "An adaptive protection for radial AC microgrid using IEC 61850 communication standard: Algorithm proposal using offline simulations," *Energies*, vol. 13, no. 20, p. 5316, Oct. 2020, doi: 10.3390/en13205316.
[35] A. A. Memon and K. Kauhaniemi, "Real-time hardware-in-the-loop testing of IEC 61850 GOOSE-based logically selective adaptive protection of AC microgrid," *IEEE Access*, vol. 9, pp. 154612–154639, 2021, doi: 10.1109/ACCESS.2021.3128370.
[36] *Deutsch Ordinance on System Services by Wind Energy Plants*. Accessed: Jul. 29, 2022. [Online]. Available: http://www.ichgmbh.com/wp-content/uploads/2016/06/doc_Deutsch_ordinance-on-system-services-by-wind-energy-plants.pdf
[37] N. Filipe, A. Leiria, and M. Louro, "Reactive power injection by wind farms during asymmetric faults-application to Portuguese distribution grid," in *Proc. CIRED 23rd Int. Conf. Elect. Distr.*, Lyon, France, Jun. 2015, pp. 15–18, Paper 0960.

AUSHIQ ALI MEMON (Member, IEEE) received the B.E. degree in electrical engineering from the Quaid-e-Awam University of Engineering, Science and Technology, Nawabshah, Pakistan, in 2006, and the M.Sc. (power engineering) degree in electrical power engineering from the Brandenburg University of Technology, Cottbus, Germany, in 2013. He is currently pursuing the Ph.D. degree with the Department of Electrical Engineering, University of Vaasa, Finland. He is also working as a Project Researcher with the Department of Electrical Engineering, University of Vaasa. Previously, he was a Lecturer with the Quaid-e-Awam University of Engineering, Science and Technology, from 2007 to 2009. He worked as a Project Researcher with the University of Vaasa, from 2014 to 2020. His research interests include power system protection, microgrids, power system transient simulations, smart grids, and power electronics applications.

MAZAHER KARIMI (Senior Member, IEEE) received the Ph.D. degree in electrical energy and power system from the University of Malaya, Kuala Lumpur, Malaysia, in 2013. He worked as a Postdoctoral Research Fellow at the University of Malaya, from 2014 to 2015, and then joined The University of Manchester as a Research Associate, from 2016 to 2017. From 2017 to 2020, he was an Assistant Professor at Gonbad Kavous University, Iran. Currently, he is an Assistant Professor at the School of Technology and Innovations, University of Vaasa, Vaasa, Finland. His current research interests include smart grid applications; wide-area monitoring, protection, and control; distributed generation; and power system stability and frequency control.

KIMMO KAUHANIEMI (Member, IEEE) received the M.S. and Ph.D. degrees in electrical engineering from the Tampere University of Technology, Finland, in 1987 and 1993, respectively. Previously, he was worked at ABB Corporate Research and the VTT Technical Research Centre of Finland. He is currently with the University of Vaasa, where he is also a Professor in electrical engineering and leads the Smart Electric Systems Research Group. His special research interests include power system transient simulation, protection of power systems, grid integration of distributed generation, and microgrids.

IEEE Access
Multidisciplinary ⋮ Rapid Review ⋮ Open Access Journal

Received 16 May 2023, accepted 29 May 2023, date of publication 7 June 2023, date of current version 14 June 2023.

Digital Object Identifier 10.1109/ACCESS.2023.3283575

RESEARCH ARTICLE

Protection of the Future Harbor Area AC Microgrids Containing Renewable Energy Sources and Batteries

AUSHIQ ALI MEMON, (Member, IEEE), AND KIMMO KAUHANIEMI, (Member, IEEE)
School of Technology and Innovations, University of Vaasa, 65200 Vaasa, Finland

Corresponding author: Aushiq Ali Memon (amemon@uwasa.fi)

This work was supported by the Future Energy Storage Solutions in Marine Installations (FESSMI) Research Project funded by the European Regional Development Fund (ERDF) through the Finnish Funding Agency for Technology and Innovation (Tekes) under Grant 3345/31/2015.

ABSTRACT A significant share of global carbon emissions is related to marine vessels running solely on fossil fuels. The hybrid or fully electrified marine vessels using battery energy storage systems (BESS) both for onboard propulsion system and for cold-ironing during docking at harbor areas will significantly reduce marine related carbon emissions. However, the transformation of marine vessels' operations from diesel engines to BESS will necessarily require charging stations and other electric power infrastructure at harbor areas. The sustainable and cheap energy of renewable energy sources like wind turbine generators (WTGs), photovoltaic (PV) systems and related BESS could be used at harbor areas for charging depleted vessel-BESS and supplying power to cold-ironing loads. For this purpose, two new harbor area smart grid or AC microgrid models have been developed by our research group. This paper presents a comprehensive analysis of three-phase short-circuit faults for one of the proposed AC microgrid models using PSCAD/EMTDC simulations. The fault study of harbor area AC microgrid-1 is done for both grid-connected and islanded modes. The main purpose of the fault study is to check if grid-connected mode overcurrent settings of intelligent electronic devices (IEDs) will also be valid for different islanded mode fault cases with different fault current contributions from converter-based distributed energy resources (DERs) including WTG, PV and BESS. The extent of fault current contribution from DERs and BESS to avoid adaptive protection settings and to ensure definite-time protection coordination and fast fuse operations during different islanded modes is investigated.

INDEX TERMS Adaptive overcurrent protection, batteries, converter-based DERs, fuse, harbor area ac microgrids, islanded mode, renewable energy sources, short-circuit faults.

I. INTRODUCTION

The battery energy storage systems (BESS) both installed onboard the vessel and offboard at harbor area provide a great opportunity for reduction of fossil fuel consumption, carbon emissions and marine pollution. The BESS installations near harbor areas will help utilize the renewable energy sources (RES) including wind turbine generators (WTGs) and photovoltaic (PV) systems up to their maximum available potential. The correctly dimensioned BESS can easily replace some or all of the diesel engines used to propel a particular type of the vessel. This will not only help improve the dynamic response of the vessel propulsion system but also increase the energy efficiency of the system. In order to achieve these goals, the required supporting infrastructure should be installed not only onboard the vessel but also in the harbor area reaching the quay. This supporting infrastructure include all necessary electrical installations supplying power to electrical propulsion systems onboard the vessel and the harbor area power supply system enabling the "shore-to-ship connection" [1] for providing power to vessel load during cold-ironing and in the future also supply power for charging the depleted vessel batteries. Furthermore, the harbor area grid can include RES and BESS, in that case we can call the system as *harbor area smart grid* (HASG) [2].

In this regard, two alternative HASG models have been developed by our research group incorporating the technical suggestions provided by all the FESSMI project

The associate editor coordinating the review of this manuscript and approving it for publication was Giambattista Gruosso.

partners: One alternative for overnight offboard slow charging of vessel-BESS and the other for onboard fast charging of vessel-BESS during cold-ironing [3]. Both solutions consider providing power to onboard ship load from the RES installed at the harbor area during the docking period. This paper is limited to the first alternative HASG-1 (Fig. 1) that is a seven-bus supply system consisting of two main-grid buses (110 kV and 20 kV), two harbor area buses (20 kV and 0.69 kV), one charger bus (0.69 kV), one port bus (0.69 kV) and one ship bus (6.6 kV). The 20 kV harbor bus is located at a distance of 5 km from the transformer-T1 substation (110 kV/20 kV) connecting the main grid with HASG-1 through a 5 km long cable. The three units of container-based vessel-BESS each of 2 MW rating are connected with the 0.69 kV charger bus. These container-based vessel-batteries are charged overnight with 0.1C slow charging rate (10 hours for full charge). The 0.69 kV charger bus is connected to the upstream 20 kV harbor bus through a 2.5 km long cable and a 20 kV/0.69 kV, 3 MVA step down transformer-T4. The PV generator of 1 MVA and a wind turbine generator (WTG) of 3 MVA are connected at the 20 kV harbor bus via 5 km and 10 km long cables, respectively. Each of the PV and WTG has its local BESS to balance the normal weather-related power fluctuations and each one of them has its own 0.69 kV/20 kV step up transformer for connection to 20 kV harbor bus. A local harbor area load of 1.5 MVA is also connected to the 20 kV harbor bus.

The main grid connection to the cold-ironing load of 2 MW, 6.6 kV with two different frequencies of 50Hz and 60 Hz is also provided via the 20 kV harbor bus. The main grid connection to cold-ironing load is provided in two voltage-conversion stages: 20/0.69 kV and 0.69/6.6 kV. A 5 MVA, 50 Hz transformer-T2 at the 20 kV harbor bus steps down the voltage to 0.69 kV for providing LV connection to a 2 MW, 50/60 Hz frequency converter at the 0.69 kV harbor bus. The LV frequency converter converts the supply frequency from 50 Hz to 60 Hz at the 0.69 kV port bus. A 3 MVA 50/60 Hz transformer-T3 at the 0.69 kV port bus steps up the voltage from 0.69 kV to 6.6 kV to match the voltage level of the cold-ironing load. The star-point of shore-side transformer-T3 is earthed via a 200 Ohm continuous rated neutral earthing resistor as per recommendations in [4] for a nominal voltage of 6.6 kV. The frequency of cold-ironing load depends on the type of the vessel, if it is a 50 Hz vessel then direct connection from 0.69 kV harbor bus to 0.69 kV port bus is provided without the need of a frequency converter in between these two buses.

A 2.5 km long cable at the secondary of 0.69/6.6 kV transformer-T3 is connected to the 6.6 kV ship bus. At 6.6 kV ship bus the 2 MW loads of 50 Hz and 60 Hz vessels are connected via a 0.2 km flexible-cable. A single 3 MVA transformer-T3 connection at 0.69/6.6 kV conversion stage dictates that only one type of vessel load either 50 Hz or 60 Hz can be supplied at a time. An additional 2 MVA BESS is also connected at 0.69 kV harbor bus, which can be used to supply cold-ironing load if connection to the main-grid and

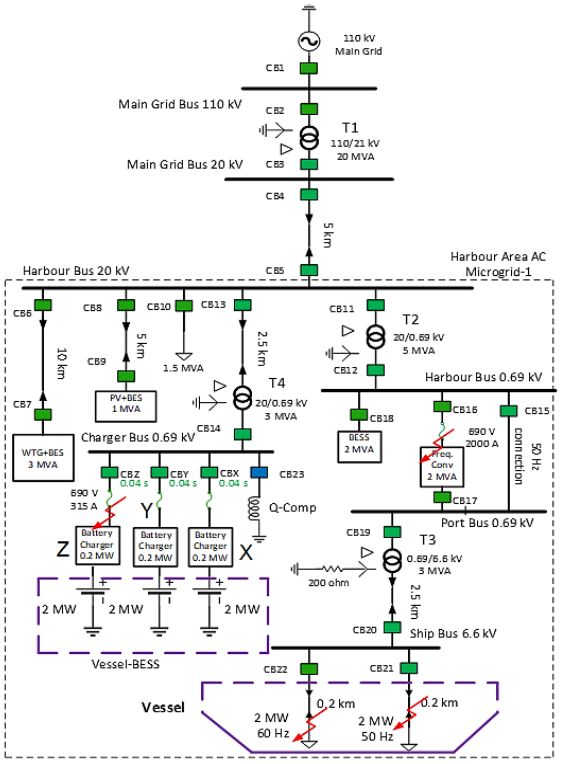

FIGURE 1. The first alternative HASG-1 model with renewable DERs and BESS (For 10 hour overnight slow charging of vessel-BESS).

distributed energy resources (DERs) is lost in case of fault at 20/0.69 kV transformer-T2. The main purpose of the DERs connected at the 20 kV harbor bus of HASG-1 is to supply charging power to container-based vessel-BESS at harbor area during night and supply power to cold-ironing load when empty container-based vessel-BESS are being replaced by charged batteries. Also, the harbor area load of 1.5 MVA connected at the 20 kV harbor bus has to be supplied by DERs depending on the available capacity. The main idea behind the HASG-1 is to use clean renewable energy available at harbor area up to its maximum available potential and reduce emissions by avoiding diesel generator operations during cold-ironing and use overnight charged batteries for hybrid vessel drives/propulsion system during the journey.

The proposed harbor area smart grid also considers importing the deficit power from the main grid if local DERs are not able to provide an adequate amount of power to cold-ironing load or vessel-BESS being charged plus local harbor area load and system losses. Normally, harbor area smart grid will be operated in grid-connected mode for a stable operation. However, during faults on the main grid, only DERs and BESS inside the harbor area smart grid will be available to supply power. In this situation, HASG-1 is said to be operating in the islanded mode. The overall structure of HASG-1 is like an AC microgrid with DERs, BESS and loads, that

can be operated in grid-connected or islanded mode. Therefore, the standards [5], [6], [7], and [8] for DERs and the standards [9] and [10] for AC microgrids are very much relevant to the proposed HASG-1 model in addition to the standards [4], [11], and [12] for "shore-to-ship connection" of marine installations. The main objective of this paper is to analyze remote three-phase short-circuit (SC) faults and investigate the operational suitability of traditional overcurrent (OC) protection schemes and fuses in the islanded mode of the proposed HASG-1 to be called from here onwards as *harbor area AC Microgrid-1* using PSCAD simulations.

The traditional protection schemes using single-setting definite-time and inverse-time OC relays, and fuses usually work quite well during the grid-connected mode of AC microgrid due to sufficient short-circuit current from the main grid. However, during the islanded mode more sensitive OC protection schemes are essentially required due to the limited available short-circuit current from DERs. It means adaptive OC settings are generally required for detection and isolation of faults in both grid-connected and islanded modes of AC microgrids with converter-based DERs [13], [14], [15], [16].

Due to the reduced/limited fault current contributions of DERs in the islanded mode, either the operation of fuse becomes very slow, or the failure of fuse operation happens. Previously in [17], the operation of fuse was practically observed within an islanded microgrid in central Finland that was fed by 120 kVA back-to-back converter. The 32 A gG type of fuse cleared different types of faults within 300-500 ms with a fault current contribution of the converter equal to its rated current. However, the results presented did not mention the size of the load being protected by the fuse. Nevertheless, the operation of fuse was quite slow therefore unsuitable for the fast fault clearance and proper maintenance of protection coordination with other backup overcurrent protection relays. Recently, a modified overrated energy storage inverter design has been proposed in [18] that provides three times the rated full load current during three-phase short-circuit fault in the islanded microgrid. The results show that the fuse (12.5 A) blows/operates within 500 ms of the three-phase fault. Although the fuse-relay and relay-relay coordination are maintained, the coordination time interval (CTI) between the fuse and backup overcurrent relay is three-times longer than the usual 200 ms. The CTI for the relay-relay coordination is even six times longer than 200 ms. The impact of energy storage devices on the control and protection system when used together with the RES generators was studied earlier in [19]. This paper diagnosed a considerable variation of fault current from the storage devices when suddenly switching from the generator mode to the load mode and vice versa. Therefore, adaptive protection scheme was suggested. Due to the lack of suitable simulation models of energy storage devices, the detailed protection coordination and fault dynamics were not analyzed.

Majority of the previous papers have only focused on the detection of short-circuit fault current and then limiting the output current of converter-based DERs to the rated current or below it either using the fault current limiters (FCL) or by adjusting the control of converters. In [20], the output current of the converter in a low voltage DC distribution network during the fault is limited by the control and then tripping is carried out within 50 ms using a non-standard controlled circuit breaker. A similar method is presented in [21] that utilizes current limiting control before isolation of different faults in an isolated AC microgrid with single DER unit. Fault detection and isolation are done using voltage and current thresholds followed by circuit breaker tripping. An output power and current limiting controls have been proposed in [22] for providing overload and overcurrent protection of directly voltage controlled DERs in an AC microgrid.

In [23], the protection of a looped AC microgrid is proposed using simple inverse-time OC devices with the same settings. The DERs close to the fault are controlled in a manner to inject relatively larger current than other DERs proportional to the measured impedance of the microgrid. The detection of the fault is based on indirect measurement of microgrid impedance. The supercapacitors of reduced sizes are used at the DC links of DER inverters for the enhancement of the fault current. Although, the results show a proper coordination between two OC devices at both ends of the fault, the backup protection is provided with either too small or too large values of CTI. Consequently, the OC devices other than the required are tripped without isolating the fault when primary OC devices fail to operate. General factors and requirements affecting the fault interruption and protection coordination for AC, DC and hybrid microgrids in distribution systems with converter-based DERs are discussed in [24]. The protection scheme for hybrid low voltage AC/DC distribution system is proposed in [25]. The proposed scheme uses high-speed DC circuit breaker for faults in remote DC section and recloser scheme using AC circuit breakers for faults in AC section near utility transformer. This way protection coordination is established between the protection devices. In our previous work [14], it was found that definite-time OC relays perform better than inverse-time OC relays for the remote faults in the grid-connected mode of AC microgrid. The performance of definite-time OC relays in terms of operating time and CTI between relays was even better during faults in the islanded mode with grid-forming BESS and grid-following DERs. However, the operation of fuse was not considered in that study.

The literature review indicates that there is still a research gap for the global protection coordination study in the islanded mode of AC microgrid. Particularly, due to the increasing applications of BESS along with the RES for an operational flexibility. This new phenomenon can enhance fault levels in distribution networks and microgrids. Additionally, with ever-increasing penetration levels of DERs the future grid codes are expected to demand large converter sizes or extra fault current sources for providing more than the

rated current during faults, particularly in the islanded mode of operation.

The evaluation of adaptive protection of AC microgrid using the current-limiting grid-following and grid-forming controls of converter-based DERs during the grid-connected and islanded modes was done in our previous paper [15] with 1.2 p.u. fixed fault current contribution. In this paper, the increased fault current contributions of converter-based DERs (1.2 p.u. and greater) are evaluated to check whether adaptive protection can be avoided in the islanded modes of AC microgrid. The details about various types of grid-forming controls of converter-based DERs can be found in [26] and [27]. In this paper, generic PSCAD-based models of grid-forming and grid-following converter-based DERs have been used. The converter-based DER models employ dq-control with inner current loop and outer power loop. The grid-forming control is implemented using voltage-controlled oscillator (VCO) in the islanded mode. The load and generation are closely balanced during islanded modes for voltage and frequency regulation. The maximum overcurrent during faults is limited by using a saturator block. The used grid-forming control is simplified version of the control presented in [28].

Considering the above factors, the focus of this paper is on the islanded-mode fault cases with different fault current limiting scenarios of DERs and BESS. Nevertheless, selected fault cases for the grid-connected mode are also presented for comparisons. In this regard, maximum load current at each OC relay has been found in different grid-connected and islanded modes of the considered harbor area AC microgrid-1. Then following questions have been addressed:

- What will be the magnitude of fault current at each OC relay during the remote three-phase SC faults in different grid-connected and islanded modes of the considered AC microgrid-1?
- In which fault cases of islanded mode operation and at what fault current levels of converter-based DERs and BESS the protection coordination and fuse operation will be ensured, and adaptive OC protection be avoided by using the same grid-connected mode definite-time OC settings of relays?

The rest of the paper is organized in a way that Section II presents the detailed fault study and evaluation of OC protection of the proposed harbor area AC microgrid-1 during both grid-connected and islanded modes with different scenarios of fault current contributions of DERs and BESS. Section III includes discussion and summary of results and Section IV concludes the paper.

II. FAULT STUDY AND EVALUATION OF PROTECTION OF THE HARBOR AREA AC MICROGRID-1

The operational modes of the proposed harbor area AC microgrid-1 (Fig. 1) can be broadly divided into two categories: (1) Grid-connected mode (2) Islanded mode. Each of the two mentioned operational modes can be subdivided into two further modes: (a) Slow-charging of container-based vessel-BESS during night with no cold-ironing load; (b) Power supply to cold-ironing load with no slow-charging of the container-based vessel-BESS. Again, during the power supply to cold-ironing load, it should be considered if the vessel type/load type is 50 Hz or 60 Hz.

If vessel type/load type is 60 Hz, then it has to be supplied through the frequency converter that can only provide fault current up to twice the magnitude of the nominal current for a duration of *two* seconds [29] or less for faults at and downstream of 0.69 kV port bus in both grid-connected and islanded modes of operation. Therefore, irrespective of grid-connected or islanded mode of operation, all OC protection relays or IEDs (intelligent electronic devices) downstream of the frequency converter need to be more sensitive for 60 Hz cold-ironing load/vessel type.

On the other hand, for the 50 Hz cold-ironing load the OC protection IEDs will need different settings for grid-connected and islanded modes. The islanded-mode settings will greatly depend upon the short-circuit current from DERs and BESS. The number of OC protection IEDs is equal to number of circuit breakers (CBs) at various locations in Fig. 1 and each CBxx is operated by the related IED referred later in this paper as IEDxx. The frequency converter and battery chargers are primarily protected with fast acting fuses and local OC protection IEDs act as backup for fuses. In this paper, only the OC function has been considered for the proposed AC microgrid-1 (Fig. 1), therefore all IEDs referred to in the following subsections are OC protection IEDs with definite-time coordination. The fault analysis and tripping response of OC devices for different operational modes are given in the following subsections.

A. FAULTS DURING GRID-CONNECTED MODE

When the proposed harbor area AC microgrid-1 is operated in the grid-connected mode, the maximum fault current contribution has to come naturally from the main grid. The fault current contributions from DERs have to be minimum in the grid-connected mode for any downstream fault within AC microgrid or any upstream fault on the main grid. In order to find the maximum possible load current at each IED, all DERs including the 2 MVA BESS at 0.69 kV harbor bus are disconnected in the first step and the load currents at all IEDs are obtained with only the main-grid connected.

Table 1 shows magnitudes of load currents, I (A) and voltages, V_{ph-ph} (kV) at all IEDs except IEDs 6-10,13-14, 16-18 and 23 when all power is supplied from the main grid and only 50 Hz cold-ironing load and harbor bus load are connected. With the final voltage level of 0.96 p.u. at 2 MW, 50 Hz ship load terminal a peak load demand of 92.5% is met with these voltage settings due to an impedance-based voltage-dependent load.

Table 2 shows magnitudes of load currents and voltages at all IEDs except IEDs 6-10, 13-15, 18 and 23 when all power is supplied from the main grid and only 60 Hz cold-ironing

TABLE 1. Currents & voltages at IEDs when only the main grid supplies power to 50 Hz cold-ironing & harbor load (no DER mode).

IED#	I (A)	V_{ph-ph} (kV)	IED#	I (A)	V_{ph-ph} (kV)
IED1	18.96	110	IED12	1647.5	0.682
IED2	18.96	110	IED15	1644	0.682
IED3	100.4	20.33	IED19	1644	0.682
IED4	100.4	20.31	IED20	171.5	6.33
IED5	101.34	20.03	IED21	171.5	6.33
IED11	57.29	20.03			

TABLE 2. Currents & voltages at IEDs when only the main grid supplies power to 60 Hz cold-ironing & harbor load (no DER mode).

IED#	I (A)	V_{ph-ph} (kV)	IED#	I (A)	V_{ph-ph} (kV)
IED1	20.1	110	IED12	1825	0.687
IED2	20.1	110	IED16	1825	0.683
IED3	106.8	20.3	IED17	1748	0.725
IED4	106.8	20.3	IED19	1748	0.725
IED5	107.5	20.02	IED20	182.6	6.72
IED11	63.25	20.02	IED22	182.6	6.72

TABLE 3. Currents & voltages at IEDs when only the main grid supplies power to depleted vessel-BESS & harbor load (no DER mode).

IED#	I (A)	V_{ph-ph} (kV)	IED#	I (A)	V_{ph-ph} (kV)
IED1	11.84	110	IED13	18.63	20.2
IED2	11.84	110	IED14	540	0.694
IED3	62.67	20.4	IEDX	299	0.695
IED4	62.67	20.38	IEDY	299	0.695
IED5	63.16	20.2	IEDZ	299	0.695

load and harbor bus load are connected. With the final voltage level of 1.02 p.u. at the 2 MW 60 Hz ship load terminal a peak load demand of 100% is met with these voltage settings. This is possible due to increased voltage of 1.05 p.u. (0.725 kV/0.69 kV) at the output of frequency converter. Table 3 gives magnitudes of load currents and voltages at all IEDs except IEDs 6-12 and 15-23 when all power is supplied from the main grid and only container-based vessel-BESS and the harbor bus load are connected.

Table 4 and Table 5 show load currents and voltages at the active IEDs in case of power supply to 50 Hz and 60 Hz cold-ironing loads, respectively when both WTG and PV system are also operating in parallel to the main grid. Table 6 shows load currents and voltages in case of power supply to depleted vessel-BESS for slow charging during the night when only the WTG is operating in parallel to the main grid. In this case it is assumed that the PV system will be naturally out of service during the night and BES (battery energy storage) at PV system may not be available. Moreover, slow charging of the depleted vessel-BESS requires less power (0.6-0.75 MW) as compared to 2 MW for cold-ironing load. Therefore, it is not feasible to charge depleted vessel-BESS by BES at PV location even if sufficient storage is available until and unless the WTG is also out of service.

First, magnitudes of load currents during different operational modes are obtained by simulations as presented in Table 1-6. Then the maximum magnitude of load current ($I_{max-load}$) at each IED (green highlight) is selected from these calculations as the basis for OC settings. Pickup

TABLE 4. Currents & voltages at IEDs when the main grid, WTG and PV supply power to 50 Hz cold-ironing and harbor load.

IED#	I (A)	V_{ph-ph} (kV)	IED#	I (A)	V_{ph-ph} (kV)
IED1	2.12	110	IED9	27.44	20.59
IED2	2.12	110	IED11	58.7	20.5
IED3	16.7	20.48	IED12	1687.8	0.701
IED4	16.7	20.48	IED15	1682.9	0.701
IED5	12.93	20.5	IED19	1682.9	0.701
IED6	82.06	20.5	IED20	176.14	6.49
IED7	79.68	20.98	IED21	176.14	6.49
IED8	28.73	20.5			

TABLE 5. Currents & voltages at IEDs when the main grid, WTG and PV supply power to 60 Hz cold-ironing and harbor load.

IED#	I (A)	V_{ph-ph} (kV)	IED#	I (A)	V_{ph-ph} (kV)
IED1	3.51	110	IED9	27.43	20.6
IED2	3.51	110	IED11	64.8	20.5
IED3	24	20.5	IED12	1870	0.703
IED4	24	20.5	IED16	1870	0.699
IED5	20.2	20.517	IED17	1790	0.746
IED6	82.03	20.518	IED19	1790	0.746
IED7	79.65	21	IED20	187	6.9
IED8	28.72	20.518	IED22	187	6.9

TABLE 6. Currents & voltages at IEDs when the main grid and WTG supply power to depleted vessel-BESS and harbor load.

IED#	I (A)	V_{ph-ph} (kV)	IED#	I (A)	V_{ph-ph} (kV)
IED1	4.1	110	IED7	79.46	21.05
IED2	4.1	110	IED13	18.25	20.56
IED3	26.65	20.5	IED14	528.5	0.709
IED4	26.65	20.5	IEDX	303.75	0.708
IED5	23.42	20.56	IEDY	303.75	0.708
IED6	81.85	20.56	IEDZ	303.75	0.708

TABLE 7. Pickup current threshold settings of all considered IEDs.

IED#	I>>	I>	IED#	I>>	I>	IED#	I>>	I>
IED1	50.3	25.15	IED8	71.8	35.9	IED21	440.4	220.2
IED2	50.3	25.15	IED9	68.6	34.3	IED13	46.6	23.3
IED3	267	133.5	IED11	162	81	IED14	1350	675
IED4	267	133.5	IED12	4675	2338	IEDX	759.4	379.7
IED5	269	134.5	IED15	4207	2104	IEDY	759.4	379.7
IED6	205	102.5	IED19	4475	2238	IEDZ	759.4	379.7
IED7	199	99.6	IED20	467.5	234	-		

I>> Threshold of OC stage (A), I> Threshold of overload stage (A)

currents of all two-stage IEDs have been set at 2.5 times $I_{max-load}$ for OC stage ($I\gg$) and 1.25 times $I_{max-load}$ for the overload stage ($I>$) as given in Table 7. The definite-time delay settings for all considered IEDs are given in Table 8. These delay settings of IEDs remain unchanged irrespective of the grid-connected or islanded mode. Relatively long time delays for IEDs related to DERs (Table 8 in red color) ensure required low voltage ride-through (LVRT) and remote backup protections for IEDs in the fault path. The DERs are set to provide fault currents up to 1.2 p.u. of base or rated current in the grid-connected mode.

1) THREE-PHASE FAULT AT 50 HZ COLD-IRONING LOAD WHEN SUPPLIED BY MAIN GRID, WTG AND PV

Protection settings of all active IEDs have been evaluated in this case during a 3-phase SC fault at 50 Hz cold-ironing

TABLE 8. Definite-time delay settings of all considered IEDs.

IED#	t_{op}	IED#	t_{op}	IED#	t_{op}
IED1	2.0	IED8	2.0	IED20	0.2
IED2	1.8	IED9	2.2	IED21	0.02
IED3	1.6	IED11	1.0	IED13	0.44
IED4	1.4	IED12	0.8	IED14	0.24
IED5	1.2	IED15	0.6	IEDX, Y, Z	0.04
IED6	2.0	IED18	2.0	FuseX, Y, Z	0.02
IED7	2.2	IED19	0.4	-	

t_{op} = Operating time (s)

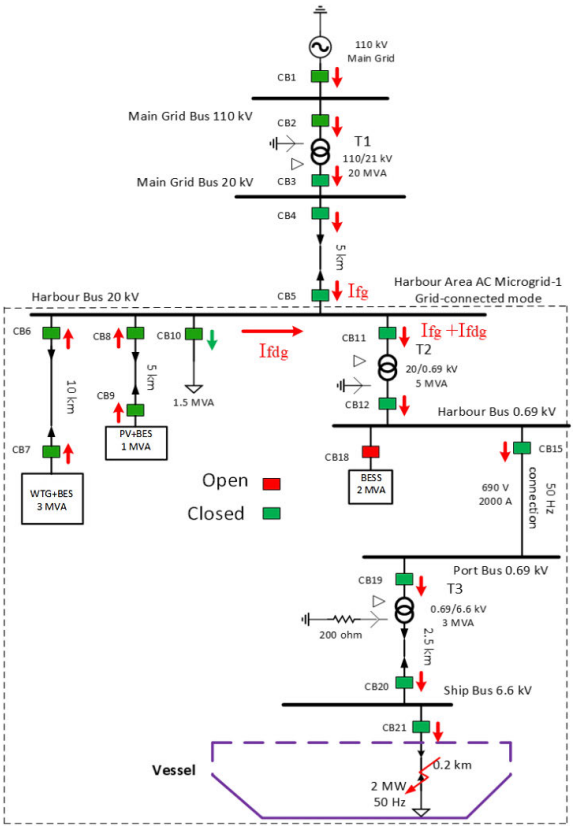

FIGURE 2. 3-phase short-circuit fault at 50 Hz cold-ironing load in grid-connected case-1.

load supplied by main grid, WTG and PV system (Fig. 2). A 3-phase SC fault is applied for a duration of 4 s, from the simulation time of 1.2 s to 5.2 s.

The rms magnitudes of fault currents at all active (green) IEDs for this case are given in Table 9. The fault current magnitudes at IEDs 1-5, 11-12, 15, 19-21 are well above the pickup settings of 2.5 x $I_{max-load}$ for OC stage of IEDs during the considered 3-phase fault. Therefore, not only the primary IED21 will pick up and trip but all upstream IEDs to IED21 will also pick up during 3-phase SC fault at 50 Hz cold-ironing load for providing backup protection in case of CB21 failure.

TABLE 9. Voltages and currents at active IEDs during 3-phase short-circuit fault at 50 Hz cold-ironing load in grid-connected case-1.

IED#	I (A)	V_{ph-ph} (kV)	IED#	I (A)	V_{ph-ph} (kV)
IED1	110.2	110	IED9	32.52	17.35
IED2	110.2	110	IED10	38.1	17.25
IED3	588	18.22	IED11	642	17.25
IED4	588	18.22	IED12	18580	0.413
IED5	591.5	17.25	IED15	18554	0.413
IED6	94.81	17.25	IED19	18561.5	0.413
IED7	92.95	17.8	IED20	1937.47	0.0975
IED8	33.55	17.25	IED21	1937.47	0.011

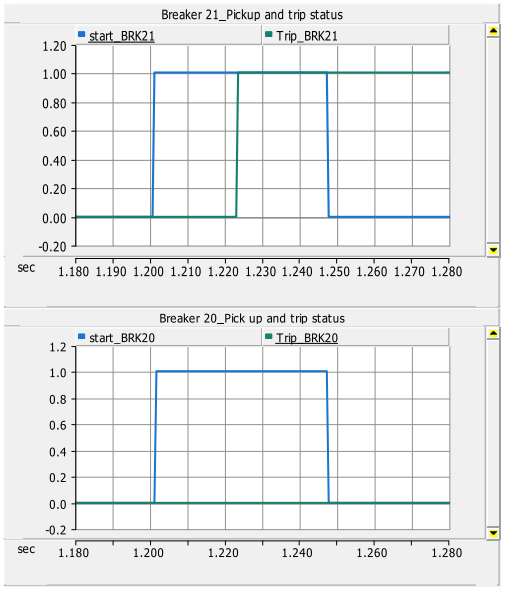

FIGURE 3. Pickup (start) and tripping status of primary IED21 & backup IED20 during 3-phase SC fault at 50 Hz cold-ironing load in grid-connected case-1 (start_BRK21 = pickup signal for IED21, trip_BRK21 = tripping status of IED21 with status 0 = closed and status 1 = open).

The pickup and tripping status signals of primary IED21 and the first backup IED20 are shown in Fig. 3. It can be observed from Fig. 3 that IED21 trips within the required 20 ms of 3-phase SC fault and backup IED20 also picks up.

The rms magnitude of fault current per phase at IED21 is shown in Fig. 4. The fault current contribution from DERs during 3-phase SC fault at 50 Hz cold-ironing load is lower than the current limiter setting (I-lim) of 1.2 p.u. of base current (Fig. 5) that is calculated at the rated voltage and rated power capacity of the DER. Therefore, IEDs 6-9 can only see the fault currents up to 1.15-1.18 times $I_{max-load}$ and these will neither pick up nor trip falsely for this fault case in grid-connected case-1.

2) THREE-PHASE FAULT AT CHARGER-Z TERMINAL WHEN SUPPLIED BY MAIN GRID AND WTG

The protection settings of all active IEDs have been evaluated in this case during a 3-phase SC fault at charger-Z terminal when supplied by main grid and WTG (Fig. 6). The rms

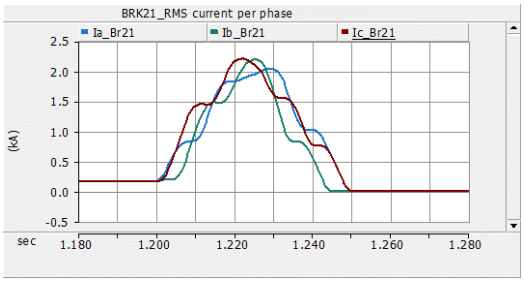

FIGURE 4. Magnitude of current per phase of primary IED21 during 3-phase SC fault at 50 Hz cold-ironing load in grid-connected case-1 (Ia_Br21, Ib_Br21, Ic_Br21 = line currents at IED21).

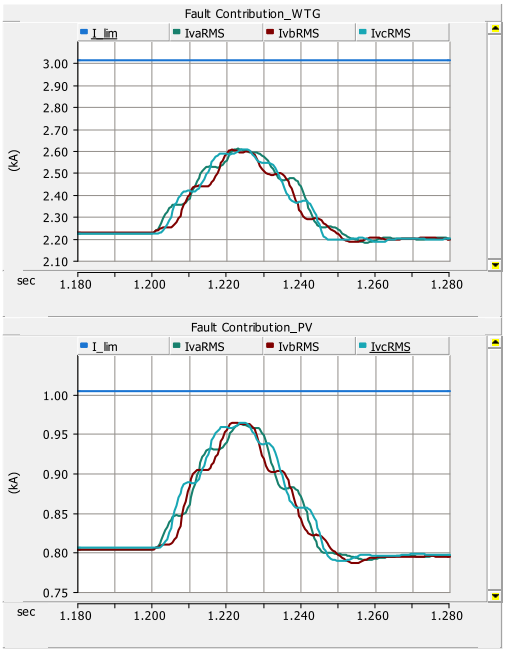

FIGURE 5. Magnitude of fault current contribution per phase by WTG and PV system during a 3-phase SC fault at 50 Hz cold-ironing load in grid-connected case-1 (I_lim = Current limiter setting of the DER, IvaRMS, IvbRMS, IvcRMS = Line currents at LV terminals of DERs).

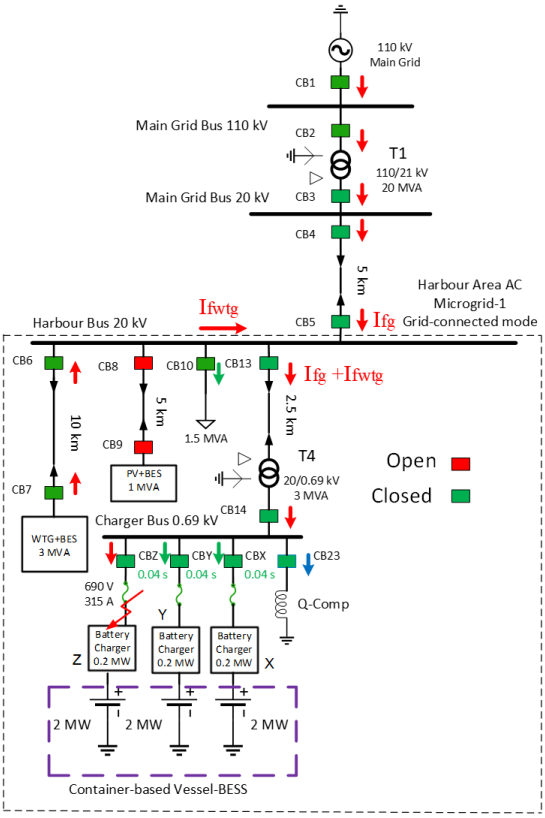

FIGURE 6. 3-phase short-circuit fault at charger-Z terminal in grid-connected case-2.

TABLE 10. Voltages and currents at active IEDs during 3-phase short-circuit fault at charger-Z terminal in grid-connected case-2.

IED#	I (A)	V_{ph-ph} (kV)	IED#	I (A)	V_{ph-ph} (kV)
IED1	213	110	IED10	30.7	14.3
IED2	213	110	IED13	1210	13.88
IED3	1144	16.95	IED14	35100	0.204
IED4	1144	16.95	IEDX	100	0.26
IED5	1145	14.3	IEDY	100	0.26
IED6	105	14.5	IEDZ	35000	decay to zero
IED7	103.5	13.9			

magnitudes of fault currents at all active IEDs are given in Table 10. The fault current magnitudes at IEDs 1-5, 13-14 and IEDZ are well above pickup settings of 2.5 x $I_{max-load}$ for OC stage of IEDs during the considered 3-phase SC fault. Therefore, not only the primary IEDZ will pick up and trip but all upstream IEDs to the IEDZ will also pick up during a 3-phase SC fault at charger-Z terminal and provide backup protection in case of CBZ failure.

The rms magnitude of fault current per phase at IEDZ during 3-phase SC fault at charger-Z terminal is shown in Fig. 7. The pickup and tripping status signals of primary IEDZ and the nearest/first remote backup of IEDZ, that is, IED14 are shown in Fig. 8. It can be seen from Fig. 8 that the IEDZ opens CBZ within the required delay of 40 ms after the fault. The pickup status of IED14 shows that it will act as a backup for IEDZ if CBZ fails to open. It should be noted that the IEDs X, Y, and Z act as backups for the fast acting fuses at these locations and these are coordinated with fuses with a coordination delay of 20 ms. The fast acting fuseZ blows within 20 ms of the 3-phase SC fault (Fig. 9).

The fault current contribution per phase from the WTG operating in parallel to the main grid during a 3-phase SC fault at charger-Z terminal is shown in Fig. 10. The WTG supplies the fault current contribution up to the current limiter setting (I-limit) of 1.2 p.u. of base current during this scenario. The IED6 and IED7 can sense the fault current magnitude of about 1.3 × $I_{max-load}$ (compared with Table 6 values) that is less

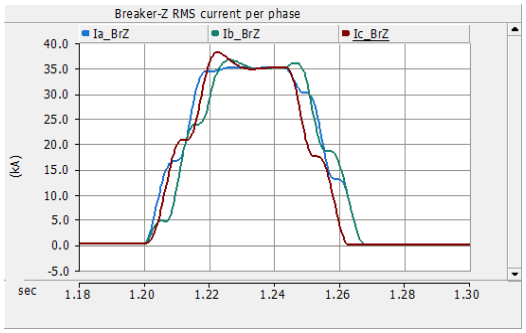

FIGURE 7. Magnitude of current per phase of IEDZ during 3-phase SC fault at charger-Z terminal in grid-connected case-2 (Ia_BrZ, Ib_BrZ, Ic_BrZ = line currents at IEDZ, Br = BRK = breaker).

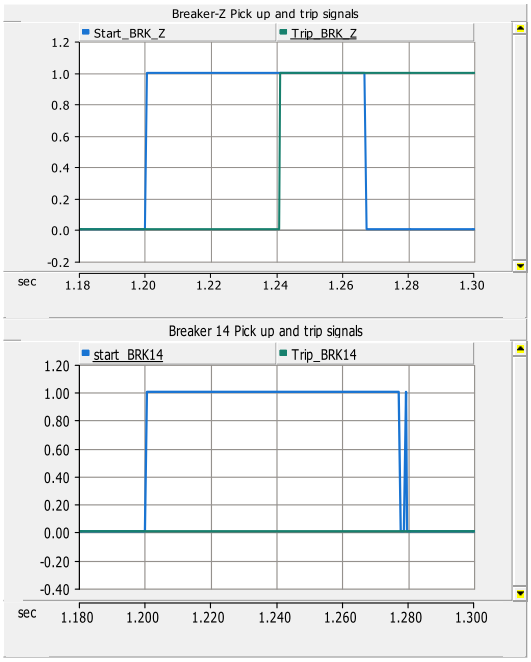

FIGURE 8. Pickup and tripping status of primary IEDZ and backup IED14 during 3-phase SC fault at charger-Z terminal in grid-connected case-2.

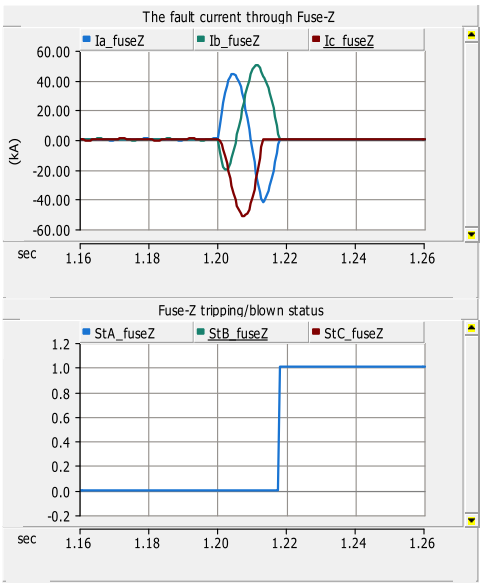

FIGURE 9. Magnitude of current per phase through fuseZ and its tripping/blown status during 3-phase SC fault at charger-Z terminal in grid-connected case-2 (StA_fuseZ = status of fuse, 1 = open, 0= closed).

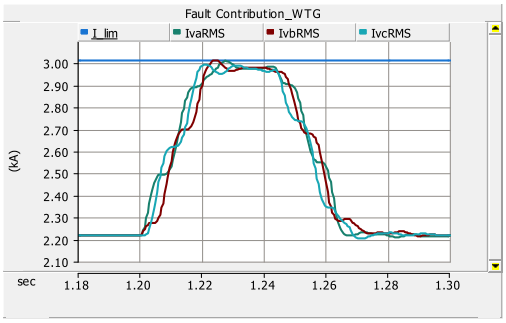

FIGURE 10. Magnitude of fault current contribution per phase by WTG during 3-phase SC fault at charger-Z terminal in grid-connected case-2.

than the set OC stage limit of 2.5 $\times$ $I_{max-load}$. Hence no OC pickup and nuisance tripping will occur at IED6 and IED7 during a 3-phase SC fault at charger-Z terminal in the grid-connected case-2.

B. FAULTS DURING ISLANDED MODE

The islanded mode operation for the proposed AC Microgrid-1 will occur when the main grid is out of service, for example, due to the maintenance or fault on any part of connecting network. In the islanded mode with CB4 and CB5 open, both WTG and PV system are normally available to supply power to the cold-ironing and the harbor area loads during the daytime and only the WTG during the nighttime when the depleted vessel-BESS are being charged.

In the islanded mode it is required to operate the largest DER source like the WTG as the grid-forming DER while the smaller sources like PV system and if required the BESS at 0.69 kV harbor bus as the grid-following DERs according to IEEE Std. 1547.4-2011. In this regard, the DERs in the islanded mode are controlled in a manner to supply the required power to the harbor bus load and the cold-ironing load while maintaining the voltage and frequency at their terminals within the allowed limits. The WTG in the islanded mode operates as the grid-forming DER and both the PV system and BESS at 0.69 kV harbor bus operate as the grid-following DERs.

The same grid-connected OC settings are used for all IEDs in six islanded mode fault cases. The fault analysis and evaluation of selected OC settings of IEDs for six islanded mode

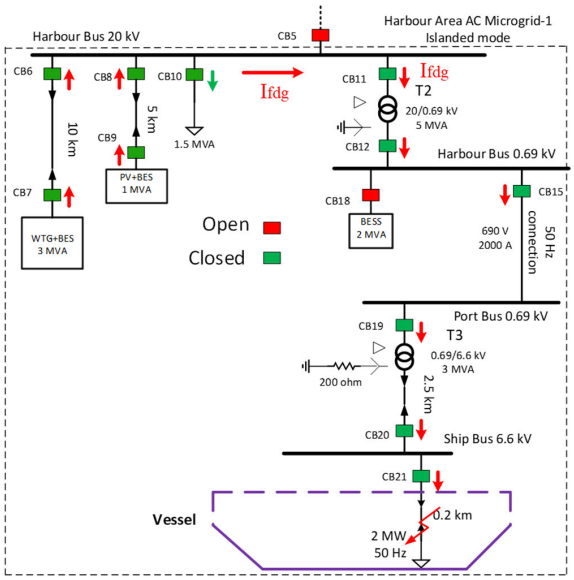

FIGURE 11. 3-phase short-circuit fault at 50 Hz cold-ironing load when supplied by WTG and PV during islanded mode 1.

cases with different scenarios of fault current contribution of DERs are explained in the next subsections. A 3-phase SC fault is applied for a duration of 4 s from the simulation time of 1.2 s to 5.2 s for most of the islanded mode cases, otherwise specified. The main purpose of all islanded mode cases is to check whether the fuses, primary OC IEDs and remote backup OC IEDs pick up and trip using the same grid-connected mode settings (2.5 x $I_{max-load}$) with different fault current contributions of DERs. If the answer is *YES*, then adaptive protection settings can be avoided in those islanded mode cases.

1) FAULTS AT 50 HZ COLD-IRONING LOAD WHEN WTG AND PV SUPPLY FAULT CURRENT

Fig.11 describes the islanded mode 1, where the green color indicates the closed or active IEDs and red color indicates the open or inactive IEDs. The combined fault current contribution of WTG and PV is denoted by I_{fdg}. The islanded mode 1 is further subdivided into two case studies: One related to fault current contribution of 1.2 p.u. from DERs and the other related to fault current contribution of 2 p.u. from DERs.

a: FULT CURRENT CONTRIBUTION OF 1.2 P.U. FROM DERs

Table 11 shows fault current magnitudes at all active IEDs in the fault path during a 3-phase SC fault at 50 Hz cold-ironing load in the islanded mode 1a. The fault current magnitudes at IEDs in Table 11 can be compared with maximum load currents (green-highlighted) of IEDs in Table 2-6. The results presented in Table 11 show that fault current magnitudes of 2.01-2.24 x $I_{max-load}$ are observed at IEDs 11-12, 15 and 19-21 in the islanded mode 1a that are lower than set OC

TABLE 11. Voltage and current at active IEDs during 3-phase short-circuit fault at 50 Hz cold-ironing load when supplied by WTG and PV during islanded mode 1A.

IED#	I (A)	V_{ph-ph} (kV)	IED#	I (A)	V_{ph-ph} (kV)
IED6	105.1	3.51	IED12	3780	0.084
IED7	103.75	3.89	IED15	3780	0.084
IED8	35	3.51	IED19	3780	0.084
IED9	34.5	3.61	IED20	395	0.0225
IED10	10.05	3.51	IED21	395	0.0225
IED11	130.5	3.51			

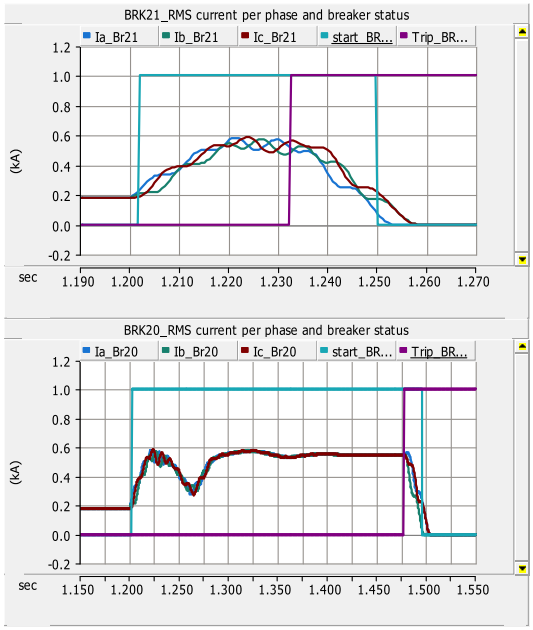

FIGURE 12. Magnitude of current per phase, pickup and tripping status of primary IED21 and backup IED20 during a 3-phase SC fault at 50 Hz cold-ironing load in islanded mode 1b.

tripping thresholds of 2.5 x $I_{max-load}$. This concludes that a fault current contribution of 1.2 p.u. from both WTG and PV system will not prevent adaptive OC settings in the islanded mode 1a. Only overload stages of IEDs will work in this mode.

b: FAULT CURRENT CONTRIBUTION OF 2 P.U. FROM DERs

Fig. 12 shows tripping responses of primary IED21 and backup IED20 during a 3-phase SC fault in the islanded mode 1b. Fig. 13 reveals that in the islanded mode 1b maximum fault current contribution comes from the nearest PV system and reduced fault current contribution comes from the WTG.

From Fig. 12 it is clear that IED21 trips within 32 ms of the 3-phase SC fault instead of the required tripping time of 20 ms (see Table 8). This means that the use of grid-connected mode settings in the islanded mode 1b causes 12 ms slower tripping response of primary IED21. This slower response of primary IED21 is due to the slower fault current ramp-up

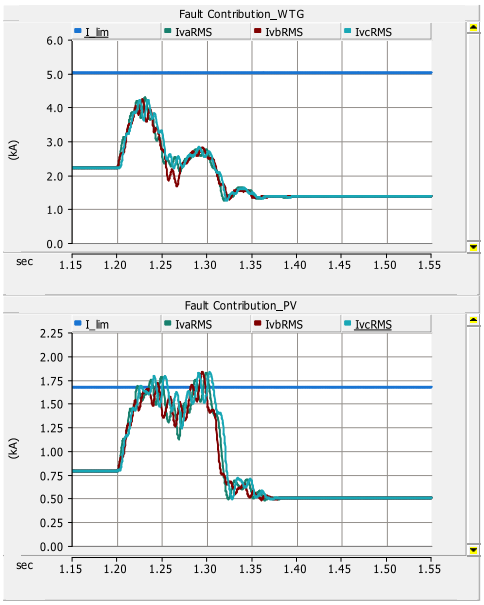

FIGURE 13. Magnitude of fault current contribution per phase by WTG and PV system during a 3-phase SC fault at 50 Hz cold-ironing load in islanded mode 1b.

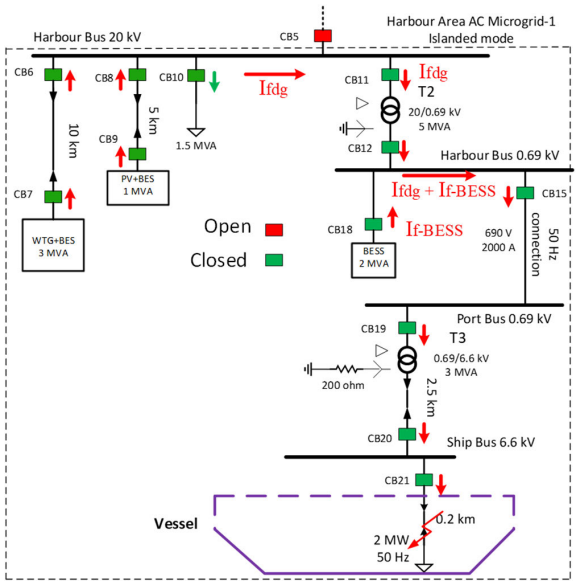

FIGURE 14. 3-phase short-circuit fault at 50 Hz cold-ironing load when supplied by WTG, PV and harbor-BESS during islanded mode 2.

time of DERs to reach to the required current level of the tripping threshold. The slower tripping responses of 75-79 ms are also observed at all backup IEDs in the fault path (IED20-19-15-12-11) that are set with a definite-time CTI of 200 ms between each primary IED and upstream backup IED. For example, Fig. 12 shows that after CB21 failure happens, the first backup IED20 will trip at simulation time of 1.475 s. It means the first backup IED20 will now trip within 275 ms instead of required 200 ms (20 ms + 180 ms) with a new CTI of 275-32 = 243 ms. In this case, the backup IED20 is 75 ms slower than set time delay. Despite the slower tripping response at each IED, the increased fault current contribution of 2 p.u. from DERs in the islanded mode 1b will potentially avoid adaptive OC settings during a 3-phase SC fault at 50 Hz cold-ironing load. For the sake of brevity, tripping responses of only primary IED and first backup IED are shown in Fig. 12.

2) FAULTS AT 50 HZ COLD-IRONING LOAD WHEN WTG, PV, AND HARBOR-BESS SUPPLY FAULT CURRENT

This is an extended case of the previous islanded mode 1 and in this case the BESS at 0.69 kV harbor bus is also used as a fault current source in addition to WTG and PV system during a 3-phase SC fault at 50 Hz cold-ironing load. In the islanded mode case 2 (Fig. 14) the BESS at 0.69 kV harbor bus is activated within 10 ms after the fault detection to provide extra fault current contribution. The purpose of connecting BESS is to check if the delayed tripping of primary IED21 and backup IEDs can be avoided.

The islanded mode 2 (Fig. 14) is further subdivided into three cases: First related to fault current contributions of 1.2 p.u. from harbor-BESS and 2 p.u. from DERs, second related to fault current contributions of 2 p.u. from harbor-BESS and DERs, and third related to fault current contributions of 3 p.u. from harbor-BESS and DERs. In Fig. 14, I_{fdg} denotes the combined fault current contribution from WTG and PV and I_{f-BESS} denotes the fault current contribution from BESS.

a: FAULT CURRENT CONTRIBUTION OF 1.2 P.U. FROM HARBOR-BESS AND 2 P.U. FROM THE WTG AND PV SYSTEM

Fig. 15 shows the tripping response of primary IED21 and backup IED20 during a 3-phase SC fault at 50 Hz cold-ironing load in the islanded mode 2a. Fig. 16 reveals that the maximum fault current contribution comes from the nearest DERs (BESS and PV system), and reduced fault current contribution comes from the distant WTG. From Fig. 15 it is clear that primary IED21 trips at simulation time of 1.232 s that is after 32 ms of the 3-phase SC fault instead of the required tripping time of 20 ms resulting in 12 ms slower tripping response in islanded mode 2a.

The first backup IED20 trips at simulation time of 1.458 s that is within an extended coordination time delay of 226 ms when IED21 or CB21 fails to trip. The second and third backups IED19 and IED15 trip within 201 ms and 196 ms coordination delay at simulation times of 1.659 s and 1.855 s, respectively. The fourth backup IED12 results in coordination delay of 217 ms because it trips at simulation time of 2.072 s instead of 2.055 s. The fifth backup IED11 trips at simulation time 2.271 s with 199 ms coordination delay. It is concluded

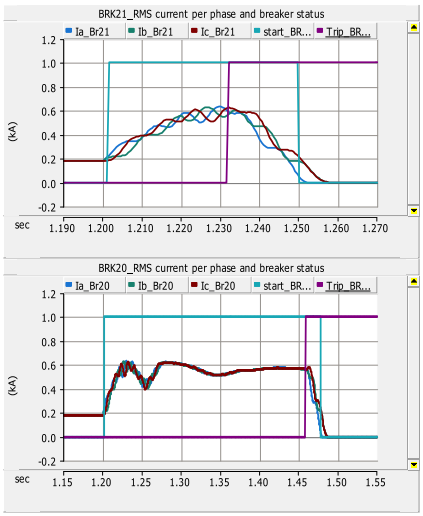

FIGURE 15. Magnitude of current per phase, pickup and tripping status of primary IED21 and backup IED20 during a 3-phase SC fault at 50 Hz cold-ironing load in islanded mode 2a.

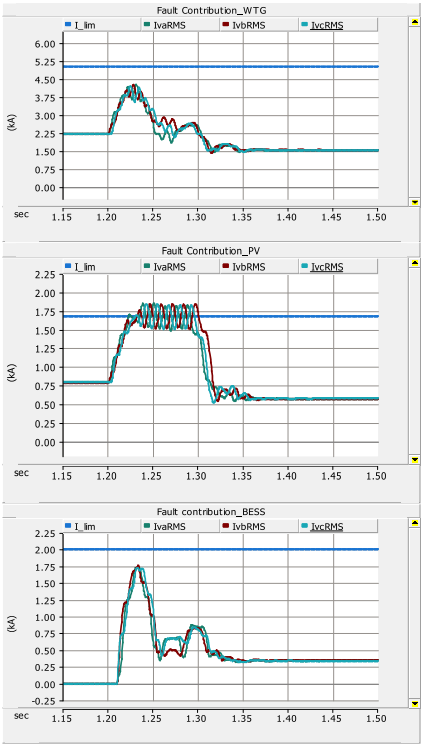

FIGURE 16. Magnitude of fault current contribution per phase by WTG, PV system and harbor-BESS during a 3-phase SC fault at 50 Hz cold-ironing load in islanded mode 2a.

that islanded mode 2a avoids both adaptive OC settings and slower tripping response of all backup IEDs in the fault path except primary IED21, backup IED20 and backup IED12.

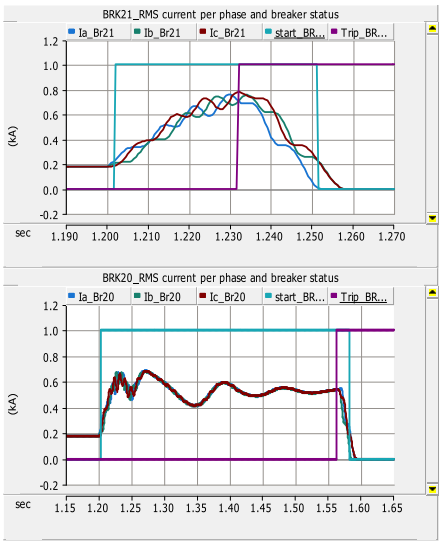

FIGURE 17. Magnitude of current per phase, pickup and tripping status of primary IED21 and backup IED20 during a 3-phase SC fault at 50 Hz cold-ironing load in islanded mode 2b.

b: FAULT CURRENT CONTRIBUTION OF 2 P.U. FROM THE WTG, PV SYSTEM, AND HARBOR-BESS

It is evident from Fig. 17 that in islanded mode 2b the tripping response of the primary IED21 is similar to that of the islanded mode 2a. The primary IED21 trips at simulation time of 1.232 s that is 12 ms slower than the required 20 ms tripping time. The first backup IED20 trips with new coordination time of 330 ms at simulation time of 1.562 s in islanded mode 2b (Fig. 17). The second and third backups IED19 and IED15 trip within 200 ms and 194 ms coordination delays at simulation times of 1.762 s and 1.956 s, respectively. The fourth and fifth backups IED12 and IED11 trip at simulation times of 2.065 s and 2.266s respectively resulting in respective coordination delays of 109 ms and 201 ms in islanded mode 2b. The fault current contributions of WTG, PV and harbor-BESS are presented in Fig. 18 for islanded mode 2b. The primary IED21 gives a similar tripping response irrespective of the fault current contribution of 1.2 p.u. or 2 p.u. from the harbor-BESS. It is concluded that in case 2b adaptive OC settings are avoided with similar coordination problems as in case 2a.

c: FAULT CURRENT CONTRIBUTION OF 3 P.U. FROM THE WTG, PV SYSTEM, AND HARBOR-BESS

From Fig. 19 it is clear that primary IED21 trips at simulation time of 1.232 s that is after 32 ms of the 3-phase SC fault resulting in 12 ms slower than required tripping response of 20 ms in islanded mode 2c. The first backup IED20 trips at simulation time of 1.412 s that is within the coordination delay of 180 ms when IED21 or CB21 fails to trip. Similarly, the second and third backups IED19 and IED15 trip within 200 ms coordination delays at simulation times of 1.612 s

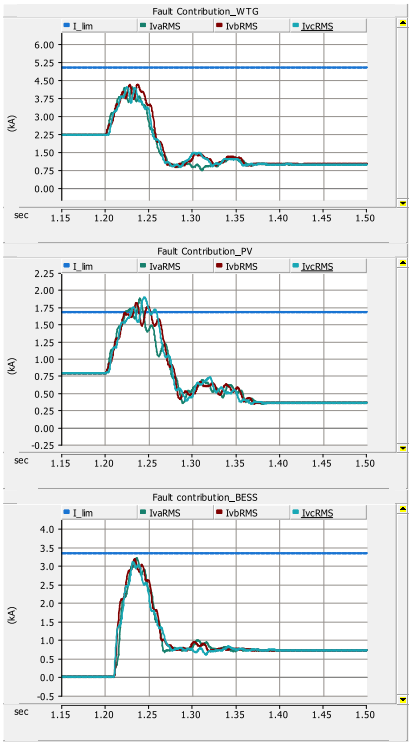

FIGURE 18. Magnitude of fault current contribution per phase by WTG, PV system and harbor-BESS during a 3-phase SC fault at 50 Hz cold-ironing load in islanded mode 2b.

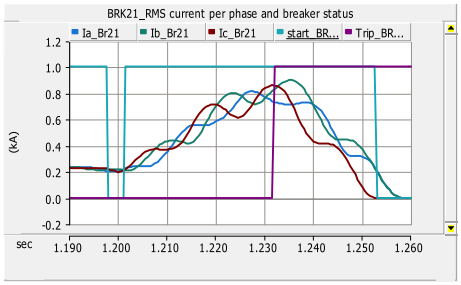

FIGURE 19. Magnitude of current per phase, pickup and tripping status of primary IED21 during a 3-phase SC fault at 50 Hz cold-ironing load in islanded mode 2c.

and 1.812 s, respectively. However, the fourth backup IED12 results in an extended coordination delay of 218 ms, that is 18 ms more than required because it trips at simulation time of 2.03 s instead of 2.012 s. The fifth backup IED11 trips at simulation time 2.23 s with 200 ms coordination delay. The results of only primary IED21 are shown in Fig. 19 and the rest of the results of islanded mode 2c are not shown for the sake of brevity. It is concluded that islanded mode 2c avoids both adaptive OC settings and slower tripping response of all backup IEDs in the fault path except one, the fourth backup IED12 that is delayed by 18 ms.

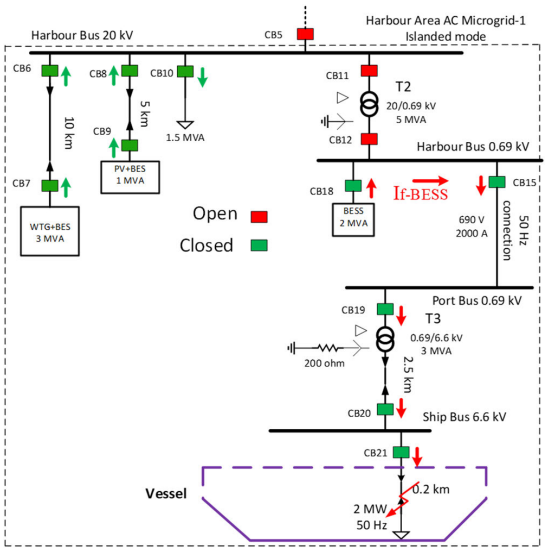

FIGURE 20. 3-phase short-circuit fault at 50 Hz cold-ironing load when supplied by only harbor-BESS during islanded mode 3.

3) FAULTS AT 50 HZ COLD-IRONING LOAD WHEN ONLY THE HARBOR-BESS SUPPLIES FAULT CURRENT

This case can be termed as an emergency case when the connection to WTG, PV system and related battery storages is lost in the islanded mode due to the fault at stepdown transformer T2 at 20 kV harbor bus. In this islanded mode 3 (Fig. 20) the BESS at 0.69 kV harbor bus can be used to supply 50 Hz cold-ironing load until the upstream fault is removed. The protection system in this case should also respond to any fault at or upstream to the cold-ironing load. Because only single DER source is available in this case so its fault current contribution should be enough to cause pickup and tripping of all the corresponding protection IEDs in the fault path.

The islanded mode 3 (Fig. 20) is further subdivided into two case studies: One related to fault current contribution of 2.5 p.u. from the harbor-BESS and the other related to fault current contribution of 3 p.u. from the harbor-BESS. In the islanded modes 3a and 3b, the duration of applied fault is 5.2 s from the simulation time of 1.2 s to the simulation time of 6.4 s to check if overload stages of IEDs also pick up and trip. Because the power rating of the cold-ironing load and the harbor-BESS is the same, that is 2 MW, therefore neither the fault current contribution of 1.2 p.u. nor the fault current contribution of 2 p.u. from the harbor-BESS will help avoiding adaptive OC settings of IED21. At 2 p.u. of the fault current contribution from harbor-BESS, only the overload stage of IED21 and backup IEDs will pick up and trip keeping the same OC settings as in the grid-connected mode.

a: FAULT CURRENT CONTRIBUTION OF 2.5 P.U. FROM HARBOR-BESS

Fig. 21 shows the tripping response of primary IED21 and backup IED20 during a 3-phase SC fault at 50 Hz

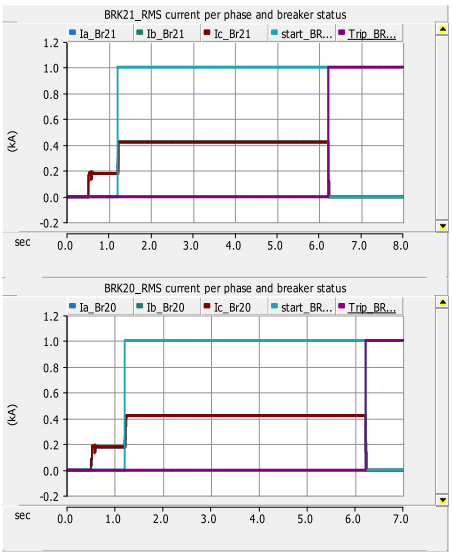

FIGURE 21. Magnitude of current per phase, pickup and tripping status of primary IED21 and backup IED20 during a 3-phase SC fault at 50 Hz cold-ironing load in islanded mode 3a.

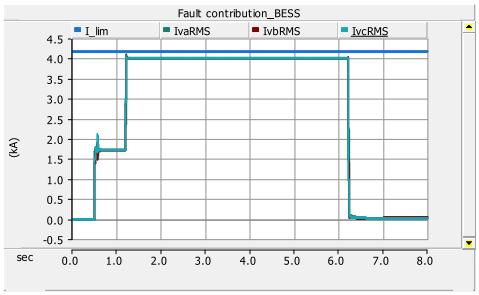

FIGURE 22. Magnitude of fault current contribution per phase by harbor-BESS during a 3-phase SC fault at 50 Hz cold-ironing load in islanded mode 3a.

cold-ironing load when harbor-BESS is set to provide fault current of 2.5 p.u. in islanded mode 3.

It is clear from Fig. 21 that only the overload stages of both primary IED21 and backup IED20 pick up and trip because harbor-BESS provides a fault current contribution of somewhat less than 2.5 p.u. in islanded mode 3a (Fig. 22). Therefore, fault current magnitudes observed at IED21 and IED20 are less than the corresponding OC setting thresholds of $2.5 \times I_{max-load}$. Other backup IEDs (IED19 and IED15) also give similar tripping response in this case. This concludes that fault current contribution of 2.5 p.u. from harbor-BESS will not avoid adaptive setting in islanded mode 3a.

b: FAULT CURRENT CONTRIBUTION OF 3 P.U. FROM HARBOR-BESS

It is observed that with a default rating or capacity of 2 MVA, the harbor-BESS is not capable of providing higher than

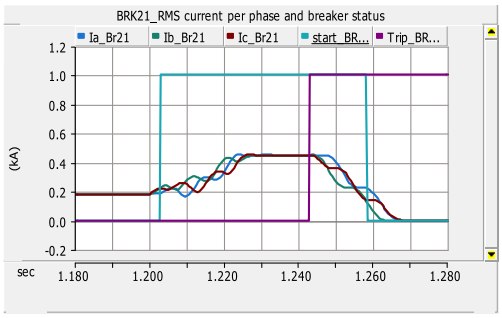

FIGURE 23. Magnitude of current per phase, pickup and tripping status of primary IED21 during a 3-phase SC fault at 50 Hz cold-ironing load when supplied by 2.2 MVA harbor-BESS in islanded mode 3b.

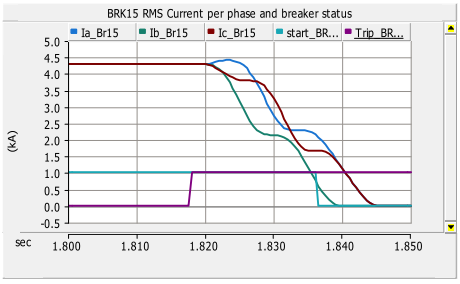

FIGURE 24. Magnitude of current per phase, pickup and tripping status of IED15 (third backup) during a 3-phase SC fault at 50 Hz cold-ironing load when supplied by 2.2 MVA harbor-BESS in islanded mode 3b.

2.5 p.u. of fault current contribution in the islanded mode 3b. It means that with a default rating the fault current contribution does not increase higher than that shown in Fig. 22 even if the maximum current limit (I-lim) is set as 3 p.u. Therefore, the tripping response of primary IED21, backup IED20 and other backup IEDs will be similar as in the previous islanded mode 3a (Fig. 21). However, with an increased rating or capacity of 2.2 MVA, the harbor-BESS is capable to provide enough fault current contribution to cause a pickup and tripping of primary IED21 during a 3-phase SC fault at 50 Hz cold-ironing load (Fig. 23). In this situation, only IED15 (third backup) will be capable of providing backup OC protection within 618 ms after the fault at simulation time of 1.818 s due to a sensed current of higher than its set tripping threshold of $2.5 \times 1683 = 4207.5$ A (see Fig. 24).

The results show that an additional installed capacity of 10 per cent of harbor-BESS will avoid adaptive OC settings with somehow slower tripping response (40 ms instead of 20 ms) of primary IED21 and limited backup OC protection only by IED15 in islanded mode 3b. The fault current contribution of 2.2 MVA harbor-BESS in islanded mode 3b is shown in Fig. 25. An additional installed capacity of 25 per cent of harbor-BESS (2 MVA+0.5 MVA) will avoid adaptive OC settings, reduce primary IED21 tripping response to 30 ms and ensure all backup IEDs (IED20, 19 and 15) pick up and trip in case of CB21 failure.

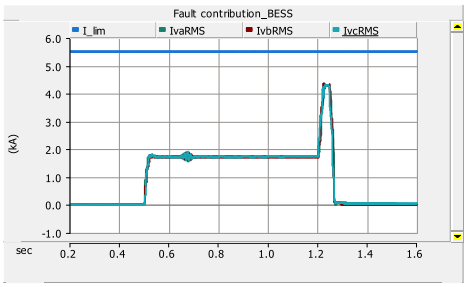

FIGURE 25. Magnitude of fault current contribution per phase by 2.2 MVA harbor-BESS during a 3-phase SC fault at 50 Hz cold-ironing load in islanded mode 3b.

4) FAULTS AT CHARGER-Z TERMINAL WHEN ONLY THE WTG SUPPLIES FAULT CURRENT

In this islanded mode only the WTG supplies power to the harbor load of 1.5 MW and three depleted vessel-BESS each of 2 MWh rated capacity. The islanded mode 4 (Fig. 26) happens when the connection to the main grid is lost during the nighttime when depleted vessel-BESS are on slow charging. This mode assumes that only the WTG is available with its full rated capacity of 3 MW and PV system together with its storage (PV+BES) is out of service. With only the WTG in service supplying the rated power not only the load at harbor area can be supplied but also a power demand of 0.6 MW for slow charging of depleted vessel-BESS can easily be met in addition to some power losses. Various types of faults may happen in this mode, but the most important type of fault is at the terminals of the battery chargers. Since the battery chargers using power electronics components are relatively costly components so their fault protection is very important. The battery chargers are protected by using both the fast-acting full-range fuses and the fast-acting breakers operated by backup IEDs. Because all of the three battery chargers (charger-X, Y and Z) are identical in capacity and construction, therefore only the faults at one charger location (charger-Z) have been analyzed.

The islanded mode 4 (Fig. 26) is further subdivided into three case studies: One related to fault current contribution of 1.2 p.u. (islanded mode 4a), the second related to fault current contribution of 2 p.u. (islanded mode 4b) and third related to fault current contribution of 3 p.u. (islanded mode 4c) from the WTG. The main purpose of selecting different fault current levels of the WTG is to check proper operation of fuses and backup IEDs during 3-phase SC fault. In islanded modes 4a-4c, the duration of applied fault is 5.2 s from the simulation time of 1.2 s to the simulation time of 6.4 s to check whether overload stages of IEDs also pick up and trip.

a: FAULT CURRENT CONTRIBUTION OF 1.2 P.U. FROM THE WTG

Table 12 shows magnitudes of currents and voltages at all active IEDs during a 3-phase SC fault at charger-Z terminal in islanded mode 4a. The results show that fault current

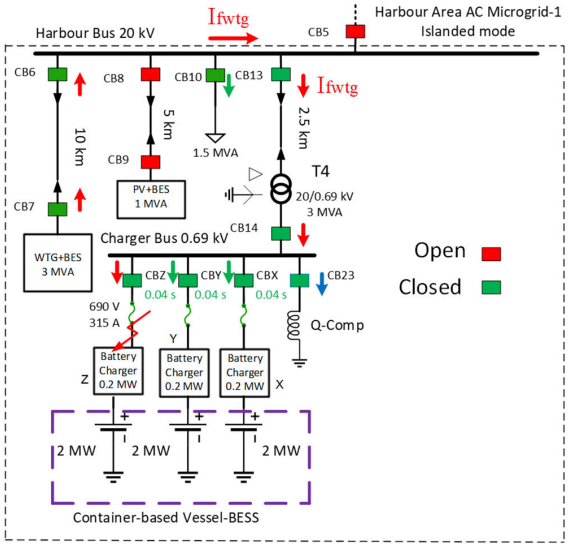

FIGURE 26. 3-phase short-circuit fault at Charger-Z terminal when supplied by only WTG during islanded mode 4.

TABLE 12. Voltage and current at active IEDs during 3-phase short-circuit fault at charger-Z terminal in islanded mode 4A.

IED#	I (A)	$V_{ph\text{-}ph}$ (V)	IED#	I (A)	$V_{ph\text{-}ph}$ (V)
IED6	105	1200	IED14	2980	20
IED7	104	1760	IEDX	80	20
IED10	3.5	1200	IEDY	80	20
IED13	102	1200	IEDZ	3000	Zero

magnitudes at the first backup IEDZ, the second backup IED14 and the third backup IED13 are greater than the set thresholds of 2.5 x $I_{max-load}$ at these IEDs. Therefore, IEDZ, IED14 and IED13 can easily trip after 0.04 s, 0.24 s and 0.44 s of the 3-phase SC fault at charger-Z terminal assuming a coordination delay of 0.2 s between each backup IED. The primary protection is provided by the fast acting fuse that is disabled in simulation to test the tripping of backup IEDs.

Fig. 27 shows magnitudes of currents per phase, pickup and tripping signals of IEDZ and IED14 during a 3-phase SC fault at charger-Z terminal in islanded mode 4a. The first backup IEDZ trips within the required 40 ms of the SC fault at simulation time of 1.24 s and the second backup IED14 also picks up to provide backup protection if IEDZ fails to trip due to any reason.

Fig. 28 reveals that the fast acting fuseZ at charger-Z terminal blows within 255 ms at simulation time of 1.455 s after the occurrence of 3-phase SC fault at simulation time of 1.2 s in islanded mode 4a. Fault current contribution of WTG during islanded mode 4a is shown in Fig. 29. The results show that in islanded mode 4a, the tripping response of fuseZ (primary OC protection) is 215 ms slower than the first backup IEDZ that trips within 40 ms of the 3-phase SC fault. The slower tripping response of fuse is unacceptable in islanded mode 4a because it creates coordination problem

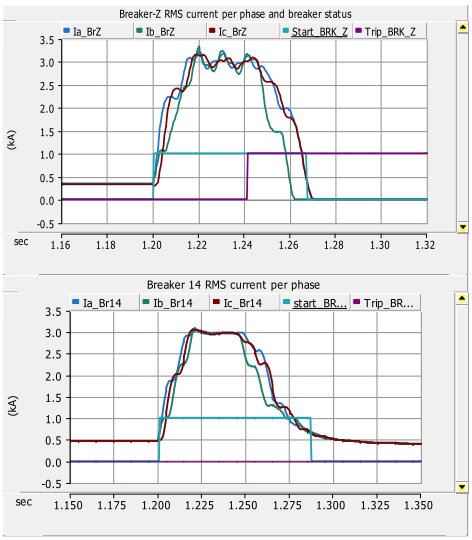

FIGURE 27. Magnitude of current per phase, pickup and tripping status of IEDZ (first backup) and IED14 (second backup) during a 3-phase SC fault at charger-Z terminal in islanded mode 4a.

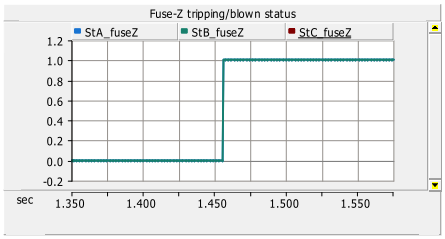

FIGURE 28. Status/tripping response of fuseZ during a 3-phase SC fault at charger-Z terminal in islanded mode 4a.

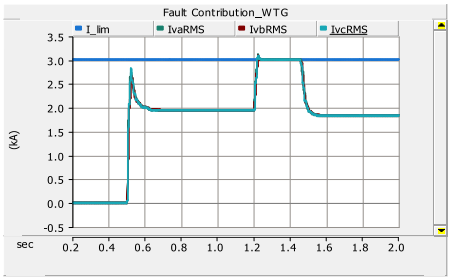

FIGURE 29. Magnitude of fault current contribution per phase by the WTG during a 3-phase SC fault at charger-Z terminal in islanded mode 4a.

between the primary OC protection (fuseZ) and backup OC protection IEDZ. For a proper protection coordination, the fuse needs to operate within 20 ms after the 3-phase SC fault instead of 255 ms. This concludes that the islanded mode 4a avoids adaptive protection settings but creates the coordination problem between fuseZ and backup IEDZ.

b: FAULT CURRENT CONTRIBUTION OF 2 P.U. FROM THE WTG

Fig. 30 reveals that the fast acting fuseZ at charger-Z terminal blows within 105 ms at simulation time of 1.305 s after the

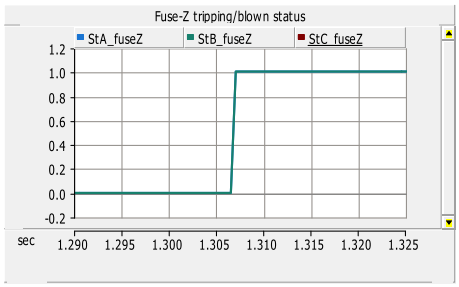

FIGURE 30. Status/tripping response of fuseZ during a 3-phase SC fault at charger-Z terminal in islanded mode 4b.

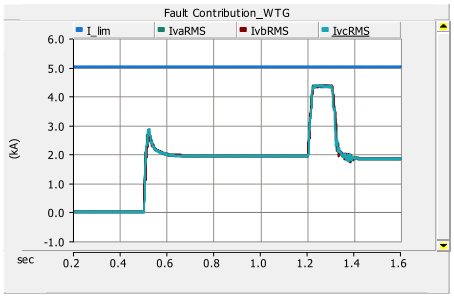

FIGURE 31. Magnitude of fault current contribution per phase by the WTG during a 3-phase SC fault at charger-Z terminal in islanded mode 4b.

occurrence of 3-phase SC fault at simulation time of 1.2 s in islanded mode 4b. It means that in islanded mode 4b, the tripping response of fuseZ (primary OC protection) is 65 ms slower than the first backup IEDZ that trips within 40 ms of the 3-phase SC fault. The obvious reason of slower than expected 20 ms tripping response of fuseZ is less than the required magnitude of fault current sensed by the fusing element due to less than 2 p.u. fault current contribution of the WTG (Fig. 31) in the islanded mode 4b due to the network impedance. Although the tripping response of fuseZ is improved in the islanded mode 4b compared with the islanded mode 4a, it still creates coordination problem between fuseZ and the first backup IEDZ.

c: FAULT CURRENT CONTRIBUTION OF 3 P.U. FROM THE WTG

Fig. 32 shows that fuseZ blows with a time delay of 33 ms when a 3-phase SC fault is applied at simulation time of 1.2 s in the islanded mode 4c. Although the tripping response of fuseZ is still 13 ms slower than the expected 20 ms, but 3 p.u. fault current contribution from the WTG will maintain protection coordination between fuseZ and first backup IEDZ though with only a coordination time delay of 7 ms between them. For more speedy tripping response of fuseZ to maintain the required coordination delay of 20 ms between fuseZ and IEDZ, the WTG must provide a fault current contribution of more than 3 p.u. Alternately, the coordination time delay between fuseZ and IEDZ should be extended from 20 ms to 40 ms.

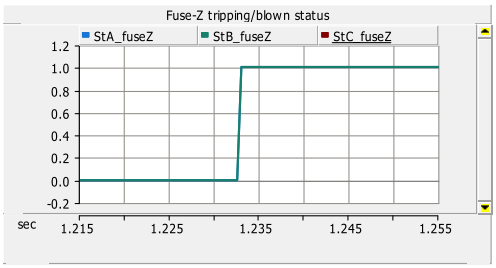

FIGURE 32. Status/tripping response of fuseZ during a 3-phase SC fault at charger-Z terminal in islanded mode 4c.

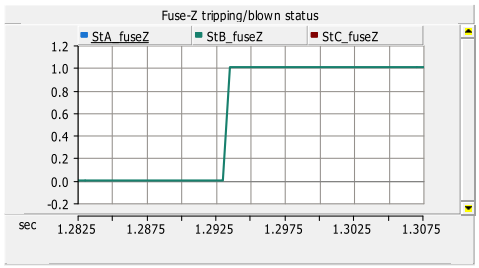

FIGURE 34. Status/tripping response of fuseZ during a 3-phase SC fault at charger-Z terminal in islanded mode 5a.

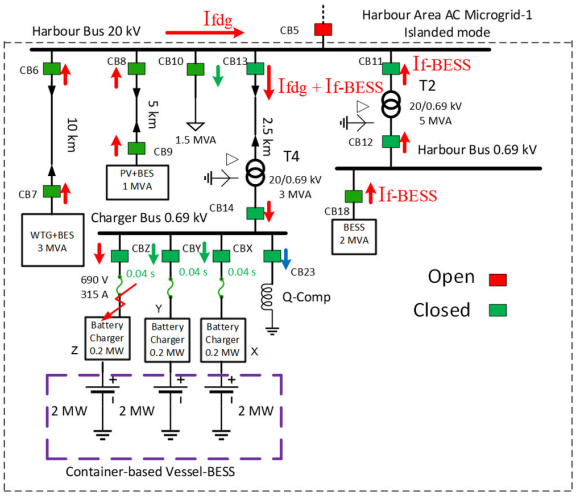

FIGURE 33. 3-phase short-circuit fault at charger-Z terminal when supplied by WTG, PV-BES and harbor-BESS during islanded mode 5.

5) FAULTS AT CHARGER-Z TERMINAL WHEN WTG, PV-BES, AND HARBOR-BESS SUPPLY FAULT CURRENT

This is an extended case for the previous islanded mode 4. In the islanded mode 5 (Fig. 33), it is checked if the fuseZ operates as fast as in the grid-connected mode during 3-phase SC fault at Charger-Z terminal when the battery energy storage at PV system (PV-BES) and BESS at 0.69 kV harbor bus are also activated within 10 ms as extra fault-current sources. The main purpose of the islanded mode 5 is to check whether protection coordination between fuseZ and IEDZ can be maintained using existing available fault current sources with different levels of fault current contributions. Hence, the tripping response of only fuseZ is presented in the results because IEDZ trips within required 40 ms even with 1.2 p.u. fault current contribution of the WTG (case 4a). Same is the case for other backup IEDs in the fault path.

The islanded mode 5 (Fig. 33) is further subdivided into four case studies: The first related to fault current contribution of 1.2 p.u. from the WTG, PV-BES and harbor-BESS, the second related to the fault current contribution of 2 p.u. from the WTG, PV-BES and harbor-BESS, the third related to the fault current contribution of 3 p.u. from the WTG and 2 p.u. from the PV-BES and harbor-BESS, and the fourth related to the fault current contribution of 2.5 p.u. from the WTG, PV-BES and harbor-BESS.

a: FAULT CURRENT CONTRIBUTION OF 1.2 P.U. FROM THE WTG, PV-BES, AND HARBOR-BESS

Fig. 34 reveals that the fast acting fuseZ at charger-Z terminal blows within 92.5 ms at the simulation time of 1.2925 s after the occurrence of 3-phase SC fault at simulation time of 1.2 s in islanded mode 5a. It means that the tripping response of fuseZ (primary OC protection) is 72.5 ms slower than expected 20 ms when each of the WTG, PV-BES and harbor-BESS provides a fault current contribution of 1.2 p.u. (Fig. 35). In this case, the first backup IEDZ will trip before fuseZ. Therefore, it can be concluded that fault current contribution of 1.2 p.u. from the DERs is not enough for maintaining a proper protection coordination between fuseZ and backup IEDZ in the islanded mode 5a.

b: FAULT CURRENT CONTRIBUTION OF 2 P.U. FROM THE WTG, PV-BES, AND HARBOR-BESS

Fig. 36 reveals that the fast acting fuseZ at charger-Z terminal blows within 53 ms at simulation time of 1.253 s after the occurrence of 3-phase SC fault at simulation time of 1.2 s in islanded mode 5b. It means that the tripping response of fuseZ (primary OC protection) is 33 ms slower than expected 20 ms when each of the WTG, PV-BES and harbor-BESS is set to provide a fault current contribution of 2 p.u. Fig. 37 shows that the fault current contribution of the distant WTG is somehow limited to less than 2 p.u. due to the increased fault current contribution from the nearby PV-BES and harbor-BESS in comparison to the islanded mode 5a. It can be concluded that a fault current contribution of 2 p.u. from the DERs is not enough for maintaining a proper protection coordination between fuseZ and backup IEDZ in the islanded mode 5b.

c: FAULT CURRENT CONTRIBUTION OF 3 P.U. FROM THE WTG, AND 2 P.U. FROM THE PV-BES AND THE HARBOR-BESS

Fig. 38 reveals that the fast acting fuseZ at charger-Z terminal blows within 18 ms at simulation time of 1.2175 s after the

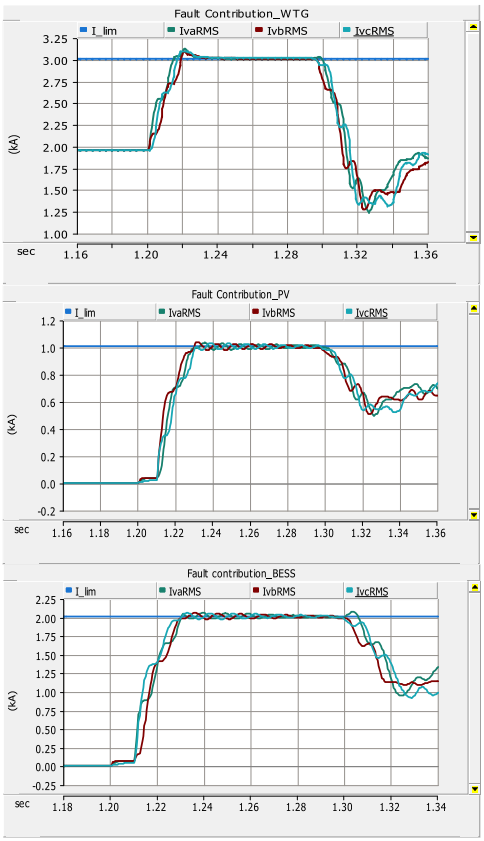

FIGURE 35. Magnitude of fault current contribution per phase by the WTG. PV-BES and harbor-BESS during a 3-phase SC fault at charger-Z terminal in islanded mode 5a.

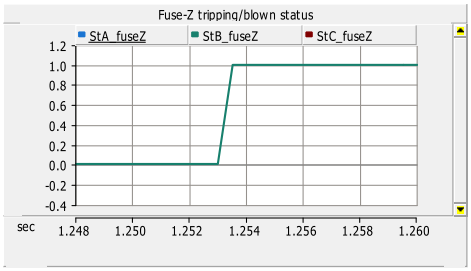

FIGURE 36. Status/tripping response of fuseZ during a 3-phase SC fault at charger-Z terminal in islanded mode 5b.

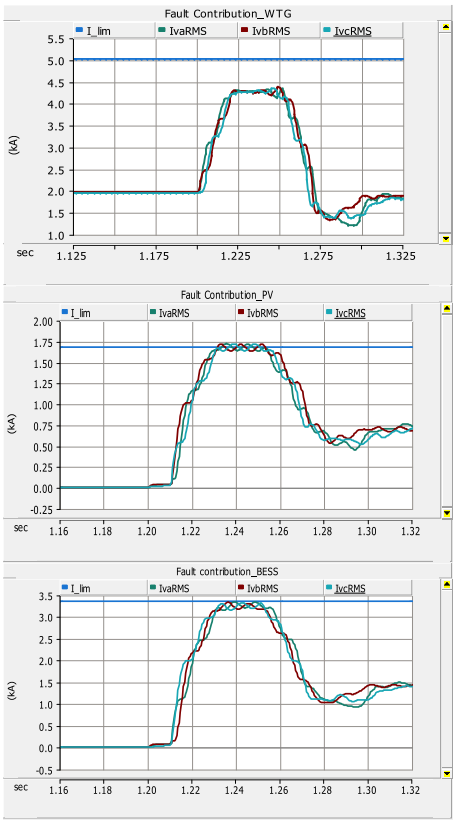

FIGURE 37. Magnitude of fault current contribution per phase by the WTG. PV-BES and harbor-BESS during a 3-phase SC fault at charger-Z terminal in islanded mode 5b.

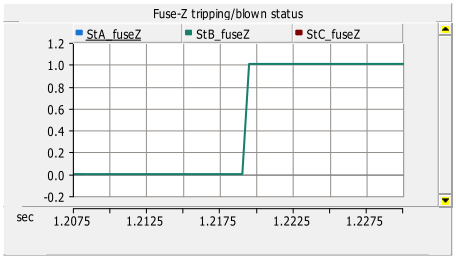

FIGURE 38. Status/tripping response of fuseZ during a 3-phase SC fault at charger-Z terminal in islanded mode 5c.

occurrence of 3-phase SC fault at simulation time of 1.2 s in islanded mode 5c. It means that the tripping response of fuseZ (primary OC protection) is 2 ms faster than the expected 20 ms when the WTG is set to provide fault current contribution of 3 p.u. and both PV-BES and harbor-BESS are set to provide a fault current contribution of 2 p.u. It is concluded that a proper protection coordination between fuseZ and backup IEDZ in the islanded mode 5c is maintained at the mentioned fault current contributions.

d: FAULT CURRENT CONTRIBUTION OF 2.5 P.U. FROM THE WTG, PV-BES AND HARBOR-BESS

Fig. 39 reveals that the fast acting fuseZ at charger-Z terminal blows within 17 ms at simulation time of 1.217 s after the occurrence of 3-phase SC fault at simulation time of 1.2 s in islanded mode 5d. It means that the tripping response of fuseZ (primary OC protection) is 3 ms faster than the expected 20 ms when the WTG, PV-BES and harbor-BESS are set to provide a fault current contribution of 2.5 p.u. Fig. 40 shows the fault current flowing through fuseZ in the islanded

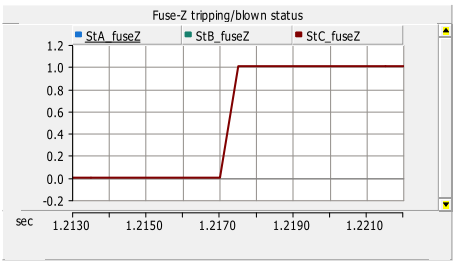

FIGURE 39. Status/tripping response of fuseZ during a 3-phase SC fault at charger-Z terminal in islanded mode 5d.

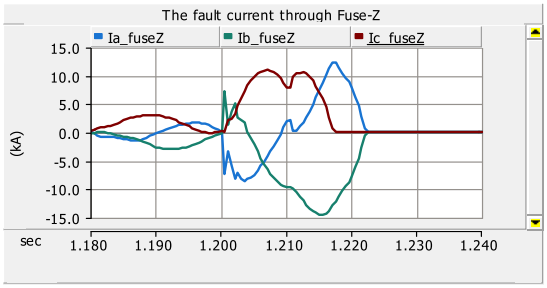

FIGURE 40. Magnitude of fault current per phase flowing through fuseZ during a 3-phase SC fault at charger-Z terminal in islanded mode 5d.

mode 5d. It is concluded that a proper protection coordination between fuseZ and backup IEDZ in the islanded mode 5d is maintained at the mentioned fault current contributions.

6) FAULTS AT CHARGER-Z TERMINAL WHEN WTG, HARBOR-BESS, AND HEALTHY CHARGING VESSEL-BESS SUPPLY FAULT CURRENT

This is an extended case for the previous islanded case 5. In this case 6 (Fig. 41) not only the WTG and harbor-BESS can be used but also the healthy container-based vessel-BESS on charge can be utilized as the extra fault-current sources during the non-availability of PV-BES. For this purpose, 0.2 MW chargers of container-based vessel-BESS need to be bidirectional type providing 1.2-3 p.u. of the rated discharging current during 3-phase SC faults for practical application in the islanded mode 6.

In the islanded mode 6, the battery chargers X and Y along with 2 MWh batteries are replaced with generic DER models each of 0.2 MVA capacity to emulate their discharging mode. The main purpose of the islanded mode 6 is to check if the protection coordination between fuseZ and IEDZ can be maintained using the mentioned fault current sources with different levels of fault current contributions.

The islanded mode 6 (Fig. 41) is further subdivided into four case studies (6a-6d) according to different fault current contributions of DERs as discussed in the following subsections. In all of the four case studies of the islanded mode 6, the harbor-BESS, vessel-BESS-X, and vessel-BESS-Y are activated with a delay of 10 ms after the fault.

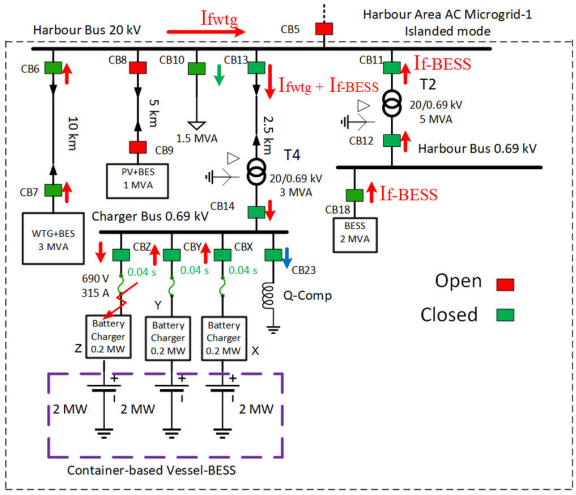

FIGURE 41. 3-phase short-circuit fault at Charger-Z terminal when supplied by WTG, harbor-BESS and healthy container-based vessel-BESS during islanded mode 6.

a: FAULT CURRENT CONTRIBUTION OF 1.2 P.U. FROM THE WTG, HARBOR-BESS, VESSEL-BESS-X, AND VESSEL-BESS-Y

Fig. 42 reveals that the fast acting fuseZ at charger-Z terminal blows within 101 ms at simulation time of 1.301 s after the occurrence of 3-phase SC fault at simulation time of 1.2 s in islanded mode 6a. It means that the tripping response of fuseZ (primary OC protection) is 81 ms slower than expected 20 ms when each of the WTG, harbor-BESS, vessel-BESS-X, and vessel-BESS-Y provides a fault current contribution of 1.2 p.u. It can be concluded that a fault current contribution of 1.2 p.u. from DERs is not enough for maintaining a proper protection coordination between fuseZ and backup IEDZ in the islanded mode 6a because backup IEDZ will trip before the fuseZ blows.

b: FAULT CURRENT CONTRIBUTION OF 2 P.U. FROM THE WTG, HARBOR-BESS, VESSEL-BESS-X, AND VESSEL-BESS-Y

Fig. 43 reveals that the fast acting fuseZ at charger-Z terminal blows within 36 ms at simulation time of 1.236 s after the occurrence of 3-phase SC fault at simulation time of 1.2 s in islanded mode 6b. It means that the tripping response of fuseZ (primary OC protection) is 16 ms slower than expected 20 ms when each of the WTG, harbor-BESS, vessel-BESS-X, and vessel-BESS-Y provides a fault current contribution of 2 p.u. It can be concluded that a fault current contribution of 2 p.u. from DERs is not enough for maintaining a proper protection coordination between fuseZ and backup IEDZ in the islanded mode 6b because the coordination time delay has become very short (only 4 ms instead of 20 ms).

c: FAULT CURRENT CONTRIBUTION OF 2.5 P.U. FROM THE WTG, HARBOR-BESS, VESSEL-BESS-X, AND VESSEL-BESS-Y

Fig. 44 reveals that the fast acting fuseZ at charger-Z terminal blows within 37 ms at simulation time of 1.237 s after the occurrence of 3-phase SC fault at simulation time of 1.2 s in

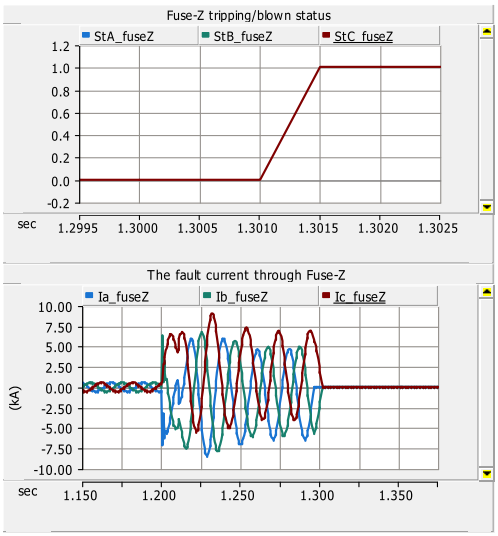

FIGURE 42. Status/tripping response of fuseZ (top) and magnitude of fault current per phase flowing through fuseZ (bottom) during a 3-phase SC fault at charger-Z terminal in islanded mode 6a.

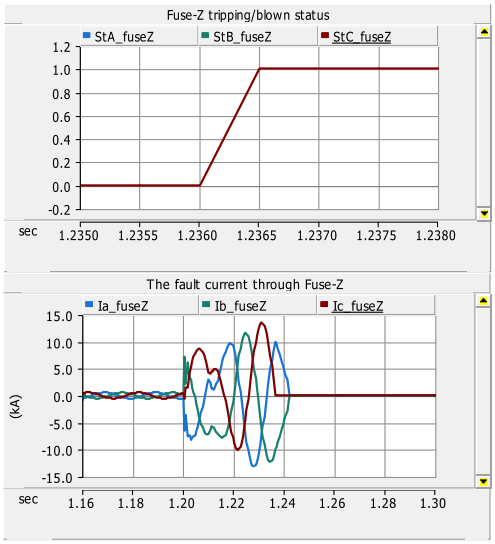

FIGURE 43. Status/tripping response of fuseZ (top) and magnitude of fault current per phase flowing through fuseZ (bottom) during a 3-phase SC fault at charger-Z terminal in islanded mode 6b.

islanded mode 6c. It means that the tripping response of fuseZ (primary OC protection) is 17 ms slower than expected 20 ms when each of the WTG, harbor-BESS, vessel-BESS-X, and vessel-BESS-Y is set to provide a fault current contribution of 2.5 p.u. This is due to the fact that in the islanded mode 6c, less than the set limit of fault current contribution from DERs is observed. It can be concluded that a fault current contribution of 2.5 p.u. from DERs is not enough for maintaining a proper protection coordination between fuseZ and backup IEDZ in

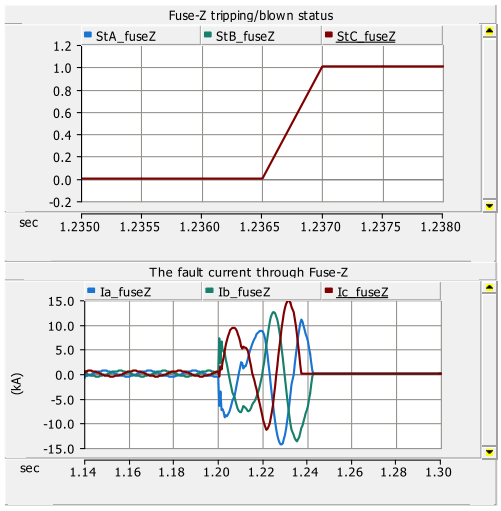

FIGURE 44. Status/tripping response of fuseZ (top) and magnitude of fault current per phase flowing through fuseZ (bottom) during a 3-phase SC fault at charger-Z terminal in islanded mode 6c.

the islanded mode 6c because the coordination time delay has become very short (only 3 ms instead of 20 ms).

d: FAULT CURRENT CONTRIBUTION OF 3 P.U. FROM THE WTG, HARBOR-BESS, VESSEL-BESS-X, AND VESSEL-BESS-Y

Fig. 45 reveals that the fast acting fuseZ at charger-Z terminal blows within 36 ms at simulation time of 1.236 s after the occurrence of 3-phase SC fault at simulation time of 1.2 s in islanded mode 6d. It means that the tripping response of fuseZ (primary OC protection) is 16 ms slower than expected 20 ms when each of the WTG, harbor-BESS, vessel-BESS-X, and vessel-BESS-Y is set to provide a fault current contribution of 3 p.u. This is due to the fact that in the islanded mode 6d, less than the set limit of fault current contribution from DERs is observed. It can be concluded that a fault current contribution of 3 p.u. from DERs is not enough for maintaining a proper protection coordination between fuseZ and backup IEDZ in the islanded mode 6d because the coordination time delay has become very short (only 4 ms instead of 20 ms).

The results show that the only way for maintaining a proper coordination in the islanded modes 6b, 6c and 6d is to increase the coordination time delay between fuseZ and backup IEDZ from the existing 20 ms coordination time delay to the new 40 ms coordination time delay. In this way, only a fault current contribution of 2 p.u. from DERs will be sufficient for the proper protection coordination, detection and isolation of 3-phase SC fault at charger-Z terminal in the islanded mode 6. There are two obvious and unavoidable time delays resulting in the slow tripping/blowing response of fuseZ in islanded mode cases 6a-6d. One is the activation time delay of 10 ms taken by extra fault current sources. The second is the ramp-up time delay of fault currents provided by DERs to reach up to their maximum values for fuse to respond.

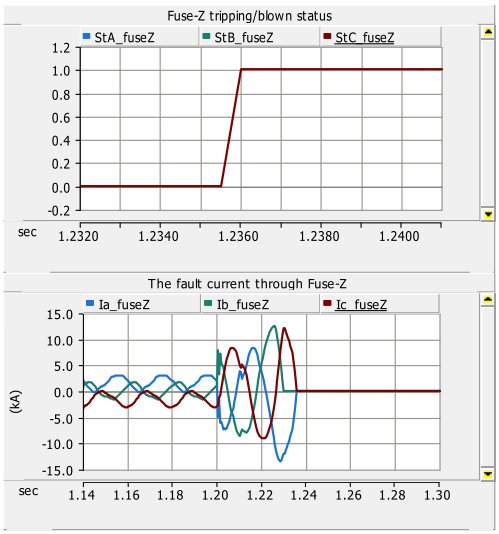

FIGURE 45. Status/tripping response of fuseZ (top) and magnitude of fault current per phase flowing through fuseZ (bottom) during a 3-phase SC fault at charger-Z terminal in islanded mode 6d.

III. DISCUSSION

Table 13 presents the summary of the islanded mode fault cases for the harbor area AC microgrid-1. The islanded mode cases 1a to 3b are related to 3-phase SC fault at the cold-ironing load whereas the islanded mode cases 4a to 6d are related to 3-phase SC fault at charger-Z terminal. In the islanded mode cases 1a to 3b it is checked if adaptive OC settings can be avoided and protection coordination between the primary and backup IEDs in the fault path can be properly maintained. In the islanded mode cases 4a to 6d the operating time of fast acting fuse is also checked in addition to avoidance of adaptive OC settings and maintenance of proper protection coordination between IEDs in the fault path.

From the summary in Table 13 and results in Table 14 it is evident that in most of the islanded mode cases adaptive OC settings can be avoided with different combinations of fault current contributions of DERs except in islanded mode cases 1a, 3a and 3b. The exceptional islanded cases 1a, 3a and 3b are obvious islanded modes with either minimum magnitudes of fault current contributions from DERs or minimum number/capacity of DERs. The adaptive OC settings can only be avoided in the exceptional islanded mode case 1a by increasing fault current contributions of DERs as done in case 1b, and in exceptional islanded mode cases 3a and 3b by adding 25 per cent extra MVA capacity.

The results indicate that in most of the islanded mode cases, the tripping time of primary IED or fuse is delayed which results in subsequent extended coordination delays between the backup IEDs. In islanded mode cases 4c, 6b, 6c and 6d the operating time of fuseZ is delayed up to 20 ms or less, therefore, a revised coordination delay of 40 ms instead of existing 20 ms between fuseZ and the first backup IEDZ may solve the coordination problem. This requires some compromise on backup IEDs' operations. In exceptional islanded cases 1a, 3a and 3b, the protection coordination between IEDs can be improved by increasing fault current contributions of DERs, using only the grid-forming control of all DERs and adding 25 per cent extra MVA capacity.

Last but not least, the avoidance of adaptive OC protection settings, the maintenance of protection coordination, and the operation of fuse within 20 ms are possible by using existing available DERs and battery storages as fault current sources during 3-phase SC fault in islanded mode cases 2c, 5c and 5d. The only concern will be to disconnect the extra

TABLE 13. Summary of islanded mode fault cases of the harbor area AC microgrid-1.

Islanded mode fault case	Fault current contribution from DERs	Are adaptive OC settings avoided?	Is protection coordination maintained?	Does fuse operate within 20 ms?
1a	WTG: 1.2 p.u. PV: 1.2 p.u.	NO	NO	-
1b	WTG: 2 p.u. PV: 2 p.u.	YES	YES (PARTIALLY)[1]	-
2a	WTG: 2 p.u. PV: 2 p.u. H-BESS: 1.2 p.u.	YES	YES (PARTIALLY)	-
2b	WTG: 2 p.u. PV: 2 p.u. H-BESS: 2 p.u.	YES	YES (PARTIALLY)	-
2c	WTG: 3 p.u. PV: 3 p.u. H-BESS: 3 p.u	YES	YES	-
3a	H-BESS: 2.5 p.u.	NO	NO	-
3b	H-BESS: 3 p.u.	NO	NO	-
		YES (25% additional MVA capacity)	YES (25% additional MVA capacity)	-
4a	WTG: 1.2 p.u.	YES	YES (PARTIALLY)	NO (Delayed)
4b	WTG: 2 p.u.	YES	YES (PARTIALLY)	NO (Delayed)
4c	WTG: 3 p.u.	YES	YES (PARTIALLY)*	NO (Delayed)**
5a	WTG: 1.2 p.u. PV-BES: 1.2 p.u. H-BESS: 1.2 p.u	YES	YES (PARTIALLY)	NO (Delayed)
5b	WTG: 2 p.u. PV-BES: 2 p.u. H-BESS: 2 p.u	YES	YES (PARTIALLY)	NO (Delayed)
5c	WTG: 3 p.u. PV-BES: 2 p.u. H-BESS: 2 p.u	YES	YES	YES
5d	WTG: 2.5 p.u. PV-BES: 2.5 p.u. H-BESS: 2.5 p.u	YES	YES	YES
6a	WTG: 1.2 p.u. H-BESS: 1.2 p.u. V-BESS: 1.2 p.u.	YES	YES (PARTIALLY)	NO (Delayed)
6b	WTG: 2 p.u. H-BESS: 2 p.u. V-BESS: 2 p.u.	YES	YES (PARTIALLY)*	NO (Delayed)**
6c	WTG: 2.5 p.u. H-BESS: 2.5 p.u. V-BESS: 2.5 p.u.	YES	YES (PARTIALLY)*	NO (Delayed)**
6d	WTG: 3 p.u. H-BESS: 3 p.u. V-BESS: 3 p.u.	YES	YES (PARTIALLY)*	NO (Delayed)**

WTG=Wind turbine generator, PV = Photovoltaic, BESS = Battery energy storage system
H-BESS = Harbor-BESS, PV-BES = PV-Battery energy storage,
V-BESS = Vessel-BESS (both X and Y), MVA = Mega Volt-Ampere.
*Can be improved by extending coordination delay between fuseZ and IEDZ to 40 ms
**FuseZ operating time is delayed up to 20 ms or less.
[1] Grid -forming control of both WTG and PV will improve the coordination delay of primary and backup IEDs closer to the setting limits in the islanded mode 1b.

TABLE 14. Operating times of IEDs in islanded mode fault cases.

Fault Cases	Operating times (ms) during 3-phase SC faults										
	IED21	IED20	IED19	IED15	IED12	IED11					
1a	I>@5	I>@5	I>@5	I>@5	I>@5	I>@5					
1b	32	275	477	675	879	1079					
2a	32	258	459	655	872	1071					
2b	32	362	562	756	865	1066					
2c	32	212	412	612	830	1030					
3a	I>@5	I>@5	I>@5	I>@5	-						
3b	40	I>@5	I>@5	618							
→	4a	4b	4c	5a	5b	5c	5d	6a	6b	6c	6d
FuseZ	255	105	33	92.5	53	17.5	17	101	36	37	36
IEDZ	40*	ms = Millisecond, SC = Short-circuit, I>@5 = Overload stage operating in 5 s.									
IED14	240*	→ Fault cases in columns, IEDs in rows.									
IED13	440*	*IEDZ, IED14 and IED13 have same operating times in cases 4a-6d.									

Primary protection devices are highlighted in green, and backups are highlighted in blue color.

activated fault current sources immediately after the fault is isolated to prevent overvoltage and related aftereffects like AC microgrid's instability or blackout due to disconnection of the required DERs by the overvoltage protection.

In general, adaptive OC protection settings may still be required for the islanded mode AC microgrids protected by the inverse-time OC function. This conclusion can be easily drawn from the results of islanded mode 6 as the operation of fuseZ, that is an inverse-time OC device, is delayed in all four cases. However, a separate coordination study for the inverse-time OC function will confirm whether the adaptive protection will be required, or it can avoided for the considered islanded modes with different scenarios of fault current contributions of converter-based DERs.

IV. CONCLUSION

The magnitudes of maximum load currents and the short-circuit fault currents at each IED during the grid-connected and islanded modes of harbor area AC microgrid-1 have been determined. The operating time and protection coordination of definite-time OC relays and fast acting fuse during the selected 3-phase SC faults in the grid-connected mode have been evaluated and found to be correct according to the settings. The evaluation of operating time and protection coordination of definite-time OC relays and fast acting fuse during the selected 3-phase SC faults for six islanded mode cases with different fault current contributions of DERs have also been done. It is found that grid-connected mode settings of definite-time OC can also be effectively used during 3-phase SC faults in the islanded modes if the active/operational DERs and freely-available quickly operated battery storage units provide at least 3 p.u. of fault current contribution. In this way adaptive definite-time OC settings can be avoided, and proper definite-time protection coordination and fast fuse operation can be ensured during 3-phase SC faults in the islanded modes of AC microgrid.

REFERENCES

[1] K. Marquart, T. Haasdijk, G. B. Ferrari, and R. Schmidhalter. (2010). Reprint ABB Review 4/2010 Shore-to-Ship Power. ABB, Switzerland, Accessed: Nov. 20, 2017. [Online]. Available: https://library.e.abb.com/public/8f916bbe49d92d1ac12579680032f273/Shore-to-ship-power-2010-low.pdf

[2] J. Kumar, O. Palizban, and K. Kauhaniemi, "Designing and analysis of innovative solutions for Harbour area smart grid," in *Proc. IEEE Manchester PowerTech*, Manchester, U.K., Jun. 2017, pp. 1–6.

[3] J. Kumar, A. A. Memon, L. Kumpulainen, K. Kauhaniemi, and O. Palizban, "Design and analysis of new Harbour grid models to facilitate multiple scenarios of battery charging and onshore supply for modern vessels," *Energies*, vol. 12, no. 12, p. 2354, Jun. 2019, doi: 10.3390/en12122354.

[4] *Utility connections in port—Part 1: High Voltage Shore Connection (HVSC) Systems—General requirements*, document IEC/ISO/IEEE 80005-1, Ed. 2.0, International Electrotechnical Commission, Geneva, Switzerland, Mar. 2019, pp. 1–74. [Online]. Available: www.iec.ch

[5] D. W. Gao, E. Muljadi, T. Tian, M. Miller, and W. Wang, "Comparison of standards and technical requirements of grid-connected wind power plants in China and the United States," Nat. Renew. Energy Lab. (NREL), Golden, CO, USA, Tech. Rep. NREL/TP-5D00-64225, Sep. 2016.

[6] *Requirements for Generating Plants to be Connected in Parallel With Distribution Networks. Part 1: Connection to a LV Distribution Network. Generating Plants up to and Including Type B*, Standard SFS-EN 50549-1:2019, European Committee for Electrotechnical Standardization, Brussels, Belgium, Feb. 2019, pp. 1–71.

[7] *Requirements for Generating Plants to be Connected in Parallel With Distribution Networks. Part 2: Connection to a MV Distribution Network. Generating Plants up to and Including Type B*, Standard SFS-EN 50549-2:2019, European Committee Electrotechnical Standardization, Brussels, Belgium, Feb. 2019, pp. 1–80.

[8] *IEEE Standard for Interconnection and Interoperability of Distributed Energy Resources With Associated Electric Power Systems Interfaces*, Standard IEEE 1547-2018, IEEE Standards Association, IEEE Standards Coordinating Committee 21, Feb. 2018, pp. 1–136.

[9] *IEEE Guide for Design, Operation, and Integration of Distributed Resource Island Systems with Electric Power Systems*, IEEE Standard 1547.4-2011, IEEE Standards Association, IEEE Standards Coordinating Committee 21, Jul. 2011, pp. 1–42.

[10] *IEEE Standard for the Specification of Microgrid Controllers*, IEEE Standard 2030.7-2017, IEEE Standards Association, IEEE Standards Coordinating Committee 21, Dec. 2017, pp. 1–41.

[11] *Amendment 1 Utility connections in Port—Part 1: High Voltage Shore Connection (HVSC) Systems—General Requirements*, document IEC/ISO/IEEE 80005-1:2019/AMD1:2022, Ed. 2.0, International Electrotechnical Commission, Geneva, Switzerland, Feb. 2022, pp. 1–7. [Online]. Available: https://www.iec.ch

[12] *Utility Connections in Port—Part 3: Low Voltage Shore Connection (LVSC) Systems—General Requirements*, document IEC/ISO/IEEE PAS 80005-3:2014, Ed. 1.0, International Electrotechnical Commission, Geneva, Switzerland, Aug. 2014, pp. 1–51. [Online]. Available: https://www.iec.ch

[13] A. A. Memon and K. Kauhaniemi, "A critical review of AC microgrid protection issues and available solutions," *Electric Power Syst. Res.*, vol. 129, pp. 23–31, Dec. 2015, doi: 10.1016/j.epsr.2015.07.006.

[14] A. A. Memon, H. Laaksonen, and K. Kauhaniemi, "Microgrid protection with conventional and adaptive protection schemes," in *Microgrids*, A. Anvari-Moghaddam, H. Abdi, B. Mohammadi-Ivatloo, and N. Hatziargyriou, Eds. Cham, Switzerland: Springer, 2021, ch. 19, pp. 523–579, doi: 10.1007/978-3-030-59750-4_19.

[15] A. A. Memon and K. Kauhaniemi, "An adaptive protection for radial AC microgrid using IEC 61850 communication standard: Algorithm proposal using offline simulations," *Energies*, vol. 13, no. 20, p. 5316, Oct. 2020.

[16] H. Laaksonen, D. Ishchenko, and A. Oudalov, "Adaptive protection and microgrid control design for Hailuoto island," *IEEE Trans. Smart Grid*, vol. 5, no. 3, pp. 1486–1493, May 2014, doi: 10.1109/TSG.2013.2287672.

[17] J. Niiranen, R. Komsi, M. Routimo, T. Lähdeaho, and S. Antila, "Experiences from a back-to-back converter fed village microgrid," in *Proc. IEEE PES Innov. Smart Grid Technol. Conf. Eur. (ISGT Europe)*, Gothenburg, Sweden, Oct. 2010, pp. 1–5.

[18] M. Ferrari and L. M. Tolbert, "Inverter design with high short-circuit fault current contribution to enable legacy overcurrent protection for islanded microgrids," in *Proc. IEEE Power Energy Soc. Gen. Meeting (PESGM)*, Denver, CO, USA, Jul. 2022, pp. 1–5.

[19] A. Cruden and G. J. W. Dudgeon, "The impact of energy storage devices used in conjunction with renewable embedded generators, on the protection and control system," in *Proc. 7th Int. Conf. Develop. Power Syst. Protection (DPSP)*, Amsterdam, The Netherlands, Apr. 2001, pp. 230–233.

[20] P. Nuutinen, P. Peltoniemi, and P. Silventoinen, "Short-circuit protection in a converter-fed low-voltage distribution network," *IEEE Trans. Power Electron.*, vol. 28, no. 4, pp. 1587–1597, Apr. 2013, doi: 10.1109/TPEL.2012.2213845.

[21] S. Gupta, S. Mukhopadhyay, A. Banerji, and S. K. Biswas, "Fault management in isolated microgrid," in *Proc. IEEE Int. Conf. Power Electron., Drives Energy Syst. (PEDES)*, Chennai, India, Dec. 2018, pp. 1–6.

[22] A. H. Etemadi and R. Iravani, "Overcurrent and overload protection of directly voltage-controlled distributed resources in a microgrid," *IEEE Trans. Ind. Electron.*, vol. 60, no. 12, pp. 5629–5638, Dec. 2013, doi: 10.1109/TIE.2012.2229680.

[23] K. O. Oureilidis and C. S. Demoulias, "A fault clearing method in converter-dominated microgrids with conventional protection means," *IEEE Trans. Power Electron.*, vol. 31, no. 6, pp. 4628–4640, Jun. 2016, doi: 10.1109/TPEL.2015.2476702.

[24] L. Qi, M. Carminati, and M. Riva, "Fault interruption and protection coordination in converter interfaced distribution systems," in *Proc. IEEE Power Energy Soc. Gen. Meeting (PESGM)*, Portland, OR, USA, Aug. 2018, pp. 1–5.

[25] C.-H. Noh, C.-H. Kim, G.-H. Gwon, M. O. Khan, and S. Z. Jamali, "Development of protective schemes for hybrid AC/DC low-voltage distribution system," *Int. J. Electr. Power Energy Syst.*, vol. 105, pp. 521–528, Feb. 2019, doi: 10.1016/j.ijepes.2018.08.030.

[26] D. B. Rathnayake, M. Akrami, C. Phurailatpam, S. P. Me, S. Hadavi, G. Jayasinghe, S. Zabihi, and B. Bahrani, "Grid forming inverter modeling, control, and applications," *IEEE Access*, vol. 9, pp. 114781–114807, 2021, doi: 10.1109/ACCESS.2021.3104617.

[27] N. Mohammed, H. H. Alhelou, and B. Bahrani, *Grid-Forming Power Inverters: Control and Applications*, 1st ed. Boca Raton, FL, USA: CRC Press, 2023, [Online]. Available: https://www.taylorfrancis.com/, doi: 10.1201/9781003302520.

[28] A. Yazdani and R. Iravani, "Controlled-frequency VSC system," in *Voltage-Sourced Converters in Power Systems: Modeling, Control, and Applications*, vol. 9. Hoboken, NJ, USA: Wiley, 2010, pp. 245–269.

[29] *Technical Catalogue PCS100 SFC Static Frequency Converter, 2UCD030000E009_d PCS100 SFC Technical Catalogue*, ABB Limted, New Zealand, 2021, Accessed: Dec. 13, 2022, pp. 1–35. [Online]. Available: https://library.e.abb.com/public/65b31251075443f09c54549966809657/2UCD030000E009_d%20PCS100%20SFC%20Technical%20Catalogue.pdf

AUSHIQ ALI MEMON (Member, IEEE) received the B.E. degree in electrical engineering from the Quaid-e-Awam University of Engineering, Science and Technology, Nawabshah, Pakistan, in 2006, and the M.Sc. degree in electrical power engineering from the Brandenburg University of Technology, Cottbus, Germany, in 2013. He is currently pursuing the Ph.D. degree with the Department of Electrical Engineering, University of Vaasa, Finland. Previously, he was a Lecturer with the Quaid-e-Awam University of Engineering, Science and Technology, from 2007 to 2009. He was a Project Researcher with the University of Vaasa, from 2014 to 2020. His research interests include power system protection, microgrids, power system transient simulations, smart grids, and power electronics applications.

KIMMO KAUHANIEMI (Member, IEEE) received the M.S. and Ph.D. degrees in electrical engineering from the Tampere University of Technology, Finland, in 1987 and 1993, respectively. Previously, he was with ABB Corporate Research and the VTT Technical Research Centre, Finland. He is currently with the University of Vaasa, where he is a Professor of electrical engineering and leads the Smart Electric Systems Research Group. His research interests include power system transient simulation, protection of power systems, grid integration of distributed generation, and microgrids.

Hardware in the loop testing for power systems

Sadegh Mahmoudi tabar[1], Aushiq Ali Memon[2], Mazaher Karimi[2], Mohammad Mohammadi[1], Kimmo Kauhaniemi[2]

[1]School of Electrical and Computer Engineering, Shiraz University, Shiraz, Iran

[2]School of Technology and Innovations, University of Vaasa, Vaasa, Finland

Abstract

Today, power systems have become very sophisticated with the significant development of hardware and software technologies. Increment the penetration level of renewable energies, the move to the smart grid, and the growth of load and consequently the growth of the grid are also investigated, nowadays. Implementation of these new technologies into the network should be tested and evaluated as close to reality as possible to prevent damage to the equipment and network to save on testing costs. The development plan of the power system can be designed, evaluated, and tested using the hardware in the loop simulation in a powerful environment. This paper describes the basic specifications of the HIL simulation in a power system.

Keywords: Electrical power system, Hardware in the loop, Power interface, Real-time simulation

1. Introduction

Power systems are very large and complex, and it is obvious that any changes in the power system have to be carefully evaluated and investigated. Therefore, the process of installing a new equipment or developing a part of the system involves several steps. This process is known as model-based testing. In model-based testing, design steps are performed at different levels from determine the general specifications to system integration tests. For example, the process of designing, developing, simulating, and testing the X-in-the-loop enables earlier testing, faster development, and as illustrated in Fig.1 consists of Model in the Loop (MIL), Software in the Loop (SIL), Processor in the Loop (PIL), Hardware in the Loop (HIL), and System in the Loop (SYSIL), respectively [1,2].

In MIL, the model runs behaviorally in a computer development environment such as Simulink. At this stage, the design is quickly corrected and the model is executed based on the processor time constant. In the SIL, which is actually a coding test, the model is compiled in C code and executed at a fixed time constant, and the design correction is slightly slower than in the previous step. In the PIL stage, the code generated from the previous step. It is loaded on a microprocessor. This step is to find possible implementation problems in the built-in environment. The speed of design correction is significantly reduced at this stage. In the HIL stage, the control system is inserted into the control loop as hardware, and the rest of the system runs in real-time on the computer system set. Finally, the integrated system is verified in the SYSIL step.

Sadegh Mahmoudi tabar, Aushiq Ali Memon, Mazaher Karimi, Mohammad Mohammadi, Kimmo Kauhaniemi,
Hardware in the loop testing for power systems, Editor(s): Jorge García,
Encyclopedia of Electrical and Electronic Power Engineering, Elsevier, 2023,Pages 294-309,
ISBN 9780128232118, https://doi.org/10.1016/B978-0-12-821204-2.00146-X.
(https://www.sciencedirect.com/science/article/pii/B978012821204200146X)

2

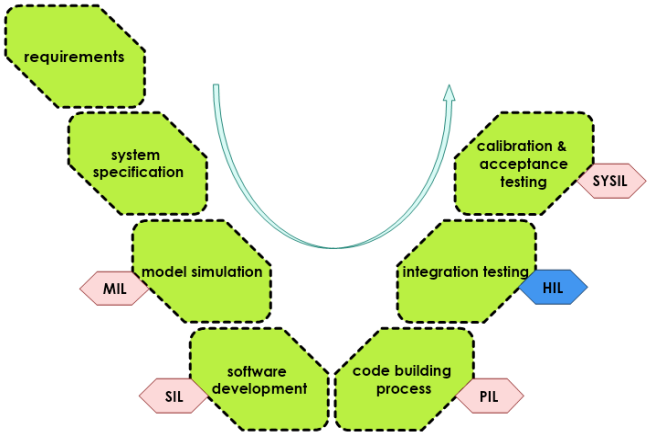

Fig. 1. The V development process including the x-in-the-loop testing phases

The structure of the article is categorized as follows: In section II, the main content of the HIL simulation definition is presented. The configuration required to implement the HIL simulation for power systems, including the types of simulators, power interfaces, and test hardware, is described and compared in Section III. In the section IV, methods for improving the stability and accuracy of HIL simulations are presented and compared. Finally, it is concluded in the section V of the article.

2. General concept

2.1. HIL

The history of HIL dates back to the 1950s with the connection of a physical controller to a real-time simulated system. Therefore, with this method, embedded systems were tested in a practical, reliable and inexpensive way. In the last few decades, the use of real-time hardware simulation has become popular in various industries such as aerospace, power systems, robotics, automotive, etc. In general, in a HIL simulation, the part of the system for which an exact model is available would be simulated in real-time, and the part of the system for which an exact model is not available is entered as HIL. Fig. 2 shows the basic concept of a HIL simulation. The face of the hardware is located in the loop. The connection between the hardware and the simulator is made by analog-to-digital (A/D) and digital-to-analog (D/A) converters without power exchange in such a way that the simulator does not sense the presence of the hardware and sees it as an aborted block [3].

A more complete way to illustrate the nature of a HIL simulation as shown in Fig. 2 (a) is a combination of hardware and real-time simulation. Therefore, the hardware and simulated components of a system can be anywhere in the system, including the controller subsystem, the plant subsystem, and the interface subsystem. Also, a variety of components of each subsystem can be simulated or physically placed in a loop. Therefore, there can be various options for how to combine an HIL simulation, which according to Fig. 2 (b) in each sub-section of physical degree or simulation can be green (hardware) or blue (simulated) of each sub system is determined.

a) b)

Fig. 2. (a) Basic concept of a HIL simulation setup (b) Physical degree of HIL simulation

2.2. The difference between Offline, Real-time, Online, and HIL simulations in power system

Computer simulation is an attempt to model the actual or hypothetical state of a phenomenon within computer programs, so that the system can function in the face of phenomena and learn how the system works.

2.2.1. Offline

Most power system simulations used in the design phase are offline. Hence, it does not interact with any of the equipment parts or controllers of the system. Offline simulations have high computational power, but their simulation speed is not real-time. Applications of offline simulation include power-flow, transient stability, design of electric machines, etc. in software such as PSCAD, EMTP, MATLAB/Simulink.

2.2.2. Real-time

In a real-time simulation, the real-time simulator used must produce the internal variables and simulation outputs exactly at the same time as its physical counterpart. In real-time simulation, when a certain time is passed from the simulation function, the same time has passed in the real world. In general, in real-time simulation, the accuracy of the calculations depends not only on the accurate display of the system dynamics, but also on the time used to produce the results. Fig. 3 shows a comparison between real-time and non-real-time (offline) simulations in a system. During a non-real-time simulation, the amount of real-time required to compute all equations and functions representing the simulation of a system over a given time step may be shorter than the simulation time step, and the overall goal achieve results in the fastest time possible. For a real-time simulation, the time step corresponds to the time step of the actual performance of the system. It will premise the real-time simulation to perform all the relevant necessary operations including driving the input and output signals, which is required for the HIL testing.

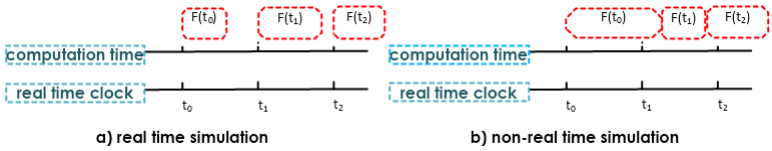

Fig. 3. The concept of real-time (a) real-time simulation (b) non real-time simulation

2.2.3. Online

In online simulations using estimation techniques or using online interaction with an online system such as SCADA, it ensures that the mode and parameter of the simulated model are as accurate as possible. For this reason, the online model can be used both to evaluate planned changes at any time, and to control, optimize and perform various operational tasks. Online simulations are used when it is not possible to find offline data for the full range of working conditions or when the workflow varies with time. Therefore, they are very suitable for transient analyzes.

2.2.4. HIL

Online or real-time simulations are closest to the real system. But if we cannot find an exact model for the controller or other system equipment or want to develop part of the system, we physically place the subsystem inside the simulation loop through the input/output interfaces and form a HIL simulation. Therefore, the important and common part of this simulation is being real-time. A real-time simulator can perform an offline simulation with an accuracy close to HIL simulation, but its great advantage is the ability to use HIL if needed.

2.3. Basic HIL simulation concept for CHIL and PHIL

If in a HIL system the controller is placed in the loop as hardware and the other components of the power system are simulated in real-time, it is called the controller hardware in the loop (CHIL). According to the Fig. 4, no power is exchanged and the controller communicates with the power system simulation part through ADC converters in the

4

low voltage and power range (+/-10V and a few milliampere) for data processing. Therefore, to design or develop power system controllers such as protection relays, electric car drivers, smart grid development platform, electronic power boards, to reduce the costs and potential risks to the physical state in the presence of the real power systems

If in a HIL system power devices such as an electric motor or a photovoltaic are placed in the simulation loop as hardware, it is called the hardware power in the loop (PHIL) [4]. In this case, according to the fig. 4, power is exchanged in the range of high voltage and power. Therefore, the signals that are sent or received from the simulator to the physical power device, in addition to A/D conversion by power interface, should be amplified and attenuated, respectively.

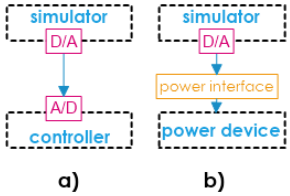

Fig. 4. HIL types in power systems (a) controller HIL (b) power HIL

3. Framework and platform

As mentioned, HIL simulation in power systems is divided into CHIL and PHIL. CHIL is a controller whose interface with the simulator section is usually ADC and DAC converters, and in PHIL the hardware section includes equipment that consumes or produces power. Therefore a power interface (PI) is required. a PHIL platform consists of three parts: 1) the RTSs, 2) HUT, and 3) the PI:

1) Real-time simulators simulate a part of the system that has an exact model or that we do not intend to develop. The simulator time constant to show the actual dynamic behavior of the system should be considered small enough depending on the application.
2) The hardware-under-test has previously been examined in detail for power system applications, including a part of the system that lacks a precise model, or that we intend to develop, or that we intend to launch a new equipment.
3) Depending on the application, the power interface includes power amplifiers (PAs), A/D converters, and feedback sensors, which are the connection between the hardware and the RTS.

3.1. Power interface (PI)

The power interface in PHIL applications consists of three parts: PAs, interface algorithms, and interface communication.

3.1.1. Power amplifiers (PAs)

Different types of PAs can be used depending on the application. PAs affect the bandwidth, accuracy and stability of HIL simulations. Therefore, the study of PA is necessary to create an optimal HIL simulation [5].

3.1.2. Interface algorithm (IA)

The interface algorithm communicates between the hardware part and the real-time simulator. The interface algorithm determines the type of signal sent, including voltage, current, speed, pressure, torque, etc., as well as signal

processing technology such as low-pass filter. The interface algorithm has a significant impact on the accuracy and stability of PHIL simulations. Below are five important interface algorithms described [6,7].

- *Ideal transformer method (ITM)*

This method is the simplest way to show the relationship between HUT and RTS as shown in Fig. 5. Its open loop transfer function is

$$-F_0(s) = \frac{e^{-sT_D} \times T_{pa}(s) \times T_M(s) \times Z_S(s)}{Z_L(s)} \tag{1}$$

Where T_D is the time delay due to the PA and the T_{pa} and T_M show the dynamic behavior of the PA and the measurement, respectively. The ratio of the simulated impedance of Z_S to the impedance of Z_L hardware indicates the stability of PHIL simulations.

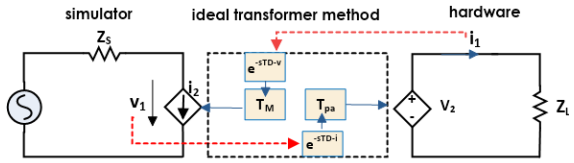

Fig. 5. Ideal transform method (ITM) interface algorithm diagram

- *Advanced ideal transformer (AIT) method*

By adding a Z_A impedance greater than zero to the RTS section as shown in Fig. 6, the stability of the ITM method increases but the simulation accuracy decreases. The open-loop transfer function of this method is

$$-F_0(s) = \frac{e^{-sT_D} \times T_{pa}(s) \times T_M(s) \times Z_S(s)}{Z_L(s) + Z_A(s)} \tag{2}$$

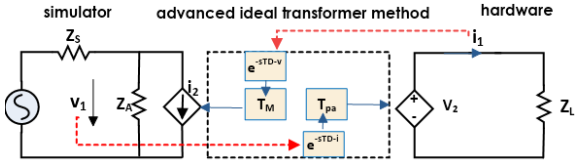

Fig. 6. Advanced Ideal transform (AIT) method interface algorithm diagram

- *Partial circuit duplication (PCD) method*

In this method, Z_B coupling impedances in RTS and HUT are added according to Fig. 7. In this method, the effect of the PA and the measurement and the time delay caused by them are negligible. The presence of Z_L significantly increases system stability but negatively affects simulation accuracy. The open-loop transfer function of this method is

$$-F_0(s) \approx \frac{Z_L(s) \times Z_S(s)}{(Z_L(s) + Z_B(s)) \times (Z_S(s) + Z_B(s))} \tag{3}$$

6

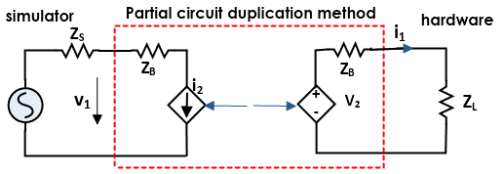

Fig. 7. Partial circuit duplication (PCD) method interface algorithm diagram

- *Damping impedance method (DIM)*

This method is a combination of ITM and PCD methods according to Fig. 8, in which a Z^* damping impedance is added to the RTS, which is a definite stability if equal to the ZH impedance, but increases the cost. The open-loop transfer function of this method is

$$-F_0(s) \approx \frac{Z_S(s) \times \left(Z_L(s) - Z^*(s) \right)}{\left(Z_L(s) + Z_B(s) \right) \times \left(Z_S(s) + Z_B(s) + Z^*(s) \right)} \tag{4}$$

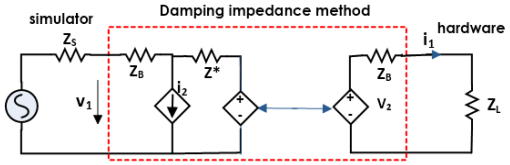

Fig. 8. Damping impedance method (DIM) interface algorithm diagram

- *Feedback current filter (FCF) method*

To increase the stability of the ITM method as shown in Fig. 9, a low-pass filter with a F_C cut-off frequency is added to limit harmonics and noise, but it affects accuracy. The transfer function of this method is in Equation (5), in which T_{FCF} represents the dynamic effect of FCF in the system.

$$-F_0(s) = \frac{e^{-sT_D} \times T_{pa}(s) \times T_M(s) \times Z_S(s) \times T_{FCF}(s)}{Z_L(s)} \tag{5}$$

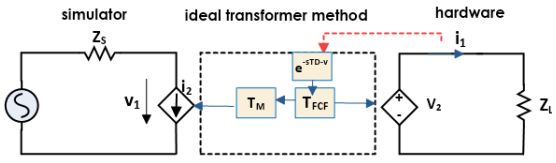

Fig. 9. Feedback current filter (FCF) method interface algorithm diagram

A summary of the interface algorithms is compared in the Table 1 [8,9].

Table 1. Comparison of PHIL interface algorithms

Interface algorithm	ITM	AIT	PCD	DIM	FCF
pros	best accuracy	high accuracy	extreme high stability	great stability	Extendible feature for IA
		easy to implement		good accuracy occure when $Z^*=Z_L$	
	easy to implement	good stability	Promising for large scale systems	method has the ability to adapt	easy to implement
cons		additional hardware	low accuracy	additional hardware	

7

low stability (depends on Z_S/Z_L)	accuracy depending on F_C

3.1.3. Ethernet-based communication

Ethernet-based protocols for proper communication and coordination of data transmission between intelligent electronic devices (IEDs) are described below.

- *IEC 61850*

The IEC 61850 communication standard offers the standardized data model structures and the rules how to exchange the data between intelligent electronic devices (IEDs). The IEDs from different vendors which support the IEC 61850 based structured data are capable of interoperating and exchanging data for monitoring and controlling the power flow in steady state operation and protecting different power system equipment during the faults. The implementation of IEC61850 standard not only ensures the interoperability between IEDs but it also reduces the integration and installation costs.

The IEC 61850 standard comprised of ten main parts starting from the IEC 61850-1-x to the IEC 61850-10. The IEC 61850-7-x defines the abstract data and service models for achieving the interoperability between IEDs independent of the communication system or related protocols. The IEC 61850-7-4 defines the logical nodes (LNs) as the smallest possible functional pieces of the logical device (relay) inside the physical device or IED that requires information exchange with other physical devices. Each logical node of the logical device contains different data sets and data attributes. Fig. 10 shows how the physical devices (IEDs) are mapped to the data models. For example, the voltage measurement of the logical node Measurement Unit #1 of the logical device Relay1 of the physical device IED is mapped to data model as IED:Relay1/MMXU1.MX.PhV, and the breaker position status of the logical node Circuit Breaker #1 of the logical device Relay1 of the physical device IED is mapped to data model as IED:Relay1/XCBR1.ST.Pos. The mapped data models for a particular IED are usually described in the substation configuration language (SCL) file called the ICD (IED capability description) file.

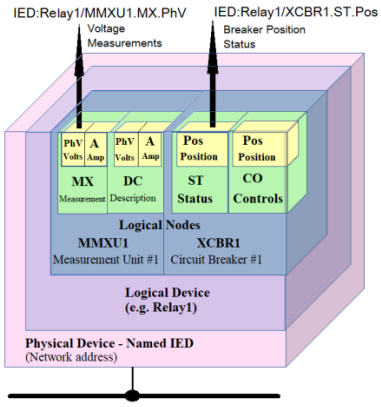

Fig. 10. Mapping of physical device to data models

The IEC 61850 standard defines two real-time peer-to-peer communication protocols: Generic object-oriented substation event (GOOSE) and sampled value (SV) messaging protocol. The GOOSE protocol can be used for exchanging both binary and analog type of data whereas the SV protocol can be used for transfer of the digitized transducer signals from the switchyard to the substation IEDs. The GOOSE and SV protocols both carry the time critical messages like fast tripping commands and the sampled values of the measured physical quantities, therefore these are mapped directly to the TCP/IP Ethernet link layer for saving the processing time.

8

The data or information exchange in IEC 61850 communication standard happens in a publisher/subscriber manner. It means an IED can publish the data to the Ethernet link with a multicast message and other IEDs need to subscribe the message in order to receive the data. For the successful subscription of a multicast GOOSE message, the subscriber IED need the GOOSE ID, application ID (AppID) and MAC (media access control) address of the published GOOSE message [10,11].

- *SPA protocol*

The SPA (Strömberg Protection Acquisition) or the SPA-bus communication protocol is an ASCII-based protocol used for the asynchronous serial communication and can be used as an alternative for the IEC 60870-5-103 communication protocol. The SPA communication is mainly used for the substation monitoring system. The data/information exchange in the SPA communication protocol is based on master/slave principle in which the computer acts as a master and any IED acts as a slave. A program is required in the master computer for interpretation of the SPA-bus codes and for translation of the data that should be sent to the IED. The master computer can be connected to the substation LAN with IEDs via the utility LAN or WAN connection.

The SPA protocol assumes that the slave does not need a self-initiated talk to the master and the master is aware of the data contained in the slaves which it can request when required. Moreover, the master can send data to the slave. The master requests the slave information using request messages performed by the sequenced polling method or only on demand. The master can send data/information to the slave in write messages. Additionally, the master can send data/information to all slaves in a common broadcast message containing time or other data. The most important settings in the IED for SPA communication are the slave number and baud rate or communication speed. In ABB 670 Series of IEDs, the slave number can be set from 1 to 899 and the baud rate can be set to between 300 and 38400 baud (bits per second) [12].

- *IEC 60870*

The IEC 60870 standard is one of the popular open communication standards particularly in Europe for the transmission of SCADA (supervisory control and data acquisition) telemetry control and information. Although IEC 60870 standard includes the general data types that can be used for a wide range of SCADA applications, however, it is primarily defined and used for the telecommunication of the electrical systems and control information. The IEC 60870 standard was defined in terms of the open systems interconnection (OSI) model using a subset of minimum three layers including the physical, data link and application layers, known as enhanced performance architecture (EPA) model. For the interoperability between equipment from different manufacturers, the IEC 60870 protocol included the detailed definition of the message structure at the data link layer and a set of data structures at the application layer.

The IEC 60870 standard structured in hierarchical manner consists of six main parts IEC 60870-1 to IEC 60870-6 and a number of companion standards. Each of the main part consists of a number of further sections. The IEC 60870-5 entitled as “Telecontrol equipment and systems-Part 5: Transmission protocols” is comprised of the five early developed sections of the IEC 60870 standard: IEC 60870-5-1 to IEC 60870-5-5 and these are considered as the core documents of the Transmission Protocols part of the standard. Four companion standards IEC 60870-5-101 to IEC 60870-5-104 are each separate application protocols intended for the specific purpose.

The IEC 60870-5-1 entitled as “Transmission frame formats” defined four frame formats or data structures suitable for telecontrol applications which include FT1.1, FT1.2, FT2 and FT3 data frames. The earlier version of IEC 60870-5-101 entitled as “Companion standard for basic telecontrol tasks” specified the use of FT1.2 frame format. The other separate open communication protocol called distributed network protocol (DNP) which was developed in parallel to IEC 60870 adopted the FT3 frame format of the IEC 60870-5-1. The companion standard IEC 60870-5-101 creates a full definition of a complete SCADA transmission protocol. This document provides all of the application-level data objects and functions necessary for SCADA operation over wide geographical areas using the low bandwidth bit-serial communication. The companion standards IEC 60870-5-102 and IEC 60870-5-103 contain data types and functions to support specifically the electrical protection systems including the distance protection, differential protection and transformer differential protection. The companion standard IEC 60870-5-104 defines the transport of

IEC 60870-5 application messages over networks. It means the companion standard IEC 60870-5-104 also includes the additional two layers of OSI model, the transport and network layers to use the TCP and IP protocols for transmission of IEC 60870-5 messages over networks. Therefore, IEC 60870-5-104 is also referred to as the network version of the IEC 60870-5, whereas IEC 60870-5-101 is referred to as the non-networked version.

The IEC 60870-5-101 supports point-to-point and multidrop communication links providing a choice of using balanced or unbalanced transmission at the link level. The IEC 60870-5-101 uses the master/slave principle for the data/information exchange. The standard assumes the hierarchical structure in a way that for any two stations communicating with each other, one is the controlling station (master) and the other is the controlled station (slave). The monitor direction and the control direction are also defined in a way that the monitored data (e.g., analog values from field) are sent in the monitoring direction and commands are sent in the control direction. In a dual-mode operation, a station can send both monitored data and commands thus acting both as the controlled and the controlling station. In SCADA systems, the master station usually consists of hardware and software infrastructure at some central location used for collecting data from various remote terminal units (RTUs) through communication system and providing an operator interface for display of information and control of remote locations. The RTUs are microprocessor based stand-alone data acquisition and control units for monitoring and controlling devices at remote locations. The RTUs usually acquire A/D data from the remote devices and transfer this data to central master station. It is also possible that RTUs can communicate with each other using peer-to-peer communication.

In IEC 60870-5-101 using the unbalanced transmission, only the master station acting as a primary on the link can initiate the communication by transmitting the data frames and the slave stations acting as secondary stations must wait until polled by the controlling station. The master station must acquire data from the slave stations by polling each in turn for data because slave stations cannot initiate transmission on their own. This simplifies the system design because there will be no need to avoid the collision problems which occur in balanced transmission when two controlled stations transmit the message simultaneously. The slave data link layer is also simple using the unbalanced transmission. The unbalanced transmission is suitable for multi-point topology or multidrop communications in which there is a master station and several slave stations. Using the balanced transmission, any station on the link can act as a primary station and initiate the communication. The balanced transmission is limited to only point-to-point topology or peer-to-peer communications in which there is a master station and only one slave station. The balanced transmission requires collision avoidance and recovery [13].

- *DNP3*

The distributed network protocol version 3.3, generally called the DNP3 protocol is an open SCADA telecommunication standard that was developed by Harris Controls Division initially as a proprietary protocol for the electrical utility applications in America. Today, the DNP3 protocol is also used in many other industrial applications including the water/wastewater, oil, gas and security industries around the world. The DNP3 protocol supported by a large number of SCADA vendors is also used in Europe along with the widely used IEC 60870-5 protocol in the region.

The DNP3 protocol defines the communication between the master stations, RTUs and other IEDs. It also offers the interoperability among devices of different manufacturers for application in different industrial systems. The DNP3 protocol is designed for the transmission of relatively small packets of data messages in a reliable and deterministic sequence compared with the TCP/IP protocol which can send large data files that are unsuitable for SCADA control. The DNP3 protocol is based on EPA model and uses the FT3 data frame defined in IEC 60870-5-1. The DNP3 protocol also uses some transport functions or pseudo-transport layers, sometimes described as the transport and network layers in a limited manner for the transmission of larger than commonly used blocks of data. Despite the common point of the origin, the IEC 60870-5 and DNP3 are completely separate protocols and not compliant with each other.

The DNP3 protocol uses the master-slave principle of data exchange and can support point-to-point or peer-to-peer (one-master one-slave), multidrop (one-master many-slaves), hierarchical master-slave with intermediate data concentrators and multiple-master communication topologies. The DNP3 supports two operational modes: polled and quiescent or reporting by exception operations. In the quiescent mode of operation, neither the polls from the master

10
station nor the responses from the slave station happen in the absence of any system change. However, an hourly periodic background poll is generally used by the master station to detect the communication failure in the quiescent mode of operation.

The capability of DNP3 protocol for supporting point-to-point or peer-to-peer and quiescent operation demands the requirement of non-master or slave stations to initiate communications, also referred to as the balanced communication. Despite the balanced communication capability, the differentiation between the master and slave stations remains necessary within the DNP3 protocol such that only the master stations can initiate requests for data or issue commands to other stations.

The DNP3 protocol offers many features including the flexibility and security. It provides time synchronization, secure configuration or file transfer, an optimum error control and rapid communication sequences by breaking message into multiple frames. It also supports broadcast messages, time stamped messages for sequence of events (SOE) recording, provides user definable objects and allows addressing for over 65000 devices on a single link [13].

- *Modbus*

The Modbus transmission protocol was developed by Schneider for the process control systems. It is considered as the de facto industrial communication standard due to its wide acceptance and applications in many industrial operations. The Modbus protocol uses the master-slave principle in which only the master initiates a transaction. One master and up to 247 slaves can be included in the Modbus transmission protocol. The transactions can either be a query/response type comprised of a single query/response data frame with single slave addressed or a broadcast/no response type comprised of a single broadcast data frame with all slaves addressed.

The information in the Modbus data frame for the transmission of message between the master and slaves includes the address of the intended receiver (address field), what the receiver must do (function field), the data needed to perform the action (data field) and a means of checking errors (error check field). The slave reads the message, performs the tasks if there is no error and sends a response back to the master. The information in the response message includes the slave address, the action performed, the result of the action and a means of checking errors. In case of the initial broadcast message from the master, no response is required from the slaves. The master can send another query as soon as it receives the response message. The timeout function ensures the continuity of the system operation when the query message is not received correctly.

In the Modbus protocol, the request frames with parity or checksum errors are ignored and no response is sent by any device. If the valid request frame contains an illegal request that is not supported by the slave unit, then an “exception response” is sent to the master. Table 2 lists the most important exception response codes in the Modbus protocol.

Table 2. Exception response codes in the Modbus protocol.

code	name	description
01	Illegal Function	Requested function is not supported
02	Illegal Data Address	Requested data address is not supported
03	Illegal Data Value	Specified data value is not supported
04	Failure in Associated Device	Slave has failed to respond to a message
05	Acknowledge	Slave is processing the command
06	Busy, rejected message	Slave is busy

Certain characteristics of the Modbus protocol are fixed like frame format, frame sequence, communication errors and exception conditions handling and the performed functions. Other characteristics like transmission medium, transmission characteristics and transmission mode (RTU/ASCII) are selectable. The RTU or the Modbus Binary mode is the preferred Modbus mode. The user characteristics set at each device cannot be changed when the system is running [13].

3.2. Real-time simulator

Power system dynamic equations can be solved using digital computers in a variety of ways. However, a huge amount of processing throughput is required to accomplish such sophisticated computations. In the past, special computers have been used, with simulation studies conducted off-line. The advancement of current microprocessors has made it possible to dedicate significant processing power to individual users at a low cost. Therefore, digital real-time simulation (DRTS) of the complex electric power system is possible using such hardware. As mentioned earlier a real-time process occurs in discrete time steps with a maximum duration and is rapid enough to affect the environment in which it occurs, such as inputs to a computing system. Some of the most important simulators are described below.

3.2.1. RTDS

The first real-time digital simulator (RTDS) based on a digital signal processor was tested in 1991 for the hardware controller of a high voltage direct current converter (HVDC) by Manitoba HVDC Research Center, Canada [14]. This simulator was then developed and is designed specifically to perform real-time electromagnetic transient simulations with a typical timestep of 50 microseconds. This simulator can be used for a wide range of power equipment and controllers and power electronics. Real-time emulators include a software component and a hardware component. The latest RTDS hardware as shown below includes units called NovaCor chassis [15]. Each chassis has an IBM RISC processor with 10 cores, each of which can work in parallel and carry out computational operations. One NovaCor chassis can model up to 600 nodes in one network solution, plus numerous embedded nodes, all within one tightly coupled subsystem. If a larger network model is required, as many as 144 NovaCor chassis can interconnected to represent extremely large grids. Each NovaCor chassis includes an Ethernet port so it can be connected to the LAN and easily accessed using a Windows PC. While running real time simulations, the NovaCor chassis do not use an OS, the processor cores run “bare metal” to provide the ultimate efficiency and determinism. The RTDS Simulator software is called RSCAD and runs on a standard Windows based PC. RSCAD consists of a number of modules through which the user designs/defines and performs the real time simulations and. The user can also interact with the real time simulation using RSCAD as well as retrieve and analyse data from the simulation.

The main purpose of a real time simulator is to test external equipment so the RTDS Simulator can be equipped with a number of I/O options. Conventional signal exchange is supported via analogue and digital input and output modules (GTIO modules). The simulator may also include GTNETx2 telecommunication cards to establish a high-level communication protocol such as IEC 61850. The GTNETx2 also supports communication protocols such as ModBus, TCP / UDP telecommunication socket, IEC 60870-5-104, IEEE C37.118 and DNP3 and Aurora (high speed serial communication).

12

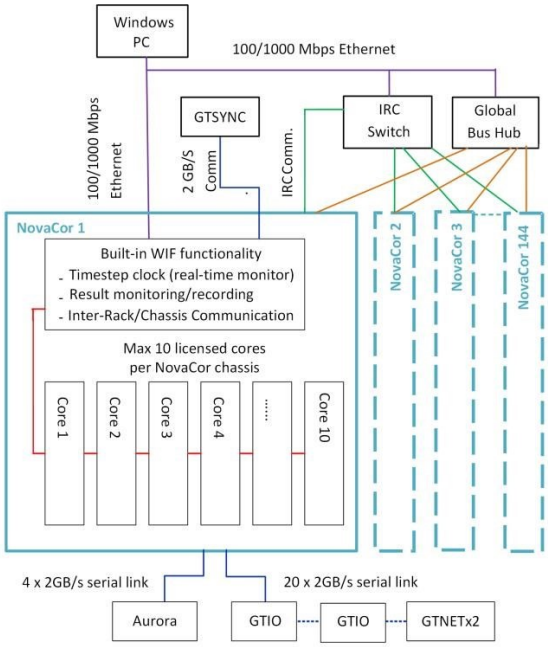

Fig. 11. Hardware architecture of RTDS simulator [15]

3.2.2. OPAL-RT

The OPAL-RT is a real-time digital simulator with Redhat Linux operating system that uses MATLAB/Simulink as the main modeling tool and RT-LAB as the real-time simulation platform. The RT-LAB is the main simulation software platform on which the most popular simulation systems/suites of OPAL-RT including eMEGASIM, ePHASORSIM and eFPGASIM are based. The RT-LAB as the main user interface software of OPAL-RT simulator enables MATLAB/Simulink models to interact with the actual devices in real-time for the development and validation of various applications. It offers customizable dashboards to control simulation parameters and visualize the simulation results in real-time providing at-a-glance behavior of the simulation models. The RT-LAB provides the code parallelization feature which can be used to distribute different sections of the simulation model on different CPU (central processing unit) cores and FPGAs. The RT-LAB software also contains various customized toolboxes and component block libraries. The OPAL-RT simulator hardware and the RT-LAB software also offer different communication protocols such as ModBus, TCP/UDP telecommunication socket, IEC 61850, IEEE C37.118, DNP3, OPC, CAN and Lin, and input/outputs (I/Os) for interfacing with other hardware/software controllers and test

equipment for HIL testing [15,16]. The results of real-time HIL testing can be saved in Mat-File using the OpWriteFile block for further offline analysis. The HIL testing platform using OPAL-RT simulator is shown in Fig. 12.

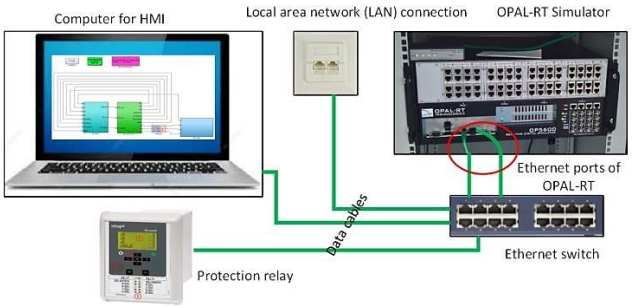

Fig. 12. The HIL testing platform using OPAL-RT simulator [10]

3.2.3. Typhoon

The most important feature of the Typhoon is the ability to test virtual HIL. Typhoon's internal libraries are full-featured in areas such as microgrids and electronics, making it easier for the user to do the simulation. The hardware of this simulator has three configurations: HIL402 with quad-core processor, HIL 604 with 6-core processor and HIL microgrid with multi-core processor. Typhoon has cards for external communication such as HIL DSP, HIL uGrid and HIL calibration. Typhoon Windows operating system and its software include schematic editor, SCADA, SUITE test and power system toolbox that also communicates with MATLAB. Typhoon supports ModBus, IEC 61850 and SunSpec telecommunication protocols [15,17].

3.2.4. dSpace

The dSpace offers different software and hardware options for rapid control prototyping (RCP), HIL and PHIL simulations. For the RCP it offers a high-performance development system called MicroLabBox hardware that includes a powerful dual-core processor with a user-programmable FPGA. This hardware offers more than hundred commonly used I/O channels for different function development, test and data acquisition [18]. For smaller RCP, it offers DS1104 research and development controller board option that includes a real-time processor and I/O interfaces which can be plugged directly into the personal computer. The real-time interface (RTI) software provides the link between the dSpace hardware and the development software (MATLAB/Simulink/Stateflow) for the RCP and HIL testing. For HIL testing of larger complex systems, the dSpace offers the modular FGPA-based hardware called dSPACE SCALEXIO. The dSPACE SCALEXIO is offered in the form of four application boxes: SCALEXIO LabBox for laboratories, SCALEXIO AutoBox for in-vehicle use, SCALEXIO off-the-shelf for HIL testing and SCALEXIO customized rack system. The main hardware of the SCALEXIO systems include the SCALEXIO processing unit and the DS6001 processor board plus application specific I/O hardware. The SCALEXIO systems are configured/implemented using a separate software called Configuration Desk. The HIL testing case studies of hybrid AC/DC power system and microgrid control using the RTDS and dSpace RT simulators are described in [19]. This simulator supports modern communication protocols and protocols such as Gigabit Ethernet PCIe, The Fieldbus Exchange Format (FIBEX), CAN and ARXML.

Other simulators include real time virtual test bed VTB-RT, HYPERSIM, speedgoat, a real-time simulator with MathWorks, Power system Online simulation Unveil Your Analysis (POUYA), Siemens' NETOMAC and more. Various HIL testing applications using different RT simulators are reviewed in [15,17], some examples are given in Table 3.

Table 3. Comparison of properties of real-time simulators.

14

RT Simulators	hardware	software	Modeling enivermoment	Application field	Case study
RTDS	PowerPC RICK Processor	OS: windows Application software: RSCAD	EMTP models, small time-step models	Power system and power electronic and equipment, controller Smart grid control	Optimal centralized voltage control, inverter evaluation.
OPAL-RT	Multi-core CPU-FPGA	OS: windows, Redhat Linux Application software: RT-Lab, Mtlab/Simulink	Simulink, code (c,c++matlab), discrete simulink solver, S-function	Power system, power electronic, Microgrid control	Intentional islanding, overcurrent relays.
dSPACE	CPU	OS: windows	Simulink, stateflow, c code models	Microgrid control	Primary & secondary control, demand response, active power curtailment.
Typhoon	FPGA	OS: windows	MATLAB, Typhoon schematic	Smart grid control (Remote lab connections), power electronic controller	Microgrid reliability, active & reactive power control at AC/DC transmission & distribution.

3.3. Hardware under test (HUT) in power system

With PHIL, electrical engineers can design, test, and install equipment related to sub-sectors of the electrical industry, including power electronics, protection, electric machines, microgrids, and etc. The following are examples and applications in these sub-sectors for the electricity industry.

3.3.1. Power electronic

Power electronics technology with conversion and control of electrical energy is used in a variety of applications including AC and DC power supplies, lighting and heating control, electric car drives, electronic welding, DC high voltage systems, flexible AC transmission systems (FACTS). Today, electronic power systems have become larger and more complex with the rapid development of semiconductors and the production of power semiconductor devices, so the development of an electronic power equipment in the power grid is a complex and long process that requires safe, cheap and fast methods. Therefore, using the HIL technique, the electronic power system can be placed as hardware in the simulation loop to check its performance and prevent damage to equipment and power grid.

An important part of electronic converters is the power of their control algorithm, which is becoming more complex every day, so in [20] to evaluate the behavior of the DC converter and inverter, HIL simulation has been used. Their control algorithm is implemented on a dedicated DSP and the model of these two converters is tested in a real-time digital simulator (RTDS). Due to the high switching frequencies of electronic power converters, the simulation time constant must be at least 100 times lower than the switching time constant [21], so for a microprocessor or a DSP with a sampling rate of 1 μs, the maximum switching frequency is 10 kHZ. For switching frequencies of medium to high power electronic converters, real-time is difficult due to the limited sampling rate of the processors as well as the minimum time required to solve the simulated model equations [22]. Therefore, in [23] the simulation of an ideal buck converter and a full-bridge converter with losses based on field programmable arrays (FPGAs) gate presentations for HIL is used, which can support up to high switching frequencies (100 kHz and above).

FPGAs has also explored various design alternatives to HIL from the perspective of different numeric formats, hardware design languages, and more.

3.3.2. Protection

Protection systems are one of the most important power grid equipment to create a reliable and efficient power grid. With the development of real-time simulators, followed by the simulation of large and complex power systems in the nearest real-time state, it has become possible to be able to protect their equipment and control algorithms in all conditions before using them in Test and evaluate the power system optimally. Now, with this possibility, it is possible to test the protection equipment, especially the relays, before installation and commissioning in the system, by increasing the reliability of the relays in the transmission and distribution systems by preventing unwanted operation. Below are some of the applications of the protection system in HIL simulation.

A communication network simulator integrated in a HIL simulation with OPAL-RT simulator to provide a test bench for evaluating security applications in power systems is presented in [24]. This test bench shows that by changing the characteristics of the modeled communication network, it affects the performance of protection systems. A new algorithm for coordination between protection equipment in an intelligent power system using HIL is presented in [25]. The smart grid in the LabVIEW environment is simulated in real-time and two protection relays are placed in the simulation loop as hardware. One of the most widely used protection devices in power systems are overcurrent relays. Incorrect settings of these relays can lead to incorrect trips resulting in false shutdown or failure to detect overcurrent and consequent lack of cut-off command for breakers and damage to the power system. Therefore, before installation in the system, they must be tested in critical conditions. In [26] a SIL simulation for overcurrent relays in MATLAB is designed and simulated with the OPAL-RT simulator. For SIL validation, hardware overcurrent relays in the form of HIL have also been simulated and compared. A distance relay to protect the feeder of a single machine system with infinite bus simulated in PSCAD software has been tested as HIL simulation in [27]. The function of this relay is implemented virtually in a commercial microcontroller.

3.3.3. Microgrids

With the development of clean and free renewable energy, the necessary ground has been provided for the development of microgrids. With microgrid, the network can be divided into small networks with renewable energy supply in case of emergency and keep the network energized. Therefore, coordination control methods and energy management systems are needed in these cases, which is almost done with software simulations, but when all the microgrids are simulated dynamically, they are not responsive. Therefore, using HIL simulation, microgrids can be tested efficiently in critical situations.

A HIL simulation to test the performance of a microgrid control algorithm under island and network-connected conditions is presented in [28]. Microgrids are implemented in hardware in a real-time RTDS simulator and control and protection algorithms. In a microgrid including diesel generator and wind turbine generator (WTG), low microgrid inertia is an important challenge for network reliability and frequency response. In [29], a model-less control strategy to evaluate the microgrid frequency response has been investigated. Diesel generator and WTG are simulated on a real-time FPGA, and the control algorithm is embedded in the simulation loop. A 50 kVA microgrid is simulated in RTDS including solar panels, wind turbines, storage and communication system with HIL simulation in [30]. A complete HIL simulation platform for microgrid testing that is able to configure the platform at multiple levels (including system level controller, equipment level controller, and microgrid equipment level) and incorporate hardware levels into HIL simulation is presented in [31].

4. Stability of HIL Experiments

Due to the existence of two separate simulated components and hardware in the PHIL system and as a result of external disturbances such as limited bandwidth, sensor noise, ripple of interface amplifier and time delay, the system

16

performance must be stable. In addition, stability must be accompanied by accurate results. The problem of stability and accuracy in a PHIL simulation depends on the simulator time constant and the interface method.

There are different ways to improve the stability of a PHIL simulation system with power interfaces. The difference between these methods is in their ease of implementation and efficiency, so each of these methods should not affect the accuracy of the simulation. These methods are based on voltage control as shown in Fig. 13, in which the main circuit is divided into two parts, the simulator and the hardware, which are connected by a PA. The amplifier receives voltage v from the simulator and delivers v to the hardware, which has an error of e. This voltage difference then leads to a different current measurement than the correct value in the hardware. Therefore in time t_k we have

$$\Delta V_2 = v, i_2 = \frac{V_2}{Z_L} \Rightarrow \Delta i_2(t_k) = \frac{v}{Z_L} \tag{6}$$

This current is sent to the simulator section through the current source, so this current error causes a further error in the voltage v. So in t_{k+1} time we have

$$V_1 = V_S - Z_S i_1 \Rightarrow \Delta V_2(t_{k+1}) = -(\frac{Z_S}{Z_L})v \tag{7}$$

Eventually the greater the error value V, the greater the error in i, and this cycle is repeated. Therefore, if the value of Z_S/Z_L is greater than 1, the increase in error will continue until we reach the hardware limit, and the PHIL simulation becomes unstable.

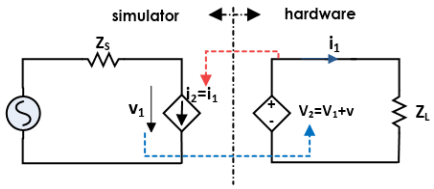

Fig. 13. The original circuit of a PHIL simulation based on voltage control

Therefore, the following methods can be used [32,33]:

4.1. Hardware inductance addition (HIA) method

The basic method to increase the stability of PHIL simulation is to add an inductance in series with the hardware part as shown in Fig. 14. This amount of inductance should be greater than the minimum value of the system stabilizer, but on the other hand the minimum amount of inductance is required for simulation accuracy. Details of this method are given in.

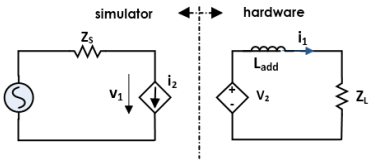

Fig. 14. Stability method based on hardware inductance addition (HIA)

4.2. Feedback current filtering (FCF) method

In the HIA method, we saw that the stability increases with increasing inductance, but decreases the simulation accuracy, and therefore inductance was the only adjustable parameter. To overcome this problem in the FCF method shown in Fig. 15, the measured current of the hardware part is properly filtered by a multiple filter block. These blocks are simulated for paternal flexibility due to the variety of hardware topologies. Therefore, by adjusting the amount of the filter block, the optimal point of stability and accuracy can be reached. Details of this method are given in.

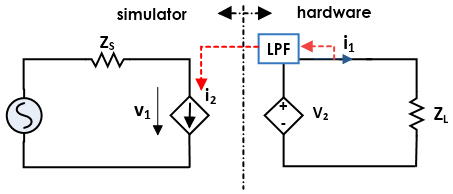

Fig. 15. Stability method based on feedback current filtering (FCF)

4.3. Multi-rate partitioning (MRP) method

In this method, according to the Fig. 16, the simulated part is divided into two fast subsystems with small time step and the slow subsystem with large time step. Now, because the stability of the whole system is directly related to the fast subsystem, first the stability of this subsystem is determined by the hardware and then the stability of all subsystems is examined by the hardware. The determination of subsystems depends on the topology of the system, which, if chosen correctly, provides the desired accuracy. This method is usually combined with FCF. Details of this method are given in.

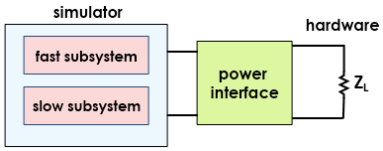

Fig. 16. Stability method based on multi-rate partitioning (MRP) method

To compare the three methods introduced above, a solar panel with a hardware inverter by a long transmission line to a low voltage network is investigated in real-time simulation, in [34]. The analytic results shown in Table 4.

Table 4. Comparison of stability methods of PHIL simulations.

Method	HIA	FCF	MRP	VERY FAST SAMPLING
Implementation effort	Low (hardware inductance needed)	Low (software filter needed)	High (multi-rate capable real-time system needed)	Very high (very fast real-time computing system needed)
Analytic complexity	Low	Medium	Very high	low
Stabilization	Always possible if inductance value is high enough	Always possible if cutoff frequency is low enough	In combination with FCF always possible	There may necessary unrealistic sampling rates for stabilization
Accuracy	Accuracy Poor	Medium	High	Very high

18

Feasibility	Always	Always	Often, depends on topology	Only for small systems

5. Conclusion

This article presents a comprehensive encyclopedia reported in the literature on HIL simulations in today's large and complex power systems. The parts required to implement a HIL simulation include power interfaces, real-time simulators, and hardware under the simulation description, and a variety of available methods are compared. PA for different power levels is introduced in terms of accuracy and stability indicators. The five interface algorithms are also compared in terms of accuracy, stability, economics and implementation difficulty. Ethernet-based high-level telecommunication protocols have been described for convenient communication between simulators and HUTs. Types of simulators are given to observe the dynamic behavior of HIL simulation in real-time. Examples of HIL simulations for power system applications are also provided. In this paper, three methods to improve the stability of HIL simulation are compared, adding an inductor in HIA and a filter in FCF. MRP requires a real-time multi-rate computing system but has the desired stability with the highest accuracy.

References

[1] Dufour, C., Soghomonian, Z. and Li, W. (2018). *Hardware-in-the-Loop Testing of Modern On-Board Power Systems Using Digital Twins*. [online] IEEE Xplore. Available at: https://ieeexplore.ieee.org/abstract/document/8445302.

[2] Nibert, J., Herniter, M. and Chambers, Z. (2012). Model-Based System Design for MIL, SIL, and HIL. *World Electric Vehicle Journal*, 5(4), pp.1121–1130.

[3] Steurer, M. (2006). *PEBB based high-power hardware-in-loop simulation facility for electric power systems*. [online] IEEE Xplore. Available at: https://ieeexplore.ieee.org/abstract/document/1709379 [Accessed 17 Jan. 2022].

[4] Barragán-Villarejo, M., García-López, F. de P., Marano-Marcolini, A. and Maza-Ortega, J.M. (2020). Power System Hardware in the Loop (PSHIL): A Holistic Testing Approach for Smart Grid Technologies. *Energies*, 13(15), p.3858.

[5] Lauss, G.F., Faruque, M.O., Schoder, K., Dufour, C., Viehweider, A. and Langston, J. (2016). Characteristics and Design of Power Hardware-in-the-Loop Simulations for Electrical Power Systems. *IEEE Transactions on Industrial Electronics*, [online] 63(1), pp.406–417. Available at: https://ieeexplore.ieee.org/abstract/document/7177085 [Accessed 17 Jan. 2022].

[6] Brandl, R. (2017). Operational Range of Several Interface Algorithms for Different Power Hardware-In-The-Loop Setups. *Energies*, 10(12), p.1946.

[7] Ren, W., Steurer, M. and Baldwin, T.L. (2008). Improve the Stability and the Accuracy of Power Hardware-in-the-Loop Simulation by Selecting Appropriate Interface Algorithms. *IEEE Transactions on Industry Applications*, 44(4), pp.1286–1294.

[8] Edrington, C.S., Steurer, M., Langston, J., El-Mezyani, T. and Schoder, K. (2015). Role of Power Hardware in the Loop in Modeling and Simulation for Experimentation in Power and Energy Systems. *Proceedings of the IEEE*, [online] 103(12), pp.2401–2409. Available at: https://ieeexplore.ieee.org/abstract/document/7289345 [Accessed 17 Jan. 2022].

[9] Nguyen, V.H., Besanger, Y., Tran, Q.T., Boudinnet, C., Nguyen, T.L., Brandl, R. and Strasser, T.I. (2017). *Using power-hardware-in-the-loop experiments together with co-simulation for the holistic validation of cyber-physical energy systems*. [online] IEEE Xplore. Available at: https://ieeexplore.ieee.org/abstract/document/8260122 [Accessed 17 Jan. 2022].

[10] Memon, A.A. and Kauhaniemi, K. (2021). Real-Time Hardware-in-the-Loop Testing of IEC 61850 GOOSE-Based Logically Selective Adaptive Protection of AC Microgrid. *IEEE Access*, 9, pp.154612–154639.

[11] Memon, A.A. and Kauhaniemi, K. (2020). An Adaptive Protection for Radial AC Microgrid Using IEC 61850 Communication Standard: Algorithm Proposal Using Offline Simulations. *Energies*, 13(20), p.5316.

[12] www.readkong.com. (n.d.). *670 series 2.0 IEC SPA Communication Protocol Manual - ABB Group*. [online] Available at: https://www.readkong.com/page/670-series-2-0-iec-spa-communication-protocol-manual-5928612 [Accessed 17 Jan. 2022].

[13] Clarke, G.R., Reynders, D. and Wright, E. (2008). *Practical modern SCADA protocols : DNP3, 60870.5 and related systems*. London: Elsevier ; Oxford.

[14] Kuffel, R., Giesbrecht, J., Maguire, T., Wierckx, R.P. and McLaren, P. (1995). RTDS-a fully digital power system simulator operating in real time. *IEEE WESCANEX 95. Communications, Power, and Computing. Conference Proceedings*, 2(19-24).

[15] Omar Faruque, M.D., Strasser, T., Lauss, G., Jalili-Marandi, V., Forsyth, P., Dufour, C., Dinavahi, V., Monti, A., Kotsampopoulos, P., Martinez, J.A., Strunz, K., Saeedifard, M., Xiaoyu Wang, Shearer, D. and Paolone, M. (2015). Real-Time Simulation Technologies for Power Systems Design, Testing, and Analysis. *IEEE Power and Energy Technology Systems Journal*, 2(2), pp.63–73.

[16] OPAL-RT. (n.d.). *Real time digital simulator | Real time system | OP5600*. [online] Available at: https://www.opal-rt.com/simulator-platform-op5600/ [Accessed 17 Jan. 2022].

[17] Noureen, S.S., Shamim, N., Roy, V. and Bayne, S.B. (2017). Real-Time Digital Simulators: A Comprehensive Study on System Overview, Application, and Importance. *International Journal of Research and Engineering*, 4(11), pp.266–277.

[18] www.dspace.com. (n.d.). *MicroLabBox Hardware*. [online] Available at: https://www.dspace.com/en/inc/home/products/hw/microlabbox.cfm#179_23629.
[19] Joseph, T., Jose, K., Ugalde-Loo, C.E., Li, G. and Liang, J. (2019). Real-Time Hardware-in-The-Loop Platform for Hybrid AC/DC Power System Studies. *2019 IEEE Milan PowerTech*.
[20] Cha, S.T., Wu, Q., Nielsen, A.H., Østergaard, J. and Park, I.K., 2012, March. Real-time hardware-in-the-loop (HIL) testing for power electronics controllers. In *2012 Asia-Pacific Power and Energy Engineering Conference* (pp. 1-6). IEEE.
[21] Zamiri, E., Sanchez, A., de Castro, A. and Martínez-García, M.S. (2019). Comparison of Power Converter Models with Losses for Hardware-in-the-Loop Using Different Numerical Formats. *Electronics*, 8(11), p.1255.
[22] Lauss, G. and Strunz, K. (2019). Multirate Partitioning Interface for Enhanced Stability of Power Hardware-in-the-Loop Real-Time Simulation. *IEEE Transactions on Industrial Electronics*, 66(1), pp.595–605.
[23] Zamiri, E., Sanchez, A., Yushkova, M., Martínez-García, M.S. and de Castro, A. (2021). Comparison of Different Design Alternatives for Hardware-in-the-Loop of Power Converters. *Electronics*, 10(8), p.926.
[24] Adrah, C.M., Kure, Ø., Liu, Z. and Høidalen, H.K., 2017, June. Communication network modeling for real-time HIL power system protection test bench. In *2017 IEEE PES PowerAfrica* (pp. 295-300). IEEE.
[25] Grillo, S., Bertolo, M. and Ragaini, E., 2018, June. Adaptive protection algorithms for smart distribution systems: Hardware-in-the-loop testing and validation. In *2018 IEEE International Conference on Environment and Electrical Engineering and 2018 IEEE Industrial and Commercial Power Systems Europe (EEEIC/I&CPS Europe)* (pp. 1-6). IEEE.
[26] Almas, M.S., Leelaruji, R. and Vanfretti, L., 2012, October. Over-current relay model implementation for real time simulation & Hardware-in-the-Loop (HIL) validation. In *IECON 2012-38th Annual Conference on IEEE Industrial Electronics Society* (pp. 4789-4796). IEEE.
[27] Camarillo-Penaranda, J.R., Aredes, M. and Ramos, G. (2021). Hardware-in-The-Loop Testing of a Distance Protection Relay. *IEEE Transactions on Industry Applications*, 57(3), pp.2326–2331.
[28] Xiao, B., Starke, M., Liu, G., Ollis, B., Irminger, P., Dimitrovski, A., Prabakar, K., Dowling, K. and Xu, Y., 2015, September. Development of hardware-in-the-loop microgrid testbed. In *2015 IEEE energy conversion congress and exposition (ECCE)* (pp. 1196-1202). IEEE.
[29] Ferrari, M., Park, B. and Olama, M.M., 2021, February. Design and Evaluation of a Model-Free Frequency Control Strategy in Islanded Microgrids with Power-Hardware-in-the-Loop Testing. In *2021 IEEE Power & Energy Society Innovative Smart Grid Technologies Conference (ISGT)* (pp. 1-5). IEEE.
[30] Jeon, J.H., Kim, J.Y., Kim, H.M., Kim, S.K., Cho, C., Kim, J.M., Ahn, J.B. and Nam, K.Y., 2010. Development of hardware in-the-loop simulation system for testing operation and control functions of microgrid. *IEEE Transactions on Power Electronics*, *25*(12), pp.2919-2929.
[31] Wang, J., Pratt, A., Prabakar, K., Miller, B. and Symko-Davies, M., 2021. Development of an integrated platform for hardware-in-the-loop evaluation of microgrids prior to site commissioning. *Applied Energy*, *290*, p.116755.
[32] Lauss, G. and Strunz, K. (2021). Accurate and Stable Hardware-in-the-Loop (HIL) Real-Time Simulation of Integrated Power Electronics and Power Systems. *IEEE Transactions on Power Electronics*, 36(9), pp.10920–10932.
[33] Lauss, G., Lehfuß, F., Viehweider, A. and Strasser, T., 2011, November. Power hardware in the loop simulation with feedback current filtering for electric systems. In *IECON 2011-37th Annual Conference of the IEEE Industrial Electronics Society* (pp. 3725-3730). IEEE.
[34] Viehweider, A., Lauss, G. and Felix, L., 2011. Stabilization of Power Hardware-in-the-Loop simulations of electric energy systems. *Simulation Modelling Practice and Theory*, *19*(7), pp.1699-1708.